

**Faculty of Science and Engineering  
Western Australian School of Mines**

**Back Analysis of Intensive Rock Mass Damage at the El Teniente Mine**

**César Pardo Mella**

**This thesis is presented for the Degree of  
Doctor of Philosophy  
of  
Curtin University**

**Sept.2015**

**To Silvana, Javiera y Renato**

## **DECLARATION**

To the best of my knowledge and belief this thesis contains no material previously published by any other person except where due acknowledgement has been made.

This thesis contains no material which has been accepted for the award of any other degree or diploma in any university.

Signed: .....

Date: .....

## **ABSTRACT**

Current mining of massive ore bodies is leading to deep operations with a requirement for an increased production. Specifically at the El Teniente mine due to copper price cycle and the current low grades of the deposit, the underground production has been increased. This has led the incorporation of new mine sectors and the expansion and consolidation of large caving sectors, such as Esmeralda and Reservas Norte mines. However, the Esmeralda operation has experienced geotechnical related damage that over years has created an impact regarding the fulfilment of production targets. The damage consists of large collapses in the central part of the caving front that have reduced its undercutting rate and forced the development and implementation of contingency plans to deliver the planned production. To this date the mechanism of the collapses are not clearly defined. Therefore, to address this issue, a systematic scientific back-analysis of Esmeralda's damage coupled with the application of numerical modeling was undertaken.

The key philosophy behind this study is the continual improvement in understanding of collapses phenomenon. This was achieved by systematic scientific back analysis of large scale damage in Esmeralda which was carried out to produce an end product encompassing a mix of theoretical research and modelling and empirical data collection and analysis.

Large scale geological data, intact rock properties, geotechnical instrumentation and observational records were reviewed and analyzed as part of methodology phase one. In parallel, and based upon Esmeralda evidence, rock mass behavior in other sectors at El Teniente Mine and the literature review, a conceptual model was created. Collapses mechanism hypothesis were performed in that phase. In addition, the conceptual model was validated by a numerical simulation of all previous extraction geometries with back analysis of documented damage.

Based on the experienced damage through the whole extraction history of the Esmeralda sector, two periods of Esmeralda collapses were identified. The first period (2001 to 2005) where a pre-undercut sequence was used as the mining method was defined. The damage was characterized by a collapse occurrence behind the undercut front. The second period (2008 to 2010) where a pre-undercut sequence with advanced developments was used as the mining method was also identified. The damage was characterized by a collapse occurrence ahead of the undercut front.

A three dimensional non-linear solution of stress, strain and energy distribution was developed to determine the deformation and damage on the extraction level and undercut level for comparison with observations during model calibration. Based on the plastic strain results (% rock mass damage), an Esmeralda scale damage was developed for its extraction evolution. By mean of this scale, the collapsed zones by periods were assessed in order to undertake the final phase of the back analysis.

Finally, the research identified that for the modified version of panel caving with pre-undercut sequence and advanced developments method the collapsed pillars located ahead of the undercut front were exposed to important stress changes and to an increased abutment stress. On the other hand, in the panel caving with pre-undercut sequence method the collapsed pillars were unconfined. For both cases, where the rock mass was affected by weak faults, this would also facilitate the pillar collapses. The model results have confirmed that the collapse mechanism is strongly related to the exploitation method used and also the conceptual models described have been validated by field observations and the model results.

## ACKNOWLEDGEMENTS

I wish to express my gratitude to the following individuals and organizations without whose help I would not have completed this project:

Professor E. Villaescusa who was my principal thesis supervisor for his technical contributions and advice during the preparation of this thesis. I am particularly grateful for giving me the opportunity to undertake this research and having faith in me. In spite of his demanding professional and personal work commitments, he was always available to discuss, critic and review all aspects of my thesis. I feel very privileged to have worked under his direct supervision.

Dr. Andres Brzovic for his friendship, encouragement and technical discussions related to cave mining. Dr. A. Brzovic provided me with the necessary support in rock mass characterization and greatly influenced the directions taken in my thesis modelling work. His constructive comments during the overall thesis are equally and greatly acknowledged and appreciated.

Dr. David Beck, Beck Engineering Pty. Ltd., for his invaluable help through our discussion regarding numerical modeling, preparing and running the numerical models and for his enthusiasm and encouragement.

Dr. Peter Cepuritis for his friendship, their ideas, and their willingness to share information on their own research.

Mr. Chris Windsor for initiating my understanding and passion for all things related to rock stress tensor. Dr. Alan Thompson for his unconditional support during my PhD studies.

I'd like to thank all my friends at WASM, especially to Dr. Ellen Morton and Luis Machuca for being my good friends, listening to my ideas and keeping my morale up at certain times.

Mr. Octavio Araneda and Mr. Mauricio Barraza, from CODELCO-Chile, for providing me with the opportunity and the support to come Australia to undertake my PhD.

El Teniente Division – CODELCO Chile for their financial support towards this research work. I wish also to thank all of the staff of the Geotechnical Team of El Teniente Division for their support and assistance in submitting the field data for the Esmeralda operation. I especially would like to thank Carlos Cifuentes, Pedro Landeros and Raynal Dunlop.

Mr. Eduardo Rojas for his constant enthusiasm and support throughout my career.

My family. Special appreciation is expressed to my wife Silvana and my children Javiera and Renato for their love, understanding and support in particular during the past three years.

# TABLE OF CONTENTS

<b>DECLARATION</b>	<b>i</b>
<b>ABSTRACT</b>	<b>ii</b>
<b>ACKNOWLEDGEMENTS</b>	<b>iv</b>
<b>TABLE OF CONTENTS</b>	<b>v</b>
<b>LIST OF TABLES</b>	<b>ix</b>
<b>LIST OF FIGURES</b>	<b>x</b>
<b>CHAPTER 1 INTRODUCTION</b>	<b>1</b>
1.1 MASS MINING .....	1
1.2 UNDERGROUND MASS MINING METHODS .....	2
1.2.1 General view .....	2
1.2.2 Caving Mechanism.....	7
1.2.3 History and Future.....	10
1.3 MAJOR HAZARDS IN CAVE MINING.....	13
1.3.1 Major Collapses.....	14
1.3.2 Rock Bursts .....	15
1.3.3 Mud Rushes.....	15
1.3.4 Water and Slurry Inrushes.....	16
1.3.5 Air Blasts.....	16
1.4 CONTEXT AND SCOPE .....	17
1.5 RESEARCH APPROACH.....	20
1.6 THESIS STRUCTURE.....	22
<b>CHAPTER 2 PANEL CAVING OPERATIONS AT THE EL TENIENTE MINE</b>	<b>23</b>
2.1 EL TENIENTE OVERVIEW .....	23
2.1.1 History.....	23
2.1.2 Location.....	24
2.1.3 Resources and Size.....	24
2.2 MINE SITE GEOLOGY .....	26
2.2.1 <i>El Teniente</i> Mafic Intrusive Complex .....	29
2.2.2 Felsic Intrusion.....	30
2.2.3 Breccias .....	30
2.2.4 Alteration.....	31

2.2.5	Structures.....	32
2.3	MINING METHODS.....	35
2.3.1	Evolution of Exploitation Method at the <i>El Teniente</i> Mine .....	35
2.4	GEOTECHNICAL RISKS AT THE <i>EL TENIENTE</i> MINE .....	41
2.4.1	Hangings.....	42
2.4.2	Collapses .....	43
2.4.3	Rockbursts.....	46
2.5	ESMERALDA MINE .....	50
2.5.1	Introduction .....	50
2.5.2	Rock Mass Characterization.....	51
2.5.3	A Review of Mine Strategy.....	54
2.5.4	Esmeralda Ore Production.....	56
<b>CHAPTER 3</b>	<b>LITERATURE REVIEW</b>	<b>57</b>
3.1	INTRODUCTION.....	57
3.2	CHARACTERIZATION OF PRIMARY ORE FOR PANEL CAVING OPERATION .....	57
3.2.1	Introduction .....	57
3.2.2	Behavior for primary intact rock.....	59
3.2.3	Behavior for Primary Rock Mass.....	67
3.3	GEOTECHNICAL HAZARDS - COLLAPSE IN CAVING OPERATIONS .....	75
3.3.1	Terminology .....	76
3.3.2	Reviewing experienced collapses.....	79
3.3.3	Reviewing collapse mechanism .....	82
3.4	NUMERICAL MODELING APPROACHES .....	86
3.4.1	Introduction – fundamentals.....	86
3.4.2	Numerical Simulations for Cave Performance.....	90
<b>CHAPTER 4</b>	<b>GEOTECHNICAL INSTABILITIES AT THE ESMERALDA PANEL CAVING OPERATION</b>	<b>96</b>
4.1	INTRODUCTION.....	96
4.2	COLLAPSES EXPERIENCED IN OTHER OPERATIONS AT EL TENIENTE MINE.....	98
4.3	REVIEWING GEOTECHNICAL INSTABILITES AT ESMERALDA OPERATION .....	101
4.3.1	Rock Bursts .....	101
4.3.2	Instabilities on Undercut Level .....	104
4.3.3	General view of experienced collapses on extraction level at Esmeralda operation .	107
4.4	DESCRIPTION OF COLLAPSED DRIFTS IN ESMERALDA .....	108

4.4.1	The Early Period of Esmeralda Collapses (1997 to 2005) .....	110
4.4.2	The Later Period of Esmeralda Collapses (2006 to 2010) .....	121
4.5	CONSEQUENCES OF EXPERIENCED COLLAPSES.....	130
<b>CHAPTER 5</b>	<b>NUMERICAL MODELLING FOR ESMERALDA PANEL CAVING OPERATION</b>	<b>132</b>
5.1	INTRODUCTION.....	132
5.2	A REVIEW OF LINEAR ELASTIC MODELLING USED AT EL TENIENTE MINE.....	133
5.2.1	Fundamentals of linear elastic modelling.....	134
5.2.2	Summary of the main models previously used at El Teniente operations.....	140
5.2.3	Linear elastic analysis for intensive rock mass damage on the later period of extraction history at the Esmeralda operation .....	144
5.3	FUNDAMENTALS OF NON-LINEAR ELASTO-PLASTIC MODELLING .....	152
5.4	WORKFLOW OF MINE SCALE NON-LINEAR MODEL.....	155
5.4.1	Geometry assembly .....	155
5.4.2	Calibration .....	157
5.4.3	Back analysis.....	158
5.4.4	Lesson learned.....	158
5.5	DATA APRECIATION AND MODEL BUILDING .....	158
5.5.1	Selection of modelling packages .....	159
5.5.2	Constitutive model .....	159
5.5.3	Model geometry and mesh discretisation .....	163
5.5.4	Extraction Sequencing and Model Step .....	167
5.5.5	In situ Stress Field.....	169
5.5.6	Faults .....	171
5.5.7	Material Assumptions .....	173
5.6	MODEL CALIBRATION.....	175
5.6.1	Selection and Bracketing.....	175
5.6.2	Detailed Fine Adjustment.....	175
5.6.3	Resulting Material Properties .....	176
5.6.4	Correlation to Measured Seismicity and Modelled Energy Release .....	184
5.6.5	Comparison with measured rock mass damage.....	187
5.6.6	Instability Criteria for Excavation Performance.....	200
5.7	SENSITIVITY ANALYSIS, UNDERSTANDING AND UNCERTAINTY .....	206
5.7.1	Material properties .....	206
5.7.2	Geometrical singularities during undercutting .....	209

5.7.3	Exercise for undercut level design .....	211
<b>CHAPTER 6</b>	<b>BACK ANALYSIS RESULTS</b>	<b>213</b>
6.1	INTRODUCTION.....	213
6.2	ASSESSING THE EARLY PERIOD OF THE ESMERALDA COLLAPSE.....	214
6.3	ASSESSING THE LATER PERIOD OF THE ESMERALDA COLLAPSE .....	220
6.4	CONFIRMING THE COLLAPSE MECHANISM .....	227
<b>CHAPTER 7</b>	<b>CONCLUSIONS AND FURTHER WORK</b>	<b>229</b>
7.1	BACK ANALYSIS OF ROCK MASS DEFORMATION EXPERIENCED AT THE EL TENIENTE MINE .....	229
7.2	MAIN FINDINGS AND ACHIEVEMENTS OF RESEARCH .....	230
7.3	LIMITATIONS AND RECOMMENDATIONS FOR FUTURE WORK.....	233
<b>REFERENCES</b>		<b>235</b>
<b>APPENDIX A –</b>	Constitutive model description for the continuum parts	<b>245</b>
<b>APPENDIX B –</b>	Rock mass properties used in the numerical simulation	<b>250</b>
<b>APPENDIX C –</b>	Representative summary of images from model results for Esmeralda simulation	<b>261</b>
<b>APPENDIX D –</b>	Benchmark of collapses for Codelco underground operations	<b>271</b>
<b>APPENDIX E –</b>	Maps of observed damage on undercut level esmeralda operation for all extraction steps (1999 - 2009)	<b>282</b>

## LIST OF TABLES

Table 2.1:	Resources inventory 2011 (Larrain et al, 2011). .....	25
Table 3.1:	Strength of the primary rock masses at El Teniente according to a traditional assessment using the Hoek-Brown method (Modified by Karzulovic, 2006b).....	69
Table 3.2:	Numerical methods used in engineering rock mechanics applications to mining (from Flores, 2005).....	89
Table 5.1:	Main features of previous numerical modelling developed for El Teniente operations.. .....	143
Table 5.2:	Elastic properties used into mine scale model (Cuello et al. 2010).....	145
Table 5.3:	Main mine model steps and their descriptions .....	167
Table 5.4:	Detailed record of major model adjustment during calibration.....	177
Table 5.5:	Esmeralda Damage scale with detailed description .....	202

# LIST OF FIGURES

## Chapter 1

Figure 1.1:	100 years of continuous growth evolution of daily production rates of selected large underground mines (Brown 2007).....	2
Figure 1.2:	Locations of block and panel caving mines (modified after Brown 2007). ....	3
Figure 1.3:	Classification of the principal methods of underground mining (after Brady and Brown 2004).....	4
Figure 1.4:	Classification of the principal mining methods by caving, according to the method of fracture of the ore column (after Flores 2005). ....	4
Figure 1.5:	Illustration of mechanized block or panel caving (Flores 2005) .....	5
Figure 1.6:	Mechanized panel caving, Henderson Mine, Colorado, USA (Doepken 1982).....	6
Figure 1.7:	Conceptual model of caving (after Duplancic and Brady 1999) .....	9
Figure 1.8:	The process of caving and cave evolution (Flores 2005) .....	10
Figure 1.9:	Block caving, Miami Mine, Arizona, USA (after Brown 2007) .....	11
Figure 1.10:	Classification of major operational hazards (Brown 2007).....	14
Figure 1.11:	Sequence of air blast at Salvador Mine, Chile (de Nicola and Fishwick 2000). ....	17
Figure 1.12:	Total collapsed area by sector and primary ore production from 1982 to 2011 (Larrain et al., 2011).....	18

## Chapter 2

Figure 2.1:	Location of the <i>El Teniente</i> mine in Chile. ....	25
Figure 2.2:	Geology of central Chile (after Skewes et al. 2002). ....	26
Figure 2.3:	Geology of the area surrounding the El Teniente copper deposit with true north (after Skewes et al. 2002).....	27
Figure 2.4:	The NE-trending Teniente Fault Zone (TFZ) is a broad zone of NE-trending faults (modified from Garrido, 1994).....	28
Figure 2.5:	Plainview with lithology of the El Teniente ore body at the Ten-5 level (2284z) and two representative photos. ....	29
Figure 2.6:	Stockwork intersected andesite rock type within primary copper ore. The white square (top photo) and the rock bolt plate (bottom photo) are 20x20 cm. (from Brzovic, 2010).....	31
Figure 2.7:	Core tray 0,7m length showing rock masses of secondary ore at the El Teniente mine (Brzovic, 2010).....	33
Figure 2.8:	East-West section at El Teniente mine showing the primary and secondary ore (Brzovic, 2010).....	33
Figure 2.9:	Faults at El Teniente mine within primary copper ore. Rock bolt plates are 20x20 cm. (Brzovic, 2010).....	34
Figure 2.10:	Typical cross section of panel caving with conventional sequence where the numerical order represents the operational sequence. ....	36
Figure 2.11:	Typical cross section of panel caving with pre-undercut sequence where the numerical order represents the operational sequence. ....	37
Figure 2.12:	Typical cross section of panel caving with pre-undercut sequence and advanced developments where the numerical order represents the operational sequence. ....	38

Figure 2.13:	Different blast designs used in Esmeralda operation : (a) John Wayne, (b) Complete Pillar and (c) Parallel holes. ....	39
Figure 2.14:	Example of the formation of a chimney-type crater immediately after a hangingwall failure affecting the Sector Inca Oeste at Salvador, on December 5, 1999 in Chile (modified from Flores & Karzulovic, 2002). ....	42
Figure 2.15:	Damage in drifts of undercutting level in Sector Teniente 4 Sur of El Teniente mine, due to a collapse occurred in 1989 (from Flores & Karzulovic, 2002). ....	43
Figure 2.16:	Gradual damage in the pillar wall of production level Esmeralda operation, due to a collapse that occurred in 2010. ....	44
Figure 2.17:	Sectors affected by collapses and the respective productive areas that were damaged vs. the production of primary ore from 1982 to 2010. ....	45
Figure 2.18:	Relation between the extraction front widths and operative area affected by collapses. ....	46
Figure 2.19:	Example of heavy damage due to rockburst in El Teniente Mine, Reno Operation, 2005. ....	47
Figure 2.20:	Example of heavy damage due to rockburst in El Teniente Mine, Pilar Norte Operation, 2011. ....	48
Figure 2.21:	Example of heavy damage due to rockburst in El Teniente Mine, Haulage level at Reno Operation, August 2012. ....	48
Figure 2.22:	Number of rockbursts per operation vs. annual production of primary ore ranging from 1982 to 2012. ....	50
Figure 2.23:	Relative location of Esmeralda operation ....	51
Figure 2.24:	Plan view with major lithology and structures at Undercut level Esmeralda operation. Where the predominant lithology is the mafic complex El Teniente (CMET or ex-andesite). ....	52
Figure 2.25:	Map of the potential disassembly of the rock mass during the mining process (Undercut Level for Esmeralda operation), map GL-10659-0 (Brzovic, 2013). ....	54
Figure 2.26:	Evolution of production of primary ore in the Esmeralda Mine ....	56

### Chapter 3

Figure 3.1:	Idealized illustration of transition from intact rock to rock mass (after Hoek and Brown, 1980). ....	58
Figure 3.2:	Some examples of brittle failure in Portland stone cores tested with confinement between 0 and 28 MPa (Farmer, 1983). ....	59
Figure 3.3:	Uniaxial stress-strain curves for six rocks (Waversik & Fairhurst, 1970) ....	61
Figure 3.4:	Two classes of stress-strain behavior observed in uniaxial compression tests (Waversik & Fairhurst, 1970). ....	61
Figure 3.5:	Idealized stress-strain curves and associated states for squeezing rocks. ....	63
Figure 3.6:	Longitudinal cut of core in primary rock CMET, showing the presence of sealed veinlets in a stockwork type of arrangement, the diameter of the core is 6". (from Karzulovic, 2006b). ....	64
Figure 3.7:	Development of a rupture plane in a Lac du Bonnet granite core. Schematics (a) to (f) show the position of the acoustic emission events in different stages of the test and indicate clearly than when exceeding $\sigma_{cd}$ a "global" plane of rupture starts forming (Martin, 1997). ....	64

Figure 3.8:	Schematic illustrating the evolution of cracking related damage in a rock core, according to results of “numerical experiments” with a model of cemented discs and using the PFC software (Diederichs, 2003).....	66
Figure 3.9:	Fracture progression and related AE hypocenter distributions. Foliation and eventual failure plane are also shown (Villaescusa et al., 2009). ....	66
Figure 3.10:	Hoek-Brown envelopes for peak strength (short term, purple dots) and stress of fracturing damage start (long term according to recommendations from Martin & Chandler, 1994, red dots). This figure also shows the straight lines defining the start condition of fracturing in the laboratory (dotted line) and in situ (thick line) for Lac du Bonnett granite (Martín, 1997).....	67
Figure 3.11:	Over-excavation in the primary rock mass at El Teniente (CMET lithology), Production Level, Sector Ten Sub 6 ( $\sigma_1/\sigma_c \approx 0.3$ ), (taken from Karzulovic, 2006). ....	70
Figure 3.12:	Over excavation observed in tunnels with different shapes and size excavated in hard rock. In each case shows the orientation of main secondary stresses in the plane of transversal section of tunnel (Martin et al, 1999).....	71
Figure 3.13:	Pre-existing discontinuities at the primary ore mass of El Teniente (CMET), Undercut Level, Esmeralda operation. ....	72
Figure 3.14:	Schematic of failure envelope for brittle failure, showing four zones of distinct rock mass failure mechanism: no damage, shear failure, spalling and unraveling (Diederichs, 2002).....	73
Figure 3.15:	Zone of potential spalling of the rock mass by the effect of the stress induced around underground excavations in hard rock (Cho et al, 2002). ....	74
Figure 3.16:	Stress path and failure modes of the rock mass, considered in Sweden for underground deposits of radioactive waste excavated in hard rock (Martin & Christiansson, 2002).....	74
Figure 3.17:	Major Collapse, Type 1, involving collapse of crown pillar (Brown, 2003). ....	76
Figure 3.18:	Major Collapse, Type 2, involving falls or large blocks from the cave back (Brown, 2003).....	77
Figure 3.19:	Major Collapse, Type 3, involving failures on and around the extraction level (Brown, 2003).....	78
Figure 3.20:	Relative frequency of area affected by one single collapse in caving operations (Flores and Karzulovic, 2002). ....	80
Figure 3.21:	Relative frequency of different main causes of collapses in caving operations (Flores and Karzulovic, 2002). ....	81
Figure 3.22:	Conceptual model to explain pillars behavior affected by collapses (Van Sin Jan, 2010).....	84
Figure 3.23:	Conceptual model to explain extraction drifts behavior affected by collapses (Van Sin Jan, 2010). ....	85
Figure 3.24:	Flowchart of rock mechanics modeling techniques (Jing and Hudson 2002). ....	87
Figure 3.25:	(a) Three-dimensional DFN, (b) the corresponding three- dimensional synthetic rock mass sample, and (c) synthetic rock mass basic components. The colors in (b) and (c) denote intact rock blocks bounded by joints (from Mas Ivars et al., 2007). ....	91
Figure 3.26:	Example of data from multiple sources visualized in a 3d collaborative workspace. The layering of modeled and measured data aids rapid model calibration, validation and improvements (from Beck et al., 2011). ....	93

## Chapter 4

Figure 4.1:	Drifts of extraction level affected by collapses at El Teniente Mine. In green color the collapsed drifts of Ten-4 Sur can be appreciated. ....	99
Figure 4.2:	Damage caused by the collapse that affected Teniente 4 Sur in October - November 1991. This picture shows C-12/Z-15 and the draw point. ....	100
Figure 4.3:	Plan view that shows in shaded color the Production Level in sector Teniente 4 Sur that were affected by a collapse in October 1984. In blue is shown the position of the caving faces by September 30, 1984 and in red the main geological faults in the sector (modified from Morel, 1986). ....	101
Figure 4.4:	Representative cross section view of the exploitation face in Esmeralda, with the relative location of damage generated by rock bursts between 1997 and 2004 (Rojas et al., 2005).....	102
Figure 4.5:	Drifts damaged by rock bursts in the undercut level of Esmeralda operation, in the period from 1997 to December 2004 (Rojas et al., 2005). ....	103
Figure 4.6:	Mapped damage located ahead of undercut front between august 1999 – dec.2004 at The Esmeralda operation.....	105
Figure 4.7:	Inclination and length of blast holes performed in the second phase of the inspection plan for pillars in Esmeralda operation (from Rubio and Seguel, 2005).....	106
Figure 4.8:	Boundaries of production drifts collapsed 2001 – 2010 along with main lithologies and the major faults in Esmeralda operation. ....	108
Figure 4.9:	The main operational milestones and area affected by collapses for the Esmeralda operation.....	109
Figure 4.10:	Location of Remnant pillars left on undercut level period 1999 to 2001.....	111
Figure 4.11:	Collapse of block affecting the roof of intersection C17/Z13, Production Level, Esmeralda Sector (view from Z13 to the North, from Karzulovic, 2003b).....	112
Figure 4.12:	Mining geometry and damage experienced on Esmeralda operation – March 2001. ....	113
Figure 4.13:	Mining geometry and damage experienced on Esmeralda operation – June 2001. ...	113
Figure 4.14:	Mining geometry and damage experienced on Esmeralda operation – Sept. 2001... ..	113
Figure 4.15:	Mining geometry and damage experienced on Esmeralda operation – Oct. 2001. ....	114
Figure 4.16:	Mining geometry and damage experienced on Esmeralda operation – Nov.. 2001.. ..	114
Figure 4.17:	Mining geometry and damage experienced on Esmeralda operation – Dec. 2001. ...	114
Figure 4.18:	Mining geometry and damage experienced on Esmeralda operation – March 2002. ....	115
Figure 4.19:	Mining geometry and damage experienced on Esmeralda operation – Aug. 2002... ..	115
Figure 4.20:	Mining geometry and damage experienced on Esmeralda operation – Dec. 2002. ...	115
Figure 4.21:	Important damage in the pillars of drift C23 with trench Z12, Production Level, Esmeralda Sector. ....	117
Figure 4.22:	Initial deformation of the external steel arc of the extraction point C23/Z12, Production Level, Esmeralda Sector. ....	117
Figure 4.23:	Mining geometry and damage experienced on Esmeralda operation – March 2003. ....	118
Figure 4.24:	Mining geometry and damage experienced on Esmeralda operation – Aug. 2003... ..	118
Figure 4.25:	Mining geometry and damage experienced on Esmeralda operation – Dec. 2003. ...	118
Figure 4.26:	Representative damage in drift C19, Production Level, Esmeralda Sector.....	119
Figure 4.27:	Mining geometry and damage experienced on Esmeralda operation – Feb. 2004....	120
Figure 4.28:	Mining geometry and damage experienced on Esmeralda operation – Jul. 2004. ....	120
Figure 4.29:	Mining geometry and damage experienced on Esmeralda operation – Aug. 2004... ..	120
Figure 4.30:	Sketch for the Esmeralda mine plan year 2007 based on three shorter fronts.....	121

Figure 4. 31:	Draw bells incorporated at Esmeralda operation during 2008. (Modified from Dunlop et al., 2010).....	123
Figure 4. 32:	Draw bells incorporated at Esmeralda operation during 2009. (Modified from Dunlop et al., 2010).....	123
Figure 4.33:	Collapsed drifts on extraction level during December 2008. ....	124
Figure 4.34:	Collapsed drifts on extraction level during November 2009.....	124
Figure 4.35:	Collapsed drifts on extraction level during January 2010. ....	125
Figure 4.36:	Collapsed drifts on extraction level during June 2010. ....	125
Figure 4.37:	Collapsed drifts on undercut level at Esmeralda operation, years 2009 to 2010 (modified from Barraza et al., 2010). ....	126
Figure 4.38:	Extent of damaged drifts to the undercut level at Esmeralda operation (modified from Barraza et al., 2010). ....	127
Figure 4.39:	Damage to C-25 as seen looking north from the XC slot (from Hustrulid et al., 2010). ....	127
Figure 4.40:	Damage to connection between C-43 –C42 as seen looking towards the Hw. ....	128
Figure 4.41:	Damage to draw point C-23 and Z-25.....	128
Figure 4. 42:	(a) Damage to C-45 as seen looking north from Z-21. (b) Floor heave and other damage to C-45. Looking to the south from Z-15.....	129
Figure 4. 43:	Changed records of damage with time to the wall panels in C-43 (Modified from Dunlop et al., 2010).....	129

## Chapter 5

Figure 5.1:	Rock mass response – constitutive model on stress-strain relationship .....	135
Figure 5.2:	(a) Relationship between elastic models and damage (Wiles, 2001), (b) showing various stress paths to over-stressing .....	137
Figure 5.3:	Reliability level for linear elastic analysis (modified from Wiles, 2006) .....	139
Figure 5.4:	General view of large-scale 3D input geometry for Map3D Modelling. ....	141
Figure 5.5:	Over-stressing distribution ahead of the undercut front from model with explicit galleries in the Reservas Norte Sector.....	142
Figure 5.6:	Numerical modelling strategy at El Teniente Mine (Pardo and Landeros, 2008). ....	144
Figure 5.7:	Tridimensional model with detailed geometry of Esmeralda Operation year 2009 (Cuello et al. 2010).....	146
Figure 5.8:	Stress distribution around modelled undercut drift and a photo with the over break observed at the same drift 2009 (Cuello et al. 2010).....	147
Figure 5.9:	Linear elastic critical stress-based criteria for different damage threshold (modified from Cuello et al. 2010). ....	149
Figure 5.10:	Linear elastic critical stress-based criteria for different damage threshold (modified from Cuello et al. 2010) .....	150
Figure 5.11:	Strain- stress relationship influenced by constitutive model (Cepuritis, 2010).....	152
Figure 5.12:	The workflow followed for numerical simulation performed. ....	156
Figure 5.13:	An example of modelled versus measured rock mass damage at one mine. Damage measured by core drilling pillars at selected locations to ground truth the model and also to better correlate the plastic strain scale with the visual impression of damage in the rock (Beck 2011). ....	162
Figure 5.14:	Model size, boundary condition, and modelled mine levels. ....	164

Figure 5.15:	Final design geometry for the Esmeralda operation, as built in Abaqus showing the higher order element mesh on the extracted surfaces. The volume is also filled with elements.....	165
Figure 5.16:	Description of the geometries modelled and their scales. ....	166
Figure 5.17:	Detailed geometries of some mine model step in the numerical model.....	168
Figure 5.18:	Principal stress orientations measured by WASM AE and CSIRO HI techniques (Windsor et al. 2006a). ....	169
Figure 5.19:	Magnitude distribution of principal stress measured by WASM AE and CSIRO HI techniques (Windsor et al. 2006a). ....	170
Figure 5.20:	Initial geological equilibrium with the stress field and initial surface topology after hypothetical ranges erosion. ....	171
Figure 5.21:	Plan view of modelled regional faults for El Teniente mine.....	172
Figure 5.22:	Esmeralda three dimensional structural model.....	173
Figure 5.23:	Uniaxial compressive strength. ....	174
Figure 5.24:	Triaxial compressive strength. ....	174
Figure 5.25:	Magnitude distribution of vertical stress during bracketing phases. ....	176
Figure 5.26:	Proxy relation between cohesion and friction angle for Hoek-Brown parameters m and s.....	178
Figure 5.27:	Changes to peak strength for CMET Fw between M05 and M17.....	179
Figure 5.28:	Changes to peak strength for CMET Hw between M05 and M17.....	180
Figure 5.29:	Changes to peak strength for Diorite between M05 and M17.....	181
Figure 5.30:	Changes to Faults properties between M05 and M17. ....	182
Figure 5.31:	Final material property sets (M17) used in calibrated model version. ....	183
Figure 5.32:	Examples of modelled energy release versus measured seismicity for three different steps, software Voxler. ....	186
Figure 5.33:	Representative example of one mapped damage ahead of undercut front for extraction geometry May 2007 (Geotechnical team, Div. El Teniente 2007).....	188
Figure 5.34:	Representative photo of significant damage in the Undercut level at Esmeralda operation.....	189
Figure 5.35:	Representative photo of Moderate damage in the Undercut level at Esmeralda operation.....	189
Figure 5.36:	Superseded results, plastic strain in the model correlated with damage threshold contoured from mapped damage for the exactly same extraction geometry modelled (first term 2001). 191	
Figure 5.37:	Superseded results, plastic strain in the model correlated with damage threshold contoured from mapped damage for the exactly same extraction geometry modelled (second term 2005).....	192
Figure 5.38:	Superseded results, plastic strain in the model correlated with damage threshold contoured from mapped damage for the exactly same extraction geometry modelled (last term 2007). ....	193
Figure 5.39:	Contoured collapsed area within undercut level and plastic strain from extraction geometry modelled (second term 2003). ....	194
Figure 5.40:	Contoured collapsed area within undercut level and plastic strain from extraction geometry modelled (last term 2003).....	195
Figure 5.41:	Contoured collapsed area within undercut level and plastic strain from extraction modelled (second term 2004). ....	196
Figure 5.42:	Location inspected pillar on undercut level for extraction geometry year 2004. ....	197
Figure 5.43:	Damage observed in drill core (Rojas et al. 2005).....	198

Figure 5.44:	Plastic strain distribution on the cross sections through assessed undercut pillar. ....	199
Figure 5.45:	Plastic strain recorded in the exactly same location of the drillhole through undercut pillar. ....	200
Figure 5.46:	Esmeralda local damage scale based on plastic strain values and associated drift deformation .....	201
Figure 5.47:	Modelled support load and contoured significant damage on extraction level, 2005204	
Figure 5.48:	Modelled support load and contoured significant damage on extraction level, 2008205	
Figure 5.49:	CMET Triaxial test results and properties finally used in the calibrated model. ....	207
Figure 5.50:	Isometric view with the cave simulated for extraction step second term 2007, Esmeralda operation. ....	209
Figure 5.51:	Plan view of modelled undercut geometry for excavation step year 2001 Esmeralda Operation along to the Remnant pillars associated to that period. ....	210
Figure 5.52:	Plan view of extraction level Esmeralda with Plastic strain modelled and contoured area for observed significant rock mass damage during year 2001. ....	210
Figure 5.53:	Plastic strain results for two different undercut designs modelled. ....	212

## Chapter 6

Figure 6.1:	Comparison between the procedures of forward and back analysis (Sakurai 1997). ....	213
Figure 6.2:	Representative cross section of Esmeralda for the earlier period of collapse (2000-2005), where panel caving with pre-undercut sequence was used. ....	215
Figure 6.3:	Cross section of modelled geometry through experienced collapse zone for early period showing contours of plastic strain associated to modelled step. ....	217
Figure 6.4:	Cross section of modelled geometry through experienced collapse zone showing contours of major and minor principal stress for each modelled step. ....	218
Figure 6.5:	Location of pillars assessed for the earlier period of Esmeralda .....	218
Figure 6.6:	Stress-strain path for four assessed pillars associated with the pre-undercut sequence, 2000-2005. ....	219
Figure 6.7:	Principal stress path for four assessed pillars associated to the pre-undercut sequence, 2000-2005. ....	220
Figure 6.8:	Representative cross section for the later period of the Esmeralda collapse (2008-2010), where a modified version of advance undercutting panel caving was used. ...	222
Figure 6.9:	Cross section of modelled geometry through experienced collapse zone for the later period showing contours of plastic strain associated with modelled step. ....	223
Figure 6.10:	Cross section of modelled geometry through experienced collapse zone for the later period showing contours of major and minor principal stress for each modelled step. ...	224
Figure 6.11:	Location of assessed pillars for later period of Esmeralda .....	225
Figure 6.12:	Stress-strain path for two assessed pillars associated with a modified version of advance undercut method, 2008-2010. ....	225
Figure 6.13:	Principal stress path for two assessed pillars associated with a modified version of the advanced undercut method, 2008-2010. ....	226
Figure 6.14:	Stress path for two representative collapsed pillars for both Esmeralda period. ....	228

## **CHAPTER 1**

### **INTRODUCTION**

#### **1.1 MASS MINING**

Although specific definitions of the term mass mining are not easy to make, its use implies that mining will be on a large scale in massive orebodies whose dimensions are extended in all three directions. Base on the production rates two types of mines may be described as mass mining (Brown 2004):

- Surface mines: production rates are more than 30,000 tonnes per day (tpd) or about 10 million tonnes per year (tpy).
- Underground mines: production exceeding 10,000 tonnes per day (tpd) or about 3 million tonnes per year (tpy).

In underground mass mining methods such as block or panel caving, sublevel caving and open stoping are commonly used. Moreover, these mass mining methods are often mechanized with a high level automation and non-selective.

The way of extracting safely and economically some of the world's most important commodities such as copper, gold, molybdenum, nickel and diamond in a large –scale represents the main feature of mass mining. The use of mass mining methods is increasing across the world and in the last decade it has been highlighted the successful application of caving methods in adverse circumstances such as strong and depth ore bodies with geotechnical issues.

Although the production rates from the world's largest open pit have grown progressively over the last 100 years, open pit depths have increased leading higher operational costs and unknowns engineer challenges in terms of open pit new designs. Additionally, the essential economic factors in open pit mining, especially in the case of deep open pits, are associated with the stability of the slopes and the efficiency of the material handling systems. Depending on the grade, distribution of the ore, the geometry and magnitude of the deposit, underground mining may, in some cases, have a lower cost than a very deep open pit mining operation. Therefore, often all these factors have favoured the underground mass mining as option. The point is reinforced by the fact that companies such as Rio Tinto and Codelco have stated that in about 15 years's time could be producing more copper from underground than from open pit. (Brown 2007).

Therefore, based on the increasing commodities demand and all the technical issues of underground methods not yet solved, the industry trends in underground mass mining show that the future will be challenging.

## 1.2 UNDERGROUND MASS MINING METHODS

### 1.2.1 General view

Due to the current trends of world mining, high production rates and low operational costs have become the key on mining business. Consequently, underground cave mining methods, such as sublevel, block or panel caving, are the only methods through which these main objectives can be achieved.

Currently these methods are being often implemented across the world. In fact, the figure 1.1 shows the evolution of production rates in tonnes of ore per day for the largest underground mines in the world. Production rates for sublevel stoping, sublevel caving and panel caving mines are included. Figure 1.1 also shows and highlights the evolution of production rate at El Teniente mine, one of the largest block caving mine around the world. Additionally, figure 1.1 shows some milestones in the development of the discipline of rock mechanics and underground mass mining research (Brown, 2007).

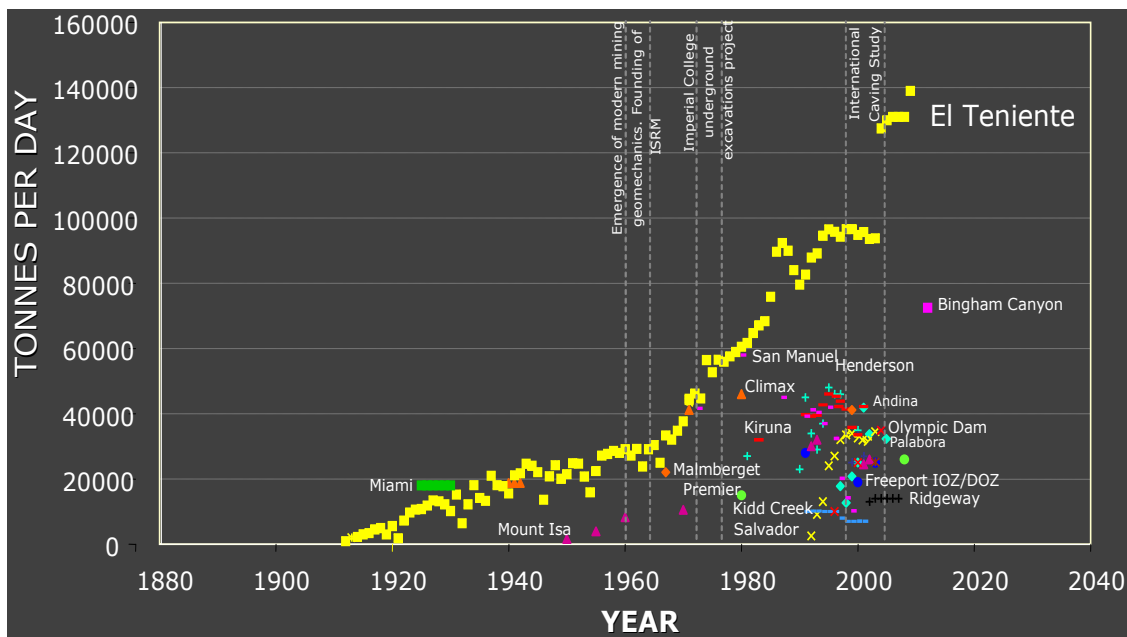


**Figure 1.1:** 100 years of continuous growth evolution of daily production rates of selected large underground mines (Brown 2007)

Additionally, figure 1.2 shows the locations of known current operations and some of future projects. Mainly block caving and panel caving mines are shown in figure 1.2.

According with the state art of current underground mass mining operations, the general classification of these methods have been generated by the literature. A division into three general classes has been identified (Brown 2007):

- Super Block Panel caving (BPC), and occasional sublevel caving, operations producing more than 25 million tpy or 75,000 tpd ore.
- Bulk BPC, Sublevel caving (SLC) and sublevel open stoping (SLOP), producing 10 to 20 million tpy or 30,000 to 60,000 tpd ore.
- Large BPC, SLC and SLOS producing 4 to 6 million tpy or 10,000 to 15,000 tpd.

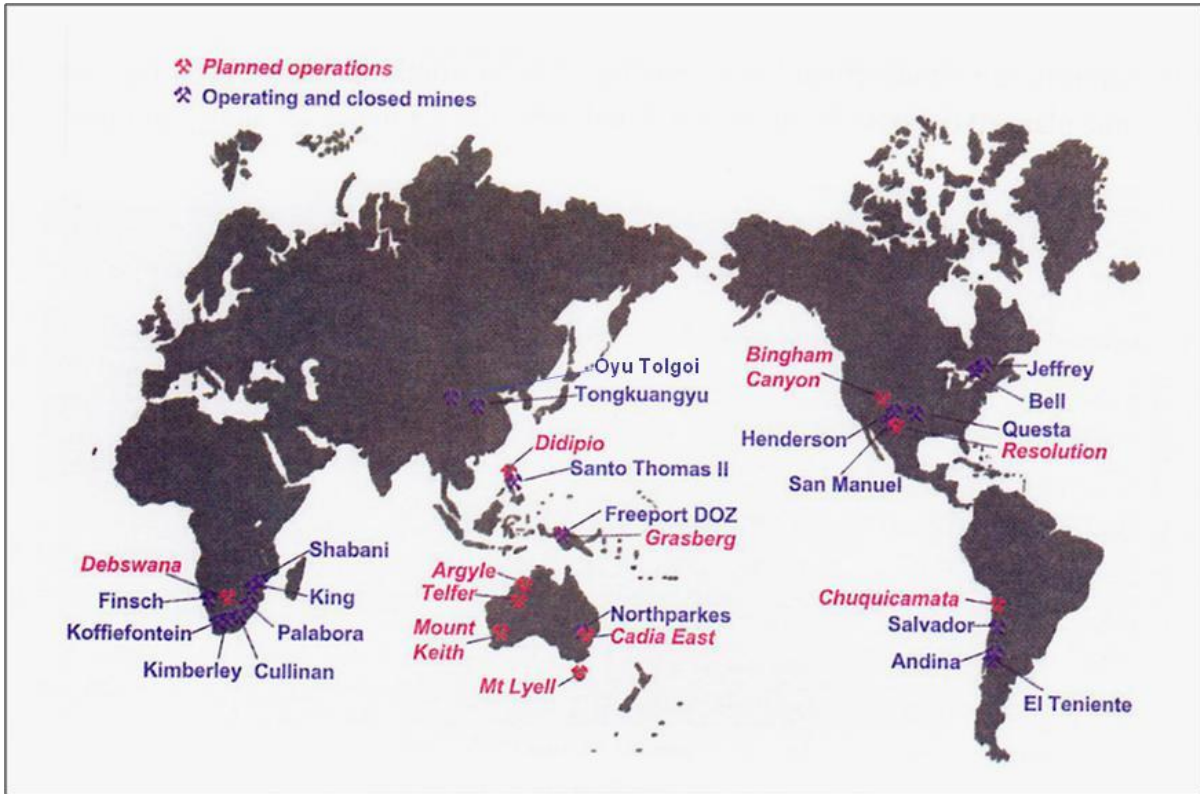


**Figure 1.2:** Locations of block and panel caving mines (modified after Brown 2007).

Other classifications of underground mining methods have been developed within the literature. As shown in Figure 1.3 the mining methods commonly employed in industrial practice are classified according to level of cavity support where the ore is extracted (Brady and Brown 2004). The caving and panel methods represent the most unsupported cave group and they experience the bigger magnitudes of displacement in the country rock with respect to the others methods. In addition, as shown the figure 1.4 the caving methods could be classified according to the ore loading method used, the way in which they induce the breakage of the column to be caved and the undercutting strategy (Flores 2005).

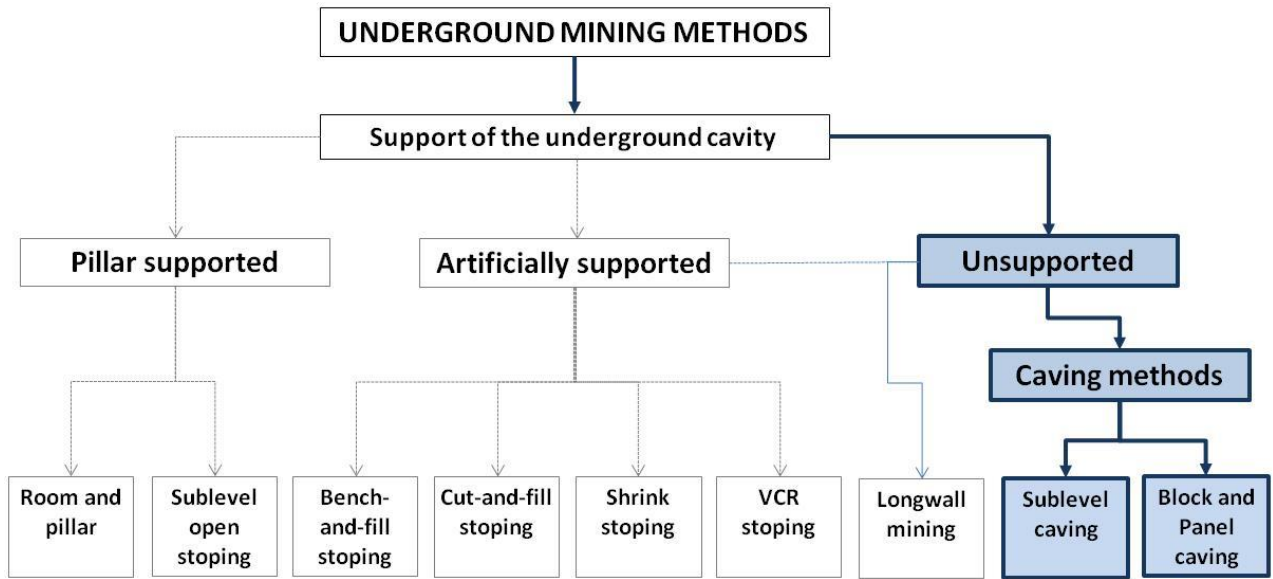


Figure 1.3: Classification of the principal methods of underground mining (after Brady and Brown 2004).

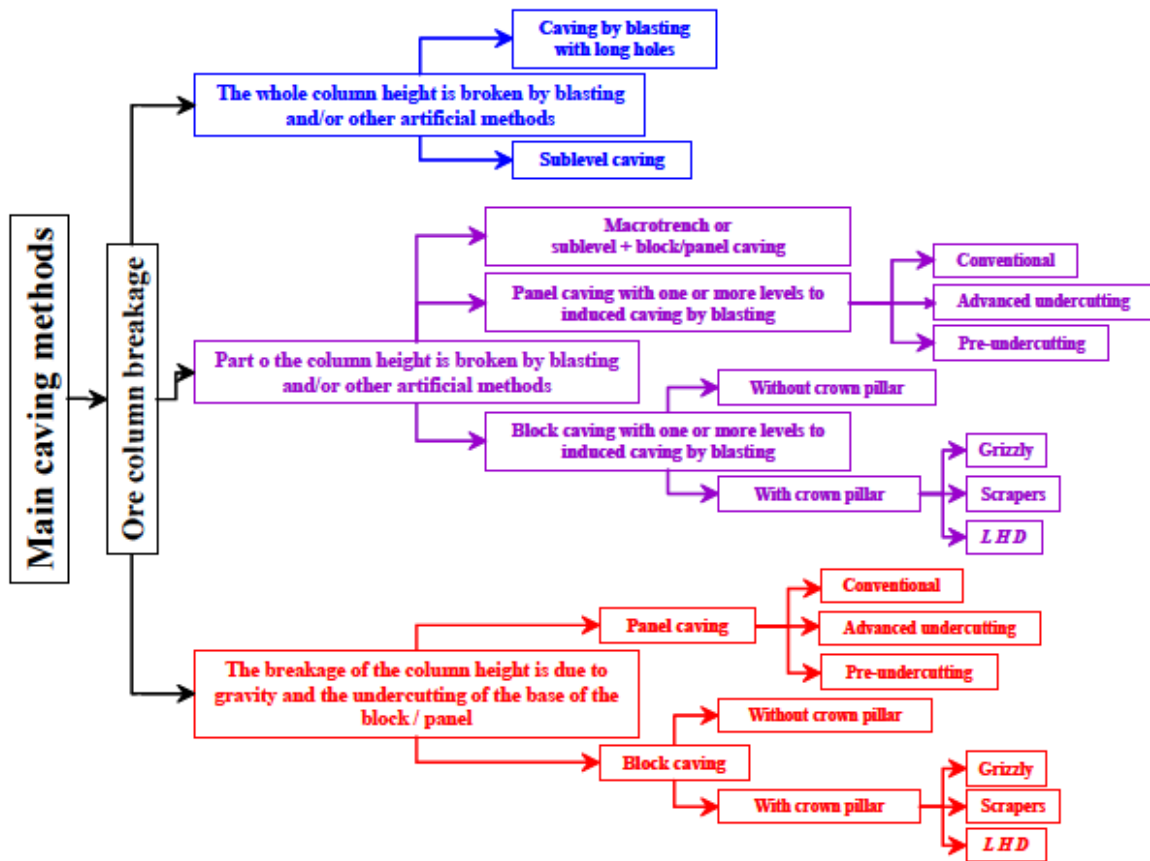


Figure 1.4: Classification of the principal mining methods by caving, according to the method of fracture of the ore column (after Flores 2005).

Cave mining is a mass method, capable of high, sustained production rates at relatively low cost per tonne. It is suitable only to big orebodies in which the vertical dimension exceeds about 100 m. The method is non selective and in general a fairly uniform distribution of values throughout the orebody is required to assure realisation of the maximum ore potential of the deposit. Although it is a low cost mining method which is capable of automation to produce an underground rock factory (Brown 2007). Intensive capital requiring considerable investment in infrastructure and development is required before production start up.

A downward displacement of the ore and overburden rock is induced in the cave mining methods. It is induced either by gravity following through undercutting of the base of the ore column to be mined in the case of block and panel caving, or, as in the case of sublevel caving by breaking the rock mass artificially using drilling and blasting methods.

Block and panel caving are mining methods in which the undercut zone is drilled and blasted progressively and some broken ore is drawn off to create a void into which initial caving of the overlying ore can take place. As more broken ore is drawn progressively following the cave initiation, the cave propagates upwards through the orebody or block until the overlying rock also caves and surface subsidence occurs. (Brown 2007)

The general features of block or panel caving method of mining can be seen in figure 1.5. The broken ore is removed through the production or extraction level developed below the undercut level and connected by drawbells through which the ore gravitates to drawpoint on the extraction level.

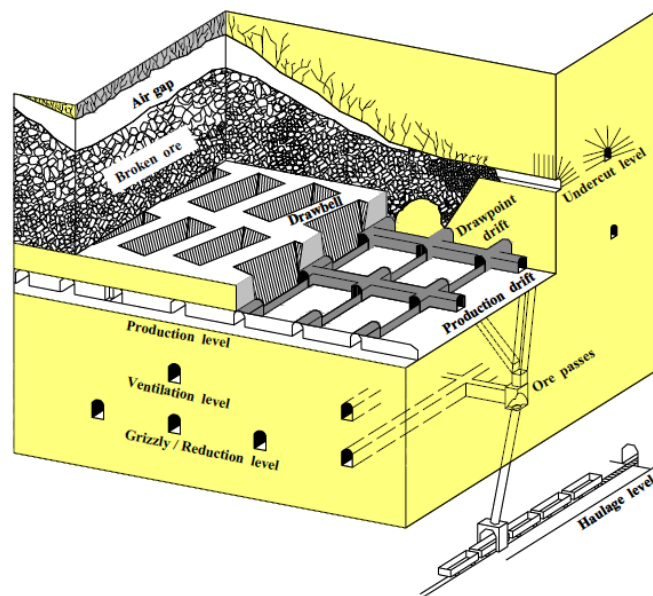


**Figure 1.5:** Illustration of mechanized block or panel caving (Flores 2005)

In the earlier block caving operations the broken material was removed using the traditional gravity based grizzly or slusher system. Currently Load Haul Dump (LHD) vehicles are used to remove the broken material from the drawpoint. From the extraction level, the ore is transported to the haulage level and out of the mine, sometimes following underground crushing.

Block and panel caving were historically used for massive, low strength and usually low grade orebodies which produced fine fragmentation. However, currently there is a tendency for block and panel caving to be used in stronger orebodies which produce coarser fragmentation than did traditional applications of the method. This enables more widely spaced drawpoints and larger equipment to be used.

In general the panel caving and others variants operate under the same fundamentals as block caving. In panel caving, the orebody or mining block is not undercut fully initially; however a panel of the orebody is undercut and allowed to cave. In the figure 1.6 can be seen the traditional panel caving sequence which include development, undercutting and mining. As a results, the cave front moves across the block at a constant angle to the direction of advance of undercut.

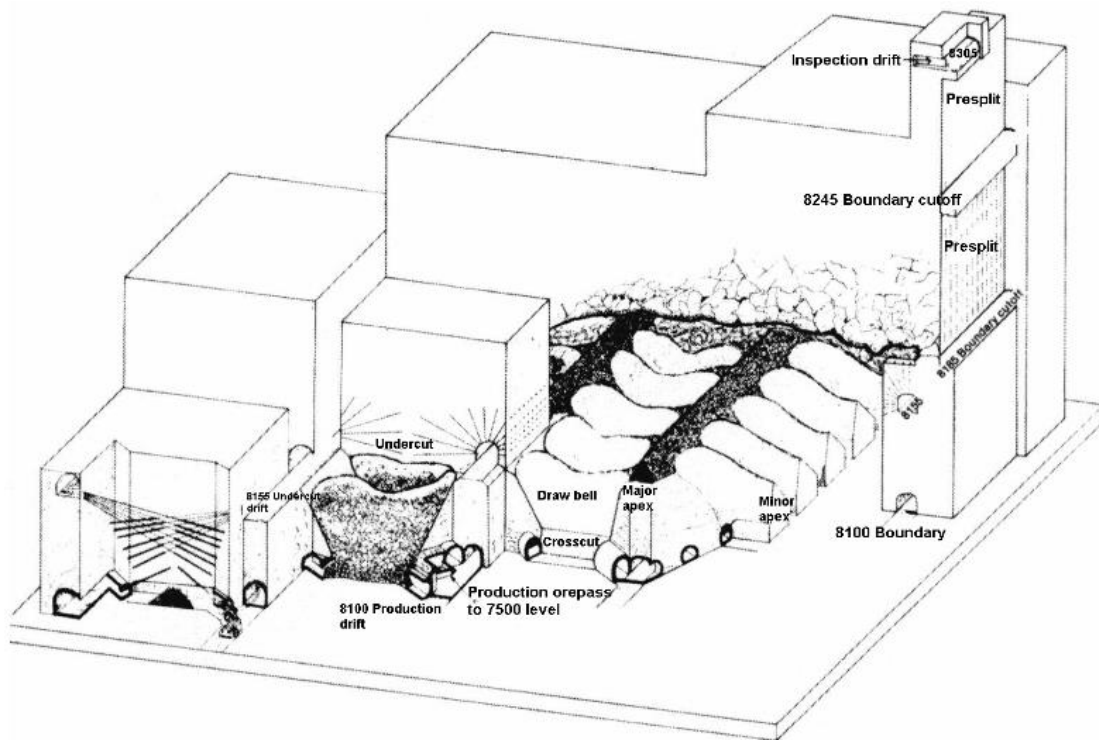


**Figure 1.6:** Mechanized panel caving, Henderson Mine, Colorado, USA (Doepken 1982).

### 1.2.2 Caving Mechanism

The essential of caving mechanism is that any unsupported rock mass cave if it is undercut over a sufficient area. Caving occurs as a result of two main influences: gravity and stress induced in the crown or back of the undercut or cave. The mechanism by which caving occurs will depend on the relations between the induced stress, the strength of the rock mass and the geometry and strength of the discontinuities.

The geomechanical methodology of block caving entails the initiation and propagation of a caving boundary through both the orebody and the overlying rock mass. At a particular elevation in the orebody, an extraction layout is developed beneath a block or panel of ore which has plan and vertical dimensions suitable for caving. An undercut horizon is developed above the extraction level. When the temporary pillar remnants in the undercut excavation are removed, failure and progressive collapse of the undercut crown occurs. The ore mass swells during failure and displacement, to fill the void. Removal of fragmented ore on the extraction horizon induces flow in the caved material, and loss of support from the crown of the caved excavation. The rock forming the cave boundary is itself then subject to failure and displacement. Vertical progress of the cave boundary is therefore directly related to the extraction of fragmented ore from the caved domain and to the swell of ore in the disintegration and caving process. During vertical flow of rock in the caved domain, reduction of the fragment size occurs (Brady et al. 2004)

For caving methods, the mining objective is the prevention of strain energy accumulation, and the continuous dissipation of pre-mining energy derived from the prevailing gravitational, tectonic and residual stress fields. Prior to caving, the rock around and above an orebody possesses both elastic strain energy and gravitational potential energy. Mining-induced relaxation of the stress field, and vertical displacement of orebody and country rock, reduces the total potential energy of the rock mass. The objective is to ensure that the rate of energy consumption in the caving mass, represented by slip, crushing and grinding of rock fragments, is proportional to the rate of extraction of ore from the active mining zone. If this is achieved, the development of unstable structures in the caving medium, such as arches, bridges and voids, is precluded. Volumetrically uniform dissipation of energy in the caving mass is important in developing uniform comminution of product ore. The associated uniform displacement field prevents impulsive loading of installations and rock elements underlying the caving mass.

It has been observed that initial and induced geomechanical conditions in an orebody determine the success of block caving. Productive caving in an orebody is prevented if the advancing cave boundary can achieve spontaneously a mechanically stable configuration, such as an arched crown, or if caved fragment sizes are too large to be drawn through the raises and drawpoints of the extraction system.

When the induced tangential stresses are high compared with the compressive and shear strengths of the rock mass and the shear strengths of the discontinuities, failure may occur at or near the boundary of the rock mass and blocks or slabs of rock may become free to fall under the influence of gravity. Under these circumstances, the dominant mechanisms of failure are brittle fracture of the intact rock and slip on discontinuities (Duplancic and Brady 1999). This form of caving is sometimes referred as stress caving (Brady 2004). A conceptual model of stress caving for this case is illustrated in figure 1.7. It was developed with data collected from early stages of caving at Northparkes Mines'. The model defines five region or zones described by Duplancic and Brady (1999):

- (a) *Caved zone:* This region consists of rock blocks which have fallen from the cave back (broken rock). Material in the caved zone provides support to the walls of the cave, but it is much softer than the rock mass.
- (b) *Air gap:* This region consists of the void existing between the broken rock filling the caved zone and the cave back. The size of the air gap depends on the breakage rate of the rock mass, the swell factor and the draw rate and draw management of the broken rock from the caved zone.
- (c) *Zone of discontinuous deformation:* This region no longer provides support to the overlying rock mass. Large-scale displacements of rock occur in this area, which is where disintegration of the rock mass occurs. No seismicity is recorded from within this region.
- (d) *Seismogenic zone:* This region is located beyond the zone of loosening, and contains a more confined rock mass that can suffer brittle failure of rock and/or shear failure and slip on discontinuities, both causing seismic events. This behaviour is due to the changing stress conditions associated with the advancing undercut and the progress of the cave.
- (e) *Surrounding rock mass or pseudo-continuous domain:* This region consists of the rock mass that surrounds and confines the seismogenic zone. The rock mass in this region is stable and behaves elastically, showing small deformations.

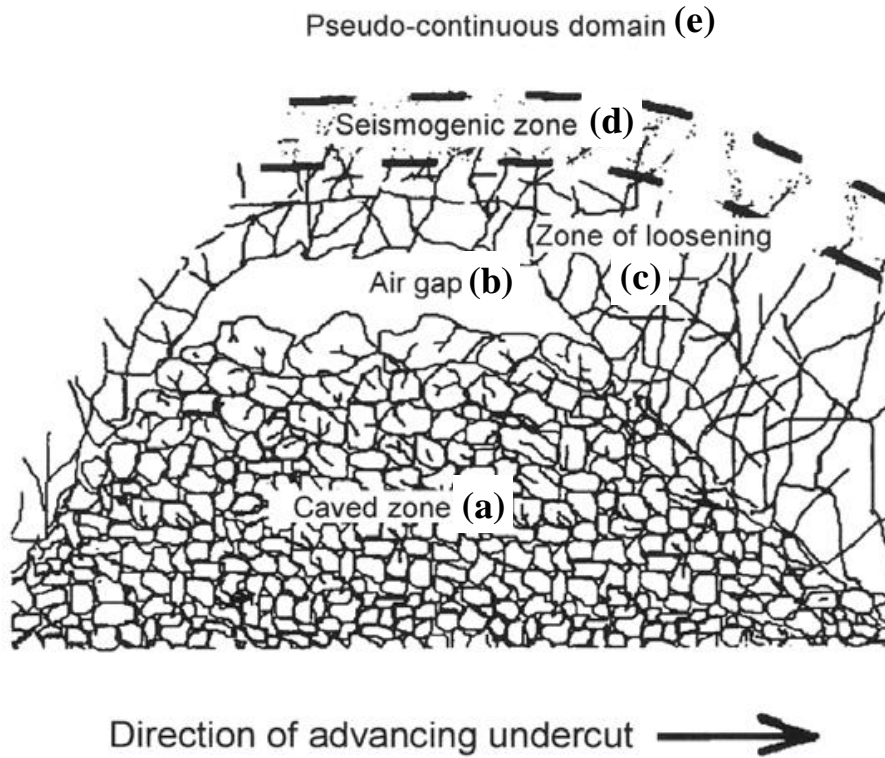


**Figure 1.7:** Conceptual model of caving (after Duplancic and Brady 1999)

There is another general case must also be considered. If the horizontal in situ stresses and the tangential stresses induced in the crown of the undercut or cave are high enough to develop clamping forces which inhibit gravity-induced caving, but are not high compared to the compressive strength of the rock mass, caving may be inhibited and a stable, self-supporting arch may develop (Brady et al. 2004).

Once continuous caving has been initiated, the rate at which the cave propagates will affect the rate of production from block or panel following draw and the creation of a small air void into which caved material may fall. Empiric evidences have shown that the cave rate will depend of the quality of rock mass, the magnitude of the induced stresses and the rate of undercutting.

The different stages of caving propagation in underground cave mining are illustrated in Figure 1.8. Once the ore body caves and the broken ore is extracted, the cave propagation process is initiated trough cave back progress upwards. The crown pillar between the cave back and the ground surface will suffer deformation and eventually the caving will connect to the surface. At the surface, some signs of these deformations may appear before the connection takes place, but ground surface deformations became significant after the connection occurs. These deformations are known as subsidence, and affect not only the ground surface but also the rock mass surrounding the cavity connected to surface, which becomes a subsidence crater (Brown 2003).

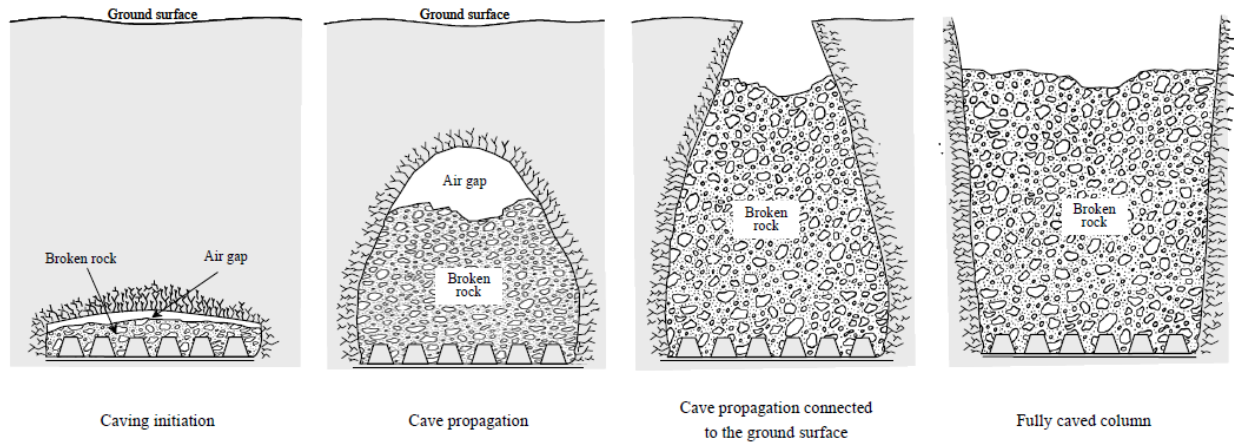


**Figure 1.8:** The process of caving and cave evolution (Flores 2005)

### 1.2.3 History and Future

By the 1920s and 30s, block caving methods were initially applied in a wide range of mines exploiting massive, weak and well fractured orebodies. During this period, the method was introduced at the King Mine which exploited asbestos in Quebe, Canada, the Climax Mine mining molybdenum in Colorado, USA, and the copper mines in Chile (Peele 1941). However, the iron ore mines of the Menominee Rangers, Michigan, USA, were the precursor of the modern block caving method of mining. The Pewabic Mine was the first to use a form of block caving from which other methods were developed (Peele 1941). In the Pewabic method, block of ore approximately 60-75 m long, 30-40 m high and the full width of the deposit (60 m) were caved in one operation (Peele 1941).

Before evolving to the use of full block caving, many mines used combined methods involving, for example, shrinkage stoping and caving methods for the subsequent mining of pillars between the primary stopes.

The first reported example of the early block caving application is provided by the Miami Copper Company's mine in Arizona. The diagram of this method can be seen in the figure 1.9 and its description was explained by Brown (2007). The block caving was introduced by 1920s, previously early mining was by top-slicing but this was replaced by shrinkage stoping with sublevel caving of pillars. Initially, caving operation involve undercutting and caving the orebody across its entire width of 150-200 m. This approach was unsuccessful and later practice was to cave and draw alternate 45 m wide panels across the entire orebody. This methodology was satisfactory for moderate thicknesses of ore averaging 60 m but was modified to true block caving where thicknesses were 90 m or more.

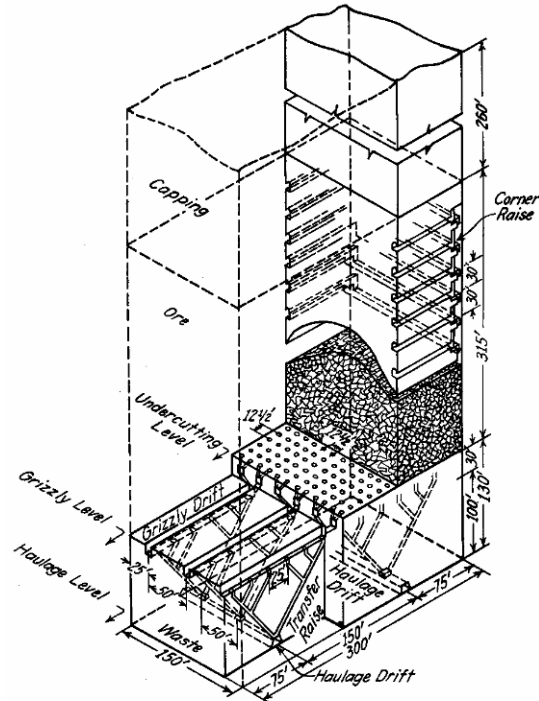


**Figure 1.9:** Block caving, Miami Mine, Arizona, USA (after Brown 2007)

The experience showed that 45 m square blocks gave better results and this block size became the standard. As shown the figure 1.9, The Miami mine used a gravity system of ore transfer to the haulage level incorporating grizzlies.

As has been indicated above, ore has been drawn throughout much of the history of block and panel cave mining by gravity or slusher methods. The availability of LHD equipment from 1960s has provided the potential for introduction of mechanised and trackless cave mining, especially for stronger ores and more coarse fragmentation in which the necessary large extraction level openings can be developed and maintained. In fact, from the 1980s block and panel caving methods began to be applied to deeper, more competent and less fractured rock masses and were being considered as a potential method for the exploitation of hard and massive rock masses (Ovalle et al 1981).

This trend has since increased, mainly due to the low production costs involved. Block and panel caving methods are currently sources of mineral production on a world scale (Brown 2007). Because of caving methods capacity and the potential that they offer for mechanization and automation, there is a current tendency to apply block caving to stronger orebodies than those to which the method has been applied in the past.

The future trends in cave mining seem to indicate that the automation and mechanisation will be essential to face a dramatic increase of extraction's rate in mines that will be placed at deeper and harder rock. In fact, mechanized continuous drawing system is being assessed in order to increase production capacity for large block caving mines (Encina et al. 2008)

Additionally, the cave mines are also being considered for the underground mining of some major orebodies that were previously, or are currently, mined by large open pits. The transition from open pit to underground mining by block and panel caving will be part of the world trends in mining methods.

### 1.3 MAJOR HAZARDS IN CAVE MINING

Decisions to exploit a particular orebody by block or panel caving methods involve a number of major risk or hazards. Caving methods involve significant amounts of capital and investment in infrastructure development before extraction can begin. Caving methods are inflexible so that, if a mistake is made, it is not easy to change or fix a problem with the mining method (Brown 2007).

Caving operations also generate a number of specific issues which constitute risks or hazards that must be addressed in mine planning and operation. Accounts of the risks associated with cave mining have been given by Heslop (2000). The following is an indicative list of some of factors requiring consideration at the various stages of a cave mining project:

- Lack of geological data in order to make recognition of orebody.
- Inadequacy of the geotechnical data available about orebody and country rock masses including major structures, discontinuities, material properties, in situ stresses and ground water hydrology.
- Poor cavability assessment.
- Cave propagation which is the ability of the cave to continue to propagate once cave has been initiated.
- The degree of fragmentation of the ore occurring as a result of caving progress.
- Caving performance which is based on the planned rate of cave propagation, rate of production, degree of fragmentation, ore grades and recovery.
- Excavation stability refers to the stability over the design life and the need for support and reinforcement on mine excavations.
- Major operational hazards including major excavation collapses, rock burst, air blasts, and mud, water and slurry inflows.
- Environmental risks
- Risks to profitability.

Specifically, the planning and operation of block or panel caving mines involve a number of major hazards. Heslop (2000) divide the area of operating risks into four further categories:

- a) Operational hazards – Rock bursts, air blasts, mud rushes and water and slurry inrushes that could led loss of life and/or premature mine closure.
- b) Design risks: those risks that have an economic impact and are the result of incorrect assessment of ground conditions or effects of stress.
- c) Draw risks: those risks that have an impact on the current and future ore and grades that will be recovered and are the result of incorrect assessments of the issue that influence draw.

- d) Automated equipment risks: risks arising from an over reliance on advanced technology to achieve critical levels of performance from LHDs and drills.

The figure 1.10 shows a classification and some of the five major operational hazards that require consideration.

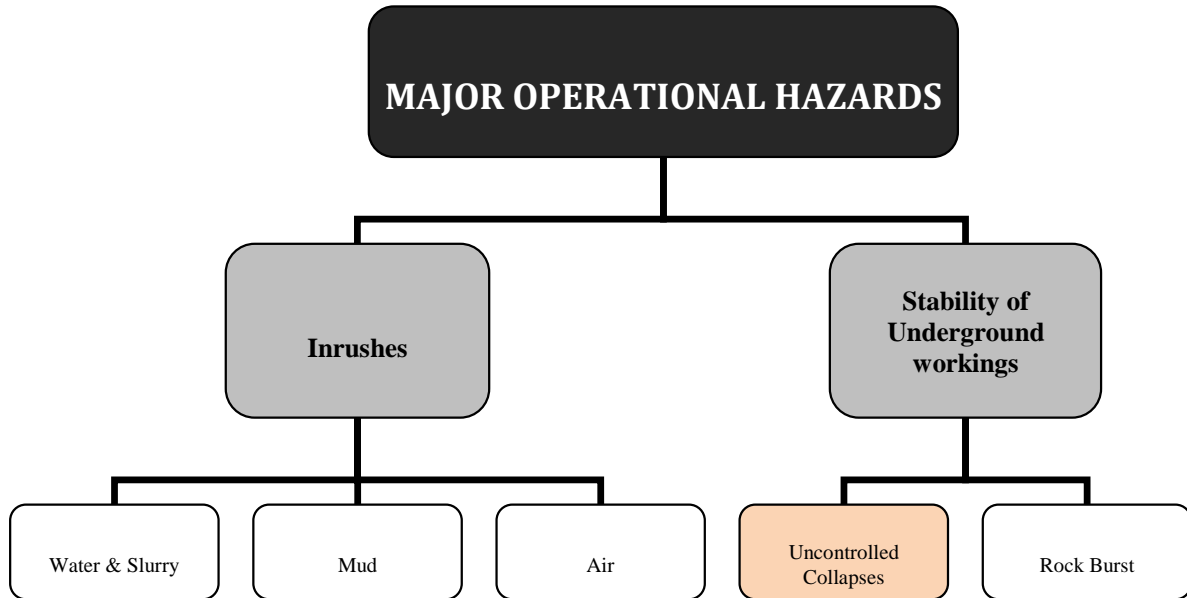


**Figure 1.10:** Classification of major operational hazards (Brown 2007).

In order to describe each of major operational hazards in cave mines, the following a detailed terminology is presented:

### 1.3.1 Major Collapses

Within the conceptual definition of collapse, Brown has described three types of major collapses in caving method:

“The uncontrolled collapse of crown or sill pillars to surface or to a mined-out overlying void (Type 1). Uncontrolled falls of large blocks or volumes of rock from the back of undercut or, more usually, the cave (Type 2); and the collapse of excavations on and above the extraction level (type 3).”

The most important aspect is that the event must cause damage to the operation. In extreme cases, collapse could result in loss of life, loss of production from a panel, or extensive damage to infrastructure. In less extreme cases, it could cause expensive delays in production or involve the need for remedial work.

The categories of major collapse listed above all relate to the undercut and extraction levels or to the cave itself. It is possible, but not likely, that major collapses having life or production threatening consequences could also occur in mine access and other items of infrastructure.

*Collapses at El Teniente Mine* have been defined as a gradual failure of the rockmass over a large area on a production level. The maximum expression is the total closure of affected drifts. As a consequence, the production area is reduced, thus leading a large impact regarding the fulfilment of production targets.

### **1.3.2 Rock Bursts**

A seismic event is a dynamic stress wave caused by inelastic deformation or failure in a rockmass. Seismic events in mines are relatively normal consequences to mining activities, particularly in hard, brittle rock. In some circumstances, significant rockmass damage, commonly called rockbursting, may accompany mining-induced seismic event. In extreme instances, severe rockmass damage may be associated with mining-induced seismicity.

Mendecki et al. (1999) define seismic event as a sudden inelastic deformation within a given volume of rock that radiates detectable seismic waves. Heal (2010) define rockburst as visible damage to an underground excavation caused by a seismic event. The severity of a rockburst may vary from minor rock spalling to catastrophic rock mass fracturing or falls of ground.

As these definitions indicate, rock bursts are a sub-set of a broader range of seismic events which arise from conditions of unstable equilibrium within the rock mass and involve the release of stored strain energy and the propagation of elastic waves the rock mass (Brady and Brown 2004).

Seismic events in mines are commonly characterized by parameters originally developed in earthquake seismology. Source parameters such as energy output, seismic moment, source radius and radiated energy may be related to the damage sustained by mining excavations. Commonly used measure of event magnitude in earthquake seismology is the Richter magnitude which is a linear function of the logarithm of the seismic moment which is obtained from the spectral analysis of body waves radiated from the source (Brady and Brown 2004).

### **1.3.3 Mud Rushes**

They are sudden inflows of mud from underground infrastructures' such as drawn points or any other openings. Generally there are two groups of mud rushes depending on the source of mud. External mud rushes are those in which the mud is produced externally to the underground cave mining

environment. Internal mud rushes are those in which the mud is produced by comminution within the cave muck pile.

The main characteristic of mud rushes are that their occurrence is sudden and the mud is liquefied by some means and flows rapidly.

#### **1.3.4 Water and Slurry Inrushes**

Water and slurry inrushes are those occurrences in which water and/or slurry enter the mining zone from some external source such as surface run-off, a water storage dam, a tailings dam or a backfilled stope (Heslop, 2000). Water and slurry inrushes can represent a different type of operational hazard from mud rushes, although they can be contributing to mud rushes.

#### **1.3.5 Air Blasts**

An air blast is the rapid flow of air through an underground opening following compression of the air in a confined space, most frequently by sudden fall of a large volume of rock (Brown 2007).

The main factors that may induce a most damaging air blasts in block caving and panel caving mines, are major collapses, such as the uncontrolled fall-off of crown pillars to a mined-out overlying void or uncontrolled falls of large blocks or rock from the back of a cave.

This type of air blast has been more common in caving mines than might be supposed (Heslop, 2000). Examples of their occurrence have been reported, for example in the latter case shown in Figure 1.11, arching has led cave propagation to be arrested. On 5 December 1999 after cave induction procedures by drilling and blasting, a plan area of approximately 4000 m<sup>2</sup> collapsed. An excess of 500 km/hr of air velocity in main access was estimated (de Nicola and Fishwick, 2000).

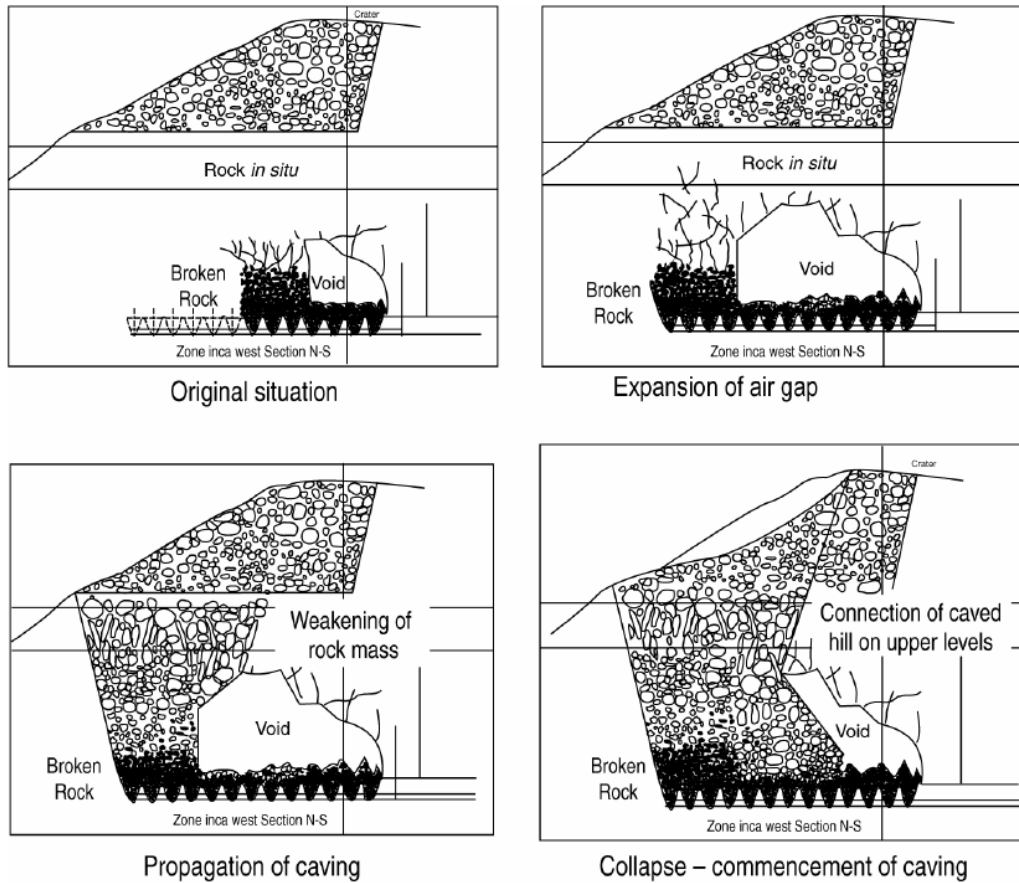


**Figure 1.11:** Sequence of air blast at Salvador Mine, Chile (de Nicola and Fishwick 2000).

#### 1.4 CONTEXT AND SCOPE

The scope of this thesis is to identify and clarify the main causes of rock mass damage during large panel caving operations at El Teniente Mine, Chile. Furthermore, it will attempt to provide guidelines for future designs of panel caving operations to minimise the extent of damage that has been observed during previous extraction.

##### *Rock mass damage and the associated impact on mining*

As operating underground mines move deeper, they encounter higher in-situ and induced stress regimes, increase of production costs associated with primary ground support, rock mass rehabilitation, ore haulage, and mine ventilation. Under these conditions, the relationship between rock mass stability and mining costs become an essential factor for a successful business, affecting directly the mine economics.

Costs that may be directly linked to rock mass damage may include rock mass rehabilitation, additional ground support, reduced access, addition of development in response to lack of access issues, and production delays. Many examples of such relationships are found at El Teniente Mine.

The most recent case occurred in one the most important sectors at El Teniente Mine called Esmeralda, where intensive rock mass damage has occurred in the central part of the caving front since 2001. Long and extensive panel caving front redistributes high abutment stresses and creates large displacements of the rock mass above and beneath the cave as the undercut front passes. The most dramatic effects will ordinarily occur in the central area of the caving front, or in areas modified by rock mass characteristics and weak major discontinuities (Ferguson 2006). Due to these conditions, the undercutting rate has been reduced in Esmeralda and contingency plans to deliver the planned production delay have been currently developed. The Esmeralda sector continues to face these difficulties, as can be seen in Figure 1.12, which shows the total collapsed area by year at the El Teniente Mine. The Esmeralda sector represents a large proportion of the damaged area during the last few years. It must be emphasized that the collapsed area are those zones in which intensive rock mass damage has occurred, affecting the extraction level stability.

El Teniente personnel have managed to cope with the difficulties by implementing various contingency plans; however, higher costs than expected were experienced (Araneda and Sougarret 2008). The research conducted during this PhD attempts to increase on understanding of the causes leading to rock mass collapse. Additionally, this project will offer alternative design criteria that will lead to a minimization of damage in panel caving method.

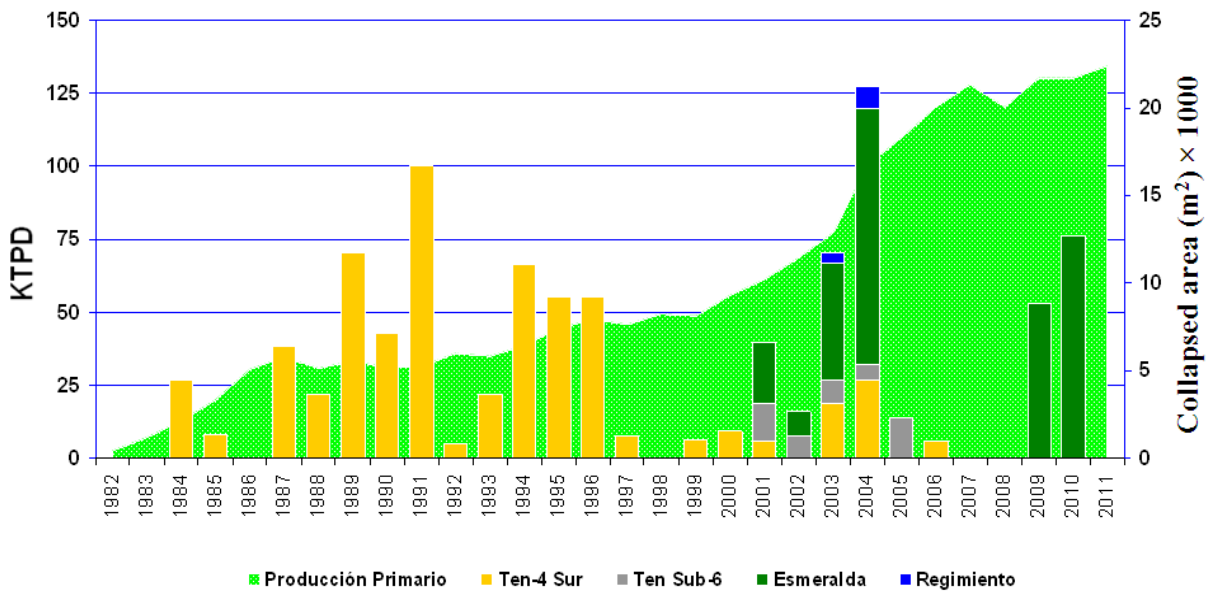


**Figure 1.12:** Total collapsed area by sector and primary ore production from 1982 to 2011 (Larrain et al., 2011).

Additionally, rock mass damage during panel caving is associated with many mechanisms, all working in conjunction to degrade the quality through fresh fracturing, extension of existing fractures and movement along planes of weakness. Many factors contribute to rock mass behaviour which can

eventually induce significant damage to mining infrastructure under certain conditions. The major goal of the current research is to identify the role and influence of each parameter on rock mass damage.

### *Panel caving projects*

The El Teniente Mine currently produces approximately 140,000 tonnes/day, 80% originating from primary ore. The last expansion program increased the copper production from 330,000 to 430,000 metric tonnes per year. In this expansion, Esmeralda sector has played an important role, reaching approximately 30,000 tonnes/day. Additionally, there is an important future project at El Teniente Mine, called New Mine Level, which has reserves of about 1548 Mton, with an average grade of 0.99% Cu. A production rate of 180,000 tonnes/day is proposed with a duty life of 50 years starting from year 2016 (Vasquez et al. 2008). This goal means reaching depths over of 1,000 meters below the surface. Within the new production levels increased geotechnical hazards are expected such as seismic activity and rock mass damage or collapses. It will therefore, be imperative to improve the design criteria for panel caving method to minimise the extent of damage compared with that has been to date.

Many caving projects are currently being studied and set up worldwide. CODELCO itself is developing two world class block cave projects at the same time: Sur Sur Underground at Andina and Chuquicamata underground (Fuentes and Adam 2008). Moreover, other projects are being studied around the world, such as Resolution copper in USA and Oyu Tolgoi in Mongolia, all of which have designed production rates of over 100,000 tonnes/day. Therefore, the successful completion of this project will also help to support all the new large caving projects around the world.

## 1.5 RESEARCH APPROACH

In order to achieve the aim and objectives of this thesis as summarized in previous section, the research approach contains three distinct phases which are carried out to produce an end product with a mix of theoretical research and modelling and empirical data collection and analysis. The following phases were taken:

- a) Carried out a comprehensive and critical review of the literature dealing with the fundamentals and geomechanical features of caving methods, rock mass response to caving methods, rock mass strength characterization, sort and scales of rock mass damage and historical caving cases around the world. Furthermore, most of the internal and consultant reports at El Teniente Mine were reviewed in order to discuss collapse phenomena and its mechanism hypothesis.
- b) Reviewed an extensive field data collection campaign that has already been undertaken at El Teniente Mine. Specifically, since 2001, several campaigns of geotechnical instrumentation and monitoring have taken place in the Esmeralda Sector. The programmes have included in situ stress field measurements, rock mass deformation data, mine seismic data, post-excavation-extraction drift surveys, and cave back geometry data.

The data collection step also included an update of geotechnical rock mass characterisation for the Esmeralda sector. This characterisation considered factors such as large scale geological data, geotechnical rock mass classification, joint mapping, principal faults, and rock mass material properties. Additionally, observational records of rock mass damage were included as field data collection. This information has been collected in mine drives by geotechnical engineers since 2001 and included rock mass damage maps and ground support conditions, for each extraction period of the Esmeralda sector.

- c) Conducted a back analysis reviewing all field data collected and previous collapse hypothesis. As a consequence, the link between field data collected and previous collapse hypothesis was used to develop a new conceptual model for collapses at El Teniente Mine, where the main goal has been the understanding mechanism of damage and collapse.

The second stage has included a back analysis of documented damage in Esmeralda. This phase involved a numerical simulation of previous extraction sequences of the mine, using the real geometries of the cavities and the previous large scale damage in the infrastructure of the Esmeralda sector. Non-linear modelling was used as analysis tool incorporating the collected field data, such as realistic geology, material properties that included post-peak behaviour, detailed excavation geometries, extraction sequences, and the stress field in order to predict the behaviour of rock mass.

Finally, based on the understanding of collapse mechanisms and the numerical modelling results, guidelines for future design were provided by the study to minimise the extent of

damage that has been observed during previous extraction. The results have been represented in forward modelling outputs using, a calibrated non-linear program.

## 1.6 THESIS STRUCTURE

The research context and objectives of this thesis are outlined in Chapter 1.

Chapter 2 of the thesis introduces background information about the caving operations at El Teniente Mine. A general overview of the mine along with mining methods and their evolution are presented. In addition, the main geotechnical risks at El Teniente Mine are reviewed. It also highlights the Mine site geology, rock mass classification and geotechnical behaviour of rock mass at El Teniente Mine.

Chapter 3 critically reviews the technical literature dealing with the geotechnical risks associated to cave mining methods. It also highlights a review about the fundamentals of intact rock damage and rock mass damage along with rock mass failure criterions. Finally, a summary of El Teniente reports about geotechnical issues is undertaken.

Chapter 4 identifies the fundamentals geotechnical issues during panel caving operations. This chapter describes background information about the Esmeralda sector and the rock mass behaviour by effect of applied cave mining method. It also includes a critically review of intensive rock mass damage in the extraction level of Esmeralda Sector defined as Collapse. In addition, it describes the collapse effects upon mining extraction and also assesses a sort of collapse mechanisms.

Chapter 5 describes the design methodology developed for conceptual collapse model that have affected the Esmeralda Sector. This model is based on a review of geotechnical and operational parameters present in Esmeralda Sector. In addition, Chapter 5 presents the numerical analysis developed to simulate the large scale rock mass damage at Esmeralda Sector. This chapter reviews previous numerical models developed at El Teniente Mine and also presents the fundamentals of linear and non linear analysis in order to simulate the rock mass behaviour. It also includes the global and local description of numerical model developed. Additionally, it describes the boundary and initial condition of model along with the geometry and sequence modelled. Finally, a model calibration and sensibility analysis are carried out.

Chapter 6 presents a back analysis of large scale rock mass damage assessing numerical model results and on site data collection. A characterizing of collapse mechanism is carried out in order to confirm the hypothesis research.

Chapter 7 summarises the main conclusions of the research and provides recommendations for future work in this field.

## **CHAPTER 2**

### **PANEL CAVING OPERATIONS AT THE EL TENIENTE MINE**

#### **2.1 EL TENIENTE OVERVIEW**

El Teniente Division is one of the mining-metallurgical complexes of the Corporación Nacional del Cobre de Chile (CODELCO) and considers amongst its main assets the underground mine called El Teniente, and the additional productive and infrastructure facilities necessary for the concentration and melting of the copper and molybdenum mineral that CODELCO markets. Currently, 135,000 tons of ore per day (tpd) are extracted and processed in order to produce approximately 409,000 tons of copper per year and 5.200 tons of molybdenum per year.

##### **2.1.1 History**

The first known owner of this land was Andrés de Torquemada, captain of the times of the conquest, the property included from the Central Valley up to the High Mountains and from the Angostura de Paine up to Rancagua, which was donated to the Jesuits later on. After the expulsion of the Jesuits in 1767, it was transferred to the State and in a public auction performed in 1771.

The mine was barely mined before the XIX century. The high altitude, low grade, bad weather and inaccessibility of the mine did not make it attractive to the owners of “Hacienda de la Compañía”. The few attempts to mine, especially made by Guillermo Blest, a business man, failed.

At the beginning of XX century, the Italian citizen Marco Chiapponi, prestigious engineer, miner and who knew the zone, studied the mine at the request by the owners and was commissioned to look for foreign investors interested in purchasing the mine. After failing in his attempts to attract foreign investors from Europe remembers an old friend and sent a letter on November 3 1903 to Mr. William Braden, a mining engineer from United States.

Braden arrived to Valparaíso at the beginning of 1904. After a week in Hacienda de la Compañía he recognized in depth its geological characteristics and fully understood the magnitude of the discovery, so he returned to the country and immediately purchased the mine. This was the exact moment when the large copper mining industry was born in Chile. The description he made of the mine, where he recognized a copper porphyry in a large volcanic chain, is perfect and incredibly accurate from the geological point of view and economic potential. The quick actions taken by Braden were remarkable. He appointed Chiapponi in charge of his interests in Chile, with the instructions to immediately build a highway from Graneros station up to the mine and when he came back to Nueva York created the

“Braden Copper Co.”. In this manner along with four other senior engineers graduated from MIT, started the production in 1905, when the operation and expansion of the mine started.

In 1915, Kennecott Copper Corporation acquired a controlling interest in the site (Baros, 1995). They raised the daily production to 34,000 tons/day by 1960. In 1967, the Chilean government acquired the mine, changed the name to El Teniente, and have been increasing productivity and delineation of the deposit ever since.

### 2.1.2 Location

The Teniente mine is located in Central Chile, latitude of approximately 34° South, and a longitude of approximately 70.3° West (Figure 2.1).

The mine workings are between 2,000m and 3,200 m elevation and the ore body is located in the first elevation of the Andes Ranges at 2,200 meters above sea level. The mine site area is surrounding by a severe topography, where difference levels greater than 1,000 meters are commonly observed.

The mine site is approximately 2 hours drive south direction from Santiago (90 kilometers), the Chilean’s capital, and 44 km to west direction from Rancagua, the nearest large town. The mine use a local coordinates system which is related with the Universal Transverse Mercator (UTM) coordinate by the follow relationship:

$$\text{Mine North} = \text{True North} + 14^{\circ}19'34'' \quad (2.1)$$

$$\text{Mine Level (z)} = \text{Elevation above sea level} - 21.36\text{m} \quad (2.2)$$

Figures where mine layouts are shown throughout this thesis refer to the mine coordinate systems.

### 2.1.3 Resources and Size

El Teniente is the largest copper- molybdenum known deposit in the world. The actual depth to which the copper mineralization extends is unknown. However, economic mineralization exists from surface, and is currently exploited down to 800m depth, and has been intersected in the deepest drilling at 1,800m below surface (Skewes et al., 2002). The 0.5% copper grade contour extends approximately 2.8 km long and 1.9 km wide at the mine level Teniente 5 (2280z). The total resources of the in situ copper ore have been estimated to be more than 28,300 million of tons with an average grade greater than 0.38%Cu as shown in Larrain et al. (2011) (Table 2.1). The hypogene or primary copper ore is chalcopyrite followed by bornite.

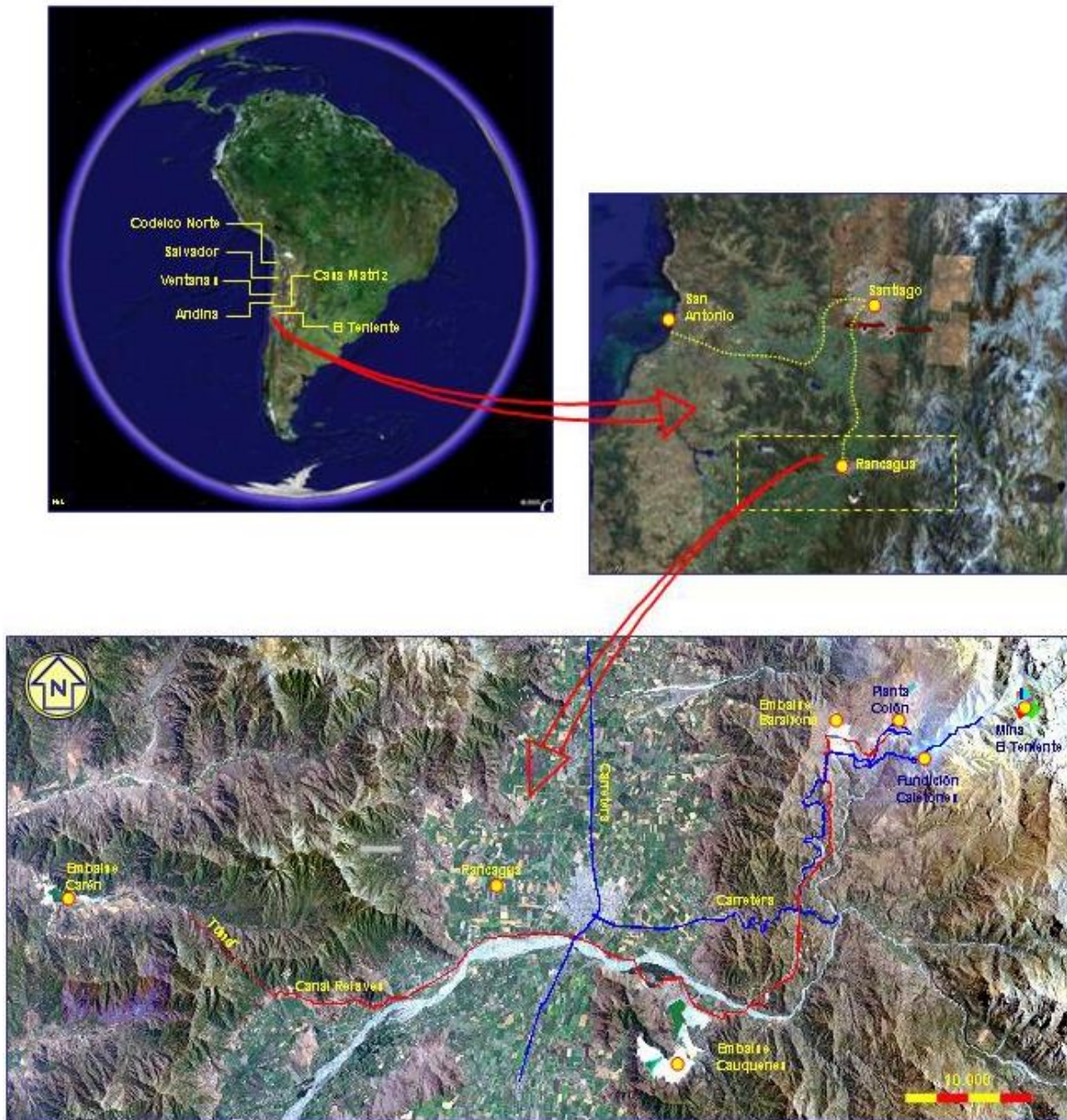


**Figure 2.1:** Location of the *El Teniente* mine in Chile.

**Table 2.1:** Resources inventory 2011 (Larrain et al, 2011).

Categories	Million tons	Copper Grade, %Cu
Measured	2,853	0.81
Indicated	3,649	0.53
Inferred	21,801	0.30
<b>Total</b>	<b>28,303</b>	<b>0.38</b>

## 2.2 MINE SITE GEOLOGY

The mineralization of copper and molybdenum along with the geology suggest an origin related to a complex evolution given by the intrusion of subvolcanic mafic and felsic bodies, deeply associated to magma and hydrothermal gaps, in an extension almost three kilometers long by two kilometers wide and recognized vertical expression of approximately two thousand meters. Therefore this ore body is classified according to recent geological literature as “Giant Ore Deposit”.

El Teniente ore deposit is placed in the belt of tertiary volcanic rock at central Chile as Figure 2.2 shown. The mining district El Teniente is formed by intrusive and extrusive rocks assigned to the Farellones Formation, from the mid to late Miocene Age. Extrusive rocks correspond mainly to a sequence of volcanoclastites and basalt and rhyolitic lava, with dams, sills and mafic stocks intrusive, the thickness of this sequence would exceed 2500m. In the surroundings of the ore body, Howell & Molloy (1960) recognized three members in rocks of the Farellones Formation, separated from each other by angular differences: the lower member, consisting on andesitic masses outflows; the middle member, with andesitic epidotic outflows and reddish lake layers and the upper member, with andesitic and basalt outflows alternated with agglomerates and pyroclastites (Figure 2.3).

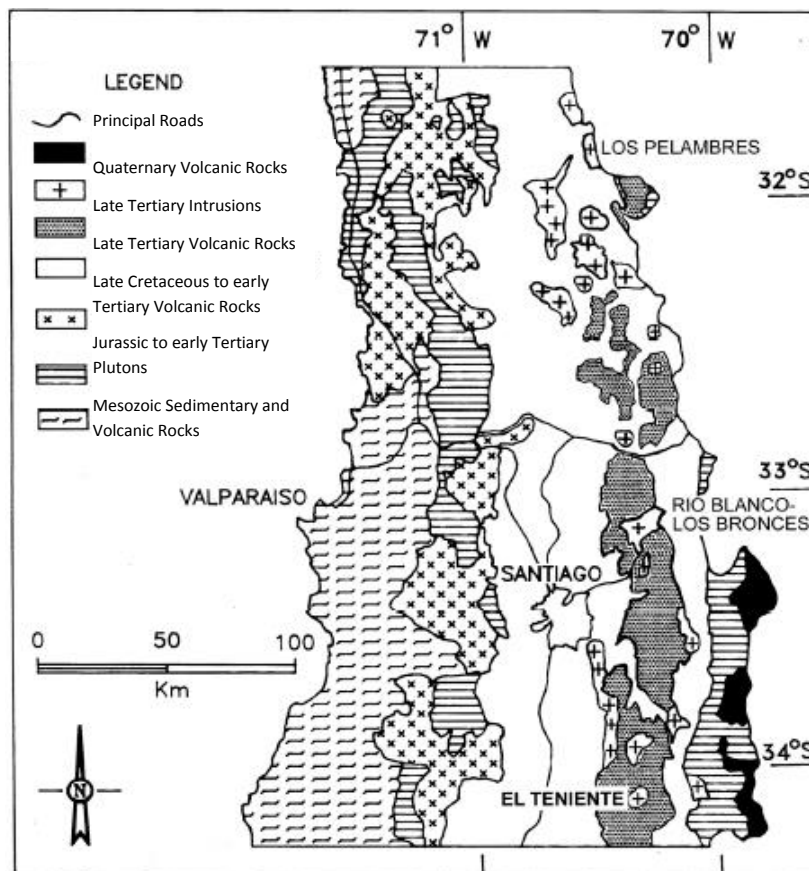


**Figure 2.2:** Geology of central Chile (after Skewes et al. 2002).

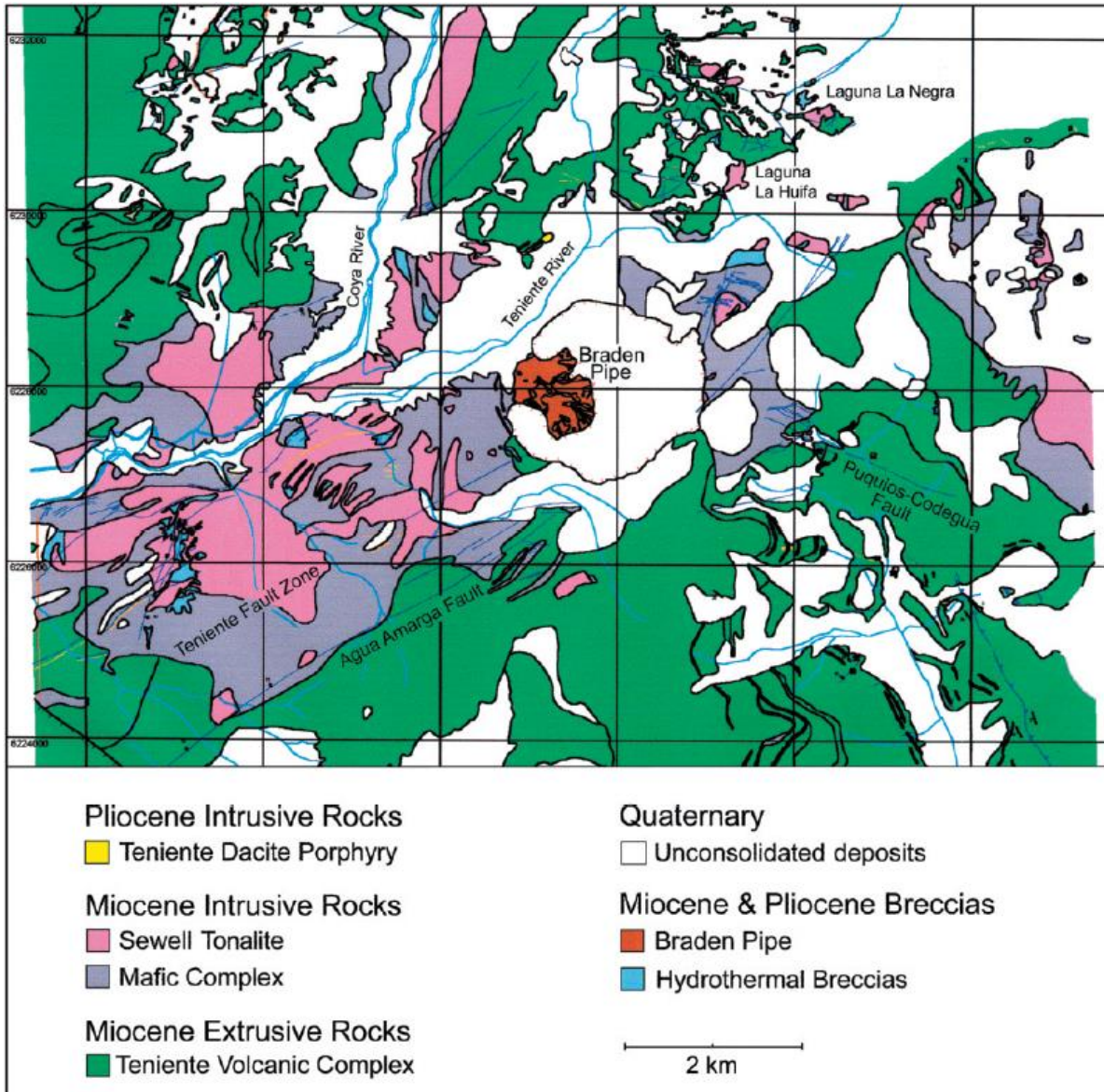


**Figure 2.3:** Geology of the area surrounding the El Teniente copper deposit with true north (after Skewes et al. 2002).

Additionally, Garrido et al. (1994) has suggested that the deposit is emplaced within the El Teniente Faults Zone (ETFZ), which is a zone of anastomosing faults trending NE-ESE. The fault zone has known dimensions of 14 km long and 3 km wide (Figure 2.4; Garrido, 1994). The eastern extent of the TFZ is poorly known, but it may terminate against the Codegua Fault. Similarly the western termination of the TFZ is not known. A predominant dextral sense of movement has been reported, producing a kilometer or more of displacement.

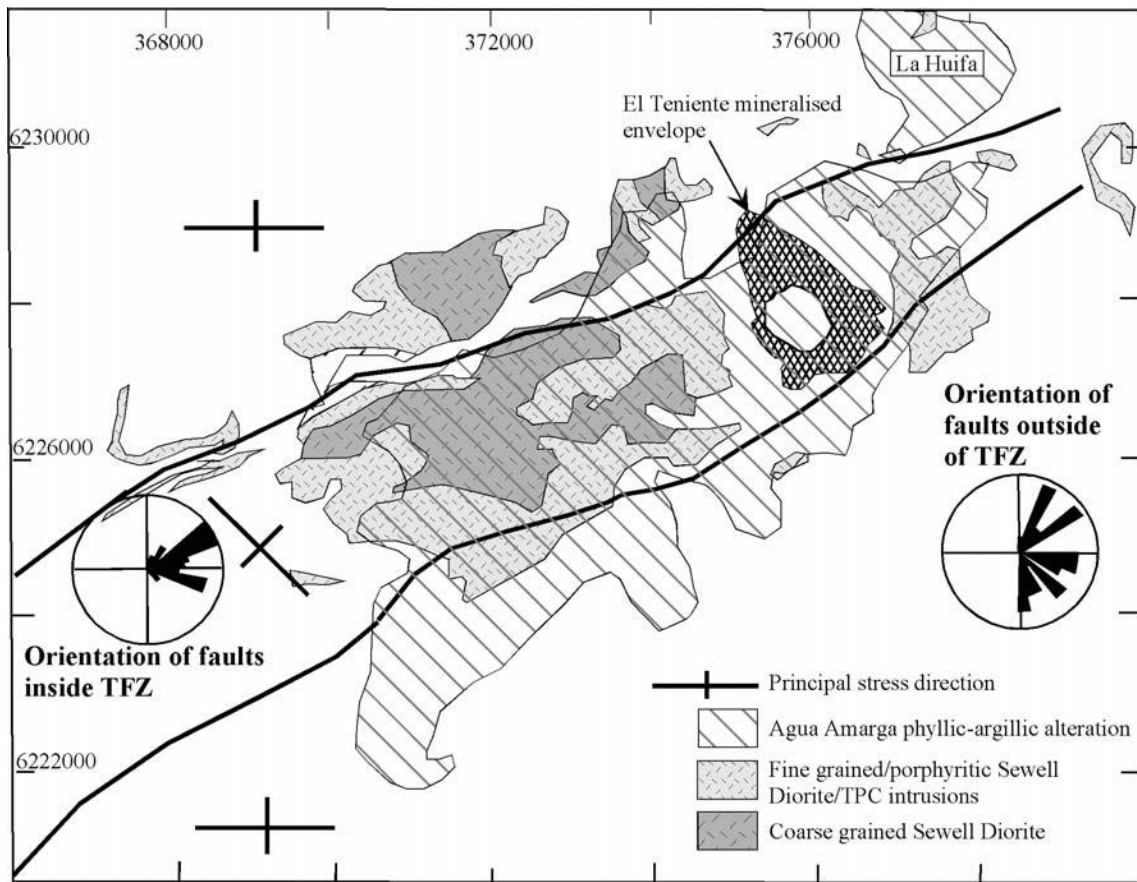


**Figure 2.4:** The NE-trending Teniente Fault Zone (TFZ) is a broad zone of NE-trending faults (modified from Garrido, 1994).

Several rock types can be identified within the ore body. Skewes et al. (2002) has described and referred the main lithology description for El Teniente mine such as: Teniente Mafic Intrusive Complex, Felsic Intrusions and Breccias. The figure 2.5 shows a plan view with the main lithologies and photos of two representative's lithology.

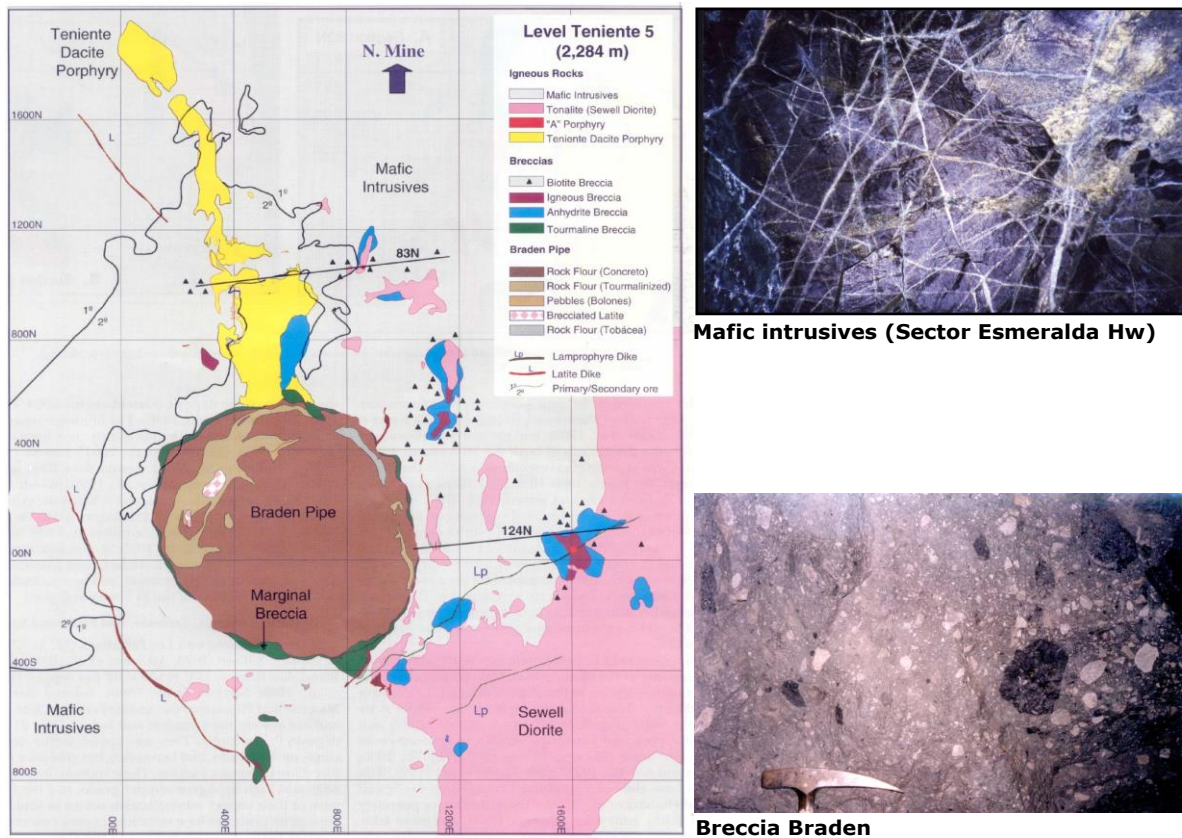


**Figure 2.5:** Plainview with lithology of the El Teniente ore body at the Ten-5 level (2284z) and two representative photos.

### 2.2.1 *El Teniente* Mafic Intrusive Complex

It corresponds to the rock with the widest distribution in the ore body, dark Brown to black in color. These rocks host 80% of the mineralization in El Teniente and have different degrees of biotization that obliterate in a microscopic way the original texture characteristics.

Its original petrological features have been obscured by an intense and overlapping alteration stage (Skewes et al., 2002). Although the name andesite suggests intermediate extrusive rocks, which have been correlated with the andesite extrusive of the Farellones Formation, it is a mafic intrusive rock. Recently studies have demonstrated that this mafic intrusive rock includes gabbros, diabases, basaltic and basaltic andesite porphyries, which have been denominated as the Mafic Intrusive Complex (Skewes and Arevalo, 1997, Skewes et al., 2002).

The Mafic Intrusive Complex has been identified as an extent laccolith of more than 2,000 meters in the Mine area. At an inferred 8.9 million of years (Ma) ago, this complex intruded rocks of the El Teniente Volcanic Complex, according to Skewes et al. (2002).

### 2.2.2 Felsic Intrusion

Various individual felsic intrusive stocks and dykes have been recognized within the deposit. The most important are the Sewell Tonalite located south-east of the Braden Pipe, and the smaller Teniente Dacite Porphyry at north of the deposit (Figure 2.5).

The Sewell Tonalite, locally referred to as a 'Diorite Porphyry' (diorite in this thesis) occurs as a large stock to the south-east of the deposit. It is a light green to white equigranular to porphyritic rock. The Sewell Tonalite consists of abundant plagioclase (oligoclase), altered amphibole, biotite, quartz and minor potassium feldspar. This unit has been dated between 7.1 and 7.4 Ma by K-Ar (Cuadra, 1986).

The Teniente Dacite Porphyry, locally referred to as a 'Dacite Porphyry' (dacite in this thesis) is a tabular dyke up to 300 meters wide that strikes north (mine coordinates) over 1,500 meters. This unit is a light green to white porphyritic rock composed of 30-50% phenocrysts, such as abundant sub-euhedral plagioclase (oligoclase-andesine), occasional rounded quartz eyes and rare mafic crystals. The groundmass is composed mainly of granoblastic quartz and K-feldspar crystals (Skewes et al., 2002). Textural varieties have been observed within this body, which have been dated between 4.6 and 4.7 Ma (Cuadra, 1986).

Smaller felsic bodies have been recognized to the East of the Braden Pipe. The most relevant are the Tonalite Apophysis, locally called 'Diorite' or 'Diorite Porphyry' (similar to the Sewell Tonalite). Those units are light grey to light green intrusive rock, which form cylindrical apophyses. Their compositions are mainly of phenocrysts of abundant plagioclase (oligoclase-andesine), minor quartz eyes and remnant biotite phenocrysts, which have been replaced by chlorite. The groundmass is aplitic.

### 2.2.3 Breccias

A number of magmatic and hydrothermal breccias have been identified at the El Teniente mine; Floody (2000) have identified mineralized and not mineralized breccias. The Braden Pipe is the largest breccia located close to the centre of the deposit. It is light grey, massive and essentially a post-mineralization polymict breccia pipe, which looks like concrete. The pipe's shape is an inverted cone and is 1,200 meters wide at surface. The walls are inward dipping at 60-70°, except on the east side, which is sub-vertical. Within this unit several facies has been recognized, each one characterized by its own relationship matrix-clasts and alteration type. These facies have been interpreted as different stages of its own evolution. The matrix is typically rock flour material plus different minerals, and a typically tourmaline breccia ring of this body is known as Marginal Breccia (Figure 2.5).

Other less extensive breccias are described within the deposit. These are found mainly surrounding the felsic intrusive rocks and the Braden pipe. They are defined as hydrothermal breccia, where the matrix is principally mineralization such as anhydrite and tourmaline, among other minerals. Where the matrix is igneous rock, they are defined as igneous breccia.

#### 2.2.4 Alteration

According with the genesis for a porphyry copper deposit, an intense fracture system takes place in the roof of the host rock and is penetrated by the fluid phase, which further extends fractures by hydraulic fracturing. Fluid migration occurs into the network and the disequilibrium between hydrothermal fluid and host rock causes physical and chemical changes in the aqueous solution leading to metal precipitation (Cline, 1995). This process may occur several times; the occurrences are named ‘first boiling’, ‘second boiling’ and so on. Therefore, several fracturing stages can take place and an intense vein network that has been called stockwork is generated (Figure 2.6).

According to Cuadra (1986), four process or stages of hypogene mineralization-alteration have been described at El Teniente mine, which can be inferred as boiling stages. These are referred as; Late Magmatic (LM), Principal Hydrothermal (PH), Late Hydrothermal (LH), and ‘Postuma’ stage.

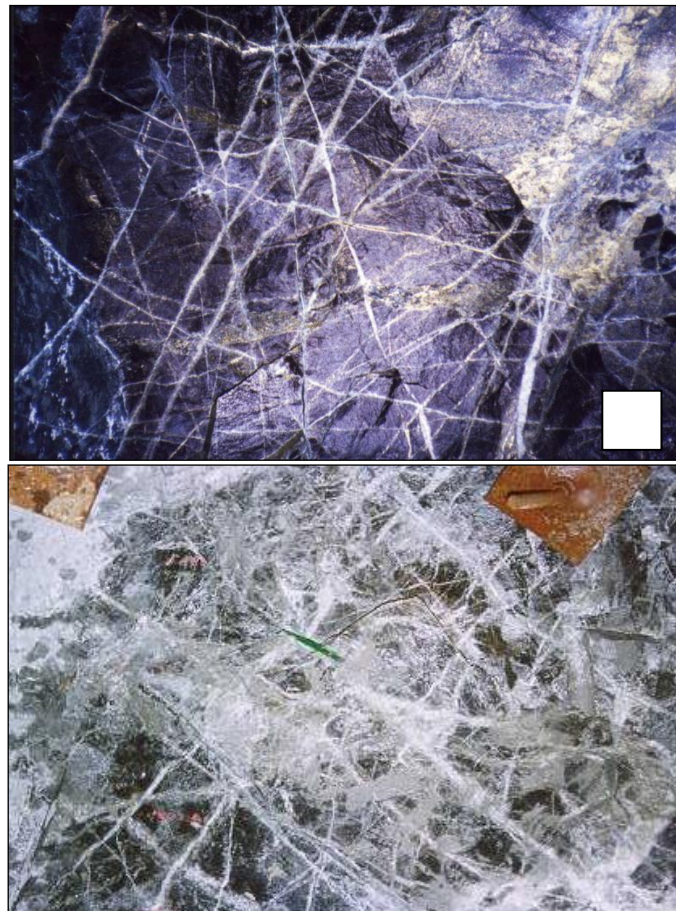


**Figure 2.6:** Stockwork intersected andesite rock type within primary copper ore. The white square (top photo) and the rock bolt plate (bottom photo) are 20x20 cm. (from Brzovic, 2010).

The Late Magmatic (LM) alteration has been characterized as potassic alteration. During this stage quartz, anhydrite and sulfide veins were formed, in association with, or preceded by a pervasive potassic alteration of the mafic rock (Zuniga, 1982). The potassic alteration is characterized by abundant biotite, chalcopyrite, Fe-oxides, and anhydrite (Skewes et al., 2002). The LM alteration stage is mainly located surrounding the Braden Pipe breccia (Zuniga 1982, Cuadra 1986).

The Principal Hydrothermal (PH) alteration has been characterized as phyllic alteration. During this stage, chalcopyrite rich veins that also contain anhydrite, pyrite, quartz and chlorite were developed (Zuniga, 1982). The Late Hydrothermal (LH) alteration has been characterized as a second stage of phyllic alteration. During this stage more diverse sulfide mineral assemblage veins were formed, and included: bornite, chalcopyrite, anhydrite, pyrite, quartz, tennantite, gypsum, chlorite and molybdenite. Quartz sericite alteration is generated as alteration halos in the wall rock.

The Late Hydrothermal alteration has major intensity (vein frequency) surrounding the Braden pipe in a ring extending from 100 to 150 meters (Cuadra, 1986), whereas the Principal Hydrothermal alteration is more intense (vein frequency) surrounding the diorite apophyses. A boundary between both alterations zones has been defined, which is called the perimeter of hydrothermal alteration zone. Consequently at the mine site, the rock types have been named by a definitional hydrothermal alteration suffix, for example, andesite located within principal hydrothermal zone is called andesite PH.

Supergene alteration has also occurred, which is not a hypogene process, coinciding mainly with the complete leaching of anhydrite and the appearance of supergene chalcocite (Brzovic, 2010). Supergene alteration that defines the secondary ore has been recognized between 100 and 600 meters below the surface (Cuadra, 1986). Secondary ore is a heavily fractured rock mass (Figure 2.7). The hypogene alteration zone, which is the original alteration without supergene alteration, is called primary ore (Figure 2.8).

### **2.2.5 Structures**

Faults are uncommon in the deposit. They are subvertical, have centimeter- to meter-scale displacement, and are millimeters to 120cm wide. Fault systems consist mainly in strike slip faults trending north-east and north-west (mine grid). These faults are the most continuous in the deposit, traceable for up to 800m (see Figure 2.9) which is associated with the late hydrothermal alteration stage. Reverse dip-slip faults are also reported (Garrido, 1994).



**Figure 2.7:** Core tray 0,7m length showing rock masses of secondary ore at the El Teniente mine (Brzovic, 2010).

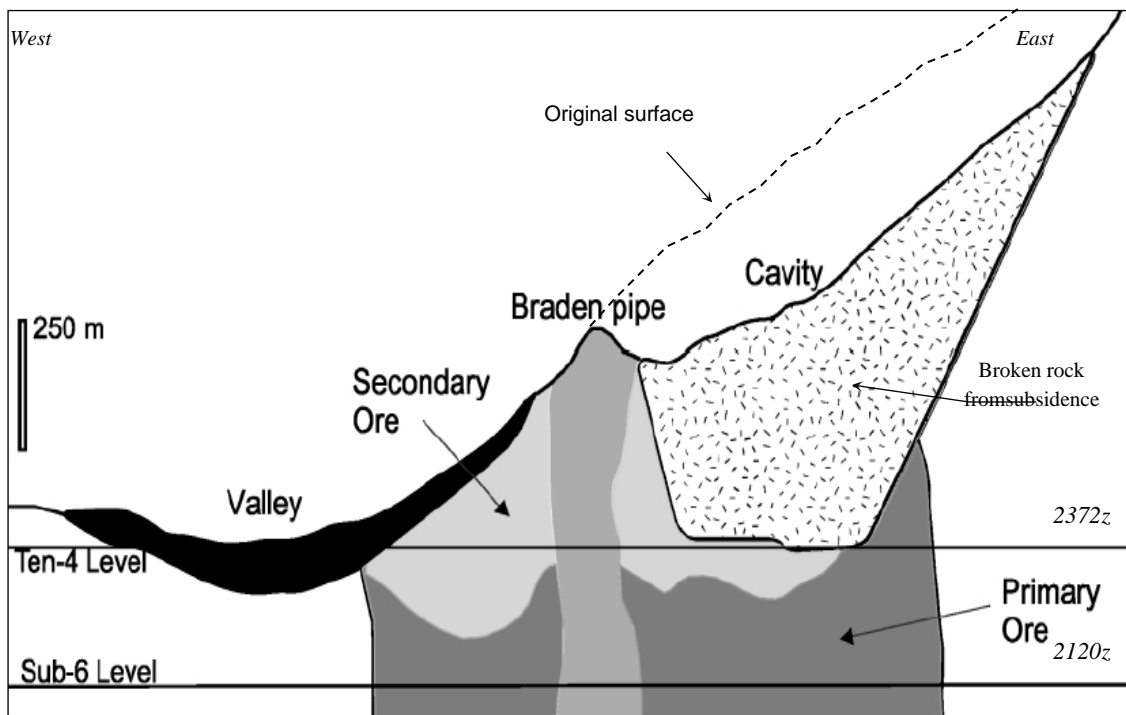


**Figure 2.8:** East-West section at El Teniente mine showing the primary and secondary ore (Brzovic, 2010)

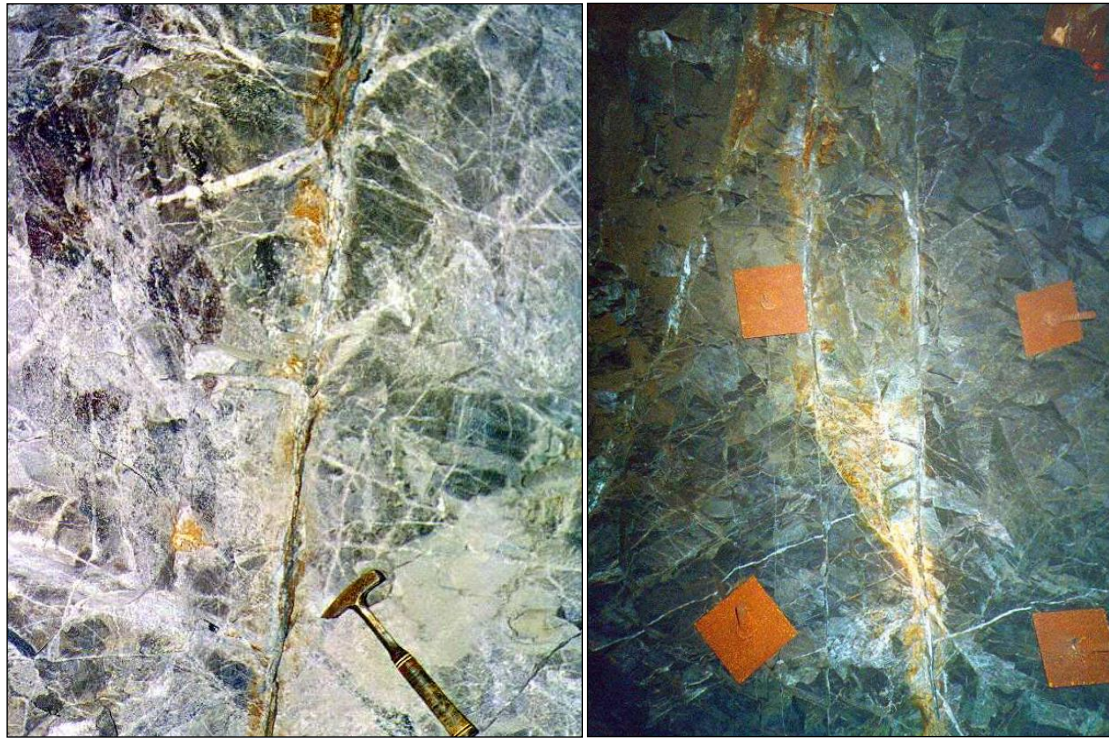


**Figure 2.9:** Faults at El Teniente mine within primary copper ore. Rock bolt plates are 20x20 cm. (Brzovic, 2010).

Two major faults have been recognized within the mine, these are called ‘Fault P’ located in the south part of deposit, and ‘Fault N1’ located in the north part (Figure 2.5). Both have been recognized with a horizontal trace length exceeding 800 meters and vertical trace length exceeding 400 meters. The gouge observed in both structures has an average thickness of 0.1 meters.

Faults are the only open discontinuities observed within the primary ore, which allow water flow through them. Copper and iron oxides may sometimes be recognized within the faults as shown Figure 2.9 (Brzovic, 2010).

## 2.3 MINING METHODS

### 2.3.1 Evolution of Exploitation Method at the *El Teniente* Mine

From the start in 1906 and up to the present days, the mining method in El Teniente has evolved, not only due to geological-geotechnical differences between secondary and a primary one, but also as a result of innovations and improvements from the experience obtained by working with different operational and mining methods.

The secondary ore corresponds to the upper part of the ore body which is higher in grade, less rigid, low hardness and finer fragmentation compared to primary ore located at depth. Nature created this difference because the weathering processes such as rain, snow, changes of temperature between day and night, and wind erosion affecting mostly the earth surface layer (Cavieres, 1999).

The first exploitations were performed in sectors emplaced in secondary ore, applying methods already in industrial form, such as Shrinkage Stopping & Pillar Caving and the current Block Caving with several variations called chute tappers, grizzlies, and scrapers for ore extraction (Chacon et al., 2004).

Later, the mining of primary ore reserves (with low grade; stiffer rock and hardness with coarse fragmentation) meant mechanizing the mining operations. This situation caused the evolution of the block caving method used in secondary ore, its main feature was manual ore transfer or semi-mechanized transference, and it evolved to panel caving with a highly mechanized ore transfer and continuous incorporation of caved area into production. In the panel caving method two mechanization varieties have been developed: one with ore transfer via “LHD” (Load-Haul-Dump) equipment used since 1982 in the first production sector that has exploited primary ore in El Teniente (case of Ten-4 Sur) and another variation introduced later that uses “Rock Pick Hammers” directly in the draw point of the extraction level (cases of Ten-4 Norte Fw and Ten-3 Isla Martillos).

When considering the operational mining sequence, there are three variations for panel caving. The typical panel caving with a conventional sequence used in modern underground operations as is illustrated in Figure 2.10. This has the following operational sequence: (1) developments are “advanced” compared to the undercutting face, at a distance that depends on the characteristics of each production sector, but this usually varies between 100 and 150 m; (2) draw bell drilling are also advanced compared to the undercutting face, at a distance that depends on the characteristics of each production sector, but that usually varies between 50 and 100 m; (3) the draw bell blasting is done in front of the undercutting face; (4) the undercutting front is delayed compared to the preparation and also compared to the blasting of opening phases of draw bells.

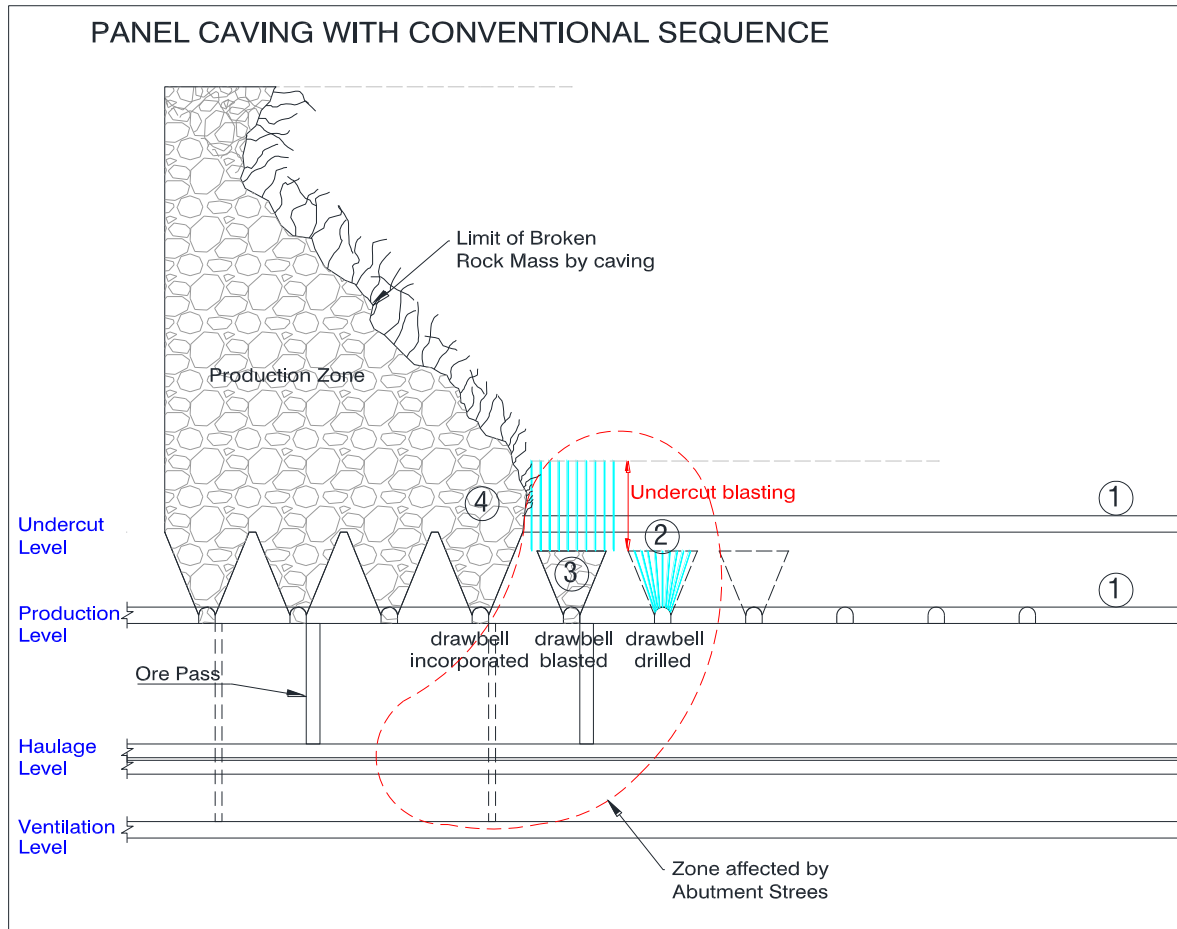


**Figure 2.10:** Typical cross section of panel caving with conventional sequence where the numerical order represents the operational sequence.

To improve this condition, moving away the abutment stress zone from the production front, El Teniente implemented two variants of this method based on pre-undercut sequence (Rojas et al., 2000) which are shown in Figures 2.11 and 2.12 (These variants do not eliminate the abutment stress zone but move it away from the production face).

The panel caving with a pre-undercut sequence (see cross section in Figure 2.11), is characterized by developing the undercutting before developing in the extraction level and includes the following operational sequence: (1) The undercut level drives are developed; (2) the undercut level is undercut, advancing with the undercut face until it is located at a certain distance ahead of the future extraction front; (3) all the excavations in the extraction level are developed, now located below the undercut area; (4) the extraction draw bells are open, below the undercut area; (5) ore extraction activities start, at a certain distance from the undercutting and preparation faces.(Rojas et al., 2000).

The panel caving with pre-undercut sequence and advanced developments (see cross section in Figure 2.12), is characterized by developing the undercutting advanced compared to the development of

some drifts and presents the following operational sequence: (1) undercut level works will be developed and just some drifts in the lower levels (e.g. just the galleries in the extraction level); (2) the undercut level is undercut, advancing with the undercutting face until it is at a certain distance ahead the future extraction face; (3) the remaining works in the extraction level are developed, in the sector now located below the undercut area; (4) the extraction draw bells are now open, below the undercut area; (5) the ore extraction activities start, at a certain distance from the undercut faces and preparation face.

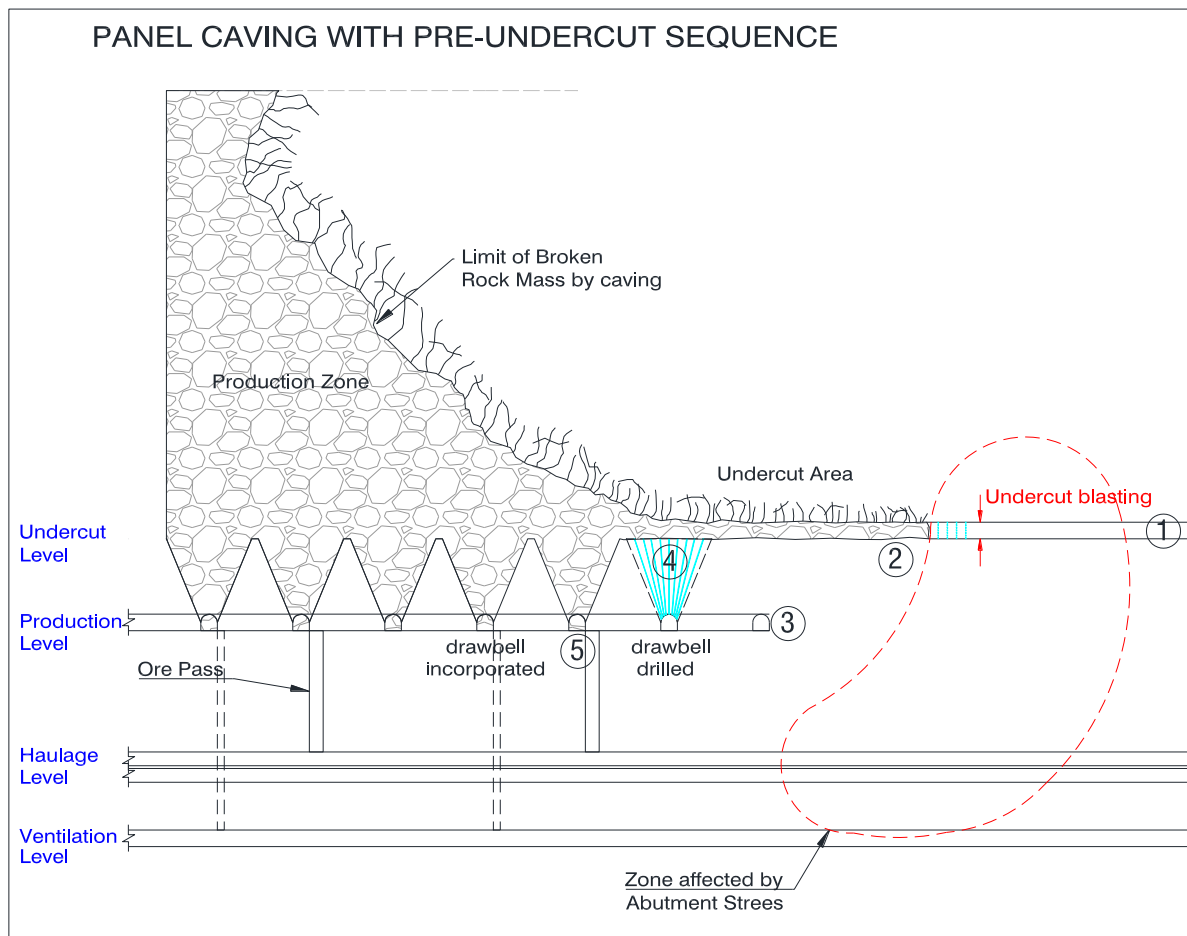


**Figure 2.11:** Typical cross section of panel caving with pre-undercut sequence where the numerical order represents the operational sequence.

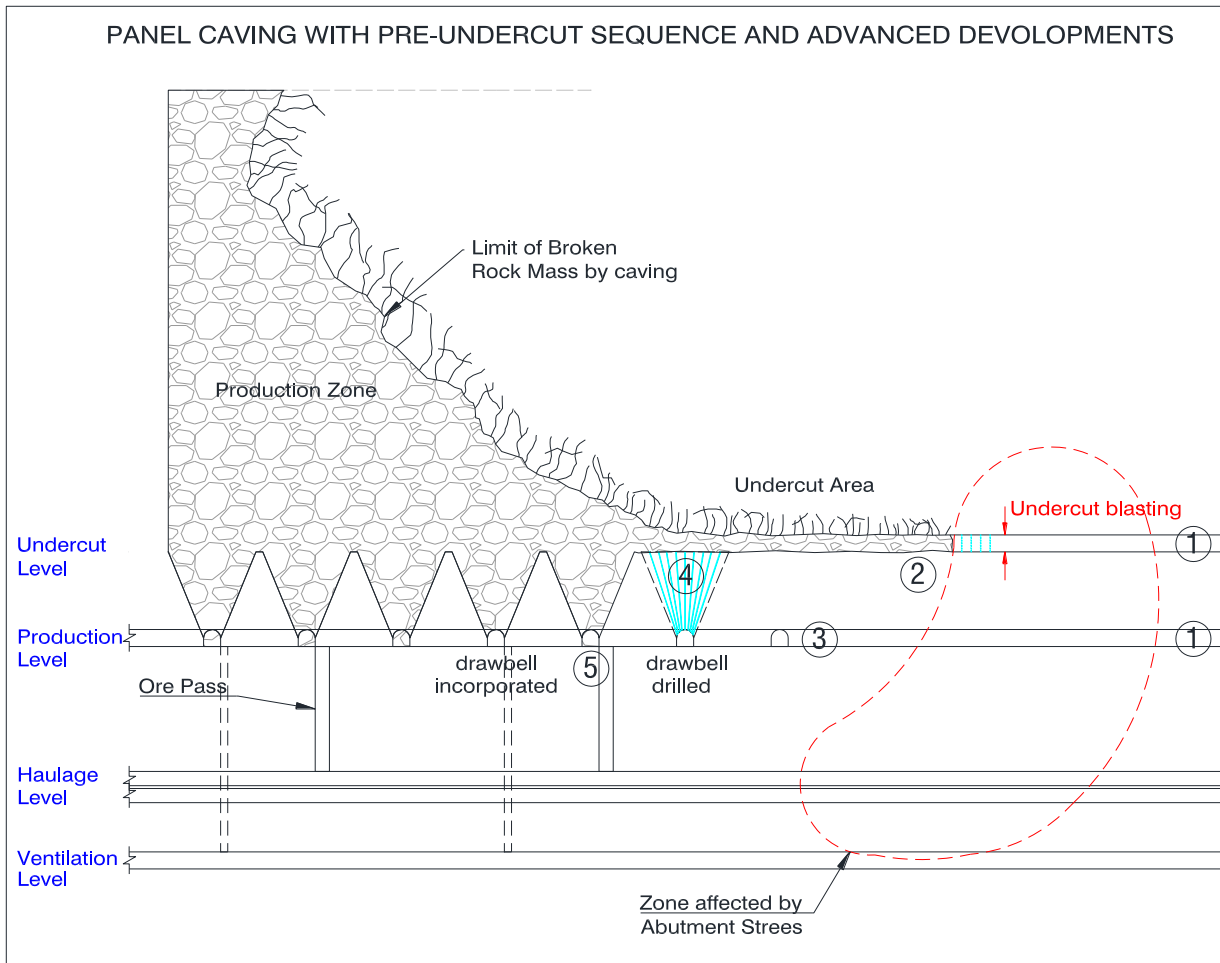


**Figure 2.12:** Typical cross section of panel caving with pre-undercut sequence and advanced developments where the numerical order represents the operational sequence.

The variants with pre-undercut sequence implemented in Esmeralda operation have used several different undercut patterns. The undercut design was based on drifts driven parallel to the extraction drifts on the production level but on 15m centers. The rib pillars between the drifts were initially removed using the “John Wayne” system. In this technique the fans of holes were drilled to both sides of the drift (see Figure 2.13a). One or two fans were blasted and swell muck was removed using remotely controlled loaders prior to blasting the next ring. Later the “Complete Pillar” system was used where fans of holes drilled through the full 15m width were drilled (see Figure 2.13b). The swell muck was removed using remote controlled loaders prior to firing the next rings. Since 2000 it was decided to try using a “Parallel hole” technique to blast the pillar. Crosscuts were driven on 30m centers leaving a pillar 26.4m in length by 11.4m in width to be blasted. Rings of parallel holes were drilled from crosscuts (see Figure 2.13c).

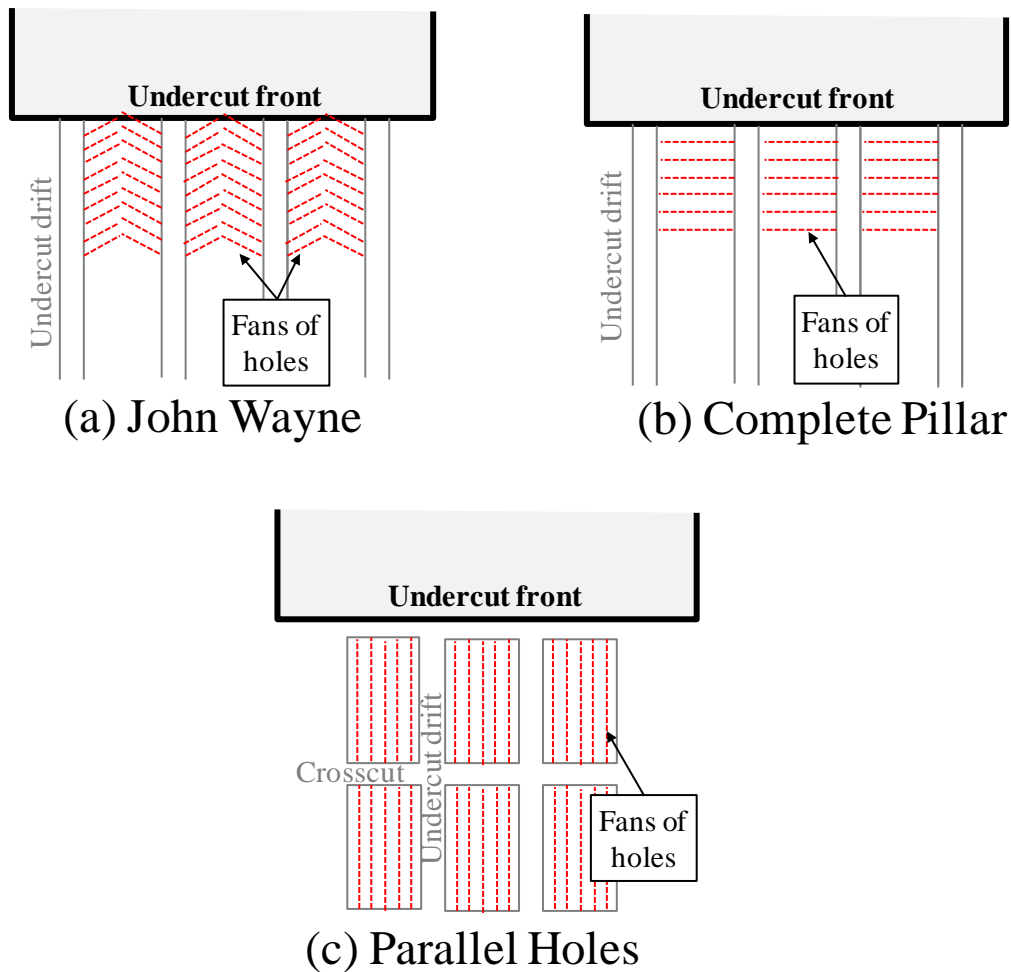


**Figure 2.13:** Different blast designs used in Esmeralda operation : (a) John Wayne, (b) Complete Pillar and (c) Parallel holes.

The evolution of the exploitation methods implemented in El Teniente mine are briefly described next (Cavieres, 1999):

(a) *Mining in secondary rock*

- Period 1906 to 1940

*Shrinkage Stopping:* This method consists on developing stopes by lifting over the ore. It was the first large scale mining method used. It was adapted to the geotechnical conditions found in the mine, mainly through variations in geometry (length and width), in the pillars between stopes, in the distance between production drifts and orientation of mining.

*Pillar Caving:* Once the ore extraction with the previous method was finished and having the stopes open, the base of the pillars was undercut between stopes to trigger the collapse and caving, which would allow extracting the ore through the ore passes and bins for later transfer to an intermediate haul level. This method was used in the upper levels of El Teniente mine.

- Period 1940 to 2000

*Block Caving without Crown Pillar:* Based on the experience obtained with shrinkage stoping and later pillar caving, it was concluded that it was enough with undercutting the base of a sector to achieve caving of secondary ore. This made unnecessary to develop stopes by rising over the ore. That was the origin of the block caving method, keeping the basic geometry of the previous methods, meaning a distance of 12 m between drifts and 6 m between chutes (alternate every 3 m).

*Block Caving with Crown Pillar:* To eliminate the stability problems affecting the production drifts, a protection pillar or crown-pillar was left between the production level and the undercutting floor, called Undercut level. This practice started in 1942 and was definitely implemented in 1947.

*Block Caving with chute tappers- grizzlies:* Once the use of crown-pillar became a standard in 1947, the exploitation system continued improving and the use of wagons pushed by hand in the production level was replaced by a system of grizzlies, located directly under the extraction funnels and connected to ore passes. This mining method allowed increasing the size of blocks, which resulted very convenient as mining, became deeper and rock became more competent.

*Block Caving with Scrapers:* A variation of the block caving method that has been used in sectors Teniente 5 Pilares and Teniente 5 Pilares Norte, with high fragmentation, consists of using scrapers instead of grizzlies.

(b) *Mining in mixed primary and secondary rock*

- Period 1970 to 1998

*Block Caving with LHD:* As the mine became deeper some primary rock became, much more massive and less fractured than secondary rock, so fragmentation was bigger in size. Therefore, some “mixed” blocks started appearing containing secondary and primary ore. At the beginning of 70’s a block caving with LHD equipment was considered. The experience from El Salvador and projects developed in Henderson were considered (Chacón, 2004).

*Forced Block Caving:* To extract mixed blocks it was also considered to use mine blasting. Radial drilling with holes de 2½” and load factors in the order of 0.7 kg/m<sup>3</sup> was used. This method of mining was implemented in sector Teniente 4 Estándar, in blocks 75 m x 75 m and 180 m high, locating the forcing level 54 m above the floor of the extraction level.

(c) *Mining in primary rock*

- Period 1982 up to present

*Panel Caving with LHD:* Mining in primary ore, with much coarser fragmentation, made necessary to modify the mining system and since May 1982, the panel caving method with LHD (Load-Haul-Dump) equipment started. Panels 100 to 280 meters high were extracted. The undercut area was incorporated in strips, along the undercutting face.

*Panel Caving with hammers:* This corresponds to a variation from the conventional method of panel caving which, instead of LHD equipment rock pick hammers located in the production level are used. This facilitates the flow of ore from the draw point to collection shafts, which download the ore to a transportation level.

*Panel caving with a pre-undercut sequence:* This variation of the panel caving method aims to move away the abutment stress zone from the extraction area and develops the production level under the undercutting level in order to achieve maximum operational safety.

*Panel caving with pre-undercut sequence and advanced developments:* This variation of the panel caving method also aims to move away the abutment stress zone from the extraction face and is similar to the previous variation; but in this case some drifts are developed in the production level before undercutting. Therefore only parts of the excavations in this level are developed under the undercut area (usually trenches and opening of draw bells).

## **2.4 GEOTECHNICAL RISKS AT THE EL TENIENTE MINE**

There are diverse geotechnical risks that can affect an underground mine due to caving methods:

- Hanging walls, that eventually can suddenly fail, thus generating air-blasts, as in the cases of Panel I in Andina and Sector Inca Oeste at Salvador, in Chile or Lift 1 of Northparkes Mine in Australia.
- Collapses, which damage drifts in the production level and cause production losses, such as the ones that have affected sectors Teniente 4 Sur and Esmeralda in El Teniente and III Panel in Andina in Chile or DOZ Block cave mine in Indonesia (Sinujahi et al., 2005).
- Excessive seismicity, induced by the caving mining itself, but which can potentially trigger rock bursts, such as the case of Sector Ten Sub 6 in El Teniente, Chile.
- Mud-water seepage, that can generate “pumping” or sudden mud flows as the ones that affected Level Ten 5 Transportation at El Teniente in Chile or Sector IOZ at Grasberg in Indonesia (Sinujahi et al., 2005).

- Subsidence problems, due to unforeseen growth of crater and/or the influence zone and that can eventually affect the underground and/or surface infrastructure.

The potential occurrence of these features can affect the production plan. Therefore, since the first engineering stages it is necessary to assess the feasibility of having such risk occurring. Special measures to minimize risk of occurrence and/or impact on the production plan need to be considered.

The rest of this chapter deals with the main types of geotechnical features that have affected underground mining at El Teniente mine.

### 2.4.1 Hangings

Hanging walls<sup>1</sup> correspond to detention of caving propagation, due to the formation of an arch or meta-stable cave that can fail suddenly, with the risk of generating an air-blast and cause significant damage in underground mining. Many times after failure of this meta-stable geometry there is connection between caving and surface, generating a crater such as the one shown in example of Figure 2.14.



**Figure 2.14:** Example of the formation of a chimney-type crater immediately after a hangingwall failure affecting the Sector Inca Oeste at Salvador, on December 5, 1999 in Chile (modified from Flores & Karzulovic, 2002).

The benchmarking study developed by Flores & Karzulovic (2002), allows making the following comments regarding hangingwalls:

- The area of a hanging wall can vary in a wide range, from less than 1,000 m<sup>2</sup> to more than 35,000 m<sup>2</sup>; however, most of the data recorded are under 15,000 m<sup>2</sup>, and the average area affected by hanging walls is 12.000 m<sup>2</sup>.

---

<sup>1</sup> This section refers to major hanging walls and not minor ones, that sometimes happen in the extraction points due to presence of significant oversize in broken material.

- Data recorded for hanging walls that triggered air-blasts in the underground mine, indicate that these are related to hanging walls affecting areas greater than 10,000 m<sup>2</sup>.

- Main causes of hanging walls, according to their relative frequency, are:

More frequent: Unexpected geological changes and underestimation of the rock mass quality.

Moderately frequent: Stress fields with very low magnitude, changes in the height of undercutting blasting.

Less frequent: Inappropriate extraction rates / extraction management, inappropriate undercutting sequence, not using measures to facilitate start of caving.

- Main remediation measures for hanging walls according to the relative frequency are:

More frequent: Increase the caved area and condition the rock mass

Moderately frequent: Weakening the edges of hanging area, extraction rate/management of extraction improved.

#### 2.4.2 Collapses

Collapses are a kind of geotechnical instability that frequently affects the extraction or production level of underground mines that use caving methods. It corresponds to gradual failure of pillars in the production and/or undercutting levels, as shown in Figures 2.15 and 2.16.



**Figure 2.15:** Damage in drifts of undercutting level in Sector Teniente 4 Sur of El Teniente mine, due to a collapse occurred in 1989 (from Flores & Karzulovic, 2002).

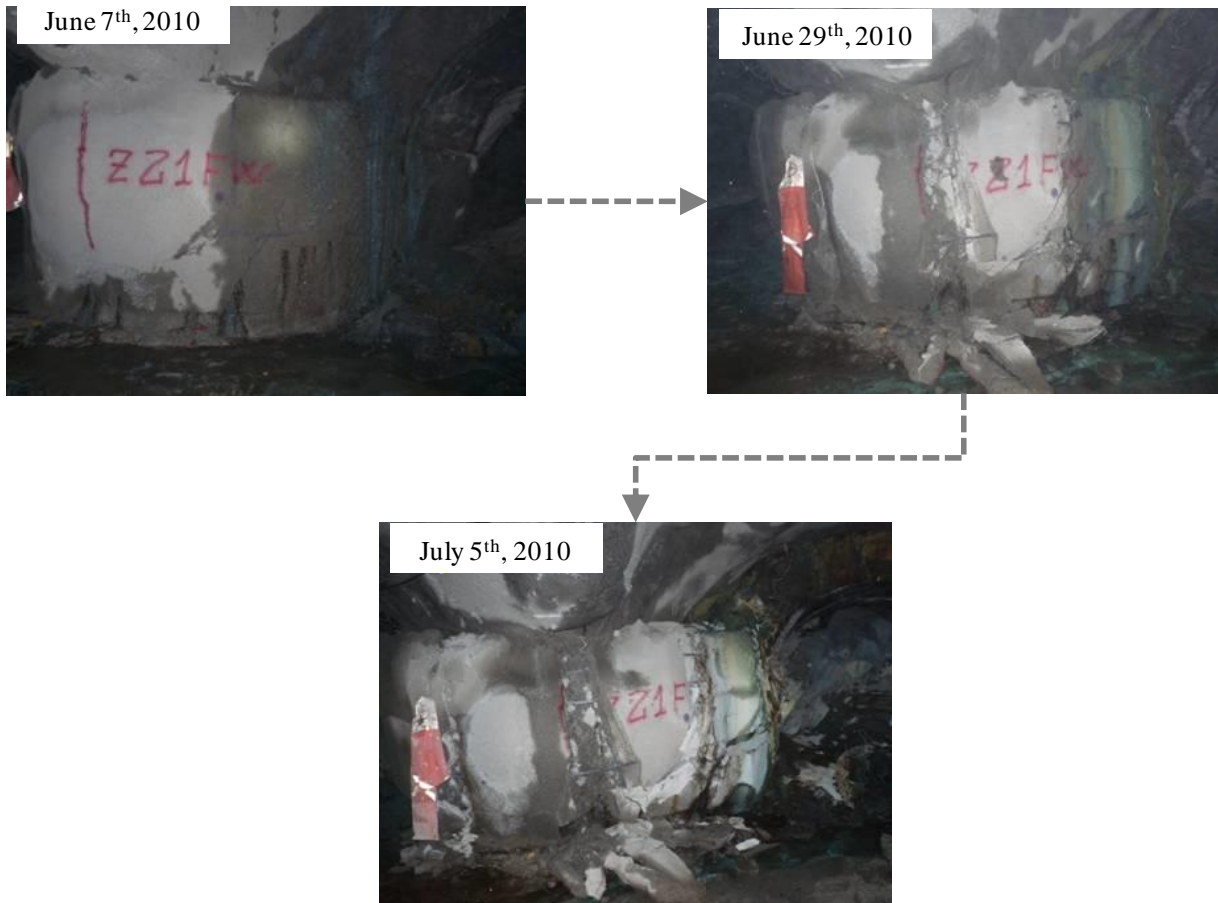


**Figure 2.16:** Gradual damage in the pillar wall of production level Esmeralda operation, due to a collapse that occurred in 2010.

The benchmark study developed by Flores & Karzulovic (2002) mentioned the following regarding collapses:

- The area affected by a collapse can vary significantly, from less than 1.000 m<sup>2</sup> to about 18.000 m<sup>2</sup>, with an average of about 4.000 m<sup>2</sup>.
- The possible causes of a collapse are: extraction rate and extraction management, presence of geological structures, and mining planning-mining sequence.
- Remedy measures to minimize a collapse are: extraction management, ground support, and improvement of the reliability of the geological-geotechnical information.

Based on a detailed review of the collapses that have affected several productive sectors of the El Teniente Mine, it can be said that the impact of the collapses has been historically important, such as

is seen in Figure 2.17, which shows the damaged areas due to collapses in the Ten-4 South, Ten Sub-6, Esmeralda and Regimiento sectors, respectively.

### Operations affected by Collapses at the El Teniente Mine

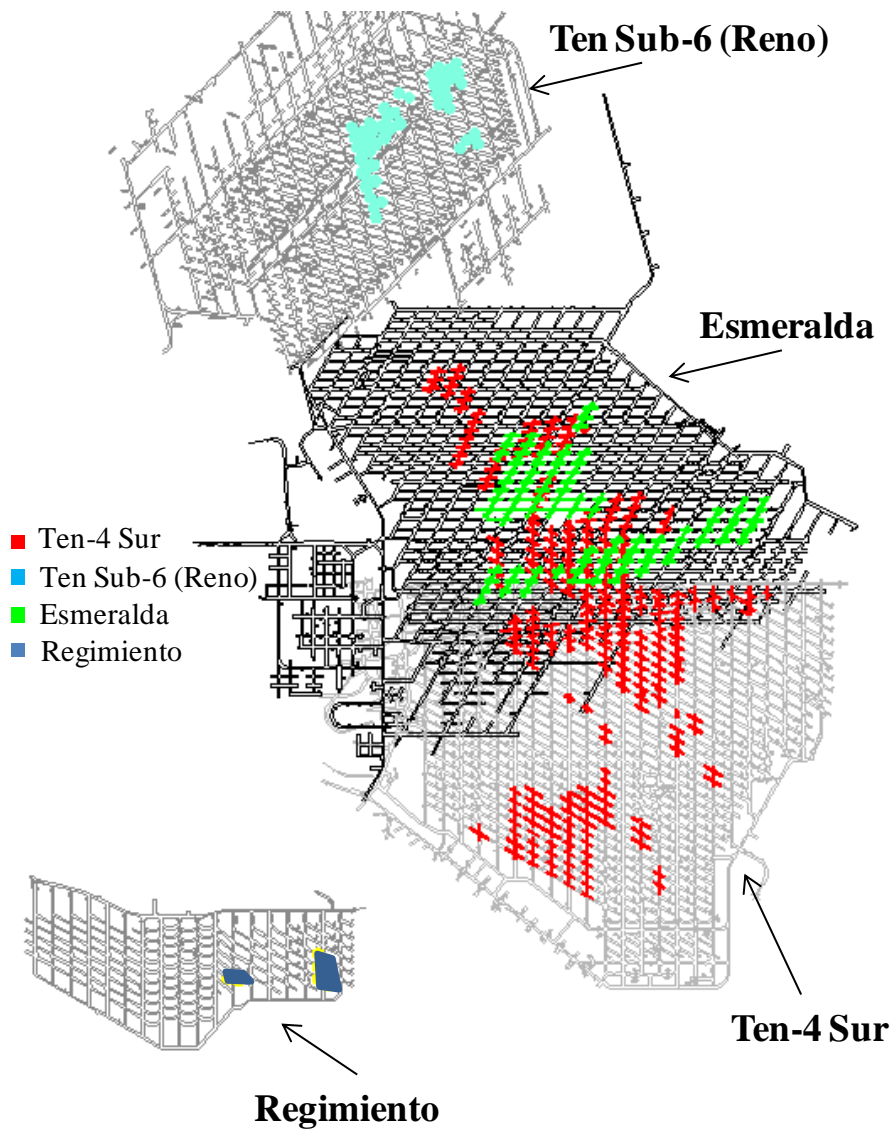


**Figure 2.17:** Sectors affected by collapses and the respective productive areas that were damaged vs. the production of primary ore from 1982 to 2010.

Additionally, taking into consideration the registration of collapses generated in the different sectors of the El Teniente Mine, a link between the width of the extraction fronts for the panel caving operations and the productive area affected by the collapse can be identified (Figure 2.18).

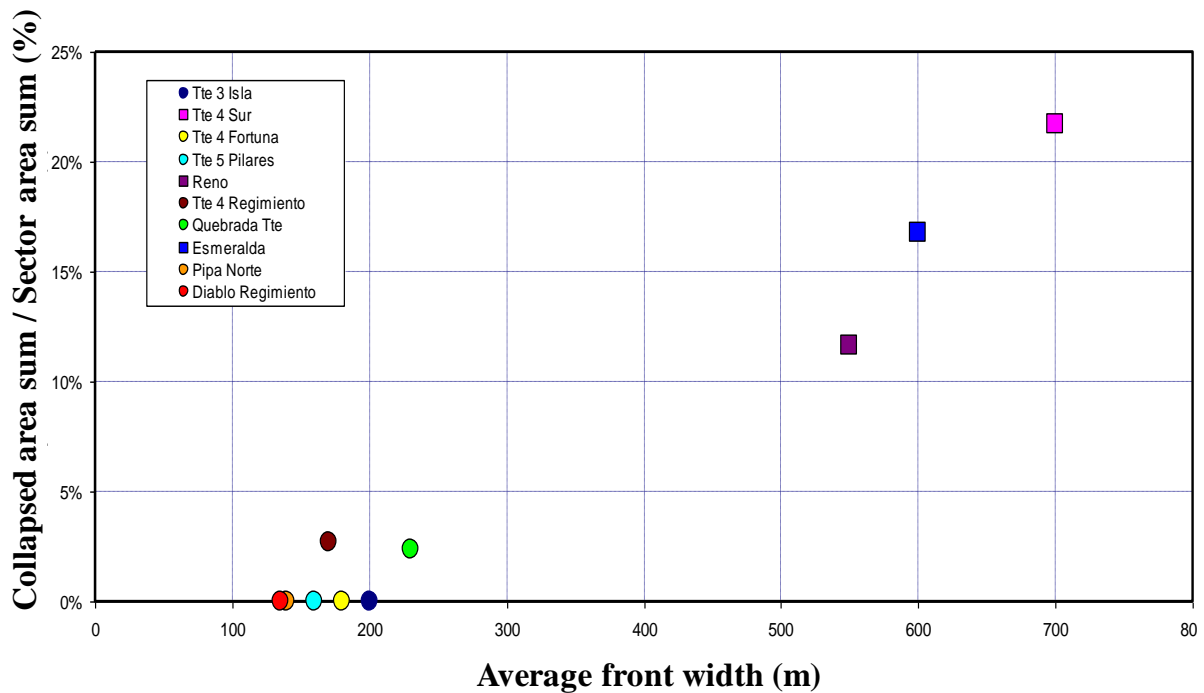


**Figure 2.18:** Relation between the extraction front widths and operative area affected by collapses.

According with Araneda and Sougarret (2008), over the last 25 years in Teniente operation, the major geotechnical problem has been associated with wide panel caving fronts, such as Ten-4 South, Esmeralda and Ten Sub-6 (Reno). All these operations have had caving front widths between 500 and 900 m.

### 2.4.3 Rockbursts

Rockburst is a seismic event caused by mining activity that produces some kind of damage. In the literature, several definitions for this phenomenon are found (see section 1.3.2).

The intensity or importance of the damages caused by a rockburst can vary significantly. In the El Teniente Mine, it is considered that a rockburst can cause three different levels of damage (Karzulovic, 2005):

- Low: Loose rock and block fall that causes some over-excavation. The fallen material does not cover more than 25% of the section of the affected area. The ground support shows signs of damage, but at least 80% of it keeps its working capacity. The work continues.
- Moderate: Loose rock and block fall that causes significant over excavation. The fallen material covers less than 50% of the section of the affected area. The ground support is

damaged, but at least 50% of it keeps its working capacity. Rehabilitation is required for work to continue.

- Heavy: Severe loose rock and block fall that causes a very significant over-excavation. The fallen material covers more than 50% of the section of the work carried out. In some cases, cracking and lifting of the floor occurs. The ground support is badly damaged and more than 50% of it has lost its work capacity. Work cannot continue operation without first undertaken large repairs.

Examples of rockburst damage in the El Teniente Mine and its levels of damage associated are shown in figures 2.19 to 2.21.



**Figure 2.19:** Example of heavy damage due to rockburst in El Teniente Mine, Reno Operation, 2005.



**Figure 2.20:** Example of heavy damage due to rockburst in El Teniente Mine, Pilar Norte Operation, 2011.



**Figure 2.21:** Example of heavy damage due to rockburst in El Teniente Mine, Haulage level at Reno Operation, August 2012.

Based on the *El Teniente* Mine experience, Dunlop (2013) suggested that the damage happens at distances in a range of 100 to 200 meters from the focus of an event. But the dimensions of seismic sources large enough to create damage are of the same order of magnitude. This fact suggests that most of the damage corresponds to the effect of rock mass deformation, movements, in the rupture zone. Radiated energy would play a secondary role damaging a limited area surrounding of the rock mass participating in the seismic source. Further research is needed to clarify this issue.

One review of the experience of the El Teniente Division mentions the following regarding rockburst that can affect underground mining by caving in the primary ore (Karzulovic, 2005):

- a) A rockburst can affect not only the extraction and undercut levels, but it can also affect other levels, and even can reach up to the Transportation or Haulage Level (See Figures 2.10, 2.11 and 2.12).
- b) The most notorious rockburst that occurred in the Ten Sub 6 Operation (year 1990 to 1992) caused different levels of damage in the various levels affected, and the damages occurred at different distances regarding the position of the undercut front.
- c) The experience of the Esmeralda Operation suggests that in a panel caving with pre undercutting sequence damages due to rockburst decrease in the production level, but increase in the undercut level, compared a panel caving with conventional sequence.

Although it has been established that seismic event are inherent to the caving method, that is, every rupture in the caving process is a seismic event (Dunlop, 2013). Efforts to reduce this risk by means of three forms are available: avoiding seismic events of high magnitude, reducing the level of damage expected (ground support) and reducing the level of personnel exposures.

The sources control has produced a reduction in the magnitude of the seismic events through the control of mining strategy and the use of pre-conditioning technology for the rock mass.

Control of damages implies the implementation of support and reinforcement systems designed by dynamic loads.

The control of exposition has been implemented though exclusion period, transition zones, and use of remote control equipment.

Finally, during the last years, in the El Teniente Mine a significant advancement was generated regarding the knowledge and control of rockburst, such as it is indicated in the graph of Figure 2.22, which evidences the decreasing of the total number of rockbursts per operation and the sustained increase of the mining of the primary ore ranging from 1982 to 2012.

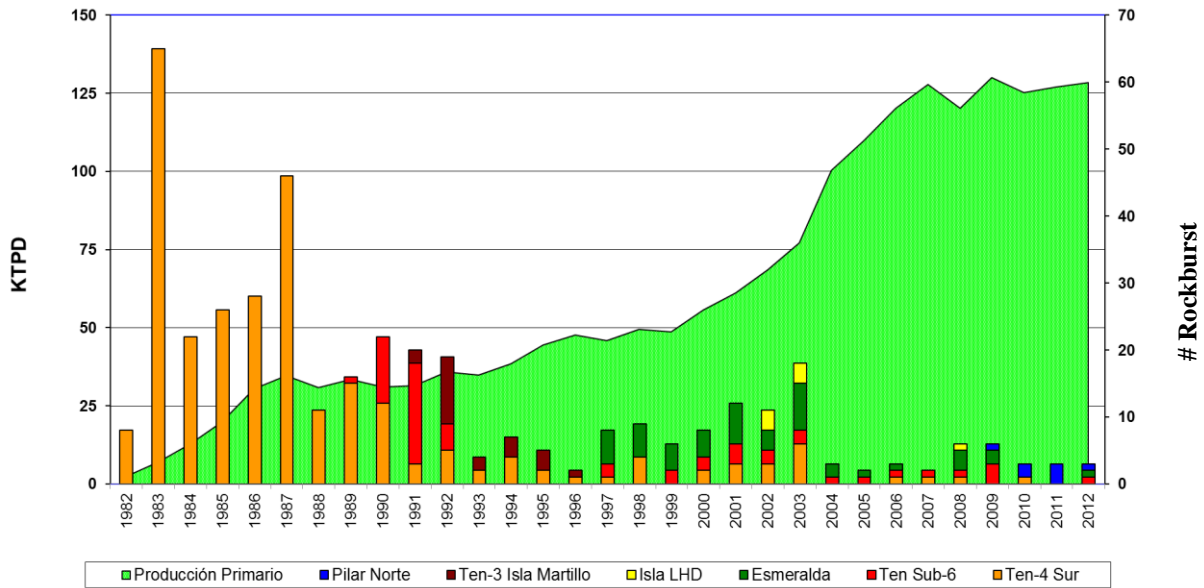


**Figure 2.22:** Number of rockbursts per operation vs. annual production of primary ore ranging from 1982 to 2012.

## 2.5 ESMERALDA MINE

### 2.5.1 Introduction

The Esmeralda operation located in the central part of the El Teniente ore body at the East part of Braden pipe (Figure 2.23), introduced panel caving with pre-undercut sequence in 1997. This operation included a production plan of 350Mtons of ore with 1% of Cu and a life span over 35 years (Barraza and Crokan, 2000).

The undercutting was initiated in October 1996, and caving initiation started one year later triggered by ore drawing at the production level. The breakthrough to the upper mine level was estimated to occur between April and May 1999, when the hydraulic radius reached a value of 26m. The effective mined area at this time was 16,800m<sup>2</sup> (Rojas et al., 2001). Caving initiation was located only 100 meters below the old Teniente 4 South mine level to reduce the seismic risk level (Barraza and Crokan, 2000).

The main geological features within the interest area are: two main rock types, andesite and diorite; two hydrothermal alteration zones, late (LH) and principal (PH); one major fault system named Fault B (Seguel, 2005). The hydrothermal alteration zones have been associated with the principal orientation reference at the Esmeralda operation, where the hanging wall sector (Hw) is related with the LH and the footwall (Fw) sector related with PH.

During the first years of mine production (until year 2000) moderate damage to the mining infrastructure occurred, which was mainly related to both; dynamics failures and stress concentration at the undercut mine level.

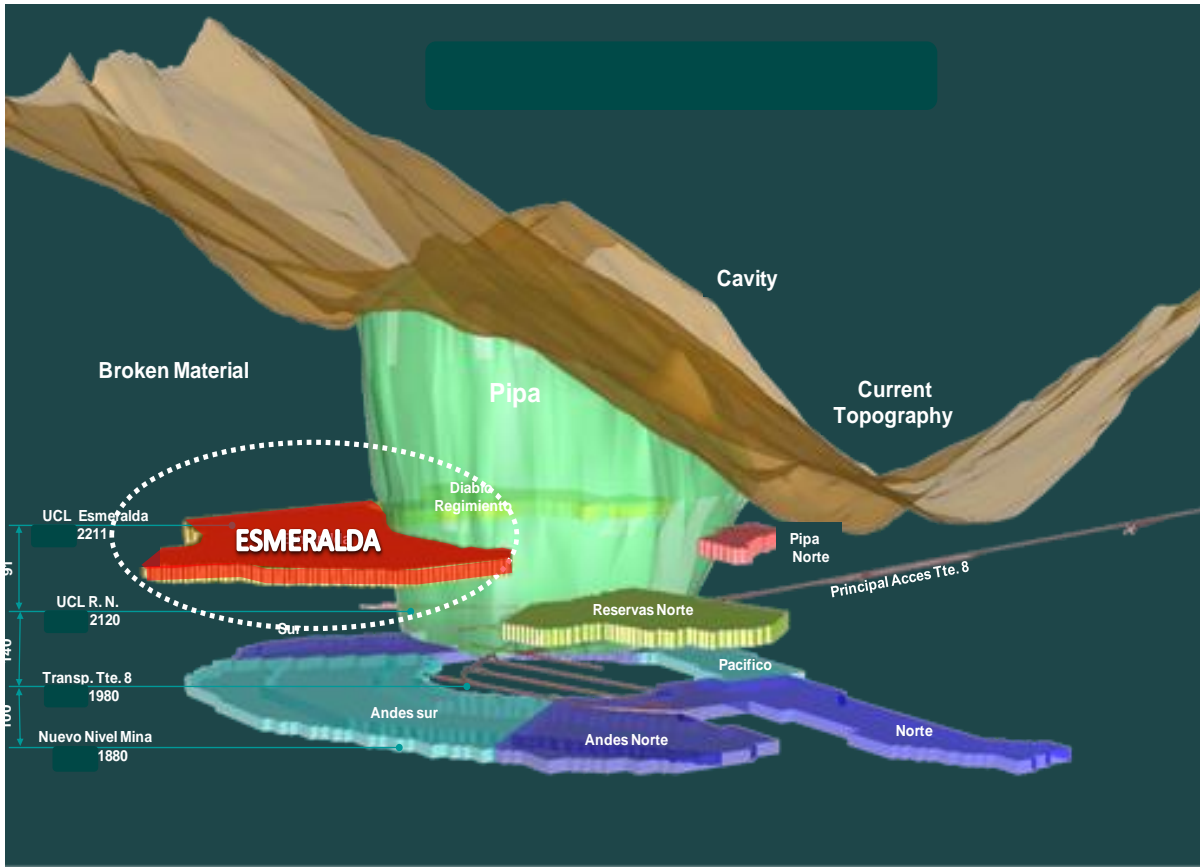


**Figure 2.23:** Relative location of Esmeralda operation

## 2.5.2 Rock Mass Characterization

The main geological units recognized in the sector correspond to: El Teniente mafic complex (ex andesites from the Mine), felsic porphyry (diorite porphyry and latite porphyry), breccia units (Braden's breccia complex, hydrothermal breccias, and igneous breccias). These units are shown in Figure 2.24 (Also see Section 2.2).

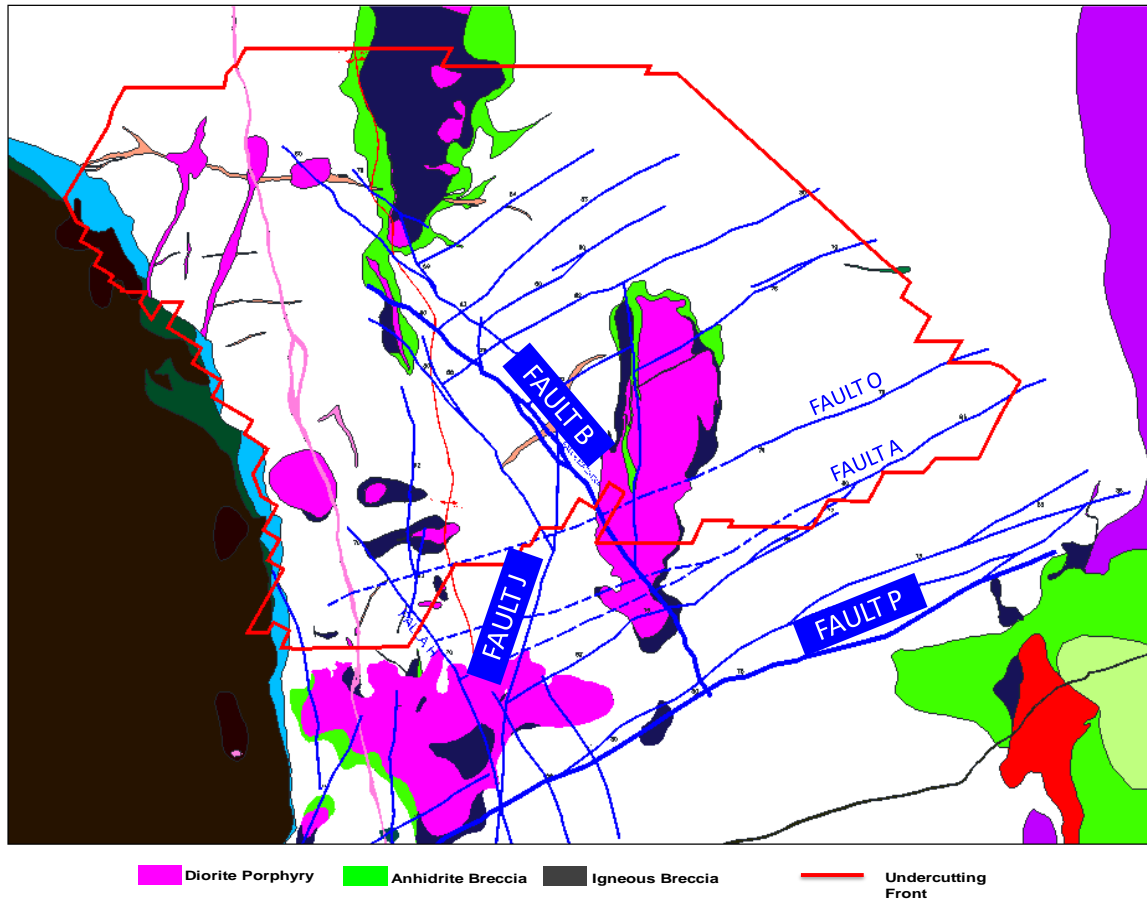


**Figure 2.24:** Plan view with major lithology and structures at Undercut level Esmeralda operation where the predominant lithology is the mafic complex El Teniente (CMET or ex-andesite).

The primary ore of the Esmeralda operation is characterized by different types of geological structures according to continuity and infill type. They could correspond to a late magmatic (TM) environment, at a main hydrothermal environment (HP) or to a late hydrothermal environment (HT). According to their trace extension, they are classified in major, intermediate, and minor structures.

The major structures at Esmeralda operation can be seen in Figure 2.24. These major structures correspond to two main systems or families (Seguel et al., 2005):

The North-West system that corresponds to the Fault B system, presents several branches and irregular traces that join and separate, both horizontally and vertically. The principal of these branches has a recognized trace of about 500 m from the TEN-4 Level to the TEN-6 Level and presents centimetric infill of carbonates, molybdenite, and gypsum. These structures have N40°W to N60°W strikes and sub-vertical dips both to the NE and to the SW:

In the North-East system to the East of the Fault B system and south-southeast of the diorite porphyries, a structural strip is developed with a N50°-60°E preferential pattern, 70° and 90° dips toward the northeast and southeast with thicknesses between 1cm and 2 cm. In this strip the Fault P

stands out, characterized by a persistence estimated at 600 m horizontally and 400 m vertically. Its thickness ranges from 2cm to 100cm with a mean value of 20 cm.

In the Esmeralda operation, the primary rock mass is competent and massive or low fractured (Seguel et al., 2005). Additionally, according to Brzovic (2010) and the implementation of traditional systems of geotechnical classification for rock masses, the rock mass quality at El Teniente mine ranges from good to very good. It does not allow the identification of the differences in behavior that have been evident in the rock mass of the Esmeralda operation during caving exploitation (Brzovic, 2008).

In response to this, a research investigation (Brzovic and Villaescusa, 2007; Brzovic, 2009; and Brzovic, 2013) has been carried out in order to determine what discontinuities are the most relevant in the rock mass disassembly process during cave mining. The infill characteristics have been used to characterize rock mass quality in different sectors, and the results are in accordance with actual observations at the mine site, especially at Esmeralda operation.

Brzovic (2013) generated a geotechnical characterization for the rock mass and a database of weak discontinuities (faults and soft veins) of the current mining sectors in production, especially the Esmeralda operation, where it has been shown that these weak discontinuities control the fragmentation, in addition to being correlated with cavability and seismicity (Brzovic and Villaescusa, 2007). Additionally, Brzovic (2013) developed a methodology to integrate the structural data of different mapping scales of the rock mass in a statistical structural model (Discrete Fracture Network Modeling). Rock structure has been characterized based on the occurrence of intermediate structures mapped in mine drives at the production and the undercut mine levels, and from small discontinuities collected using large diameter core samples.

As result of this investigation a representative map with geotechnical zones was developed (potential disassembly of the rock mass) for the undercut level at Esmeralda operation and it can be seen in Figure 2.25 (Brzovic, 2013). In the plan view six geotechnical units were defined, which were differentiated in function of the following parameters:

- Lithology
- Frequency of soft veins of thickness  $\geq 1$  mm
- Alteration environment and dominant soft mineral – drifts.
- Alteration environment and dominant soft mineral – drill holes.

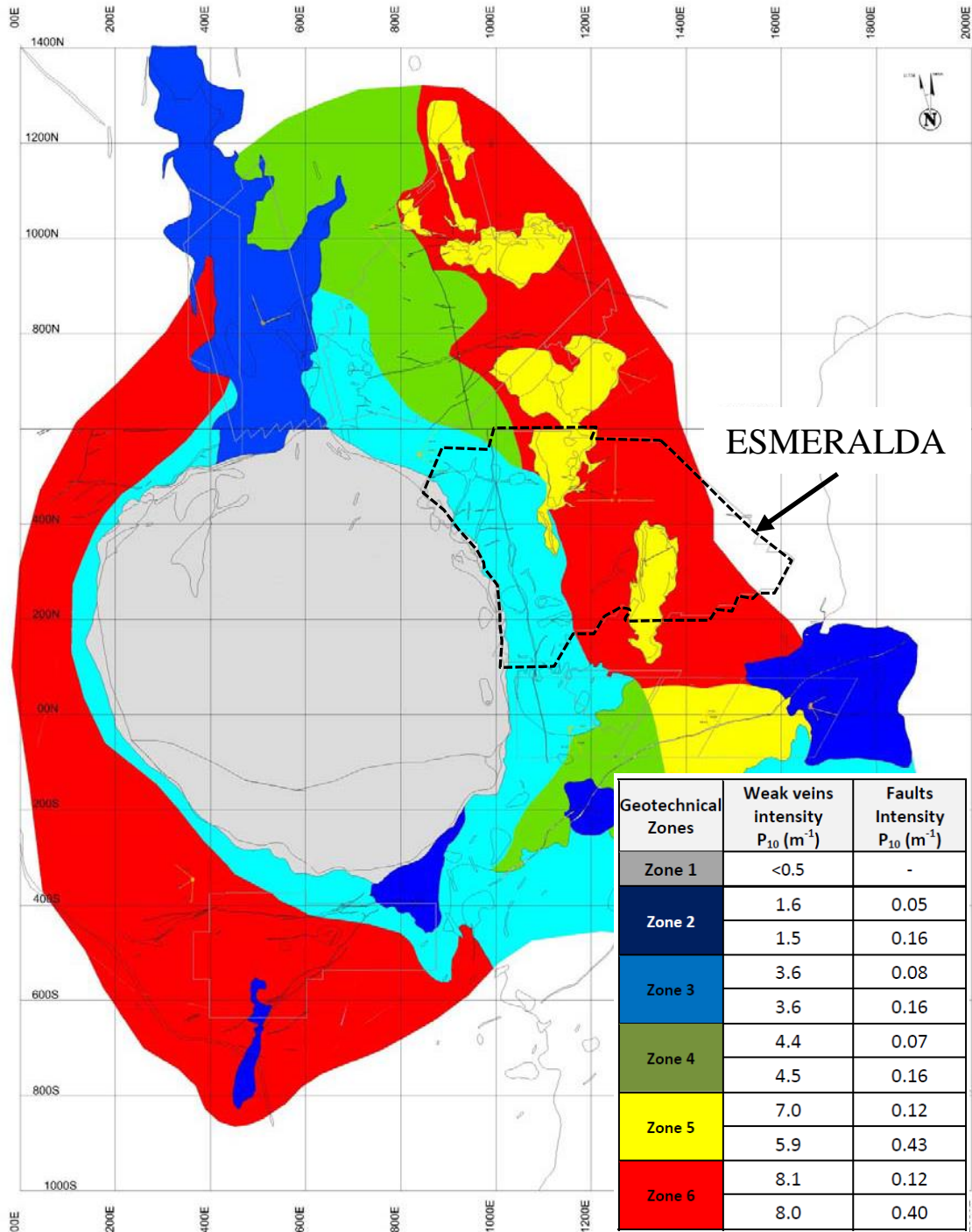


**Figure 2.25:** Map of the potential disassembly of the rock mass during the mining process (Undercut Level for Esmeralda operation), map GL-10659-0 (Brzovic, 2013).

### 2.5.3 A Review of Mine Strategy

The Esmeralda project is the third panel replaced totally in primary ore that has been developed by El Teniente Mine and Codelco Chile. The pre-feasibility study was performed during the years 1992

and 1993, based mainly on the experience and knowledge acquired during the mining of the Teniente 4 South Operation and the failure of commissioning of the Teniente Sub-6 Operation.

During the year 1997 the panel caving with pre-undercut sequence (Figure 2.12) started to be used, with the commissioning of the sector, with a growth rate of 6.000 tons per day/year and a projected production of 45.000 tons/day, for the year 2005.

During the first period of implementation of the project (1997 – 1999) a high quality standard was reached, both in compliance with its milestones, as in the quality of the productive infrastructure, thus, it is an undisputed referent of world mining due to the success reached at the end of the 90s (Rojas, 2000).

From the year 2001 Esmeralda Mine was affected by a complex situation mainly associated to delays in preparation and the beginning of loss of productive area due to collapse processes. As a result of this, a series of impacts in the projection of future growth that indicated the impossibility of fulfilling the production regime (45.000 tons/day) for the year 2005 occurred. To reduce the deficit in production, the contingency projects name Extensión Hw (2003) and Extensión North (2004) were implemented.

Given the events and the impact of the collapse phenomenon generated between the years ranging from 2001 to 2004, the decision to implement a change of variant for exploitation method was made. A modified version of panel caving with pre-undercut sequence and advanced developments (see Figure 2.13) began to be used. This period of implementation is characterized by a production regime that did not surpass 30.000 tons/day.

From 2009, the occurrence of collapses in the productive infrastructure of Esmeralda started again, until the year 2010 that finally a great part of the active front collapsed, affecting completely the advancement and growth of the Esmeralda operation.

Currently, the operation is comprised of areas that are depleted and that support the current production of the sector (current front and HW extension). For its growth the commissioning of the zone named Esmeralda South parting from the year 2011 was considered, using a mining strategy through blocks that considered the implementation of panel caving with conventional sequence (see Figure 2.10), along with the application of pre-conditioning of the rock mass (Baez, 2011 and Zepeda et al., 2008). Also, the incorporation of the Panel 1 operation parting from the year 2013 was considered, located 14 m under the current production level, allowing for the recovery of ore reserves from the central zone (Larraín et al., 2011).

### 2.5.4 Esmeralda Ore Production

The graph on Figure 2.26 shows the historical evolution of the ore extraction from the Esmeralda operation. In the graph an important break of sustained growth largely associated to geotechnical instabilities can be seen, especially periods of collapse of the infrastructure in the year 2004 and later on in the year 2010.

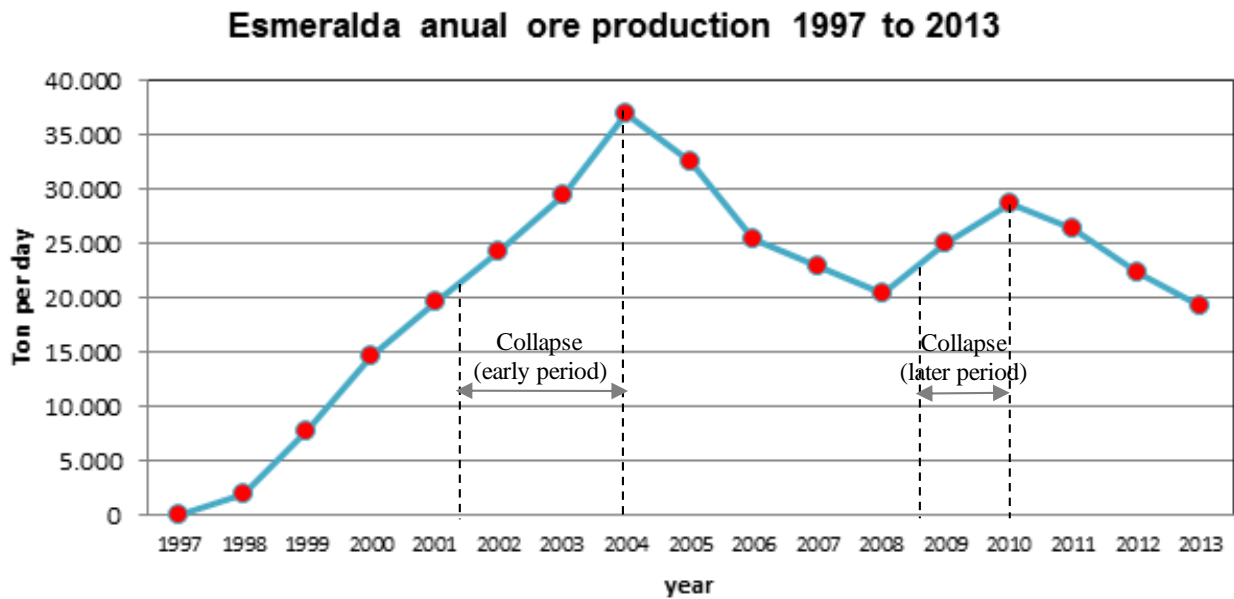


**Figure 2.26:** Evolution of production of primary ore in the Esmeralda Mine

According to Larraín et al. (2011), in the year 2011 a production of 25.090 tons/day was achieved and the further mine plan considered to reach the production regime between the years of 2017 and 2025 with a production around 41.000 ton/day, later on its rhythm will start decreasing around the year 2028 with 7.000 ton/day (closure year).

## **CHAPTER 3**

### **LITERATURE REVIEW**

#### **3.1 INTRODUCTION**

This chapter presents a review of the literature available in these three key areas with the view of assessing the current understanding of these processes which constitute the response of the rock mass during caving operation.

This chapter also includes a discussion on behavior of brittle intact rock and its implications for rock mass failure during cave mining operation. This is because it is necessary to understand the behavior or the response of the intact rock at a massive scale, to evaluate and interpret the infrastructure damages associated to caving operations by using numerical simulation tools that integrate in an approximate manner the complex mining geometry and conditions of the surrounding media.

#### **3.2 CHARACTERIZATION OF PRIMARY ORE FOR PANEL CAVING OPERATION**

##### **3.2.1 Introduction**

The start of mining in primary rock at El Teniente, early 70's, allowed detecting significant differences about mining in secondary rock:

- The rock mass presented a much lower cavability and coarser fragmentation.
- The draw points started showing operational problems and became inefficient.
- The productivity decreased in production sectors. In fact, the draw point performance by turn in secondary ore varied from 111 to 213 tons and in primary ore it diminished to 20 – 30 tons at Level Ten 4 (Ovalle & Codoceo, 1977).
- On set of seismicity.

Exploitation of the experimental block XC8-14AN in Level Ten 4, partially located in primary rock, and which extraction started in March 1972, allowed concluded that (Kvapil et al, 1982):

- The primary rock can be exploited by using caving method.
- Propagation or caving progress in primary ore was slower than in secondary rock. In fact, it was indicated that “the primary ore needs longer time to be fractured to achieve proper caving”.

- The extraction layout in primary rock should be larger than in secondary rock, because primary rock presented coarser fragmentation.
- The rock mass experienced much less cavability.

All the aforesaid made necessary to modify the classic mine designs and caused the evolution of planning and design of mines by caving methods, that varied from block caving to panel caving and recently to variations of the latter method (which are still evolving).

Karzulovic (2006b) pointed out a series of definitions associated to the concept of primary rock material. Two of the most prominent definitions are described below:

*El Teniente Primary Ore:* The primary ore forms a rock mass with high cohesion, dry and hard with high strength to breaking, and with the main characteristic being its intact original mineralogy. Its main mineralogical constituents are plagioclase, biotite, sericite, quartz, anhydrite and tourmaline. Meanwhile, the sulphide mineralogy consists of chalcopyrite and pyrite, with lower amounts of bornite, tennantite and molybdenum (Cuadra & Puig, 1991).

*Primary Rock mass (El Teniente):* Important volume of rock totally or partially intercepted by geological structures, being these faults and stockwork veinlets sealed and with different types of mineralogy infill (Brzovic, 2001).

Also to facilitate a discussion about the mechanical behaviour of the primary intact rock and primary rock mass, Hoek and Brown (1980) illustrated an idealized representation of the intact rock transition to a highly fractured rock mass, through increase of sample size (see Figure 3.1).

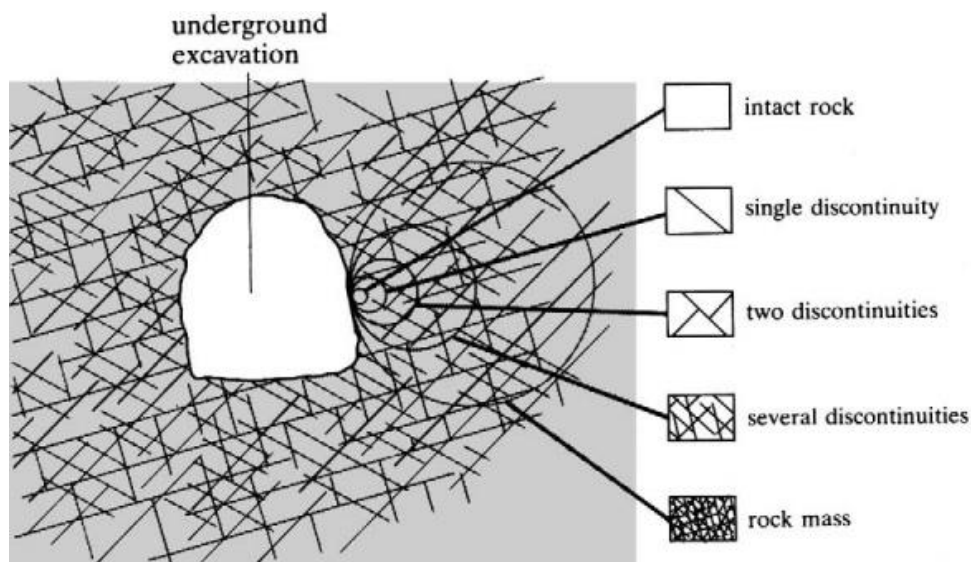


**Figure 3.1:** Idealized illustration of transition from intact rock to rock mass (after Hoek and Brown, 1980)

Complementarily Brady and Brown (2004) suggested a series of concepts and definitions clarifying the terminology about rock “strength” and failure:

*Fracture:* is the formation of separation plans in the rock material. This implies the separation of joints to form new surfaces.

*Strength or peak strength:* is the maximum stress, usually averaged over a plane that the rock can take under certain conditions. After the peak is exceeded, the rock specimen still could have some load or strength capacity. The minimum or residual strength is achieved generally only after considerable post peak deformation.

*Brittle fracture:* is the process by which sudden loss of strength occurs across a plane following little or no permanent (plastic) deformation. It is usually associated with strain-softening or strain-weakening behaviour of the specimen.

*Failure:* It is often said to occur at the peak strength or be initiated at the peak strength (Jaeger and Cook, 1979). An alternative engineering approach is to say that the rock has failed when it can no longer adequately support the forces applied to it or otherwise fulfill its engineering function.

### 3.2.2 Behavior for primary intact rock

One of the most important aspects related to the behaviour of primary intact rock is its rupture mode. This is determined experimentally by rock mechanic tests (typically uniaxial and triaxial compression tests), and based on those results parameters are determined to define a failure criterion, which is considered to be representative of rock strength.

Karzulovic (2006b) established that the primary intact rock shows a brittle type of rupture (see examples in Figure 3.2), that includes failures due to shear and also tensile failure, frequently with recent fractures which may or may not interact with sealed veinlets already existing in the core. Thus, the load-deformation curve of primary rock shows a significant loss of strength in post-peak strength.

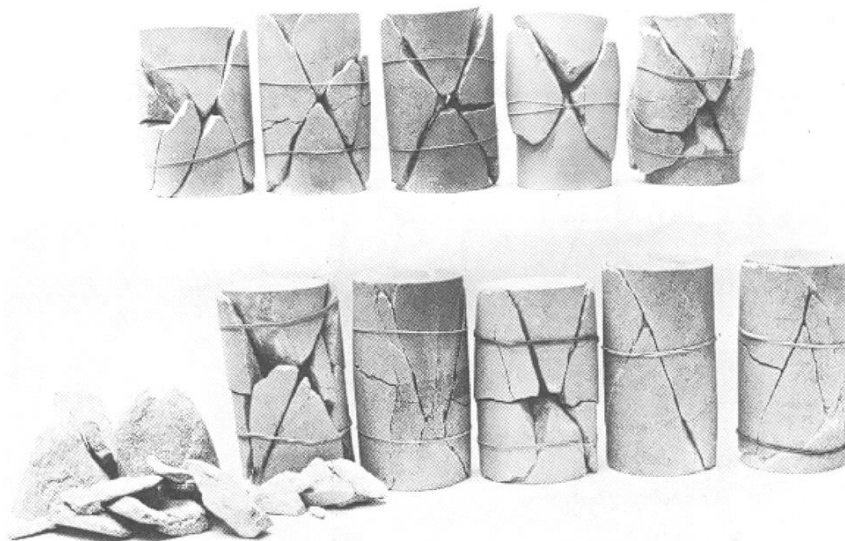


**Figure 3.2:** Some examples of brittle failure in Portland stone cores tested with confinement between 0 and 28 MPa (Farmer, 1983).

However, Mogui (1966) investigated that the failure mode in triaxial compression test can vary from brittle to ductile, depending on the confining pressures. Mogui (1966) concluded that majority of rocks could be expressed by the ratio:

$$\sigma_1 = 3.4 \sigma_3 \quad (3.1)$$

where  $\sigma_3$  is the minor principal stress (confining pressure) and  $\sigma_1$  is major principal stress. There would be a brittle rupture when this happens for values of  $\sigma_1$  lower than 3.4 times the confinement pressure and ductile behaviour in the opposite case.

Additionally, Mogui (1966) indicated that typically the confinement pressure necessary for transition of brittle behaviour to ductile is associated to the rock strength.

Based on the conclusions of Mogui (1966), Karzulovic (2006b) suggested that considering the magnitudes reached by main stress in caving mining at El Teniente mine; it can be conclude that primary rock at El Teniente shows brittle behaviour for the range of stresses with practical interest. Also Karzulovic (2006b) pointed out that in the case of a collapse the behaviour of the rock mass is mostly ductile, but this is because the rock is already damaged and fractured (the start of the collapse usually happens as cracking corresponding to brittle behaviour).

The brittle rupture mechanism was also studied by Waversik & Fairhurst (1970), who obtained complex load-deformation curves for different rock types (see Figure 3.3) and observed that the post-peak behaviour of the rock could be divided in two classes, as illustrated in the schematic in Figure 3.4:

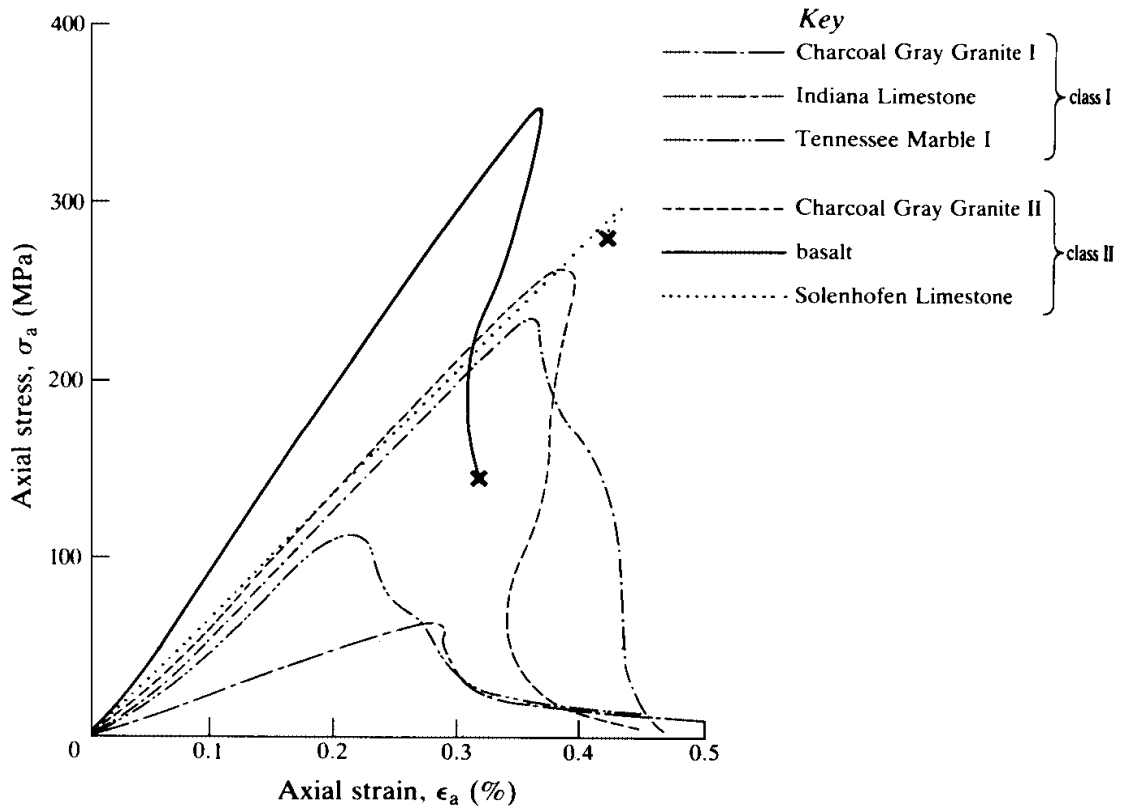


Figure 3.3: Uniaxial stress-strain curves for six rocks (Waversik & Fairhurst, 1970)

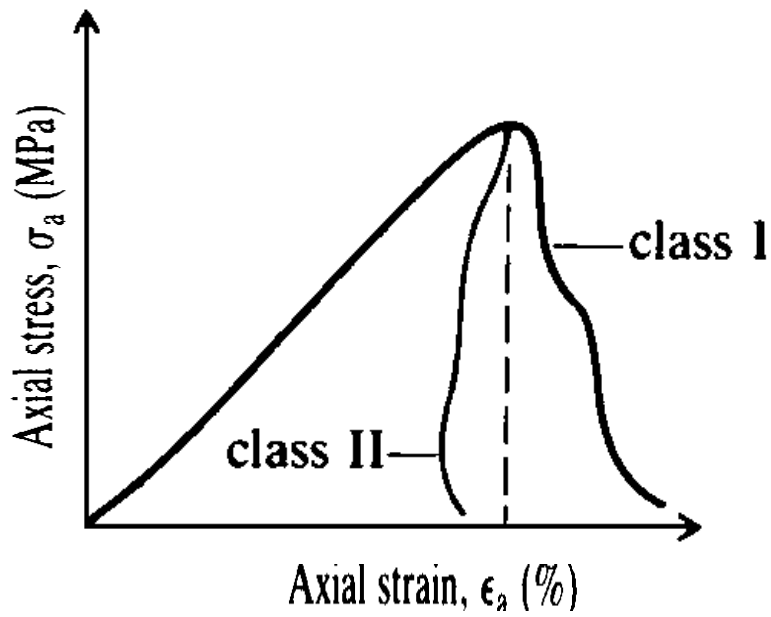


Figure 3.4: Two classes of stress-strain behavior observed in uniaxial compression tests (Waversik & Fairhurst, 1970)

For class I behavior, fracture propagation is stable in the sense that work must be done on the specimen for each incremental decrease in load-carrying ability. For class II behavior, the fracture process is unstable or self-sustaining; to control fracture, energy must be extracted from the material.

The experiments of Wawersik and Fairhurst (1970), and of subsequent researchers, indicate that, in uniaxial compression, two different modes of fracture may occur:

- (a) Local 'tensile' fracture predominantly parallel to the applied stress;
- (b) Local and macroscopic shear fracture (faulting).

The relative predominance of these two types of fracture depends on the strength, anisotropy, brittleness and grain size of the crystalline aggregates.

In very heterogeneous rocks, sub-axial fracturing is often the only fracture mechanism associated with the peaks of the  $\sigma - \epsilon$  curves for both class I and class II behavior. In such rocks, shear fractures develop at the boundaries and then in the interiors of specimens, well beyond the peak. This observation is at variance with the traditional view that through-going shear fracture occurs at the peak. Generally, these shear fractures, observed in 'uncontrolled' tests, are associated with sudden unloading in a soft testing machine.

On the other hand, and relating the behaviour with class I proposed by Wawersik and Fairhurst (1970), Aydan et al. (1993) suggested that many experiments have demonstrated that macroscopic stress-strain curves of rocks tested are strongly related to the internal status of the species. Aydan et al. (1993) established that hypothetically it is possible to distinguish 5 different specimen statuses during a full test. Stress-strain curves of rocks and soil obtained from uniaxial and triaxial tests for low levels of confinement pressure (i.e.  $\sigma_3/\sigma_c \leq 0.1$ ) are modelled and several deformation levels were defined as shown in Figure 3.5.

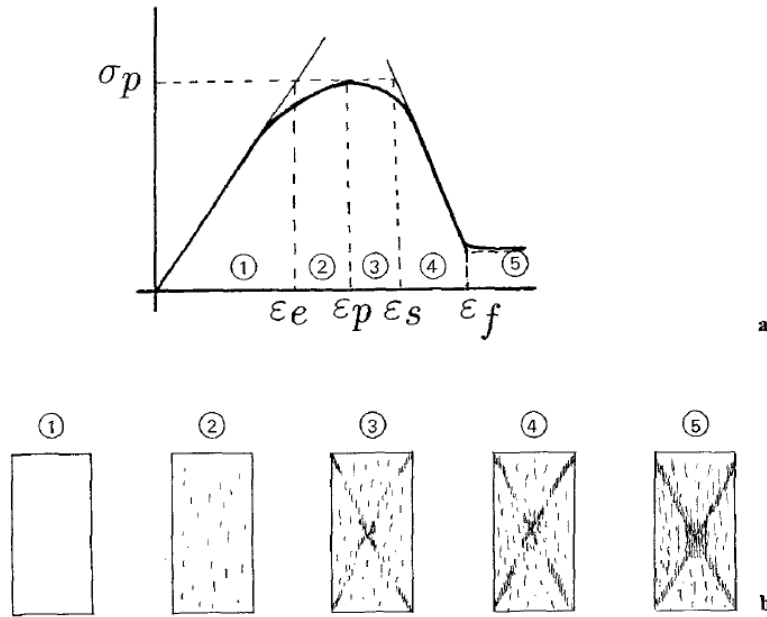


**Figure 3.5:** Idealized stress-strain curves and associated states for squeezing rocks.

These five states are characterized as:

- 1) Elastic state: Rock behaves almost linearly and no-cracking is visible.
- 2) Hardening state: Microcracking starts to occur and the orientations of microcracks generally coincide with the maximum loading direction.
- 3) Yielding state: After exceeding the peak of the stress-strain curve, micro-cracks tend to coalesce to initiate macro-cracks.
- 4) Weakening state: Initiated macro-cracks grow and align in the most critical orientations.
- 5) Flowing state: Macro-cracks along the most critical orientations completely coalesce and constitute sliding planes or bands, and fractured material flows along these planes.

The primary intact rock of El Teniente mine is characterized as heterogeneous as it presents sealed veinlets in a stockwork kind of arrangement, as illustrated in example of Figure 3.6 and can also present clasts (e.g. igneous breccias, hydrothermal breccias, etc.). These veinlets are sealed with infill with strength that varies from very high (e.g. quartz) to low (e.g. molybdenite); however, moderate-high to high strength infill are predominant (Karzulovic, 2006b).

Although the primary intact rock of El Teniente mine presents a characterization different from other rocks studied commonly in literature, we can consider the behaviour observed in similar rocks: hard ones and brittle rupture ones, especially regarding the observations made since the early 90's in granite Lac du Bonnet, in Canada. Martin (1997) established that for the range of confinement pressures usually experienced in primary rock mining, hard rocks and brittle rocks show strong softening or post-peak strength loss. This is due to the development of ruptures caused by “global”

cuts at core scale, which occur once the stress of damage due to fracturing is exceeded,  $\sigma_{cd}$ , as illustrated in example of Figure 3.7.



**Figure 3.6:** Longitudinal cut of core in primary rock CMET, showing the presence of sealed veinlets in a stockwork type of arrangement, the diameter of the core is 6". (from Karzoluvc, 2006b).

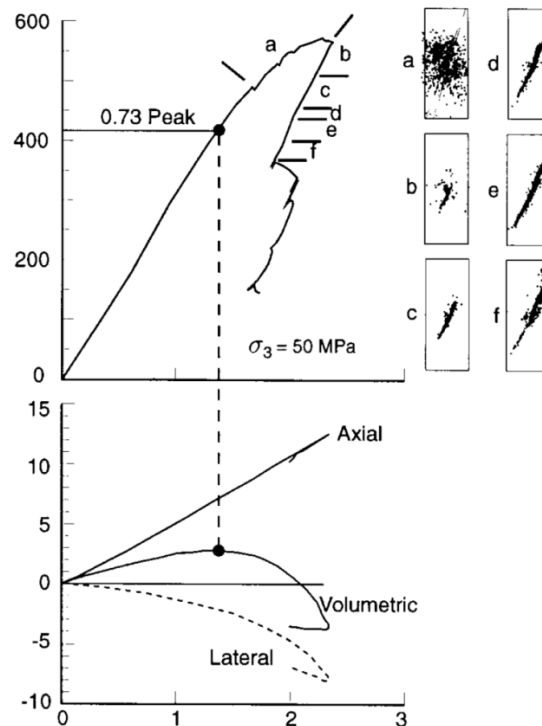


**Figure 3.7:** Development of a rupture plane in a Lac du Bonnet granite core. Schematics (a) to (f) show the position of the acoustic emission events in different stages of the test and indicate clearly than when exceeding  $\sigma_{cd}$  a "global" plane of rupture starts forming (Martin, 1997).

To complement the characterization of primary intact rock associated to the brittle rupture behaviour, based on test with species of Lac du Bonnett granite, Martin and Chandler (1994) presented the following interpretation:

- Cohesion starts decreasing once the extension of cracks starts increasing, meaning once the axial stress exceeds value  $\sigma_{cd}$ .
- As the core still can take an increase of axial stress (peak strength  $\sigma_c$  has not been reached), this means that concurrently with decrease of cohesion there must be an increase in friction.
- As deformation continues increasing more friction is mobilized, until reaching the peak strength of rock,  $\sigma_c$ , for axial deformation  $\epsilon_{peak}$ .
- As deformation of the core continues increasing the “interlocking” of rock elements limited by cracks starts decreasing, so the magnitude of the “total” friction angle also starts decreasing.
- For deformations large enough it may be assumed that the “interlocking” component would be null or very small and the “total” friction angle would tend to “basic” or “residual” friction angle.

This interpretation and conclusions were in agreement with the presentation by Diederichs (2003), who defined the evolution of damage due to cracking in a rock core as illustrated in Figure 3.8 based on “numerical experiments” where he models the rock as a set of cemented discs, using the PFC software (Itasca, 1995).

Diederichs (2003) indicated that after the start of cracking there is a uniform cracking period but without interaction between cracks (see Figure 3.8) and that the start of interaction between cracks defines really the start of “true damage” or deviation from the stress-strain linear behaviour.

However, Villaescusa et al. (2009) demonstrated based on a number of laboratory testing experiments conducted under triaxial conditions that the brittle intact rock response is different to the modelling by Diederichs (2003). In the Villaescusa et al. (2009) experiments, all specimens were cyclically loaded to determine the in situ stress and also to study the fracture process in order to identify any precursory characteristic for detecting the final stages of failure. A high speed acoustic emission (AE) monitoring system was used to record the maximum amplitude and waveform for the AE signals. The detailed damaging process as stress was increased was determined by monitoring the complete spatial-temporal distribution of micro-cracking events. The results showed that fine-grained brittle rock having a strong foliation structure, the cracking activity was very low and no significant dilatancy was observed prior to final failure (See Figure 3.9). As one of the main conclusion, the mechanism of ‘strain-softening’ in brittle rocks was identified through the migration of AE clustering along pre-existing geological features identified by short term fluctuation on b-value and AE rate.

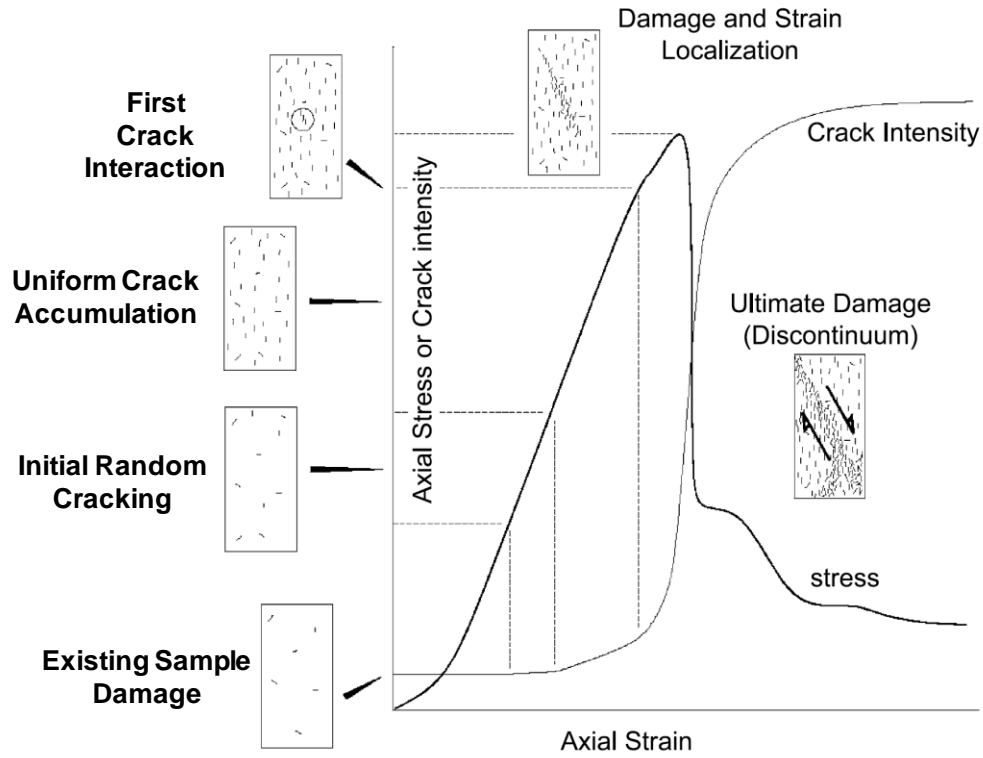


**Figure 3.8:** Schematic illustrating the evolution of cracking related damage in a rock core, according to results of “numerical experiments” with a model of cemented discs and using the PFC software (Diederichs, 2003).

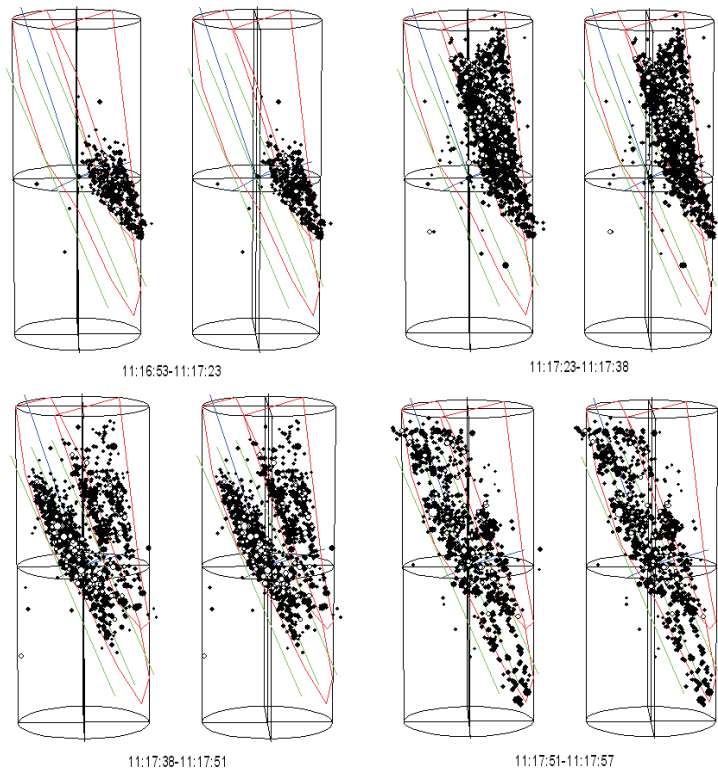


**Figure 3.9:** Fracture progression and related AE hypocenter distributions. Foliation and eventual failure plane are also shown (Villaescusa et al., 2009).

Brittle rock behaviour suggests that the “typical” failure envelope, for example according to non-linear Hoek-Brown criterion, only represents the peak strength in short term condition. This does not necessarily correspond to long term strength. Therefore, it does not provide information about the condition in which fracturing will start (which could define the long-term strength according to Martin & Chandler, 1994). This is illustrated in Figure 3.10 for the case of Lac du Bonnett granite.

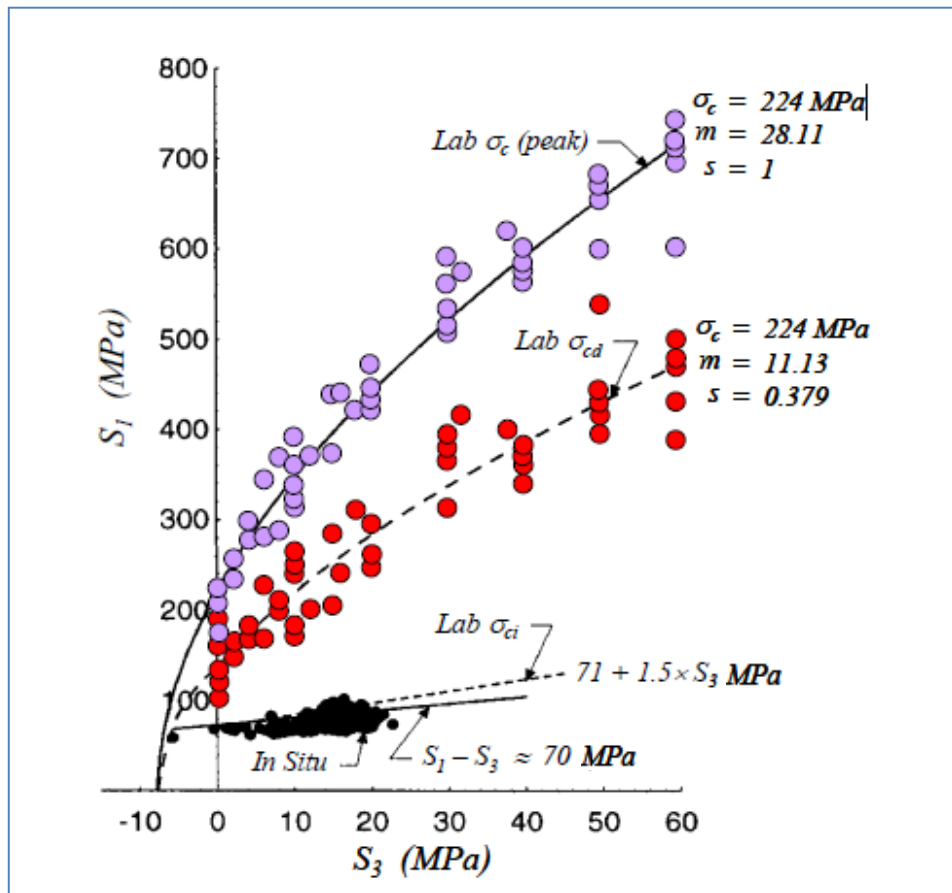


**Figure 3.10:** Hoek-Brown envelopes for peak strength (short term, purple dots) and stress of fracturing damage start (long term according to recommendations from Martin & Chandler, 1994, red dots). This figure also shows the straight lines defining the start condition of fracturing in the laboratory (dotted line) and in situ (thick line) for Lac du Bonnett granite (Martín, 1997).

### 3.2.3 Behavior for Primary Rock Mass

#### *General Considerations*

Brady and Brown (2004) suggested that the determination of the global mechanical properties of a large mass of discontinuous in situ rock remains one of the most difficult problems in the field of rock mechanics. Stress-strain properties are required for use in the determination of the displacements induced around mine excavations also according with Brady and Brown (2004).

Because of the difficulty of determining the overall strength of a rock mass by measurement, empirical approaches are generally used. An attempt to allow for the influence of rock quality on rock mass strength was made by Bieniawski (1976) who assigned Coulomb shear strength parameters,  $c$  and  $\phi$ , to the various rock mass classes in his geomechanics classification. Correlations have also been proposed between other rock mass classification schemes and rock mass strengths (e.g. Barton, 2002, Laubscher, 1990, Laubscher and Jakubec, 2001).

The most completely developed of these empirical approaches is that introduced by Hoek and Brown (1980). Brady and Brown (2004) suggested that the Hoek-Brown empirical rock mass strength criterion was soon adopted by rock mechanics practitioners, and sometimes used for purposes for which it was not originally intended and which lay outside the limits of the data and methods used in its derivation. Because of this, Hoek and Brown (1997) consolidated the changes made to that time and gave a number of worked examples to illustrate the application of the criterion in practice. A further update was given by Hoek et al. (2002).

In effective stress terms, the generalized Hoek-Brown peak strength criterion for jointed rock masses is given by:

$$\sigma_1 = \sigma_3 + \sigma_c \left( m_b \frac{\sigma_3}{\sigma_c} + s \right)^a \quad (3.1)$$

where:

$$m_b = m_i \exp \left( \frac{GSI-100}{28-14D} \right) \quad (3.2)$$

$$s = \exp \left( \frac{GSI-100}{9-3D} \right) \quad (3.3)$$

$$a = \frac{1}{2} + \frac{1}{6} \left[ \exp \left( \frac{-GSI}{15} \right) - \exp \left( \frac{-20}{3} \right) \right] \quad (3.4)$$

The influence of blast damage on the near surface rock mass properties has been taken into account in the 2002 version of the Hoek-Brown criterion (Hoek et al., 2002) where  $m_b$  is the reduced value of the material constant  $m_i$  for the rock mass, and  $s$  and  $a$  are parameters which depend on the characteristics or quality of the rock mass. The values of  $m_b$  and  $s$  are related to the GSI for the rock mass.  $D$  is a factor which depends on the degree to which the rock mass has been disturbed by blasting or stress relaxation.  $D$  varies from 0 for undisturbed in situ rock masses to 1.0 for very disturbed rock masses. For good quality blasting, it might be expected that  $D \approx 0.7$ .

Specifically concerning the primary rockmass at El Teniente mine, Karzulovic (2006b) highlighted the fact that the rock mass presents few or no “open” structure. Hence, the traditional methods of scaling up the rock strength to define the strength of the mass results are less than sensible to allow differentiating in an adequate manner the different types of primary ore mass which appear at El Teniente.

In a complementary manner Karzulovic (2006b) applied this methodology (see Hoek et al., 2002) for strength estimation to the different primary rock masses representative of El Teniente mine (see Table 3.1). So in the case of massive rock masses GSI is typically higher than 75, and in the case of primary rock mass in El Teniente the mean values range from 80 to 85. On the other hand, Karzulovic (2006b) estimated that blasting damage affects typically no more than 0.5 m in the labour and evidently is not present in caving propagation, so as a first approximation, can be assumed that  $D \approx 0$ . This gives:

$$m_b = 0.49 \text{ to } 0.59 \quad m_i \approx 0.54 \quad m_i$$

$$s = 0.11 \text{ to } 0.19 \approx 0.15$$

$$a \approx 0.5$$

and primary rock mass strength is given by

$$\sigma_1 = \sigma_3 + \sigma_c \left( 0.54 \frac{\sigma_3}{\sigma_c} + 0.15 \right)^{0.5} \quad (3.5)$$

Karzulovic (2006b) used the values of  $\sigma_c$  and  $m_i$  mentioned for the different lithology units present in El Teniente (Celhay et al, 2005) and calculated the strength for confinement conditions equal to 5 MPa (in the surroundings of underground caves) and 30 MPa (inside the rock mass), as shown in Table 3.1.

**Table 3.1:** Strength of the primary rock masses at El Teniente according to a traditional assessment using the Hoek-Brown method (Modified by Karzulovic, 2006b).

Lithology unit	$\sigma_c$ (MPa)	$m_i$	$\sigma_1$ (MPa)	
			$\sigma_3 = 5$ MPa	$\sigma_3 = 30$ MPa
Gabro	160	6.8	87	177
CMET	159	5.7	84	166
Diorite Porphyry	182	11.4	108	226
Dacite Porphyry	150	33.2	135	320
Latite Porphyry	105	13.3	79	186
Igneous Breccia of CMET	148	5.3	79	156

According to Karzulovic (2006b) these results show that little differentiation is achieved among the different types of primary rockmass when applying the Hoek-Brown method. He suggested exactly the same when evaluating the little differentiation between the different deformability modules for the types of rock masses in El Teniente.

Brady and Brown (2004) recognized that the Hoek-Brown rock mass strength criterion is a short-term peak strength criterion and not a crack initiation or long-term strength criterion. Furthermore, it applies only to sensibly isotropic rock masses and it should not be used when failure is governed by a single discontinuity or by a small number of discontinuities.

*Observed Behavior*

The practical experience in hard rock mining (e.g. Hoek & Brown, 1980) indicated that it is possible to estimate the damage in the surroundings of an underground excavation considering the ratio  $\sigma_1/\sigma_c$ , where  $\sigma_1$  is the main major stress in situ (i.e. in pre-mining condition) and  $\sigma_c$  is the uniaxial compressive strength of the rock. If  $\sigma_1/\sigma_c \leq 0.1$  the rock mass behaves elastically and no damages are produced in the surroundings of the excavation. When  $\sigma_1/\sigma_c \approx 0.2$  some degree of cracking is produced in the surrounding of the excavation, reducing the strength of the rock mass in the damaged zone. When  $\sigma_1/\sigma_c \approx 0.3$  the rock mass in the surroundings of the excavation will suffer enough damage to produce slabbing and spalling and underground excavation will reach an over-excavated geometry but stable (unless later mining induces other changes in the stress field), as seen in the example of Figure 3.11. When  $\sigma_1/\sigma_c > 0.5$  the damage process is propagated significantly increasing the extension of the damaged zone, which is observed in deep excavations.

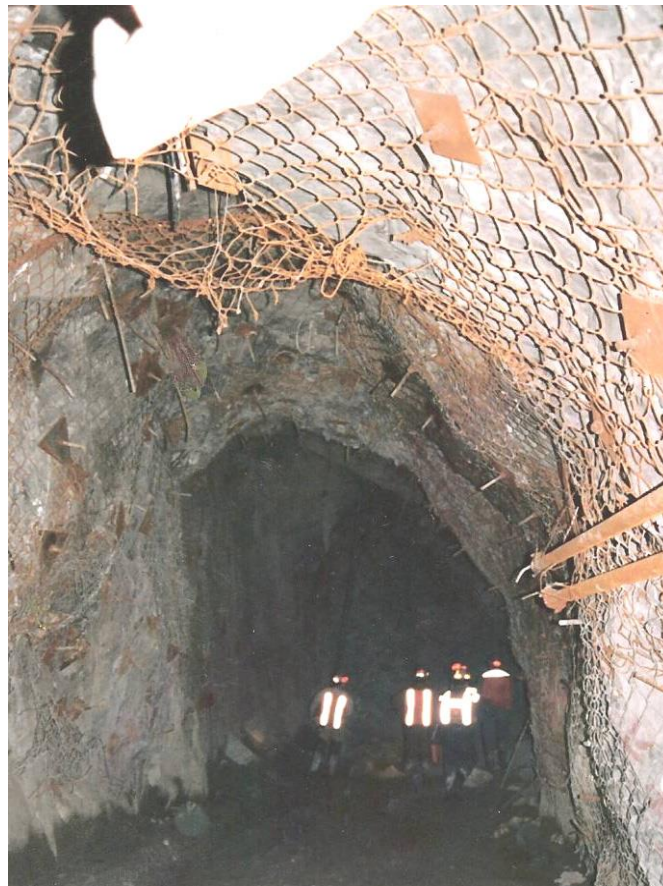


**Figure 3.11:** Over-excavation in the primary rock mass at El Teniente (CMET lithology), Production Level, Sector Ten Sub 6 ( $\sigma_1/\sigma_c \approx 0.3$ ), (taken from Karzulovic, 2006).

Besides the behaviour observed in the primary rock mass of El Teniente it is convenient to consider also the behaviour observed in hard rock massive masses, especially regarding observations made since mid 90's in Lac du Bonnet granite in Canada.

Field observations indicate that independent from the geometry and final shape of the tunnel, over-excavation tends to form a notch, as seen in the examples in Figure 3.12 (obviously this shape can be affected partially by the presence of veinlets with soft infill in the rock mass, in the case of the primary mafic complex in El Teniente). This over-excavation is due to the brittle rupture of the rock mass and expressing the Hoek-Brown criterion we obtain the following failure condition:

$$\sigma_1 - \sigma_2 = \sqrt{s \times \sigma_c^2} \quad (3.6)$$

According to this Martin et al (1999) suggested defining the strength of the rock mass for a brittle rupture condition considering the following parameters by Hoek-Brown:  $m = 0$  and  $s = 0.11$  (this is equivalent to assuming that strength is purely frictional). It is important to indicate that this only defines the start of damage due to fracturing and does not determine the extension this damage could reach due to the evolution of the slabbing process and spalling previously described.

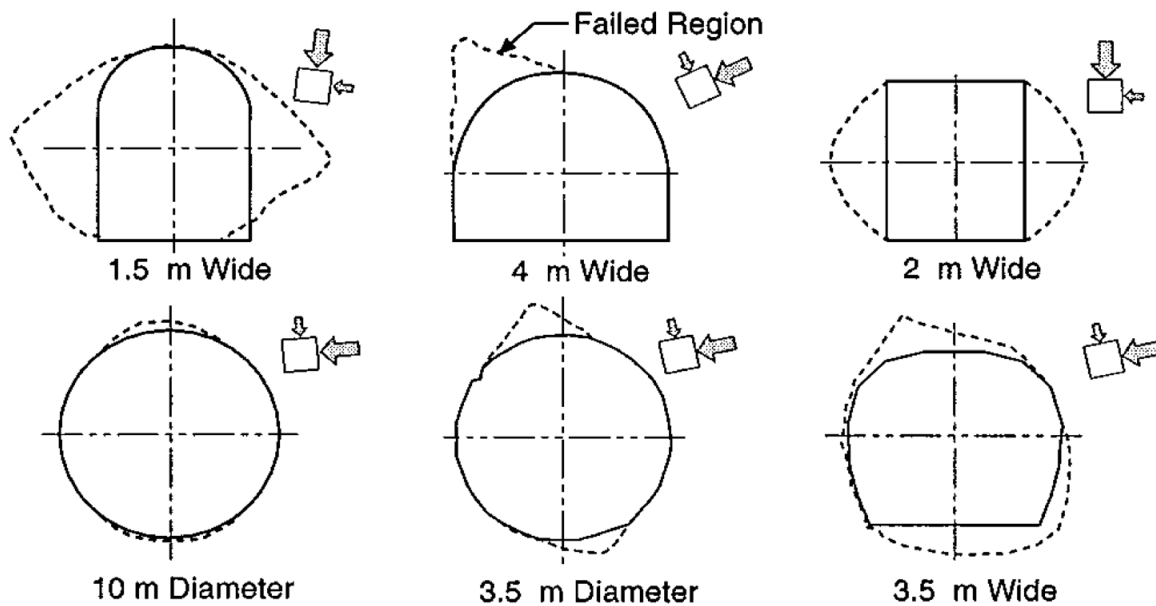


**Figure 3.12:** Over excavation observed in tunnels with different shapes and size excavated in hard rock. In each case shows the orientation of main secondary stresses in the plane of transversal section of tunnel (Martin et al, 1999).

Everitt and Latjai (2004) studied the influence of geological characteristics of the rock mass on the over excavation observed in experimental tunnels excavated in Lac du Bonnet granite. This affects the genesis and propagation of fractures induced by development of an underground excavation in a massive rock mass. Foliation planes and other pre-existing discontinuities act as weakness planes, in

one or more directions, generating anisotropy in the strength of the rock mass and influencing the development and propagation of over excavation.

In this sense, Karzulovic (2006b) suggested that in the case of the rock mass in El Teniente mine, the potential effect of changes in the rock factory over the behaviour of the rock mass can result especially significant in igneous breccias and hydrothermal breccias and similar to what was observed in the Lac du Bonnet granite in the dacite and diorite porphyry.

Furthermore, the effect of pre-existing discontinuities would be especially significant in the case of rocks in the mafic complex El Teniente (CMET), which present a stockwork of veinlets with infill that in many cases have less strength than the rock (see Figure 3.13).



**Figure 3.13:** Pre-existing discontinuities at the primary ore mass of El Teniente (CMET), Undercut Level, Esmeralda operation.

Diederichs (2002) analysed the effect of accumulation of induced damage on massive hard rock masses where, due to unconfinement produced in the surroundings of underground excavations, compressive rupture occurs by extension fractures. This causes slabbing and spalling commonly

observed in excavations in this type of rock masses. Diederichs (2002), quantified the “non uniformity” as the percentage of the cave surroundings with tensile zones for different values of ratio  $\sigma_1/\sigma_3$ .

Diederichs (2002) developed “limits” for the zone where the rock mass fails due to spalling. Such limits are important because they define a “rational connection” between the upper envelope of the rock mass strength, defined by the interaction among cracks and the inferior envelope, defined by the beginning of the cracking. Figure 3.14 summarizes this concept, and the same has been applied to URL tunnels, in the massive mass of Lac du Bonnet granite, and in the case of the Brunswick mine pillars in Canada (Diederichs et al, 2002).

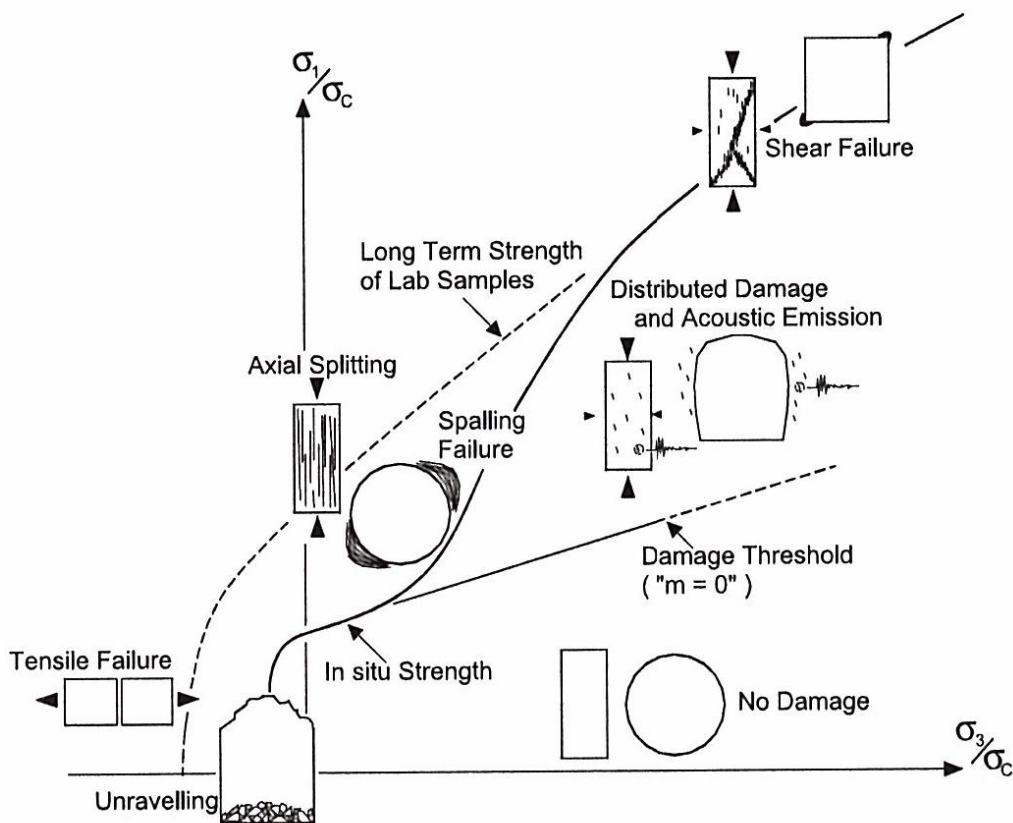


**Figure 3.14:** Schematic of failure envelope for brittle failure, showing four zones of distinct rock mass failure mechanism: no damage, shear failure, spalling and unraveling (Diederichs, 2002).

Based on considerations of fracture mechanics, Cho et al (2002) suggested that the potential excavation spalling is defined by the relation  $\sigma_3/\sigma_1 = 0.05$ , as shown on Figure 3.15. Martin and Christiansson (2002) applied similar criterion to hard rock excavations in deposits of nuclear waste in Sweden (see Figure 3.16), and show that failure modes correspond to instabilities with structural control, due to the relation of the rock mass, slabbing and spalling.

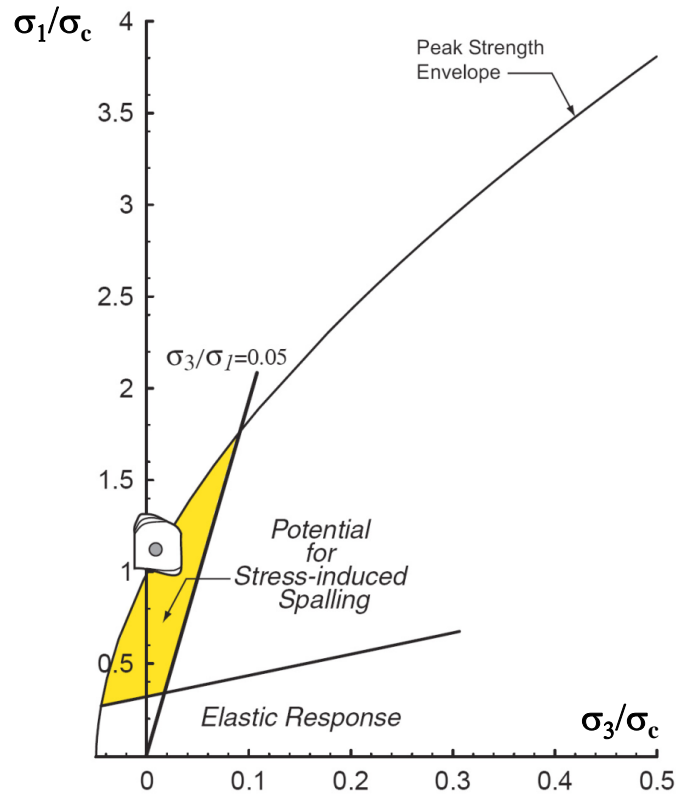


**Figure 3.15:** Zone of potential spalling of the rock mass by the effect of the stress induced around underground excavations in hard rock (Cho et al, 2002).

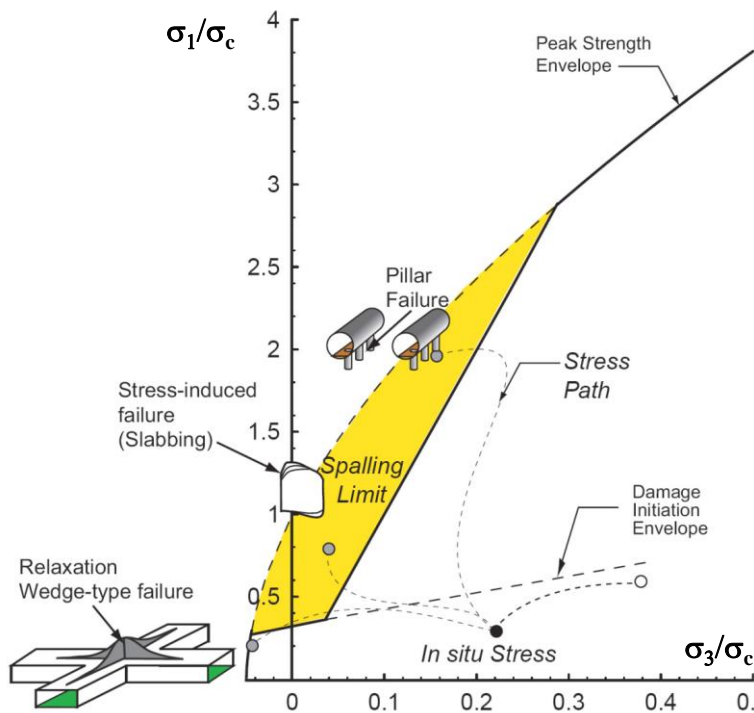


**Figure 3.16:** Stress path and failure modes of the rock mass, considered in Sweden for underground deposits of radioactive waste excavated in hard rock (Martin & Christiansson, 2002).

Finally, most published work suggested that Hoek-Brown criterion would not be applicable to the case of rock masses in hard rock, meaning when  $GSI > 75$ , because it does not incorporate in an appropriate manner the brittle failure condition. On the other hand, importance of the effect of low confinement on this type of brittle rupture of the rock mass has been mentioned by several writers including: Stacey and Page (1986), Wagner (1987), Castro et al (1996), Grimstad and Bhasin (1997) and Diederichs (1999). All of them have shown based on back analyses that fracture induced damage in hard rock tunnels begins when the tangent stress to the tunnel is 0.3 to 0.5 times the strength in uniaxial compression of the rock and that failure condition is almost independent of confinement.

Especially Karzulovic (2006b) suggested that induced damage in rock mass by development of underground excavations depends on the stress trajectory, being the field condition typically more unfavourable than the condition of lab tests. In fact, presence of a free face defined by the contour of the cavity facilitates propagation of cracks, as there is no restriction to dilatance. Damage to the rock mass can get worse by asymmetry of the stress field compared to the orientation of excavation, by rotation of stresses (as is common in underground mine), by presence of structures (as the case of stockwork in the CMET unit in El Teniente) and for heterogeneities of the rock mass (which could be the case of igneous breccias and primary hydrothermal breccias in El Teniente).

### **3.3 GEOTECHNICAL HAZARDS - COLLAPSE IN CAVING OPERATIONS**

Brown (2003) suggested that the planning and operation of panel caving mines involve a number of major risks or hazards. Caving methods involve significant amounts of capital and investment in infrastructure development before extraction can begin. Therefore, caving methods are inflexible so that, if a mistake is made, it is not easy to change or fix a problem with the mining method.

Caving operations also generate a number of specific issues which constitute risks or hazards that must be addressed in mine planning and operation (Heslop, 2000). The uncontrolled large scale ground collapses emphasized because they are a major possible cause of air blasts, and could lead to losses of life and production risk in any caving operation.

### 3.3.1 Terminology

Globally, mining the rock mass is defined as fracturing or disintegration of the rock mass resulting in loss of bearing capacity. When failure is accompanied by a substantial discontinuous displacement of rock, it is referred to as rock mass collapse (Szwedzicki, 2001).

Part of the literature associated to the theme of geomechanics for cave mining (Brown, 2003) proposed a simplified classification of collapses having dimensions, without being referred to or proposing models for mechanisms. In particular it presents the three following types of collapses:

- Type 1: Uncontrolled collapse of crown pillar or sill pillar to surface or to a sector already mined (large size slab between the cave and field surface or sector already mined); see Figure 3.17.

Brown (2003) suggested that the major collapse described as Type 1, involving collapse of the entire crown pillar, is the most dramatic of the major collapses to be considered. They occur when the height of the crown pillar reduces to such an extent that failure can happen through different mechanism. This may include progressive unraveling, chimneying, buckling or snap through instability and shear failure on vertical boundaries of the crown pillar.

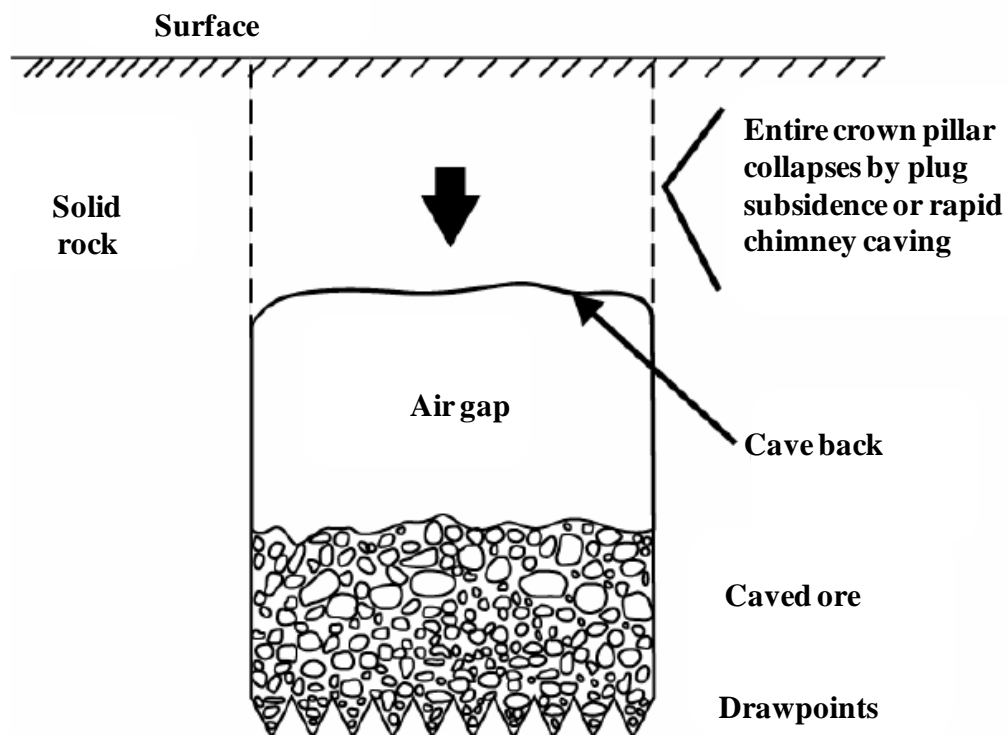


**Figure 3.17:** Major Collapse, Type 1, involving collapse of crown pillar (Brown, 2003).

- Type 2: Uncontrolled failure of large blocks or rock volumes from the undercutting back or more usually, from cave back, see Figure 3.18.

Brown (2003) stated that the second type occurs when a block or a large volume of rock is isolated by the surface of the undercut or caveback and discontinuities. It is caused by the induced stresses, and falls or slides under gravity influence.

Brown (2003) also suggested that this collapses are more likely when the back of the cave is convex downwards that when it is concave.

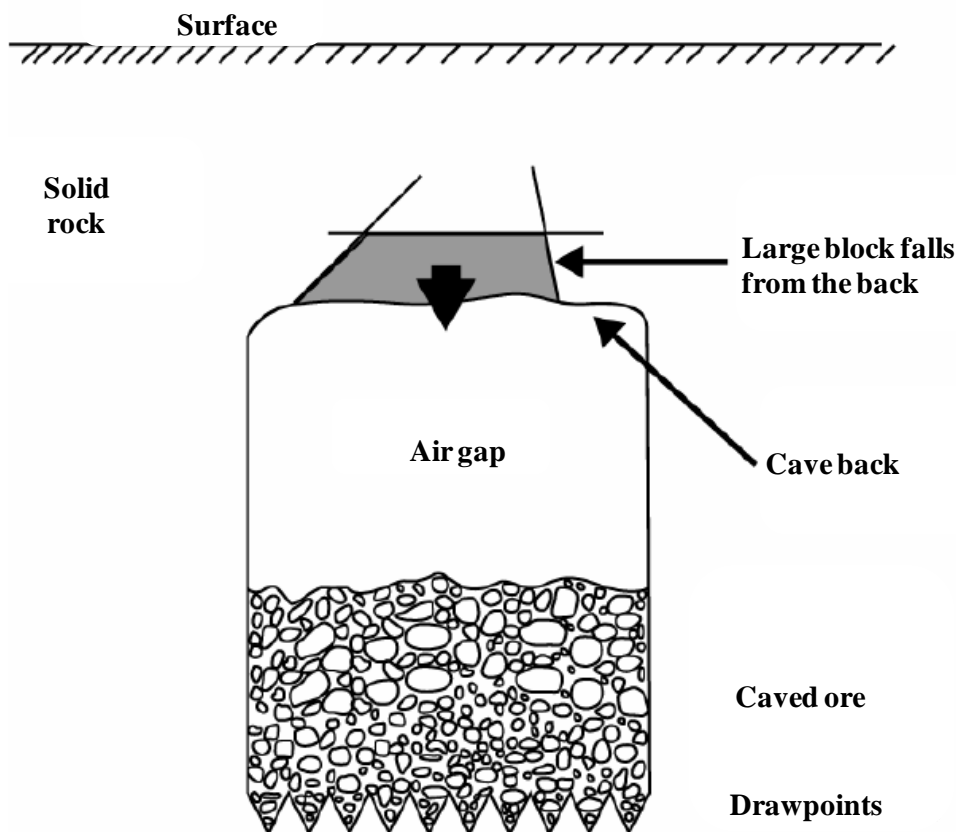


**Figure 3.18:** Major Collapse, Type 2, involving falls or large blocks from the cave back (Brown, 2003).

- Type 3: Collapse, progressive or otherwise, of excavations at or above the extraction level (production level); see Figure 3.19.

Brown (2003) highlighted that the third type of collapses are stress-induced, however they may be exacerbated by faults or other major and persistent discontinuities present. Collapses of this type have been experienced in many caving operations (Cavieres, 1995; Krstulovic, 1997; Dunlop and Pereira, 1998; Diaz and Tobar, 2000; Flores and Karzulovic, 2002; Hannweg et al., 2004; Karzulovic, 2003b; Rojas et al., 2005; Karzulovic, 2006a; Villegas,

2008; Dunlop et al., 2010), usually ahead of the cave as a result of the stress abutment concentrated ahead of the undercut.

According with Diaz and Tobar (2000) and Diaz et al. (2009) a major collapse of Type 3, is a phenomenon that involves failure of the rock mass in a significant area of the undercut level and/or production level, with partial or total closing of excavations, due to excessive deformation or occurrence, predominant or not, of instabilities with structural control. This phenomena can happen and develop a gradual velocity (slow – months to years) or very fast (days).

As shown in Figure 3.19, they involve failure of the pillars left on and above the extraction level.

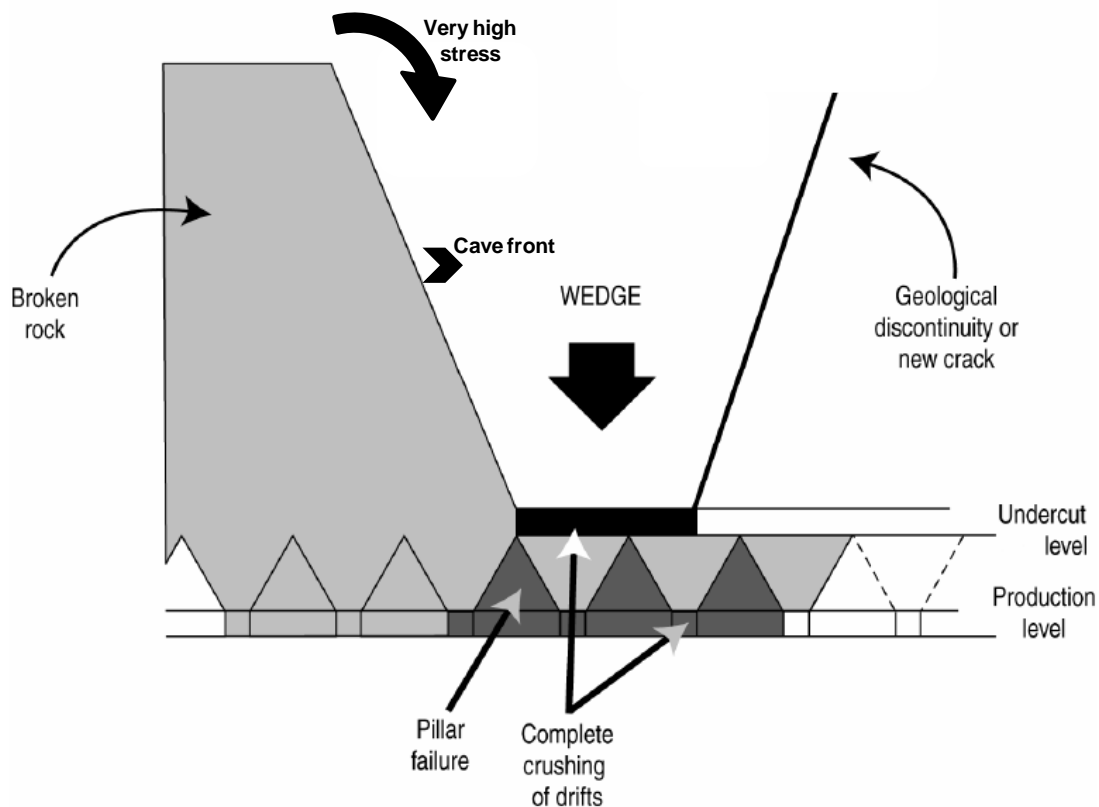


**Figure 3.19:** Major Collapse, Type 3, involving failures on and around the extraction level (Brown, 2003).

The most important aspect is that the event must cause damage to an operation. In extreme cases, collapse could result in loss of life, loss of production from a panel, or extensive damage to infrastructure. In less extreme cases, it could cause expensive delays in production or involve the need for remedial work.

According to Brady and Brown (2004), the natural discontinuities in a rock mass have a dominant effect on the post-peak deformation properties of the medium, and may control the potential for global mine instability. A collapse may have total, partial or no structural control and may occur at a range of speeds from very gradual to very rapid.

Additionally, Flores et al. (2004) defined the collapses as a relatively slow failure of undercut level and or extraction level, which triggers crown pillar failure and in the worst case drift closure.

Finally, Brown (2003) suggested that just as the effects of these major collapses are many and varied, so are the means of preventing them and ameliorating their effects. Generally, they can be mitigated by careful planning, design and operation of a mine.

### **3.3.2 Reviewing experienced collapses**

Karzulovic et al (1991) analyzed an example of a slow, structurally controlled collapse on the extraction level in Panel II operation Andina Division in CODELCO Chile. In this case, a large pyramidal key block was formed by geological structures and the cave front. The process of undercutting relieved the confining stresses, making the base of the block unstable. The unstable key block failed slowly, resulting in complete collapse of production and draw point drifts in the affected zone. The problem was back analyzed successful trough block theory (Goodman and Shi, 1985) and currently this theory is used by Andina mina to identify potentially unstable key blocks during the caving process.

Additionally, and based on the classification realized by Brown (2003) for different types of collapses, the massive collapse occurring as second type have usually produced air blasts. One example has been reported by Van As and Jeffrey (2000) at Northparkes E26 Mine, NSW, Australia. Where a massive air blast resulting from the collapse of the “crown pillar” into a large air voids when caving propagated into a weak leached zone led to the death of four men in late 1999. Furthermore, examples of this type are discussed by de Nicola and Fishwick (2000) and Ross and Van As (2005).

Szwedzicki (2001) reviewed documented cases of large-scale ground collapse in underground showing that geotechnical precursors to rock mass failure appear over time. Ten case studies of ground collapse on a large-scale were studied by Szwedzicki (2001), where the case of a block caving operation called San Manuel Mine was highlighted by a ground caving collapse marked by two general stages: a preliminary one of tensional fracturing together with gentle settlement of the ground surface followed by a final stage of sinkhole development. It took 24 months for ground to collapse after being undercut and ore draw commenced.

Unfortunately, Szwedzicki (2001) identified that geotechnical precursors have not always been recognized as warning of potential failures. Literature on geotechnical precursors is limited and geotechnical reports on rock mass failure are often confidential and not widely circulated.

Other different case that involved large-scale rock mass movement which caused major cracking and drift closure in the Koffietonte in Mine, South Africa, was reported by Hannweg et al.,(2004). The front cave was operated quit successfully until February 2003 when a major collapse occurred on the undercut level, and significant movement was recorded on an upper sub-level cave. Hannweg et al. (2004) suggested that the cause was uncertain, however a number of factors contributed to the sudden massive failure experienced, production constrains and requirements may have contributed to the failure of the cave front.

A bench marking for caving operations around the world was undertaken by Flores and Karzulovic (2002) where geotechnical hazards such as Collapse were included. The conclusion from the data on collapses analyzed by Flores and Karzulovic (2002) were mentioned in Section 2.5.2. The figure 3.20 shows a summary with the relative frequency of area affected by one collapse in caving operations and the figure 3.21 shows a relative frequency of main causes of collapses in caving operations.

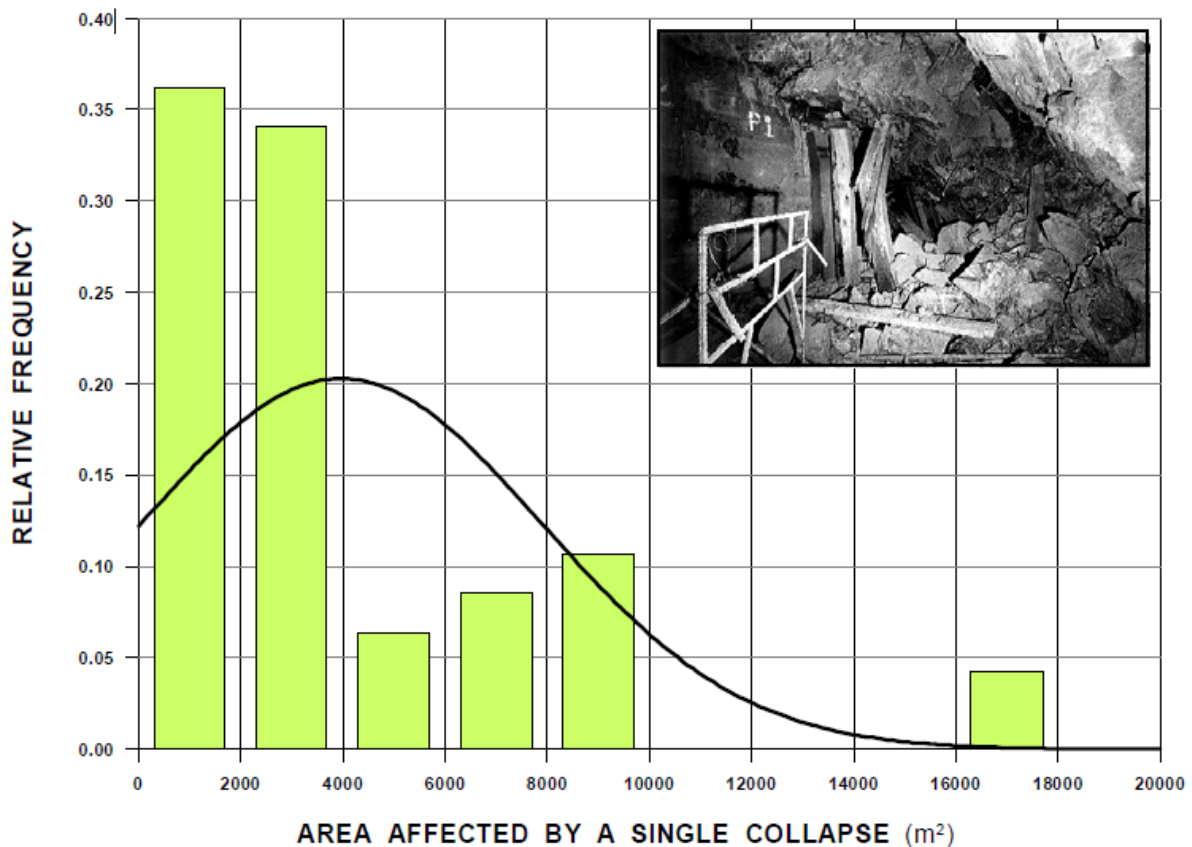


**Figure 3.20:** Relative frequency of area affected by one single collapse in caving operations (Flores and Karzulovic, 2002).

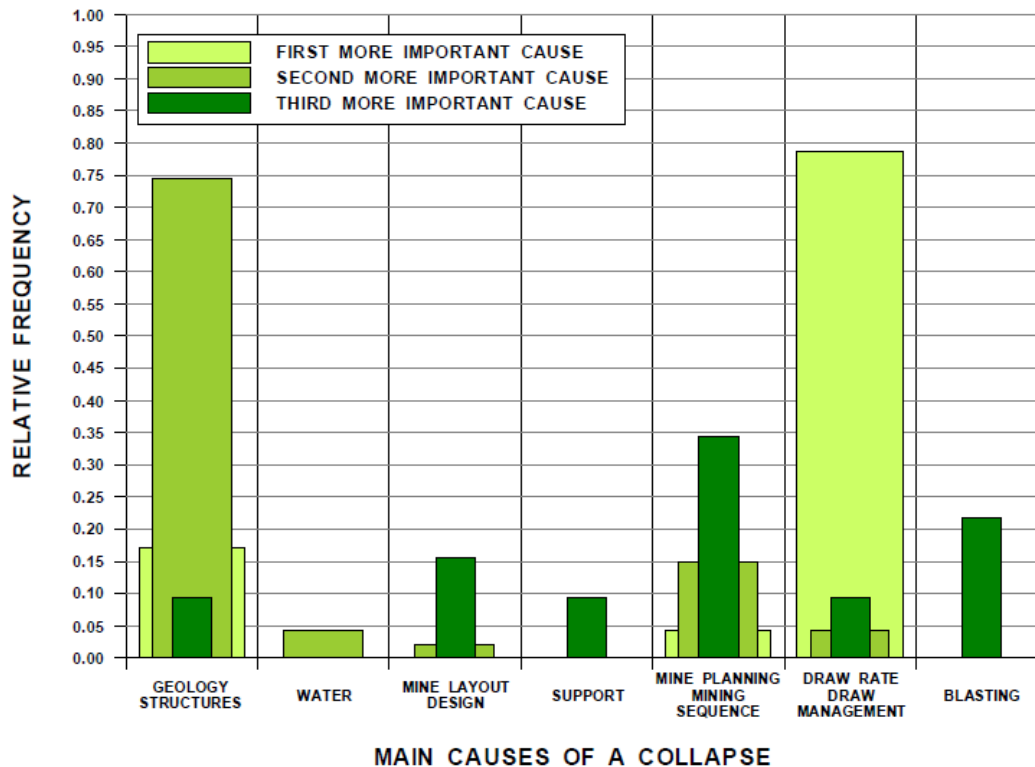


**Figure 3.21:** Relative frequency of different main causes of collapses in caving operations (Flores and Karzulovic, 2002).

Another bench marking of collapses associated to large caving operations in Chile was performed by Diaz et al. (2009). This study considered records by Pasten (1999), Flores and Karzulovic (2002) and Villegas (2008) amongst others. Based on review of all data, Diaz et al (2009) it concludes that:

- The collapse phenomenon affected different front widths (135 to 700 m) in different productive sectors, which present different geotechnical structural conditions.
- Sector Teniente 4 Sur of El Teniente mine, shows that the geotechnical event collapse has accompanied almost all the production life of the sector. This shows evidence that a panel caving method is capable of tackling and facing this type of instabilities within its schedule. Panel caving can provide high production rates (up to 50,000 tons per day) with an expected area affected by collapse could be up to 15% of the open area in the production sector.
- There have been collapses generated in areas affected between 650 and 32,245 m<sup>2</sup>, meaning, from irrelevant sizes (“negligible”) to significant dimensions (critical), with an average of 3,187 m<sup>2</sup>. These collapses have affected different sizes in production sectors with open areas between 24,000 and 98,000 m<sup>2</sup>.
- It is frequent to see the presence of ore passes in the damaged areas.

Regarding to the experienced collapses at the El Teniente Mine, Villegas (2008) reviewed all data information about collapses generated in the different operations at the El Teniente mine between 1986 a 2004, highlighting the following conclusions:

- There were 8 episodes of collapse located more than 70 meters behind the undercutting face. In those cases the draw percentage had exceeded 100% of block column extraction.
- 11 collapses occurred less than 50 meters from the undercutting face. In some cases, there was evidence of block mobilization with opening of structures in the undercut levels. Sometimes the cracks crossed more than two drifts.
- Two collapses occurred in front of the caving face, without undercutting of the sector.
- More than 60 % of collapses were located next to an old collapse.
- Approximately 45% of draw points collapsed had less than 10 meters of extracted column.

### **3.3.3 Reviewing collapse mechanism**

Other research projects have discussed different parameters that could induce a collapse of a large area. For instance, experience in South African mines has shown that undercutting is one of the most important aspects in cave mining. The undercutting process is the key for a successful cave mining operation. It is essential that the undercut is continuous and caving should not be advanced if there is a possibility of remnant pillars being present. This rule, which is often ignored owing to the problems of re-drilling holes, in difficult conditions results in pillars being left and the collapse of large areas and high ore losses.

Regarding the collapses experienced at the El Teniente Mine prior to 2000. A number of studies were conducted to understand the causes of this phenomenon (Cavieres, 1995; Krstulovic, 1997; Dunlop et al., 1998; Lorig and Gomez, 1998 and SRK, 1999) in order to apply actions to mitigate the observed damage. The following points are the main common conclusions from those studies regarding to the collapse causes (Villegas, 2008):

- Structural conditions and discontinuities. The presence of major faults.
- Excess of stresses around cave front.
- Operational mistakes.

According with the subsequent observations, preventive actions included strict draw control and increased draw within a collapsed areas to avoid creating a potential big structural wedge. In other cases, previous ore reserves losses associated to collapses were recovered through new production level located under the affected area. In those recovery sectors, the new extraction level is located approximately 15 m below the old collapsed extraction level. Most of the experiences of recovery

sector have achieved successful fulfillment production targets without geotechnical instability problem associated (Villegas, 2008).

Collapses of increased frequency continued to occur even after 2000. Esmeralda is one of the sectors that were affected more intensively by the phenomenon. According to Hustrulid (2004), the pre-undercutting system in the Esmeralda sector (a variant of panel caving) worked quite well until 2003 when a collapse on the production level was experienced. This required a series of remediation actions to be taken to isolate the area and to progress the cave once again. Investigations revealed that there were a number of different factors which could have contributed, related to the design, geology, planning, and coordination of development and construction. In addition, internal reports from El Teniente Mine, specifically Rojas, et al. (2005), have described the main parameters that could lead a collapse in Esmeralda sector such as: geologic conditions, deficient blasting, and global geometry of the cave front and the extraction angle (cave back geometry). Short term factors are related to operation and undercutting practices; the medium term factors deal with design singularities; and long term factors are the effects of geologic conditions, such as structures and induced stress.

In recent years, many studies have been conducted to characterize the observed collapses and their causes. Most of the research has analyzed the different mining parameters that could induce a collapse and also the actions to mitigate the effects. For instance, Fernandez (2008) suggested that the generation and propagation of a collapse process could mainly be associated with loads that were transmitted through remnant and abandoned pillars in the mining infrastructure. According to Araneda and Sougarret (2008) some lessons were learned from Esmeralda experience. Araneda and Sougarret (2008) discussed the relationship between the exploitation variant and the recovery of collapses, for instance Esmeralda used the panel caving with pre-undercut sequence with a reduce distance between the production and haulage levels. This configuration imposed difficulties in the recovery of collapses below the production level which had been a successful practice in other sectors of the mine as example Teniente 4 Sur Sector.

One of the latest studies carried out in order to identify the collapse mechanism for the last event at Esmeralda Sector in 2009 was developed by Van Sin Jan (2010). Based on the onsite observations and some simple numerical analysis, this study suggested an understanding model (Conceptual model) of pillar behavior as shown in Figure 3.22. In addition, different failure mechanisms were identified as acting during the different exploitation stages at Esmeralda sector.

Van Sin Jan (2010) also suggested a simple model in order to explain the local behavior of extraction drifts affected by intensive damage during collapse process. A summary scheme can be seen in Figure 3.23.

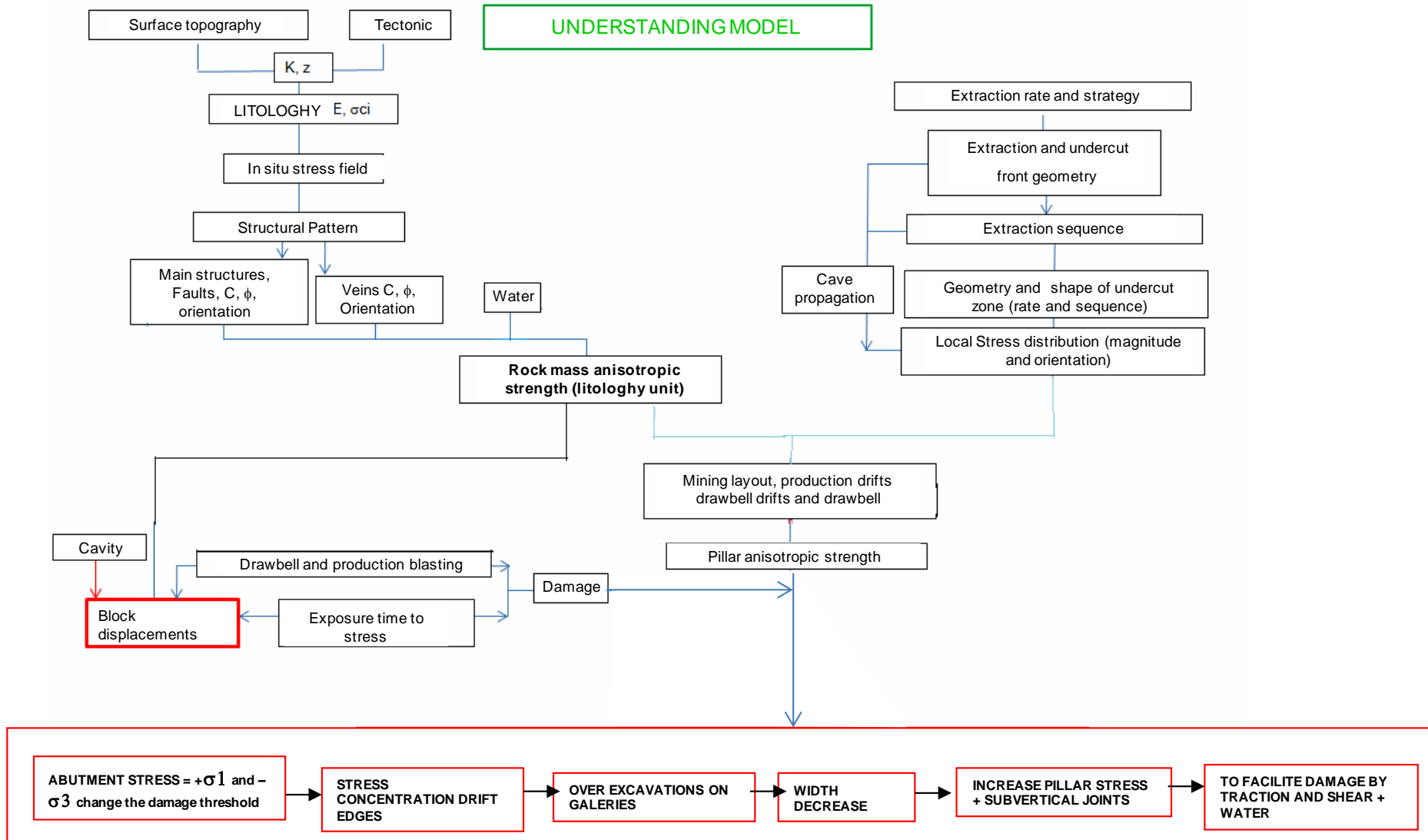
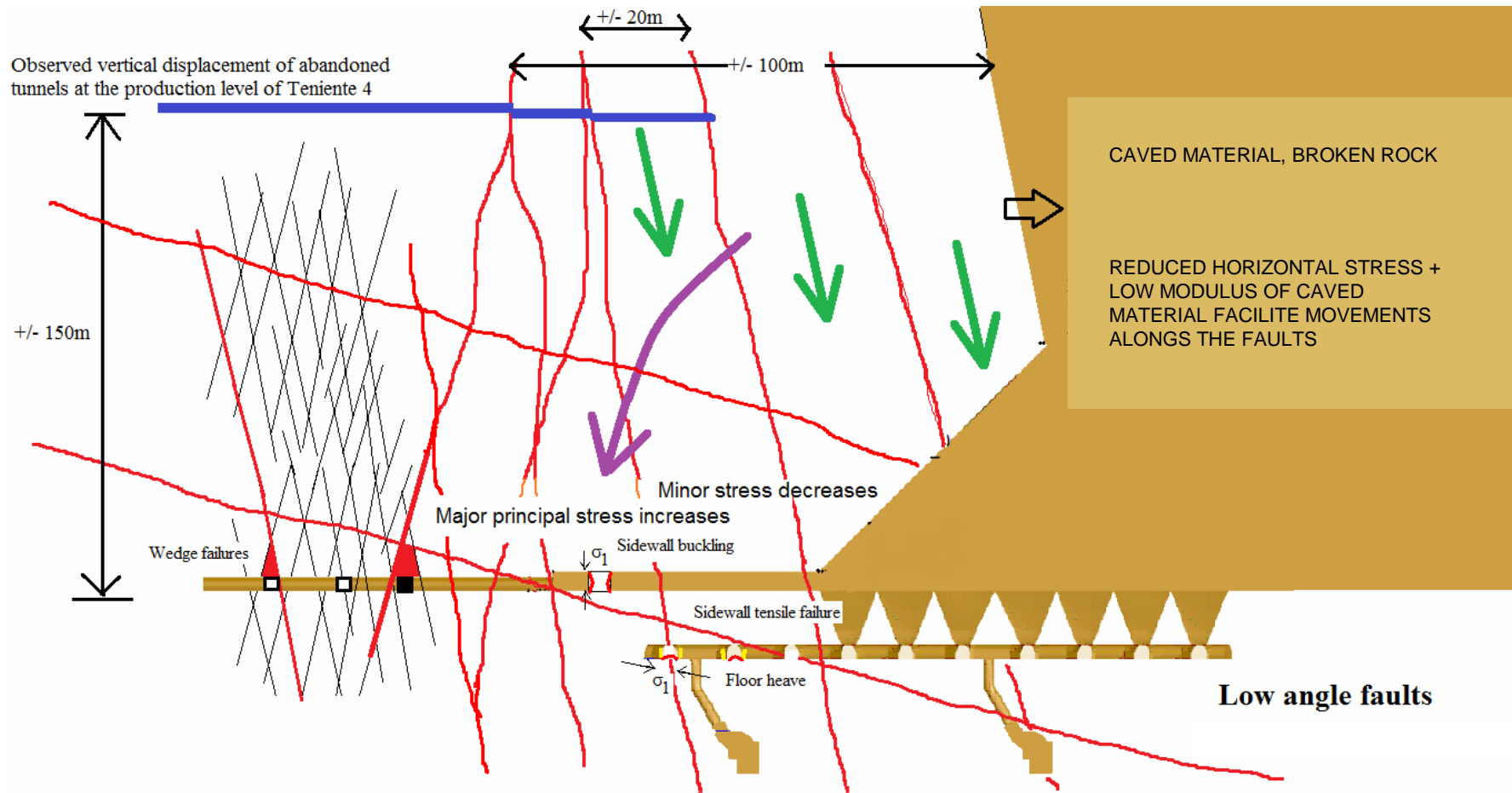


Figure 3.22: Conceptual model to explain pillars behavior affected by collapses (Van Sin Jan, 2010)



**Figure 3.23:** Conceptual model to explain extraction drifts behavior affected by collapses (Van Sin Jan, 2010).

### 3.4 NUMERICAL MODELING APPROACHES

#### 3.4.1 Introduction – fundamentals

Many design problems in rock mechanics practice involve complex geometries involving a nonlinear constitutive behavior of the medium. Actually, solutions to the more complex mining design problem may usually be obtained by use of computational procedures (Brady and Brown, 2004).

Computational methods continue to be used routinely in rock engineering in feasibility studies and in mine design, to assess failure mechanisms, and to predict potential ground control problems. They are also useful in identifying critical geological, geotechnical or mining factors that control the failure and also to provide simulation tools to assess measures for controlling or preventing ground problems (Board et al 2001).

The fractured rock mass comprising the upper crust of the ground is a discrete system. Consistent approach solutions do not exist for such problems and numerical methods must be used for solving practical challenges. Jing (2003) suggested that due to the differences in the underlying material assumptions, different numerical methods have been developed for continuous and discrete system.

Jing (2003) pointed out that the most commonly applied numerical methods for rock mechanics problems are:

- *Continuum methods*
  - The Finite Difference Method (FDM),
  - The Finite Element Method (FEM),
  - The Boundary Element Method (BEM).
- *Discontinuum methods*
  - Discrete Element Method (DEM),
  - Discrete Fracture Network (DFN) methods.
- *Hybrid continuum/discontinuum models*
  - Hybrid FEM/BEM
  - Hybrid DEM/BEM,
  - Hybrid FEM/DEM, and
  - Other hybrid models.

In addition, Brady and Brown (2004) have divided the computational methods of stress analysis into two categories – differential methods and integral methods. In differential methods, the problem

domain is discretized into a set of sub-domains or elements. A solution procedure may then be based on differential equations of equilibrium, the strain–displacement relations and the stress–strain. For the integral methods of stress analysis the problem is specified and solved in terms of surface values of the field variables of traction and displacement. Since the problem boundary only is defined and discretized, the so called boundary element methods of analysis effectively provide a unit reduction in the dimensional order of a problem. The implication is a significant advantage in computational efficiency, compared with the differential methods. The most commonly used integral method in rock mechanics is the boundary element method (Brady and Brown 2004).

Considering their applicability, Board (2001) subdivided them into two basic classes: (1) those that assume the rock mass is elastic (i.e., there is no failure load limit, and stress concentrations are controlled by extraction ratio and geometry of the excavations), and (2) those that assume that the rock mass may fail and shed its load to surrounding regions.

As rock mechanics modeling has been designed for rock engineering structures under different circumstances and for different purposes, and because different modeling techniques have been developed, there exists at present a wide spectrum of modeling and design approaches. One of these approaches was developed by Jing and Hudson (2002) that includes a categorization into eight techniques based on four methods and two levels as shown in Figure 3.24.

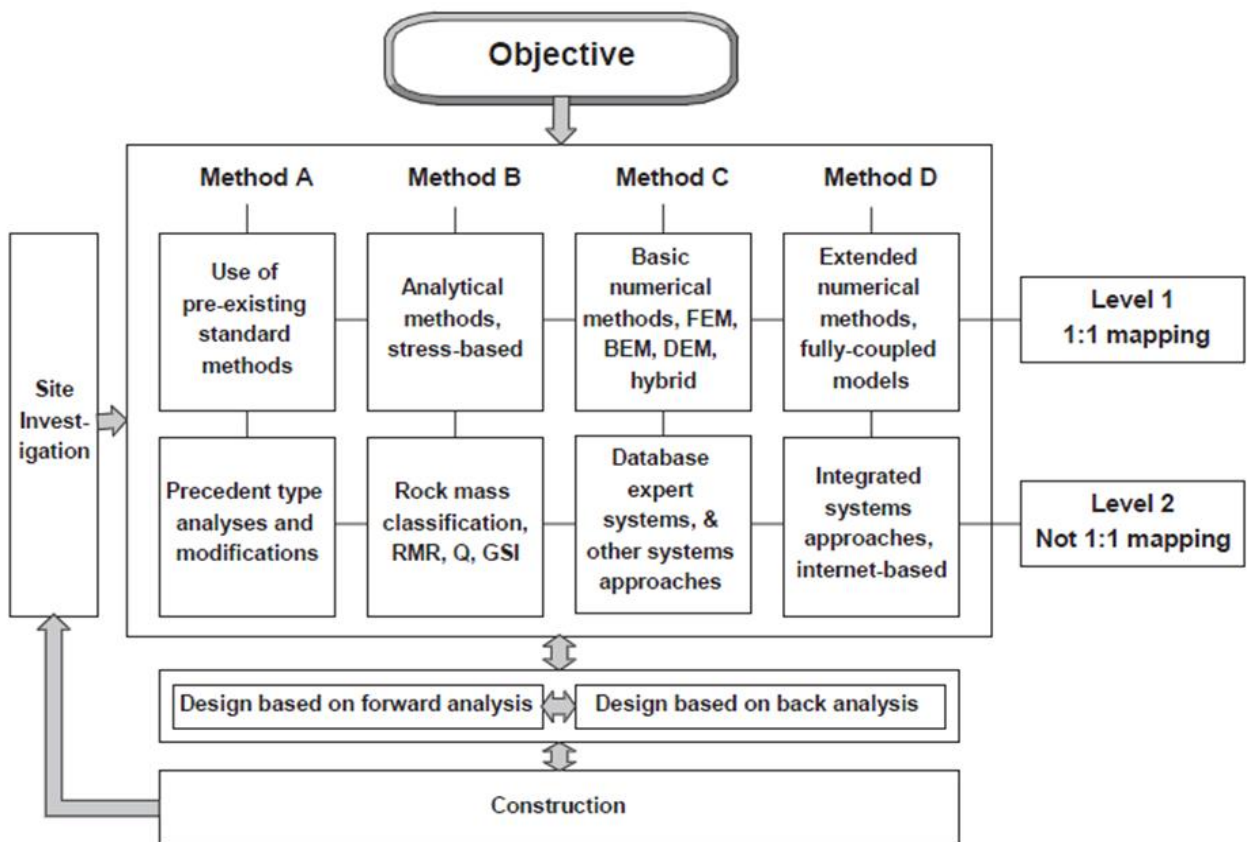


**Figure 3.24:** Flowchart of rock mechanics modeling techniques (Jing and Hudson 2002).

The purpose of this flowchart is to include the basic categories of modeling within the framework of the project objective, site investigation, design and construction. The modeling and design work starts with the objective and the four columns represent the four main modeling methods. Level 1 includes methods in which there is an attempt to achieve one – to one mechanism mapping in the model. The geotechnical risk associated to a panel caving operation and discussed in this study is directed to Methods C and D in the top row, central box, of level 1 in Figure 5.12. Nowadays an integrated approach is needed, incorporating the parallel and sequential use of analysis methods harmonizing the rock engineering design with the host rock character. The integrated modeling should be a process of cognition – calibration and modification – re cognition to capture the rock engineering system behavior (Hudson and Feng 2007).

Based on work developed by Lorig (1999), the most commonly numerical methods used in engineering rock mechanics applications to mining were summarized by Flores (2005) in Table 3.2.

Considering the technical issue described here, the inverse solution technique must be reviewed during this chapter. This technique is a large and relevant class of numerical methods in rock mechanics and civil engineering practice. Jing and Hudson (2002) suggested that the key of the inverse solution approach is to derive unknown material properties or system geometry, and boundary or initial conditions. This is based on a limited number of laboratory or usually in situ measured values of some relevant parameters, using either least square or mathematical programming techniques of error minimization. In the rock engineering case, the most common applied inverse solution technique is back analysis using measured displacements in the field. This includes displacements measured by extensometers and the convergence of tunnel walls. This technique was initiated by Sakurai (1997) for displacements back analysis and has been extensively used in rock engineering.

On the other hand, despite all the advances, the current computer methods and codes described can still be inadequate when facing the challenge of some complex geotechnical problem. This is especially true when adequate representation of rock fracture systems and fracture behavior are a precondition for successful modeling (Jing and Hudson, 2002). There are a number of limitations still associated with applying computational methods, including (Jing and Hudson 2002):

**Table 3.2:** Numerical methods used in engineering rock mechanics applications to mining (from Flores, 2005).

Method	Description	Media Modelling	Numerical Method	Characteristics
Integral	Divides the boundary of excavations into elements and the interior of the rock mass is represented mathematically as an infinite continuum.	Continuum	<ul style="list-style-type: none"> <li>▪ Indirect (boundary element)</li> <li>▪ Direct (boundary integral equation)</li> </ul>	<ul style="list-style-type: none"> <li>▪ Elastic material behaviour</li> <li>▪ Limited number of material types</li> <li>▪ Static analysis</li> <li>▪ Two-dimensional problems are fast to set up and run</li> <li>▪ Three-dimensional problems are large due to fully populated matrices</li> </ul>
		Discontinuum	<ul style="list-style-type: none"> <li>▪ Displacement discontinuity</li> </ul>	
Differential	Divides the interior of the rock mass into geometrically simple elements, and solves the problem by considering each element and the whole set of elements.	Continuum	<ul style="list-style-type: none"> <li>▪ Finite elements</li> <li>▪ Finite differences</li> </ul>	<ul style="list-style-type: none"> <li>▪ Linear and non-linear material behaviour</li> <li>▪ Multiple material types</li> <li>▪ Static and dynamic analysis</li> <li>▪ Mesh generators necessary to reduce set-up time</li> <li>▪ Far-field boundary location/condition determined by user</li> </ul>
		Discontinuum	<ul style="list-style-type: none"> <li>▪ Distinct elements</li> </ul>	
Hybrid	Combines boundary and domain methods to form hybrid methods, which are designed to maximize the advantages and minimize the disadvantages of each of the former two methods.	Continuum	<ul style="list-style-type: none"> <li>▪ Direct or indirect boundary elements and finite elements</li> </ul>	<ul style="list-style-type: none"> <li>▪ Linear and non-linear material behaviour</li> <li>▪ Multiple material types</li> <li>▪ Static and dynamic analysis</li> <li>▪ Mesh generators necessary to reduce set-up time</li> </ul>
		Discontinuum	<ul style="list-style-type: none"> <li>▪ Displacement discontinuity boundary elements and finite element</li> </ul>	

- Systematic evaluation of geological and engineering uncertainties.
- Understanding and mathematical representation of large rock discontinuities.
- Quantification of fracture shape, size, connectivity and connectivity.
- Representation of rock mass properties and behavior as an equivalent continuum.
- Representation of interface behavior.
- Scale effects, homogenization and upscaling methods.
- Numerical representation of engineering processes, such as mining geometry sequence.
- Time effects; and
- Large-scale computational capacities.

However, the computational methods continue being used widely in rock engineering especially associated to the mining industry.

### **3.4.2 Numerical Simulations for Cave Performance**

Numerical modeling holds the possibility of providing a more fundamental and rigorous assessment of cave initiation and propagation than empirical methods. Brown (2003) proposed that the variety of analysis for caving mechanism involves non-linear and discontinuous rock mass behavior. Therefore, the numerical methods commonly used to tackle this type of caving analysis are governed by non-linear partial differential equations where the problem domain is not homogeneous. Because of the discontinuous nature of the caving process, discontinuum or distinct element approaches are attractive for use in the assessment of cavability according with Brown (2003).

Several numerical approaches have been developed to predict the cave performance and all the associated geotechnical aspect, such as: rock mass characterization, cavability and cave propagation, fragmentation, block cave stability and gravity flow (Chitombo, 2010).

Focused on cave mining industry and their geomechanical problems, a number of methods are being developed to provide viable alternative design and optimization methodologies. They are expected to gain more significance as cave mining operations increase in size and depth, as they all attempt to incorporate the governing physics associated with the different caving processes (Chitombo 2010).

Some of these approaches about numerical simulations described on literature are discussed:

### *Rock mass characterization and response*

The synthetic rock mass (SRM) has become an important approach to characterize and predict the large-scale response of the rock mass to caving. This methodology was developed within the MMT project to quantify rock mass behavior at the scale of 10-100 m, which is impossible to assess directly in the laboratory or field, when failure is important (Cundall, 2008).

The SRM uses the bonded particle model (based on the discrete-element code PFC3D, Itasca, 1998) for rock to represent intact material and the smooth-joint contact model (SJM) to represent the in situ joint network. The ability to obtain predictions of rock mass scale effects, anisotropy, and brittleness, properties that cannot be obtained using empirical property methods, is described by Mas Ivars et al. (2007). One example about the SRM concept is shown in Figure 3.25.

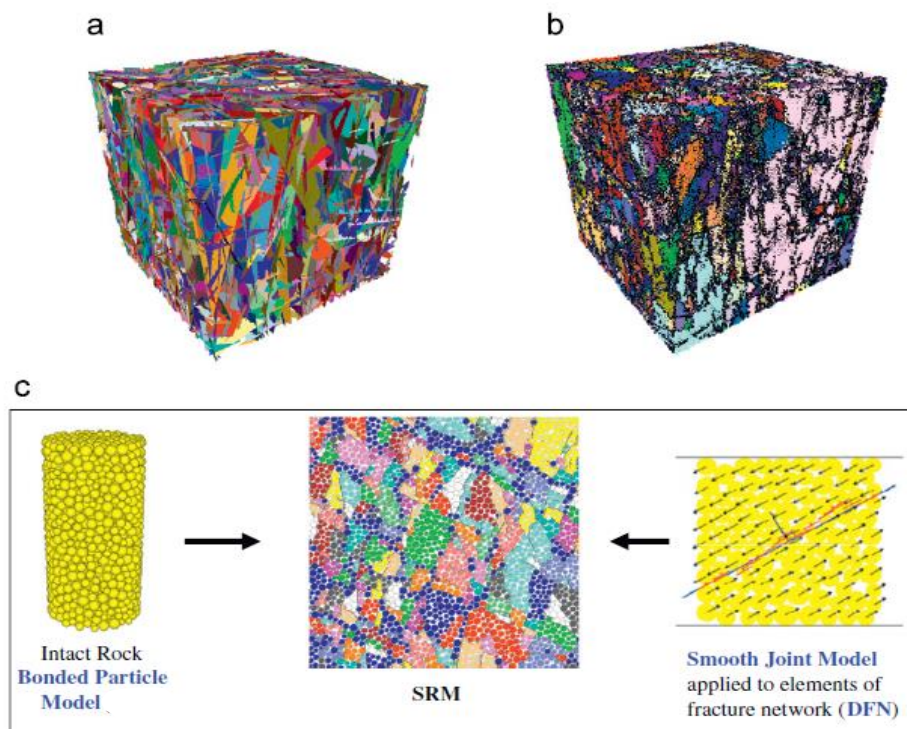


**Figure 3.25:** (a) Three-dimensional DFN, (b) the corresponding three-dimensional synthetic rock mass sample, and (c) synthetic rock mass basic components. The colors in (b) and (c) denote intact rock blocks bounded by joints (from Mas Ivars et al., 2007).

To date, the method has been used to derive rock mass properties for use in large-scale continuum models of cave mining, to estimate fragment size distribution, to quantify the impacts of scale on rock mass strength, and to study the influence of veining in intact rock strength. For instance one application case was reported by Mas Ivars et al. (2007) referred to a back-analysis study of caving behavior at Rio Tinto's Palabora mine in South Africa.

The SRM methodology works based on the rock mass strength, discontinuity characteristics and one concept called “discrete fracture network” (DFN). This is integral part of rock mass characterization and modeling (Chitombo, 2010).

To complement the DFN definition, Elmo and Stead (2009) suggested that the use of a stochastic discrete fracture network (DFN) approach provides the best option for creating realistic geometric models of fracturing, reflecting the heterogeneous nature of a specific fractured rock mass. The basis of DFN modeling is the characterization of each discontinuity set within a structural domain using statistical distributions to describe variables such as orientation, persistence and spatial location of the discontinuities. Moreover, the use of discontinuity data from mapping of exposed surfaces, boreholes and or other sources of spatial information is maximized by DFN approach (Elmo and Stead, 2009). A fracture representation (DFN) is also shown in Figure 3.26.

Additional description and application of DFN approaches regarding to rock mass characterization are discussed by Elmo et al. (2008a) and Rogers et al. (2010) where a DFN approach was developed to define in situ primary and secondary fragmentation distributions for Cadia East panel cave project.

Although the concept was originally developed within the framework of the discrete element method, recently the approach has been adapted to multi-scale, continuum-discontinuum finite element (FE) models. For instance, Beck et al. (2009) investigated some homogenization concepts for mine problems, the load-deformation response of some discontinuous rock masses at an example mine were simulated using Explicit, finite element models. The effects of specimen size and confining stress on strength, dilation and comminution were analyzed.

### ***Caving process***

Chitombo (2010) reviewed the main aspect associated to SRM approach for cave mining. The capacity to estimate cavability, propagation prediction and subsidence estimation was also highlighted.

However, other methodologies and numerical techniques have been recently developed to simulate cave initiation and propagation. Coupled, granular flow-deformation simulations were undertaken to simulate cave initiation, propagation and gravity flow. The tool combines a Newtonian Cellular Automata (NCA) representation of the cave muck pile (Sharrock et al. 2004) with an explicit Discontinuum Finite Element (DFE) model of the rock mass mine scale and incorporate high resolution input data such as large numbers of explicit structures in the rock mass and a very large numbers of small particles in the cave muck pile (Beck et al., 2011).

Beck et al. (2011) pointed out that the coupled DFE-NCA simulation procedure enables rapid simulation of cave propagation, flow and induced deformation, driven by the cave draw schedule. The method can be calibrated directly using observations of cave back location, grade and recovery,

seismicity, tunnel damage, tomography and or ground movement. At several mines, including Newcrests Ridgeway Mine (as shown the Figure 3.26), the results of DFE-NCA analysis closely conformed to field measurements suggested by Beck et al. (2011).

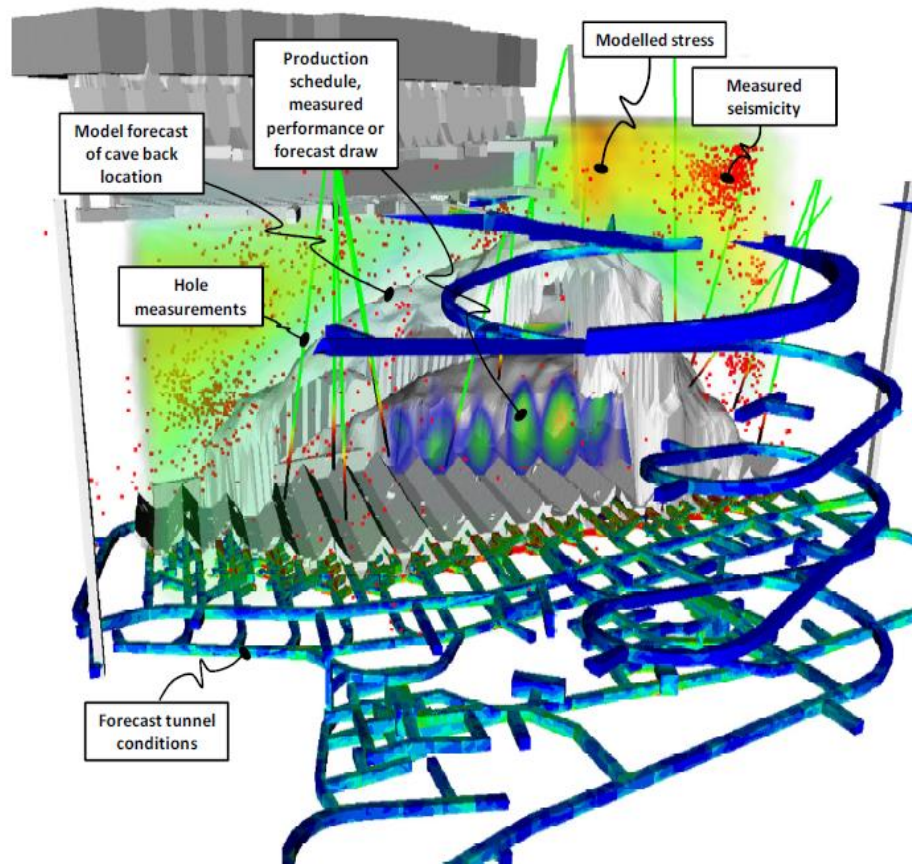


**Figure 3.26:** Example of data from multiple sources visualized in a 3d collaborative workspace. The layering of modeled and measured data aids rapid model calibration, validation and improvements (from Beck et al., 2011).

As a complement a brief review of seismicity and the caving process was carried out on this literature review. Some of these are discussed.

As part of SRM development, Reyes-Montes et al. (2007) and via MMT caving mechanics research, developed a novel seismology and micro seismic analysis techniques. Additionally, a numerical modeling technique that involved large-strain, 3d discontinuum, strain softening dilatant behavior (DFE modeling) was implemented for simulating seismic effects of mining. The approach estimated the energy released throughout the mine at each extraction step, and was validated for its intended purpose using data from mine sites (Beck et al., 2007).

Regarding to flow simulation or gravity flow for caving mining, a rapid emulator based on PFC3D (REBOP) was developed via MMT research. Chitombo 2010 defined REBOP as a numerical modeling tool that provides rapid analysis of the movement and extraction of fragmented rock under draw in mine operations that use block or panel caving. Pierce (2009) developed a complete description of this tool and its applications.

### ***Block cave stability***

Block cave stability at increasing depths has become one of the most significant issues particularly with relatively complex rock mass behavior. The stability of extraction and undercut levels has always been an engineering constraint on block cave design. Anecdotally, stability issues have become even more important for those operations where the rules of thumb are showing signs that they have reached their limits of applicability.

Chitombo (2010) suggested that the emerging tools in the arena of multi-scale modeling of mines, taking into account the physics and the characterization of key geometrical structures governing a rock mass response, is becoming a powerful addenda to current design and operation of cave mines.

Many cases of cave stability analysis have been recently performed using emerging technologies such as DFN, SRM or multi-scale analysis, to improve stability assessment. Some of these representative examples are discussed:

- Beck et al. (2006) developed a numerical analysis to analyze a conceptual sequence for a block cave in an extreme stress and deformation environment. The case analyzed options for a potential block cave for the Perseverance Deeps mine in Western Australia. A calibrated three dimensional Finite Element (3-D FE) non-linear, strain-softening, dilatancy model of the Perseverance environment was performed. The calibrated mine-scale model was able to test the effect of sequencing variables on drive survivability, however sufficient field data must be required for an efficient calibration task.
- Elmo et al. (2008b) analyzed pit wall deformation induced by block-caving extraction using a combined FEM/DEM –DFN synthetic rock mass approach. By coupling a DFN approach with hybrid FEM/DEM model it was possible to define synthetic fractured rock properties capturing the effects of block cave mining, in terms of increased simulated inward displacements (i.e. deformation) of the pit wall (Elmo et al., 2008b).
- Swanepoel et al. (2008) developed a back analysis of the failed Advance Undercut at Cullinan Mine from De Beers in South Africa. This analysis was carried out in order to better understand the complex evolution of loads on the production and undercut horizons. The sequence of events was back analyzed using a 3D strain softening dilatant, Finite Element (FE) model. The main effort of the back analysis was to establish root engineering causes so they may be avoided in the future.
- Hormazabal et al. (2010) performed a geomechanical evaluation of macro-block caving options using three dimensional numerical modeling at Chuquicamata underground project-Chile. Based on the geotechnical characterization of the site, a 3D elastic-plastic model was developed using the FLAC3D code (Itasca, 2005) to assess the stability for the macro-block

caving options proposed. The aims were to quantifying stress concentrations in certain critical areas of the planned infrastructure.

Some of the most important geotechnical risks for caving mines were shown to be significant, and in some case simply dependent on mine scale extraction sequencing and geometry. Cases of cave stalling, plug collapse and infrastructure failures at some mines were also found to be a consequence mainly of the geometry of the mine and the excavation sequencing (Beck et al., 2013). Therefore, the use of large three-dimensional numerical models, sufficient scale and detail of geological units, structures and the precise description of the regional stress field is allowing simulation of realistic displacements and energy release for mining progresses. It also has the ability to simulate the damage accumulated as a consequence of progressive excavation process (Beck, 2008).

The most significant improvement in modeling has come from a move towards calibrated, multi-scale non-linear modeling. Many mine deformation modeling approaches assume physical phenomena of different length scales cannot, or do not, affect each other. In fact, gross deformation simulated at one scale, relying on a set of simplified material assumptions, can be used to frame the loading system, or boundary conditions for a smaller length scale model incorporating a more advanced material model.

Massive, strain-softening, dilatant analysis is the most obvious approach for multi-scale analysis in rock. Nowadays using the off-the shelf strain-softening, dilatants Finite Element (FE) codes and parallel computing, models with more than 10 million degrees of freedom and higher order elements are frequently being employed in both small and large projects (Beck et al., 2013). Run and built times for very large, life of mine, mine scale problems are short enough to allow application in roles very similar to that usually fulfilled by much simpler, but less featured 2D and elastic analysis on mine sites.

A large number of projects around the world have performed multi-scale analysis. The greatest improvements have been the rationalization of the use of sub-models and a major step change in the ability to correctly replicate displacements (at all length scales). This has become an important modeling tool to greater rigor in calibration. Additionally, an immediate consequence is the ability to use velocity, displacement and rock damage as criteria for stability (Ceputitis, 2010). Finally, the mechanisms of damage and deformation that affect stability at each mining geometry step are successfully captured by the use of massive multi-scale approach.

## **CHAPTER 4**

# **GEOTECHNICAL INSTABILITIES AT THE ESMERALDA PANEL CAVING OPERATION**

### **4.1 INTRODUCTION**

The Esmeralda sector is the third large panel completely located in primary ore developed by El Teniente Mine. Feasibility studies were performed during 1992 and 1993, mainly based on experience and knowledge acquired during exploitation of sector Teniente 4 Sur and failure of the start in sector Teniente Sub-6. This operation, totally located in primary rock- that started production in 1989, stopped its operations temporarily in 1992, due to the occurrence of rock bursts that caused fatalities, infrastructure damages and significant economic losses associated.

The Esmeralda sector introduced a change in the operations sequence of panel caving, called “Panel caving with pre-undercut sequence”. This consists basically on advancing the caving face preferentially in front of the developments and preparation of the production level, thus preventing damage to the drifts and mining infrastructure. During 1997 this variant started being applied with the start up of the sector, with a growth rate of 6,000 tpd/year and a projected production of 45,000 tpd, for 2005.

The first period of implementation of the project was during 1997 – 1999 where a high standard of quality was achieved in compliance with landmarks, as well as quality of production infrastructure. In this period, attention was initially focused on the caving start-up phase (connection). During this process there were some rock bursts and their consequences were efficiently managed by the work groups supporting the start up of the operation. Later the focus was on instabilities generated in the undercut level –with damage to the pillars- which caused the loss of blast holes and later incomplete undercutting. Since the beginning of the exploitation, damages in the undercut level have made difficult the process of undercutting..

Until 2004, The Esmeralda operation was characterized by sustained growth and compliance with a committed production reaching 93,5 % of planned production (Rojas et al., 2005). However, since 2000 there have been delays in the incorporation of the area and mining preparation. The effects related to this were compensated with over extraction (approximately 13% of accumulated production) and incorporation of marginal expansions to the north and east of the sector.

Since 2001 Esmeralda operation was affected by a complex situation associated mainly to delays in preparation and start of losses in the production area due to collapses on the extraction level. This

brings as a consequence a series of impacts on projections of future growth, which generate non compliance with production goals of 45,000 tpd for 2005.

Hustrulid (2004) suggested that the panel caving with pre-undercut sequence worked quite well until 2003 when an extensive area of the central part at Esmeralda Sector was finally collapsed. This required a series of remedial actions to be taken to isolate the area and to progress the cave once again. The following factors were listed by Hustrulid (2004), which could have been involved in the collapse process until 2004:

- Design
- Geotechnical/Geology
- Planning
- Operational
- Coordination – development, construction and operation

The collapse severely interrupted the mining rhythm on both the extraction and undercut levels. Eventually, mining activities on both levels were resumed. However, as the undercut was moved to the east (toward the mountain), very severe pillar stability problems were experienced making it impossible to complete the undercut drilling and blasting. This area was labelled “abandoned” and the undercut was moved to the south, where severe pillar instability was once again experienced.

An attempt to recover part of the collapsed area was carried out in the period January 2005 until November 2006. During the extraction, an increase of damage was observed in some extraction drifts which also were recorded by geotechnical monitoring. Damage evolution in the sector of the central collapsed area (2001 to 2004) resulted in operations being temporarily abandoned.

Since 2007 the sector has been extracted by two cave faces working independent, sector Hw and sector Fw respectively. However from mid 2008, stability problems have started again at the extraction level.

During 2008, 2009 and 2010 at Esmeralda operation there were 3 episodes of collapse in the production and undercut levels. These collapse processes are particular, as they occurred in areas that have not been incorporated to production, meaning they have not had draw bells built and pillars have not been yet undercut. This phenomenon was different from previous collapses, where instabilities had been generated in sectors incorporated or where the undercutting face had already passed.

The last episode of collapse occurred in the extreme Fw of the Esmeralda Mine approximately between extraction drifts 43 and 45 and trenches 18 to 22. The negative consequences for mining resulted in closure of the face in sector Fw with a delay in the incorporation of the area.

The collapses especially those generated ahead of the caving face have compromised the mining plan, as it is impossible to undertake production from sectors affected. Consequently, the need to establish a new strategy to face the exploitation in that sector has arisen.

## **4.2 COLLAPSES EXPERIENCED IN OTHER OPERATIONS AT EL TENIENTE MINE**

A database (bench mark) of collapses associated to exploitation of sectors with block and panel caving has been completed based on the information collected by Diaz et al. (2009): This information is presented in Appendix D.

This set of data has been incorporated and included in the assessment records of El Teniente mine (Pasten, 1999; Villegas, 2008 and Cifuentes, Dunlop, 2010)), Andina mine (Díaz et al, 2000; Karzulovic & Lledó, 2004), El Salvador mine and others. Each record indicates the productive sector and location, according to drift, trench and draw point affected. The start month and start year for each event is also included. The data indicates the square meters of area effectively affected in the collapse and annual accumulative, also indicating the draw points involved. Finally, the width of the caving face is associated to the existing open area.

From the information collected, and especially about the experience in El Teniente Mine, it is concluded that historically one of the most affected sectors by this phenomenon has been Sector Ten-4 Sur. As indicated in the graph of figure 2.22.

Sector Ten-4 Sur, started its production in 1982 and according to the records, it shows that collapses events have been present almost all the productive life. A record of approximately 119,000 m<sup>2</sup> of production area was affected by collapses, corresponding to 25% of the total area in the sector. Figure 4.1 shows coloured drifts of the extraction level affected by collapses at el Teniente mine. The highlighted color green represents collapses associated to Ten-4 Sur.

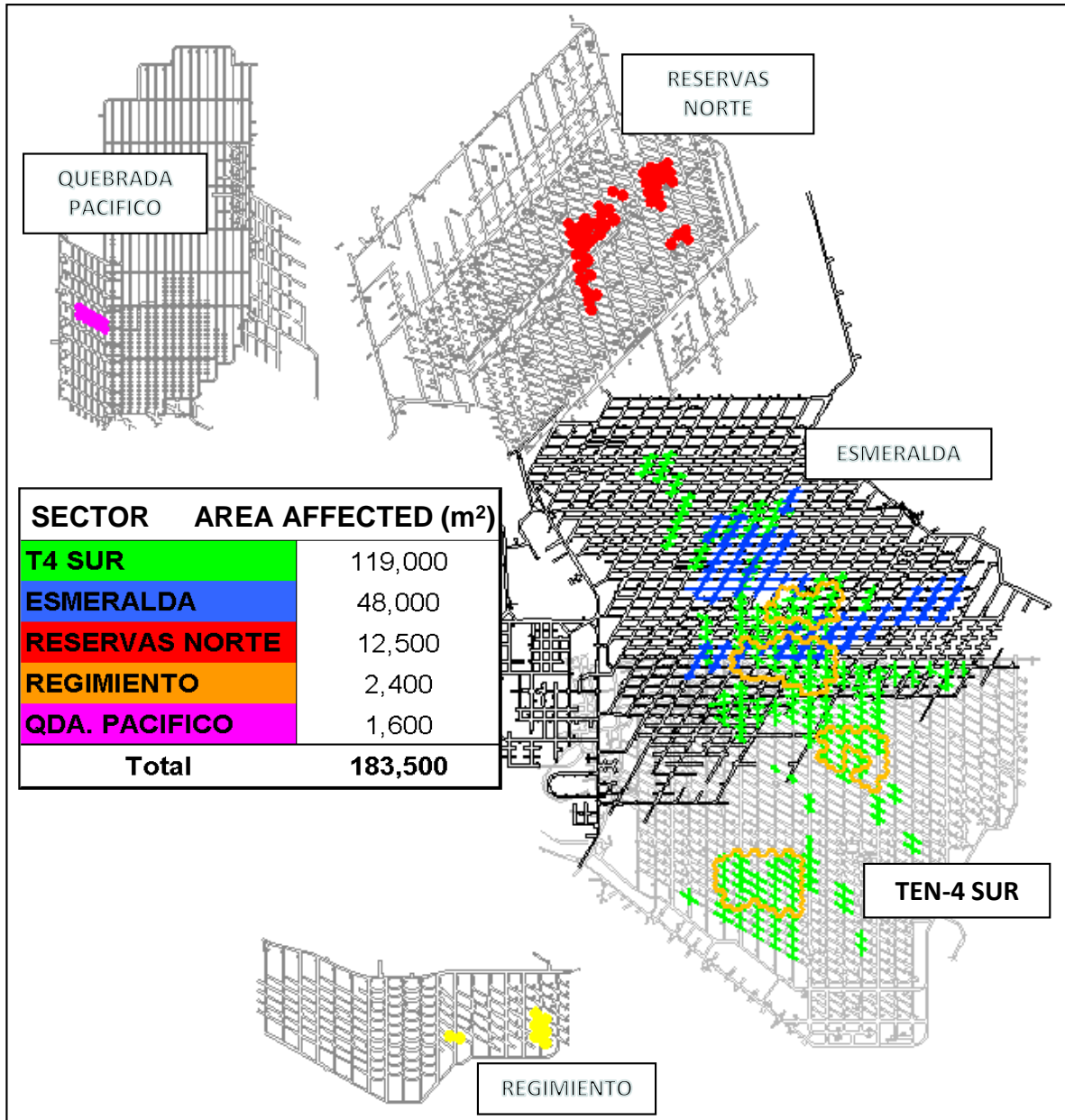


**Figure 4.1:** Drifts of extraction level affected by collapses at El Teniente Mine. In green color the collapsed drifts of Ten-4 Sur can be appreciated.

This kind of problems have a relatively slow evolution, and their effect on production can become extremely important due to the damage caused, which are illustrated with the example represented in Figure 4.2.

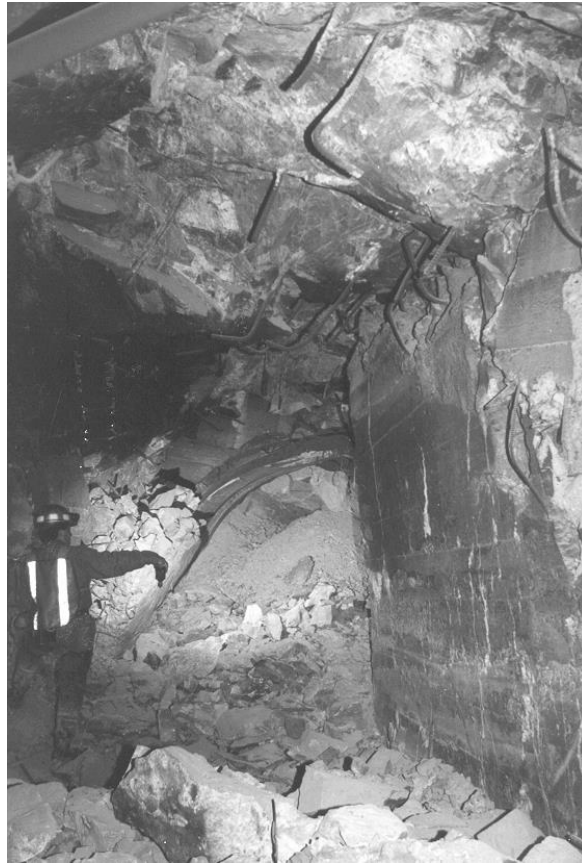


**Figure 4.2:** Damage caused by the collapse that affected Teniente 4 Sur in October - November 1991. This picture shows C-12/Z-15 and the draw point.

To explain the causes of this phenomenon, multiple studies with a relatively partial and/or local vision of the problem, were performed between 1986 and 1999. Amongst these studies one can mention the ones developed by: Morel (1986), Cavieres (1995), Krstulovic (1997), Dunlop and Pereira (1998), Lorig (1998), SRK Consultores (1999) and Dunlop (1999). From these we can derive three essential conclusions about the precursors of the phenomenon associated to sector Ten-4 Sur:

- Structural condition, major faults.
- Excessive stress in the caving face, caused by large blocks or other agents.
- Operational abnormalities.

From these, the structural condition was identified early by Morel (1986). Morel (1986) indicated that major structures had been one of the main causes of the collapse that affected the sector Teniente 4 Sur in October 1984, as shown in Figure 4.3. This feature is also mentioned by Karzulovic (2003b), who identified an agreement between the cause identified by Morel (1986) for Ten-4 Sur and generation of the first collapse in Esmeralda.

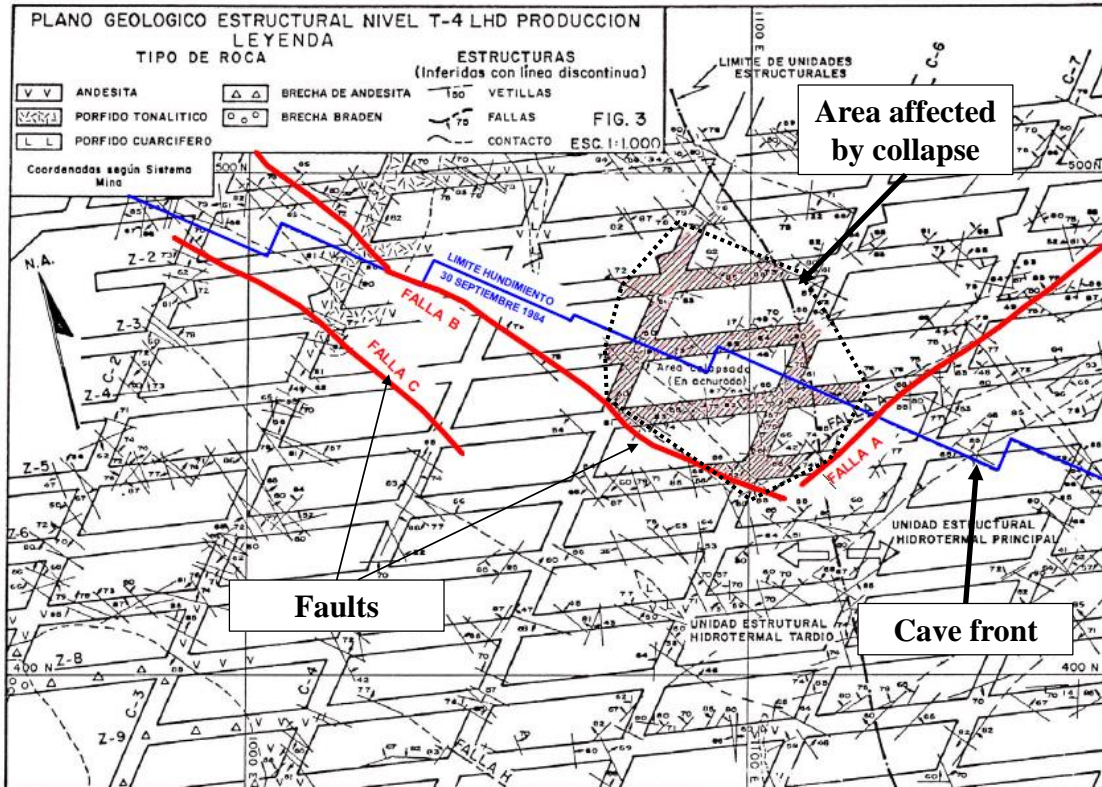


**Figure 4.3:** Plan view that shows in shaded color the Production Level in sector Teniente 4 Sur that were affected by a collapse in October 1984. In blue is shown the position of the caving faces by September 30, 1984 and in red the main geological faults in the sector (modified from Morel, 1986).

### 4.3 REVIEWING GEOTECHNICAL INSTABILITES AT ESMERALDA OPERATION

The Esmeralda sector has been historically affected by geomechanical events that have caused impact on the normal development of the mining process (preparation and extraction). Some of the most relevant geomechanical events that have occurred are:

- Rock bursts
- Undercut instabilities
- Collapses experienced on extraction level

A representative summary of the situation with one of the events is presented below. The collapses in the production level and instabilities in the undercut level are emphasized, as these have generated the biggest effects in the sector.

#### 4.3.1 Rock Bursts

Rock bursts have generated damage in the rock mass and in the drifts of different levels, causing in some cases the interruption of mining operations. Despite the rock bursts being experienced during

the whole history of exploitation of the Esmeralda sector, the main effects have been concentrated during the first years of operation, especially in the period from 1997 to 2004.

Rojas et al (2005) reviewed the information associated to rock bursts generated until December 2004. It must be mentioned that there were 35 rock bursts, from which 27 were minor, 5 were minor to moderate, 2 were moderate and 1 minor to moderate and major (2004) according to the classification described in section 2.5.3. Spatial distribution of damage relates the caving face. Damage has always been contained within the limits of the abutment stress zone. Also, damage has involved all levels, as indicated in Figure 4.4.

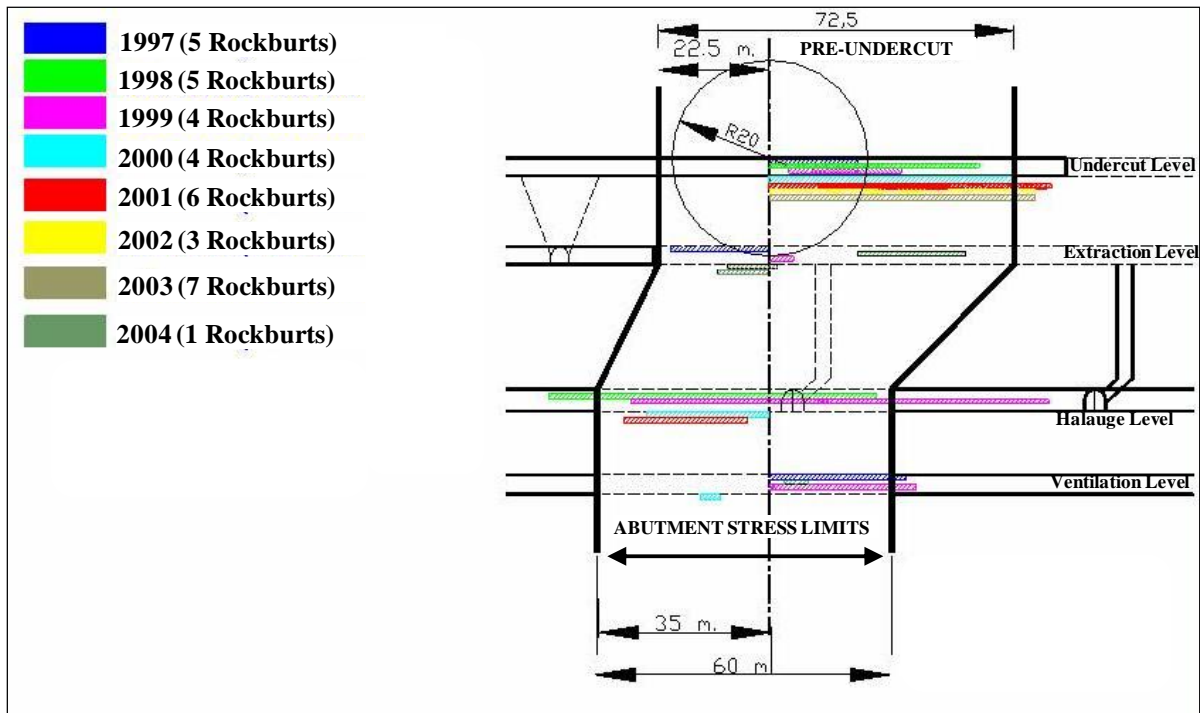


**Figure 4.4:** Representative cross section view of the exploitation face in Esmeralda, with the relative location of damage generated by rock bursts between 1997 and 2004 (Rojas et al., 2005).

Additionally Rojas et al. (2005) reviewed the information provided by preliminary reports of rock bursts, occurred between 1997 and December 2004, from which the following is derived:

- Regarding the damage per level
  - Undercut: 50 % of damages.
  - Extraction: 16 % of damages.
  - Haulage: 12 of damages.
  - Ventilation: 22 % of damages.

- Regarding the causes of rock bursts
  - 49% has occurred after undercut blasting (3 before connection to the crater).
  - 17% has been associated to extraction.
  - 23% has been associated to extensive distance between extraction and undercut fronts.
  - 11% due to other factors.

Figure 4.5 shows damage associated to rock bursts in the caving level of Esmeralda Mine, in the period between 1997 and December 2004.

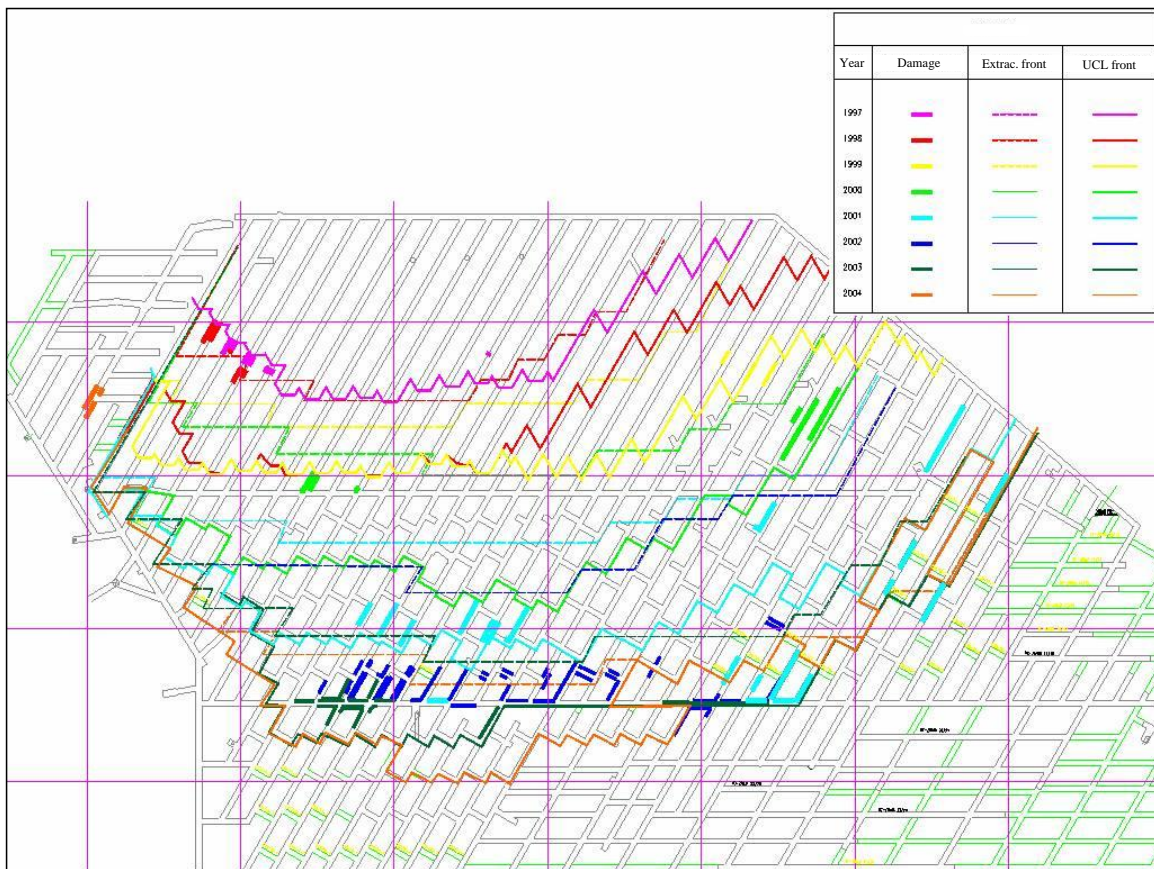


**Figure 4.5:** Drifts damaged by rock bursts in the undercut level of Esmeralda operation, in the period from 1997 to December 2004 (Rojas et al., 2005).

Based on the distribution of damage due to rock bursts in the undercut level and its association with the three different techniques of undercut blasting implemented between 1997 and 2004 (described in Section 2.31), Rojas et al. (2005) concludes that:

- There was practically no evidence of damaged drifts due to rock bursts by implementing through undercutting from half pillar to full pillar. This relates to extraction before 2000.

- During the period 2000 – 2002. A greater concentration of damage due to rock bursts was experienced in the caving level. In this period the undercutting blasting was done by connections.

#### **4.3.2 Instabilities on Undercut Level**

The undercut level in Esmeralda operation started showing a halo of damage ahead of the undercut front in sectors Centre-Fw (specifically to the East of drift 19), since mid 1998. This damage had been periodically mapped by the geotechnical team at El Teniente Mine.

Since the start of deterioration of the rock mass (1998) until 2010, an increase in the extension and severity of damage had been observed. In some case abandonment of pillars occurred. A damaged area of 14,300 m<sup>2</sup> is presented by December 2004 (Rojas et al., 2005). In other cases Dunlop et al (2010) had reported draw bells that had been incorporated to production with a special design (locally called high draw bells) because of the amount of damage in the undercut level making it impossible to have a successful undercutting over them.

Progress of damage around the undercut face is shown representatively in the schematic of Figure 4.6. This figure summarizes the mapping of damage in the undercut level for different periods until 2004. However in Appendix E all the damage mapping records for the caving level reported quarterly since 1998 until 2010. It is worth mentioning that this information has been used in this thesis as background for calibration of the back analysis modelling developed.

Rojas et al. (2005) suggested that there were two conditions that have influenced the increase of deterioration in the undercut level: irregular geometry of the face (convex to the cave) and a long distance between extraction and undercut fronts exceeding 120 meters.

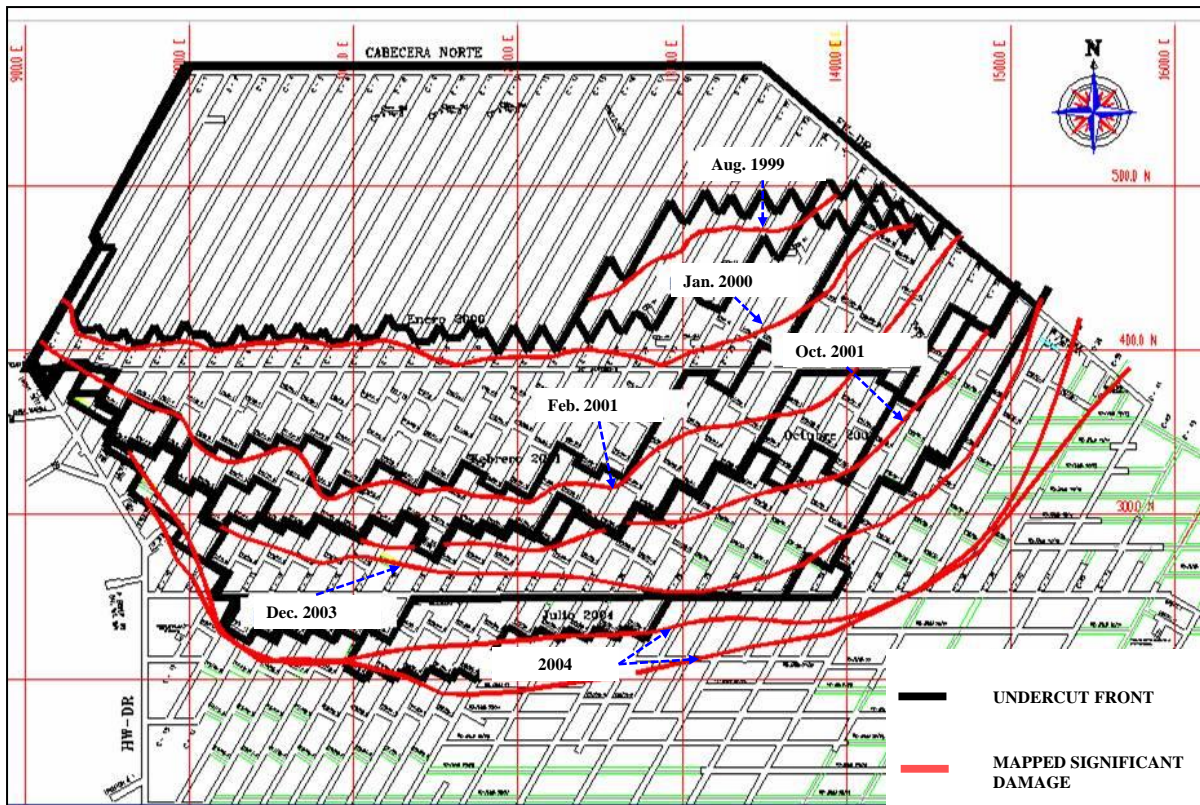


**Figure 4.6:** Mapped damage located ahead of undercut front between August 1999 – Dec. 2004 at The Esmeralda operation.

The status of the rock mass deterioration within the pillars in the undercut level, has strong influence in the success of the drilling and blasting of the base cut. In many cases there has been incomplete undercutting, generating remnant pillars that have acted as load transmission points from the undercut level to the production level.

A borehole camera inspection of blasting holes complemented with diamond drilling cores, coupled with geological-geotechnical mapping of cores recovered in pillars of caving level was performed by Rubio and Seguel (2005).

The plan was divided in two phases, considering the pillars located between 0 and 50 meters to the south of the undercutting face, in the strip corresponding to the abutment stress zone.

Based on the realization and inspection of horizontal blasting oriented North-South and East-West, Rubio and Seguel (2005) concluded for the first phase of the plan that:

- Pillars located around the caving face present severe damage, reflected in a progressive deterioration of the undercut drill holes.
- In both orientations of core recovery (North-South and East-West), the damage condition inside the pillar was similar (intensive damage).

- The severity of damage indicated that induced stress was of such magnitude that caused the disking phenomenon. This was confirmed by the observations with bore-hole camera.
- Close to the undercutting face, a predominant factor in the increase of induced deformation and deterioration of holes over time was experienced. As part of the information obtained in the field, it was found that after 24 hrs drilling the borehole, the blast holes showed damage, which was intense in the center of the pillar.

Regarding the second phase of the plan performed by Rubio and Seguel (2005), it can be said that in order to evaluate the condition of damage in the roofs of drifts of the undercut level, inclined vertical boreholes were drilled (5°, 45°, 60°, 90°). Boreholes 10 meters long were drilled and 75 mm in diameter within the inclination range mentioned. Drill holes were distributed in the abutment stress zone of the undercut level, with the undercutting face stopped. The time elapsed between the drilling of holes and the inspection was between 1 and 3 weeks. The inclination and length of drilling performed is shown in Figure 4.7

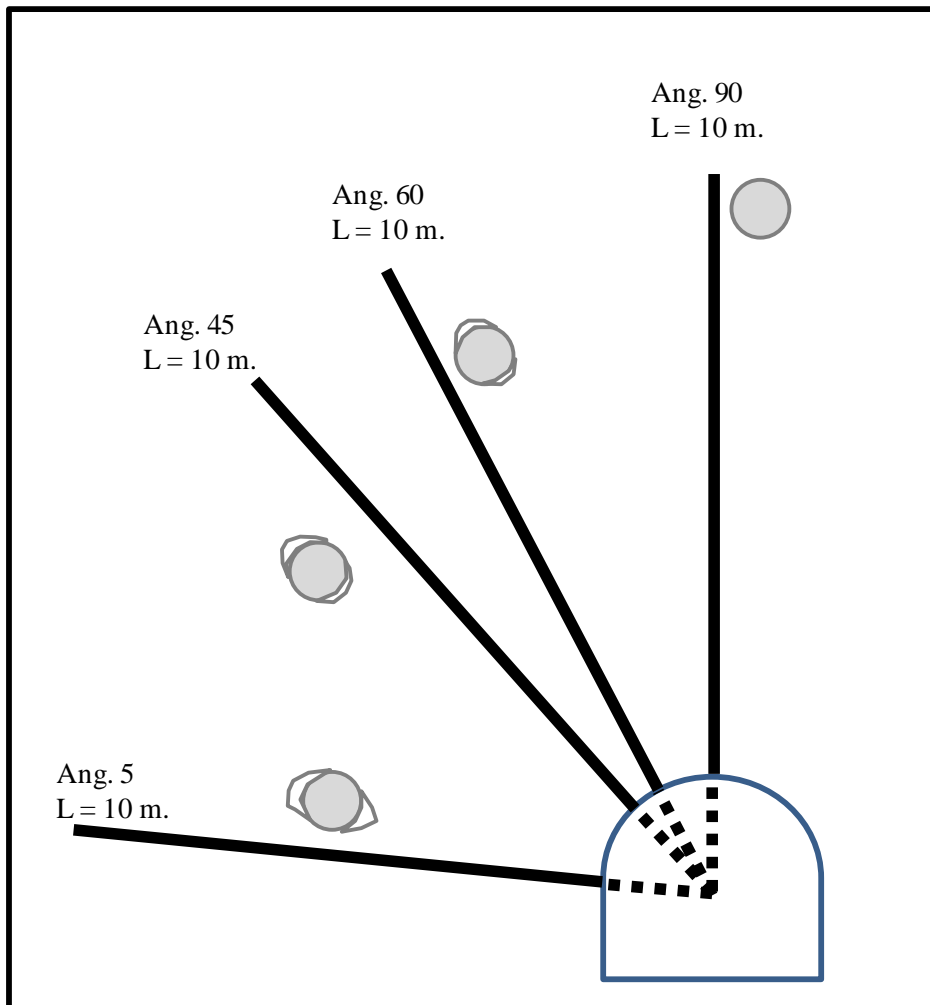


**Figure 4.7:** Inclination and length of blast holes performed in the second phase of the inspection plan for pillars in Esmeralda operation (from Rubio and Seguel, 2005).

Regarding the second phase of the plan, Rubio and Seguel (2005) concluded that:

- Drilling with inclinations of 90°, 60° and 45° did not present major differences in terms of damage. Slabbing was observed and specific deformations within the first 3 meters of length, probably associated to the effect of excavating the drift. Condition of deterioration of these drilling is clearly less compared to the horizontal ones, due to the semi-parallel nature of those compared to the orientation of the major principal stress.
- Drilling with an inclination of 5° showed more deterioration. This was due to the major principal stress acting in a semi-perpendicular manner to the blast hole. Opening of structures and deformation of drilling were experienced.
- Blast holes of 5° present an unfavourable condition that is increased over time.

Finally Rubio and Seguel (2005) summarize the global conclusion of the plan:

- All cores register values of RQD index of less than 40%.
- Blast holes in pillars located near the caving face ( $d < 30$  m) present over-excavations that become equal to the radius of the blast hole, which indicates a very high level of stress in the body of these pillars. On the other hand, blast holes located in pillars further away from the undercutting face ( $d > 45$  m) present over-excavations up to 25% to 30% of the blast hole radius, which indicates stress values significantly lower in the body of these pillars.
- Blast holes drilled in pillars adjacent to the undercutting face suffer damages in less than 24 hours since the drilling and the increase rate of these damages is such that in 2 weeks part of the blast hole length is lost. On the other hand, blast holes drilled in pillars located further away from the undercutting face ( $d > 45$  m) present minor damages after 24 hours and the increase of these damage is relatively lower (10%) after 25 days.

#### **4.3.3 General view of experienced collapses on extraction level at Esmeralda operation**

One of the sectors that have been affected more intensively by the collapse phenomenon is Esmeralda extraction level. Since 2001, this sector has suffered with collapses in the central part of the caving front, which have reduced its undercutting rate and forced the development and implementation of contingency plans to deliver the planned production. A brief scheme with the historical evolution of collapsed drifts in Esmeralda production level is shown in the Figure 4.8. Moreover, the area collapsed is displayed along with main lithologies and the major faults within the area.

In general, the collapses located in the central sector of the Esmeralda mine ( collapses from 2001 to 2004) occurred behind the undercutting face. On the other hand, collapse episodes during 2008 to 2010 have occurred ahead of the caving face. Such failures were concentrated mainly in the east sector (Fw side).

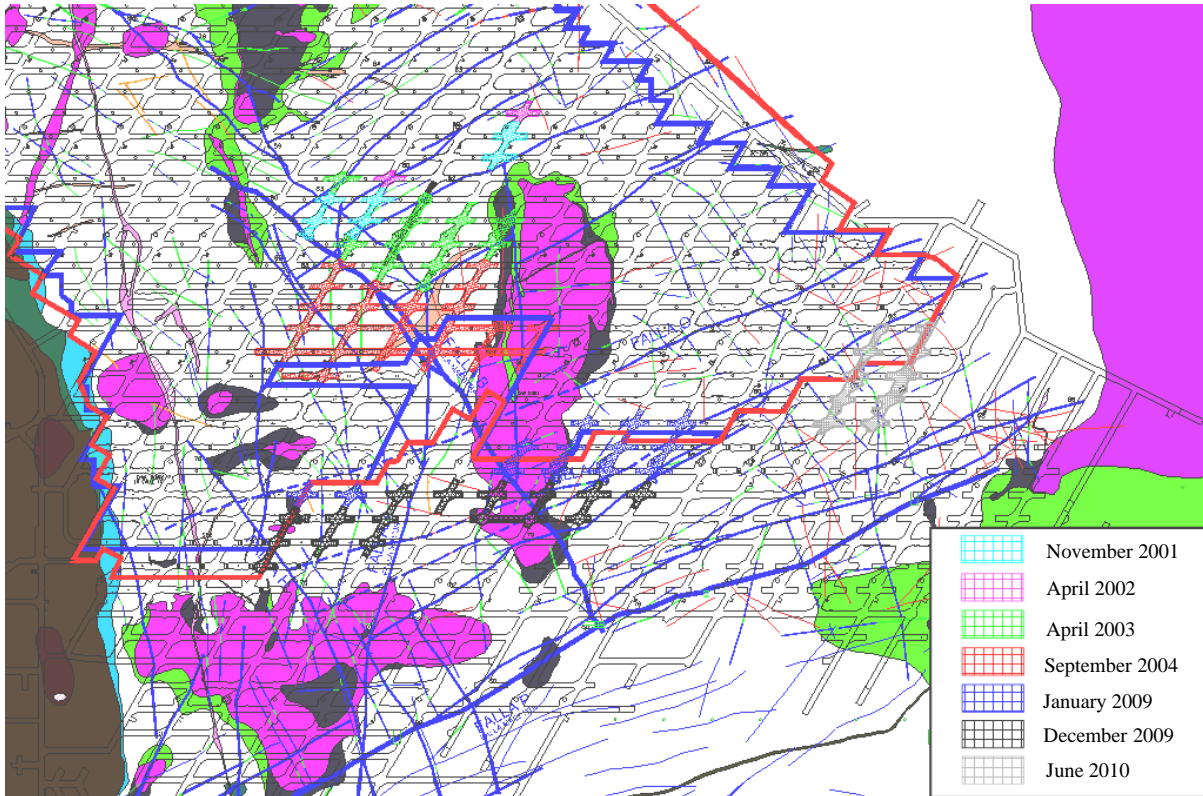


**Figure 4.8:** Boundaries of production drifts collapsed 2001 – 2010 along with main lithologies and the major faults in Esmeralda operation.

#### 4.4 DESCRIPTION OF COLLAPSED DRIFTS IN ESMERALDA

Before describing in detail the historical evolution of collapses that have affected the Esmeralda sector, it is required to review the main operational and geotechnical landmarks of the operation between 1997 and 2010. Figure 4.9 shows in detail the main operational and/or geotechnical landmarks that describe the behavior of Esmeralda sector.

Based on the schematic presented in Figure 4.9, a number of important steps can be identified:

- Initially, the “John Wayne” and “Pilar completo” techniques were used to blast the pillars and complete de undercut. In 2000 this was changed to a technique based on the use of parallel holes (described in section 2.31).
- The Panel caving with pre-undercut sequence worked quite well until 2003 when an important extraction area was affected by collapse. At the same time, very severe pillar stability problems were observed on the undercut level to the east. This problem made impossible to complete the drilling and blasting of the undercut and the area was labelled as “abandoned”.

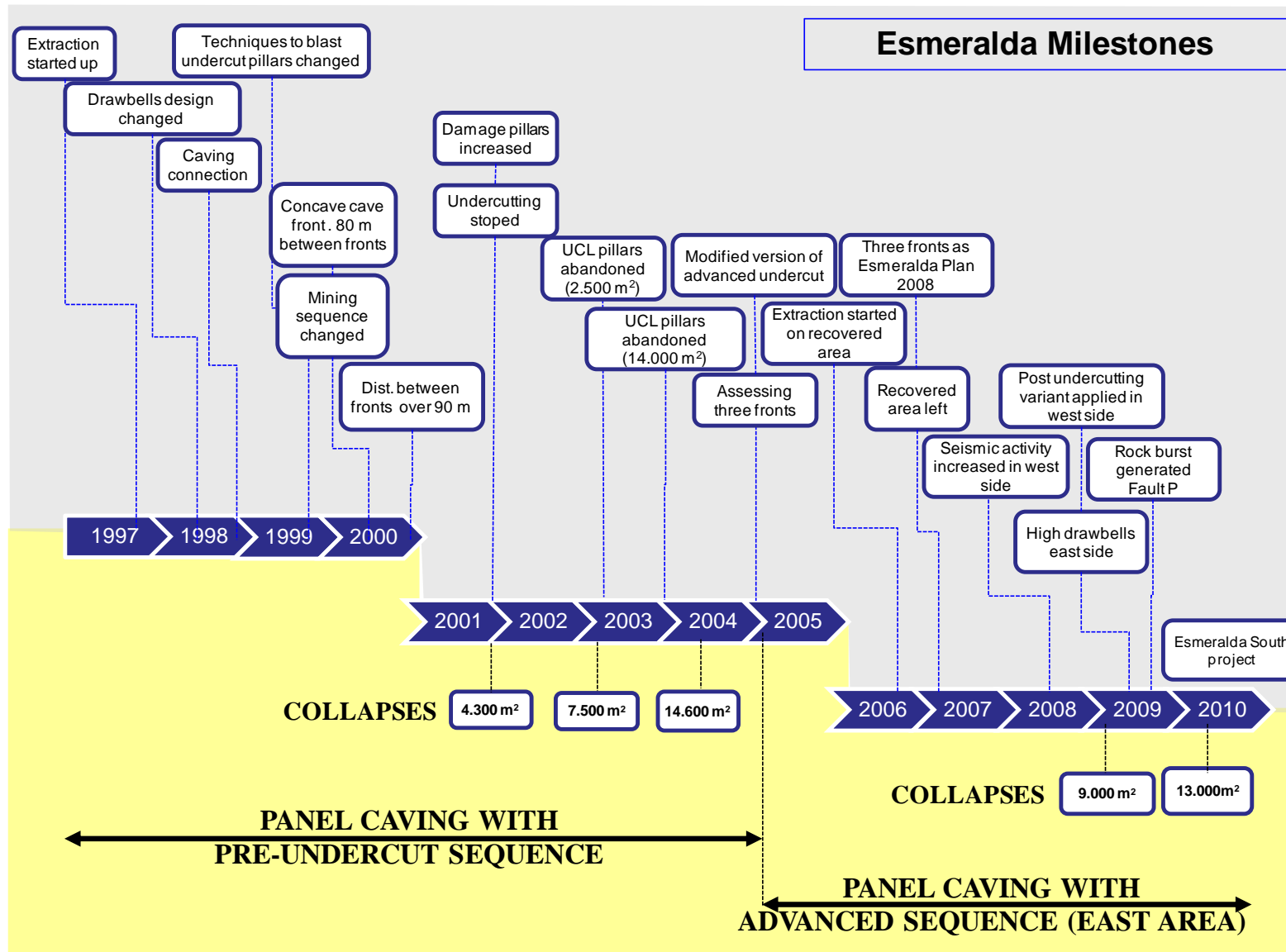


Figure 4.9: The main operational milestones and area affected by collapses for the Esmeralda operation.

- At the beginning of 2005 a modified version of Panel Caving with pre-undercut sequence and advanced developments was applied in the east side of Esmeralda.
- A panel caving with conventional sequence is adopted in the west side
- Finally, between the years 2008 and 2010, a collapse occurrence ahead of undercut front which affected almost the entire cave front at the Esmeralda operation.

#### **4.4.1 The Early Period of Esmeralda Collapses (1997 to 2005)**

Initially, based upon the damage experienced through the whole extraction history of Esmeralda sector, the early period of Esmeralda collapses has been identified between years 2000 till 2005. This period is characterized essentially by a collapse occurrence behind the undercut front and the Panel Caving with pre-undercut sequence as extraction method used.

Based on the information and analysis developed for the problem of collapses in Esmeralda operation during this period (Molina and Catalano, 2002; Celis and Rubio, 2003; Karzulovic et al., 2003 and Rojas et al., 2005), is possible to summarize the sequence of the main events associated to the stability condition in the sector as follows;

1999:

- The first damage signs were observed in the undercutting level, as well as the presence of remnant pillars to the east of drift C19. The location of these remnant pillars are shown in Figure 4.10.

2001:

- In January it was concluded that the draw bells had a 40% delay to achieve a 30% column extraction.
- Between April and August a number of a rock bursts damaged the undercut level. Seismicity increased and reached the elevation in Level Ten 5, expanding further to the north compared to the undercutting level.
- In September the presence of more remnant pillars in the sector was detected. In addition, some damage was observed in drift C23 of Production level. By the end of this month the roof has descended 0.5 meters in the intersection drift C23/ draw bell drift Z8.

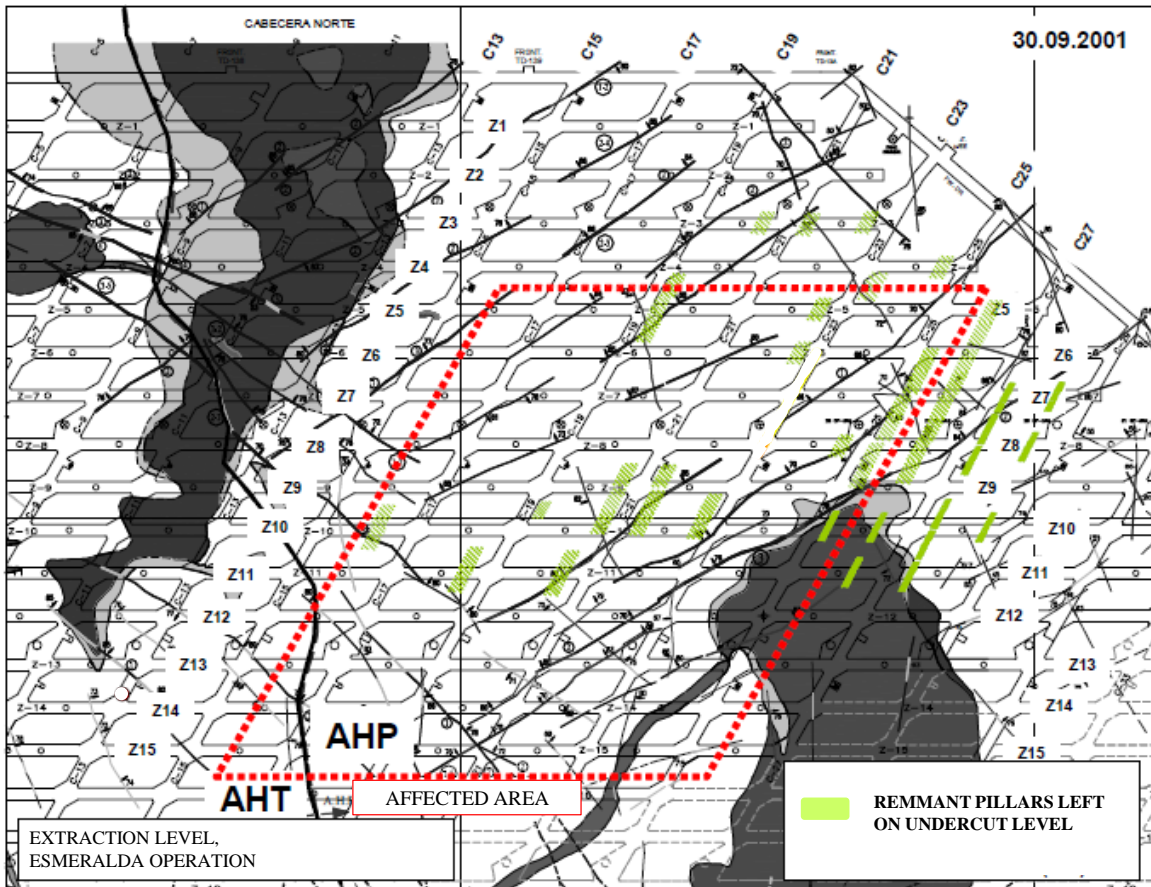


**Figure 4.10:** Location of Remnant pillars left on undercut level period 1999 to 2001.

- In November an increase in damage in the Ventilation Sublevel was detected. There was a significant increase of damage in the Production Level, which affected mainly drifts C17, C19 and C21. A 180 tons block fell on intersection drift C17/ draw bell drift Z23. See Figure 4.11.
- In December there was a collapse of drifts C17 and C19, between draw bell drifts Z11 and Z13 in the production level.
- Evolution of damage along with the mining condition associated during 2001 can be seen in the sequence of figures 4.12 to 4.17.



**Figure 4.11:** Collapse of block affecting the roof of intersection C17/Z13, Production Level, Esmeralda Sector (view from Z13 to the North, from Karzulovic, 2003b).

2002:

- In January the roof of drift C23 decreased greater than 1 m obstructing the way for equipment.
- In March a collapse in drift C23 occurred, between draw bell drifts Z6 and Z10.
- In April a block fell on intersection drift C23/ draw bell drift Z7.
- During the year 2002 some recovery works in collapsed drifts were developed, recovering 100% of drift C19, 80% of drift C17 and 70% of drift C 23.
- A summary of the damage evolution along with the mining condition associated during 2002 could be seen in the sequence of Figures 4.18 a 4.20

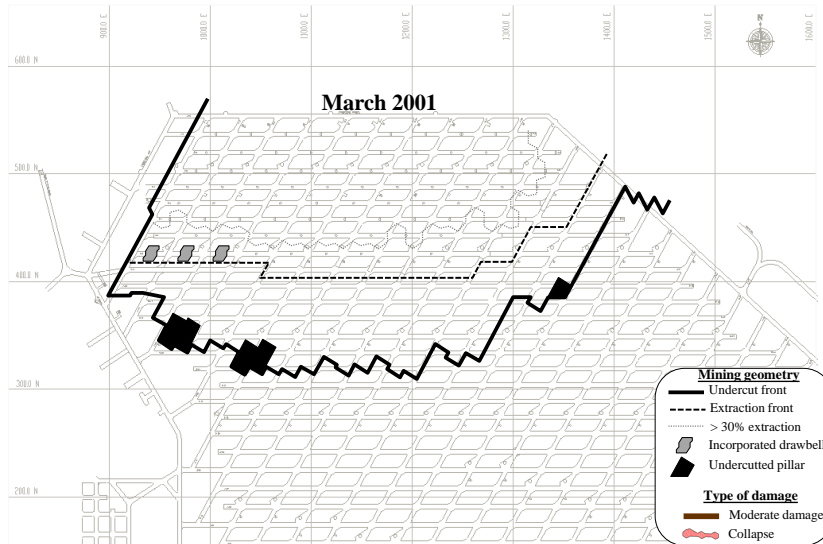


Figure 4.12: Mining geometry and damage experienced on Esmeralda operation – March 2001.

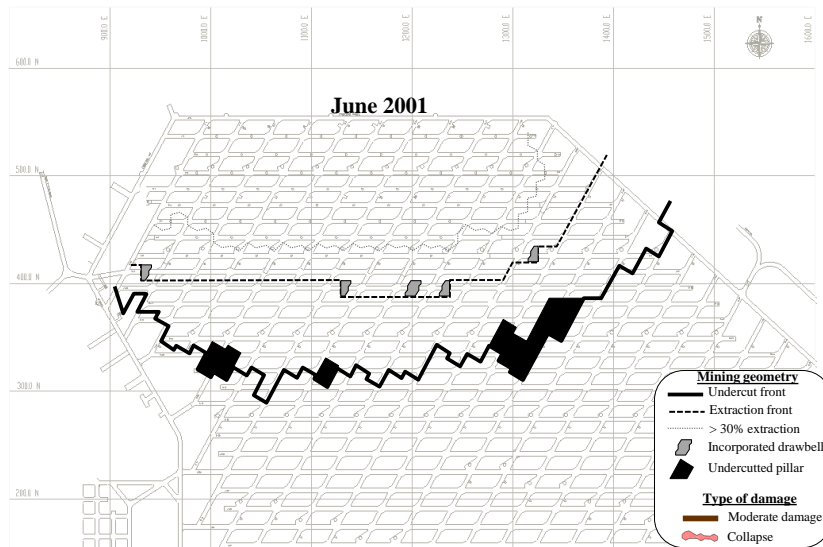


Figure 4.13: Mining geometry and damage experienced on Esmeralda operation – June 2001.

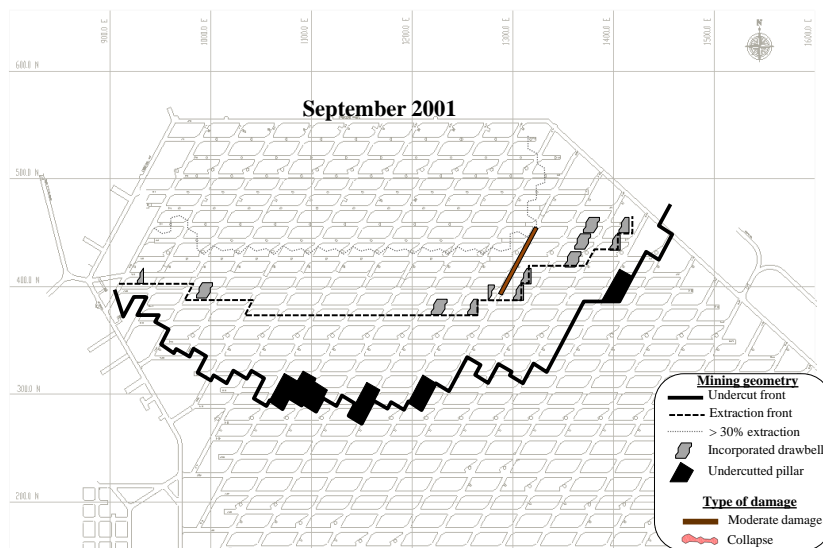


Figure 4.14: Mining geometry and damage experienced on Esmeralda operation – Sept. 2001.

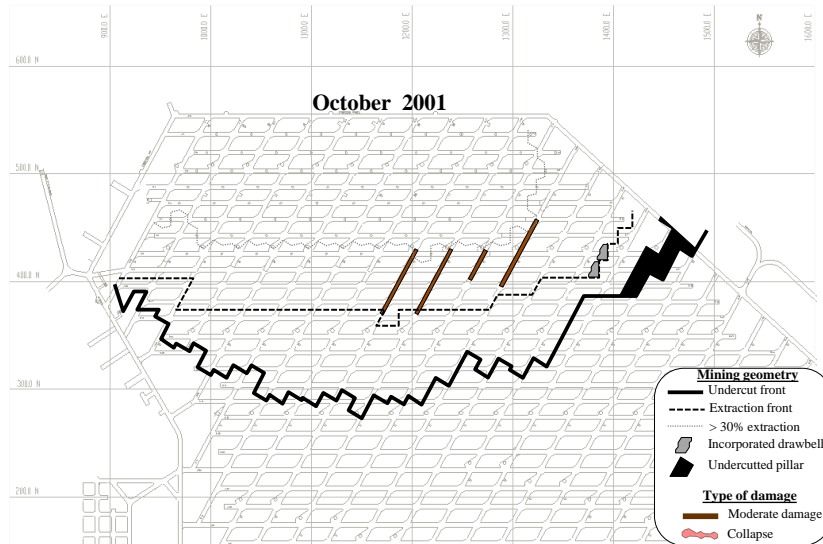


Figure 4.15: Mining geometry and damage experienced on Esmeralda operation – Oct. 2001.

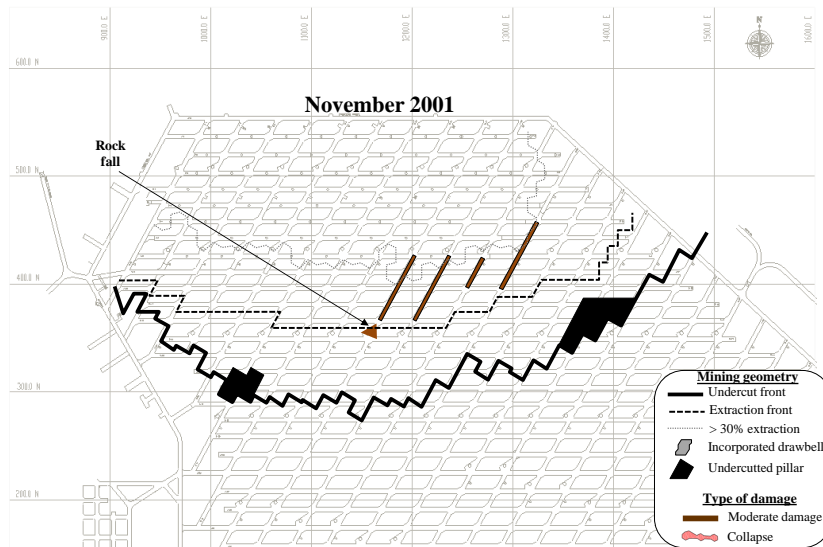


Figure 4.16: Mining geometry and damage experienced on Esmeralda operation – Nov.. 2001.

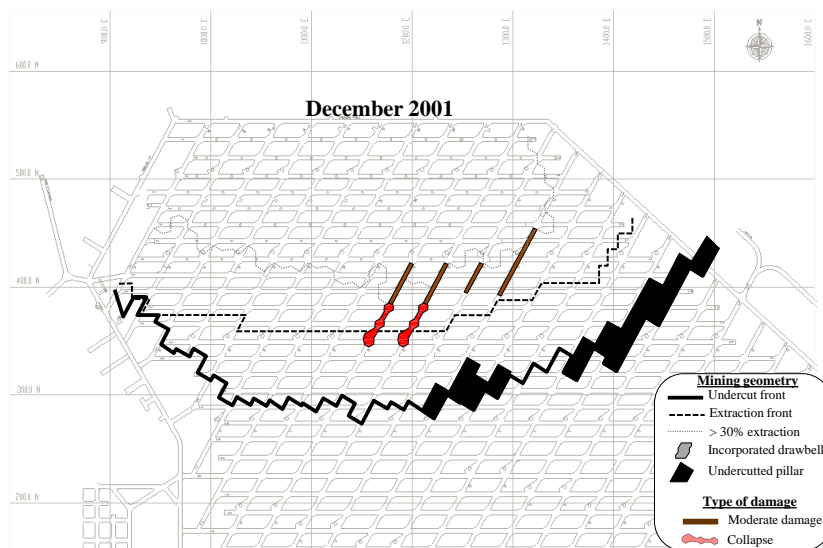


Figure 4.17: Mining geometry and damage experienced on Esmeralda operation – Dec. 2001.

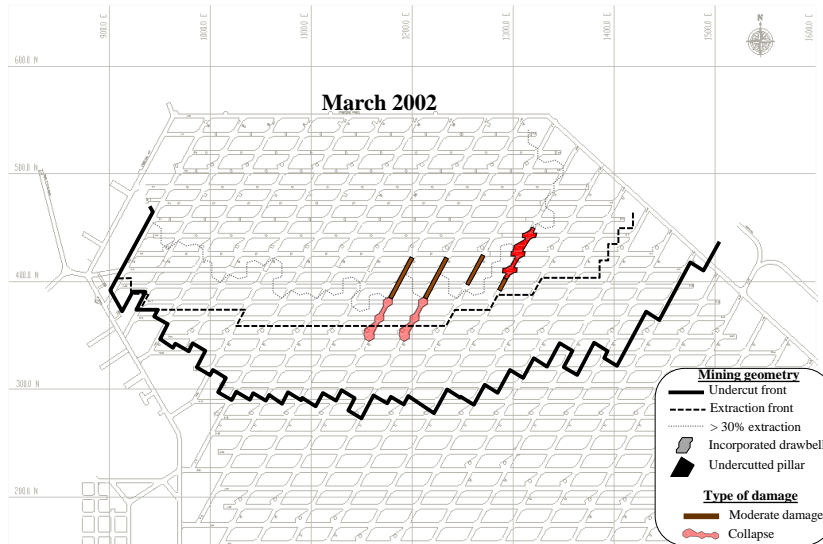


Figure 4.18: Mining geometry and damage experienced on Esmeralda operation – March 2002.

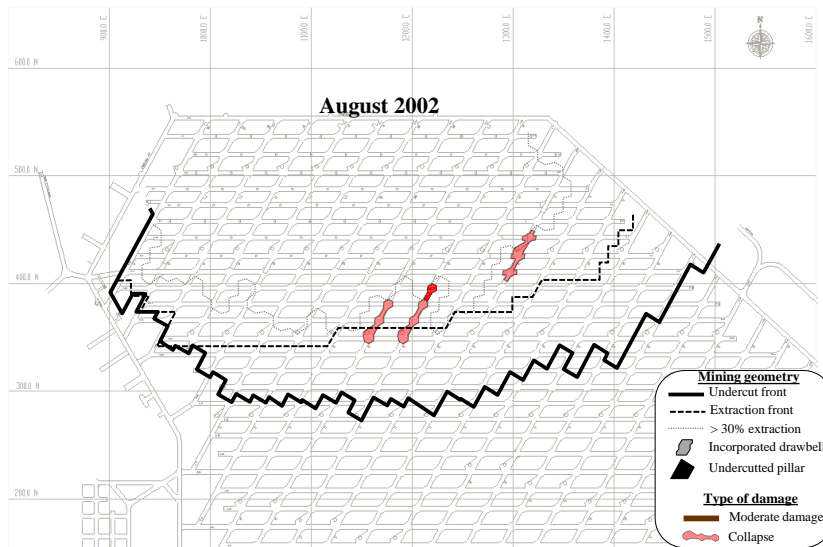


Figure 4.19: Mining geometry and damage experienced on Esmeralda operation – Aug. 2002.

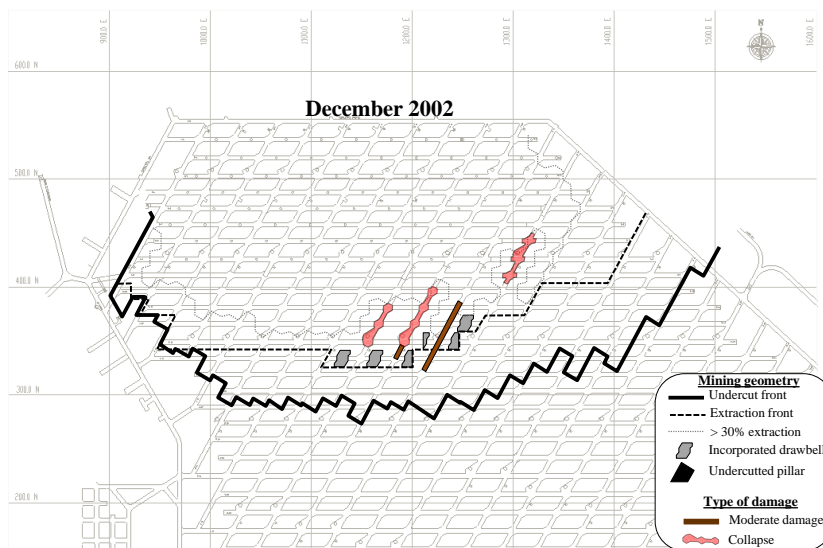


Figure 4.20: Mining geometry and damage experienced on Esmeralda operation – Dec. 2002.

2003:

- In January there was a collapse of drift C21, between draw bell drifts Z12 and Z15 in the production level.
- In April there was a collapse of drift C23, between draw bell drifts Z12 and Z15 in the production level. See representative damages in Figures 4.21 and 4.22.
- There was an accelerated incorporation with poor connection between draw bells during the breaking process from both ends and later closure of extraction ahead of the collapse zone.
- Different authors (Rojas et al., 2005 and Karzulovic, 2003b) suggested that there was inadequate coordination between the preparation and construction work ahead of the collapsed zone and the activities associated to re-hauling of ore.
- Operational interferences generated deficiencies in mining preparation performance.
- Undercutting of pillars was done before completing the closure of incorporation ahead of the collapsed zone, which generated an increase in the distance between extraction and undercut fronts (March 2003).
- An abandonment of pillars was decided following a strong to severe damage in drifts- in the sector between drifts C25 and C29 immediately north of access cross-cut XC-2. These abandoned pillars were located above the damaged drifts in the production level.
- A summary of the evolution of damage along with the mining condition associated during 2003 can be seen in sequence of Figures 4.23 a 4.25.



**Figure 4.21:** Important damage in the pillars of drift C23 with trench Z12, Production Level, Esmeralda Sector.



**Figure 4.22:** Initial deformation of the external steel arc of the extraction point C23/Z12, Production Level, Esmeralda Sector.

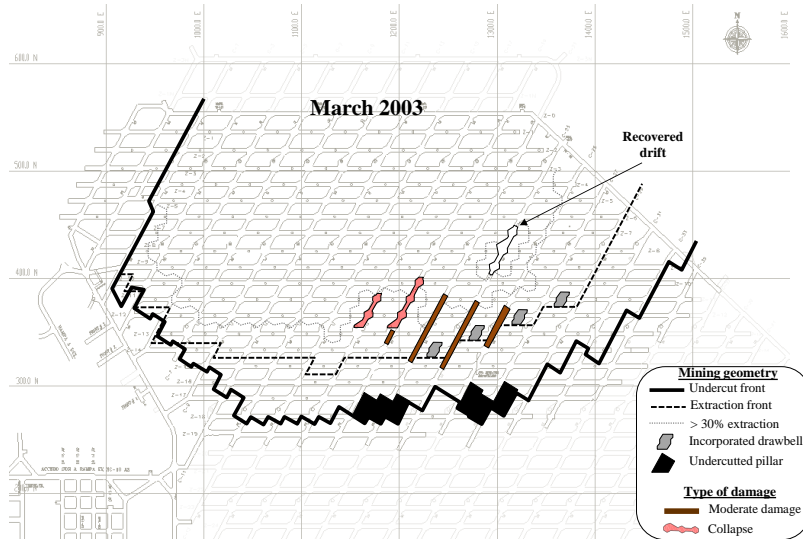


Figure 4.23: Mining geometry and damage experienced on Esmeralda operation – March 2003.

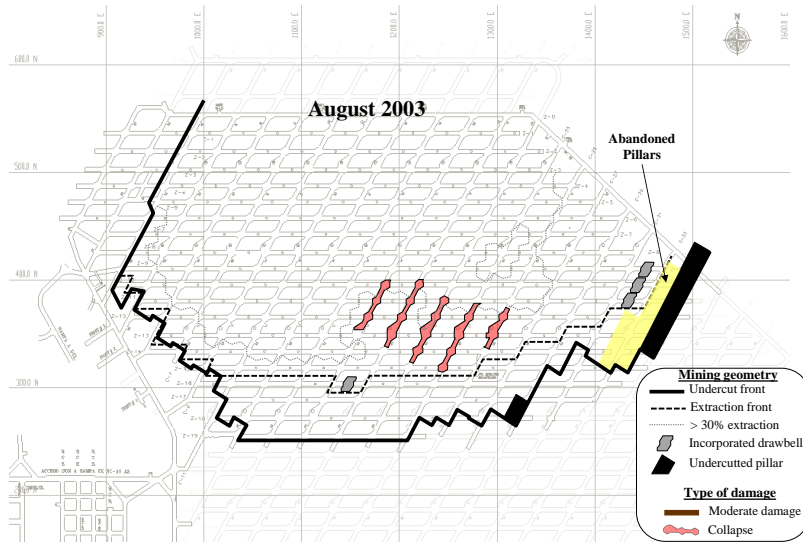


Figure 4.24: Mining geometry and damage experienced on Esmeralda operation – Aug. 2003.

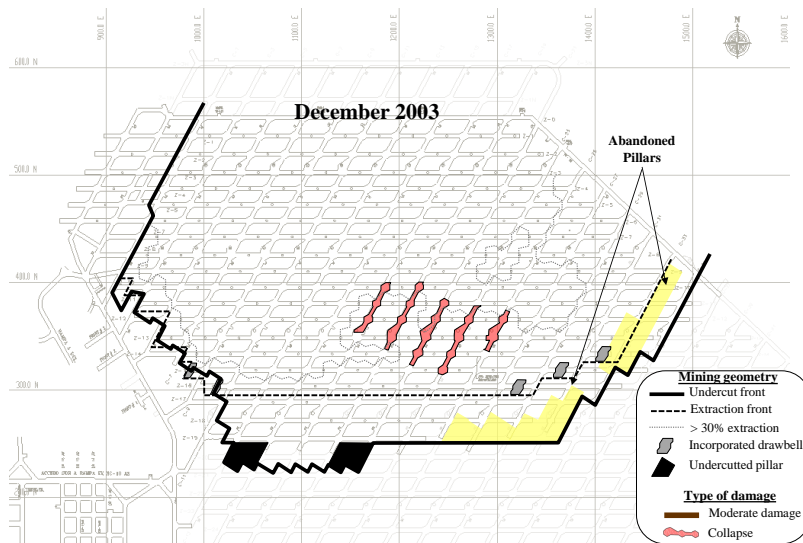


Figure 4.25: Mining geometry and damage experienced on Esmeralda operation – Dec. 2003.

2004:

- Rojas et al. (2005) suggested that the collapse generated during 2004 is different from the ones occurred in the period 2002 – 2003, as there is a zone without presence of damage which separated them. The collapsed zone corresponded to developments excavated in the abutment stress zone.
- The zone collapsed was located below the area damaged by rock bursts occurred on August 2002.
- Part of the evidenced collapse involves the sectors affected by the rock burst occurred on February 17, 2004 (See Figure 4.26).
- The sector with damage in the production level between drifts C17 and C29, draw bell drifts Z17 to Z19, experienced a concentration of remnant pillars in the undercut level.
- There were deficiencies in the connection between draw bells, mainly in the line of draw bell drift Z18 due to the loss of blast holes caused by deterioration of the rock mass in the sector. See representative condition in Figure 4.26
- A total of 80% of the extraction points collapsed in the production level having less than 10% column extraction.
- The total area collapsed during 2004 was 14,600 m<sup>2</sup>.
- An example of damage along with mining condition associated during 2004 can be seen in the sequence of Figures 4.27 to 4.29.



**Figure 4.26:** Representative damage in drift C19, Production Level, Esmeralda Sector.

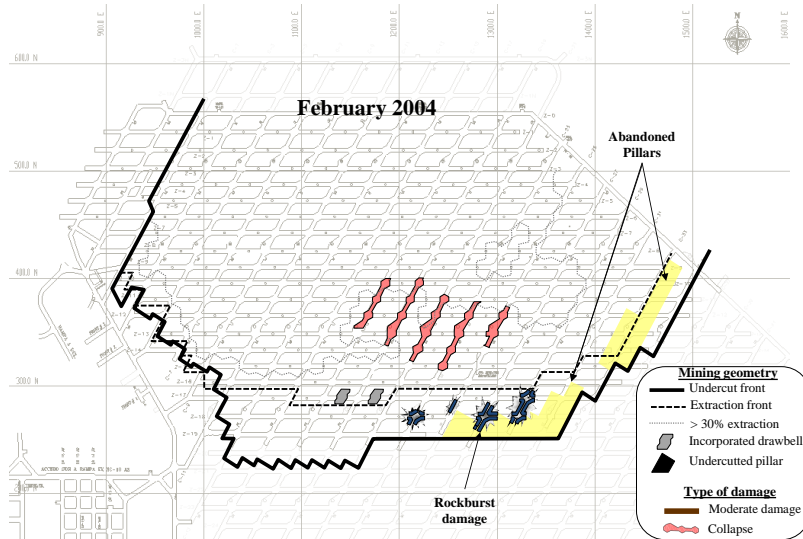


Figure 4.27: Mining geometry and damage experienced on Esmeralda operation – Feb. 2004.

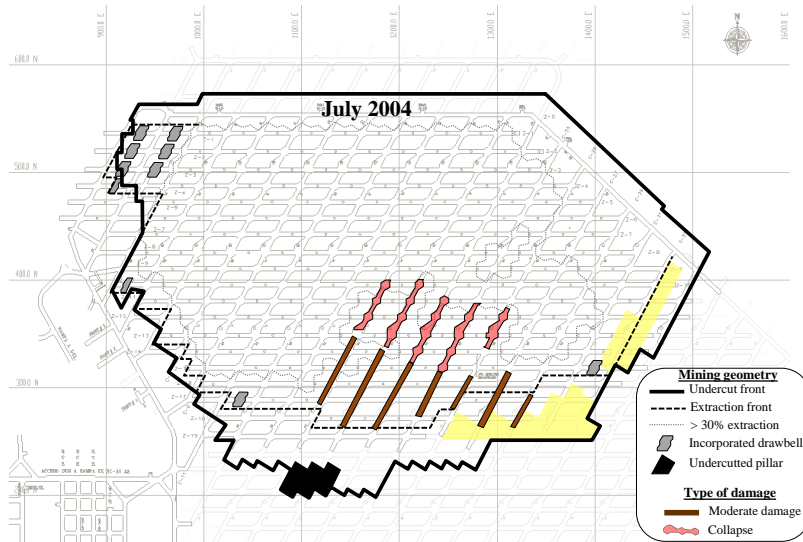


Figure 4.28: Mining geometry and damage experienced on Esmeralda operation – Jul. 2004.

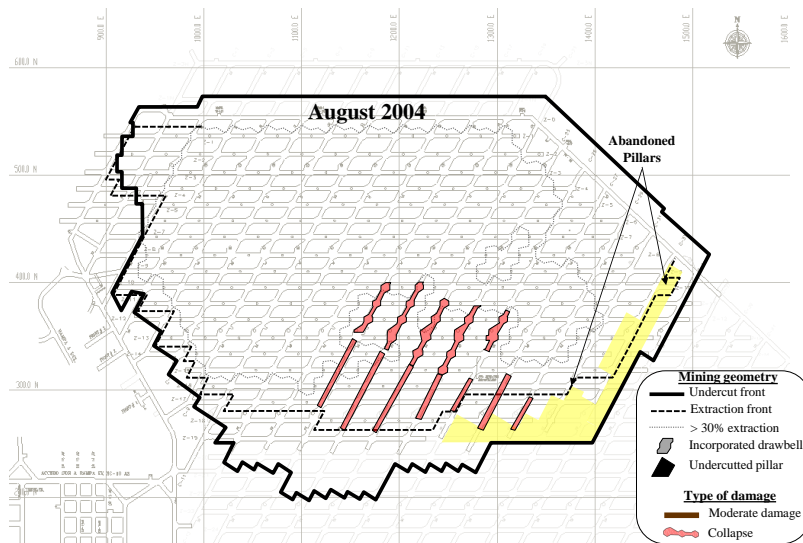
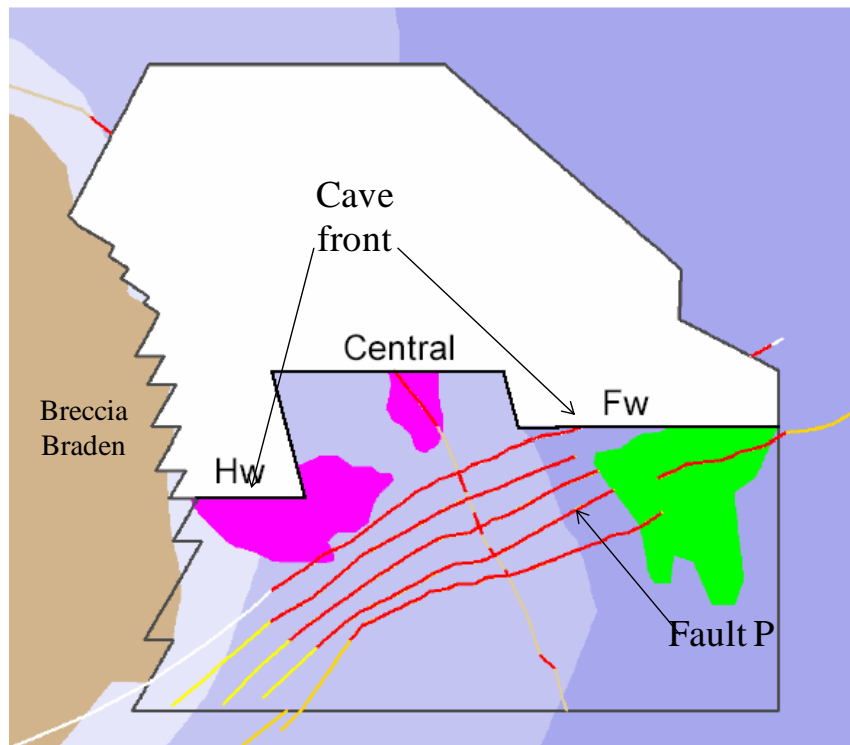


Figure 4.29: Mining geometry and damage experienced on Esmeralda operation – Aug. 2004.

#### 4.4.2 The Later Period of Esmeralda Collapses (2006 to 2010)

Unfortunately, throughout its lifetime, the sector has been plagued with a series of unfortunate stability problems, which has meant that it has never reached its production potential/expectation (Hustrulid, 2010). The later period of Esmeralda collapses was identified between the 2008 and 2010 years. This period is characterized essentially by collapse occurrence ahead of the undercut front where nearly the entire production front was affected by collapses on the undercut level, the production level or both.

The latest instability event was in June 2010. On that period, the production rate was in the order of 22,000tpd or roughly 15% of the total production from the mine. Hustrulid (2010) pointed out that in 2008, because of the continuous stability problems; it was decided to divide the overall production front into 3 shorter fronts. The thought being that the shorter fronts would provide better control and a better advancing rhythm. The hanging wall and footwall fronts (west and east fronts respectively) would advance first followed by the central front, however this plan was never implemented (See Figure 4.30).



**Figure 4.30:** Sketch for the Esmeralda mine plan year 2007 based on three shorter fronts.

Unfortunately, the hanging wall area of the sector suffered collapses in December 2008/January 2009 and again in December 2009/January 2010. Development was stopped and a detailed planning study is in process to expand the front to the south and to the east. The footwall front had experienced

problems in the past but it has been rehabilitated and was being advanced as planned. Most of the problems were associated with collapses/instabilities occurring behind the undercutting front. As the footwall front approached the P-fault, problems were expected. They have materialized in the form of collapses ahead of the advance undercut. Progress on this front was stopped. This situation forced a reconsideration of the entire action (Hustrulid, 2010).

According with Hustrulid (2010) there was no question that the entire sector was in extremely poor condition around 2010. There were various stability issues of varying magnitude both ahead of and behind the undercut. Parts of the sector experienced similar problems during the mining of Ten-4 (see Figure 4.1) although the causes may or may not have been the same.

Dunlop et al. (2010), Barraza et al. (2010), Hustrulid (2010) and; Seguel and Millan (2009a) have developed analyses of the collapses occurred in Esmeralda Mine during this period. Based on this literature, below there is a description and evolution of the damage recorded in UCL and production level at Esmeralda operation, along with the mining condition associated.

The east zone of Esmeralda incorporated an area by the special methodology of draw bells with high cut design due to severe damage observed in the undercut level, that made impossible to generate undercutting.

During 2009 there were seismic events recorded that caused rock bursts in Fault P (see Figure 2.29), this situation caused the wait of the incorporation of draw bells to extraction and installation of more ground support. Figure 4.31 shows the blasted draw bells, emphasizing the high draw bells blasted during the period 2008. Figure 4.32 shows the incorporation of draw bells during 2009, in sector Fw of Esmeralda Mine. Here, it is possible to see that draw bells between Drifts C43 and C45 and draw bells drifts Z16 to Z18 which were incorporated as draw bells with special design and high cut.

Figures 4.33 to 4.36 show the evolution of the collapsed area in the extraction level during the period 2008 to 2010. It can also be observed the extraction and undercutting faces at the time the collapses were generated along with the main lithological bodies and structural faults.

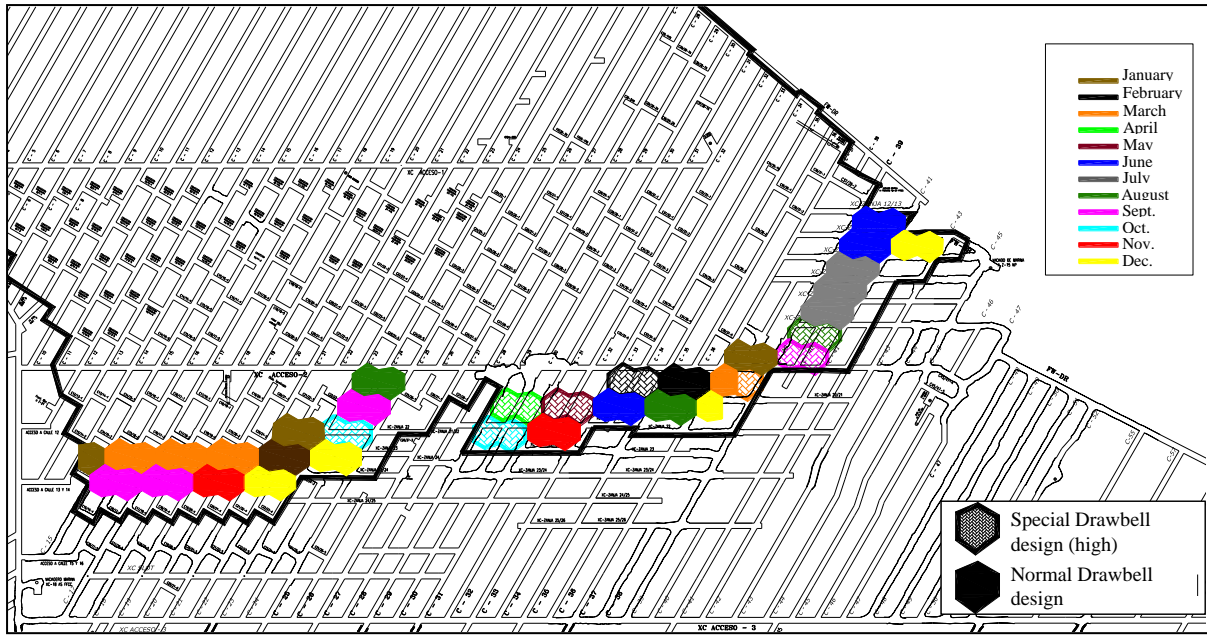


Figure 4.31: Draw bells incorporated at Esmeralda operation during 2008. (Modified from Dunlop et al., 2010).

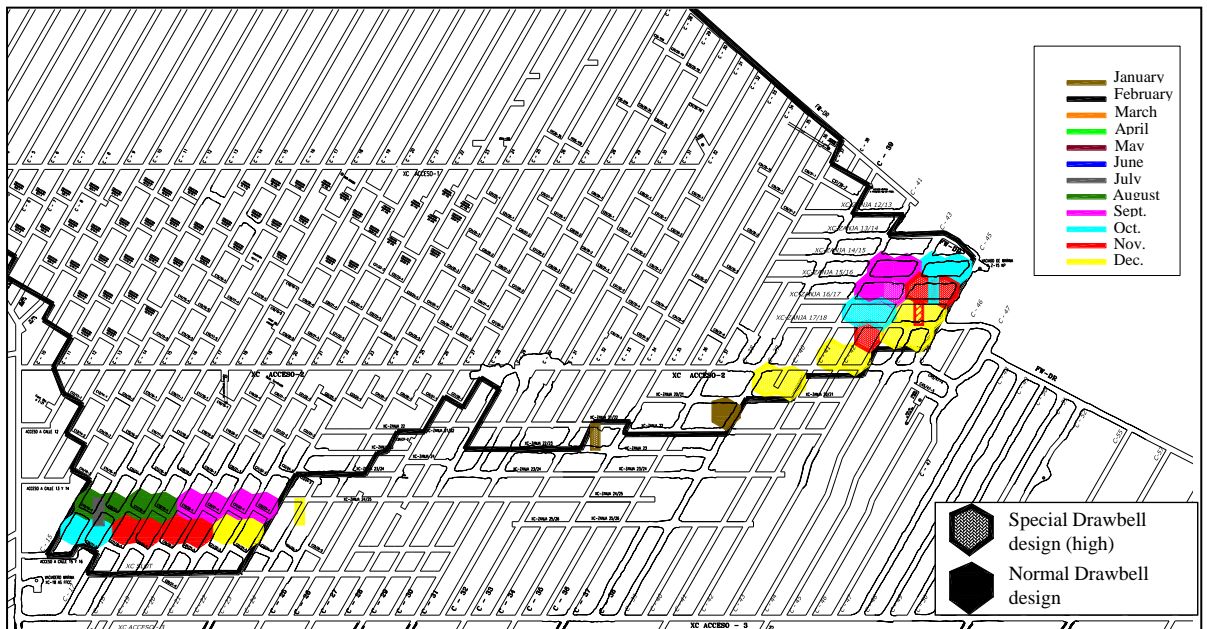


Figure 4.32: Draw bells incorporated at Esmeralda operation during 2009. (Modified from Dunlop et al., 2010).

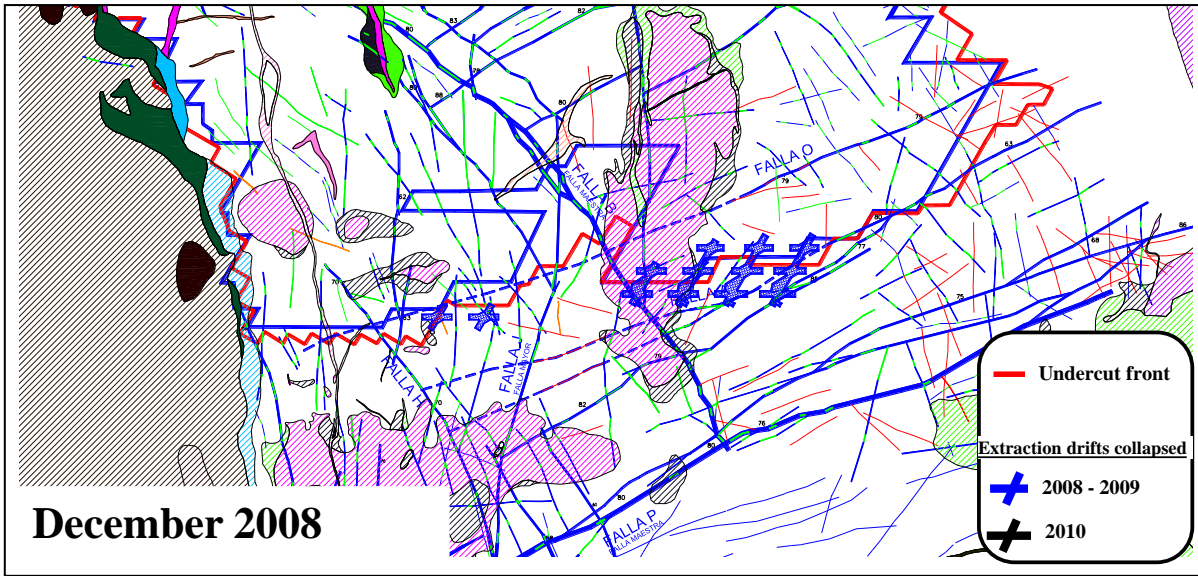


Figure 4.33: Collapsed drifts on extraction level during December 2008.

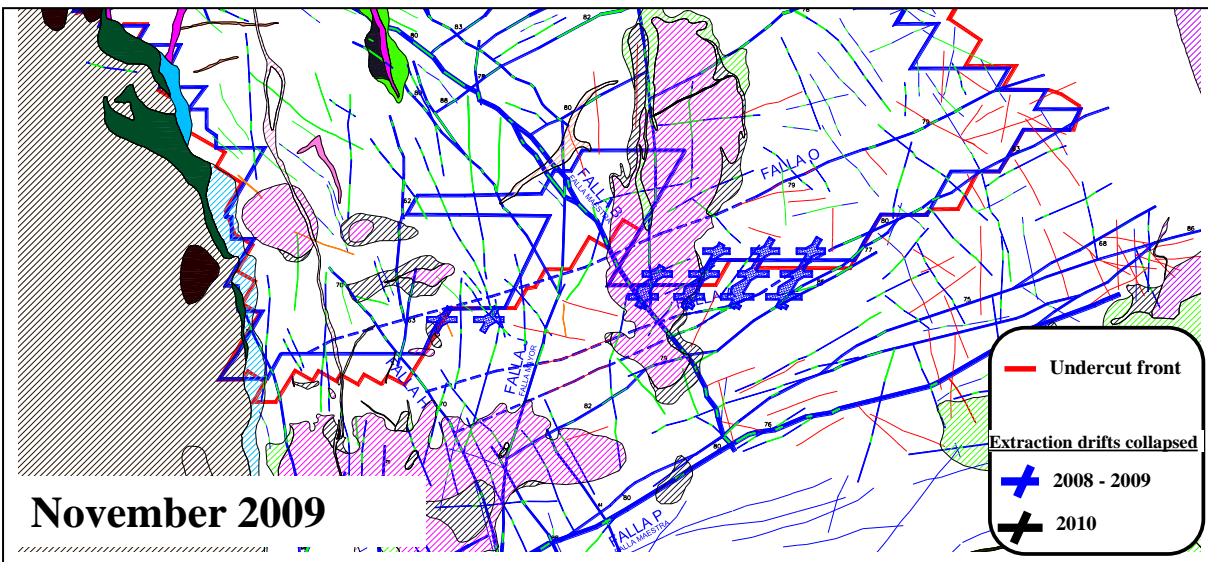


Figure 4.34: Collapsed drifts on extraction level during November 2009.

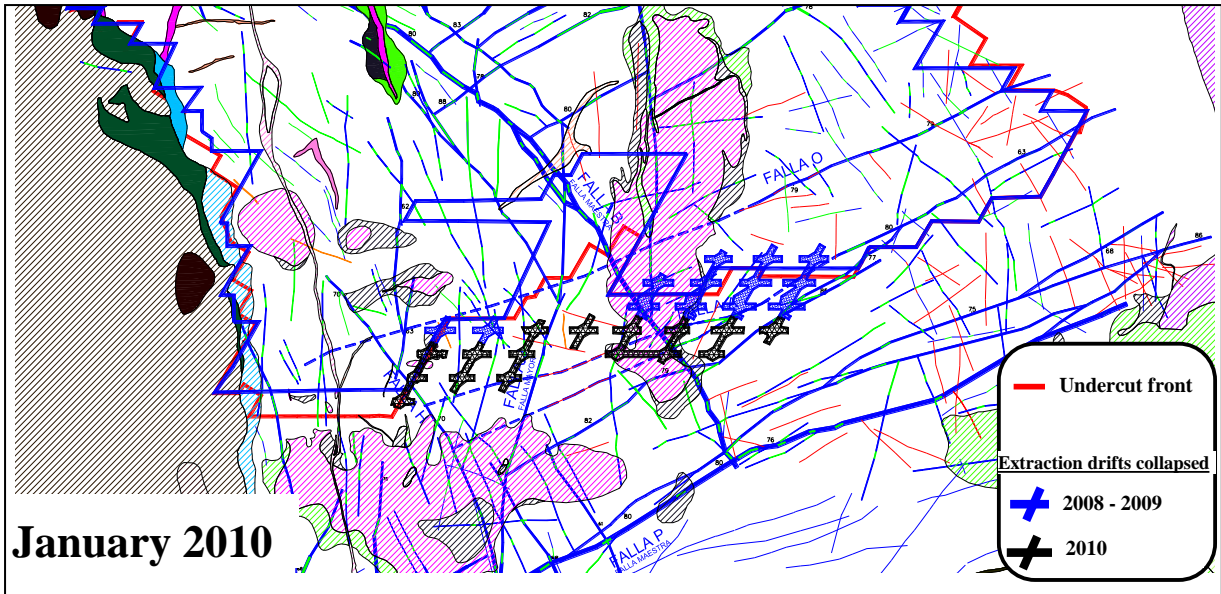


Figure 4.35: Collapsed drifts on extraction level during January 2010.

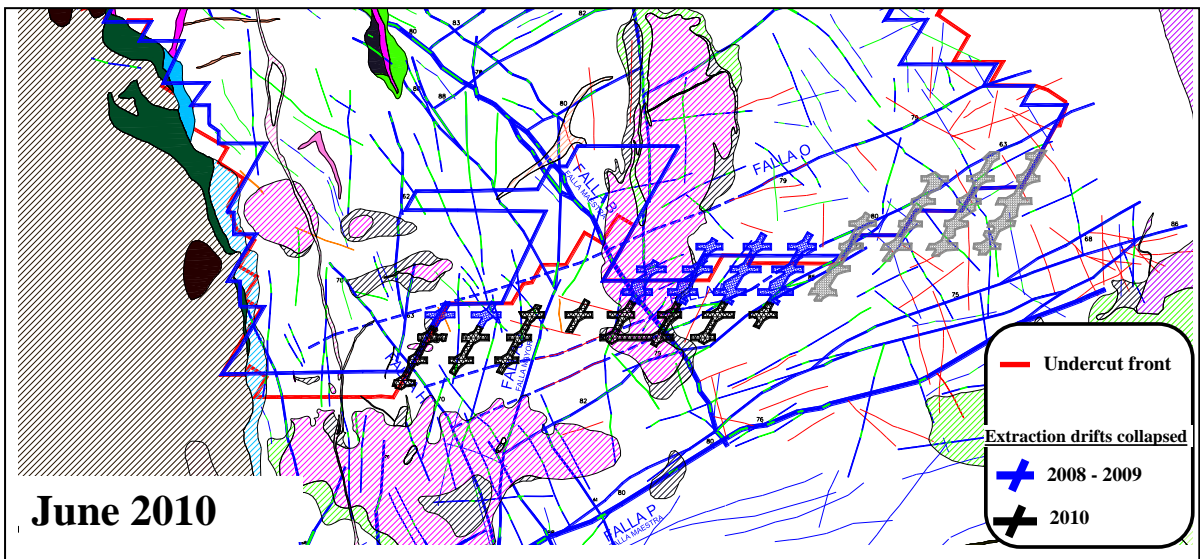
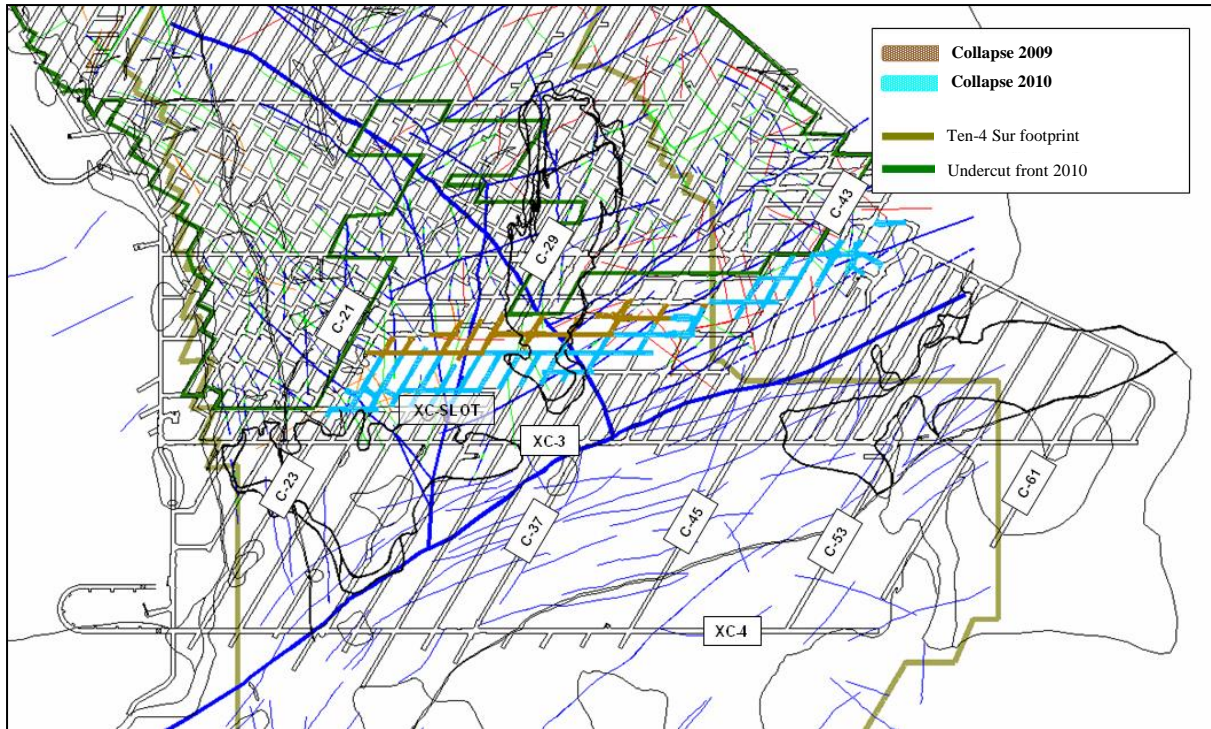


Figure 4.36: Collapsed drifts on extraction level during June 2010.

Additionally, the area declared as collapsed in the undercut level during the last period is shown in Figure 4.37. Barraza et al (2010) emphasized the propagation and expansion of the collapse during the last episode registered in June 2010, which compromised the growth from C-23 to C-47.



**Figure 4.37:** Collapsed drifts on undercut level at Esmeralda operation, years 2009 to 2010 (modified from Barraza et al., 2010).

Once the collapse evolved to June 2010, the record of the global condition of the status of the rock mass ahead of the undercutting face also showed a large damaged extension. Figure 4.38 shows the status of the damage recorded in the undercut level in September 2010. It must be mentioned that the sector Fw, north of XC-3 from drifts C-38 to C-53, represents the greater amount of area compromised by damage in the undercut level and that practically extend to the entire face and more than 70 m ahead of the undercutting face.

The different types of representative damage associated to collapses at Esmeralda operation are shown in the following pictures. First of all, the damage on the UCL can be seen in the Figures 4.39 y 4.40. The representative damage on the UCL in the Hw zone is shown in Figure 4.39 and for the Fw zone in the figure 4.40. Additionally, the damage on the Extraction level is shown in the Figures 4.41, 4.42 and 4.43. So the representative damage for draw points in the Hw zone is shown in Figure 4.41. Figure 4.42 shows the traditional damage on the extraction drifts along to a representative floor heave in the Fw zone, and finally, the damage evolution to the wall panel in C-43 (Fw zone) is represented by three photos taken during June and July on 2010 in Figure 4.43.

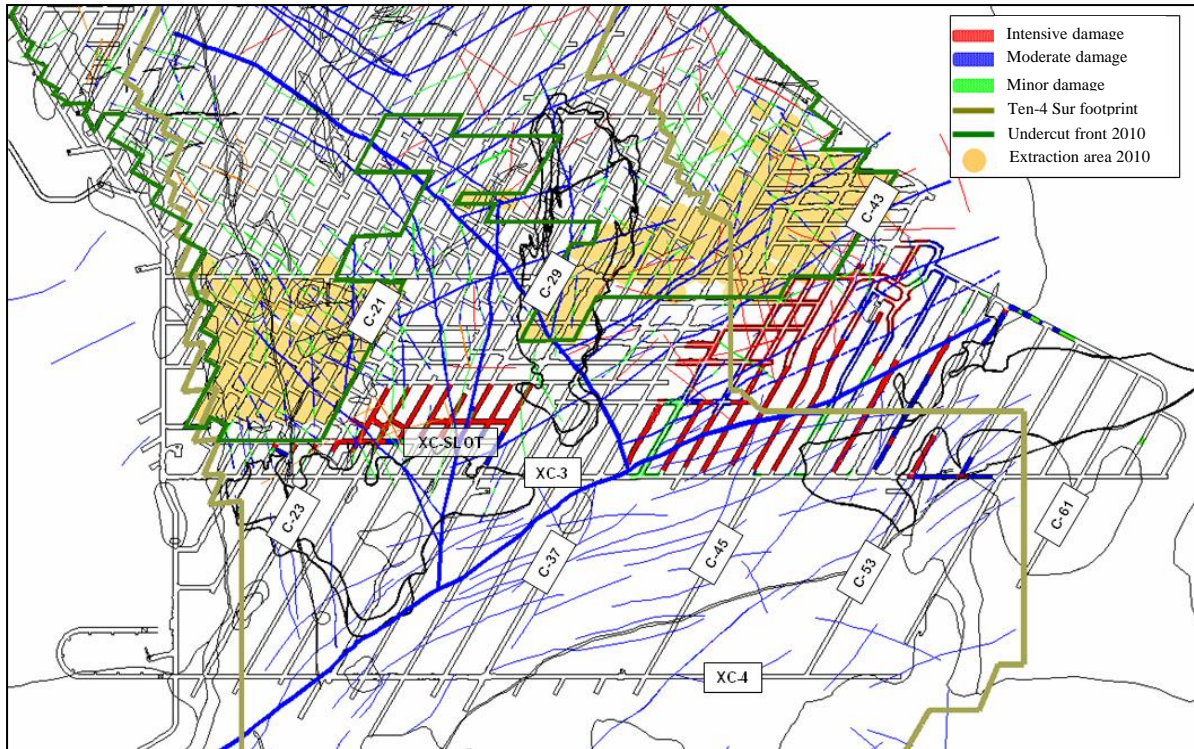


**Figure 4.38:** Extent of damaged drifts to the undercut level at Esmeralda operation (modified from Barraza et al., 2010).



**Figure 4.39:** Damage to C-25 as seen looking north from the XC slot (from Hustrulid et al., 2010).



**Figure 4.40:** Damage to connection between C-43 –C42 as seen looking towards the Hw.



**Figure 4.41:** Damage to draw point C-23 and Z-25.

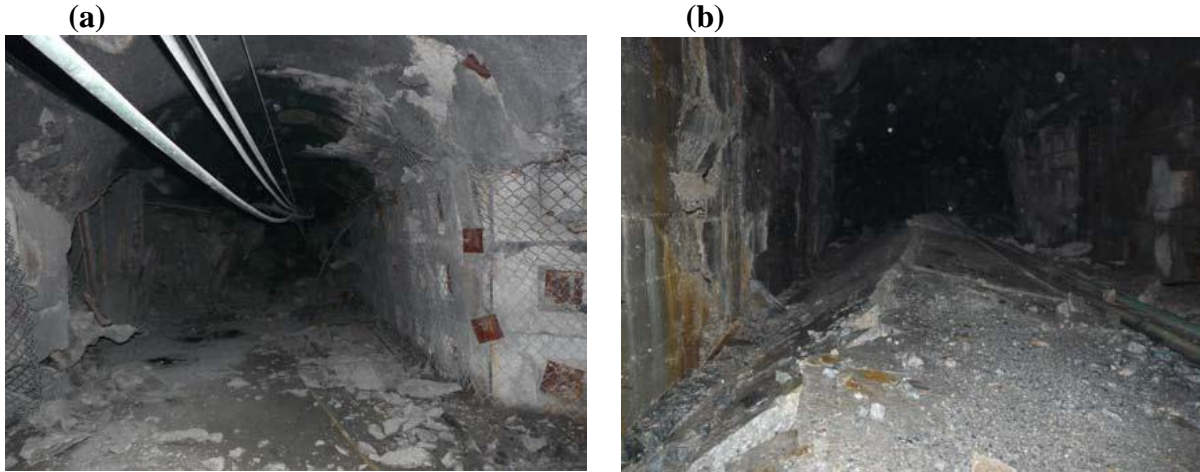


**Figure 4.42:** (a) Damage to C-45 as seen looking north from Z-21. (b) Floor heave and other damage to C-45. Looking to the south from Z-15.

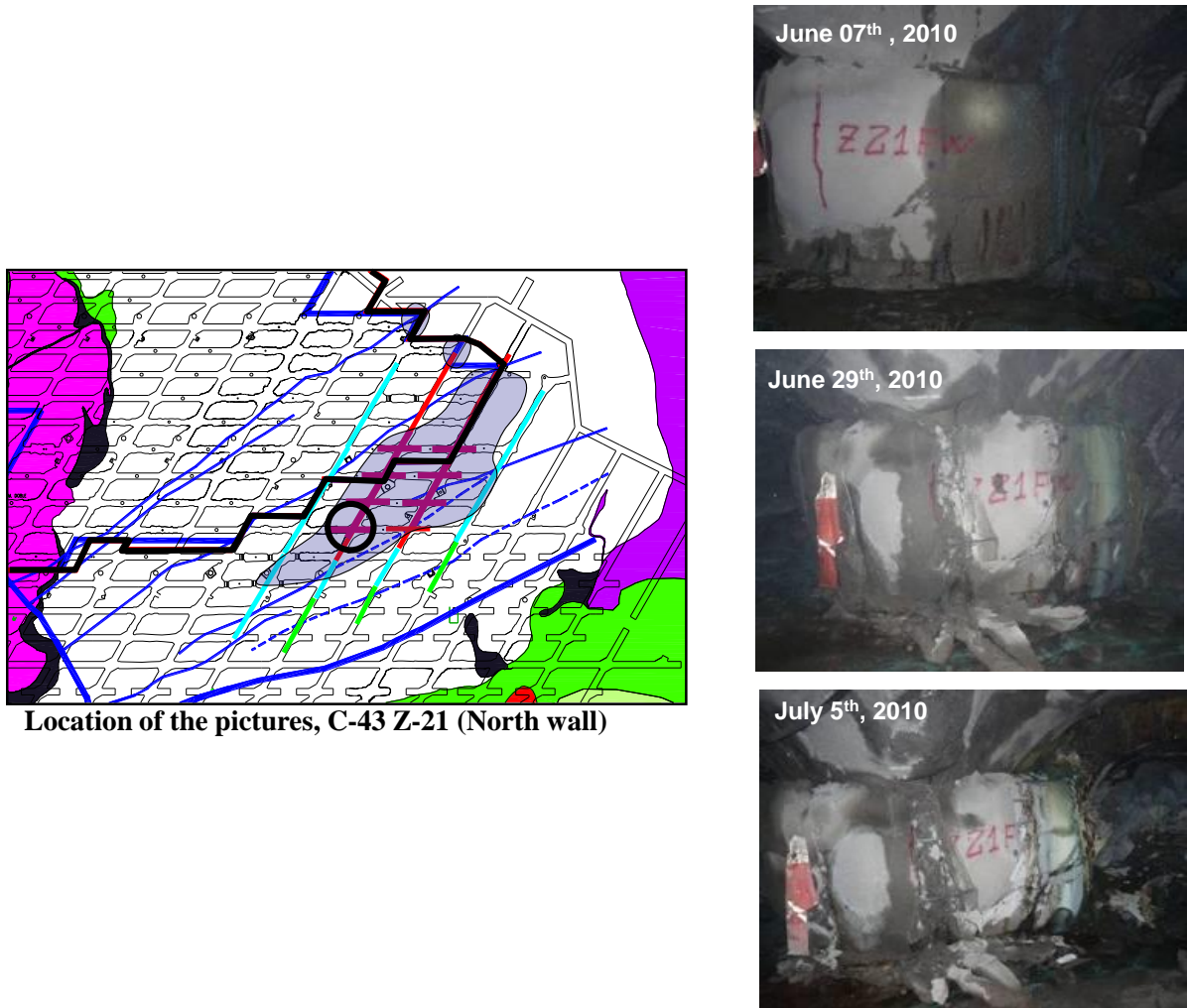


**Figure 4.43:** Changed records of damage with time to the wall panels in C-43 (Modified from Dunlop et al., 2010)

#### 4.5 CONSEQUENCES OF EXPERIENCED COLLAPSES

A direct and generic consequence of the collapse phenomenon in El Teniente Mine (regardless of the analysis period) is the reduction of production area due to lost accesses and no extraction of reserves as per the mining plan. This has happened during all events previously analysed in this study.

“Direct” economic costs are translated into:

- Loss of infrastructure.
- Costs of operational interference due to partial loss of a production sector.
- Loss due to non-extraction of ore committed.
- Costs of extracting ore through contingency projects that support the extraction of reserves as per the mining plan.

However, local and particular impacts associated to each period identified of the collapse phenomenon (early and later period) were identified. Therefore, for the period between 2001 and 2004, where finally 26,000m<sup>2</sup> of the area in the production level were affected by collapses, Rojas et al (2005) concluded that the sector complied with the flow of ore committed in the project, but delayed incorporation of the area. Up to 2004 there was an accumulative deficit of 60,000 m<sup>2</sup> (equivalent to two years), which has been stressed by the loss of area due to collapses and equivalent to 11.6 Mt (millions of tonnes) of reserves. A consequence of this was the inability to comply with production goals (45,000 tons/day) in 2005, with a trend to decreased future production capacity due to the deficit of broken reserves affecting future projections. To reduce the deficit in production contingency projects called Extension Hw (2003) and North Extension were implemented (2004).

Rojas (2013) estimated that economic impact due only to interferences and repairs during the period between 2001 and 2003 was approximately MUS\$ 20. For the period between 2003 and 2004 the estimated economic impact due to deviation from mining plan and additional investment per contingency project exceeded MUS\$ 50.

Regarding the last period characterized by the presence of collapses (later period 2008 – 2010), it can be said that this new instability situation made impossible to continue growing with the incorporation of the area to production and generated an important decrease of broken reserves for the sector, which are the ones sustaining the production commitments. This new process of instability is different from the event recorded between 2001 and 2004, as the damages and loss of infrastructure are located ahead of the extraction face and that makes even more difficult to continue with the current plan (PQ2010). This made necessary to make the decision to declare the loss of this area that makes a total of 30,605 m<sup>2</sup> and therefore defining a new concept of growth for Esmeralda sector through the block growth scheme (Barraza et al., 2010).

A new strategy to face the exploitation of this sector was conceptualized. In this manner the Esmeralda Sur project was originated, which consisted on the incorporation of three exploitation blocks located at approximately 150 m to the south of the area affected by collapses.

Finally, Rojas (2013) estimates that the economic impact due to deviation from the mining plan and the cost of repair associated to period 2008 to 2010 exceeded MUS\$ 50.

.

## **CHAPTER 5**

# **NUMERICAL MODELLING FOR ESMERALDA PANEL CAVING OPERATION**

### **5.1 INTRODUCTION**

During previous chapters it has been shown that geomechanical related intensive damage upon extraction levels is strongly related to the standard operation at any version of panel caving method. Historically, the intensive rock mass damage at El Teniente mine has been associated to the different versions of Block or Panel caving operations. Based on all the reviewed information from the totality of the extraction history of Esmeralda operation, two different collapse mechanisms have been identified and stated as the research hypothesis. Although these assessed collapse mechanisms are based on a large amount of empirical information and observations throughout 15 years of extraction history, a numerical simulation of observed experiences during caving performance at Esmeralda operation was carried out in order to validate and confirm collapse mechanisms mentioned before.

The panel caving design is based on a sound understanding of the potential rock mass failure modes that may de-stabilise excavation performance and in a worst case scenario, also affect part of the extraction level performance. Rock mass failure modes governed by panel caving operations are classified into a combination of failure through the rock mass substance and translation and rotation of rock blocks (Cepuritis 2010). Actually numerical methods represent one of the most important tools of engineer design in order to assess the likely modes of failure incorporating additional complexities. The traditional empirical and analytical methods are complemented by numerical methods to recreate a best simulation of any rock mechanism issue. In addition, they are able to capture the rock reality incorporating a variety of physical or engineering properties, such as effects of in situ and induced stresses, complex excavation geometries, non linear material behaviour, material anisotropy and the influence of complex rock structure (Brady and Brown, 2004).

Modern computational capacity allows for the simulation of realistic displacements and energy release of any mining progresses the use of large three-dimensional numerical models, where detailed geology units, geological structures and the precise description of the stress field are included. Advances in computational efficiency and capacity mean that significant improvement in modelling practice for mines is possible. Perhaps the most significant improvement will come from a move towards calibrated, multi-scale non-linear modelling.

Although the use of large three-dimensional numerical simulation allows improved geomechanical approaches, the practical use of numerical modelling in panel caving mining processes is limited by a number of factors associated with the complex combination of constituents and its long history of

formation of rock masses. This makes it a difficult material for mathematical representation via numerical modelling. Ultimately, the choice of modelling approach is constrained by (Modified from Cepuritis 2010);

- The features of the numerical code and availability of input data.
- The ability of the selected code to adequately model the rock mass characteristics and anticipated rock mass behaviour.
- Complexity of problem geometry – whether the problem geometry can be satisfactorily represented in two dimensions or whether a three-dimensional approach is required.
- The complexity of model construction, general ease of use of modelling package and licensing costs.

The following sections briefly describe some previous numerical modelling for different operations at El Teniente mine. In addition, the fundamentals and principles approaches of non-linear numerical simulation used in this study are described below. Finally, a current mine scale model was developed to assess the state of stress around excavations, rock mass deformation and energy release extraction during the whole extraction history of the Esmeralda operation.

Given the complex nature of the topic analysed and the requirement of three-dimensional numerical modelling, the decision was made to include external expert modelling services to the development of this research. Thus, Beck Engineering, experts in numerical simulations for rock-mechanics matters, was incorporated. This external expert was commissioned to provide the software and hardware infrastructure and to develop the finite element grid for the geometric problem modelled. Furthermore, the expert support was required to define a constitutive model adequate enough for the conditions that required representation through modelling, prioritizing the numerical representation of the caving process.

## **5.2 A REVIEW OF LINEAR ELASTIC MODELLING USED AT EL TENIENTE MINE**

During the last decade mainly linear elastic simulations have been carried out to model the mining extraction geometries at El Teniente Mine in order to improve the knowledge about rock mass behaviour by panel caving operation. Boundary element codes were essentially used due to their efficiency modelling large areas and easier model building. This type of numerical tool has been used as a complement to solve different geomechanical issues experienced at El Teniente Mine, especially part of intensive rock mass damage experienced at Esmeralda operation during the last period of its extraction life (years 2008 to 2010).

### 5.2.1 Fundamentals of linear elastic modelling

Numerical modelling attempts to simulate from a Mathematical point of view the way the rock mass responds to mining. The numerical methods provide predictions of stresses, strains and displacements based on a combination of 4 essential components: loading conditions, geometry and geology, elasticity and flow rule (Jing and Hudson, 2002). While modelling by itself is reasonably straight forward, it is the interpretation of the modelling results that is the real challenge, looking for the best match between model predictions of stress, strain and displacement and observed behaviour and recorded data.

In addition, numerical modelling achieves simulation by using physical constraints on how the rock mass can respond. First of all, the applied forces must always balance one another at all locations in the model, which is called “equilibrium”. Second, in the rock mass continuum, the mass of material must be maintained, which is called “continuity”. Third, at locations where the stresses do not exceed the strength, the rock deforms in a linear elastic manner, that means stresses varying in direct proportion to the strains. Finally, at locations where the stresses are concentrated to the point where they exceed the strength, the rock will yield to these loads and deform, this is called “non-linearity”. All the equations of equilibrium and continuity are differential equations. This must be solved to integrate them over the rock mass volume such that the appropriate boundary conditions are satisfied. There are many ways of accomplishing this. The most popular three-dimensional BEM codes integrate the equations analytically, and then use a numerical approximation to satisfy the boundary conditions. FEM and FDM packages use a numerical integration scheme to integrate the differential equations (Jing, 2003). Both of these equations constitute a mathematical description of how the rock mass responds. All numerical models use some variation on this approach.

The continuum and discontinuum analysis are the most common methods for mining applications. As a primary approach to predict how the rock mass will respond to mining, the continuum methods tend to be more popular, with the most common three-dimensional BEM codes being Map3D (Wiles, 1993) and Examine3D (Rocscience Inc. 1990). The fundamental choice of continuum over discontinuum approaches can be related to the amount of parameters that control the modelling reliability. In a discontinuum approach there is more uncertainty with the control parameters, even with the faults and joints properties (Jing, 2003).

A key of the rock mass behaviour is to define or quantify the rock mass failure and its behaviour after the failure. First of all, the constitutive behaviour of the material needs to be selected and it provides the relation between stresses and strains that can be sustained by a rock mass.

#### *Constitutive models*

Constitutive relationships range from simple isotropic linear elastic models to anisotropic non-linear inelastic models. Isotropic linear analysis has been carried out to date at the El Teniente Mine. This is due to the fact that only few parameters need to be specified and there has been uncertainty about anisotropic parameters. With this type of modelling the material response can be associated to linear elastically behaviour. Considering, for instance, a bit of rock being loaded, in the early stages of loading the rock behaves more or less elastically. This means that deformations occur without causing any damage to the rock. The rock will spring back “linearly” to its original shape when unloaded and the stress will increase linearly with increasing strain. See Figure 5.1.

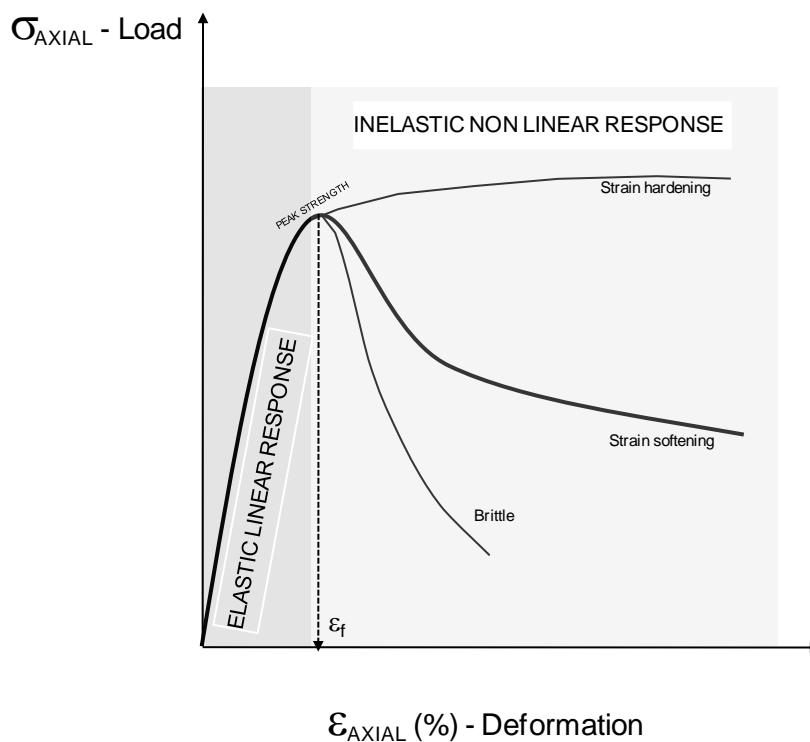


**Figure 5.1:** Rock mass response – constitutive model on stress-strain relationship

At some point the loads increases, so that the rock begins to crack and the deformation is no longer entirely elastic. After unloading, part of the deformation is recoverable due to internal structure damage. This means that a non-linear deformation has occurred.

So, in order to look for the best approach of rock mass behaviour by mining effects, the constitutive model selection is essential as it will govern the scope and reliability of any analysis.

***Rock mass Failure Criteria***

Cepuritis et al. (2010) suggested that for purposes of excavation design using equivalent continuum yield models, the following definitions of “failure” may be used:

- Peak Strength: in terms of static stress-based criteria, peak strength is the ultimate stress level that the rock mass can sustain.
- Yield strain or Critical strain: the point at which the rock mass material is observed to display non-linear behaviour, expressed either in terms of stress or strain.
- Damage: rock mass damage is the irrecoverable static strain. Dynamic strains (i.e. due to blasting etc.) are not considered.

Linear elastic BEM modelling packages such as MAP3D have been commonly used to predict different levels of damage during panel caving operation at El Teniente mine. Wiles (2001) suggests that rock mass damage can be related to linear elastic overstress according to the criterion shown in Figure 5.2. In addition, the facility to use this modelling package and the few number of parameters controlling the analysis, have facilitated its implementation as a planning and prognosis tool.

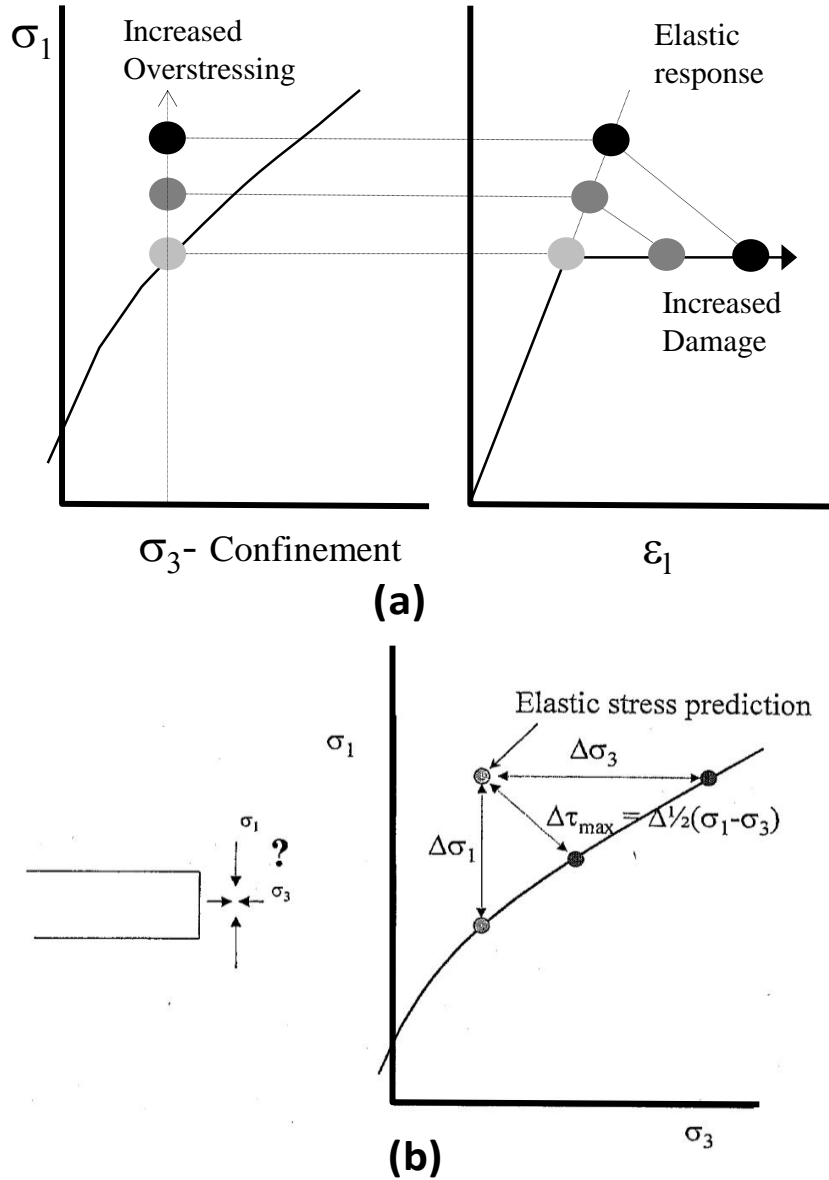


**Figure 5.2:** (a) Relationship between elastic models and damage (Wiles, 2001), (b) showing various stress paths to over-stressing

The results are interpreted assuming that there is correspondence between over-stressing and damage (Figure 5.2). This model anticipates that below the site-specific damage threshold the response is elastic and usually little damage can be observed. As the level of over-stressing increases, the observed damage should increase too. Increased over-stressing beyond this level leads to driven failures and eventually rock mass may become unsupportable.

Wiles (2001) suggests that this methodology could be incorporated into a back analysis technique to assist in quantitative mine design. This criterion could be useful in order to assist in mine planning activities, as numerical modelling can then be used to identify the potential damage zone extent for different mining configurations.

The main assumption with this “damage criterion” is that there is a direct relationship between the amount of observed damage and the amount of over-stressing. Although this criterion has some limitations when applied in areas where loss of confinement causes the change in the loading conditions that trigger the failure, it could achieve a proper adjustment when the rock damage is caused by increases of the major principal stress.

***Reliability using linear elastic modelling***

Back analysis using numerical modelling is more efficient than using empirical methods. It could be argued that the back analysis procedure quantifies the reliability of the entire predictive system rather than any of its individual components (Wiles, 2006). For linear elastic analysis, Wiles (2006) suggests using the coefficient of variation around the line of best fit for Mohr-Coulomb rock mass strength envelope (equation 5.1) as a measure of reliability.

$$\sigma_1 = B + q\sigma_3 \tag{5.1}$$

In this case, the distance from any stress point to the best-fit line for a linear criterion is given by:

$$\Delta\sigma_1 = \sigma_1 - B - q\sigma_3 \tag{5.2}$$

where  $\Delta\sigma_1$  is positive above the line and negative below the line (see figure 5.3)

The standard deviation for the back analysis data points for  $\sigma_1$  and  $\sigma_3$  can be written:

$$s_1 = \sqrt{\sum (\sigma_1 - \bar{\sigma}_1)^2 / (n - 1)} \tag{5.3}$$

$$s_3 = \sqrt{\sum (\sigma_3 - \bar{\sigma}_3)^2 / (n - 1)} \tag{5.4}$$

where  $\bar{\sigma}_1$  and  $\bar{\sigma}_3$  represent the mean values of  $\sigma_1$  and  $\sigma_3$  and n represents the number of back analysis points. The combined standard deviation can be written:

$$s = \sqrt{(s_1^2 - q^2 s_3^2)(n - 1) / (n - 2)} \tag{5.5}$$

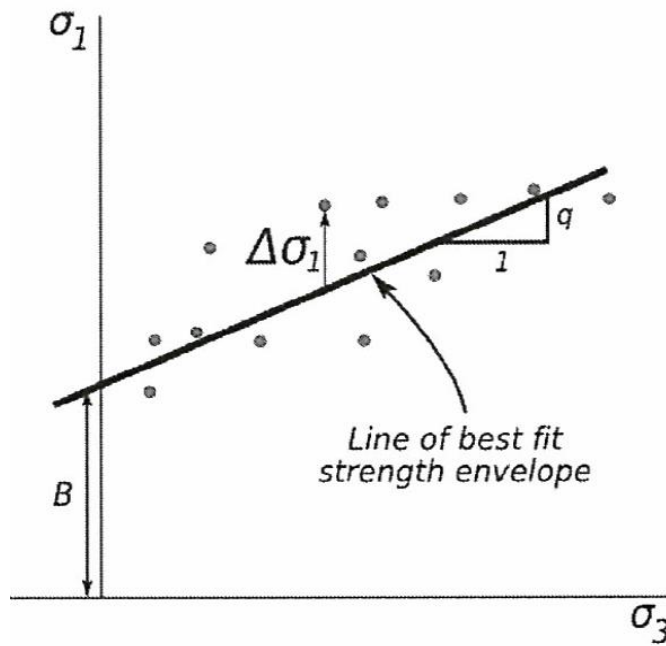


**Figure 5.3:** Reliability level for linear elastic analysis (modified from Wiles, 2006)

With the coefficient of variation for the predictive system defined by:

$$C_v = \frac{s}{\bar{\sigma}_1} \quad (5.6)$$

The variation coefficient can be used to establish the reliability of the criteria. If values are assumed to follow a normal distribution, then confidence intervals around the mean can be established (Wiles, 2006). Wiles (2006) also suggests that if the variation coefficient is large (greater than 30%), then alternative approaches may need to be adopted.

Wiles (2006) suggests that some sources of variability in back analysis may include, but not limited to:

- Incorrect pre-mining stress state orientation or stress ratio assumptions
- Geometric construction errors in the model between actual and modelled geometries
- Chaotic rock mass behaviour
- Role of large scale geological features
- Significant rock mass strength heterogeneity across the study area.

The elastic techniques seem to be an attractive tool to evaluate design criteria reliability; however, there are some aspects that must to be considered. Because of the limitations of linear elastic modelling, a rock mass can be over-stressed beyond a damage threshold line and without knowing the damage threshold in advance, the precise degree of over-stressing is unknown.

### 5.2.2 Summary of the main models previously used at El Teniente operations

Diagnosis was carried out for Esmeralda operation in relation to intensive and large rock mass damage (Rojas et al. 2005). The studies have been conducted to characterise the observed intensive rock mass damage and its causes. Furthermore, simple numerical analysis were developed evaluating different proposed mining alternatives in the medium and long term horizon.

Different authors between 2006 and 2010 carried out these studies. They applied numerical techniques through two and three dimensional analysis, applying different evaluation criteria and, for the first time at El Teniente mine, a Map3D (linear elastic boundary code) model was carried out. All of them were focused to the main geotechnical issue of large intensive rock mass damage at the Esmeralda operation.

The following points include a brief summary for each one of these projects:

- a. Karzulovic (2006a) developed a geomechanical evaluation for the different proposed mining alternatives in the Esmeralda Sector. Based on a previous internal analysis about pillar stabilities and the large-scale stability condition at the Esmeralda Sector, Karzulovic (2006a) analysed the advance of the Esmeralda extraction geometry to the Southern front by means of exploitation of three different cave fronts that were considered independent at that time. The study was carried out using two-dimensional numerical analysis FEM code with the software Phases2D. Karzulovic (2006a) suggested that the best chance would be to divide the large front into three independent fronts matching the geological and geotechnical conditions in the Esmeralda Sector. Sensitivity analysis with undercut front sizes and faults effects were performed. Finally, the study suggested that the best option is the simultaneous advance of the Western and Eastern fronts, delaying a central advance front.
- b. Villegas and Landeros (2007) developed a geomechanical approach for intensive rock mass damage at the Esmeralda operation. The analysis considered an evaluation criterion similar to Karzulovic (2006a); however the most important comparative difference in relation to previous analysis was that a Map3D numerical analysis (linear elastic boundary element code) was performed for the first time. A three dimensional model was developed in order to represent the Esmeralda geometries. A large-scale model was conceived to provide a general idea about stress conditions around the mine scale geometry (see Figure 5.4). This study analysed different future extraction geometries for Esmeralda. Cave fronts disconnected were modelled and stress measurements and observed damages were used for calibration purposes. This study attempted to create the best match between observed behaviour and recorded data. Finally, the study discussed the potential extent of the damage zone for each of the sequences analysed. An advance strategy was recommended considering the distances between the different fronts (Eastern, Central and Western).

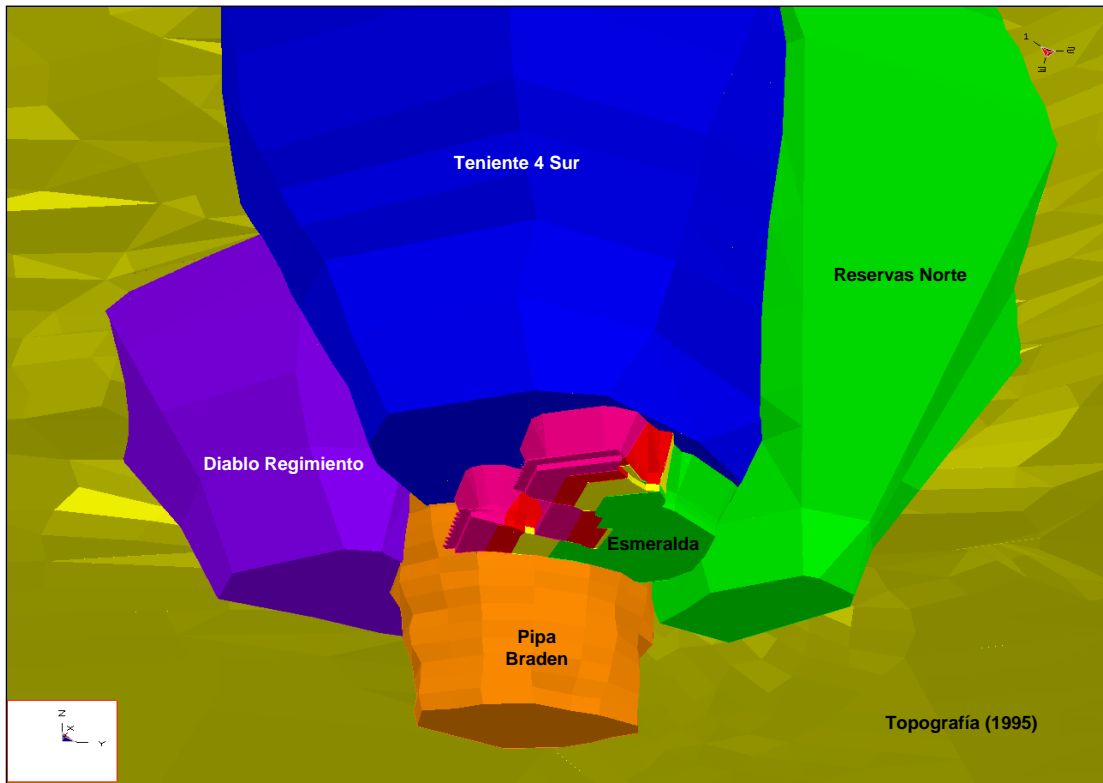


**Figure 5.4:** General view of large-scale 3D input geometry for Map3D Modelling.

- c. Landeros and Pardo (2008). The large-scale model geometry was updated and some calibrations were carried out with emphasis on the Reservas Norte and Pilar Norte Sectors. For the first time in the Teniente model, explicit galleries were included. Due to including galleries in the Reservas Norte sector, the match between observed damage ahead of undercut front and the over-stressing model results was improved (see figure 5.5). The reliability of the model, mainly in the Northern area of the deposit, was improved. However, the geometry in the Esmeralda sector was not updated and no new sensibility analysis was carried out. Although the improvements were not done at the Esmeralda operation, the reliability of the global model was evident and, therefore, some mining sequence decisions were taken based on the model results.

As a summary, the next table 5.1 shows the main features for the majority of models described previously.

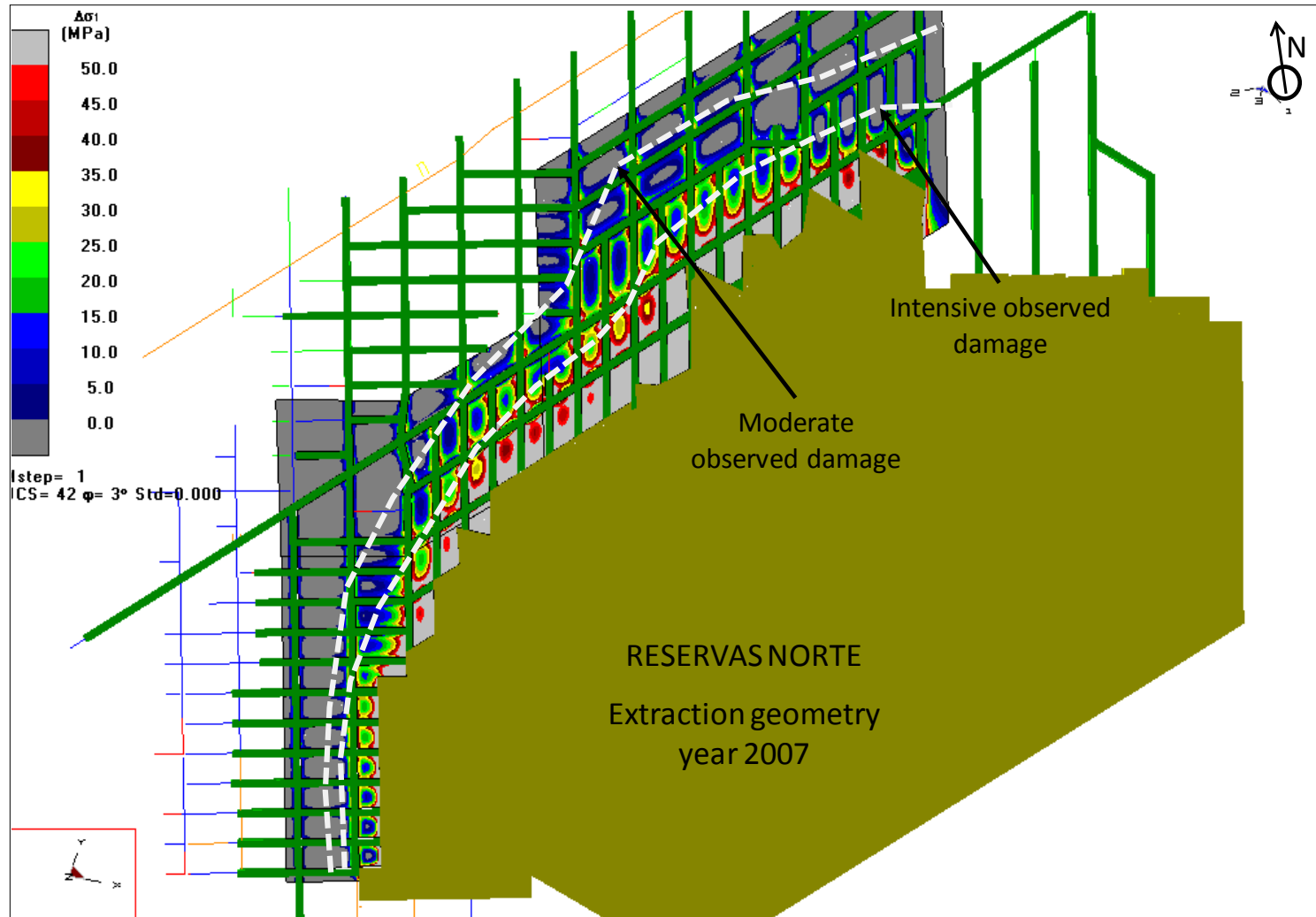


**Figure 5.5:** Over-stressing distribution ahead of the undercut front from model with explicit galleries in the Reservas Norte Sector.

Chapter 5: Numerical Modelling for Esmeralda Panel Caving Operation

Year	Type of Modelling	Objectives	Mining Geometry used	Type of Calibration	Main Results	Conclusions and Recommendations	Limitations	Author
2006	<i>Linear and nonlinear 2-dimensional finite element analysis. (Phases<sup>2D</sup>)</i>	<ul style="list-style-type: none"> <li>• Feasibility study in order to evaluate different sequence options for the Esmeralda Southern advance.</li> <li>• To compare three fronts alternative versus original case of unique front.</li> <li>• To evaluate effect on main geological faults.</li> </ul>	<p>Considered use of one general Esmeralda plan view section and five cross sections across Esmeralda.</p> <p>Different mining sequences according with the three front options.</p> <p>Geometries since year 2006 until year 2028.</p>	<p>The study doesn't describe a formal calibration method.</p> <p>The study just makes a relationship between model abutment stress results ahead of cave front with observational records in Undercut pillars.</p>	<ul style="list-style-type: none"> <li>• Sensibility analysis for width of central front.</li> <li>• Values for abutments stress</li> <li>• Yield zones for sequences advances</li> <li>• Stress distributions over main faults</li> </ul>	<ul style="list-style-type: none"> <li>• To divide the unique front into three independent fronts. It allows a better match to geological-geotechnical conditions in Esmeralda.</li> <li>• The study recommends that the Western front goes ahead of the others and the Central front goes delayed.</li> <li>• The width of Central front must be bigger than 240 m.</li> </ul>	<ul style="list-style-type: none"> <li>• The study doesn't apply a systematically calibration method.</li> <li>• Bi-dimensional numerical analysis may lead to biased results.</li> </ul>	Karzulovic et al. (2006)
2007	<i>3-dimensional linear elastic boundary element analysis (Map3D)</i>	<ul style="list-style-type: none"> <li>• To evaluate the effects of the stress distribution effect due to disconnected fronts in Esmeralda</li> <li>• To carry out a back analysis based on observational damage records and modelling results.</li> </ul>	<p>The main cavities at El Teniente mine are modelled.</p> <p>The Breccia Braden and CMET are considered as geotechnical units</p> <p>The caving geometries for Esmeralda were modelled yearly from 2001 to 2004 to carry out back analysis. Afterwards, the planned geometries for Esmeralda are modelled from 2008 to 2014.</p>	<p>Validation process through matches between modelled stress state and conventional stress measurements.</p> <p>Damage criterion is found by selecting the minor and major principal stresses at the boundaries where damage was recorded during the years 2001 to 2004.</p>	<ul style="list-style-type: none"> <li>• Selective damage criteria are found for Western, Central and Eastern front. They are applied as prognosis in mining geometries from 2008 to 2014.</li> <li>• Stress distributions and risk zones are identified in Haulage and ventilation levels.</li> </ul>	<ul style="list-style-type: none"> <li>• The Central front must start where the Eastern front is located 70 m ahead and the Western front is located 150 m ahead.</li> <li>• The major damage vulnerability zone is evidenced ahead of the Central front. (Central part of Esmeralda).</li> <li>• Potential damage zones are identified in the level located below the production level.</li> <li>• The main conclusion of previous analysis about the disconnect front are confirmed</li> </ul>	<ul style="list-style-type: none"> <li>• Elastic assumption negates the possibility of modelling post-peak behaviour of rock.</li> <li>• Does not include explicit main faults neither their effects.</li> <li>• Only considers two geotechnical units, breccia Braden and CMET.</li> <li>• Without explicit galleries</li> </ul>	Landeros and Villegas (2007)
2008	<i>3-dimensional linear elastic boundary element analysis (Map3D)</i>	<ul style="list-style-type: none"> <li>• To improve the large scale model geometry</li> <li>• To improve the calibration criteria towards the Northern sectors.</li> </ul>	<p>The main cavities at El Teniente mine are modelled with emphasis on the Northern sectors.</p> <p>The caving geometries for Reservas Norte are modelled to carry out a back analysis including explicit drives in Undercut and Production levels.</p>	<p>Validation process through matches between modelled stress state and conventional stress measurements.</p> <p>Damage criterion is found by selecting the minor and major principal stresses at the boundaries where damage was recorded</p>	<ul style="list-style-type: none"> <li>• Improve the matches between the damage criterion and the mapped damage at Reservas Norte.</li> <li>• Improve the large scale model reliability; therefore the accuracy of stress distribution in Esmeralda Sector is better.</li> </ul>	<ul style="list-style-type: none"> <li>• A better prediction damage criterion is developed for the Esmeralda Central front. It is based on improved general modelling.</li> </ul>	<ul style="list-style-type: none"> <li>• Elastic assumption negates the possibility of modelling post-peak behaviour of rock.</li> <li>• Does not include explicit main faults neither their effects.</li> <li>• Only considers two geotechnical units, breccia Braden and CMET.</li> <li>• Without explicit drives in Esmeralda Sector.</li> </ul>	Landeros and Pardo (2008)

**Table 5.1:** Main features of previous numerical modelling developed for El Teniente operations

### 5.2.3 Linear elastic analysis for intensive rock mass damage on the later period of extraction history at the Esmeralda operation

After 2008, a new philosophy behind numerical modelling strategy was applied for all the new numerical developments on any El Teniente operation geometry to be modelled. It was based on creating evidence through calibrated models. The aim was to create a model providing the best match between observed behaviour and recorded data. Once, the numerical model showed a satisfactory match between numerical results and observed and recorded data, the model could then be used as a geotechnical-planning tool. A summary of this strategy can be seen in Figure 5.6. (Pardo and Landeros, 2008).

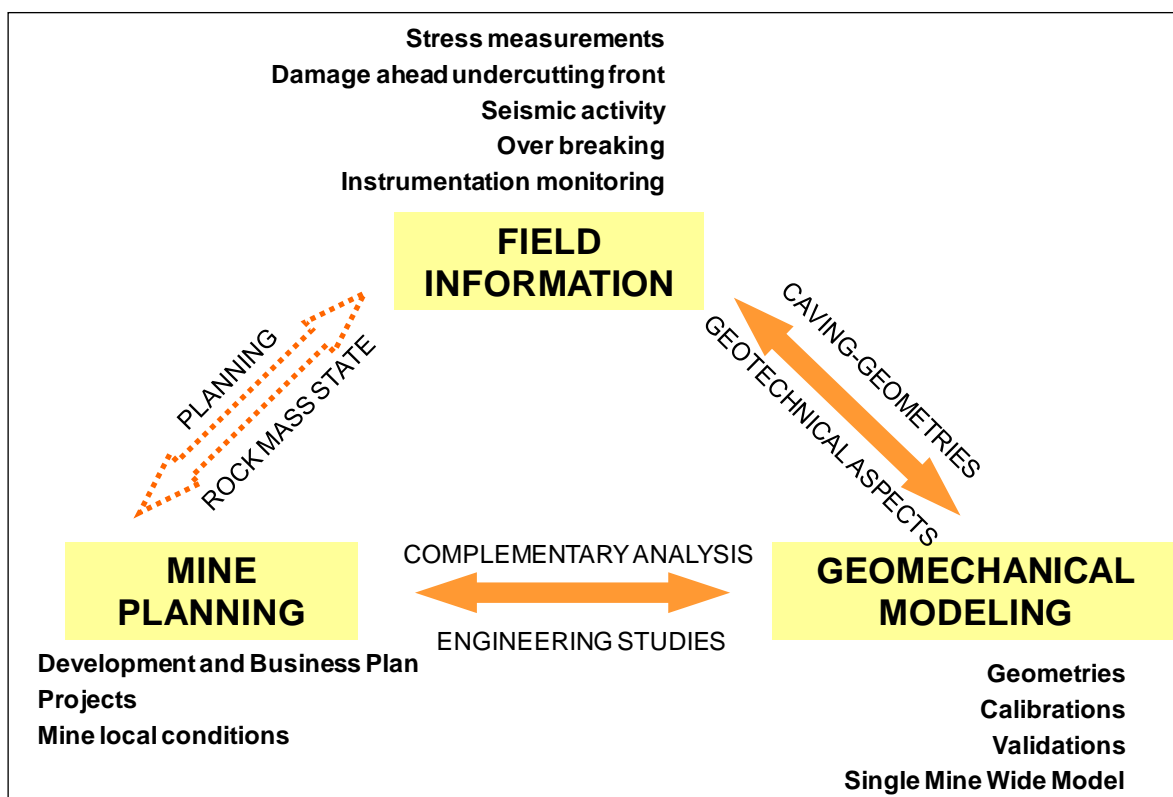


**Figure 5.6:** Numerical modelling strategy at El Teniente Mine (Pardo and Landeros, 2008).

Currently, a large-scale model has been conceived to provide a general idea about stress conditions around the whole mine. Nevertheless, when applied to specific areas such as Esmeralda, the model required a major level of detail, including a layout of the area of interest and a better geometrical definition of the cave. Based on those ideas, a new local model was built, calibrated and validated in order to improve the numerical tool that supports the planning decisions at the Esmeralda Sector.

In order to clarify the causes of the intensive rock mass damage and collapse generated ahead of the undercut front at the Esmeralda operation during the more recent period (2008-2010), a 3D linear

numerical modelling was developed by Cuello et al. (2010). At this time a local criterion from damage ahead of undercutting was introduced, including explicit galleries. Further analysis searched for continuous improvements, considering explicit galleries and improving calibrations in terms of stresses, damage and new source of calibration, such as information from preconditioning by hydrofracturing (Cuello, 2010).

***Data Appreciation and modelling development***

Map 3D software (Wiles, 1993) was selected as the model package, which is based on the BEM code alongside a rock mass characterised by linear elastic behaviour. Esmeralda stress measurements, observed rock mass damage and recorded seismic events were used to calibrate and validate the model. Moreover, the record of hydraulic fracturing pressure was used as validated information. The hydraulic fracture technique was undertaken as part of rock mass pre conditioning applied in the Western area of the Esmeralda operation.

Considering the linear elastic solution as constitutive model, the principal stress field, Young’s modulus (E) and Poisson’s ratio ( $\nu$ ) are considered as the only input parameters into the analysis. The small number of input parameters and less time of modelling represent one of the most important features of the linear elastic solution.

The predominant material corresponds to CMET lithology, which was used as host material in the model. Elastic properties utilised for the model are shown in Table 5.2

**Table 5.2:** Elastic properties used into mine scale model (Cuello et al. 2010).

Young’s Modulus	60 Gpa
Poisson’s Ratio	0.25

Due to mathematics formulation of the model package that assumes that the excavations are undertaken inside a continuum and endless material, the stress field must be defined by gradients function and identified values in a specific known point. In this type of mine scale model, this known point is identified in some specific point of surface topography. Cuello et al. (2010) indicate that the utilised values of stress field are sensitised in order to find the best match between model and reality, which means less dispersion between the stress interpretation from the model and the in situ stress measurements carried out at the Esmeralda operation.

In relation to the geometries developed for this linear elastic analysis, 3 models were developed that are associated to different steps of global extraction geometry. The geometries modelled correspond

to the mining global cavities for 1997, 2005 and 2009. Each model included: surface topography, cavities associated to the modelled year and, for the model year 2009 alone, part of explicit undercut and extraction drifts. As an example, the geometry modelled for 2009 is shown in Figure 5.7.

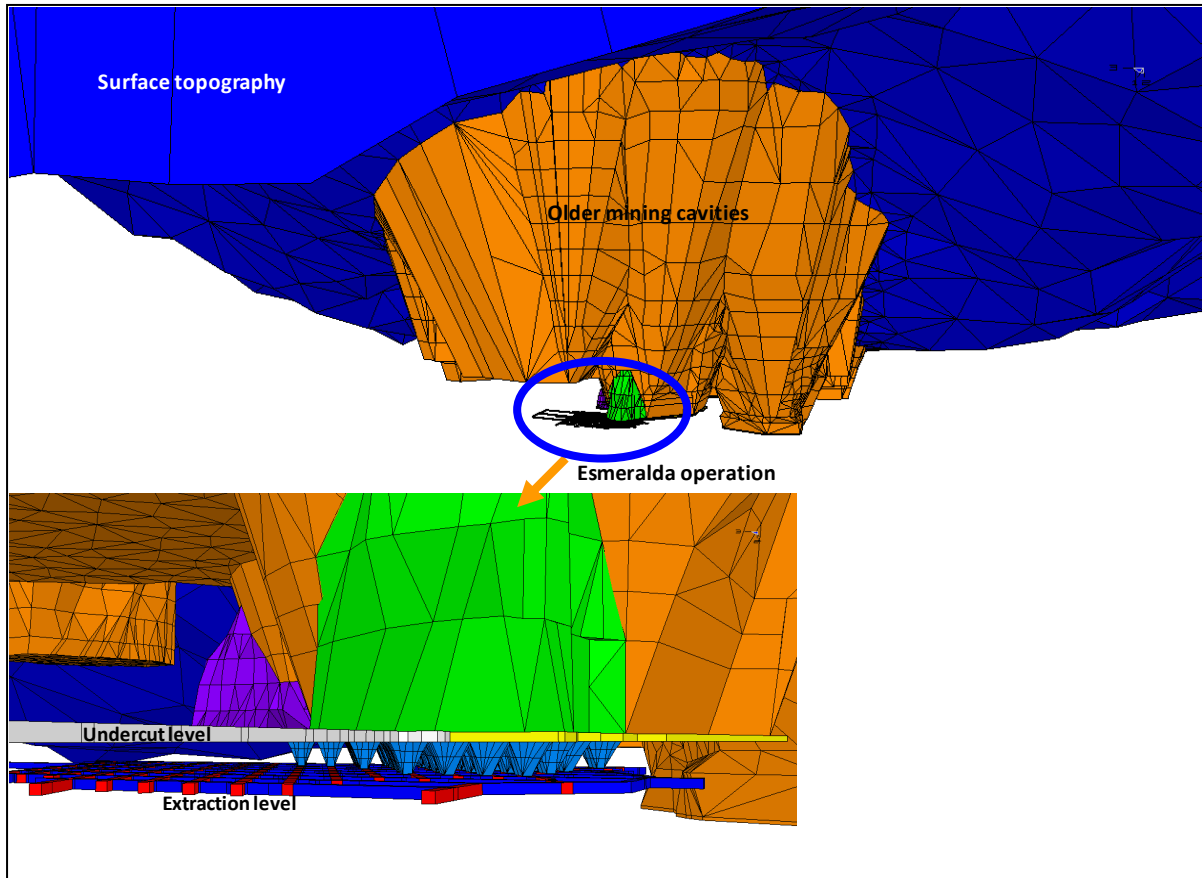


**Figure 5.7:** Tridimensional model with detailed geometry of Esmeralda Operation year 2009 (Cuello et al. 2010).

### ***Calibration***

In order to achieve a reliable analysis of the modelled Esmeralda operation geometry, a calibration methodology was carried out through the following correlative steps:

- a. *Selection of pre mining stress field associated to the Esmeralda operation area before its exploitation.* A total of 13 stress measurements that were undertaken between 1995 and 1997 surrounding the Esmeralda operation were used to define a representative initial pre mining stress field previous to caving initiation at the Esmeralda operation.
- b. *Validation with measured stress field associated to the Esmeralda extraction geometry in 2009.* A statistical Point estimate method was used to generate different scenarios of stress field distribution associated to the Esmeralda extraction geometry in 2009. The model was sensitised with each scenario generated; finally the resulting model was compared with stress measurements carried out ahead of the Esmeralda cave front in 2009.

- c. *Adjustment of stress field distribution on the model by comparing the results of rupture pressure of Hydraulic fracturing.* Once a representative and reliable stress field distribution was defined for the modelled Esmeralda 2009 geometry, the estimated stress induced around the cavity was compared with the record of propagation pressure of Hydraulic fracturing technique. This technique was part of the rock mass precondition that was carried out in the Western area of the Esmeralda operation during 2009.
- d. *Matching between observed damage located on undercut and extraction level ahead of undercut front and prediction of stress induced by the model.* A qualitative match between induced over stress around the modelled drifts and the observed over break of the Eastern undercut drifts was assessed. As an example, figure 5.8 shows the stress distribution around the drift and the over break observed in the same modelled undercut drift.

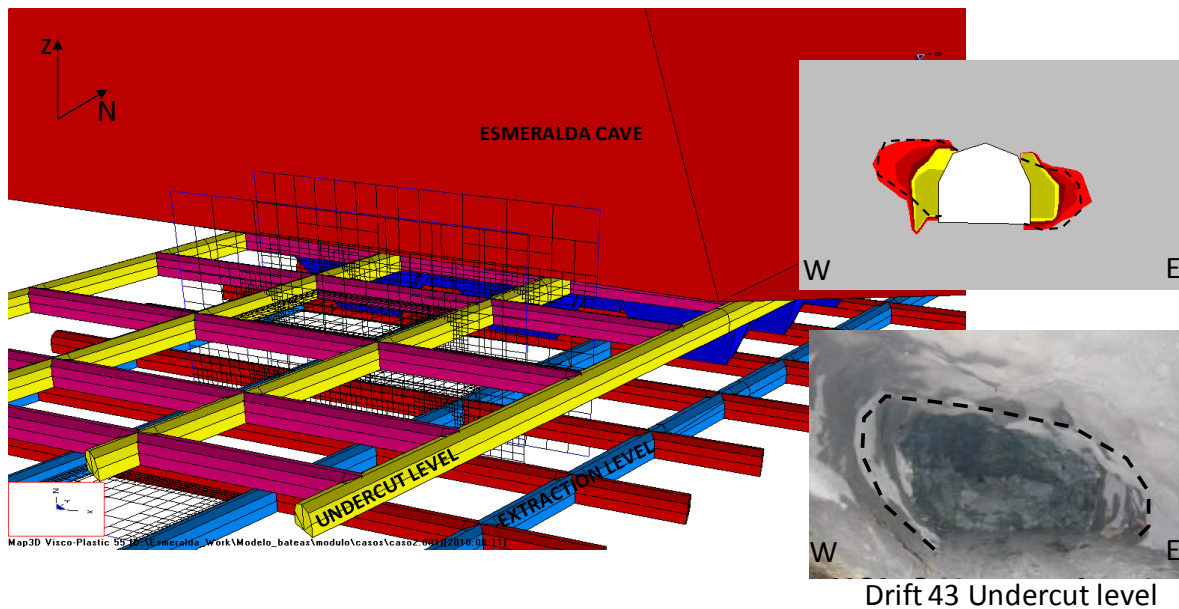


**Figure 5.8:** Stress distribution around modelled undercut drift and a photo with the over break observed at the same drift 2009 (Cuello et al. 2010).

### ***Rock mass damage interpretation***

As alluded to in Chapter 4, the rock mass damage experienced and observed on extraction and undercut drifts during the later period of Esmeralda extraction history (2008-2010) was assessed according to level of intensity and effects generated. In fact, the intensive rock mass damage defined as a failure of the rock mass over a large area on extraction level shows its maximum expression with the total closure of the affected drifts.

The results obtained for the last calibrated model associated with the Esmeralda extraction geometry in 2009 were analyzed within damaged areas either on extraction or undercut level located ahead of the cave front. These zones contain areas with very intensive rock mass damage that have been

identified as Collapses. Based on the methodology proposed by Wiles (2001) where the fundamental assumption with the linear elastic “damage criteria” method is that there is a direct correspondence between the amount of over-stressing and the amount of observed damage, simple plots of  $\sigma_1$  versus  $\sigma_3$  were created for different observed damage thresholds. Finally, these plots were generated in order to establish a site-specific linear elastic damage criterion (simple failure criterion), such as the Mohr-Coulomb rock mass strength envelope, as described in equation (5.1). The estimated regression plot for each damage threshold can be seen in Figure 5.9.

The rock mass damage interpretation primarily developed the initial damage threshold. Villaescusa et al. (2003) suggest that the initial damage threshold is defined as:

$$\sigma_1 - \sigma_3 = A \quad (5.7)$$

This has also been suggested by Martin (1997) and Diederichs et al. (2004) and is characteristically manifested by the onset of observed seismicity in massive brittle rocks. An initial damage criterion was developed with the seismic events recorded on later period at Esmeralda operation. The plot can be seen in Figure 5.9.

Secondly, plots of  $\sigma_1$  versus  $\sigma_3$  were also contoured by data points in the rock mass where moderate damage (described in Chapter 4) has occurred as direct result of induced stresses exceeding the local rock mass strength (Wiles 2001), which in turn, is manifested as high deformation at this location but still operative (Figure 5.9). The local moderate rock mass damage criterion was approximated by:

$$\sigma_1 = 1.27 \sigma_3 + 54 \quad (5.8)$$

Finally, plots of  $\sigma_1$  versus  $\sigma_3$  were also contoured by data points in the rock mass where closure of drifts (described in Chapter 4) has occurred as direct result of induced stresses exceeding the local rock mass strength (Wiles 2001), which in turn, is manifested as intensive deformation exceeding intensively rock mass strength at this location (Figure 5.9). The local intensive rock mass damage criterion was approximated by:

$$\sigma_1 = 3 \sigma_3 + 54 \quad (5.9)$$

Additionally, an example of principal stress induced by Esmeralda extraction cavity 2009 associated with moderate rock damage criteria (equation 5.8) is shown in Figure 5.10. This example shows the match between observed collapsed areas to model results for one of the local failure criterion.

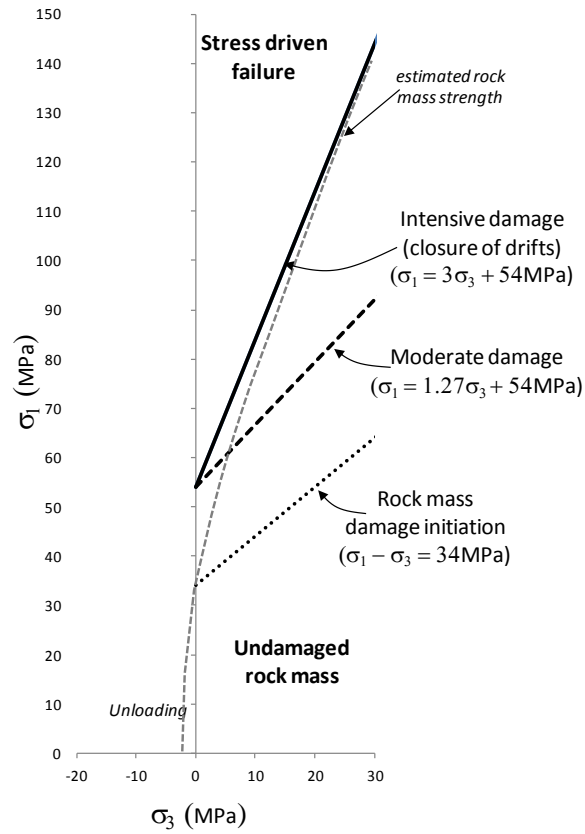


**Figure 5.9:** Linear elastic critical stress-based criteria for different damage threshold (modified from Cuello et al. 2010).

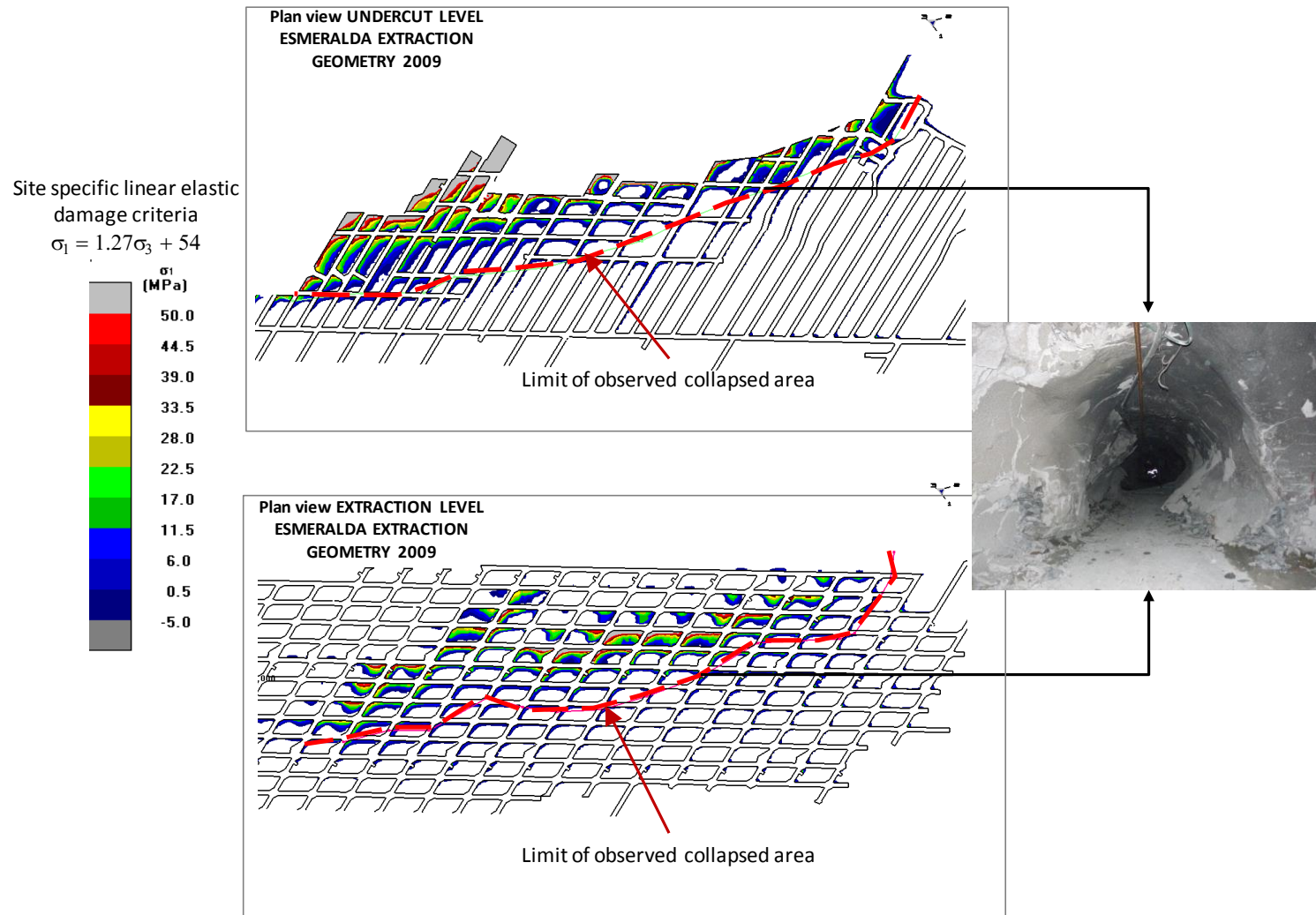


**Figure 5.10:** Linear elastic critical stress-based criteria for different damage threshold (modified from Cuello et al. 2010)

### ***Conclusion***

The exercise above has shown that, if the rock mass is represented as continuum without the presence of discontinuities facilitating instability, it's possible for linear elastic results to provide a reasonable match between observed rock mass damage and linear elastic stress-damage. This represents a continuum methodology that can provide reasonable reliability for simple geomechanical stability problems to be analysed.

Although a reasonable correlation was carried out to simulate intensive rock mass damage assessed during the later period of Esmeralda extraction history (year 2009), the analysis was just undertaken for one specific representative extraction geometry without including the rock mass degradation by caving advance associated with previous extraction geometries at Esmeralda. The relationships between over-stressing and rock mass response are fundamentally dependent on the post peak properties of a rock mass, therefore, elastic assumption negates the possibility of modelling post-peak behaviour of rock. When using excavation steps in linear elastic continuum modelling, the extent and amount of rock damage is not considered and included for each subsequent step. Rock mass damage and resultant redistribution of stress therefore, cannot be accurately represented using linear elastic modelling.

The study carried out by Cuello et al. (2010) generated predictions based on direct comparisons to stress states well correlated with observed conditions found at existing Esmeralda sector. However according to Wiles (2010) this has only been studied for collapse conditions ahead of the undercut front, not behind.

Yielding of the rock mass may not be solely attributed to stress-induced rock mass damage, yet may be caused by other influences such as weak geological discontinuities or poor drill and blast practices. It is suggested that improvement in reliability of continuum modelling may be gained using more sophisticated material models, such as non-linear inelastic models.

### 5.3 FUNDAMENTALS OF NON-LINEAR ELASTO-PLASTIC MODELLING

In order to understand the post-yield behaviour of a rock mass, the choice of constitutive model is essential. As shown in Figure 5.11, the main feature of the constitutive model is whether the material behaves elastically or in-elastically. The critical strain value ( $\epsilon_{critical}$ ) represents the point up to where the model behaviour has been elastically linear. As it has been mentioned previously, in the linear elastic model the stress increases linearly with increasing strain, however non-linear inelastic models are incapable of sustaining stress in this fashion. For the non-linear elastic model, the strain at peak stress ( $\epsilon_f$ ) is irrecoverable and can become very significant.

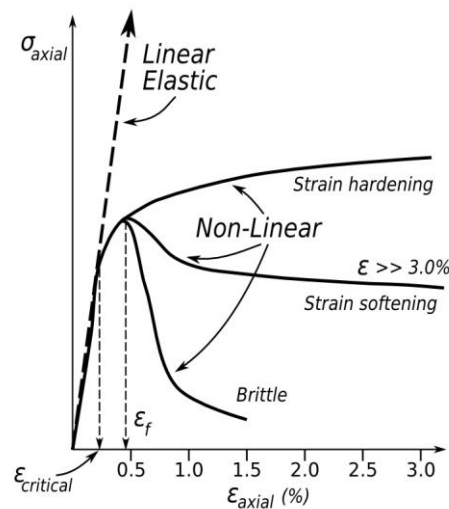


**Figure 5.11:** Strain- stress relationship influenced by constitutive model (Cepuritis, 2010)

The benefits of using non-linear elasto-plastic constitutive models over linear elastic models are the ability to model irrecoverable inelastic strains, as well as rock mass behaviour in the 'post-peak' region (Cepuritis 2010).

The early development of plasticity theory of geo-materials has been performed upon this foundation achieved in metal plasticity. Unlike metal plasticity, however, modelling plastic behaviour of geo-materials is highly controlled by volume changes during loading. Plasticity and elasto-plasticity models have been developed and widely applied to fractured rocks since 1970's, based mainly on the classical theory of plasticity, with typical use of the Mohr-Coulomb and Hoek-Brown failure criteria as the yield functions and plastic potentials (Jing 2003).

Once a suitable stress-strain relation is developed, it needs to be combined with equilibrium equations and compatibility conditions for solving geotechnical boundary value problems. In general, these governing equations are too complex to be solved analytically. Analytical solutions are possible only

for problems with very simple geometry and boundary conditions such as cavity expansion problems solved by Hill (1950) and Yu (2000). From mainly a practical point of view, however, numerical methods (e.g. finite element method, finite difference methods, boundary element methods, and discrete element methods) are required (Yu, 2006).

In the past, geotechnical stability analysis has been undertaken based on a perfectly plastic behaviour after yield. This is because the slip line method and bound theorems of limit and shakedown analysis developed in the classical plasticity theory allow the failure and stability calculations to be carried out in a relatively simple manner (Hill, 1950). In addition, geo-materials generally display dilatant characteristics (i.e. positive increases in volumetric strain) at yield. The confinement effect can influence the post-yield strain behaviour (Cepuritis, 2010). Strain-hardening and strain-softening are the two main features of plastic behaviour of rocks, with the latter more often observed under uniaxial compression test conditions.

The failure criteria of rocks are important components of constitutive relations and usually used as yield surfaces or/and plastic potential functions in a plasticity model. Besides the most well-known and perhaps also the most widely used Mohr-Coulomb and Hoek-Brown criteria, a number of strain-softening and dilatant constitutive models have been developed specifically for geo-materials, looking for assessing accumulated damage, which means that as strain increases the material softens, weakens and dilates. One recent model is the LR2 constitutive model (Levkovitch et al. 2010). The yield criterion in LR2 uses a modified form of the Menetrey/Willam strength criterion (Menetrey and Willam, 1995). Essentially their main feature is that each geotechnical domain can vary at different rates with respect to strain changes, including a dilatancy parameter. This allows for the approximation of complex stress-strain behaviour. A full description of the material model is provided in Appendix A.

With respect to deformation analysis, past practice has been based on elastic analysis. This is now recognised to be inaccurate for many cases as experimental research suggests that behaviour of geo-materials is highly nonlinear and plastic (Yu 2006), even at very small strain. Therefore, Yu (2006) suggests that an appropriate deformation analysis should be carried out using nonlinear elasticity and accurate plastic stress-strain relations.

Additionally, there is no doubt that a most important development over the last three decades in geotechnical analysis has been the widespread application of finite element methods in both stability and deformation calculations. Finite element analysis is particularly popular because it is very general and is capable of incorporating any material stress-strain relations. The FE method can easily account for both material and geometric nonlinearities, which are often present in boundary value problems facing the geotechnical engineer.

It is well known that some of the most important geotechnical risks for caving mines are simply dependent on mine scale extraction sequencing and geometry. Cases of cave stalling, plug collapse and infrastructure failures at some mines were found to be a consequence mainly of the geometry of the mine and the excavation sequencing (Beck et al, 2013). Therefore, the use of large three-dimensional numerical models, sufficient scale and detail of geological units, structures and the precise description of the regional stress field has allowed simulation of realistic displacements and energy release as mining progresses. It also has the ability to simulate the damage accumulated as a consequence of progressive excavation process (Beck and Duplancic, 2005).

The intent of this research is to replicate the induced deformation associated with a caving operation. A back analysis process has been performed using non-linear modelling under the doctrine described early. This type of modelling uses measurements or observed damage to be calibrated with modelled displacements, plastic strain and energy. In particular, a scalar approximation of plastic strain tensor can be utilised (Cepuritis 2010, Coppola et al. 2009).

$$\varepsilon_p = \sqrt{\frac{2}{3}} \sqrt{\varepsilon_1^2 + \varepsilon_2^2 + \varepsilon_3^2} \quad (5.10)$$

where  $\varepsilon_1$ ,  $\varepsilon_2$ ,  $\varepsilon_3$ , are the principal strain components. The calibration procedure requires observed damage to be replicated in terms of when in the mining extraction step it occurs and its location. This damage can then be matched to equivalent plastic strain levels confirming that the fundamental mechanisms of damage and deformation were captured (Beck and Duplancic, 2005).

The keys to all modelling doctrines used on this study and based on multi-scale approaches, can be summarised as follows:

- Only higher order elements can be used
- Very small excavation steps are needed to capture the stress path
- 2D modelling is now the exception, and 3D the rule
- Anisotropic, strain-softening, dilatants constitutive models for rock masses and structure
- Multi-scale analysis based on the assumption that phenomena at different length are coupled
- Rigorous calibration, and homogenisation of material properties

By ensuring realistic displacements, the models are able to interpret rock mass phenomena using displacement, strain and energy, rather than indirect correlates with stability.

## **5.4 WORKFLOW OF MINE SCALE NON-LINEAR MODEL**

The sequence of geotechnical risks and events experienced at the Esmeralda operation and described in detail in Chapter 4 were back analysed using a 3D strain softening, dilatant, Finite Element model with geotechnical enhancements including an improved constitutive model for underground problems (Levkovitch et al. 2010). The work flow for the simulation consisted of several and parallel phases of geometry assembly, calibration, adjustment and back analysis. These phases are each a critical milestone in the development of the numerical simulation and are summarised below in Figure 5.12.

The simplest measure of effects on the extraction sequence and cave growth, in detail, in the back analysis model is the comparison of observed damage with model results. Interpreting extraction and undercut pillar condition using plastic strain is consistent with standard geotechnical practice. Conventional theorems of plastic collapse for limit analysis are well documented (Yu 2006; Hill 1951).

### **5.4.1 Geometry assembly**

The model geometry incorporated all major geological domains, all prior mining, as well as surface topography, regional discontinuities represented by major faults, detailed extraction sequence and cave growth of the Esmeralda operation allowing for the simulation and back analysis of the global and local observed rock mass damage. The analysis required two scales of model sequencing with a total of 200 extraction steps:

- Mine global scale to generate the regional deformation caused by all previous extraction cavities at El Teniente Mine. This phase includes the entire mine and a large margin of the terrain surrounding the mine and recreating the complete extraction history at El Teniente Mine.
- The Esmeralda operation block scale, which included all lithology bodies, three scales of structural sets and detailed extraction history from 1996 to 2010.

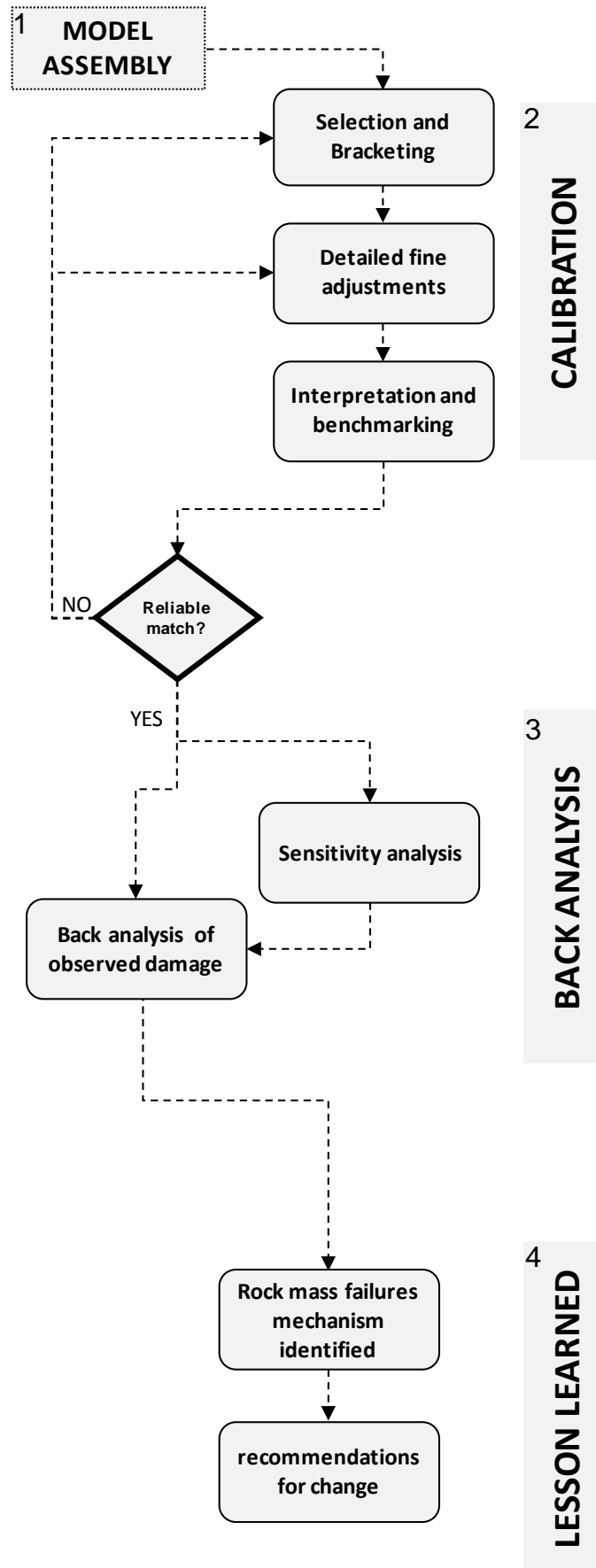


**Figure 5.12:** The workflow followed for numerical simulation performed.

## 5.4.2 Calibration

The purpose of calibration is to identify model inputs that produce the best match to measured data, and to assist in quantifying the resolution and precision of the model. The calibration method consists of sequential tasks which often merge together into a continuous process of model improvement, and is largely driven by the experience of the mining and applied mechanics engineers and their intuitive understanding of the influence of material properties on rock mass behaviour:

- a. *1<sup>st</sup> calibration stage: Selection and bracketing.* The purpose of selection and bracketing is to appreciate the geomechanical problem, to identify the governing physics that must be captured, to select the modelling approach, to set model fundamentals and sufficiency requirements and then ultimately to identify initial model variables.

At the end of this stage, the modelling approach will be propped and preliminarily tested.

- b. *2<sup>nd</sup> calibration stage: Detailed fine adjustments.* The purpose of the detailed fine adjustment phase is to further refine the model fundamentals and variables, to improve precision and quality or quantity the model error.

An example of a detailed fine adjustment is the incremental adjustment of the frictional strength of a particular fault or a particular geological unit in the model. It also includes the geometric shape of excavation steps considering more detailed sequencing than in the global model to better match dissipated plastic energy (DPE) and seismic measurements.

At the end of this stage, the model variables are largely selected.

- c. *3<sup>rd</sup> calibration stage: Interpretation and benchmarking.* The purpose of the interpretation and benchmarking phase is to aid interpretation of the model by identifying relationships between correlated modelled quantities, but not direct measures of expected real world occurrence. An example is the correlation between dissipated plastic energy (DPE) and seismic event probability; DPE is measured in  $J/m^3$ , but event is measured in events/ $m^3$ /month (Beck and Duplancic, 2005). The expected nature of this correlation can be used to assist in calibrating the model, and a close correspondence can be achieved, however a final interpretation of relationship is needed to convert the modelled value in to a real-world estimate of occurrence.

The main benchmarking focus was to establish an instability criterion based on observed and measured damage on either extraction or undercut level during the whole extraction history at the Esmeralda operation. The focus was to validate as well the relation between modelled support pressure and plastic strain to excavation performance, to establish relationships between stress, energy and strain.

At the end of this stage, the definitions and criteria for interpreting the model results are developed.

### **5.4.3 Back analysis**

The back analysis is considered as parameter identification, so that they are only adequate when the models are well defined and fixed. However, according to Sakurai (1997) in the back analysis of geotechnical engineering problems, the mechanical model should not be assumed, but should be determined by back analysis. This means that for the current research study, the particular back analysis should not only be capable of identifying the main geotechnical parameters, but also the instability mechanism itself.

The back analysis phase assessed the developed failure criterion upon major instability zones at the Esmeralda operation, evaluating the stress-strain relationship in order to identify failure mechanisms and better understand the complex evolution of loads on the production and undercut of horizons.

Additionally, a sensitivity analysis was carried out during this phase in order to quantify the differentiated effect of each main geotechnical parameter acting upon generated instability.

### **5.4.4 Lesson learned**

Finally, the purpose of this last phase was to assess the rock mass failure mechanisms identified and to generate future guidelines about the relationships between mining strategies and rock mass failure mechanisms.

## **5.5 DATA APPRECIATION AND MODEL BUILDING**

The requirements of the problem under discussion (Chapter 4) constrained the analysis to a three dimensional, strain softening, dilatant, discontinuum simulation. This means that the rock mass in the model degrades due to over stressing, faults are represented and can slip and separate, and the rock mass can dilate as it degrades.

The following sections describe the key elements of model development, inputs and assumptions used for the nonlinear simulation to study post-peak rock mass behavior and to study the influence of large-scale discontinuities by direct incorporation into the numerical model. Moreover, the mining sequence also had to be represented in very small steps to replicate the stress path as closely as possible, including the sequential development extraction to match the real schedule. From this numerical modelling work, an instability criterion was developed based on assessed drifts that have experienced different grades of damage. These instability criteria have been used during the back analysis process in order to identify the main geotechnical parameters acting upon the rock mass damage experienced, and also the instability mechanisms themselves.

### 5.5.1 Selection of modelling packages

A model of this complexity consists of several parts:

- CAD: the models include all geometries, surface topography, previous mining cavities, and components of the geological and structural models without substantive simplification. The geometric complexity requires the use of modern CAD software to facilitate the sequencing and construction of the refined model geometry. Modelling software does not typically have the required functionality for this task.
- Solution of the stress, strain and energy distribution using the Abaqus Explicit solver which is a general purpose, 3D, non-linear, discontinuum finite element (FE) analysis product. Abaqus has been adapted especially for analysis of problems where there is potential for significant plasticity, high levels of deformation, large strain gradients and large numbers of material discontinuities (Arndt et al., 2007, Beck and Duplancic, 2005, Beck et al., 2011).

This approach was selected for this study for the discontinuum and large strain abilities of the package and the large size needed to represent the geometry and faults at the selected resolution.

- Results visualisation using software 3<sup>rd</sup> Voxel and the Abaqus viewer.

### 5.5.2 Constitutive model

Both continuum and discontinuum components of the numerical model were modelled using the Levkovitch Reusch (LR2) constitutive framework (Levkovitch et al., 2010) with the Hoek-Brown (HB) yield criterion. Indeed, the LR2 model itself is a constitutive framework for discontinuum models that can incorporate any common yield criterion and represents a package of approaches to handle the continuum parts and the discontinuities in geotechnical problems.

Although a full description of the material model is provided in Appendix A, the LR2s main features are detailed below:

- The continuum parts (ie, the rockmass between explicit structures) are modelled as a strain softening dilatant material. This means that as strain increases the material softens, weakens and dilates. Each geotechnical domain has its own set of material properties, and all parameters for each domain can vary at different rates with respect to strain changes, including the dilatancy parameter. This allows for the approximation of very complex stress-strain behaviour.

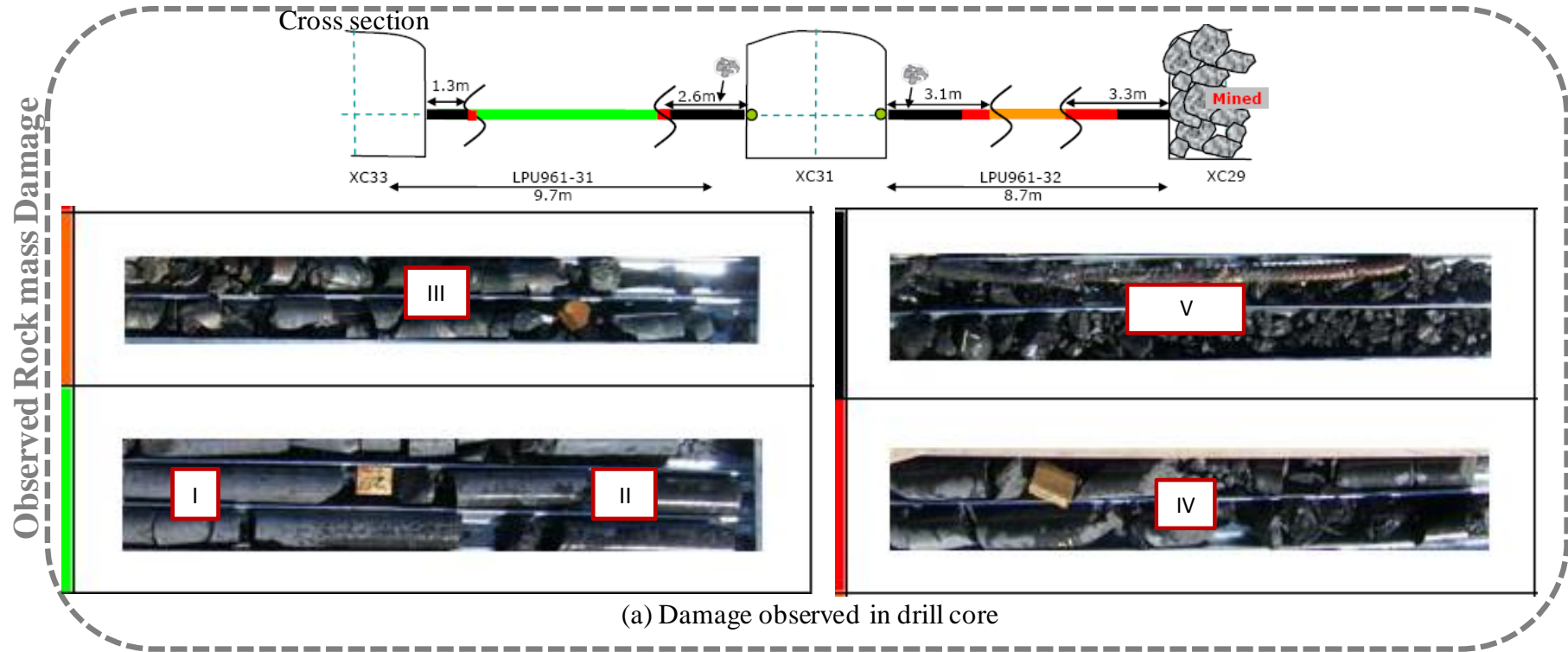
In a well-calibrated strain-softening model, rock mass damage is an output of the model, so it can be directly compared to the observed damage in mine development.

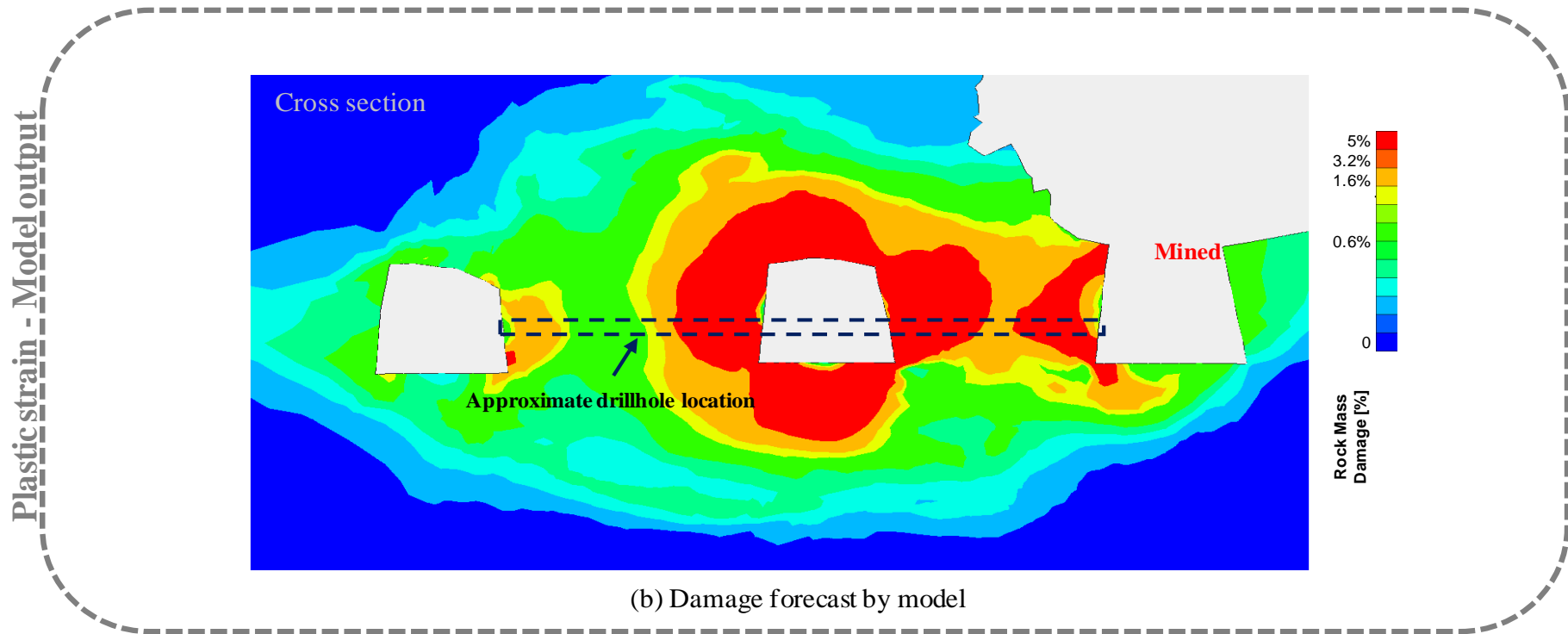
- All normal model outputs such as stress, displacement and strength loss are produced, but in addition, the plastic strain (damage) tensor is available. For ease of viewing, the dilation component of the plastic strain tensor is typically plotted, as this is a scalar for which a simple colour scale can be used.

For strong rock masses, such as those at El Teniente mine (Brzovic and Villaescusa 2007), the damage level is interpreted at the surface of excavations and settling on qualitative descriptions at a mine is usually simple. A local damage classification can then be carried out based on the match between perceptions of damage levels and plastic strain scalar from the calibrated model.

It must be noted that the % rock mass damage is not % tunnel closure. It is the % dilation of the rock at that location in the model. Some mines carry out diamond drill cores through damaged pillars to better understand the relation between qualitatively observed rock mass condition and swell, as shown in a mine uses as an example in Figure 5.13 (Beck 2011).

From this point in this thesis, this scalar of the rock damage tensor will be referred to as 'plastic strain', PS or generically, as modelled rock mass damage.





(b) Damage forecast by model

**Figure 5.13:** An example of modelled versus measured rock mass damage at one mine. Damage measured by core drilling pillars at selected locations to ground truth the model and also to better correlate the plastic strain scale with the visual impression of damage in the rock (Beck 2011).

A trouble with this approach is that it is also difficult to estimate the extent to which underestimating damage in any part influences deformation and stability in other parts. The main effort of this calibration methodology is to match the modelled and measured extent of damage, so that higher order effects and coupling between different areas of the mine can be better captured and understood.

- Discrete structures that are explicitly represented in the model are performed by contact-cohesive elements. Cohesive elements can have any valid constitutive formulation in LR2. Their purpose is to allow very large dislocations and separations on discontinuities while providing the correct kinematics of contact between the adjacent fault surfaces. The faults and shear zones are free to dislocate and dilate and the faults surfaces can dilate and degrade, and if needed, particles may flow dynamically. The main benefit is that the mechanics and kinematics of contacts between solid continuous parts bound by cohesive elements are very well resolved and robustly solved; that is, the representation of stress-strain behaviour within rock parts need not be compromised in order to incorporate discontinuum behaviour.

### **5.5.3 Model geometry and mesh discretisation**

The model geometry is based on the electronic meshes and wireframes that include the complete mining and extraction history at the El Teniente mine, surface topology, the geological boundaries and regional and local fault systems. The model was built using higher-order tetrahedral elements, based on geometries assembled such as: the whole mining geometry to be modelled (pre and post mining activity with regional and local geometries), cave shapes which mean subsidence geometries, tridimensional lithology bodies and structural sets either regional or local.

The model was built taking into account the multi-scale design; therefore a large regional scale model (see Figure 5.14 a) was developed including the hilly topology and the main regional faults. The dimensions of this scale model were 14km × 14 km × 4 km. Subsequently, the “old” mining geometry of 9 different sectors was built explicitly to account for historic mining and also to recreate their stress path previous to recent mining. Following this, a refined volume for model calibration was carried out (red square in Figure 5.14 b) that included the recent mining history (since the mid nineties) represented essentially by the extraction history at the Esmeralda operation, Reno operation and Ten-4 operation. In addition, greater resolution was considered within a second refined volume that only included the Esmeralda extraction history.

In summary the main features of the model are described in the following points:

- Model size 14 km x 14 km x 4 km
- Greater than 2.000.000 CD310 non-linear tetrahedral elements

- Greater than 700.00 cohesive elements for discontinuum representation of structures
- A total of 250 local structures built + regional faults
- Equilibrium step + old mining sectors + previous mining since 1995
- Esmeralda , Ten-4 Sur and Reno operations - sequence built in >80 steps

The mesh discretisation is optimised to ensure that the element size is small enough, so that the results are not affected at the length scale that is being interpreted, or other smaller and larger scales that would affect the result. For the modelled Esmeralda area that included extraction history and all development associated with the extraction and undercut levels. The mesh discretisation points were placed 1.0 m apart, as shown in Figure 5.14.

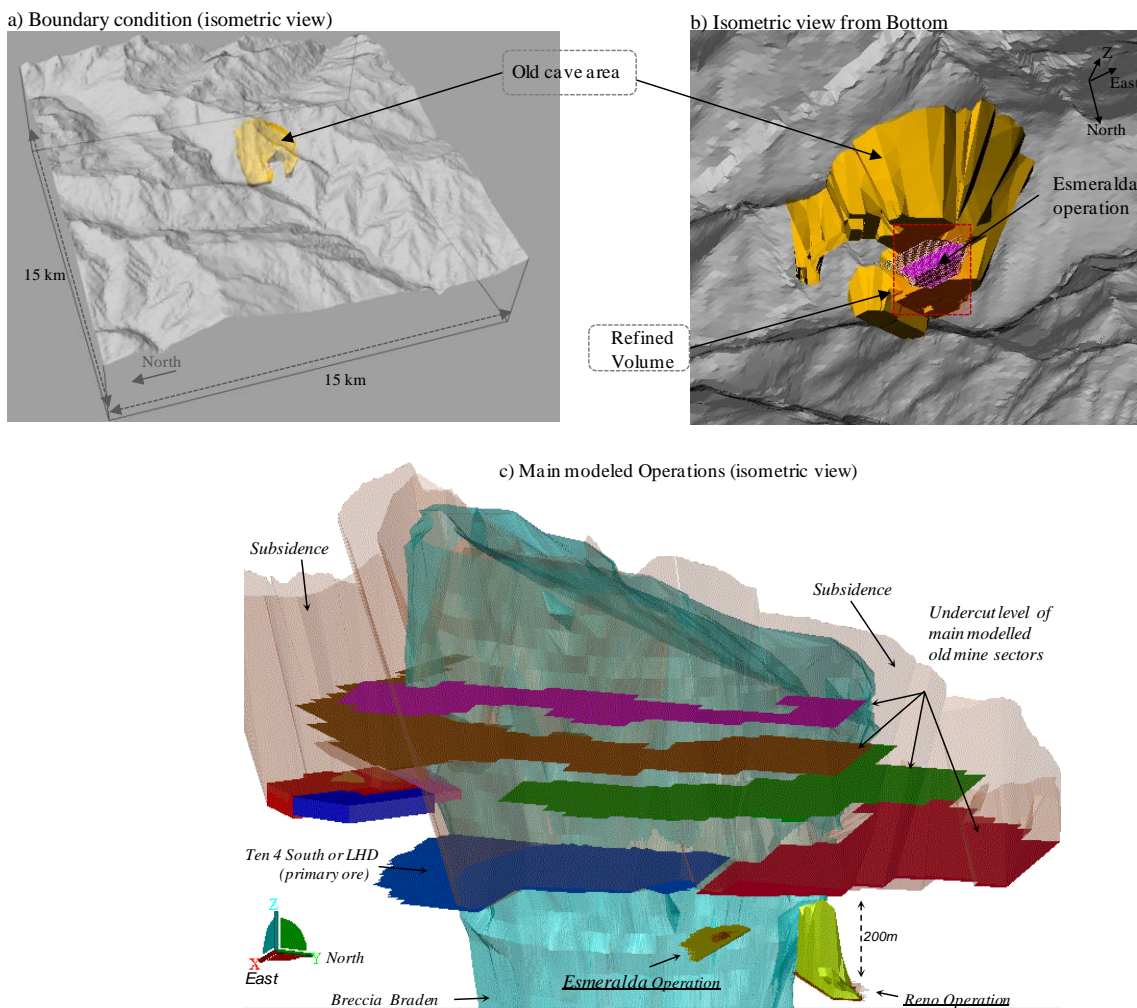


**Figure 5.14:** Model size, boundary condition, and modelled mine levels.

Generally, the interpreted length scale is underground 'global scale'. This means that the model is conditioned to produce sufficient similitude for the pillars within the model, but that it is the average behaviour of large areas of the mine that must be interpreted.

In this instance, this exercise included in the model all of the main faults assessed. However, smaller scale structures that would affect local pillar stability were not included and this limits the model to average global resolution.

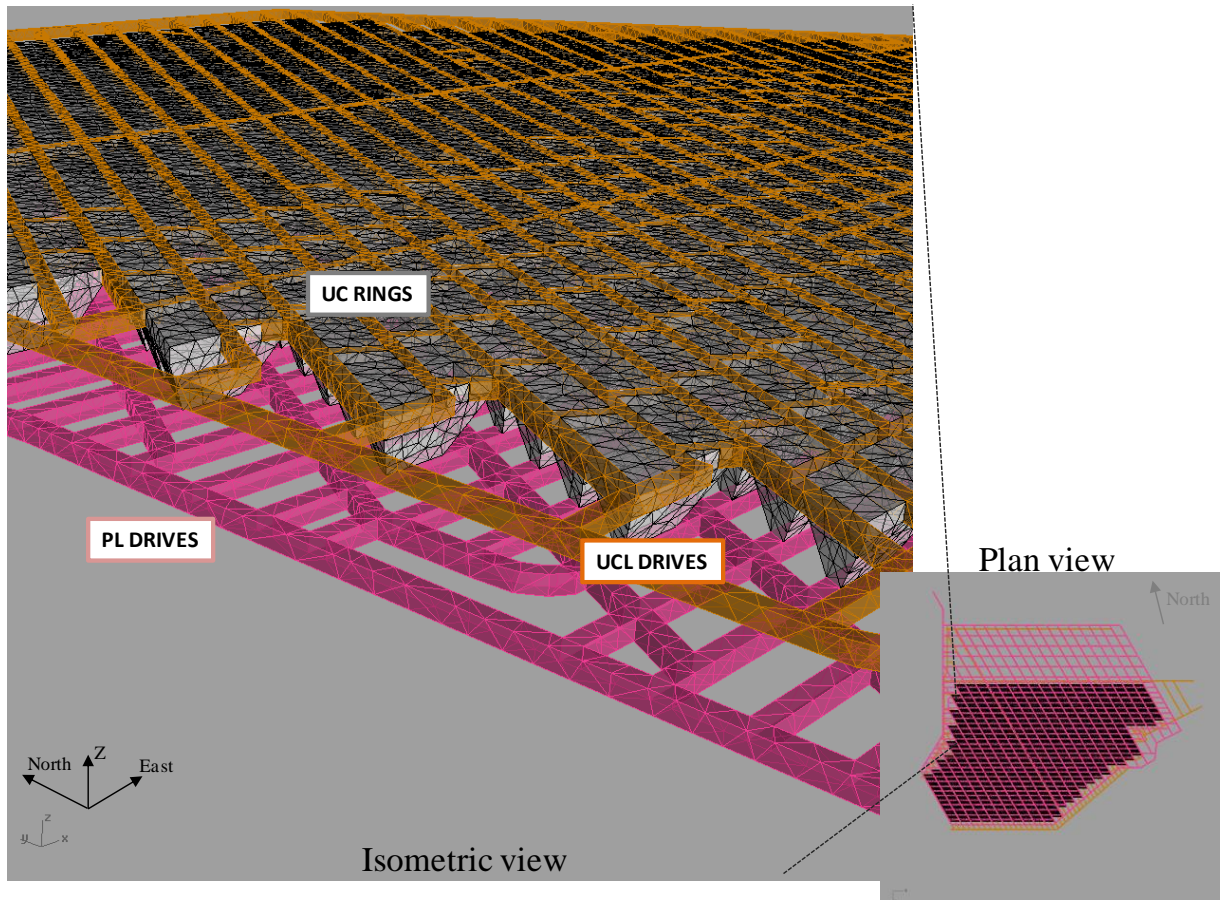


**Figure 5.15:** Final design geometry for the Esmeralda operation, as built in Abaqus showing the higher order element mesh on the extracted surfaces. The volume is also filled with elements.

Finally, once the geometry modelled and their mesh discretisations have been described, it is necessary to explain the different scales of modelling. Consequently, for the purpose of clarifying the geometry developed in the modelling, the whole mine scale model was characterised by three different levels of resolution (geometric scales), that can be seen in Figure 5.16. Firstly, the large global scale that included regional faults and surface topology with lower resolution was used to achieve the initial geological equilibrium with the stress field. Secondly, the El Teniente mine cavity scale where the “old” mining geometry of different sectors is located was carried out explicitly to account for historic mining and also to recreate their stress path immediately before the recent mining. Finally, the detailed geometry of the whole extraction history of the Esmeralda operation was undertaken alongside developments associated with each extraction step, all of them built with high resolution. Furthermore, the geology units and a tridimensional distribution of structural sets representative from Esmeralda rock mass were also included at this stage.

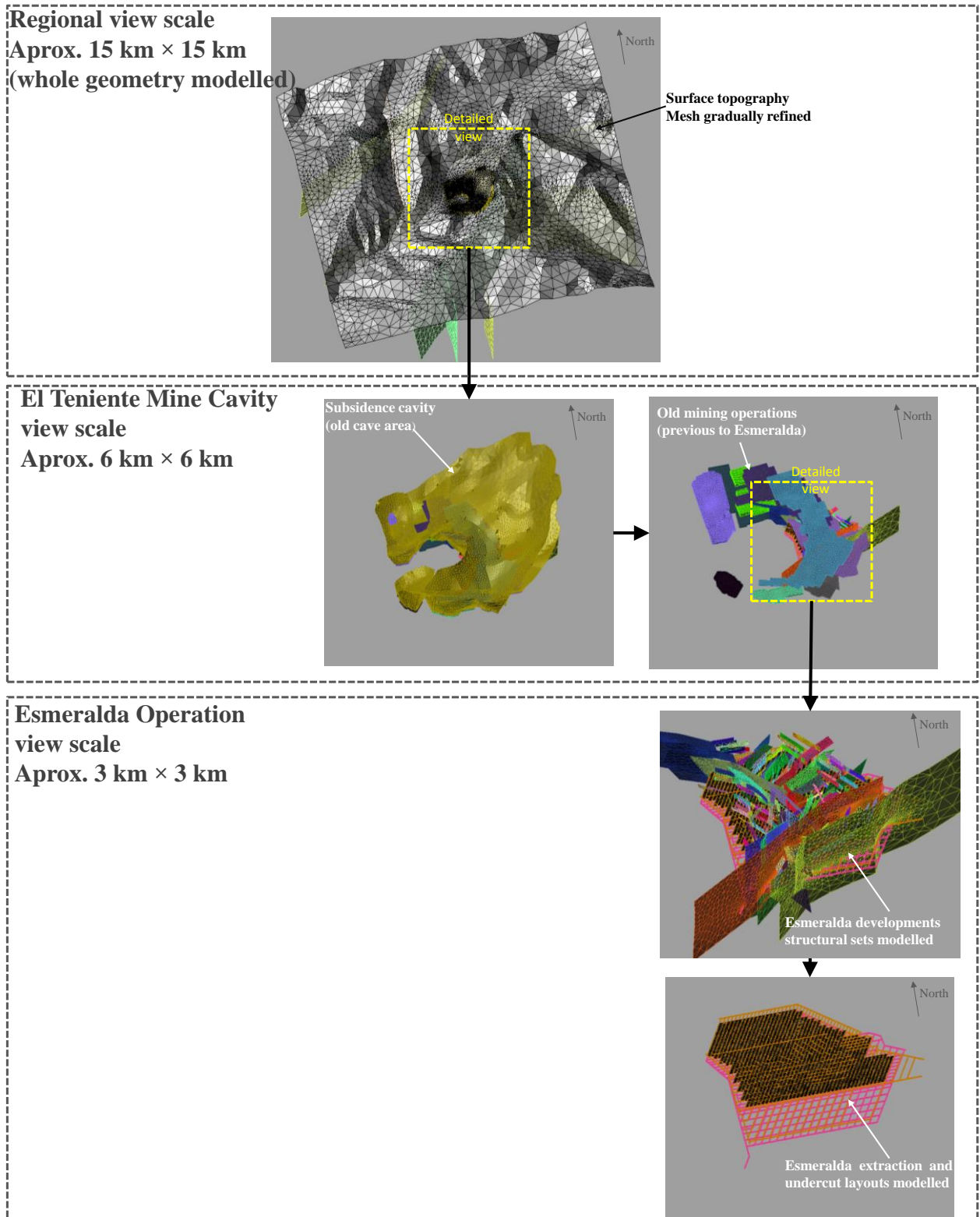


**Figure 5.16:** Description of the geometries modelled and their scales.

#### 5.5.4 Extraction Sequencing and Model Step

The total model sequence included in excess of 90 mining steps. Some particular features of model geometries built (model steps), which included descriptions, geometries, and dates are presented in Table 5.3. As an example, some representative extraction geometries modelled are shown in Figure 5.17. Due to a large number of extraction steps, it is necessary to ensure that the stress path throughout the Esmeralda operation is captured. The extraction sequence (extraction and undercutting steps) at the Esmeralda Operation was modelled in quarterly steps between 2000 and 2010 only.

**Table 5.3:** Main mine model steps and their descriptions

Steps	Dates	Mine sector / Comment
1-6		Geological equilibrium
7-34	1917-1970	Secondary ore exploitation, general mine sequence from up to down, and north to south
40	1990	Reno mine sector started using panel caving mining method – Ten 4 sur extraction step
47	31/12/1996	2 months of undercutting at Esmeralda mine sector, Reno and Ten- sur extraction step
50	31/12/1997	2 months of drawing generate the first modelled cave volume at Esmeralda mine sector
56	31/12/1998	Extraction step for Esmeralda – Reno and Ten-4 Sur
59	31/12/1999	Extraction step for Esmeralda – Reno and Ten-4 Sur
63	2000	Extraction step for Esmeralda – Reno and Ten-4 Sur
66	2001	Extraction step for Esmeralda – Reno and Ten-4 Sur
69	2002	Extraction step for Esmeralda – Reno and Ten-4 Sur
72	2003	Extraction step for Esmeralda – Reno and Ten-4 Sur
75	2004	Extraction step for Esmeralda – Reno and Ten-4 Sur
78	2005	Extraction step for Esmeralda – Reno and Ten-4 Sur
81	2006	Extraction step for Esmeralda – Reno and Ten-4 Sur
84	2007	Extraction step for Esmeralda – Reno and Ten-4 Sur
87	2008	Extraction step for Esmeralda – Reno and Ten-4 Sur
90	2009	Extraction step for Esmeralda – Reno and Ten-4 Sur
93	2010	Extraction step for Esmeralda – Reno and Ten-4 Sur

The undercutting and extraction sequence for Esmeralda, Reno and Ten-4 Sur operations were built based on mine survey data. Caves geometries anywhere in the mine site may be considered as an unknown parameter since these have not been properly measured. The model included mine drives, infrastructure opening, and excavations at extraction and undercut levels just for the Esmeralda operation; caved zones and the undercut volumes were included for the Reno and Ten-4 Sur operations.

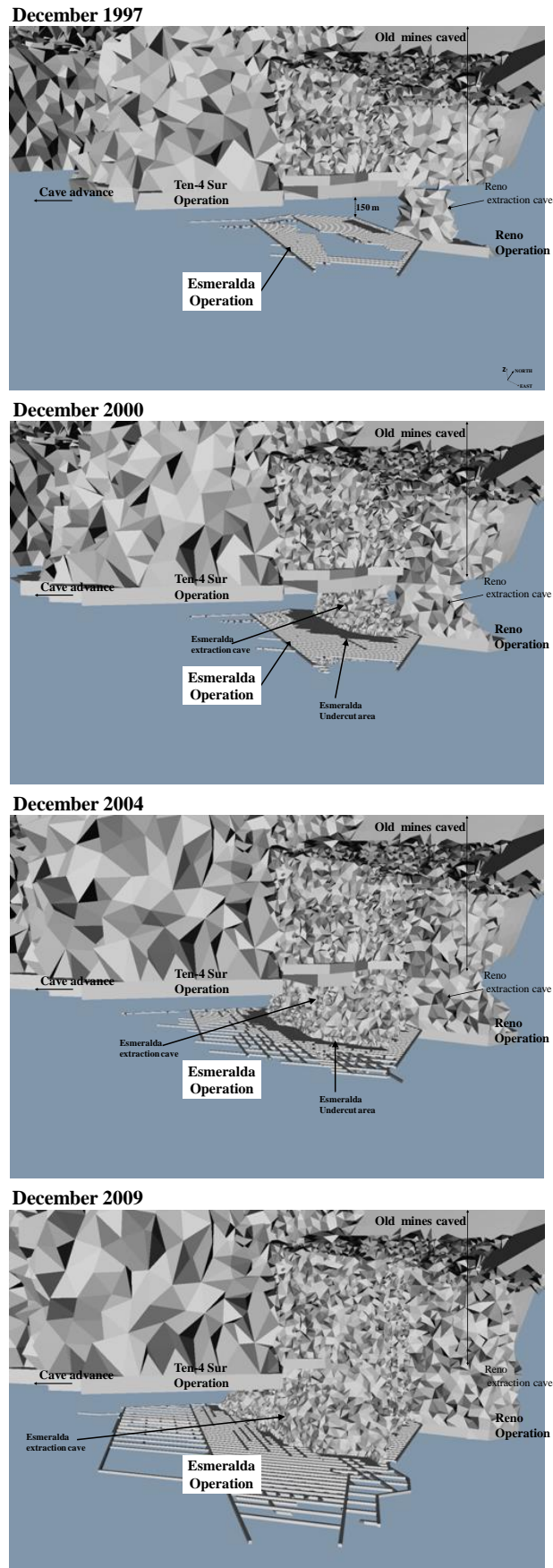


**Figure 5.17:** Detailed geometries of some mine model step in the numerical model.

### 5.5.5 In situ Stress Field

The stress orientation and magnitude are critical model inputs, and in some circumstances a small error in the orientation can be critical to the assessment of the geotechnical performance of a mine site. The accuracy by the current estimation of the stress field needs to be considered when interpreting any model results, or any other form of analysis of the mine (empirical or experience based).

Generally, a larger number of stress measurements are needed for the current multi-scale simulation that covers a wider area. A large stress tensor database from El Teniente Mine was reviewed. Those measurements were taken in different positions across the whole mine using mainly the Hollow Inclusion method, and also deeper stress measurements using the WASM acoustic emission technique (Villaescusa and Machuca, 2007).

Windsor et al. (2006) analyzed the El Teniente stress database in an attempt to define the contemporary stress field. Essentially, the strain, the structures and the stresses within the mine region were reconciled. This approach is used in this study as input parameter by the model as it represents a consistent analysis of the stress magnitude distribution with depth and accuracy estimation of principal stress orientations. Figures 5.18 and 5.19 show the El Teniente Mine principal stress orientations and their magnitude with depth respectively.

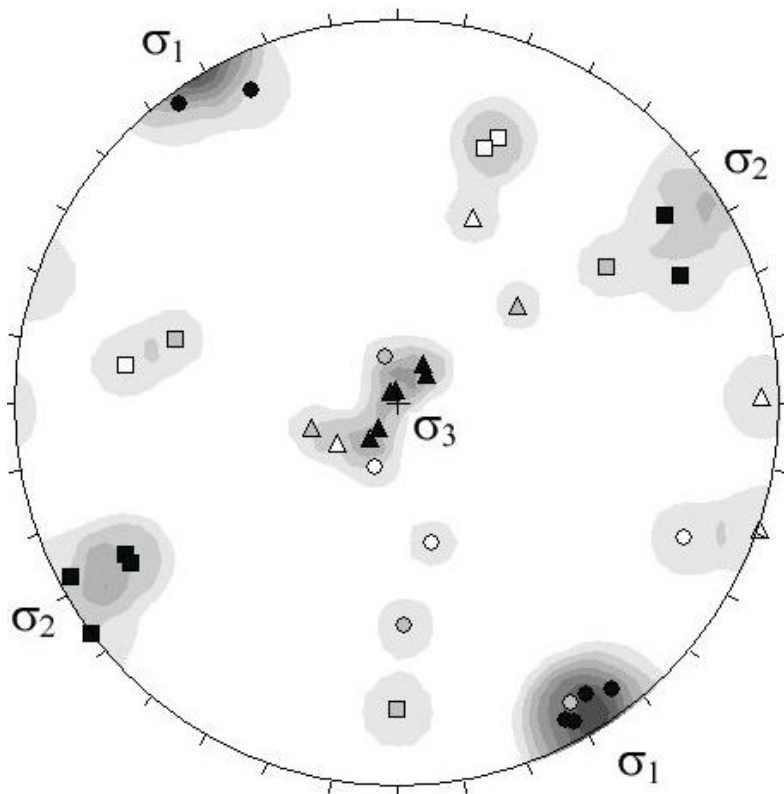


**Figure 5.18:** Principal stress orientations measured by WASM AE and CSIRO HI techniques (Windsor et al. 2006a).

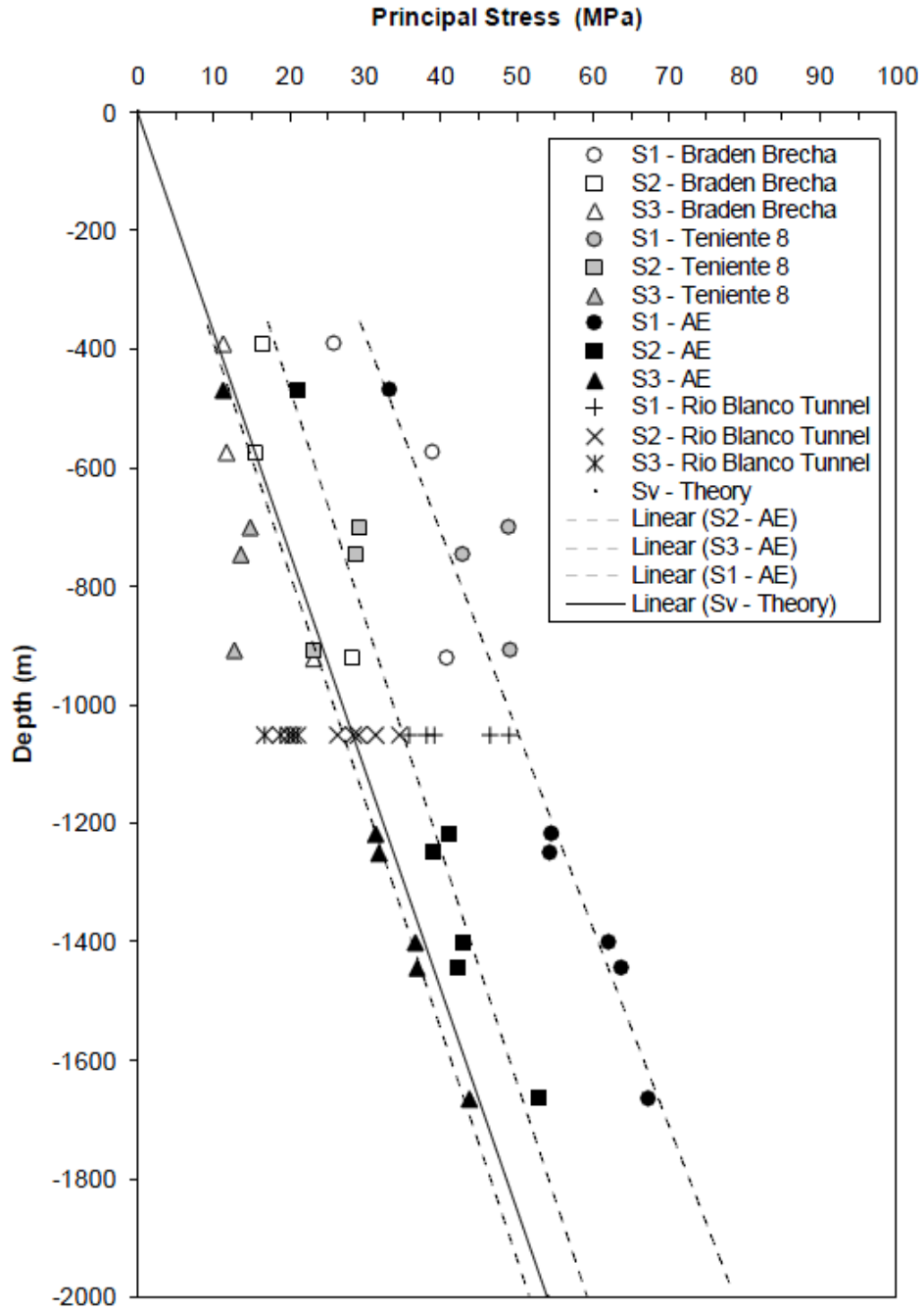


**Figure 5.19:** Magnitude distribution of principal stress measured by WASM AE and CSIRO HI techniques (Windsor et al. 2006a).

During the initial modelling step, in situ stress field, main rock types, and initial surface topology (without mining excavations) were all setup to reach geological equilibrium. A hypothetical erosion of the Andes region surface as far as 20km wide from the mine site was simulated in this process (Figure 5.20) to reach in situ stress field at the mine site used in the model.

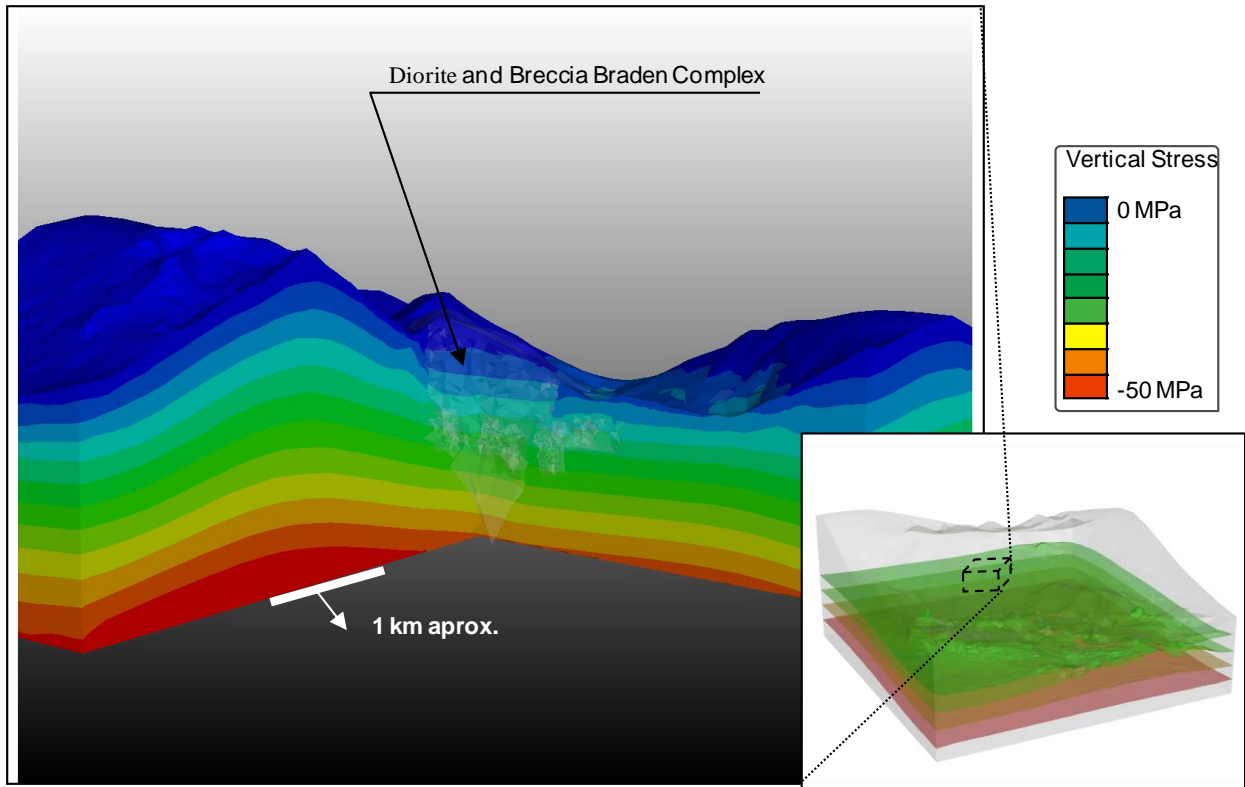


**Figure 5.20:** Initial geological equilibrium with the stress field and initial surface topology after hypothetical ranges erosion.

### 5.5.6 Faults

Experience in block caving and other underground mining methods has clearly highlighted the role of discontinuities upon rock mass behaviour, in particular the location, orientation and nature of discontinuities regarding rock mass response. It was concluded that discontinuum analysis, and a sufficient representation of structure to an appropriate scale was essential. So the representation of faults in the model is essentially identical to the current geological model of large scale structures at El Teniente.

The faults were represented in the model as explicit contact discontinuities which define blocks that can slide and separate. The coupling of a model that can accommodate discontinuous deformation, as well as simulate the gradual degradation of a rock mass is very important for capturing the evolution of stress, seismicity and strain in a working area.

Although the geological structures associated to rock mass at El Teniente mine were reviewed in Section 2.6, the selected main regional faults are shown in Figure 5.21. They were included in the model in order to reproduce the most realistic geology within the mine area.

Additionally, a structural model (tridimensional fault sets) was developed for the Esmeralda operation with the purpose of including it in a numerical simulation representing the most realistic geotechnical

characterisation of the Esmeralda rock mass. Brzovic (2011) developed the structural model taking into account the historical map fault interpretation for 4 plan views of different mine levels around the Esmeralda operation. For each plan view, the faults were identified considering their importance (trace and dimension). This was the main criterion of selection during the building of the 3D volumetric fault system or the discrete fracture network of faults associated to rock mass at the Esmeralda operation. Finally, for the purpose of this study, the interpreted faults were classified into three “local” categories, basically differentiated by their length:

- Major Faults: They represent features in which the same trace length has been recognised across all levels reviewed. This means over 150 m in height. Three major faults have been recognised, named P, B and J. Given that faults do not have infinite size, in three dimensions, they should be considered with respect to observed rock bridge in plan view. Figure 5.22 (red colour).
- Intermediate Faults: This represents the larger structures up to 100 m, but in average they are around 70 m in height. This type of faults does not cross through all levels, but their pattern does. Figure 5.22 shows (blue colour).
- Minor Faults: This represent the structures up to 50 m, but in average they are around 35 m in height. Minor faults are the ones that their vertical length is limited to several meters, for instance, not all minor faults seen in the production level appear in the undercut level (which is only 18 m away). Figure 5.22 (green colour).

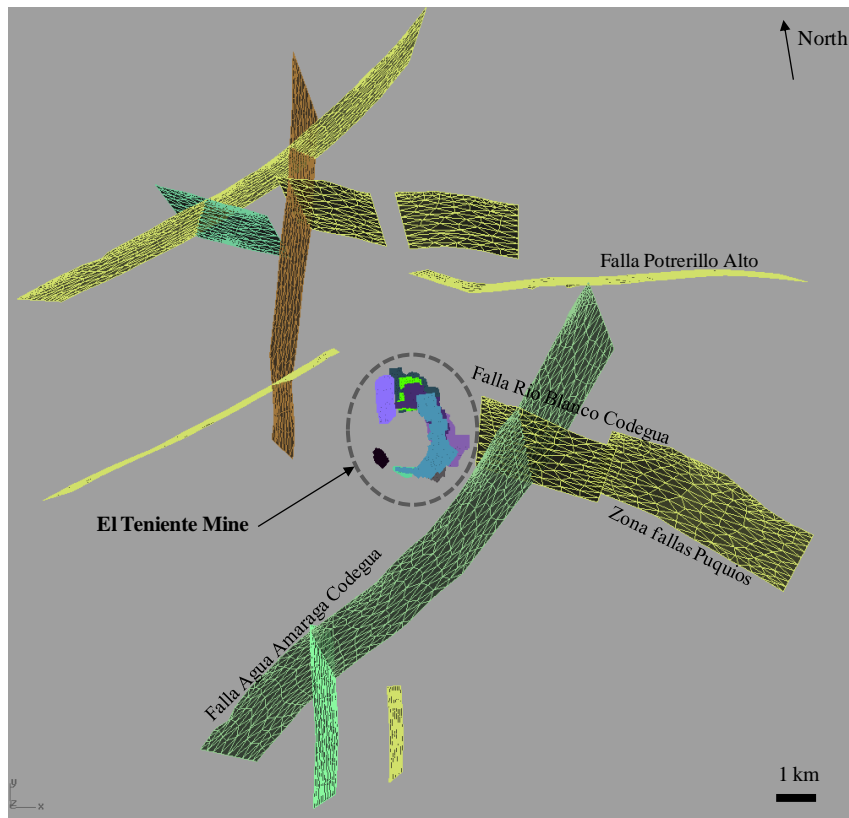


**Figure 5.21:** Plan view of modelled regional faults for El Teniente mine

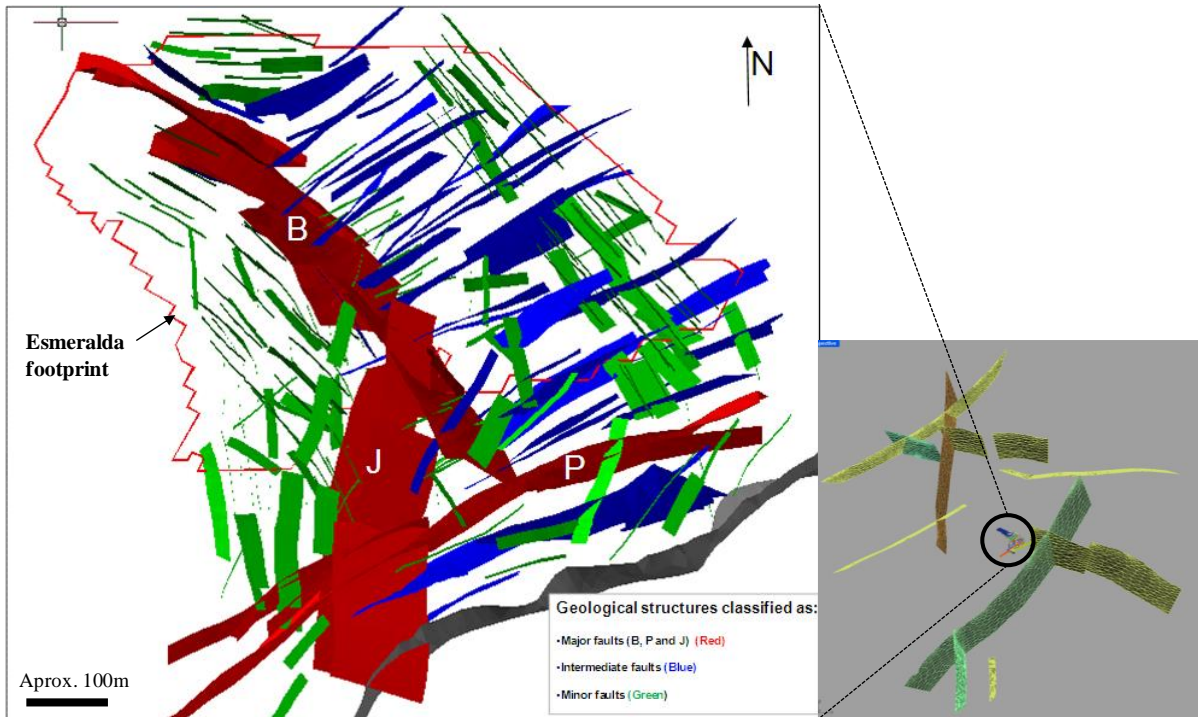


**Figure 5.22:** Esmeralda three dimensional structural model

### 5.5.7 Material Assumptions

The Levkovitch Reusch (LR2) constitutive framework (Levkovitch et al., 2010) was used in the model together with the Hoek-Brown (HB) yield criterion. The inelastic constitutive model for continuum material assumes that each material has peak and residual strength and elastic properties. In the model, yield results in dilation, and once the peak strength is exceeded, residual properties are introduced. Cohesion, friction angle, stiffness and compressive strength are all reduced as a result of yield, and then a dilation angle for yielded materials is calibrated.

All the representatives major rock type of the rock mass at El Teniente mine were described in Section 2.5 together with the rock mass properties used in the simulation. CMET (andesites), diorites and different breccia were included in the model as the most representative lithology bodies of El Teniente Mine. In addition, a specific characterisation was done for the predominant lithology at the Esmeralda operation. This corresponds to the CMET and divided in two geotechnical units called CMET hangingwall (Hw) and CMET footwall (Fw). This lithology has been described as having different mechanical behaviour (Brzovic, 2010).

In order to improve the rock properties knowledge of the Esmeralda rock mass, triaxial compression tests for the predominant lithologies CMET Hw and CMET Fw were undertaken by the WASM laboratory (Villaescusa and Machuca, 2011). These included 3 uniaxial compression tests and 9

triaxial compression tests with different confinement levels for each unit. The peak and residual strength of each rock material was determined.

The Uniaxial compressive strength (UCS) testing results and the Triaxial testing results are detailed in Figure 5.23 and Figure 5.24 respectively.

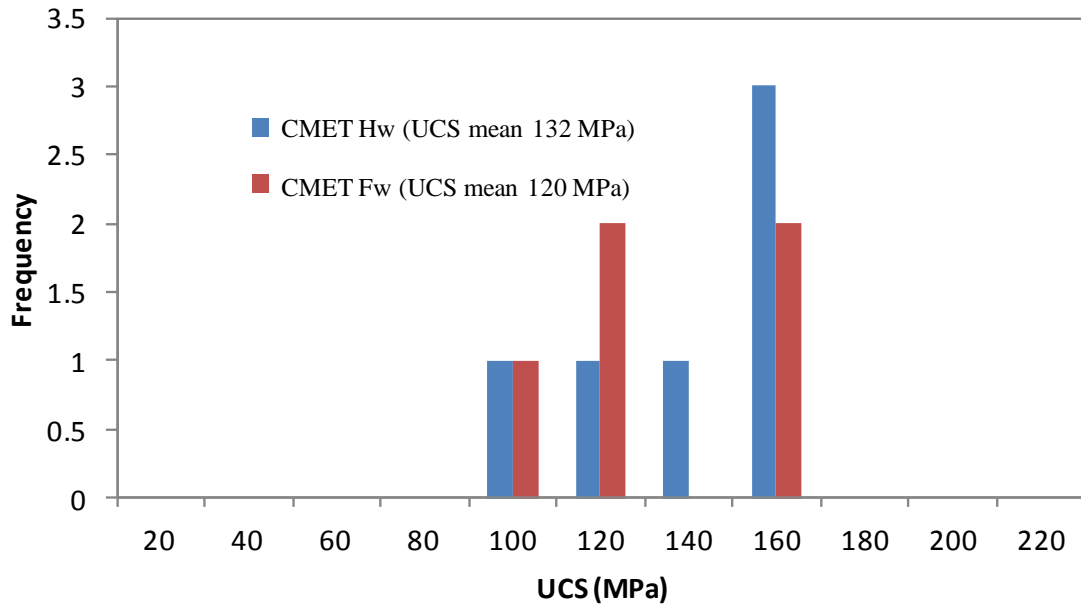


Figure 5.23: Uniaxial compressive strength.

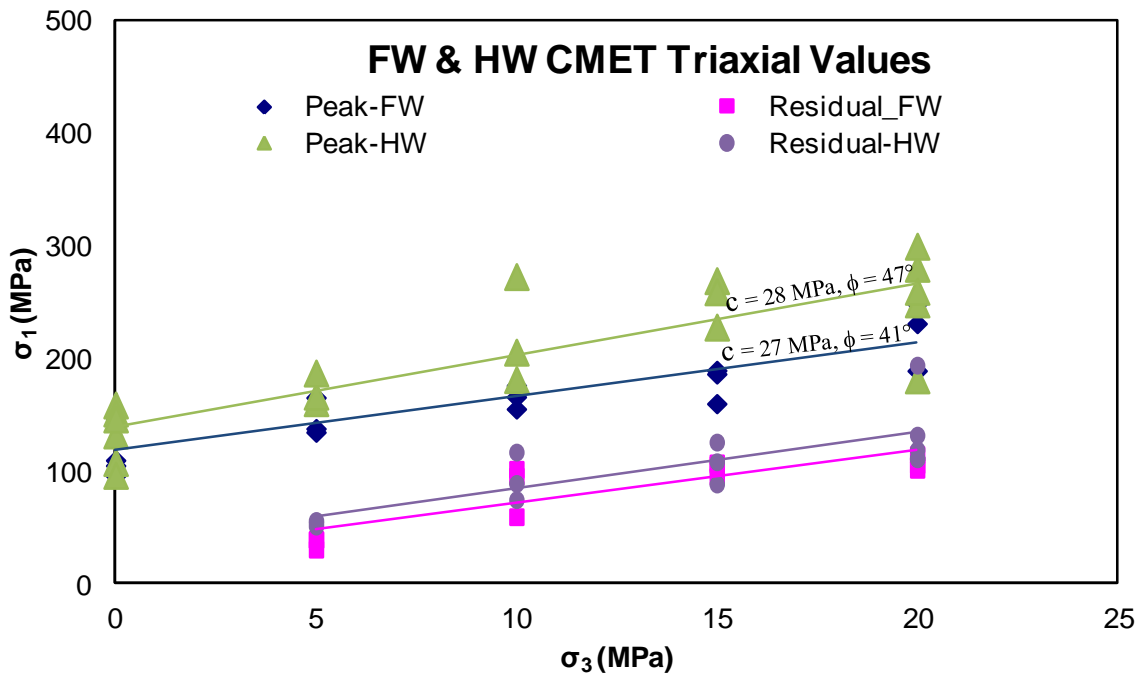


Figure 5.24: Triaxial compressive strength.

## 5.6 MODEL CALIBRATION

### 5.6.1 Selection and Bracketing

This task is a definitional stage: the governing physics of the problem are identified first to aid in setting the model fundamentals, which include:

- The match between modelled and actual estimated in situ stress field.
- The constitutive model – the match between the model and the governing mechanism.
- Mesh composition and quality, if applicable
- Dimensionality, geometry and stress path.
- Numerical solution scheme.

For the selection and bracketing stage many of the constraints and freedoms governing the setting of the model fundamentals were analyzed in previous sections.

An example of the final stress field distribution and geological equilibrium reached after those empirical material properties, in situ stress field and surface topology were all setup as part of the bracketing stage as shown in Figure 5.25. The image shows an isometric view of the global model with the vertical stress distribution after the hypothetical erosion of the Andes region surface was simulated in this process. The magnitude distribution of vertical stress for initial and final bracketing step can be seen in Figure 5.25.

### 5.6.2 Detailed Fine Adjustment

The detailed adjustments involve careful adjustments of material properties and geometric parameters to achieve a better match to specific observations. The procedure involves iterative identification of incongruities that highlight couplings between parts of the model and particular material properties. This iterative process is based on comparing measured observations to modelled results.

The model for the Esmeralda operation was firstly calibrated by correlating modelled rate of energy release (RER) and the measured seismic events. The measured observational rock mass damage was then compared to modelled damage in order to develop a local scale of damage upon the extraction and undercut levels at the Esmeralda operation.

The final calibration was achieved after 24 runs of models where global and local adjustments were done. A detailed record of the major adjustments done during calibration process is shown in Table 5.4.

Finally, the main phases of this iterative process named calibration for the Esmeralda model are detailed in the following points. These phases were classified on a detailed description of material

property adjustments, correlation between modelled RER and measured seismicity and comparison of measured damage and model.

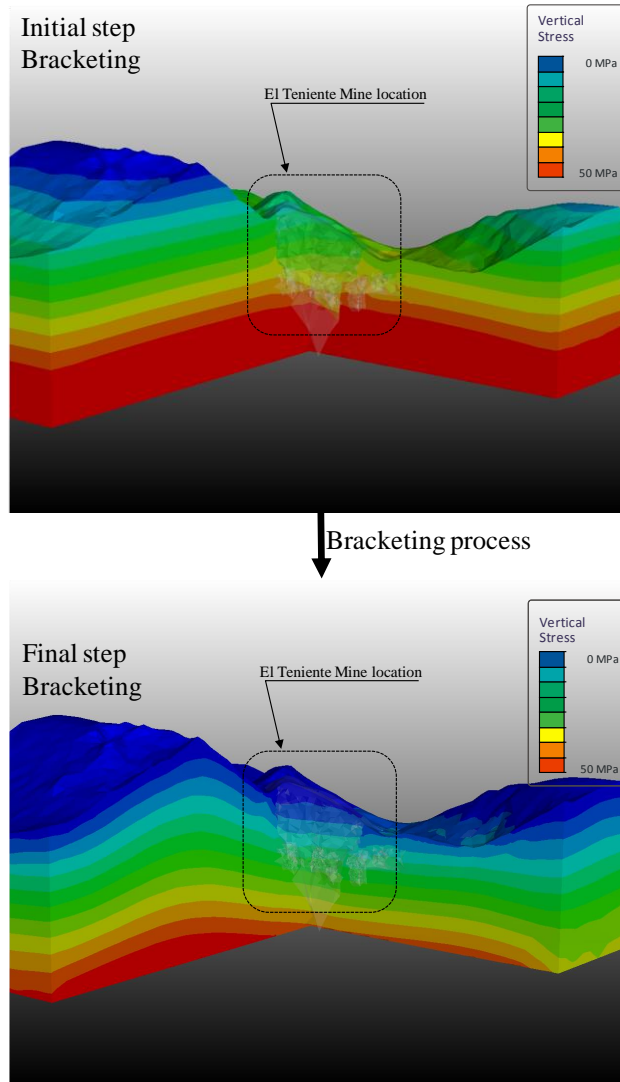


**Figure 5.25:** Magnitude distribution of vertical stress during bracketing phases.

### 5.6.3 Resulting Material Properties

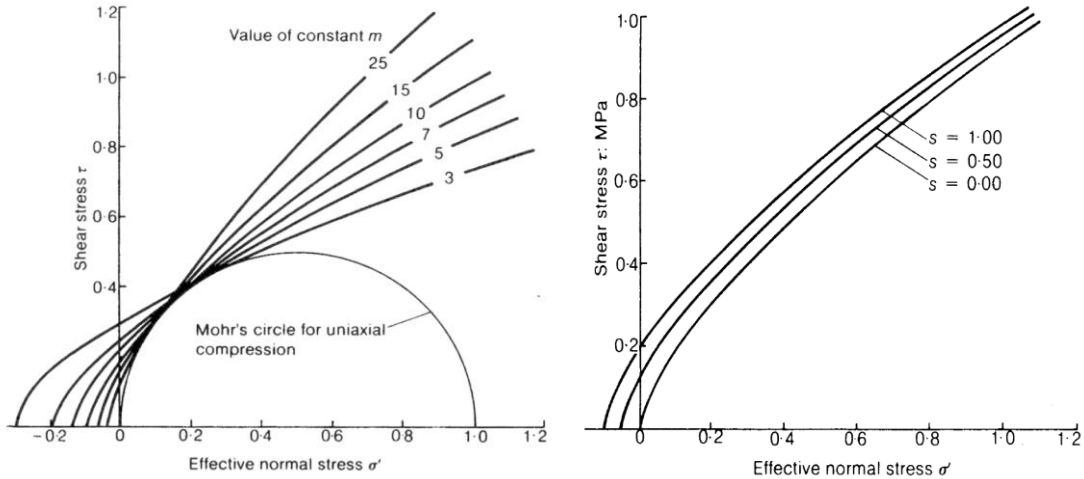
Several iterations of the model have settled on a preliminary estimate of material properties for the main geological domains. Knowledge of the stress path, plastic strain and RER in this model enables detailed adjustments of material properties.

Figure 5.26 shows how the Hoek and Brown (HB) yield envelope varies with changes in parameters  $m$  and  $s$ : increasing  $m$  approximates increase in friction angle and increasing  $s$  approximates increases in cohesion without a change in friction angle. Changing  $m$  or  $s$  parameters in isolation will change

the shape of the HB curve, so a compensatory adjustment may be necessary to maintain a good correlation across the range of stress, but it is generally a simple task. Tools such as ROCLAB, or a spread sheet scripted to show the shape of the HB curve for small changes in m or s can be used to aid achieving the necessary adjustments.

**Table 5.4:** Detailed record of major model adjustment during calibration

<b>Model</b>	<b>Run</b>	<b>Detailed description about adjustment of modelling parameters</b>
M01	Bracketing	Initial test run with extraction of old cave sections only. Material properties are a 1:1 conversion from MC to HB.
M02	Bracketing	Full sequence with corrected properties (UCS and GSI reduced accounting for scale dependence)
M03	Bracketing	Full sequence with corrected properties (UCS and GSI reduced accounting for scale dependence), M03 has some weaker UCS and GSI
M04	Bracketing	Under cut block are now modelled with very low extraction ratio. Same is very similar to M04.
M05	1	New approach using computator scheme with UCS and GSI of M04.
M06	2	Moderate changes to CMET and HOST with respect to M05.
M06SG	3	Using M06 with a self grwoing (SG) cave and a criterion of DU=60mm
M07SG_60mm	4	Using M07 (a completely new approach) with a self grwoing (SG) cave and a criterion of DU=60mm
M07SG_90mm	5	Using M07 (a completely new approach) with a self grwoing (SG) cave and a criterion of DU=90mm. Not enough cave growth.
M07SG_35mm	6	Using M07 (a completely new approach) with a self grwoing (SG) cave and a criterion of DU=35mm and refined sequence. Excessive cave growth.
M07SG_45mm	7	Using M07 (a completely new approach) with a self grwoing (SG) cave and a criterion of DU=45mm and refined sequence. Ok cave. Starts off to slow.
M07SG	8	Introducing SEQ06 which is a less-1-year sequence now.
M08SG	9	Make Brechia Braden a little bit weaker. Correct on stiffness error on LAT material.
M09SG	10	Make blue faults a little bit stronger. Introducing SEQ07 with remanent pillar.
M10SG	11	Keep properties from M09. Make slow moving cave stiffer.
M11SG	12	Make diorite a little bit stronger and red faults a little bit weaker. Cave made stiffer. (Factor is now 0.04)
M12SG	13	Red faults a little bit weaker. Cave stiffness half way back. (Factor is 0.03)
M13SG	14	CMETFW has 2 additional weaker zones
M14SG	15	CMETFW has 2 additional weaker zones. Elastic module is not changed.
M15SG	16	CMETFW has 2 additional zones
M15SG	17	Collapsed cave region introduced that reached out into the SUR4 region.
M16SG	18	Collapsed cave region made stiffer.
M17SG	19	New stress field introduced.
M17SG	20	CMETFW has 2 additional weaker zones
M17SG	21	CMETFW has 2 additional weaker zones. Elastic module is not changed.
M17SG	22	CMETFW has 2 additional zones
M17SG	23	Sequence information was corrected. Some UC drives were added. SEQ10
M17SG	24	The UC drives which were added are removed again but this time as part of the UC block, i.e. they got a different timing. SEQ12



**Figure 5.26:** Proxy relation between cohesion and friction angle for Hoek-Brown parameters  $m$  and  $s$ .

Although over seven material property sets representatives of El Teniente mine were used to develop the global model, only the adjustments of the geology units (CMET Hw, CMET Fw and Diorite) representatives of the Esmeralda operation and geology faults are reported here. Indeed these predominant lithologies and structural sets have been characterised to have different mechanical behaviour and they have controlled the rock mass damage experienced upon the extraction level and undercut level at the Esmeralda operation.

As part of the resulting calibration process the changes from models developed (from M05 until M17) for peak strengths HB properties are shown in the following figures. Figure 5.27 shows the changes from M05 to M17 for unit CMET Fw; Figure 5.28 shows the changes from M05 to M17 for unit CMET Hw and Figure 5.29 shows the changes from M05 to M17 for unit Diorite. In addition, Figure 5.30 shows the changes from M05 to M17 for modelled Esmeralda faults.

Over the course of the detailed calibration from M05 to M17 the overall changes were small but important; the following controls were observed and will be expanded in the next sections:

- Faults strength: These partitions and concentrates damage on undercut and extraction level
- Material properties: these control gross behaviour; however the unit CMET Fw has been identified as the most sensitive unit controlling the rock mass damage experienced.
- Cave geometry and scheduling: have a major influence on seismicity, extraction and undercut damage, footprint loading.

Finally, the representative properties with which the final calibration was achieved are shown in Figure 5.31 and also the changes over the entire process, from M01 to M17 are collected in Tables included in the Appendix B.

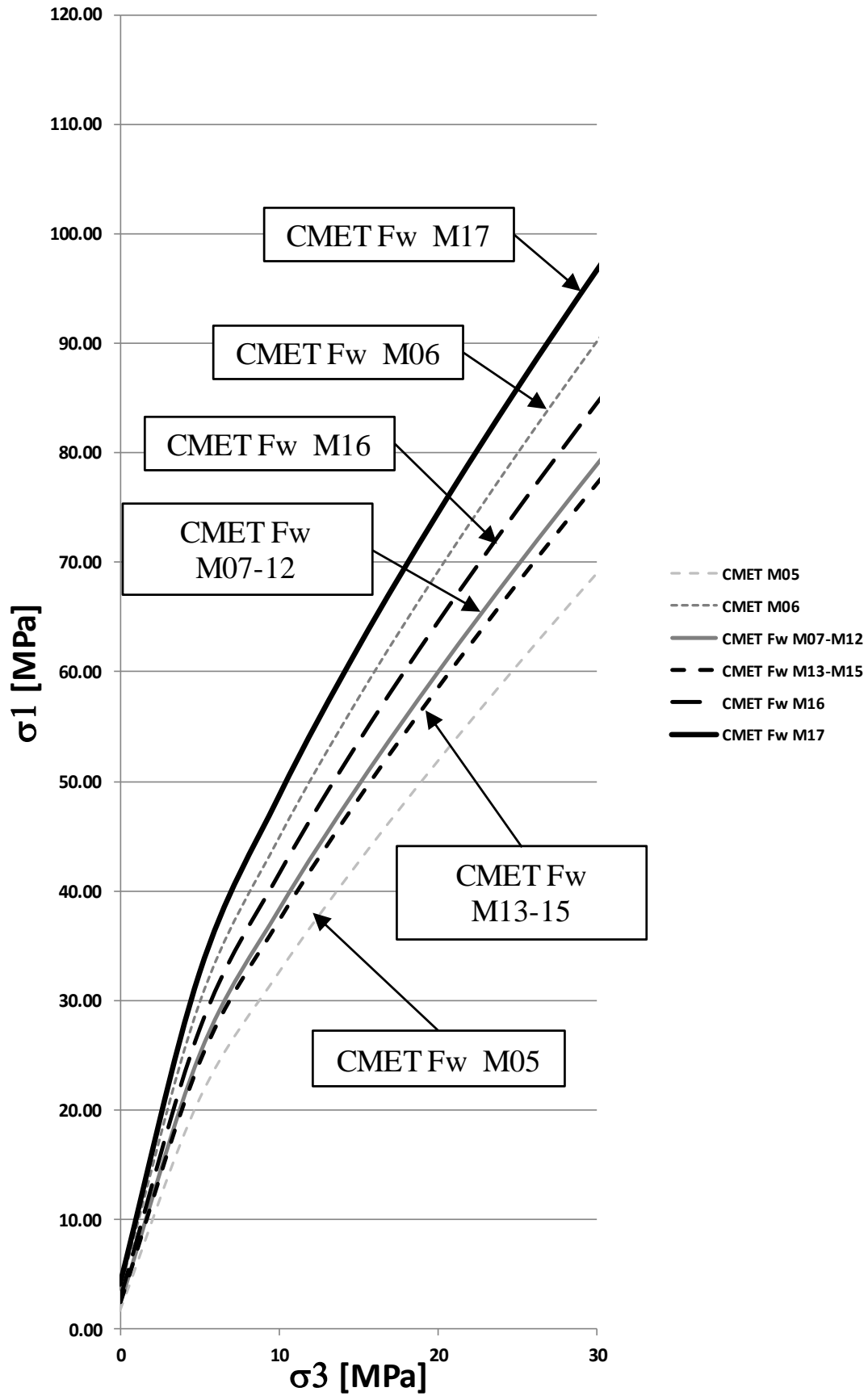


Figure 5.27: Changes to peak strength for CMET Fw between M05 and M17.

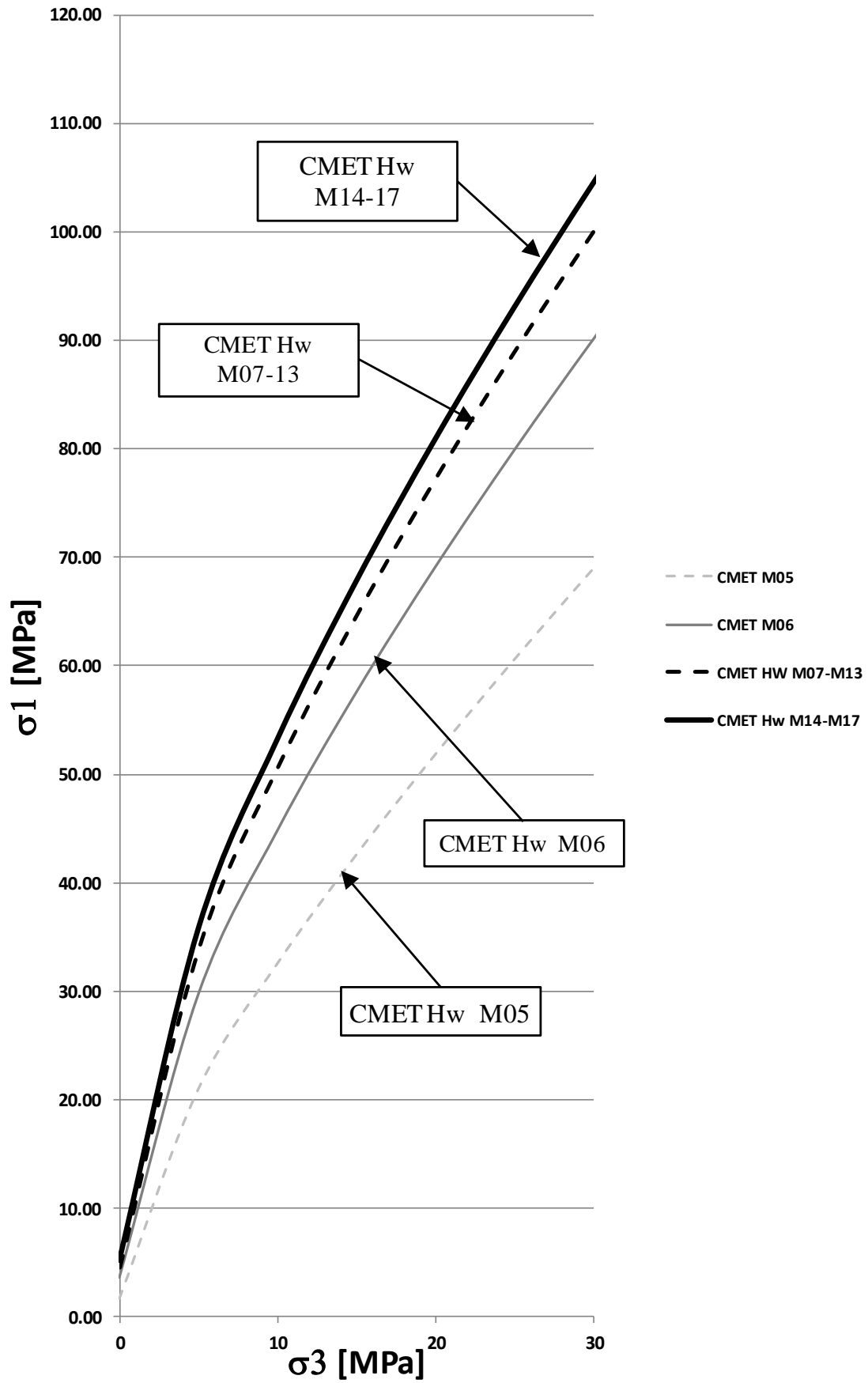


Figure 5.28: Changes to peak strength for CMET Hw between M05 and M17

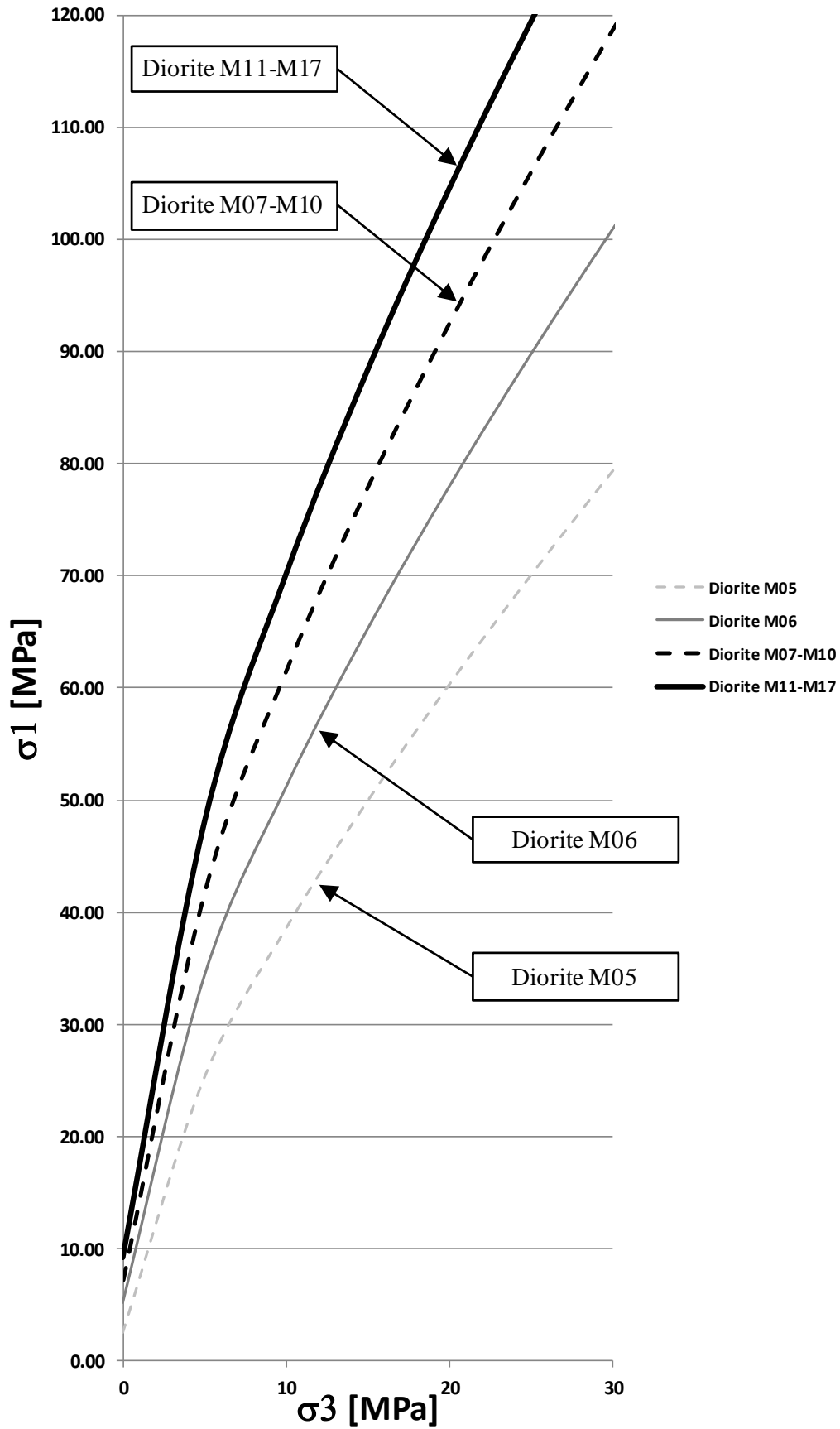


Figure 5.29: Changes to peak strength for Diorite between M05 and M17.

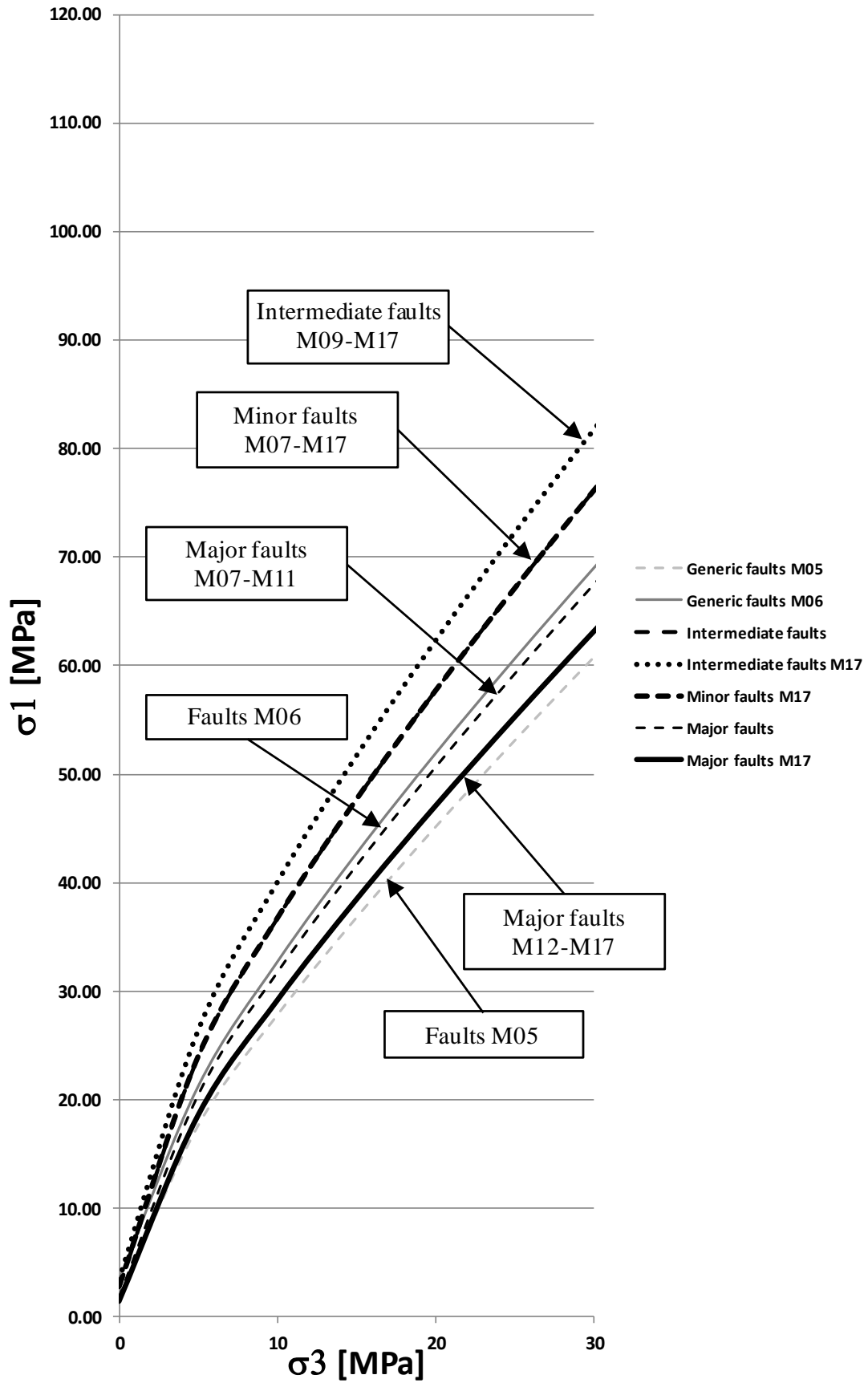


Figure 5.30: Changes to Faults properties between M05 and M17.

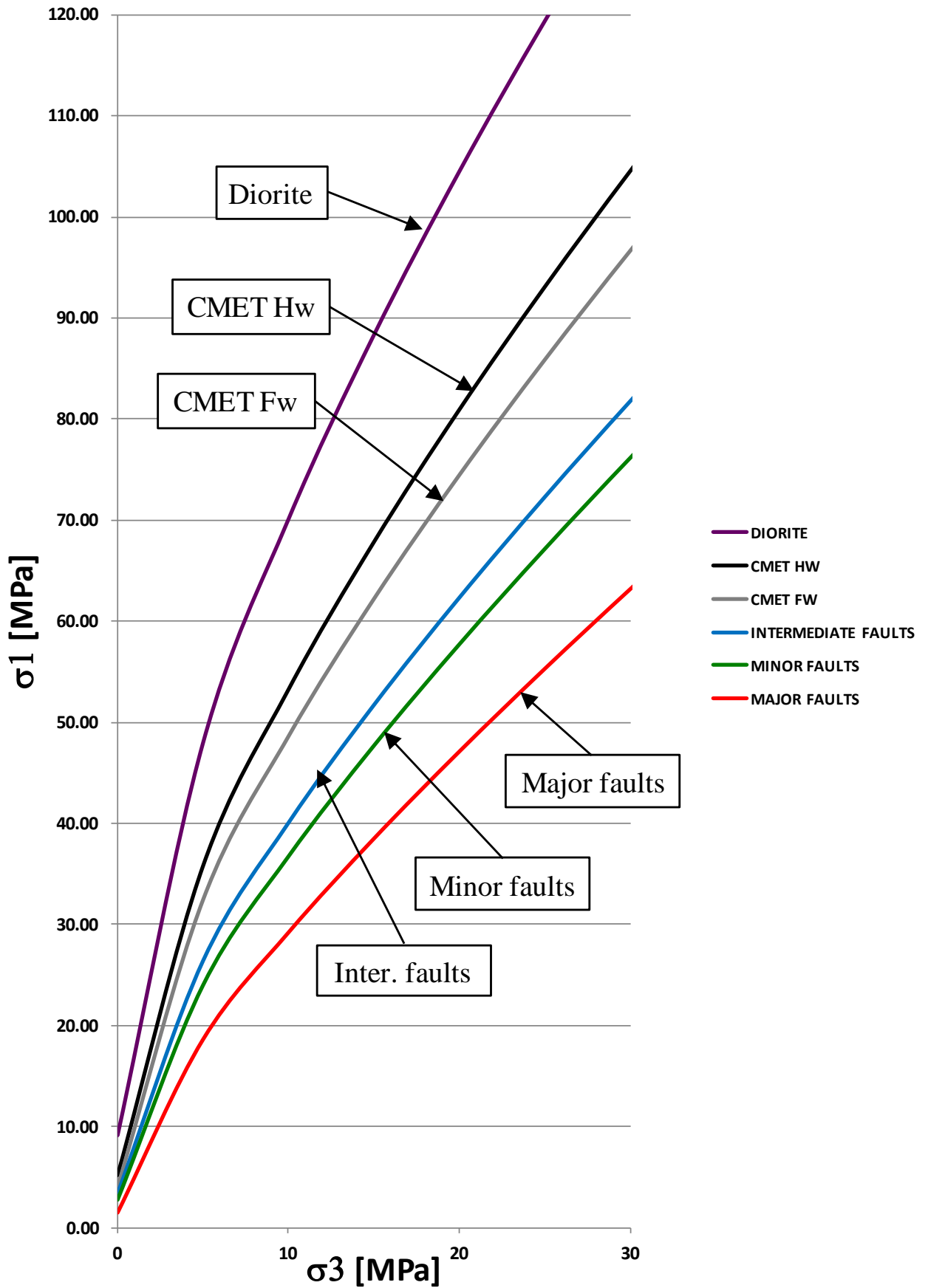


Figure 5.31: Final material property sets (M17) used in calibrated model version.

#### 5.6.4 Correlation to Measured Seismicity and Modelled Energy Release

The mining of excavations in rock re-distributes stress and causes damage to the rock mass and discontinuities. The resulting reduction in strength and degradation in stiffness of the damaged rock and structures leads to further deformation and release of stored elastic strain energy. One portion of this released energy is consumed by the damage process - frictional sliding and the creation of new surfaces. This energy cannot be retrieved, so is counted as 'dissipated'. If the value of the released elastic energy is higher than the energy dissipated by the irreversible damage, the surplus is emitted into the surrounding rock. These release events are seismic events.

The magnitude (and/or the rate) of the released energy during these events can be measured in a mine using a seismic monitoring system or calculated using a model. The instantaneous, peak (i.e. maximum) rate of energy release from a volume of rock (i.e. the energy that is not dissipated) is the Rate of Energy Release (RER).

A direct comparison between energy changes in the model and actual seismicity was carried out during this stage. The purpose was to capture the connectedness between different parts of a mine by simulating degradation and distortion of the rock mass and faults, along with the output of the dynamic nature of the movements with a close match to measured seismicity. Thus a match both for seismic and aseismic zones across time and the areas of interest is performed.

A correlation is carried out between the modelled Rate of Energy Release (RER) and measured seismic events; RER is measured in  $W/m^3$  or  $W/m^2$  and the intensity of events is measured within clusters of seismicity represented by inter-event (IE) distance iso-surfaces of approximately 10 – 20 m. The expected nature of this correlation can be used to assist initially to calibrate the model.

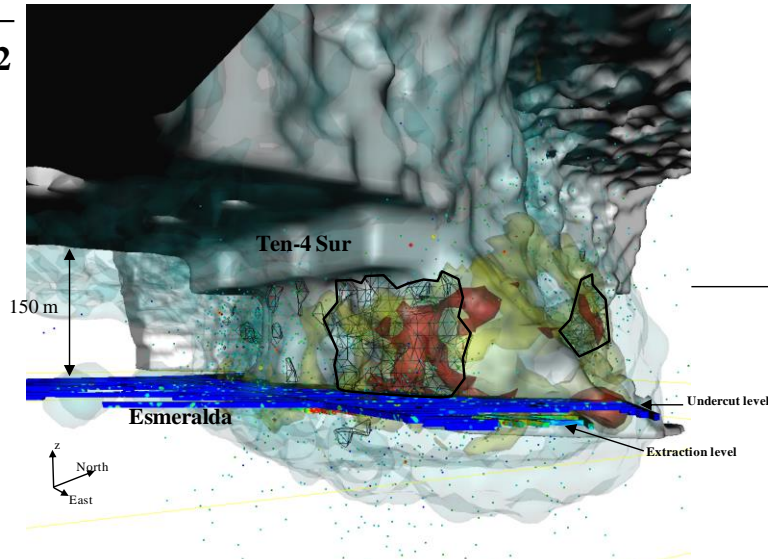
The comparison of modelled and measured seismicity for the calibration period represents a preliminary stage of the entire calibration process. Furthermore, this process has also been used to validate the final material properties during the whole modelling of the extraction geometries modelled. This is done qualitatively by visually comparing the intensity of events within clusters of seismicity to the modelled measures of nucleating, coalescing and faults slip seismicity.

To establish an approximate relation between RER and seismic potential, the isosurfaces for high intensity seismic activity defined as a cluster with an IE distance of  $< 5m$ , were compared to various RER levels until the estimated best fit shown in the images was found. Although this approach was undertaken assessing the results for the whole Esmeralda extraction history modelled between 1996 and 2010, Figure 5.32 shows the most representative examples for a comparison of modelled and measured data associated with each one to one extraction geometry or period modelled (model step) that simulate a quarter span. In addition, a detailed summary of images for each period can be seen in Appendix C.

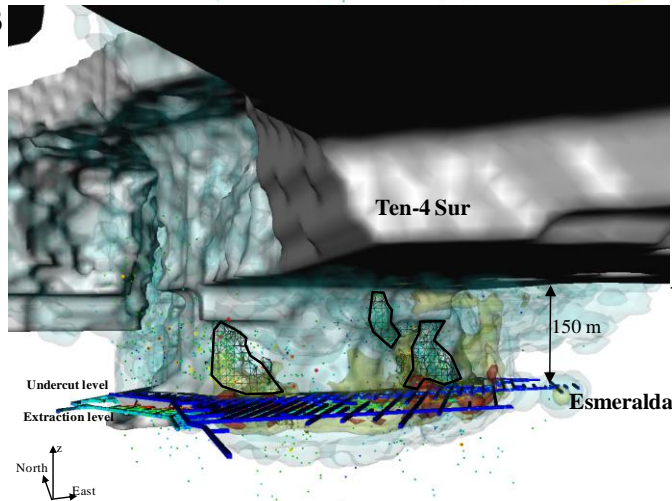
Cross-checking of modelled energy release and seismicity in each assessed period indicated a close match between dense event clusters and the intense modelled energy release for most mining areas across most model steps. The issue highlights that the model is best used for global simulations, and it needs to account for the possibility that certain structures have not been mapped, but which may pose a significantly elevated seismic risk.

After this comparison, it was concluded that the model was fit for the purposes of preliminary simulating global seismic response. A model with this resolution also highlights areas where additional data collection is required to provide input to subsequent modelling phases to improve resolution and reliability.

Late 2001 –  
Early 2002



May 2003



Mid 2008

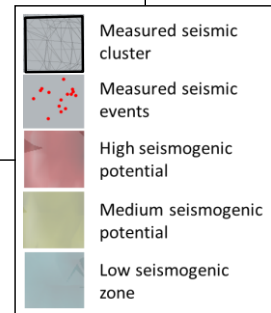
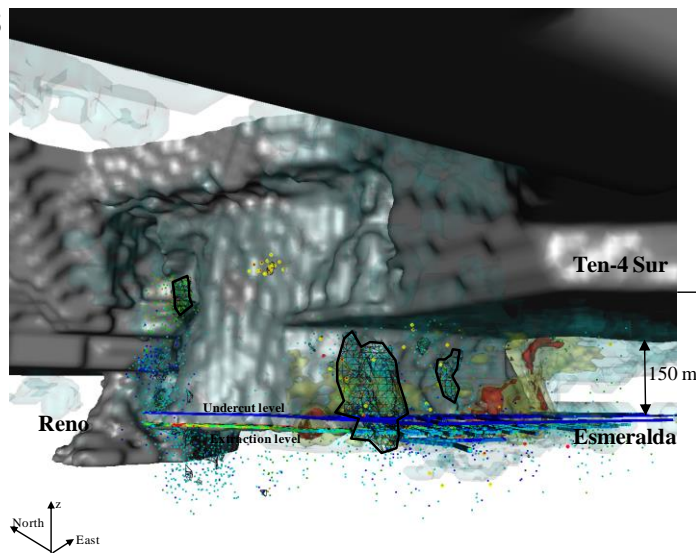


**Figure 5.32:** Examples of modelled energy release versus measured seismicity for three different steps, software Voxler.

### 5.6.5 Comparison with measured rock mass damage

A certain critical threshold of displacements or velocity generally defines the criteria for instability. These criteria occur within a certain time frame and can be measured using instrumentation, such as extensometers, TDR cables or topography surveys. However, other criteria such as Strain can be qualitatively assessed as visual rock mass damage (Beck and Duplancic 2005) but cannot be measured quantitatively during operations.

Numerical modelling provides a way to estimate the levels of strain accumulated during mining by means of use of plastic strain value discussed in Section 5.3. The estimated value of plastic strain is used to infer damage in underground excavations where the rock mass will yield as a results of mining.

As part of calibration process and to achieve the most reliable simulation of global deformation for extraction history at the Esmeralda operation, an iterative assessment from numerical modelling using the plastic strain values was carried out for the observed rock mass damage during operations at Esmeralda. In order to achieve the best approach between damage measured (observed) and plastic strain modelled, all the modelled extraction geometries discussed in Section 5.5.4, were assessed for each material property set evaluated. Indeed, different types of observed rock mass damage were used in this approach and they were recorded during the whole extraction history of the Esmeralda operation.

First of all, the mapped rock mass damage ahead of the undercut front associated to any extraction geometry was used to correlate to the plastic strain generated by exactly the same extraction geometry modelled. Although the damage mapping ahead of the undercut front was discussed, the main classification and damage scale used in this approach is highlighted in the following points and one representative example of the mapped damage associated to extraction geometry May 2007 is shown in Figure 5.33:

- Significant damage: Multiple shotcrete slabbing, failure behind mesh and failure of mesh are evidenced. Failed corners and brown, hole problems. Rehabilitation is required to maintain access. Multiple cracks and up to 2.0 m of over-break and dripping of rain water influx could be observed. A representative photo the Undercut level at Esmeralda operation is shown in Figure 5.34.
- Moderate damage: Shearing on existing structures, visible yield. Shotcrete slabbing, exposed embedded mesh with isolated broken spots is evidenced. Increased load in rock bolt plates. Up to 1.0 m over-break and dripping condition of water influx could be observed. Drive still safe for travel. A representative photo the Undercut level at Esmeralda operation is shown in Figure 5.35.

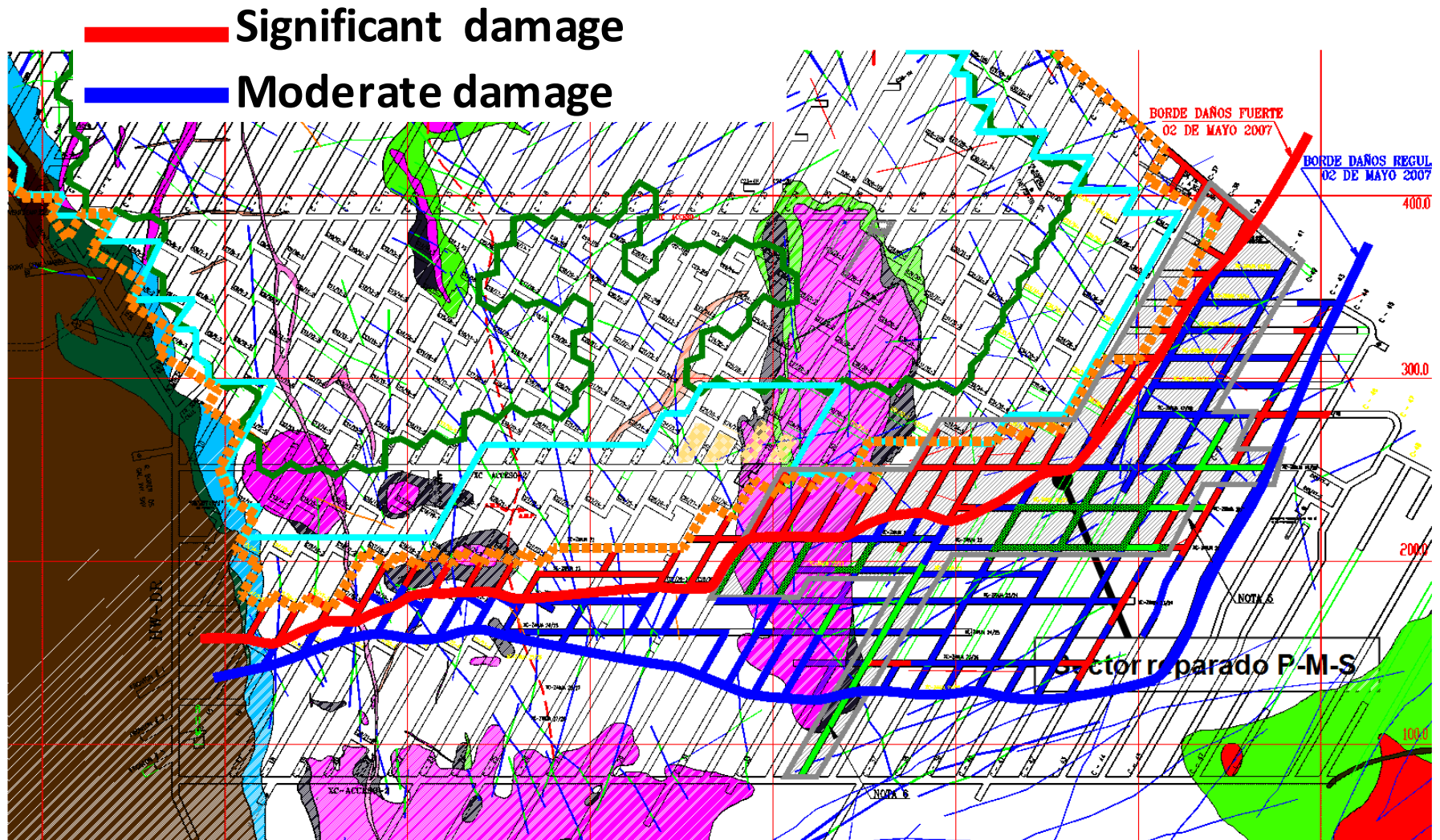


Figure 5.33: Representative example of one mapped damage ahead of undercut front for extraction geometry May 2007 (Geotechnical team, Div. El Teniente 2007).



**Figure 5.34:** Representative photo of significant damage in the Undercut level at Esmeralda operation.



**Figure 5.35:** Representative photo of Moderate damage in the Undercut level at Esmeralda operation.

The damage maps for Esmeralda extraction geometries were generated by term between 1997 and 2010. The majority of these maps were correlated with the plastic strain generated by the model; in fact a detailed summary can be seen in Appendix C.

The most representative example developed can be seen in Figures 5.36, 5.37 and 5.38 below, where for exactly the same geometry modelled, the mapped damage thresholds are superseded upon the plastic strain distribution in the Undercut level.

The same plastic strain distribution generated by the model was compared with the records of the undercut area (Pillars) which were significantly affected by extensive damage that resulted in invalidating the intended function of the excavation or in other words collapse of undercut areas. During 2003 and 2004 detailed observations of the high intensive damage were undertaken by geotechnical team at El Teniente mine, where part of the pillars located ahead of the undercut front in the Eastern zone and associated to the CMET Fw geology unit were collapsed and identified as abandoned pillars. According with the El Teniente mine classification, this type of damage is characterised by massive failure of shotcrete and mesh strands, significant cracks and open rock blocks and multiple failures of rock bolts.

By definition, pillar instability is reached when the strain in the pillar core reaches a critical level. At the critical level, pillar deformation will continue to occur at constant (or decreasing) stress. Interpreting pillar core conditions using plastic strain is consistent with standard geotechnical practice. Conventional theorems of plastic collapse for limit analysis are well documented (Yu 2006; Hill 1951). The only possible interpretation of very significant plastic strain in pillar cores is pillar collapse.

The superseded results of observed abandoned undercut pillars (collapsed undercut pillars) and the plastic strain value on undercut level for exactly the same extraction geometry modelled are shown in Figures 5.39, 5.40 and 5.41. The sequence shows the damage evolution experienced between 2003 and 2004 on the undercut level of the Esmeralda operation.

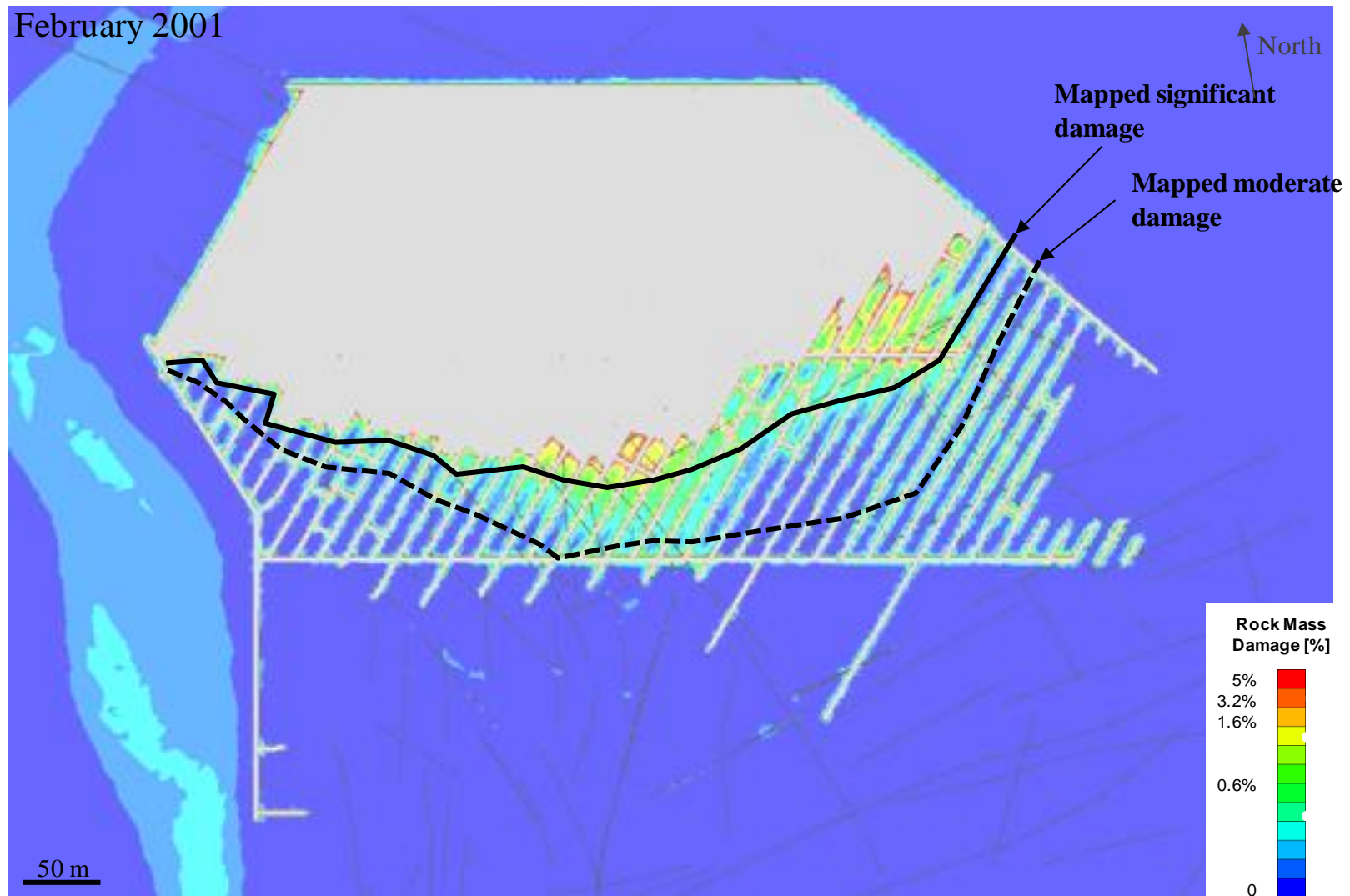


**Figure 5.36:** Superseded results, plastic strain in the model correlated with damage threshold contoured from mapped damage for the exactly same extraction geometry modelled (first term 2001).

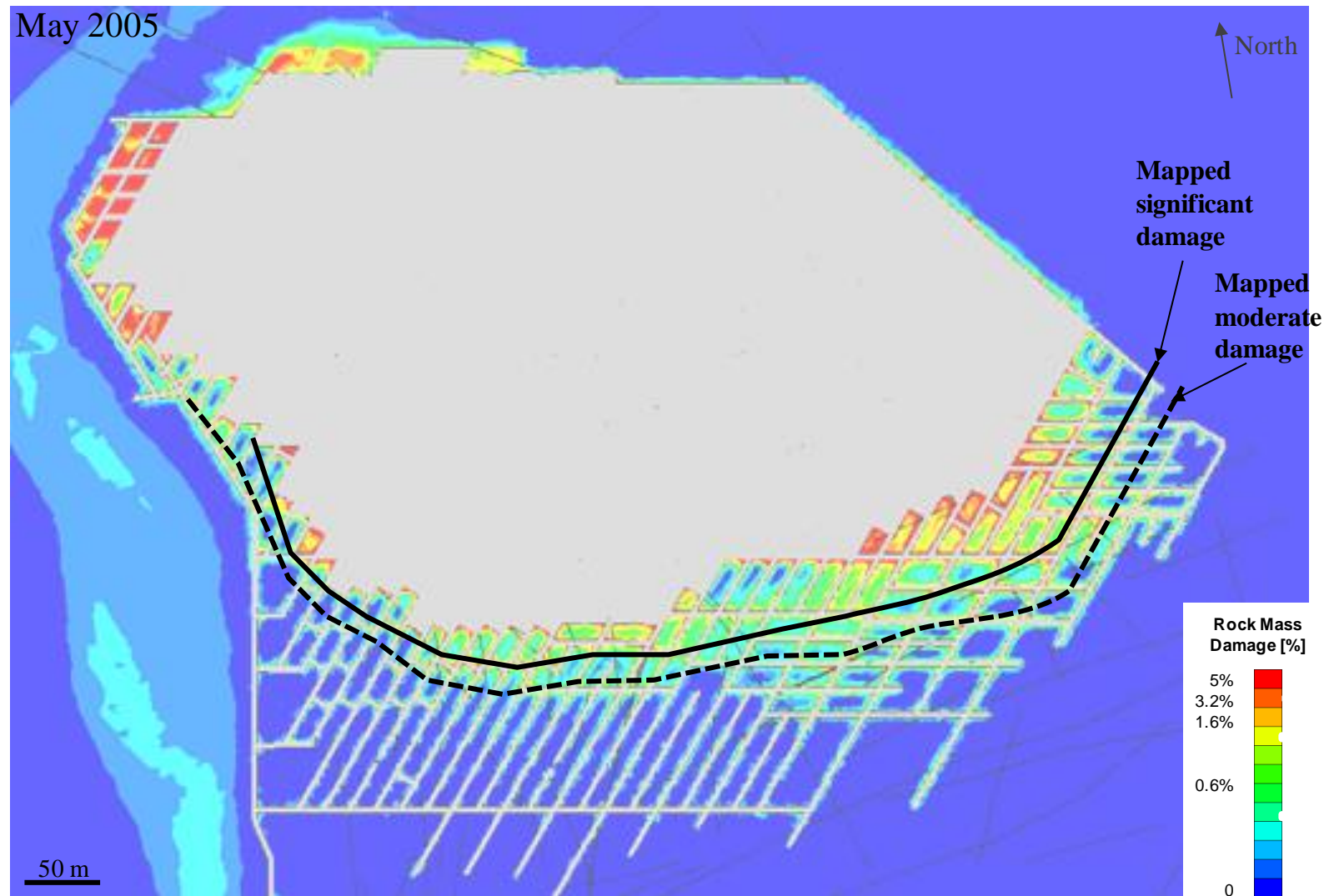


**Figure 5.37:** Superseded results, plastic strain in the model correlated with damage threshold contoured from mapped damage for the exactly same extraction geometry modelled (second term 2005).

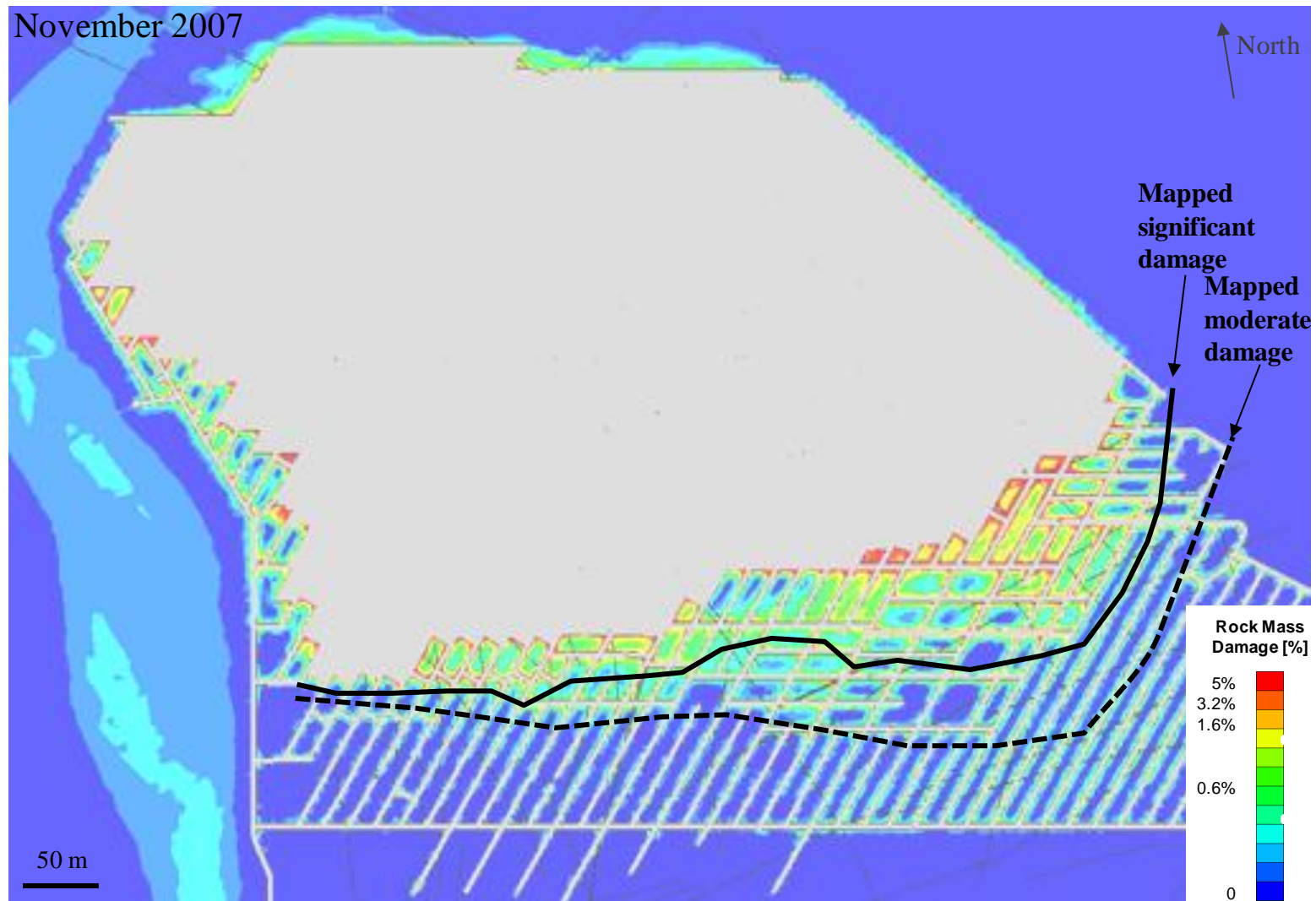


**Figure 5.38:** Superseded results, plastic strain in the model correlated with damage threshold contoured from mapped damage for the exactly same extraction geometry modelled (last term 2007).

August 2003

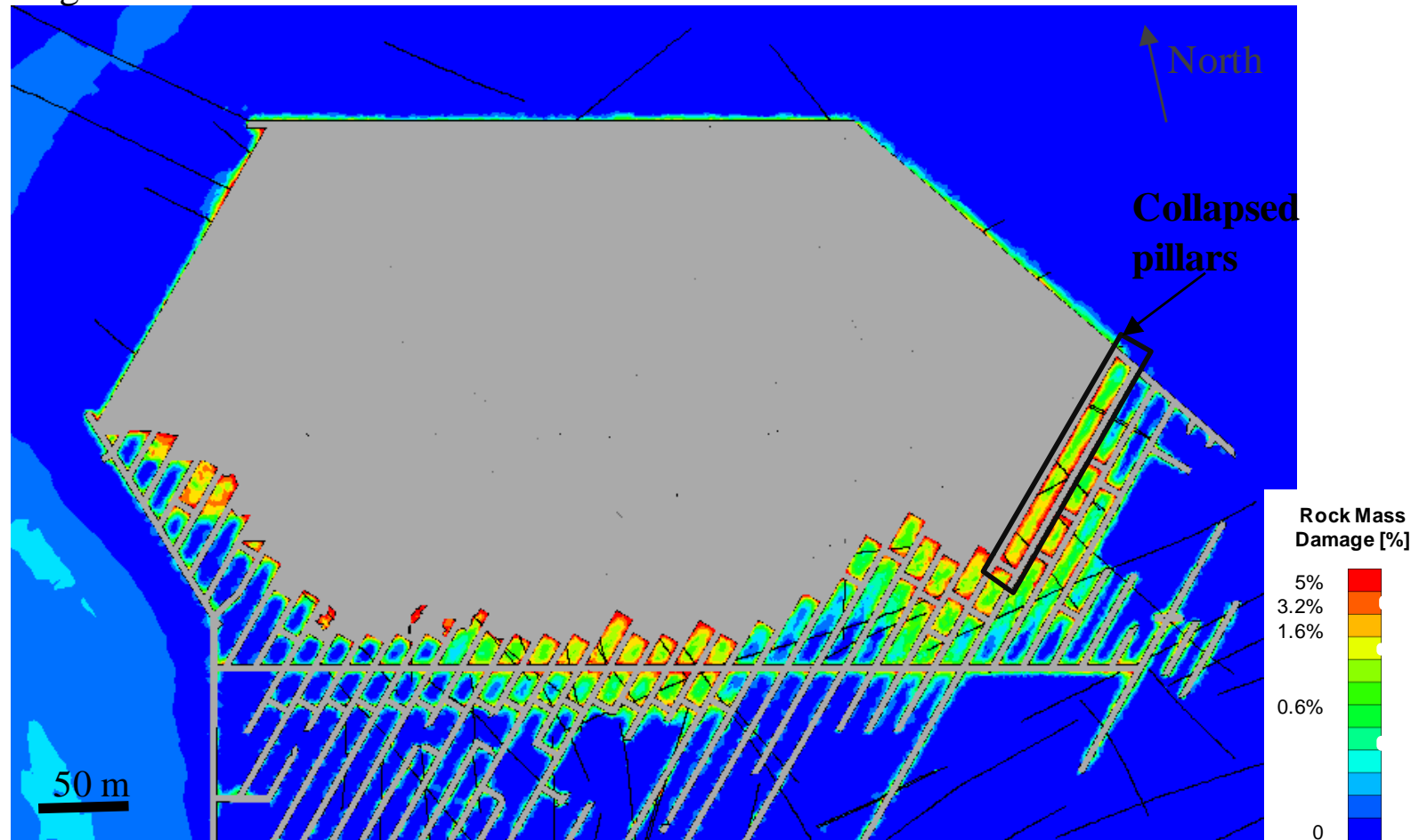


**Figure 5.39:** Contoured collapsed area within undercut level and plastic strain from extraction geometry modelled (second term 2003).

December 2003

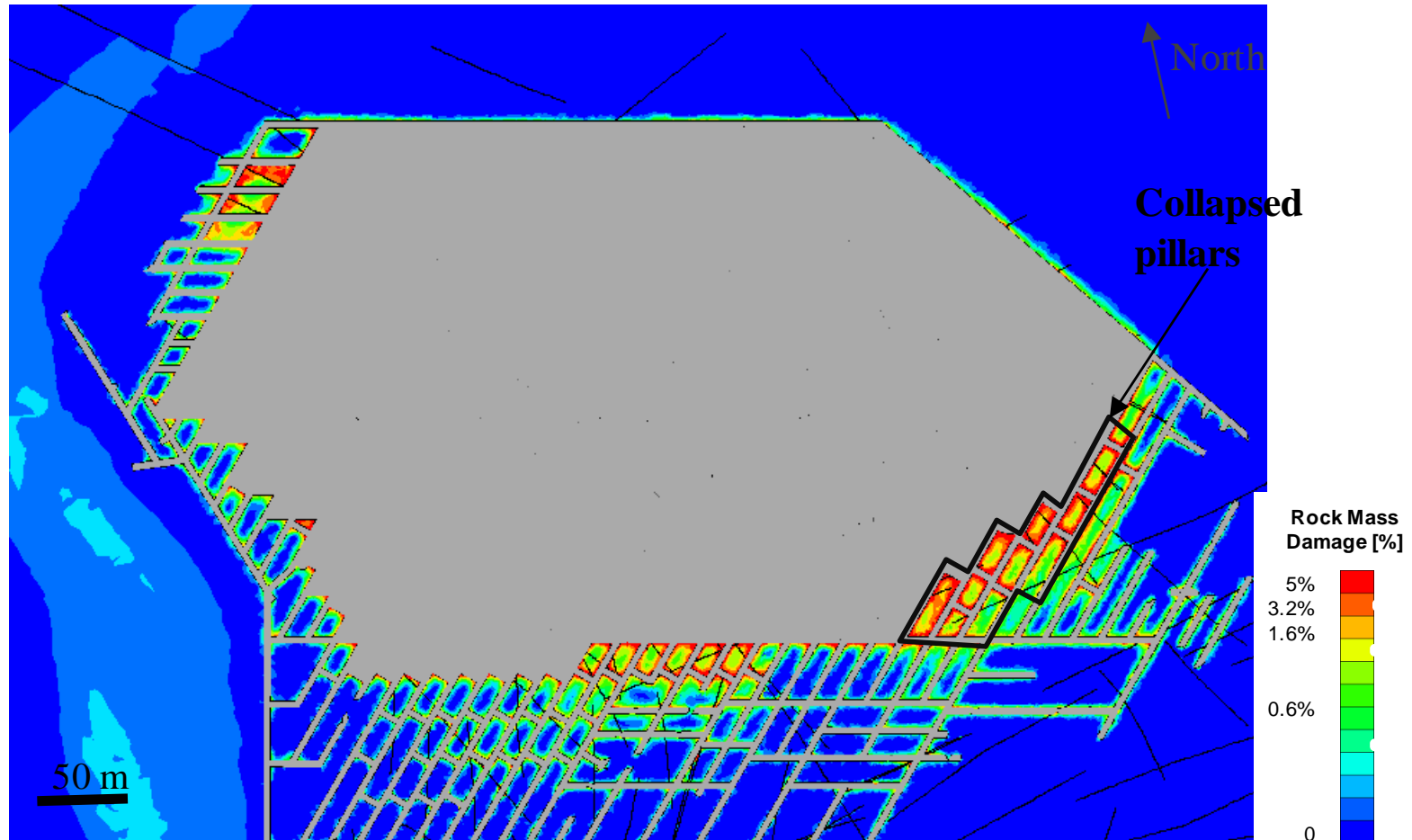


**Figure 5.40:** Contoured collapsed area within undercut level and plastic strain from extraction geometry modelled (last term 2003).

May 2004

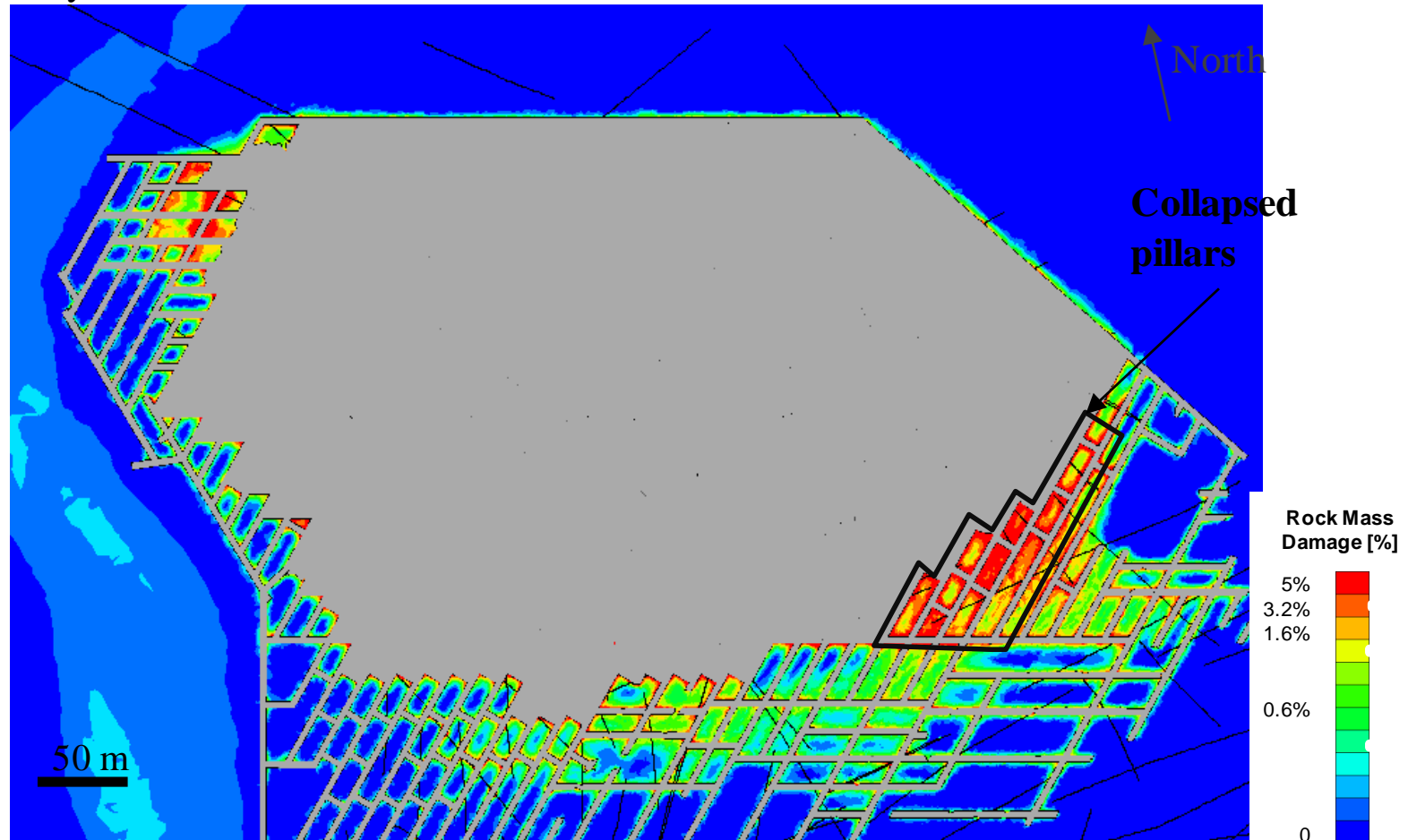


**Figure 5.41:** Contoured collapsed area within undercut level and plastic strain from extraction geometry modelled (second term 2004).

Finally, in order to assess the damage behaviour internally within undercut pillars, the plastic strain distribution was correlated with the results of diamond core through damaged pillar at selected locations. The selected pillar was located close to the undercut front and characterised by evident significant damage according to the El Teniente mine classification. The internal pillar condition was measured by core drilling in 2004 and the observed damage for the drill core was assessed by Rojas et al. (2005) concluding that the core evidenced significant damage (RQD less than 40%). The core showed slightly higher damage than observations using borehole camera. Moreover, the effect of accumulative damage was evident by the inspection of intensive hole over-break and the increased vertical stress, close to the undercut front. Figure 5.42 shows the location of inspected pillars and the core drilling carried out. The observed damage in drill core can be seen as well in Figure 5.43.

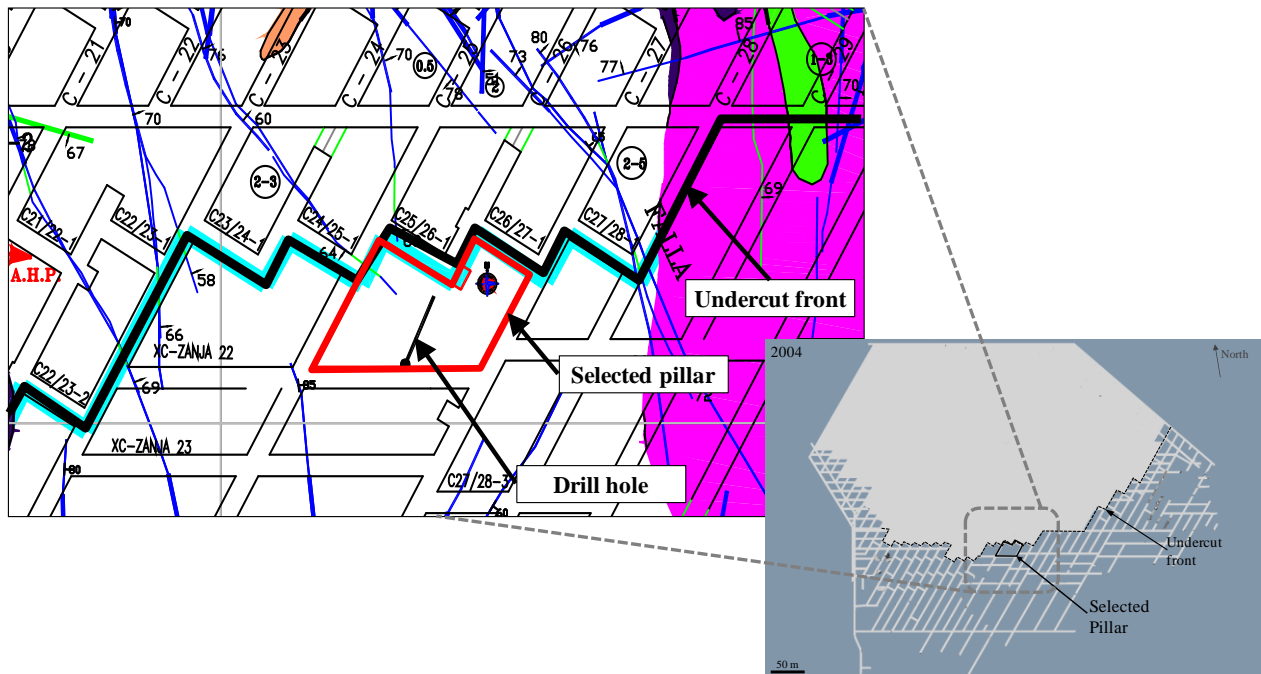


**Figure 5.42:** Location inspected pillar on undercut level for extraction geometry year 2004.



**Figure 5.43:** Damage observed in drill core (Rojas et al. 2005)

The damage experienced within the pillar affected by the undercut front advance was reflected by the inspection drill holes and also by diamond drilled core inspection. This condition was compared with the plastic strain generated by the extraction geometry modelled. This modelled extraction step was exactly the same real extraction geometry when the core drilling was undertaken. Figure 5.44 shows three East-West cross sections and one North-South cross section for plastic strain distribution along the assessed undercut pillar. In addition, Figure 5.45 shows the plastic strain values recorded from the model alongside the drill hole, the points were recorded every 1.5 m alongside the drill hole position attempting to correlate the detailed plastic strain values with the drill core condition.

It can be concluded that the plastic strain distribution along the drill hole position evidences consistent results regarding the pillar behaviour assessed by Rojas et al. (2005). On this case, the moderate plastic strain values through the pillar should be associated with a step change in adjacent tunnel deformation. However, the pillar instability has not been yet evidenced, as the strain core has not reached yet a critical level.

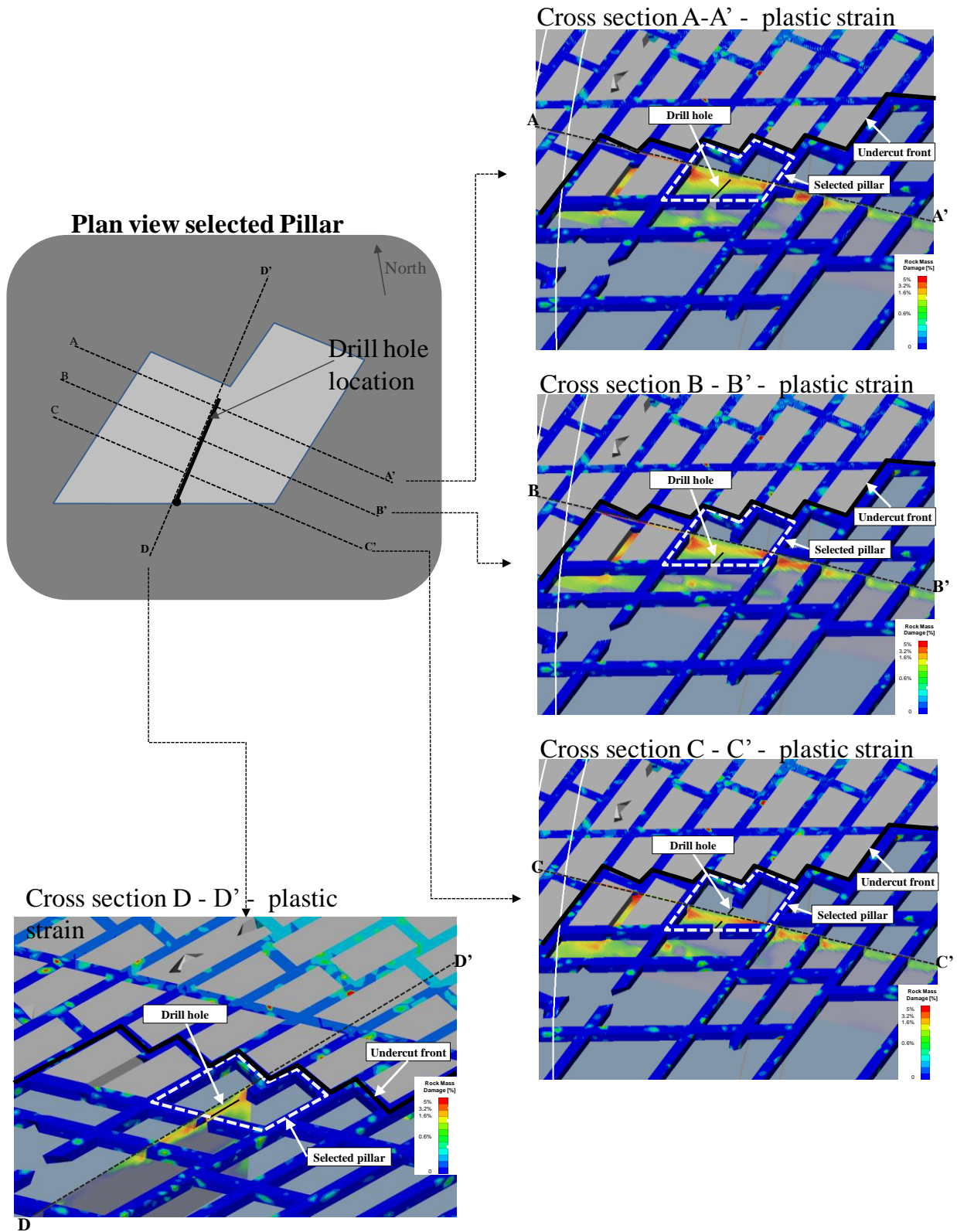


**Figure 5.44:** Plastic strain distribution on the cross sections through assessed undercut pillar.

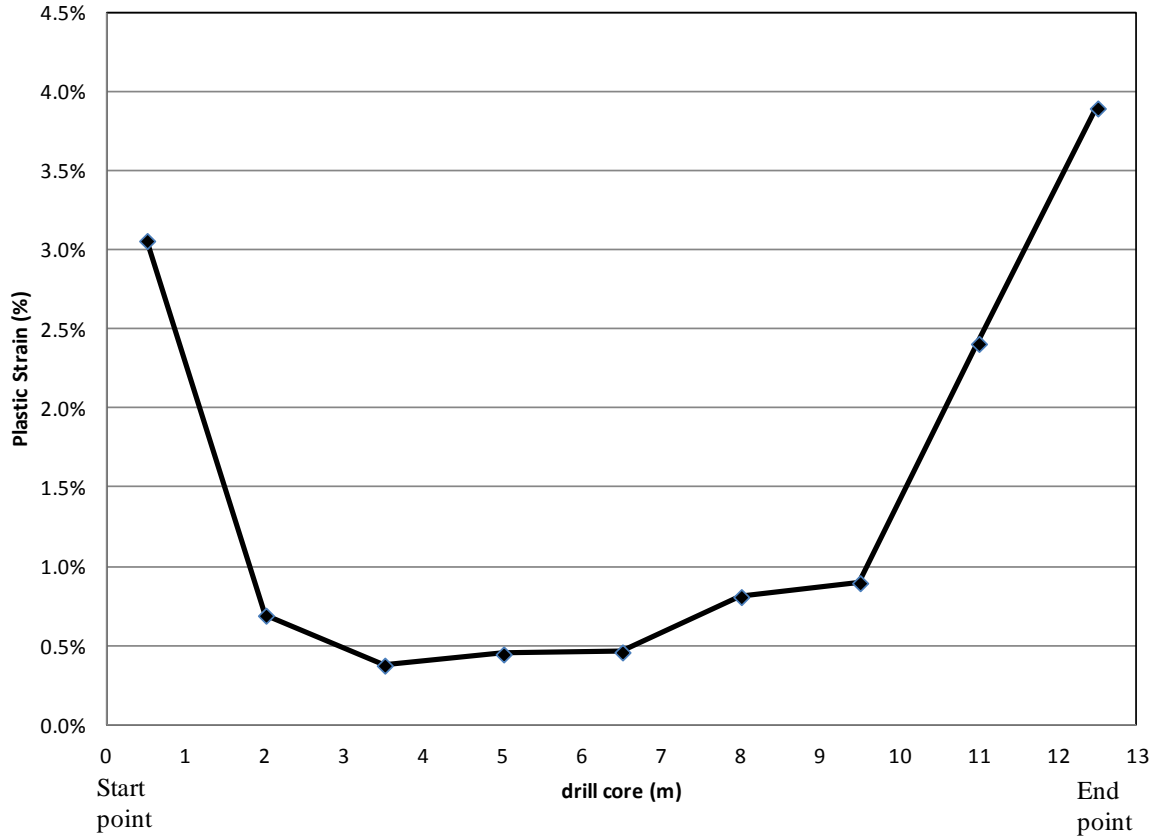


**Figure 5.45:** Plastic strain recorded in the exactly same location of the drillhole through undercut pillar.

### 5.6.6 Instability Criteria for Excavation Performance

After 24 run models, and once a reliable simulation was obtained from calibration procedure described in the previous section, the results were analysed by each extraction step modelled. A local and common Esmeralda damage scale was developed for its whole extraction history. The local scale was designed based on the qualitative and quantitative comparison between plastic strain results (or % rock mass damage) and rock mass damage experienced during the Esmeralda extraction history. As detailed in Section 5.6.2, rock mass damage experienced at Esmeralda used in this approach was determined according to the following evidence:

- Undercut damage maps from each extraction step modelled for the Esmeralda operation
- Collapsed undercut pillars recorded during some extraction steps for the Esmeralda operation
- Pillar core drilling at selected location for undercut level of the Esmeralda operation

The Local damage scale (LDS) based on the relationship between plastic strain and the rock mass damage experienced (or observed drift deformation) is shown with examples in Figure 5.46 where the coloured contours for plastic strain are used consistent throughout the thesis. Moreover, the detailed description of damage associated for each class of LDS can be seen in Table 5.5. It must be noted that

plastic strain values beyond 1.5 % plastic strain represent significant damaged rock mass for mining areas. It shows a reasonably good correlation between plastic strain and drift instability for a global deformation analysis.

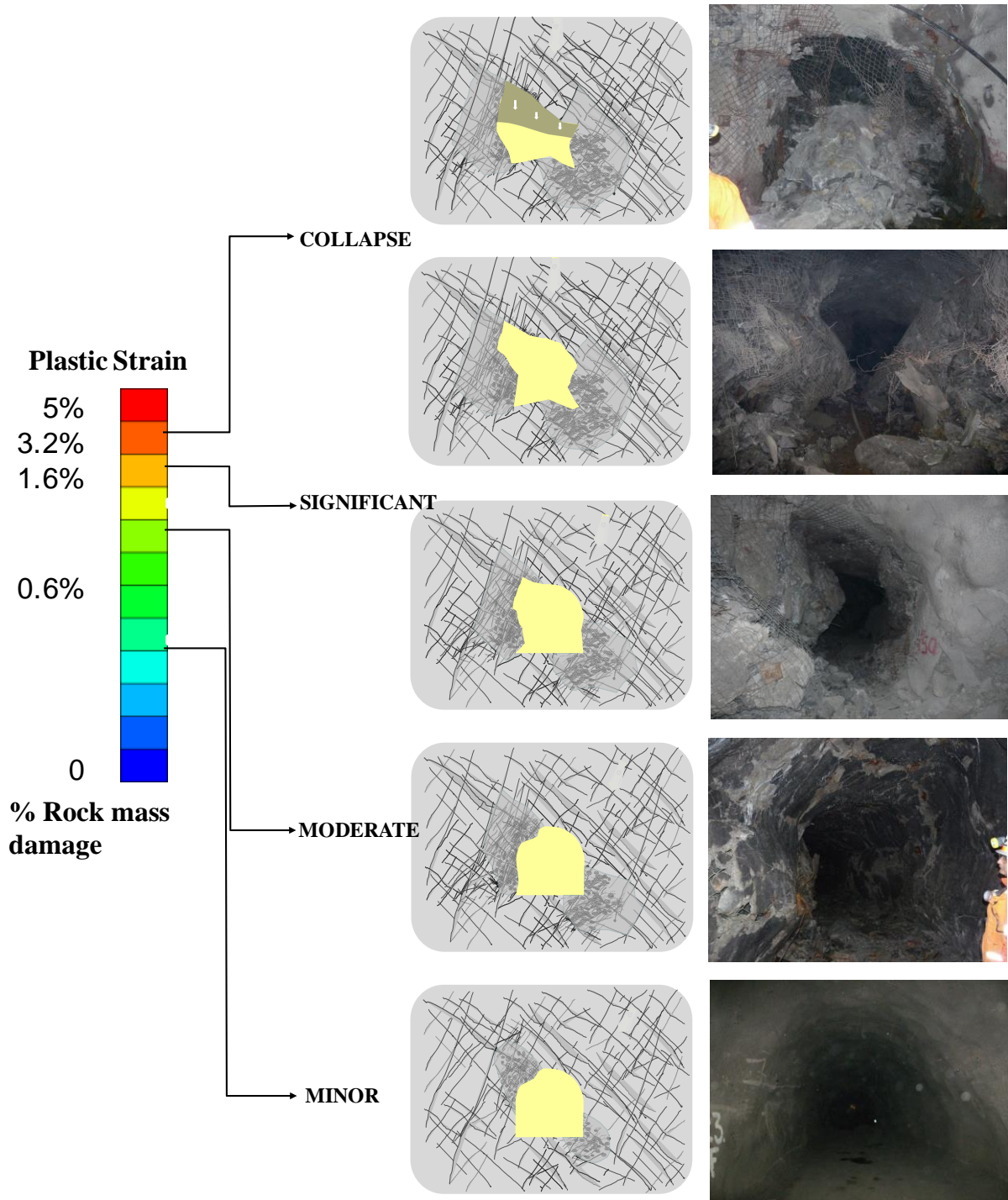


Figure 5.46: Esmeralda local damage scale based on plastic strain values and associated drift deformation

**Table 5.5:** Esmeralda Damage scale with detailed description

<b>Class</b>	<b>Detailed damage description (Observed at Esmeralda Operation)</b>	<b>Interpreted pillar core stability (Beck 2009)</b>
<b>COLLAPSE</b>	Drive surface heavily deformed. In the worst case the total closure of drifts is observed. Massive failure of support and reinforcement elements. Significant cracks and open rock blocks are observed. Over break is usually higher than 2.0 m.	<i>Pillar cores with significant damage should be interpreted as having failed. As the core is significantly deformed, so too will the adjacent excavations be deformed.</i>
<b>SIGNIFICANT</b>	Multiple shotcrete slabbing, failure behind mesh and failure of mesh are evidenced. Failed corners and brow, hole problems. Rehabilitation is required to maintain access. Multiple cracks and up to 2.0 m of over-break and dripping to rain water influx could be observed.	
<b>MODERATE</b>	Multiple cracking, shearing on existing structures, visible yield. Shotcrete slabbing, exposed embedded mesh with isolated broken spots is evidenced. Increased load in rock bolt plates. Up to 1.0 m over-break and dripping condition of water influx could be observed. Drive still safe for travel. Re drilling is required sometimes due to holes condition.	<i>Some pillars will be interpreted as failed. In these pillars degradation of pillar strength has increased but the actual deformation is still only moderate. The adjacent drives should not be significantly deformed, though additional loads will easily lead to increased damage and deformation in the pillar and the adjacent excavations</i>
<b>MINOR</b>	Minor signs of strain or deformation are observed, minor and spot cracking, commencement of shotcrete slabbing and minor mesh deformation. No rehabilitation is required.	<i>Pillar cores with minor damage should be expected to be stable. Calibration at a number of mines suggest that at this level of damage, the rock mass is commencing to yield but a significant degradation in strength has not occurred. Also, as the deformation is low, deformation in the adjacent excavations will also be low</i>

It must be highlighted that other damage scales such as Beck and Duplancic (2005) and Fernandez et al. (2010) have compared the modelled strain with excavations performance; however for this specific approach a detailed damage assessment from the Esmeralda operation was carried out where the strain levels were evaluated only for local rock mass behaviour.

Although the plastic strain parameter was explored as potential instability criteria and showed reliable simulation of the observed rock mass behaviour during the Esmeralda extraction history, the support load parameter is also used as complementary instability criteria for specific conditions and specific areas at the Esmeralda operation.

Ground support is used to stabilize the tunnels in an underground operation. Deformations induced by mining after installation of the support and to a lesser extent, rock mass creep, cause additional loads

to be developed. This ‘support load’ is estimated following an approach incorporating ground characteristic curves (Brady and Brown 2006). Ground characteristic curves compare the load-deformation response of an excavation boundary to the load-deformation response of a ground support system.

To calculate support loads, the support load-deformation curves for each candidate support system are derived by numerically testing the stiffness of the complete support system in test sections of tunnels in a three-dimensional finite element model.

Next, the representation of support system is ‘installed’ in the mine-scale model to simulate the effects of induced deformation on the support. This is done within a model with detailed mining steps to ensure the stress path is simulated correctly. The excavation of the tunnel by blasting is represented by element removal and a substitute material stiffness representing the support system is introduced, following equilibrium, in a strain free configuration.

Subsequent mining induces the deformation and yield in the rock mass that load the support. In the example shown in Figure 5.47, the observed drift performance on the extraction level for a specific area at the Esmeralda operation is compared with the estimated support load during exactly the same modelled extraction geometry in 2005. It was found that the rehabilitation of ground support was required almost universally where modelled support load reached over 600 KPa. In fact, the highlighted area shown in Figure 5.47 for extraction geometry 2005 was affected by damage classified as intensive or even collapse in some specific areas.

In the example shown in Figure 5.48, exactly the same procedure was carried out to compare drifts performance with modelled support load for Esmeralda extraction geometry during 2008 on extraction level. It was found that significant damage in extraction level was observed where modelled support load reached over 600 KPa.

Finally, the good correlation obtained from some extraction geometries modelled such as excavation steps in 2005 and 2008 allows using the support load scale as complementary instability criteria for excavation performance during back analysis of intensive rock mass damage at the Esmeralda operation.

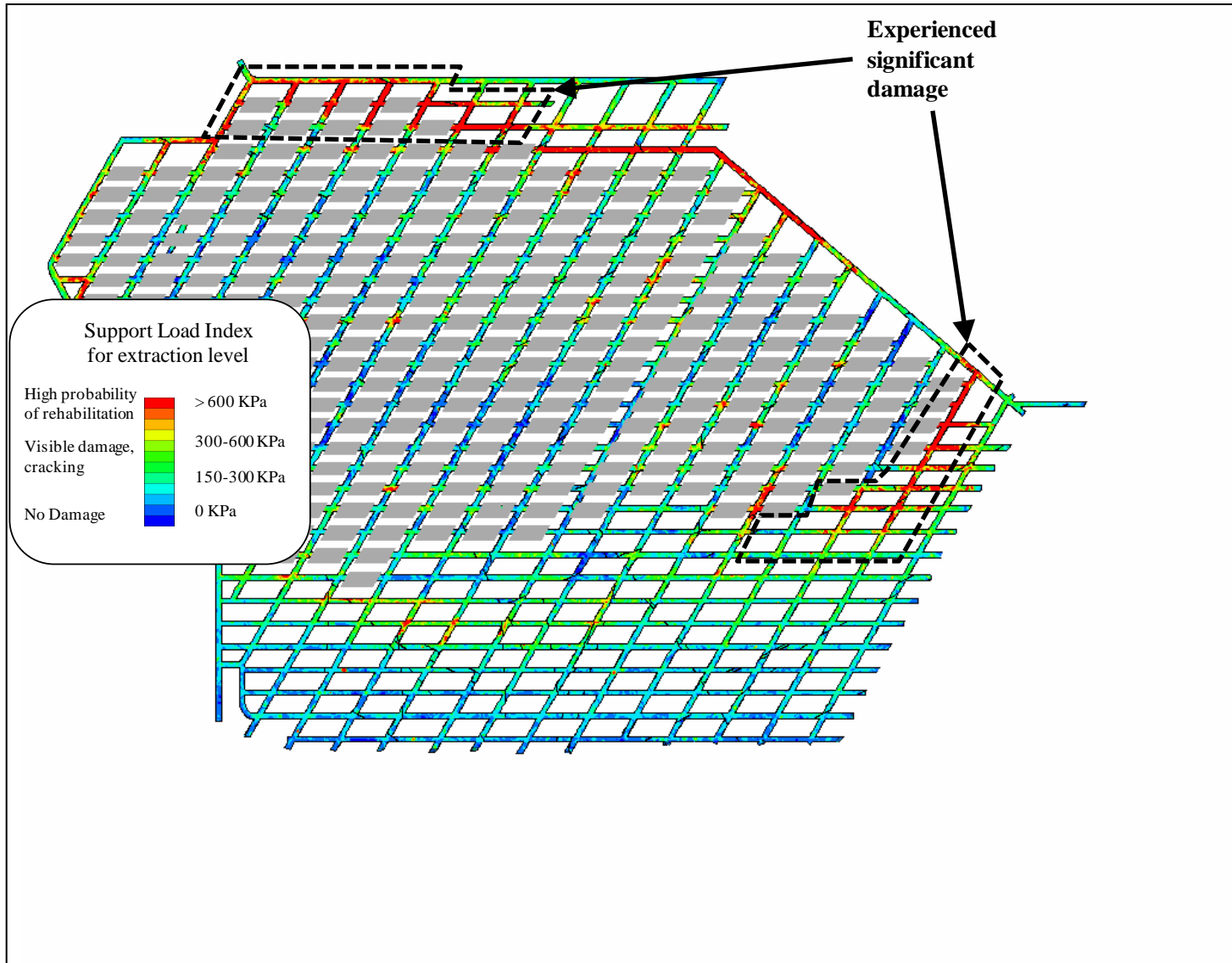


**Figure 5.47:** Modelled support load and contoured significant damage on extraction level, 2005

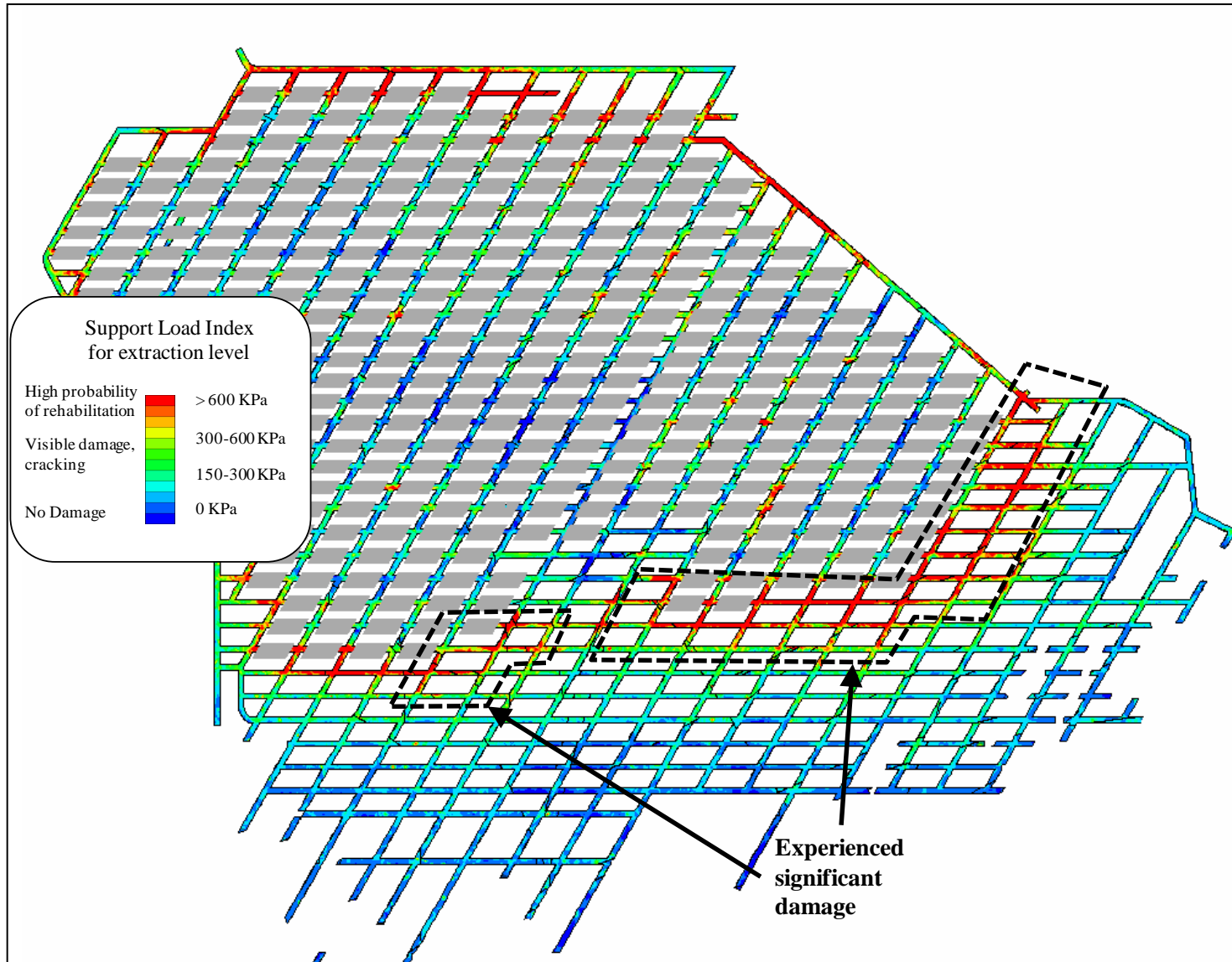


Figure 5.48: Modelled support load and contoured significant damage on extraction level, 2008

## **5.7 SENSITIVITY ANALYSIS, UNDERSTANDING AND UNCERTAINTY**

As the instability issue analysed in this study involves many parameters acting on the collapse mechanism, a sensitivity analysis was undertaken as part of the calibration process. The most relevant and sensible geotechnical parameters were selected to modify their values and to quantify their effects.

During the global sensitivity process the following guidelines have been identified for the representativeness of the model:

- The model can be considered no more precise than the geotechnical block model plus any limitations arising from the lack of small-scale structure. This is in fact, somehow limits the model interpretation at a global scale, which was one of the intended purposes.
- At a global scale, the model is representative of the expected outcome for the best interpretation of geotechnical conditions available. For the scope of this study only the performance of the extraction level and undercut was specified (i.e. other aspects of global deformation such as subsidence were not part of this study).
- Drive scale detail can only be interpreted at the Esmeralda operation scale - i.e. by looking at the range of conditions across its footprint.

Drive scale conditions are interpreted in this scale of model by interpreting the conditions in the pillars adjacent to them. Given the level of uncertainty in the geotechnical parameters, only obviously failed or obviously stable pillars are interpreted with any high degree of confidence.

The greatest uncertainty at this stage is associated to knowledge of the rock mass, in fact the characterisation of the structural sets for Esmeralda have been identified as one of the most relevant geotechnical parameters playing an important role upon collapse mechanisms. In addition, other focus of uncertainty has been related to the simulated cave shape and its associated effects.

For all of the many draw point pillars and many square kilometres of undercut simulated within a representative environment at the Esmeralda operation, several numerical tests were carried out to better understand the range of conditions in which the most reliable back analysis could be obtained. A detailed assessment of geometrical issues of undercutting process, cave shape and simulation mechanism and finally design of undercut level (pillars size) was undertaken during this stage. The description for each one of them is discussed in the following sections.

### **5.7.1 Material properties**

As a consequence of the sensitivity process for peak strength HB properties undertaken during calibration steps and detailed in section 5.6.2, Figure 5.49 shows a representative summary about the

property adjustments undertaken, especially for the most important geotechnical units at Esmeralda CMET Hw and CMET Fw. Triaxial test results representing the starting point of the calibration are compared with the definitive properties version used for the calibrated model. This summary highlights the initial and final point for the calibration process in relation to the material properties used.

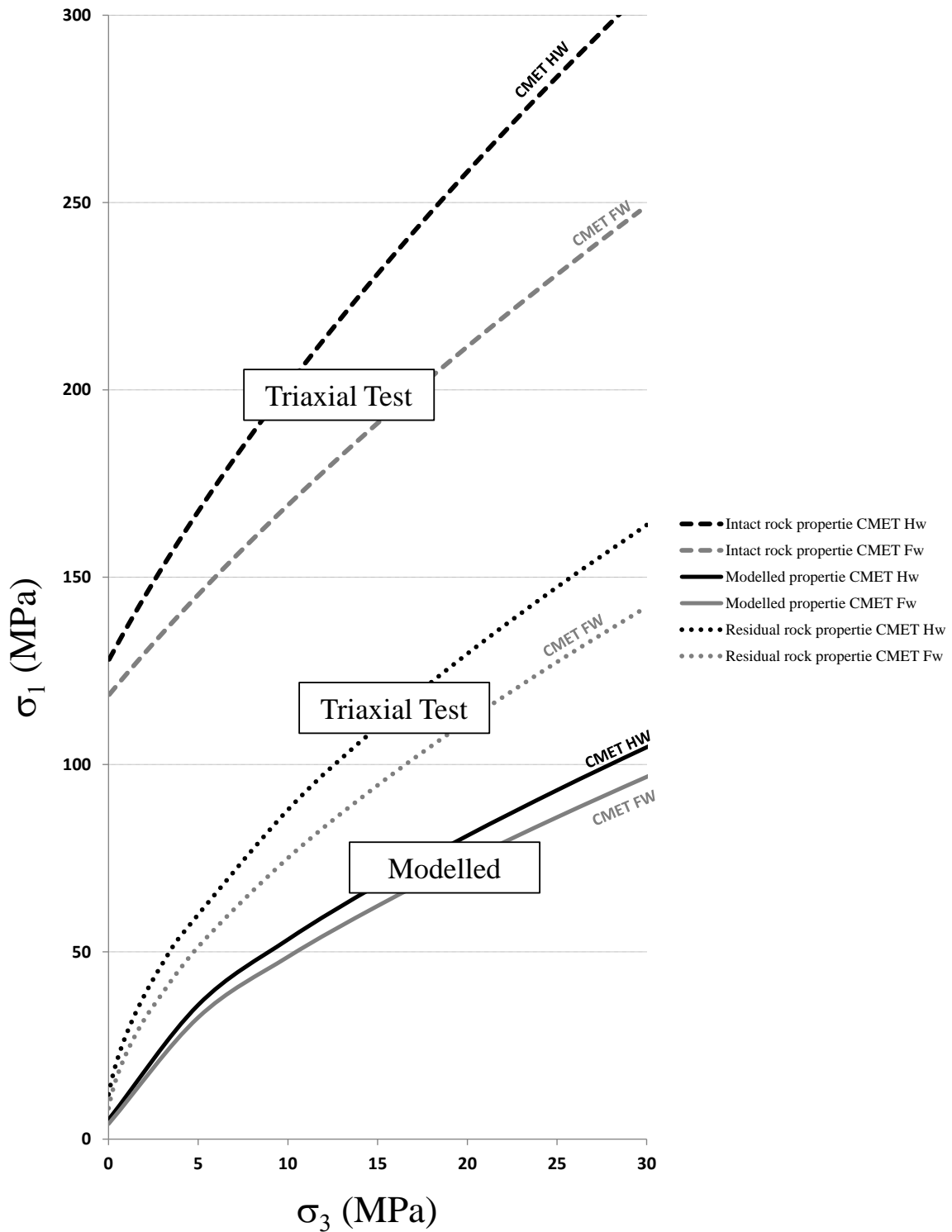


Figure 5.49: CMET Triaxial test results and properties finally used in the calibrated model.

### **Cave simulation mechanism**

The model was designed as a static model that must be able to describe the quasi static deformation behaviour of intact or degraded rock and also the deformation behaviour of highly fragmented rock like the muck pile in the cave. This study was never interested in investigating the dynamic process of rock material degradation. Sophisticated continuum models are known to be able to do this for a very wide range of degradation states, i.e. from very strong rock to very degraded materials. The strength and stiffness properties of an equivalent continuous media that sufficiently represent the cave are the result of a calibration process of this study.

The original procedure for cave simulation consisted of:

- Mapping the historic (i.e. measured) cave shapes in small increments. This involved converting the rock to cave material at the time when the records indicated its occurrence. This was achieved by changing the properties from intact rock to caved material.
- The equivalent continuum properties for the cave were of course adjusted, as part of the calibration process.

The first cave simulations were carried out originally based on the associated full historical data base of ore drawn height by drawn points. The cave shape associated to each excavation step was represented by one surface determined by ore drawn until the modelled step. However, the assessment of this approach was not successful mainly in terms of matching the observed and modelled behaviour. Therefore, the cave initiation and propagation was finally simulated based on the instability criterion that allowed the reproduction of the best cave shape by itself during the global simulation.

The discontinuum finite element (DFE) program generates an unstable zone, as a consequence of its solution for a particular excavation step. For example, at the end of a prior step, completed at time  $T$ , the DFE model provides an estimate of the unstable zone that is likely to make the transition from loosened rock mass to cave material over the following coupling period of time length ( $t_c$ ), set as small as computationally possible.

The criterion for instability in the DFE model was based on velocity. Experience shows that above a critical velocity ( $V_{crit}$ ) the material can be considered unstable. The particular value for  $V_{crit}$  was established in the calibration stage comparing modelled and observed behaviour.

Figure 5.50 show an example of cave shape performed by instability criterion for extraction step second term 2007 at the Esmeralda operation.

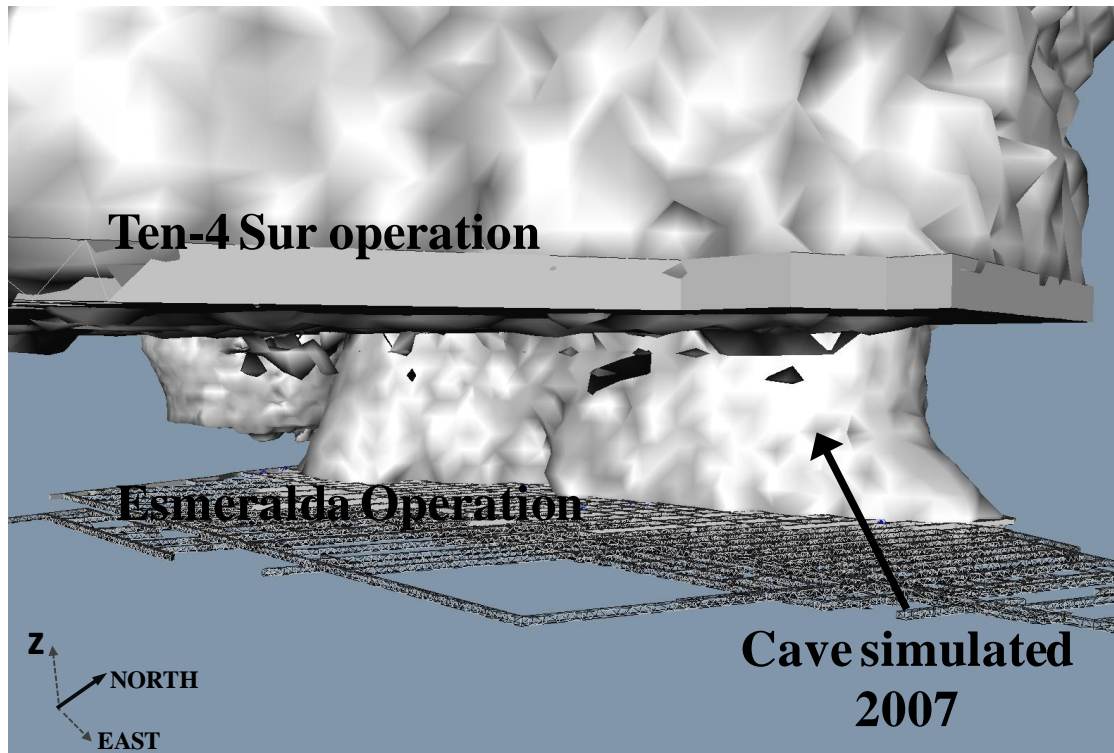


**Figure 5.50:** Isometric view with the cave simulated for extraction step second term 2007, Esmeralda operation.

### 5.7.2 Geometrical singularities during undercutting

One of the sources of intensive rock mass damage on the extraction level could be associated with the point load transfer located in the undercut level. The identified point load at the Esmeralda operation has been described as remnant pillars due to deficient drill and blast practices during the undercutting. In fact, during the period between 2000 and 2005 part of the remnant pillars left in the undercut level have been recorded by the geotechnical team and one remnant pillars map was generated on that time.

As part of the sensitivity analysis, the recorded remnant pillars were explicitly included as part of the geometry modelled, and thus the results were assessed based on observed damage on the extraction level. The plastic strain parameter was analysed as part of calibration process and iterative numerical tests were undertaken in order to achieve the best matching between observed and modelled.

Figure 5.51 shows the undercutting geometry modelled for one representative excavation step for 2001 which explicitly has a remnant pillars mapped. Additionally, the plastic strain distribution on the extraction level associated with exactly the same geometry modelled can be seen in Figure 5.52. It can be concluded that the model that included the remnant pillars achieved a better matching with observed damage especially on the extraction level during 2000 – 2001, where the first collapse evidences were identified, as can be seen in Figure 5.52.

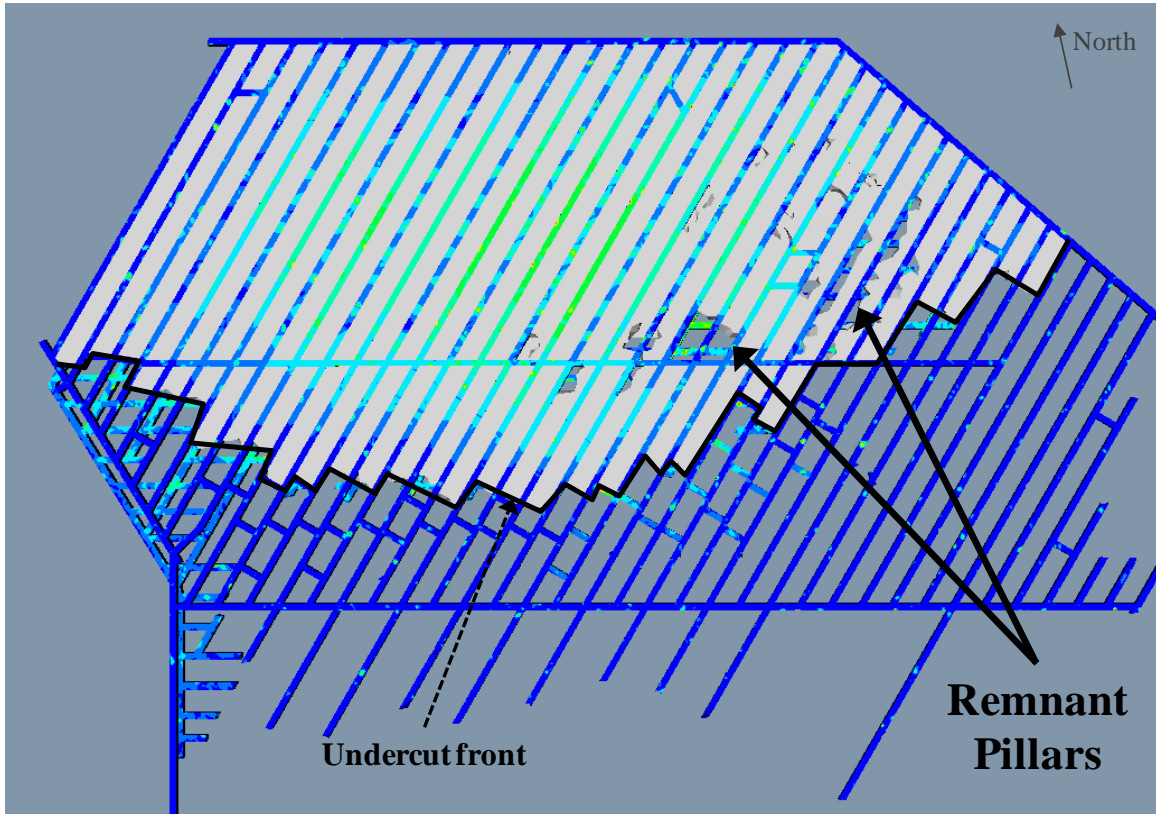


**Figure 5.51:** Plan view of modelled undercut geometry for excavation step year 2001 Esmeralda Operation along to the Remnant pillars associated to that period.

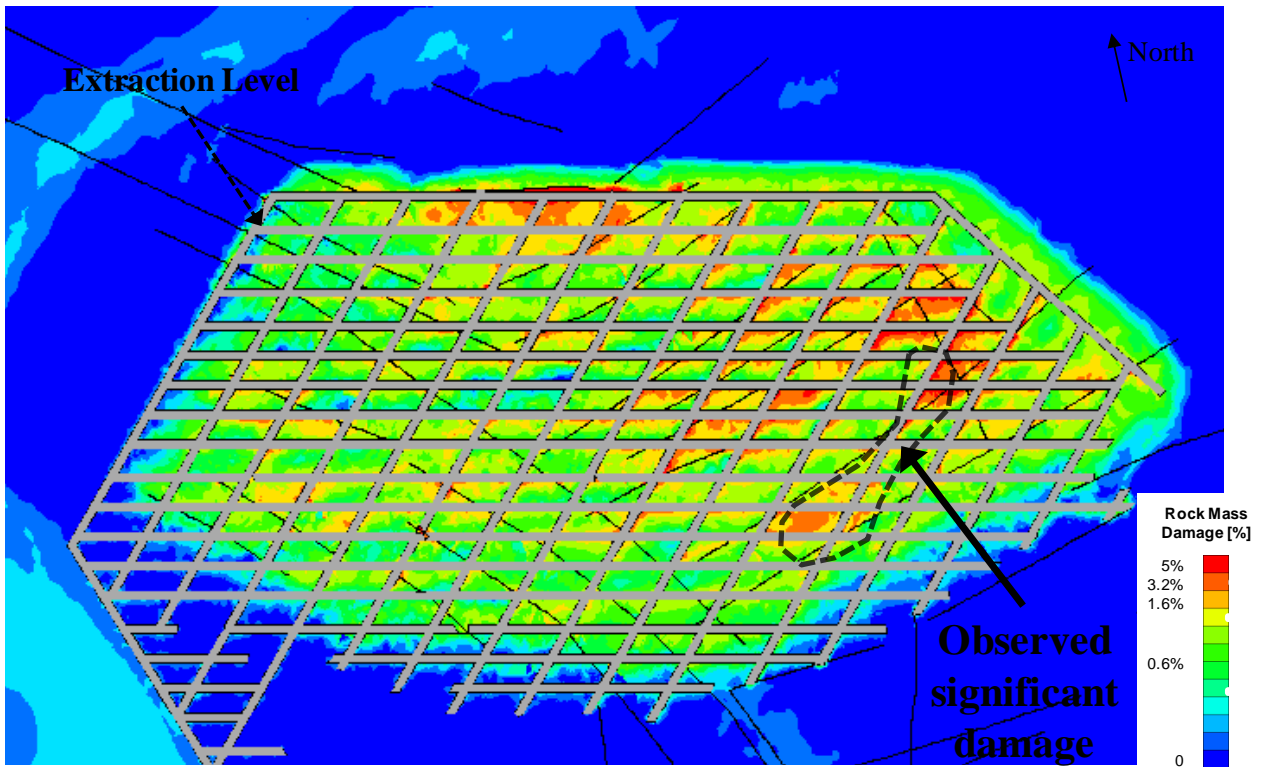


**Figure 5.52:** Plan view of extraction level Esmeralda with Plastic strain modelled and contoured area for observed significant rock mass damage during year 2001.

### 5.7.3 Exercise for undercut level design

The undercut design, especially related to the pillar dimension, has been identified as one of the factors that would also prompt a pillar collapse. The instability on undercut pillars has been experienced frequently during the full extraction history at the Esmeralda operation, as detailed in Chapter 4.

Although the modelling was performed including the original and definitive undercut layout in order to reproduce exactly the rock mass damage experienced during Esmeralda operation, some numerical exercises were undertaken with different options of undercut designs, especially including smaller pillars within vulnerable geotechnical zones such as the eastern zone (CMET Fw) of Esmeralda.

Figure 5.53 shows the results for both cases modelled: (a) the undercut design really used at Esmeralda and (b) design alternative characterised by including smaller pillars. According to the plastic strain values and the instability criteria detailed in Section 5.6.3, clearly the design alternative modelled evidence the worst behaviour. In fact, almost all group of pillars located ahead of undercut front and exposure to abutment stress are collapsed. Therefore, it can be confirmed that pillar dimension represents one of the most sensible parameters affecting the stability of undercut and extraction levels, especially within unfavourable geotechnical conditions such as present a the Eastern zone of Esmeralda.

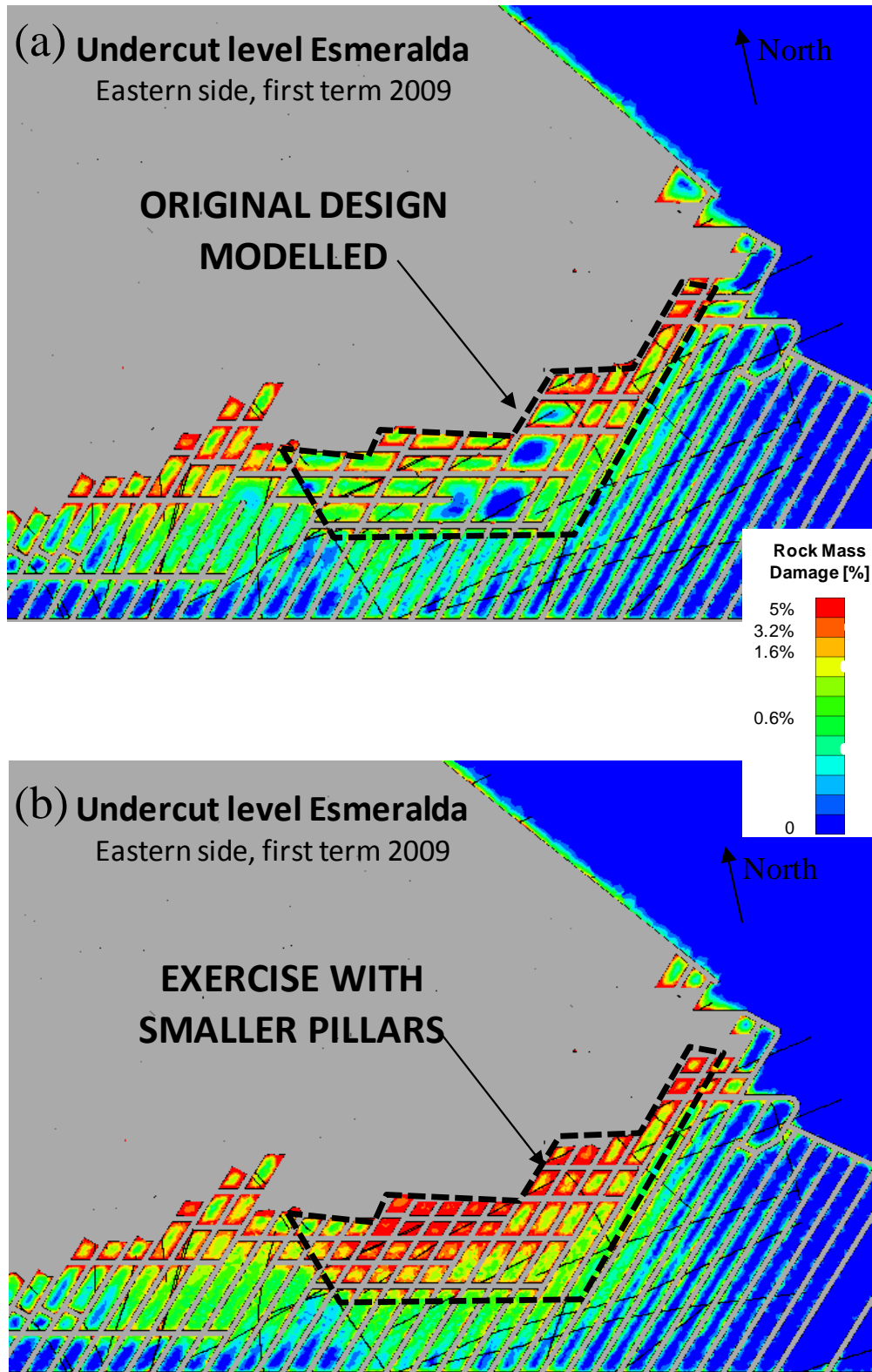


Figure 5.53: Plastic strain results for two different undercut designs modelled.

## CHAPTER 6

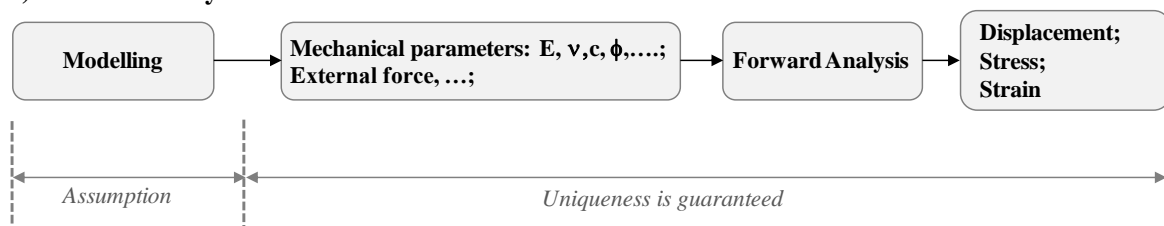
### BACK ANALYSIS RESULTS

#### 6.1 INTRODUCTION

The results shown within the previous chapters have shown that a rock mass response can be effectively modelled to simulate a reliable approach of rock mass behaviour associated with a panel caving operation. Generally, this has been achieved by carrying out a site specific back analysis where observable rock mass response is correlated with outputs from a calibrated model.

The aim of the back analysis or inverse solution approach is to identify unknown system properties or perturbation parameters, through direct application of numerical methods to derive unknown material properties, system geometry, and boundary or initial conditions (Jing 2003). The technique was representatively applied by Sakurai (1981) for back-analysis of displacement and has been widely used in rock engineering. In back analysis, only the rock mass response and excavation geometry are given, with no knowledge of the exact failure model. In fact, the same observed response may eventually be derived by multiple failure models and from a range of input parameters, which means that the uniqueness of the solution in back analysis cannot be confirmed (Sakurai 1997) as illustrated in Figure 6.1. On the other hand, in forward analysis all input parameters, boundary conditions and excavation geometries are given, and considering a specific failure model, the uniqueness of the solution is guaranteed.

##### 1) Forward Analysis



##### 2) Back Analysis

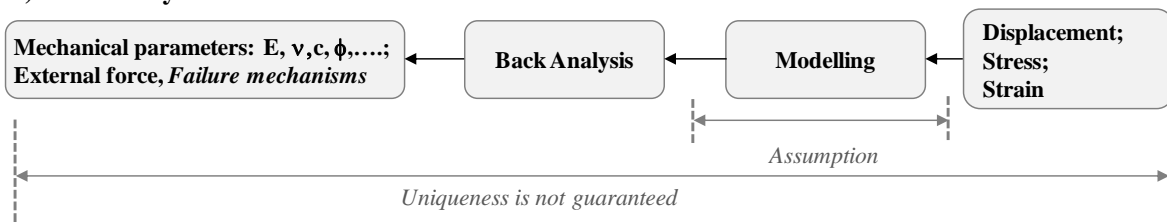


**Figure 6.1:** Comparison between the procedures of forward and back analysis (Sakurai 1997)

The aim of the back analysis in this study was to reproduce the rock mass behaviour associated to a panel caving operation determining the most appropriate failure mode for the observed rock mass response. This will be highlighted in the following sections.

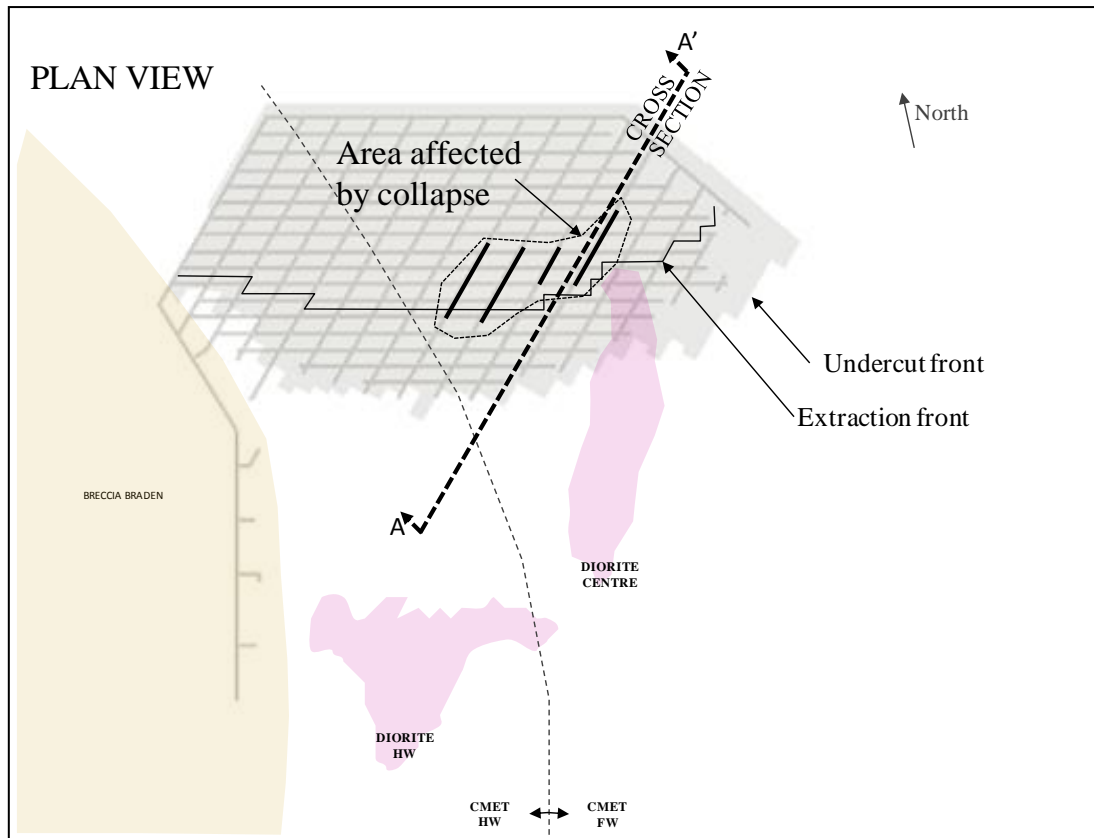
## **6.2 ASSESSING THE EARLY PERIOD OF THE ESMERALDA COLLAPSE**

Chapter 4 described the intensive rock mass damage experienced on the extraction and undercut levels at the Esmeralda operation. In addition, geotechnical precursors were identified as part of the conceptual modelling analyzed. Finally, two conceptual hypotheses about collapse mechanism at the Esmeralda operation were carried out taking into account the whole assessed evidence of the sector.

Based on the significant damage evidenced through the whole extraction history of the Esmeralda operation, the early period of Esmeralda collapses has been identified between 2000 and 2005. The geotechnical precursors identified through observations and geotechnical monitoring have characterised this early period by a collapse occurrence behind the undercut front. Moreover, it must be highlighted that the panel caving method with pre-undercut sequence was used during this period at the Esmeralda operation. The sequence of geotechnical precursors (geotechnical and geometric parameters) leading to deterioration in ground conditions and concluding with uncontrolled collapse are summarised in the list below and are also illustrated in a representative vertical cross section of the Esmeralda operation for the same period, as it can be seen in Figure 6.2. This illustration attempts to integrate the geotechnical precursors and the representative mining state on that period showing the relative location of the most significant rock mass damage represented by collapsed drifts with respect to the mining front advance.

- Undercut and extraction front parallel to weaker structural sets, identified as intermediate faults in section 5.5.6
- Span between undercut and extraction fronts exceeded typical standards
- Remnant pillars associated to deficient blasting were formed
- Draw strategy facilitate an unfavourable stress condition
- Loss of confinement within collapsed area
- Pillar strength was exceeded by the load acting

The most relevant numerical results from modelled extraction geometry from earlier period were reviewed; in fact exactly the same representative cross section detailed in Figure 6.2 was evaluated with numerical results where the majority of characterised geotechnical precursors described above were assessed through the plastic strain values and principal stress values distribution.



**CROSS SECTION**

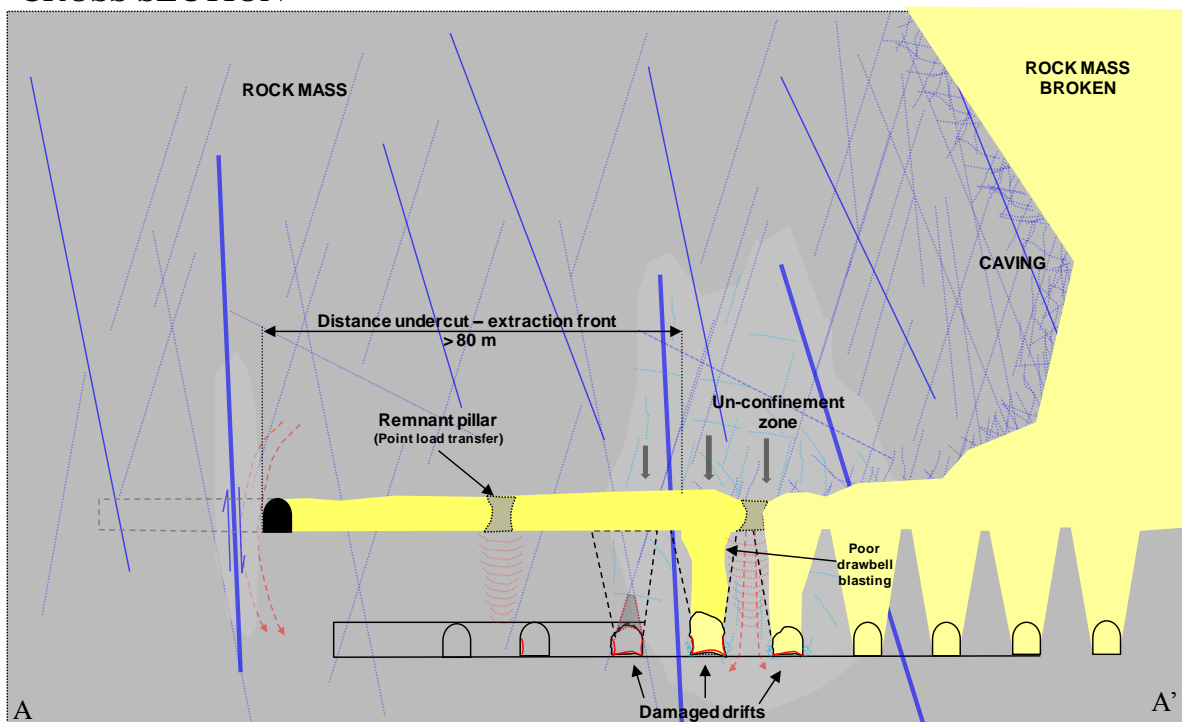


**Figure 6.2:** Representative cross section of Esmeralda for the earlier period of collapse (2000-2005), where panel caving with pre-undercut sequence was used.

Figures 6.3 and 6.4 show the numerical results for a representative cross section during the earlier period of collapses at Esmeralda. A sequence of changes and effects associated with the rock mass damage experienced can be seen in Figures 6.3 and 6.4, where the most representatives' modelled geometries between 2000 and 2002 were considered.

The results have partially confirmed that geotechnical precursors and their sequence effectively are leading to deterioration in ground conditions and conclude in uncontrolled collapses. First of all, the zone identified with the highest plastic strain values is delimited by two intermediate faults that were activated by the front advance. Secondly the modelled span between undercut and extraction fronts facilitated faults activation and generated favourable conditions to point load transfer when remnant pillars are left. Also this was incorporated in the numerical solution. Thirdly, the mining strategy modelled induced a considerable loss of confinement on the extraction level, just when the undercut has passed and draw-points and draw-bells are mined. The cave loads can still affect pillars, which show only minor or moderate damage prior to extraction of the draw-bells. The combined effect is a step change in the horizon capacity to bear loads after the draw points and draw-bells are extracted. This occurs because pillars are mostly or almost only uniaxially loaded from that point onwards and the strength of a pillar, or its capacity can be halved or more than halved even though it was 'de-stressed' by undercutting and the rock was not in a residual state. Finally, the combined effects of all assessed geotechnical precursors integrated in the model can be appreciated especially in Figure 6.3 where the evaluated area shows that the pillar strength is exceeded by the load acting according to the instability criteria detailed in section 5.6.6. In addition, the Figure 6.4 shows the contours of major and minor principal stress for each modelled step.

Furthermore, during the early period of the Esmeralda operation (2000-2005) with extraction by panel caving with pre-undercut sequence, four representative extraction pillars were selected to evaluate their stress-strain path during all the extraction steps modelled. Two of them were identified as collapsed pillars according to their observed behavior and two represented stable pillars without any evidence of significant damage. The location of the pillars assessed is shown in Figure 6.5 alongside their relative location to mining fronts (extraction and undercut fronts) for the period when they were definitively declared as collapsed/stable.

In order to assess the pillars behaviour during the whole extraction history modelled, first of all the plastic strain path versus principal stress is detailed in the Figure 6.6 for the four evaluated pillars. It can be seen that the representative collapsed pillars experienced significant plastic strain values and this is confirmed according to the instability criteria detailed in section 5.6.6, while the stable pillars experienced less than 0.5% plastic strain.

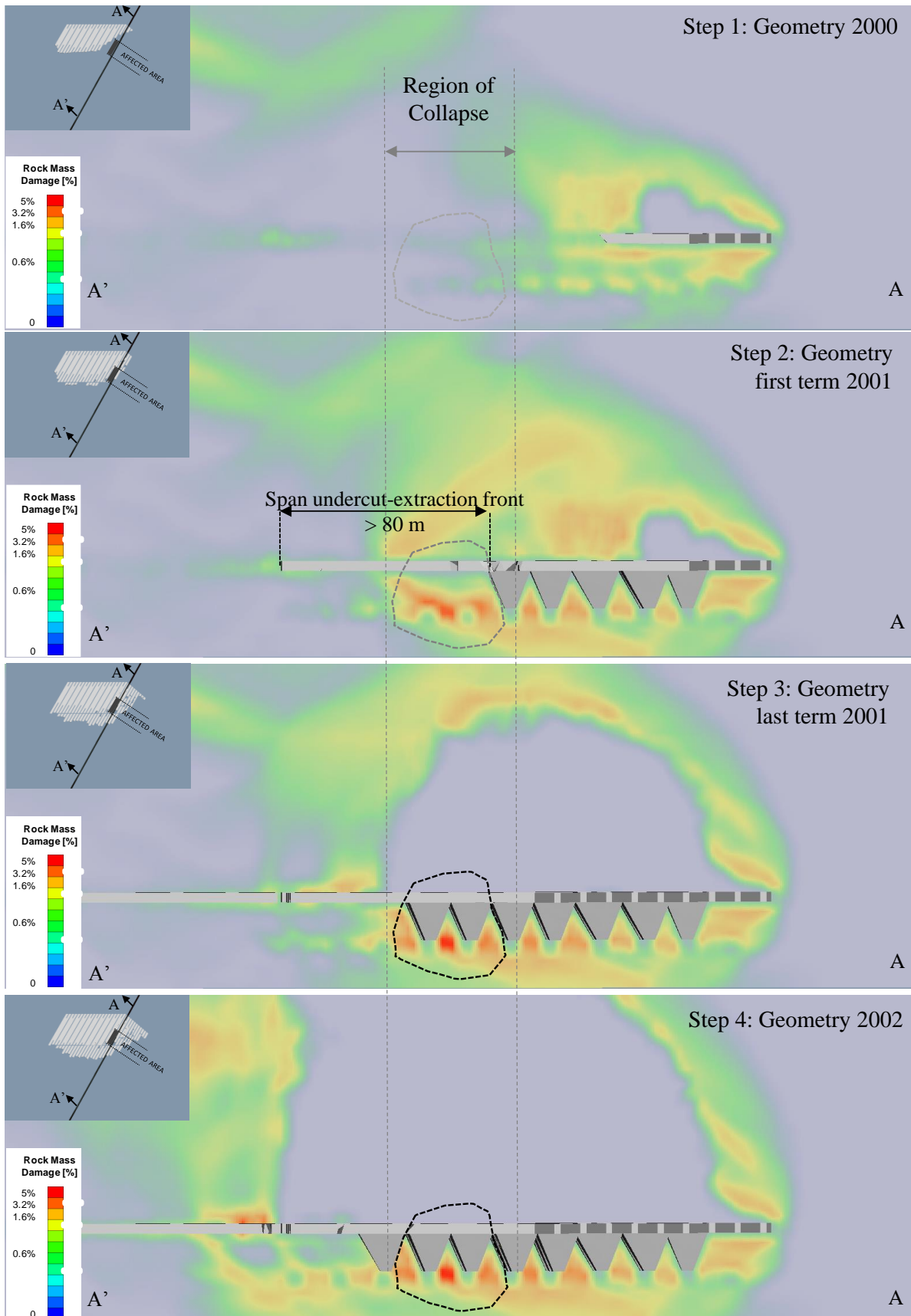


**Figure 6.3:** Cross section of modelled geometry through experienced collapse zone for early period showing contours of plastic strain associated to modelled step.

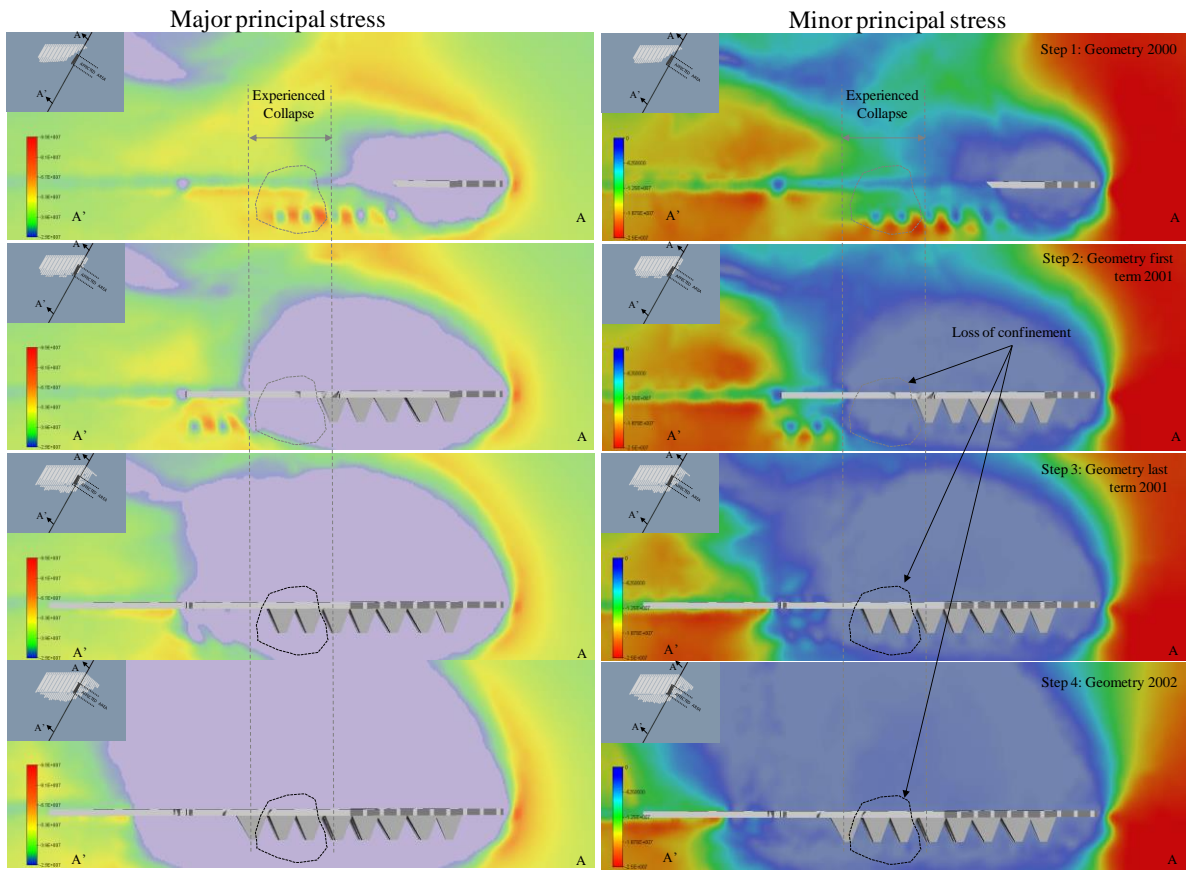


**Figure 6.4:** Cross section of modelled geometry through experienced collapse zone showing contours of major and minor principal stress for each modelled step.

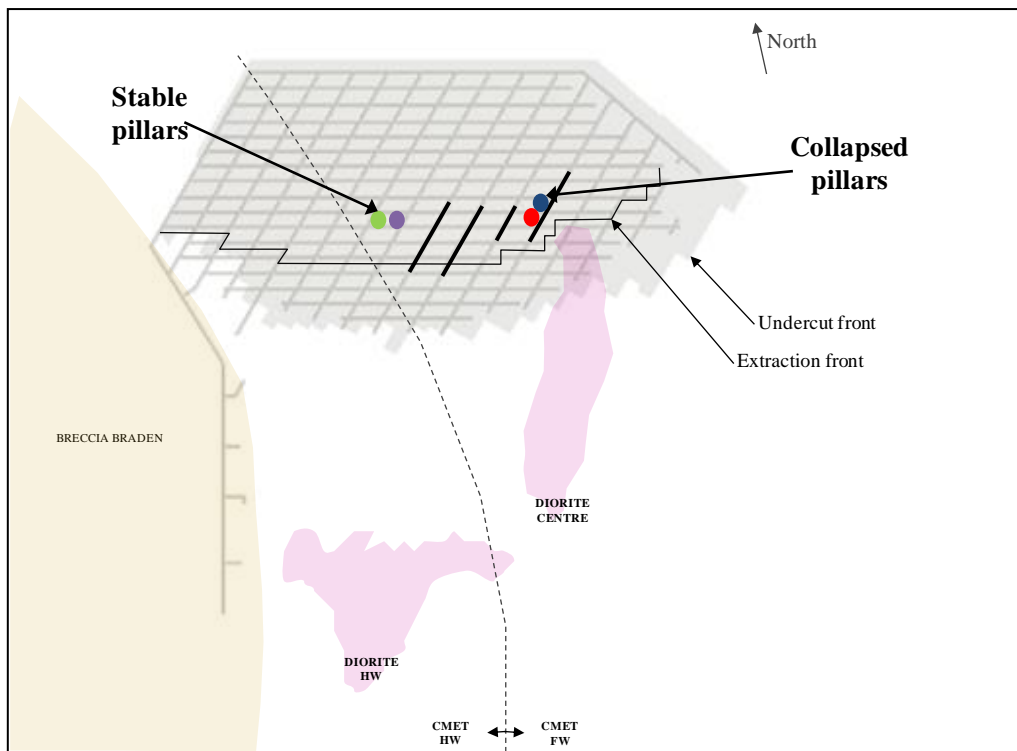


**Figure 6.5:** Location of pillars assessed for the earlier period of Esmeralda

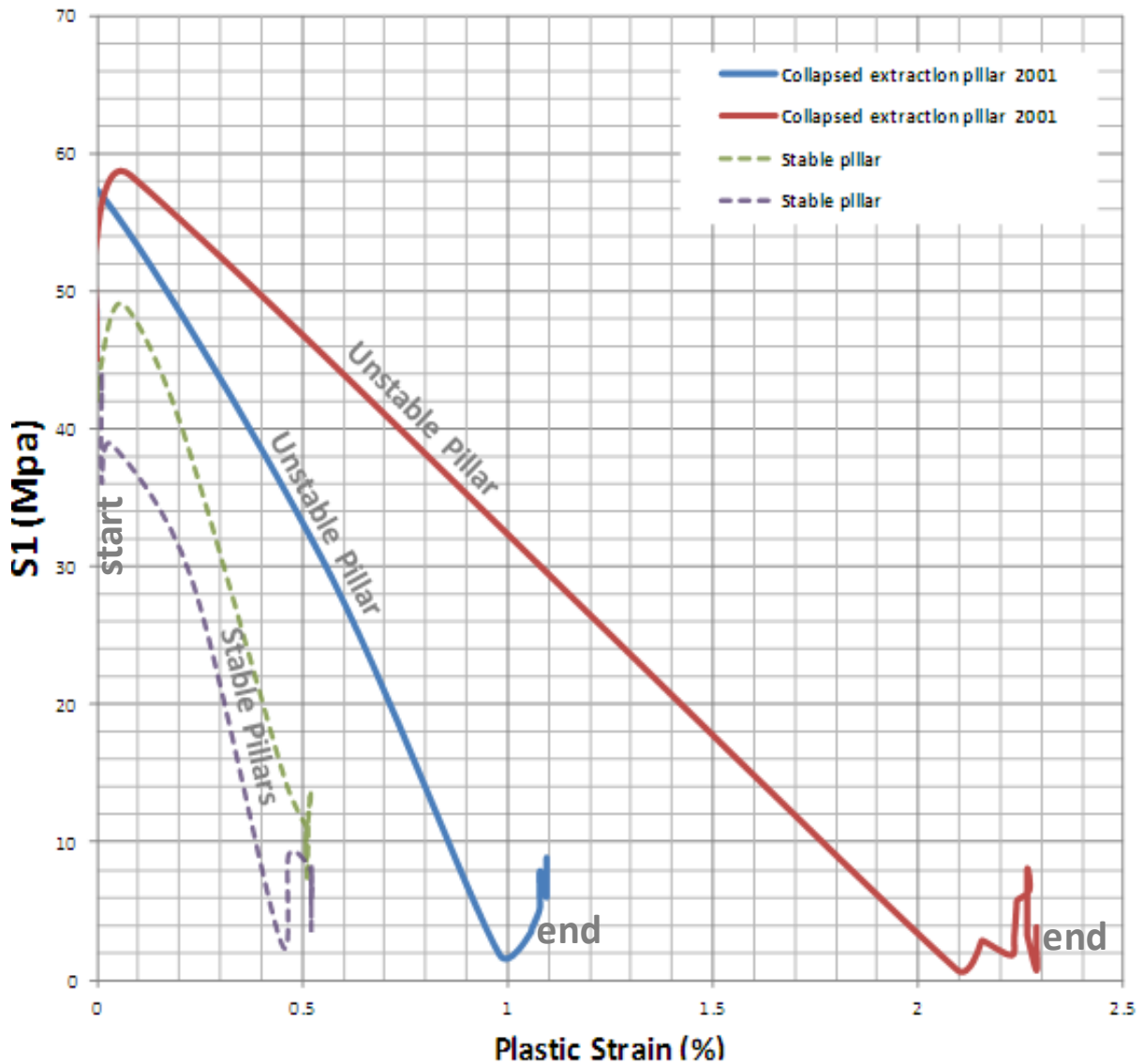


**Figure 6.6:** Stress-strain path for four assessed pillars associated with the pre-undercut sequence, 2000-2005.

For the earlier period and exactly the same representative assessed pillars, the principal stress paths were also reviewed. Figure 6.7 shows the principal stress paths associated with the whole extraction geometries modelled. The different behaviour between collapsed and stable pillars can be seen. An increased load was experienced within collapsed pillars, which should be an evidence of the remnant pillar effect which was modelled in the undercutting. Therefore, according to the observational records and conceptual model, numerical results do confirm that the remnant pillar evidence facilitates the collapse propagation, or in other words, it may be a confirmed collapse precursor.

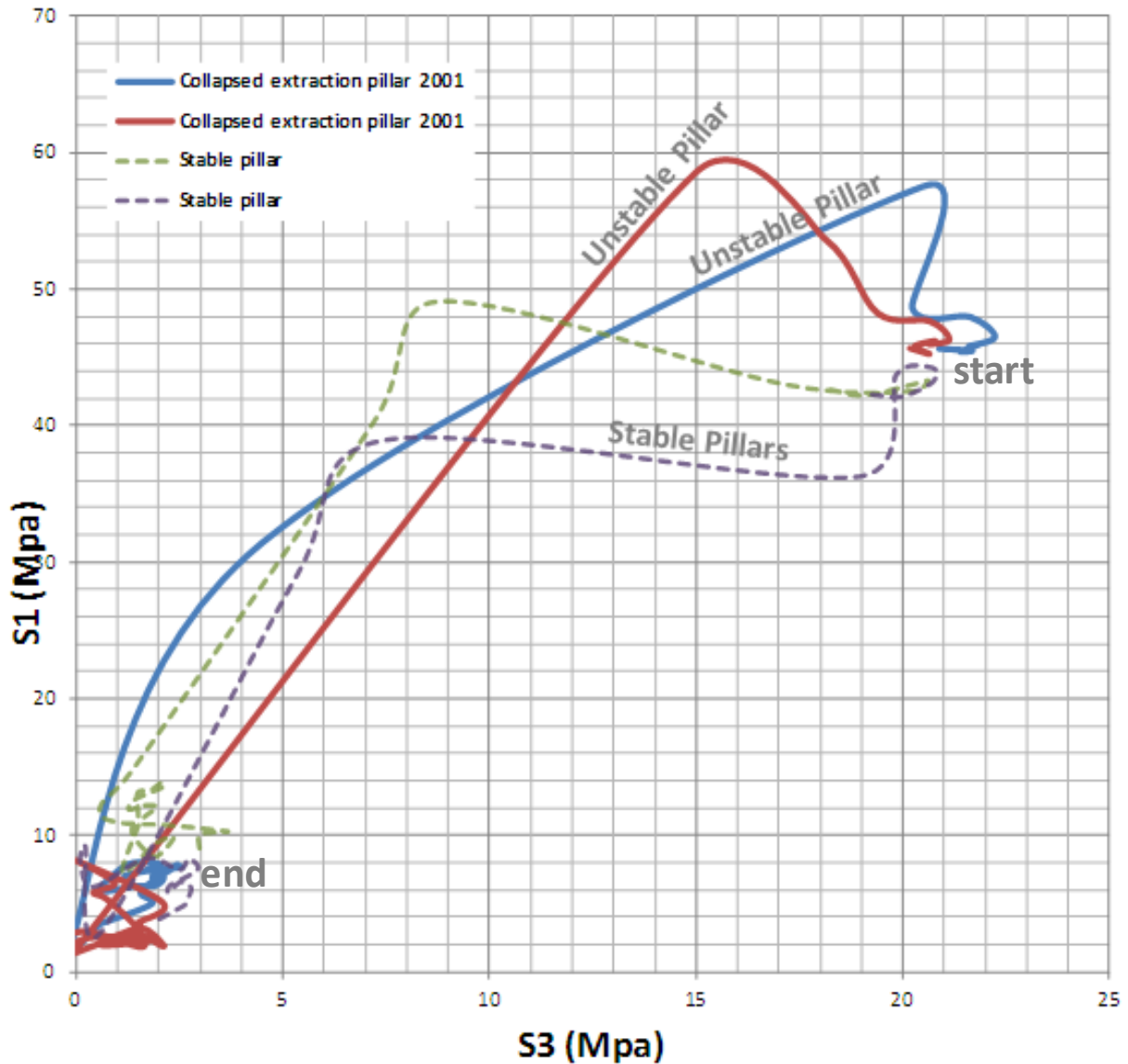


**Figure 6.7:** Principal stress path for four assessed pillars associated to the pre-undercut sequence, 2000-2005.

### 6.3 ASSESSING THE LATER PERIOD OF THE ESMERALDA COLLAPSE

Based on the significant damage experienced through the full extraction history of the Esmeralda operation, the later period of the Esmeralda collapses was identified between 2008 and 2010. The geotechnical precursors identified through observations and geotechnical monitoring characterised this later period by a collapse occurrence ahead of the undercut front. Moreover, it is important to highlight that the panel caving method with a modified version of pre undercut sequence and advanced developments was used during this period at the Esmeralda operation. The sequence of geotechnical precursors (geotechnical and geometric parameters) leading to deterioration in ground conditions and concluding in uncontrolled collapse of the crown pillar at the Esmeralda operation are

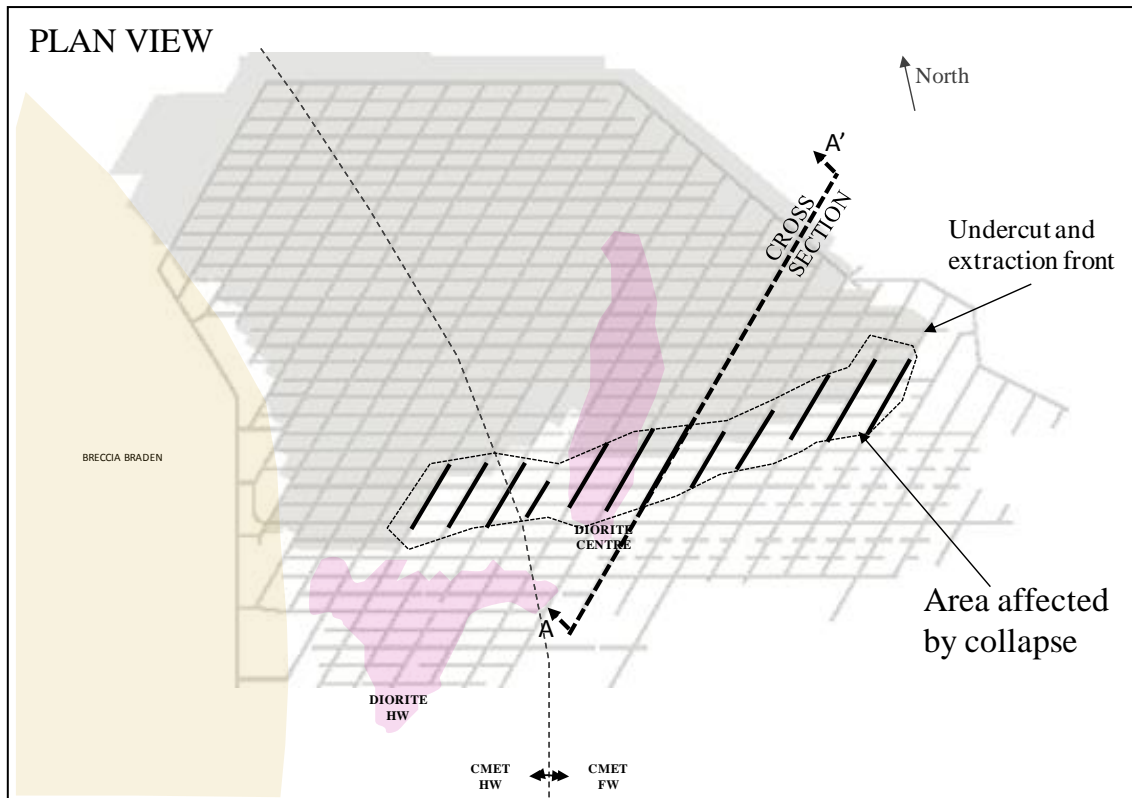
summarized in the following list and they also are illustrated in a representative vertical cross section of Esmeralda operation for this later period, as can be seen in Figure 6.8. This illustration attempts to integrate the geotechnical precursors and the representative mining state on that period showing the relative location of the most significant rock mass damage represented by collapsed drifts with respect to the mining front advance.

- Large cave front parallel to the main structural set (intermediate faults and one of the major faults detailed in Section 5.5.6)
- Faults activation by stress distribution
- Increased on abutment stress
- Pillar strength is exceeded by the load acting

The most relevant numerical results from modelled extraction geometry of the later period were reviewed. In fact, exactly the same representative cross section detailed in Figure 6.8 was evaluated with numerical results where the majority of characterized geotechnical precursors described above were assessed through the plastic strain values and principal stress values distribution.

Figures 6.9 and 6.10 show numerical results for a representative cross section during the later period of collapses at Esmeralda. A sequence of changes and effects associated with experienced rock mass damage can be seen in Figures 6.9 and 6.10, where the most representative modelled geometries between 2008 and 2010 were taken into consideration.

Results confirmed that geotechnical precursors and their sequence are effectively leading to deterioration in ground conditions and conclude with uncontrolled collapses. First of all, the zone identified with the highest plastic strain values is affected by the intersection between the undercut front and the parallel fault set that induced damage propagation by fault activation. Secondly the modelled geometry (large cave geometry) and the geotechnical condition generated an increased abutment stress ahead of the undercut front exceeding 90 MPa in some zones. The intensive abutment stress together with fault activation deteriorated ground conditions around the front. Thirdly, the mining strategy modelled caused considerable change in the confinement condition on the extraction level ahead of the undercut front. Finally the combined effects of all assessed geotechnical precursors integrated in the model can be appreciated especially in Figures 6.9 where the area under evaluation shows that pillar strength is exceeded by load acting according to the instability criteria discussed in Section 5.6.6.



CROSS SECTION

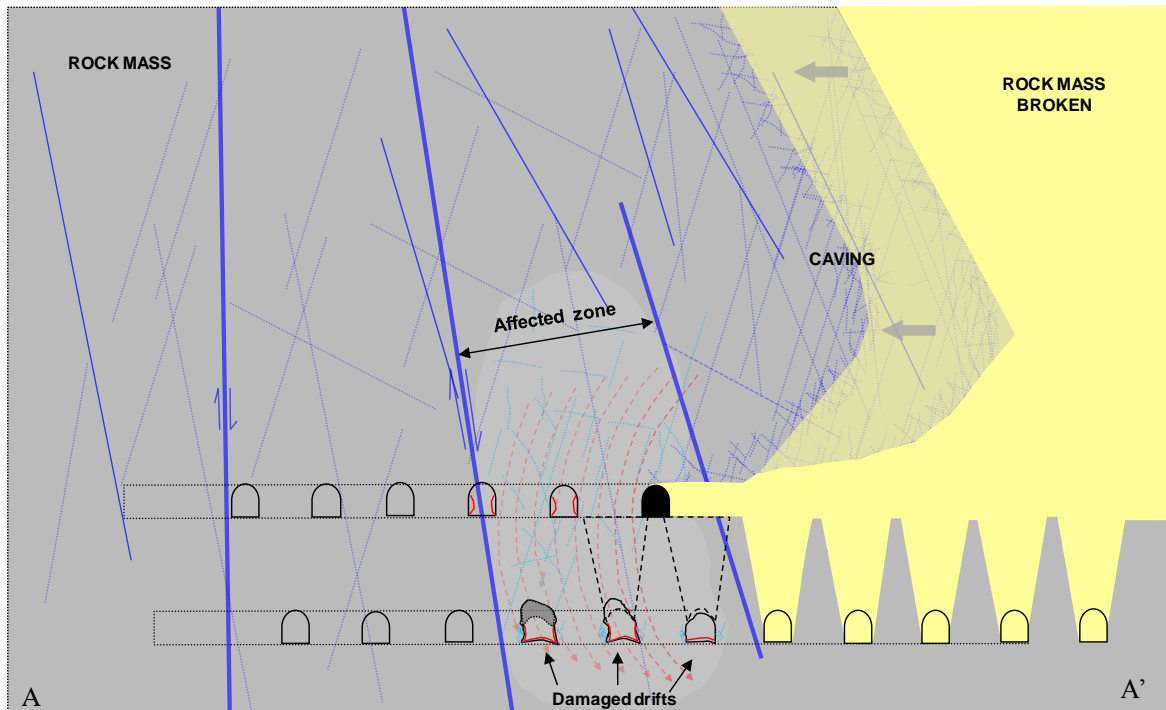


**Figure 6.8:** Representative cross section for the later period of the Esmeralda collapse (2008-2010), where a modified version of advance undercutting panel caving was used.

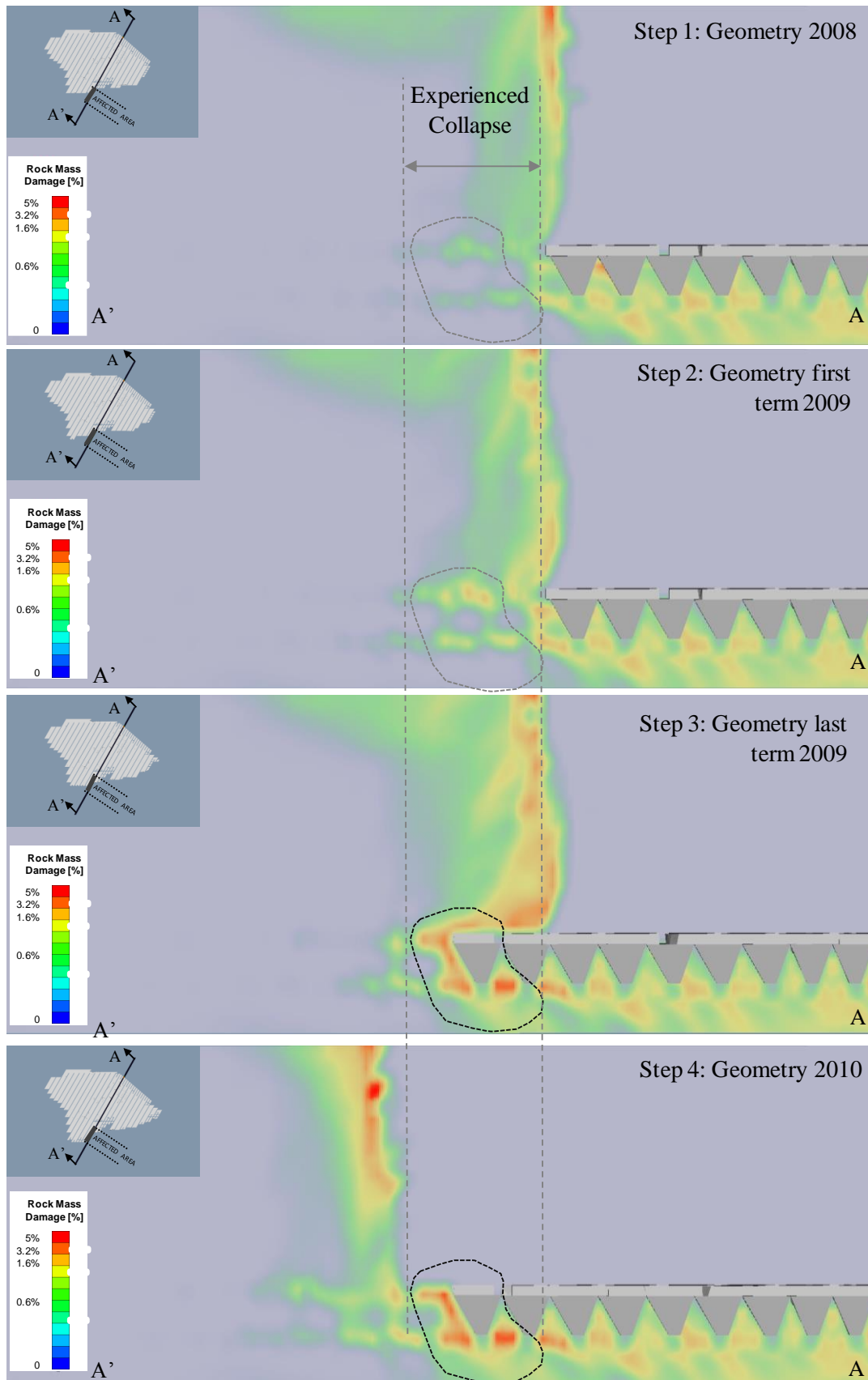


**Figure 6.9:** Cross section of modelled geometry through experienced collapse zone for the later period showing contours of plastic strain associated with modelled step.

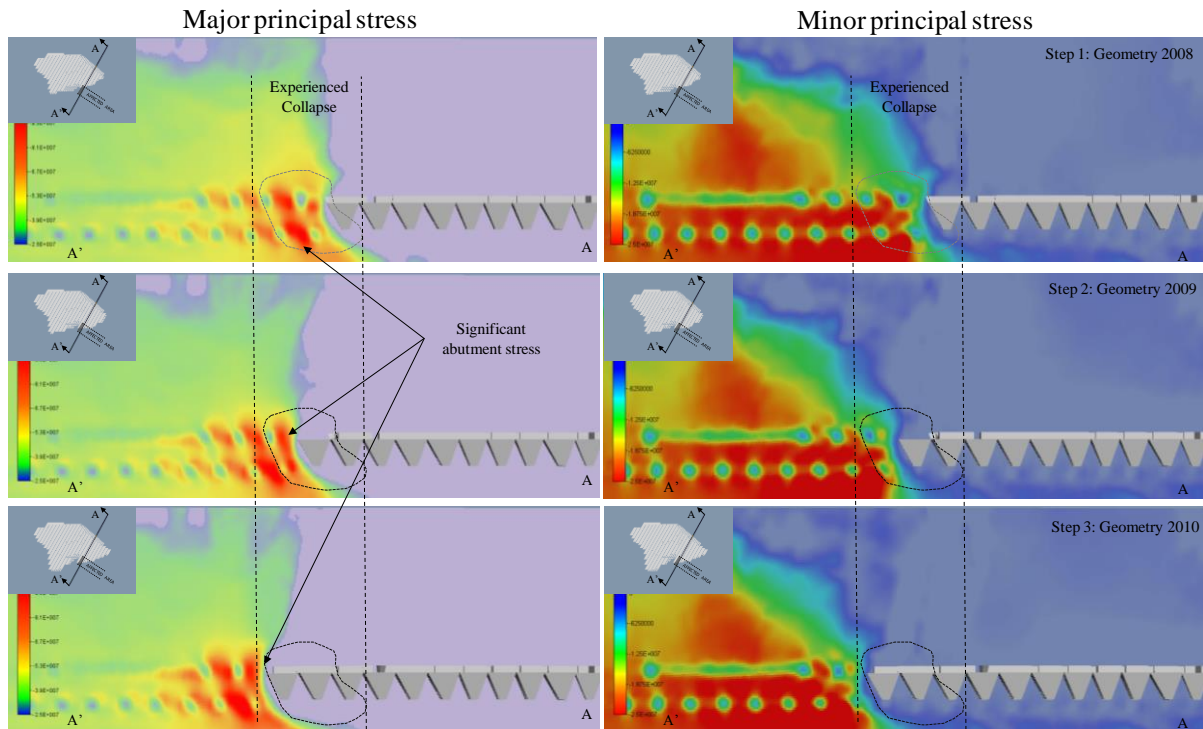


**Figure 6.10:** Cross section of modelled geometry through experienced collapse zone for the later period showing contours of major and minor principal stress for each modelled step.

In addition, during the later period of the Esmeralda operation (2008-2010) with extraction by panel caving with modified version of pre undercut sequence and advanced developments, two representative extraction pillars were selected to evaluate their stress-strain path during all the extraction steps modelled. They were identified as collapsed pillars according to observed behaviour. The location of assessed pillars is shown in Figure 6.11 alongside their relative location to mining fronts for the period when they were definitively declared as collapsed.

In order to assess the pillars behaviour during the whole extraction modelled history, all the plastic strain path versus principal stress for the two evaluated pillars is detailed in the Figure 6.12. It can be seen that the representative collapsed pillars experienced significant plastic strain values and this is confirmed according to the instability criteria detailed in section 5.6.6, where at least one of them shows plastic strain values exceeding 2%.

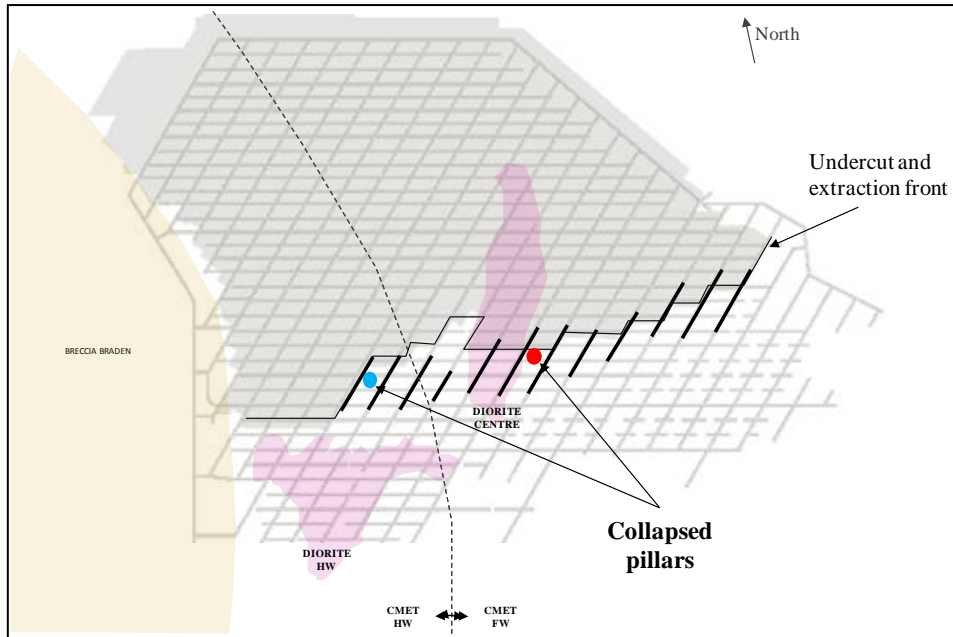


Figure 6.11: Location of assessed pillars for later period of Esmeralda

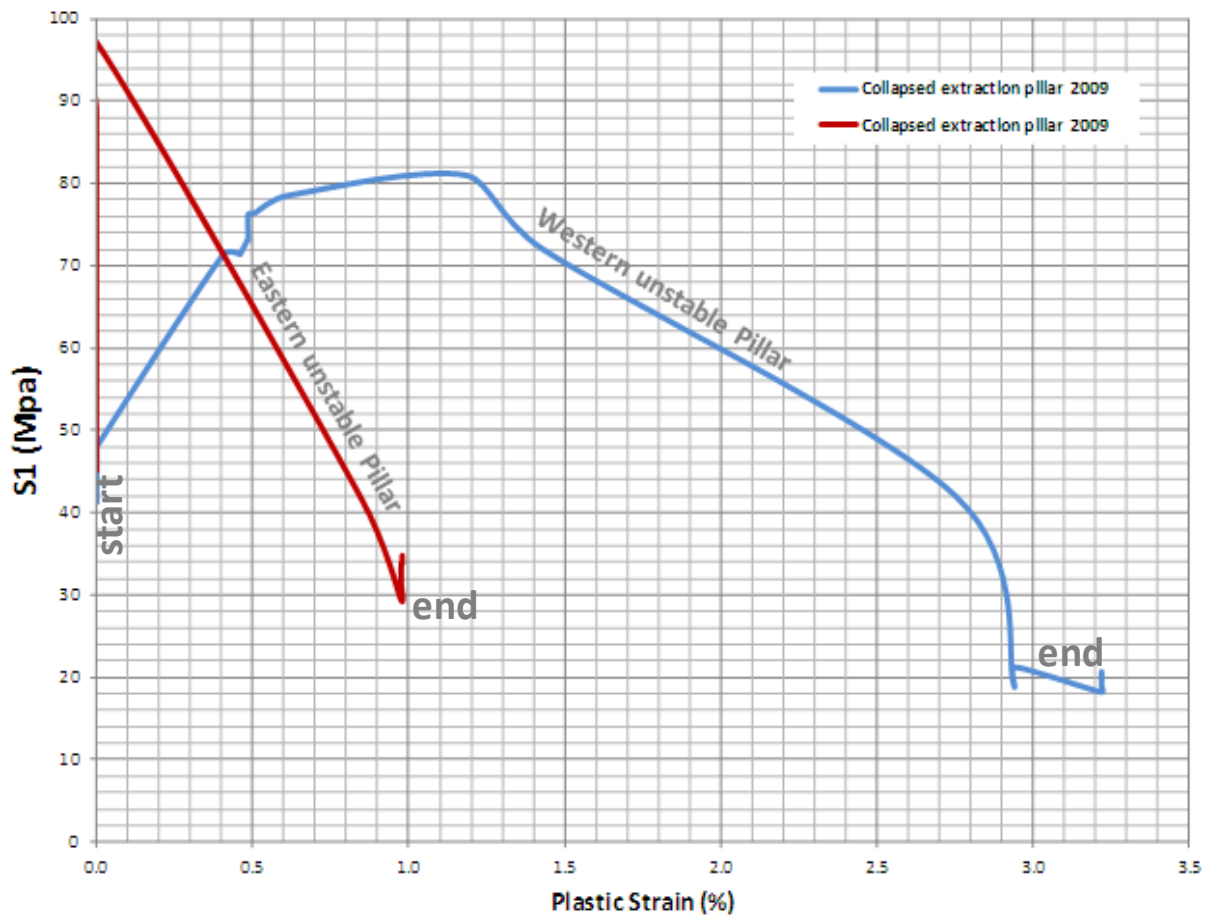
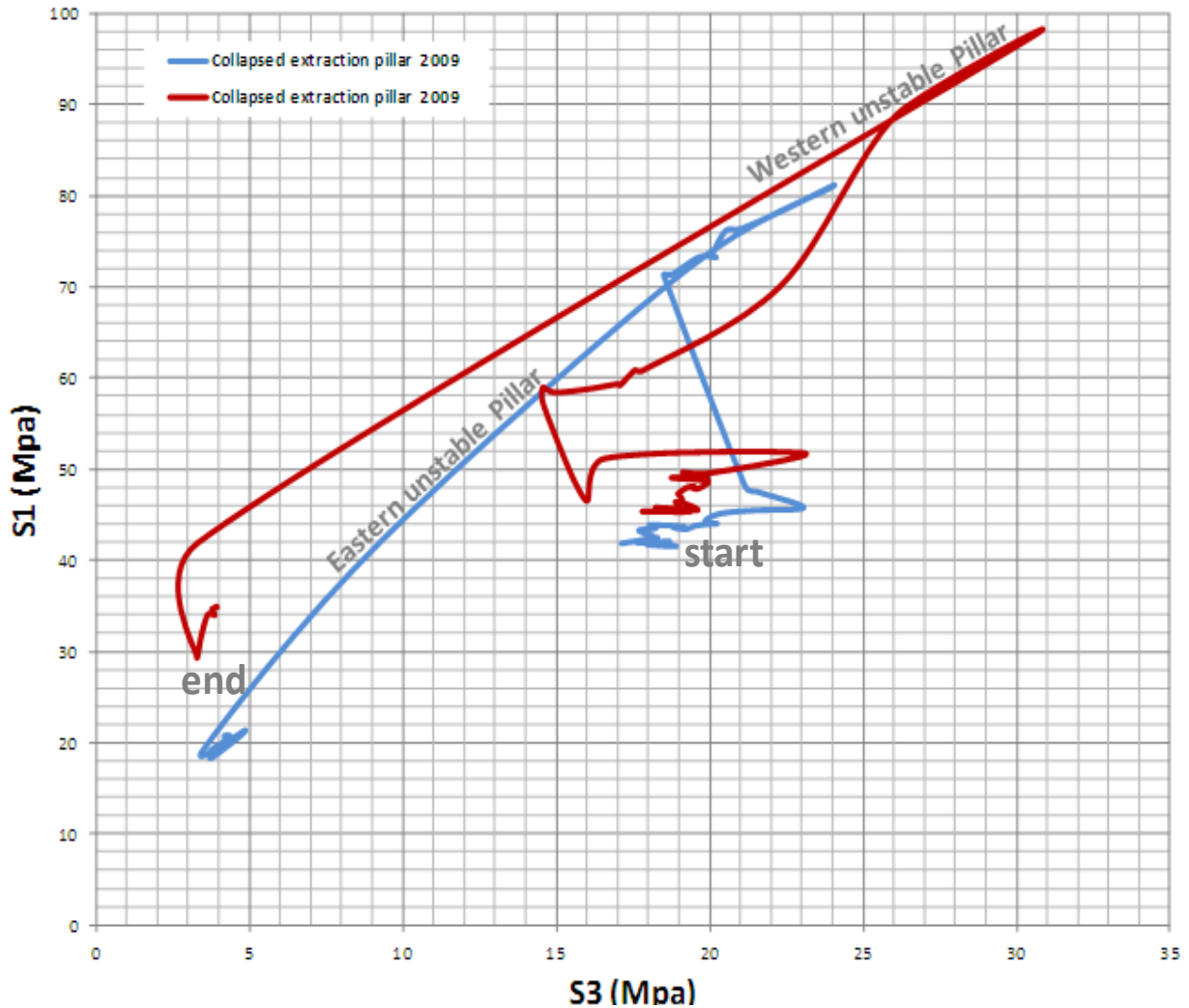


Figure 6.12: Stress-strain path for two assessed pillars associated with a modified version of advance undercut method, 2008-2010.

For the later period and exactly the same representative assessed pillars associated to the advanced undercutting method, the principal stress paths were also reviewed. Figure 6.13 shows the principal stress paths associated with complete extraction geometries modelled. An important increase of abutment stress ahead of undercut front can be seen. Indeed the whole collapse experienced associated with this period was located within the affected area through intensive stress evidences. This increased stress induced may confirm one of the main causes of collapse for pillars located ahead of the undercut front and may also confirm the conceptual hypothesis.



**Figure 6.13:** Principal stress path for two assessed pillars associated with a modified version of the advanced undercut method, 2008-2010.

#### **6.4 CONFIRMING THE COLLAPSE MECHANISM**

Two different collapse mechanisms were identified during the complete extraction history at the Esmeralda operation. These two mechanisms have been conceptually stated based on the complete geotechnical evidence associated with this operation and also the empirical analysis carried out within this chapter.

To confirm this conceptual hypothesis about the collapse mechanisms, two representative collapsed pillars were compared in terms of their stress path, as shown in Figure 6.14. The first pillar was collapsed during the earlier period (2003) and was associated with the panel caving with pre undercut sequence. The second pillar was collapsed during the later period (2009) and was associated with a panel caving with a modified version of pre undercut sequence and advanced developments. Although both representative pillars were finally collapsed and experienced similar significant damage, their stress path and therefore their geotechnical behavior is completely different. In the modified version of the advanced undercutting panel caving method, pillars located ahead of the undercut front were exposed to important stress changes and to an increased abutment stress, on the other hand, in the pre-undercut method, pillars were completely unconfined. In both cases, the weak fault sets assessed in the analysis played a relevant role on the amount of damage experienced and this might have also facilitated the collapse of pillars.

The numerical simulation confirmed that the collapse mechanism is strongly related with the mining method used and conceptual models were validated by the model results.

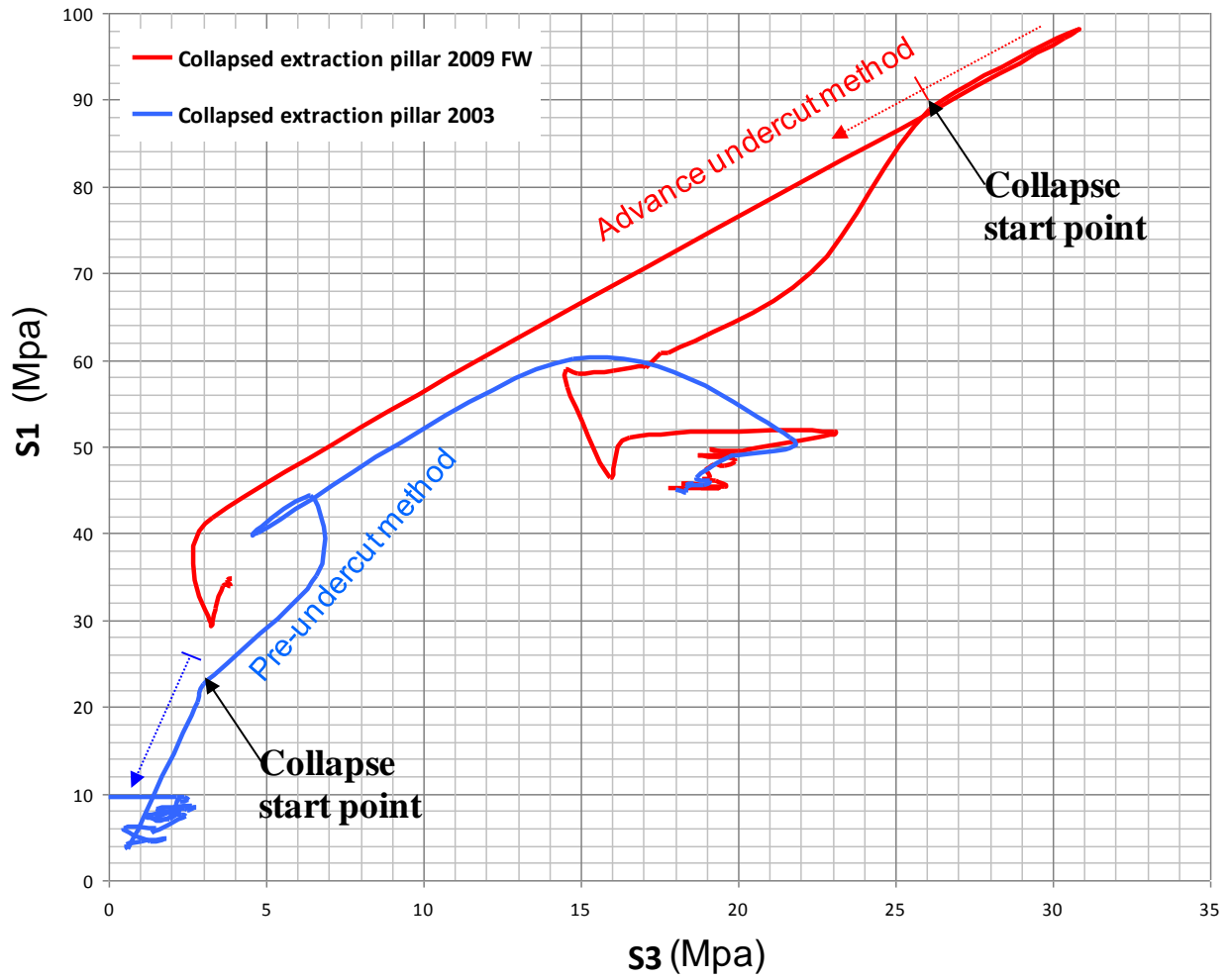


Figure 6.14: Stress path for two representative collapsed pillars for both Esmeralda period.

## **CHAPTER 7**

### **CONCLUSIONS AND FURTHER WORK**

#### **7.1 BACK ANALYSIS OF ROCK MASS DEFORMATION EXPERIENCED AT THE EL TENIENTE MINE**

Modern panel caving design is based on a sound understanding of the potential rock mass failure mechanisms that may affect excavation performance at the extraction, production levels and surrounding infrastructure of a caving operation (Brown, 2007). Rock mass failure can be experienced as a combination of failure through the rock mass substance with translation and rotation of rock blocks which are defined by geological structures.

El Teniente mine is a representative application of modern panel caving design. Their larger operations have experienced geotechnical related damage that over years has created an impact regarding the fulfillment of production targets. The rock mass failure affecting excavations performance around extraction infrastructure has been identified as large collapses in the central part of a caving front. This has reduced the production area due to lost accesses and no extraction of reserves committed in the mining plan. The systematic back analysis of rock mass deformation, was undertaken because to the mechanism of the collapses were not clearly defined.

This thesis contributes to the understanding of block caving failure mechanisms which is achieved by systematic back analysis of large scale failure in Esmeralda operation. This is carried out to produce an end product encompassing a mix of theoretical research and modelling and empirical data collection and analysis. This investigation involved review of large scale geological data, intact rock mass properties, geotechnical instrumentation and observational records in order to develop a numerical simulation of previous extractions geometries with back analysis of documented damage.

Advances in computational efficiency and capacity mean that significant improvement in modelling practice for cave mines is now possible. Perhaps the most significant improvement will come from a move towards calibrated, multi-scale non-linear modeling, such as the one employed here. Therefore, the rock mass deformation experienced at the Esmeralda mine site to date coupled with the application of numerical methods will be a valuable tool and it will lead to improved design methodology of other block caving mines.

## 7.2 MAIN FINDINGS AND ACHIEVEMENTS OF RESEARCH

With respect to the rock mass failure in modern panel caving, the key aims of the proposed integrated back analysis were to develop a work methodology based on continual improvement in understanding of the collapses phenomenon. In this regards, large scale geological data, intact rock properties, geotechnical instrumentation and observational records were reviewed and analyzed as part of a phase one methodology. In parallel, and based upon literature review, Esmeralda evidence and rock mass behavior in other sectors at El Teniente Mine, a conceptual model was created. In addition, the conceptual model was validated by a numerical simulation of all previous extraction geometries with back analysis of documented damage. The key steps of the proposed methodology were:

1. Assessment of Esmeralda evidence: literature review, field data collection since 1997 to 2010 based on observational records, geotechnical instrumentation and monitoring.
2. Empirical conceptual model development: generic hypothesis for types of collapses based on all evidences and empirical information from Esmeralda extraction steps.
3. Numerical simulation through three-dimensional non-linear model to reproduce as best as possible the rock mass deformation and stress distribution which have been experienced at the Esmeralda operation to date.
4. Understanding of the learned lesson from back analysis in order to provide guidelines for future mine design.

Some specific achievements of the research in relation to these aims and objectives are described below.

### **Rock mass characterization**

A detailed revision of the methods for geotechnical classification of the rock mass was performed. Considering the most representative lithologies at the El Teniente mine, different classification methods were applied, concluding that these techniques cannot reflect and/or capture the differences in the behavior of the rock mass at El Teniente mine. However, work performed by Brzovic (2010) allows a better classification of the differences in the behavior of the rock mass at El Teniente by assessing the type of vein infill forming the rock mass. Based on such analyses, this study included the geotechnical differentiation of the rock mass in the Esmeralda sector as input for back analysis, allowing a more realistic differentiation of results.

The geotechnical characterization was complemented with triaxial testing performed for representative lithologies present at Esmeralda operation. This information was also used as input parameter for the development of the back analysis. Although the two lithologies tested show a different mechanical behavior in the field, while the resulting envelopes from the intact rock testing do not differ from each other significantly. This conclusion is consistent with the literature reviewed;

where criteria such as Hoek–Brown do not reflect differentiation for the rock mass types from El Teniente mine (Karzulovic, 2006b).

The study developed a three-dimensional structural model representative of the mine sectors analyzed. This included faults at different scales recognized in the different levels in the surroundings of the Esmeralda operation. With this information processed as input in the numerical modeling, it was possible to confirm some of the hypothesis proposed for the conceptual model of collapse mechanisms. The Study and results showed that the presence of intermediate and major faults have a facilitating effect on the large scale damage, such as collapsed areas.

### **Rock mass failure**

The study showed that collapse as a type of the rock mass failure is present during almost the complete history of a large panel caving exploitation, particularly in those operations with wide mining front exceeding 300 m. These types of panel caving have been characterized by not complying with operational standards and design associated to the exploitation method. A detailed revision of the collapses in different conditions and operations, confirmed the presence of these damages in panel caving sectors that do not advance continuously, with irregular extraction strategies and essentially with singular designs associated either to engineering or failure in the quality of implementation of the method. The thesis concludes that a relevant aspect which facilitates the propagation of collapse damage is related to the operational discipline associated to the implementation of an exploitation method being used.

Regarding to Esmeralda operation and its analysis, the thesis also identified that there were two different periods of intensive rock mass failure during the whole history at Esmeralda operation. This was achieved taking into account the assessed evidence of the sector along with the literature reviewed. Firstly, the early period of Esmeralda collapses has been identified between the years 2000 until 2005. This period was characterized essentially by a collapse occurrence behind the undercut front and the panel caving with pre-undercut sequence as exploitation method used. The main geotechnical and geometric parameters acting upon the generated collapse were identified and analyzed in order to develop a conceptual sequence of the likely causes for that type of collapse. Secondly, a later period of Esmeralda collapses has been identified between the 2008 and 2010 years. This period is characterized essentially by collapse occurrence ahead of the undercut front and the implementation of modified version of panel caving with pre-undercut sequence and advanced developments as exploitation method. Finally, the main parameters (geotechnical precursors) affecting the generated collapse for both periods listed as follows:

- Undercut and cave front were parallel to the weaker structural sets (called intermediate faults)
- Distance between undercut front and extraction front exceeded typical standards

- Remaining pillars associated to deficient blasting were formed
- Draw strategy facilitated an unfavorable stress condition
- The large cave front was parallel to main structural set (intermediate faults and one of the major faults)
- Faults were activated by stress distribution
- A large increase on abutment stress was experienced due to the shape of cave front.

### **Numerical modeling**

The key study output was a reliable calibrated, three dimensional, non-linear numerical model with emphasis in the behavior of Esmeralda. This model was capable of capturing the evolution of rock mass damage (yielding) and displacements over the entire panel caving history at Esmeralda.

The model captured changes in the nature of modeled seismic potential and the interaction between a particular cave geometry and previous mining. The model also considered the effect of major structures in large scale damage, such as collapsed areas. The model accounts for deformation on major structures, including the changes in seismogenic potential, as the undercut advances, and the cave initiates, propagates and breaks through to previous cavities.

The thesis designed a local and common Esmeralda damage scale for its whole extraction history, based on the qualitative and quantitative comparison between plastic strain results (or % rock mass damage) and rock mass damage experienced during the Esmeralda extraction history. This scale was created once a reliable simulation was obtained from the calibration procedure.

Another important result included the determination of the material properties for the rock mass at a large scale and properties for major, intermediate and minor faults, based on calibration using the mine-global model.

Finally, by doing a sensitivity analysis in the model, the study showed the importance of scaling the material properties from triaxial tests to the rock mass scale. Also, the work developed allowed the assessment of the effect of remnant pillars during the undercutting process. These pillars were critical to facilitate the rock mass failure process in the drifts of the extraction level.

### **Back analysis**

The thesis also identified two conceptual hypotheses about collapse mechanism at the Esmeralda operation. The geotechnical precursors identified through observations and geotechnical monitoring have characterized each hypothesis that also has been associated to two periods of Esmeralda extraction history. For both periods, this work confirmed that geotechnical precursors and their sequence effectively lead to deterioration in ground conditions and end-up in uncontrolled collapses.

Finally, two representative collapsed pillars geometries were compared in term of their stress path. The first pillar collapsed during the earlier period (2003) and was associated with the panel caving with pre-undercut sequence. The second pillar collapsed during the later period (2009) and was associated with a modified version of panel caving with pre-undercut sequence and advanced developments. Although both representative pillars were finally collapsed and experienced similar significant damage, their stress path and therefore their geotechnical behavior is completely different. In the modified version of panel caving with pre-undercut sequence and advanced developments, pillars located ahead of the undercut front were exposed to important stress changes and to an increased abutment stress, on the other hand, in the panel caving with pre-undercut sequence, the pillars were completely unconfined. In both cases, weak faults sets assessed in the analysis played a relevant role on the amount of damage experienced and this may have also facilitated their collapse.

The simulation process has confirmed that the collapse mechanism is strongly related to the exploitation method used and also the conceptual models described have been validated by the model results.

#### **Summary of Contributions to knowledge**

- (a) Review and analysis of large amounts of geological data, geotechnical instrumentation and observational data at a mine scale.
- (b) Development of damage criterion which was calibrated using observations used as input to calibrate the results of numerical modelling.
- (c) Numerical model calibration of mine-scale problem. This required a large numbers of iterations.
- (d) Conceptual model of pillar collapses leading to large unstable regions within the mine.
- (e) Pillar collapse linked to mining method chosen:
  - Collapse occurrence behind the undercut front associated to Panel caving with pre-undercut sequence.
  - Collapse occurrence ahead of the undercut front associated to a Panel caving with pre-undercut sequence and advanced developments.
- (f) Guidelines for future mine extraction under similar depth and conditions

### **7.3 LIMITATIONS AND RECOMMENDATIONS FOR FUTURE WORK**

The greatest uncertainty of this study is associated to knowledge of the rock mass, in fact the characterization of the structural sets for Esmeralda have been identified as one of the most relevant geotechnical parameters playing an important role upon collapse mechanisms. Therefore, in order to improve the estimation and forecast of possible collapses, it is necessary to improve the structural geological recognition of a sector of interest.

Other focus of uncertainty has been related to the simulated cave shape and its associated effects. For any future analysis, an improved understanding based on systematic monitoring of the cave shape is required for a sector of interest.

For the El Teniente mine situation, the calibrated model can now be used for detailed forward modeling of adjacent areas such as Esmeralda Sur (Blocks 1 and 2), New Mining Level and other areas such as Pilar Norte.

The simulation process has established a framework for a more reliable numerical modeling of a complete cave extraction at the El Teniente Mine in the future. This provides the opportunity for comparison of cave variants and optimization of existing approaches at El Teniente, including a better understanding of ground support performance.

## REFERENCES

- Araneda, O., and A. Sougarret. 2008. Lessons learned in cave Mining: El Teniente 1997-2007. *Proc. 5th International Conference and Exhibition on Mass Mining - MassMin 2008*, 9-11 June, Luleå, Sweden. pp. 43-52. Luleå University of technology Press.
- Arndt, S., D. Beck, F. Reusch, I. Thin, i., C. Stone, M. Heap, and D. Tyler. 2007. Deep and High Stress Mining – Deformation and Seismicity. *ABAQUS Users' Conference*.
- Ayden, Ö., T. Akagi and T. Kawamoto. 1993. The Squeezing Potential of Rocks Around Tunnels; Theory and Prediction. *Rock Mech. Rock Engng.*, 26 (2), 137-163.
- Baez, F. (2011). *Preacondicionamiento del Macizo Rocoso, Desarrollo Tecnológico 1999-2010*. Codelco – Chile.
- Baros, M. C. (1995) *El Teniente. Hombres del Mineral, 1905-1945*, Santiago, Grafica Andes.
- Barton, N., Lien, R and Lunde, J. 1974. Engineering Classification of rock masses for the design of tunnel support. *Rock Mech.*, 6(4), pp.189-236.
- Barton, N. 2002. Some new Q-value correlations to assist in site characterisation and tunnel design. *Int.J.Rock Mech. Min. Sci.*, 39(2): 185-216.
- Barraza, M. and Crorkan, P. 2000. Esmeralda mine exploitation project. *Proc. MassMin 2000*, 29 October – 2 November, Brisbane, Australia (Ed: G Chitombo). pp. 267-278. The Australasian Institute of Mining and Metallurgy.
- Barraza, M., Vega, H., Cuello, D., Cifuentes, C., Quezada, O. and J. Millan. 2010. Esmeralda Sur definiciones de crecimiento. Internal report DPL-I-009/2010, División El Teniente, CODELCO-Chile.
- Beck, D., and Duplancic, P. 2005. Forecasting Performance and Achieving Performance Indicators in High Stress and Seismically Active Mining Environments. In Y. Potvin and M. Hudyma (ed.), *Proceedings of the 6th International Symposium on Rockbursts and Seismicity in Mines*, Perth, Australia, 9-11 March, pp. 409-418.
- Beck, D. A. 2008. Multi-scale, non-linear numerical analysis of mining induced deformation, in *Proceedings 42nd US Rock Mechanics Symposium and 2nd U.S.-Canada Rock Mechanics Symposium*, San Francisco, California, June 29–July 2.
- Beck, D A, Kassbohm, S & Putzar, G, 2010. Multi-scale simulation of ground support designs for extreme tunnel closure. In Y Potvin (ed), *Caving 2010, Proc 2nd Int Symp on Block & Sublevel Caving*, Perth, 20-22 April, 441-453. Australian Centre for Geomechanics, Perth.
- Beck, D. A., G. Sharrock, and G. Capes. 2011. A coupled DFE-Newtonian Cellular Automata scheme for simulation of cave initiation, propagation and induced seismicity. *45th US Rock Mechanics / Geomechanics Symposium – ARMA*, 26-29 June, San Francisco, CA.
- Beck, D.A. and Putzar, G. 2011. Coupled Flow- Deformation Simulation for Mine Scale Analysis of Cave initiation and Propagation. *In proceedings of the International Society of Rock Mechanics 2011 Conference*, Beijing.
- Beck D.A, Lilley C.R, Levkovitch, V and Reusch. F. 2013 An empirical method for estimation of strain softening, dilatant material properties of rock. Published on [www.beckengineering.com.au](http://www.beckengineering.com.au).
- Bieniawski, Z. 1973. Engineering Classification of Jointed Rock Masses. *Transactions of the South African Institute of Civil Engineering*, 15, pp.335-344.
- Bieniawski, Z. 1976. Rock mass classifications in rock engineering. *Exploration for Rock Engineering* (ed. Z. T. Bieniawski), 1:97-106. A. A. Balkema: Cape Town.

- Brady, B. H. G., and E. T. Brown. 2004. *Rock Mechanics for Underground Mining*. 3<sup>rd</sup> ed. London: Klumer Academic Publishers.
- Brown, E. T. (Ed.) 1981. *Rock Characterization Testing and Monitoring, Suggested Methods*, London, International Society of Rock Mechanics.
- Brown, E. T. 2007. *Block Caving Geomechanics*. 2<sup>nd</sup> ed. Brisbane: Julius Kruttschnitt Mineral Research Centre, the University of Queensland.
- Brzovic, A. 2001. Fundamentos Geológicos para un Sistema de Clasificación Geotécnico del Macizo Rocosó Primario de Mina El Teniente. Internal report SGL-I-187/2001, División El Teniente, CODELCO-Chile.
- Brzovic, A. and E. Villaescusa. 2007. Rock mass characterization and assessment of block-forming geological discontinuities during caving of primary copper ore at the El Teniente mine, Chile. *Int. J. Rock. Mech. Min. Sci.*, 44, pp.565-583.
- Brzovic, A. 2008. Rock mass disassembly during caving propagation at the El Teniente mine, Chile. *Proc. 5th International Conference and Exhibition on Mass Mining - MassMin 2008*, 9-11 June, Luleå, Sweden. pp. 1014-1022. Luleå University of technology Press.
- Brzovic, A. 2009. Rock Mass Strength and Seismicity during Caving Propagation at the El Teniente Mine, Chile. *International Symposium on Rockburst and Seismicity in Mines 2009 (RaSiM7)*. C.A.Tang (ed), 21-23 August Dalian, China.
- Brzovic, A. 2010. *Characterisation of primary copper ore for block caving at the el Teniente mine, chile*. PhD Thesis, Western Australian School of Mines of Curtin University of Technology.
- Brzovic, A. 2011. Modelo Estructural Mina Esmeralda. Unpublished internal report, Division El Teniente, CODELCO – Chile.
- Brzovic, A. 2013. Informe de avance n°1 api T10E202 Plano Desarme Potencial Macizo Rocosó Nivel Hundimiento. Internal report SGL-I-059/2013, División El Teniente, CODELCO-Chile.
- Cavieres, P. 1995. Análisis geomecánico del Nudo Isla. Internal report SPL-I-028/1995, División El Teniente, CODELCO-Chile.
- Cavieres, P. 1999. Evolución de los Métodos de Explotación en la Mina El Teniente. Curso Gestión de la Innovación Tecnológica, Programa de Especialización en Innovación Tecnológica Geomecánica y Geotecnia Aplicada a la Minería, Universidad de Chile.
- Cellhay, F., J. Pereira, and L. Burgos. 2005. Geología y Recursos para proyecto NNM, Ingeniería Conceptual. Internal report SGL-I-030/2005, Division El Teniente, CODELCO – Chile.
- Cepuritis, P. M. 2010. *An Integrated Approach to Span Design in Open Stope Mining*. PhD Thesis, Western Australian School of Mines of Curtin University of Technology.
- Chacon, J., Gopfert, H. & Ovalle, A. 2004. Thirty years evolution of block caving in Chile. *Proceedings MassMin 2004*, Santiago, (Eds: A Karzulovic and M Alfaro), 387-392. Chilean Engineering Institute: Santiago.
- Chitombo, G. P. 2010. Cave mining – 16 years after Laubscher’s 1994 paper ‘Cave mining – state of the art’, *Proc. 2nd Int. Symp. on ‘Block and sublevel caving’*, (ed. Y. Potvin), April 2010, Perth, Australia, Australian Centre for Geomechanics, 45–61.
- Cho, N., Martin, C. D. and Christiansson, R. 2002. Suppressing fracture growth around underground openings, *MINING AND TUNNELLING INNOVATION AND OPPORTUNITY, Proc. 5<sup>th</sup> North Am Rock Mech Symp & 17th Tunn Assn Can Conf, Toronto* (eds R Hammah, W Bawden, J Curran and M Telesnicki), Vol 2, pp 1151-1158. University of Toronto Press: Toronto.
- Cline, J. 1995. Genesis of porphyry deposits: the behavior of water, chloride, and copper in crystallizing melts. IN PIERCE, F. W. & BOLM, J. G. (Eds.) *Porphyry Copper Deposits of the America Cordillera*. Arizona Geol. Soc., digets Arizona.

- Coppola, T., L. Cortese and P. Folgarait. 2009. The effect of stress invariants on ductile fracture limit in steels *Engineering Fracture Mechanics*, Volume 76, Issue 9, 1288-1302.
- Cuadra, P G & Puig, A G (coordinadores). 1991. Visita Yacimiento El Teniente, Excursión Geológica IC-1, 6° Congreso Geológico Chileno.
- Cuadra, P. 1986. Geocronología K-Ar del yacimiento El Teniente y áreas adyacentes. *Revista Geologica de Chile*, 27, 3-26.
- Cuello, D., P. Cavieres, S. Diaz, and M. Gallardo. 2010. Ingeniería Geomecánica Proyecto Esmeralda Sur. Internal report SGM-I-029/2010, Division El Teniente, CODELCO – Chile.
- Cundall, P.A., Pierce, M.E. and Mas Ivars, D. (2008) Quantifying the Size Effect of Rock Mass Strength, in *Proceedings First Southern Hemisphere International Rock Mechanics Symposium (SHIRMS)*, Y. Potvin, J. Carter, A. Dyskin and R. Jeffrey (eds), 16–19 September 2009, Perth, Australia, Australian Centre for Geomechanics, Perth, Vol. 2 – Fundamental and Petroleum, pp. 3–15.
- De Nicola, R and Fishwick, M, 2000. An underground air blast - Codelco Chile – Division Salvador. *Proceedings MassMin 2000*, Brisbane, (Ed: G Chitombo), 279-288. Australasian Institute of Mining and Metallurgy: Melbourne.
- Deere, D U, Hendron, A J, Patton, F D & Cording, E J. 1967. Design of surface and near surface excavations in rock, *Proc 8th US Symp Rock Mechanics: FAILURE AND BREAKAGE OF ROCK* (ed C Fairhurst), pp 237-302, AIME: New York.
- Diaz, G. and P. Tobar. 2000. Panel Caving Experiences and Macrotrench – an Alternative Exploitation Method at the El Teniente Mine, Codelco, Chile. *Proceedings MassMin 2000*, Brisbane, (Ed: G Chitombo), 235-248. Australasian Institute of Mining and Metallurgy: Melbourne.
- Diaz, J., Villegas, F. and P. Lledo. 2009. Estudio Geotécnico de Potencial de Colapso, Chuquicamata Subterráneo. Technical Report, VCP, CODELCO-Chile.
- Diederichs, M S. 2003. Rock fracture and collapse under low confinement conditions, *Rock Mech Rock Engng*, 36(5):339-381.
- Doepken, W. G. 1982. The Henderson Mine. *Underground Mining Methods Handbook*, (Ed: W A Australid), 1:990-997. Society of Mining Engineers, AIME: New York.
- Dunlop, R. and J. Pereira. 1998. Conceptos sobre mecanismos de generación de Colapsos. Internal report PL-I-073/1998, Division El Teniente, CODELCO – Chile.
- Dunlop, R. 1999. Mecanismos generación de colapsos. Internal report PL-I-093/1999, Division El Teniente, CODELCO – Chile.
- Dunlop, R., D. Cuello, C. Cifuentes, and R. Parraguez. 2010. Hipótesis causal de los colapsos delante del frente de socavación, Mina Esmeralda. Internal report SGM-I-031/2010, Division El Teniente, CODELCO – Chile.
- Dunlop, R. 2013. *Seismic Monitoring and Induced Seismicity at the El Teniente Mine*. Master of Engineering Science Thesis (unpublished), Western Australian School of Mines of Curtin University of Technology.
- Duplancic, P. and B. H. Brady. 1999. Characterization of caving mechanisms by analysis of seismicity and rock stress. *Proceedings 9th International Congress on Rock Mechanics*, Paris, (Eds: G Vouille and P Berest), 2:1049-1053. Balkema: Rotterdam.
- Elmo, D., Stead, D. and S. Rogers. 2008a. Quantitative analysis of fractured rock masses using a discrete fracture network approach: Characterisation of natural fragmentation and implications for current rock mass. *Proc. 5th International Conference and Exhibition on Mass Mining - MassMin 2008*, 9-11 June, Luleå, Sweden. pp. 1023-1032. Luleå University of technology Press.

- Elmo, D., Vyazmensky, A., Stead D. and J. Rance. 2008b. Numerical analysis of pit wall deformation induced by block-caving mining: A combined FEM/DEM - DFN synthetic rock mass approach. *Proc. 5th International Conference and Exhibition on Mass Mining - MassMin 2008*, 9-11 June, Luleå, Sweden. pp. 1073-1084. Luleå University of technology Press.
- Elmo, D. and Stead, D. 2009. An integrated numerical modelling – discrete fracture network approach applied to the characterisation of rock mass strength of naturally fractured pillars, *Rock Mechanics and Rock Engineering*, DOI 10.1007/s00603-009-0027-3.
- Encina, V., F. Baez, F. Geister, and J. Steinberg. 2008. Mechanized continuous drawing system: A technical answer to increase production. *Proc. 5th International Conference and Exhibition on Mass Mining - MassMin 2008*, 9-11 June, Luleå, Sweden. pp. 553-562. Luleå University of technology Press.
- Everitt, R. and Latjai, E. 2004. The influence of rock fabric on excavation damage in the Lac du Bonnett granite. *Int J Rock Mech Min Sci & Geomech Abstr.* 41(8):1277-1303.
- Farmer, I. 1983. *ENGINEERING BEHAVIOUR OF ROCKS*, 2nd ed. 208 p. Chapman and Hall: London.
- Ferguson, G. 2008. Macrosecuencia Management RENO & Esmeralda Sectors. Technical Report, El Teniente Division, CODELCO-Chile.
- Ferguson, G. 2006. Breaking the Cycle – A Way Forward. Internal report, Division El Teniente, CODELCO – Chile.
- Fernandez, F., P. Evans, and R. Gelson. 2010. Design and implementation of a damage assessment system at Argyle Diamonds Block Cave project. *Caving 2010*. (Ed: Y. Potvin). pp. 65-82. Australian Centre for Geomechanics, Perth.
- Fernandez, F., P. Garay, and H. Constanzo. 2008. Análisis de Colapso sector recuperado calles 19 a 25 entre zanjas 15 y 18, nivel de producción Mina Esmeralda. Internal report SPM-I-004/2008, División El Teniente, CODELCO-Chile.
- Flores, G and Karzulovic, A, 2002. Benchmarking Report. Prepared for International Caving Study, Stage II, JKMR: Brisbane.
- Flores, G., Karzulovic, A. and E. T. Brown. 2004. Current practices and trends in Cave Mining. *Proceedings MassMin 2004*, Santiago, (Eds: A Karzulovic and M Alfaro), 83-90. Chilean Engineering Institute: Santiago.
- Flores, G. 2005. *Rock Mass response to the transition from Open Pit to Underground Cave Mining*. PhD Thesis (unpublished), University of Queensland, 246p.
- Fuentes, S., and E. Adam. 2008. Chuquicamata underground mine. *Proc. 5th International Conference and Exhibition on Mass Mining - MassMin 2008*, 9-11 June, Luleå, Sweden. pp. 461-470. Luleå University of technology Press.
- Garrido, I., Riveros, M., Cladouhos, T., Espineira, D. & Allmendinger, R. (1994). Modelo geológico estructural yacimiento El Teniente. *VII Congreso Geológico Chileno*. Antofagasta.
- Hannweg, L., Lorig, L., van Hout, G. and A. Guest. 2004. Koffiefontein mine front cave - Case History. *Proceedings MassMin 2004*, Santiago, (Eds: A Karzulovic and M Alfaro), 393-396. Chilean Engineering Institute: Santiago.
- Heal, D. P. 2010. *Observations and Analysis of Incidences of Rock burst Damage in Underground Mines*. PhD Thesis, the University of Western Australia, 223p.
- Heslop, T. G. 2000. Block caving – controllable risks and fatal flaws. *Proc. MassMin 2000*, 29 October – 2 November, Brisbane, Australia (Ed: G Chitombo). pp. 437-456. The Australasian Institute of Mining and Metallurgy.
- Hill, R. 1950. *The mathematical theory of plasticity*. New York:Osford University Press Inc.

- Hill, R. 1951. On the state of stress in a plastic-rigid body at the yield point. *Philosophical Magazine Series 7*, 42:331, pp.868-875.
- Hoek, E. and E. T. Brown.1980. *Underground Excavation in Rock*. London: Institute of Mining and Metallurgy.
- Hoek, E. 1988. The Hoek-Brown Failure Criterion - a 1988 Update. 15th Canadian Rock Mechanics Symposium, pp. 31-38.
- Hoek, E, 1994. Strength of rock and rock masses. *ISRM News J*, 2(2): 4-16.
- Hoek, E. and Brown, E. 1997. Practical Estimates of Rock Mass Strength. *Int. J. Rock. Mech. Min. Sci.*, 34, pp.1165-1186.
- Hoek, E. and Diederichs, M. 2006. Empirical estimation of rock mass modulus. *Int J Rock Mech Min Sci.* 43(2):203-215.
- Hoek, E., Marinos, P.G. and Marinos, V. P. 2006. Characterization and engineering properties of tectonically undisturbed but lithologically varied sedimentary rocks, under publication, *Int J Rock Mech Min Sci.*
- Hormazabal, E., Villegas, F., Rovira, F. and C. Carranza-Torres. 2010. Geomechanical evaluation of caving macro-block options at Chuquicamata Underground Project in Chile using three-dimensional numerical modelling. *Proc. 2nd Int. Symp. on 'Block and sublevel caving'*, (ed. Y. Potvin), April 2010, Perth, Australia, Australian Centre for Geomechanics.
- Howell, F. H. & Molloy, S. (1960). Geology of the Braden orebody, Chile, South America. *Economic Geology*, 70, 863-905.
- Hudson, J. A., and X. T. Feng. 2006. Updated flowcharts for rock mechanics modelling and rock engineering design. *Int. J. Rock. Mech. Min. Sci.*, 44, pp. 174-195.
- Hustrulid, W. 2004. Some Input Regarding Panel Caving in the Esmeralda Sector El Teniente Mine. Technical Report, El Teniente Division, CODELCO-Chile.
- Hustrulid, W. 2006. Teniente Technical Advisory Board – Report, July 24. Technical Report, El Teniente Division, CODELCO-Chile.
- Hustrulid, W. 2010. Technical report Review of the Esmeralda South Analysis and Strategy. Technical Report, El Teniente Division, CODELCO-Chile
- Itasca. 1995. *PFC Particle Flow Code, Modelling Software*. Itasca, Inc: Minneapolis.
- Itasca. 1998. *PFC3D Particle Flow Code in 3 dimensions, version 2.0*. Itasca consulting.
- Jing, L., and J. A. Hudson. 2002. Numerical methods in rock mechanics. *Int. J. Rock. Mech. Min. Sci.*, 39, pp. 409-427.
- Jing, L. 2003. A review of techniques advances and outstanding issues in numerical modelling for rock mechanics and rock engineering. *Int. J. Rock. Mech. Min. Sci.*, 40, pp. 283-353.
- Karzulovic, A., Galeb, M. and L. Quiñones. 1991. Experiencia adquirida durante el desarrollo, construcción y operación de los Panales I y II mina Rio Blanco. Technical report, Andina Division, CODELCO – Chile.
- Karzulovic, A. 1997. Modelo Geomecánico del Macizo Rocosó Primario de Mina El Teniente. Conceptos Fundamentales. Technical Report, El Teniente Division, CODELCO-Chile.
- Karzulovic, A. 2001. Altura roca primaria en minería por panel caving. Technical Report, El Teniente Division, CODELCO-Chile.
- Karzulovic, A. 2003a. Aplicabilidad de los Sistemas de Clasificación Geotécnica en Roca Primaria. Technical Report, El Teniente Division, CODELCO-Chile.

- Karzulovic, A. 2003b. Evaluación geomecánica Colapso calles 17, 19, 21 & 23 nivel de producción sector Esmeralda, informe de opinión. Technical Report, El Teniente Division, CODELCO-Chile.
- Karzulovic, A. 2005. Aplicabilidad Métodos de Explotación al Nuevo Nivel Mina de el Teniente. Technical Report, El Teniente Division, CODELCO-Chile.
- Karzulovic, A. 2006a. Continuación Minería Sector Esmeralda Consideraciones Geomecánicas. Technical Report, El Teniente Division, CODELCO-Chile.
- Karzulovic, A. 2006b. Criterios de Homologación para una Minería en Roca Primaria. Technical Report, El Teniente Division, CODELCO-Chile.
- Karzulovic, A. 2006c. Continuación minería sector Esmeralda consideraciones geomecánicas. Technical Report, El Teniente Division, CODELCO-Chile.
- Kvapil, R, McMorran, J, Petersen, L, Placet, J, White, D and Holubec, M. 1982. El Teniente Concept. Level 4 – Primary Ore. Technical Report, Geomines, Inc. Tucson, Arizona.
- Krstulovic, G. 1997. Análisis geomecánico al secuenciamiento minero del sector Ten-4 Sur y su empalme Nudo Isla. Technical Report, El Teniente Division, CODELCO-Chile.
- Larrain, M., Cuevas, J., Barraza, M. and F. Hernandez. 2011. Plan Minero PND 2011 Informe Final. División El Teniente CODELCO-CHILE, Internal report SDS-I-033/2010.
- Laubscher, D. 1973. Class distinction in rock masses. *Coal, Gold + Base Miner. South. Afr.*, 23.
- Laubscher, D. 1990. A geomechanics classification system for rating of rock mass in mine design. *J. S. Afr. Inst. Min. Metall.*, **90**(10):257-73.
- Laubscher, D. and J. Jakubec, J. 2001. The MRMR rock mass classification for jointed rock masses. *Underground Mining Methods: Engineering Fundamentals and International Case Studies* (eds W. A. Hustrulid and R. L. Bullock), 475-81. Society for Mining, Metallurgy and Exploration: Littleton, Colorado.
- Levkovitch, V., F. Reusch, and D. Beck. 2010. Application of a non-linear confinement sensitive constitutive model to mine scale simulations subject to varying levels of confining stress. *Proceedings of the European Rock Mechanics Symposium*. (Ed: In J. Zhao, V. Labiouse, J. Dudt and J. Mathier), Lausanne, Switzerland, 15-18 June, pp. 161-164.
- Li, J. 2004. Critical strain of intact rock and rock masses. PhD Thesis, Western Australian School of Mines, Curtin University of Technology. 186p.
- Lorig, L. J. 1998. Análisis cualitativo de los colapsos del sector Ten- 4 Sur LHD, Itasca Consulting group. Technical Report, El Teniente Division, CODELCO-Chile.
- Lorig, L. J. 1999. Modelamiento Numérico en Geomecánica. Course notes, Post-título en Geomecánica y Geotecnia, Departamento Ingeniería de Minas, Universidad de Chile, Santiago.
- Martin, C D & Chandler, N A. 1994. The progressive fracture of Lac du Bonnett granite, *Int J Rock Mech & Mining Sciences*, 31(6):643-659.
- Martin, C. D. 1997. Seventeenth Canadian Geotechnical Colloquium: The effect of cohesion loss and stress path on brittle rock strength, *Can Geotech J*, 34(5):698-725.
- Martin, C. D. and Christiansson, R. 2002. Rock mechanics considerations in the siting of Sweden's nuclear waste repository. *MINING AND TUNNELLING INNOVATION AND OPPORTUNITY, Proc. 5th North Am Rock Mech Symp & 17th Tunn Assn Can Conf, Toronto* (eds R Hammah, W Bawden, J Curran and M Telesnicki), Vol 2, pp 1199-1206. University of Toronto Press: Toronto.

- Mas Ivars, D., Deisman, N., Pierce, M. and Fairhurst, C. 2007. The Synthetic Rock Mass Approach – A Step Forward in the Characterization of Jointed Rock Masses, in *The Second Half Century of Rock Mechanics*, 11th Congress of the International Society for Rock Mechanics, Lisbon, July 2007, L. Ribeiro e Sousa, C. Olalla, and N. Grossmann (eds), London, Taylor & Francis Group, Vol. 1, pp. 485–490.
- Mendecki, A. J., G. Van Aswegen, and P. Mountfort. 1999. A guide to routine seismic monitoring in mines. *Handbook on Rock Engineering Practice for Tabular Hard Rock Mines*, (Ed: A. J. Jager and J. A. Ryder), Creda Communications, Cape Town, South Africa.
- Menetrey P. and Willam K.: “Triaxial failure criterion for concrete and its generalization”, *ACI Structural Journal*. 92(3): 311-317, 1995.
- Millan, J. 2010. Antecedentes geológicos geotécnicos entre XC acceso 3 y XC acceso 4 Mina Esmeralda. Internal report SGL-I-083/2010, División El Teniente, CODELCO-Chile.
- Mogi, K. 1966. Pressure dependence of rock strength and transition from brittle fracture to ductile flow. *Bull Earthquake Research Inst, Japan*, (44):215-232.
- Morel, R. 1986. Incidencia de las estructuras geológicas en la explotación del mineral primario sector central del yacimiento El Teniente. *Minerales*, 40(172):5-12.
- Ovalle, A. W. and Codoceo, J A. 1977. Factores que inciden en la productividad de un bloque en la mina El Teniente, *Revista Minerales*, 139:5-30.
- Ovalle, A. W. and H. R. Albornoz. 1981. Block caving with LHD equipment at El Teniente. *Design and Operation of Caving and Sublevel Stopping Mines*, (Ed: D R Stewart), 355-361. Society of Mining Engineers, AIME: New York.
- Pardo, C. and P. Landeros. 2008. Numerical modeling at El Teniente Mine. Internal report TTAB 2008, Division El Teniente, CODELCO – Chile.
- Pardo, C. and E. Villaescusa. 2012. Methodology for back analysis of intensive rock mass damage at the el Teniente Mine. *Proc. 6th International Conference and Exhibition on Mass Mining - MassMin 2012*, 10-14 June, Subdury, On, Canada.
- Pardo, C., Villaescusa, E., Beck, D. and A. Brzovic. 2012. Back analysis of intensive rock mass damage at the El Teniente mine. *Proc. Australian Mining Technology Conference, CRC Mining*, Perth WA.
- Pasten, O. 1999. Evaluación de la Socavación de Baja Altura en Teniente 4 Sur, Bachelor thesis, Universidad de Santiago de Chile.
- Peele, R. 1941. *Mining Engineers' Handbook*, 3<sup>rd</sup> edition. New York: John Wiley and Sons.
- Pierce, M. 2009. *A model for gravity flow of fragmented rock in block caving mines*, PhD thesis, The University of Queensland.
- Reyes-Montes, J.M., Pettitt, W.S. and Young, R.P. (2007) Validation of a Synthetic Rock Mass model using excavation Induced microseismicity, in *Rock Mechanics: Meeting Society's Challenges and Demands*, 1st Canada-U.S. Rock Mechanics Symposium, Vancouver, May 2007, E. Eberhardt (ed), London, Taylor & Francis Group, Vol. 1: Fundamentals, New Technologies and New Ideas, pp. 365–369.
- Rogers, S., Elmo, D., Webb, G. and Catalan, A. 2010. A discrete fracture network based approach to defining in situ, primary and secondary fragmentation distributions for the Cadia East panel cave project, *Proc. 2nd Int. Symp. on 'Block and sublevel caving'*, (ed. Y. Potvin), April 2010, Perth, Australia, Australian Centre for Geomechanics, 425–439.
- Rojas, E, Molina, R, Bonani, A and Constanzo, H, 2000. The pre-undercut caving method at the El Teniente Mine, Codelco – Chile. *Proceedings MassMin 2000*, Brisbane, (Ed: G Chitombo), 261-266. Australasian Institute of Mining and Metallurgy: Melbourne.

- Rojas, E., Molina, R. and Cavieres, P. 2001. Preundercut caving in El Teniente mine, Chile. IN HUSTRULID, W. R. & BULLOCK, R. (Eds.) *Underground Mining Methods; engineering fundamental and international case studies*. Colorado, SME.
- Rojas, E., S. Gaete, E. Leiva, R. Quiroz, J. Rubio and, J. Seguel. 2005. Diagnostico Mina Esmeralda-Grupo de Trabajo Proyecto Esmeralda. Internal report SGM-I-024/2005, Division El Teniente, CODELCO – Chile.
- Rojas, E. 2013. Presentación Riesgos alto impacto comité de auditoría, compensaciones y ética Directorio Codelco, mayo 2013.
- Ross, I. and As, A. 2005. Northparkes Mines – design, sudden failure, air-blast and hazard management at the E26 block cave. *Proceedings Ninth Underground Operators' Conference*, Perth, 7-18. AuIMM: Melbourne.
- Rubio, J., Seguel, J. and E. Rojas. 2005. Auscultación de pilares en zona de transición nivel de hundimiento mina Esmeralda. Internal report SGM-I-001/2005, Division El Teniente, CODELCO – Chile.
- Sakurai, S. 1981. Direct strain evaluation technique in construction in underground openings. In, *Proceedings of the 22nd U.S. Rock Mechanics Symposium*, pp. 278-282.
- Sakurai, S. 1997. Lessons Learnt from Field Measurements in Tunnelling. *Tunneling and underground Space Technology*, 12 (4), pp.453-460.
- Schwartz, A. E. 1964. Failure of rock in the triaxial shear test. *Proc 6th US Symp Rock Mech*, Rolla, Missouri, pp 109-135.
- Seguel, J. 2005. Antecedentes geologicos y geotecnicos al norte XC-3 ucl Esmeralda. Internal report, Division El Teniente, CODELCO – Chile.
- Seguel, J. and J. Millan. 2009a. Incidencia estructuras geológicas en los daños del sector FW nivel de hundimiento mina Esmeralda. Internal report SGL-I-019/2009, División El Teniente, CODELCO-Chile.
- Seguel, J. and J. Millan. 2009b. Antecedentes geológicos geotécnicos sector Brecha FW mina Esmeralda. Internal report SGL-I-090/2009, División El Teniente, CODELCO-Chile.
- Sharrock, G., Beck, D., Booth, G. and Sandy, M. 2004. Simulating gravity flow in sub-level caving with cellular automata, in *Proceedings MassMin 2004*, A. Karzulovic and M. Alvaro (eds), 22–25 August, Santiago, Chile, Instituto de Ingenieros de Chile, Santiago, pp. 189–194.
- Sinuhaji, A., Flint, D. and O. Rindriatmoko. 2005. Pillar Stability Issues at DOZ Block Cave Mine. *Ninth Underground Operators' Conference*, 7 – 9 March, Perth, WA, Australia.
- Skewes, M. A. and Arevalo, A. (1997) Andesitas de la mina, El Teniente. *VIII Congreso Geologico Chileno*. Antofagasta.
- Skewes, M. A., Arevalo, A., Floody, R., Zuñiga, P. & Stern, C. R. (2002). The giant El Teniente breccia deposit: Hypogene copper distribution and emplacement. *Economic Geology*, 9, 299-32.
- SRK, 1999. Análisis cinemático inestabilidades nivel de producción Ten-4 Sur LHD, SRK Consultores. Technical Report, El Teniente Division, CODELCO-Chile.
- Stokes, W. L. & Varnes, D J. 1955. GLOSSARY OF SELECTED GEOLOGIC TERMS WHIT SPECIAL REFERENCE TO THEIR USE IN ENGINEERING. 165 p. The Colorado Scientific Society, Denver, Colorado.
- Swanepoel, T., Van Strijp, T., Holder, A., Swarts, B., Beck, D. and P. Bartlett. 2012. Remediation of the Failed Cullinan Advance Undercut. *Proc. 6th International Conference and Exhibition on Mass Mining - MassMin 2012*, 10-14 June, Subdury, On, Canada.

- Szwedzicki, T. 2001. Geotechnical precursors to large-scale ground collapse in mines. *International Journal of Rock Mechanics & Mining Sciences*, 38 (2001) 957–965.
- van As, A and Jeffrey, R G, 2000. Hydraulic fracturing as a cave inducement technique at Northparkes Mines. *Proceedings MassMin 2000*, Brisbane, (Ed: G Chitombo), 165- 172. Australasian Institute of Mining and Metallurgy: Melbourne.
- Van Sint Jan, M. 2010. Estudio Geomecánico de pilares mina Esmeralda - Modelo de Entendimiento. Technical Report, El Teniente Division, CODELCO-Chile.
- Vargas, J. 1989. Criterios de diseño en puntos de extracción. Sistema panel caving LHD mina El Teniente. Nivel Teniente 4 Sur, *Revista Minerales*, 187:29-46.
- Vásquez, P., J. Rubio, and P. Cavieres. 2008. Methodology for estimating the “serviceability” of the UCL pillars at El Teniente mine, new mine level Project, Codelco Chile. *Proc. 5th International Conference and Exhibition on Mass Mining - MassMin 2008*, 9-11 June, Luleå, Sweden. pp. 783-792. Luleå University of technology Press.
- Villaescusa, E. 2007. *Underground Rock Engineering*, Master of Mining Geomechanics Class Notes. Western Australian School of Mines.
- Villaescusa, E. and L. Machuca. 2007. Stress measurement from oriented core using the Acoustic Emission method, El Teniente mine. Technical report WASM, Curtin University.
- Villaescusa, E., Lei, X., Nishizawa, O. and Funatsu, T. 2009. Laboratory testing of brittle intact rock – Implications for in situ stress measurements and rock mass failure. *Proc. Australian Mining Technology Conference, CRC Mining, QLD. 27 – 28 Oct, 2009. 226-239. Melbourne: AusIMM.*
- Villaescusa, E., and L. Machuca. 2011. Report of Intact Rock Properties Values for Codelco Chile Div. El Teniente. Technical report Western Australian School of Mines, Geomechanics Laboratory, Kalgoorlie, Australia.
- Villegas, F., Montecino, M., Arce, C., Alvial, J., Seguel, J., Molina, R. and E. Rojas. 2003. Informe técnico de Colapsos Mina Esmeralda, Grupo de Tarea Colapso Esmeralda. Internal report SPL-I-055/2003, Division El Teniente, CODELCO – Chile.
- Villegas, F. 2008. Prevención de Colapso en una mina de hundimiento por paneles en ambiente de roca primaria. Tesis magister en Minería, Universidad de Chile.
- Waversik, W R & Fairhurst, C. 1970. A study of brittle rock fracture in laboratory compression experiments. *Int J Rock Mech Min Sci & Geomech Abstr.* 7(5):561-575.
- Wiles, T. 1993. MAP3D User Manual. Mine Modelling Report, Copper Cliff, Ontario, Canada.
- Wiles, T. 2006. Reliability of numerical modelling predictions. *Int. J. Rock. Mech. Min. Sci.*, 43, pp.454-472.
- Wiles, T. 2010. Informe Experto Internacional en Modelamiento Numérico. Internal report, Division El Teniente, CODELCO – Chile.
- Wiles, T. 2007. *Numerical Modelling*. Master of Mining Geomechanics Class Notes. Western Australian School of Mines.
- Windsor, C.R., Cavieres, P., Villaescusa, E. and J. Pereira. 2006a. Rock Stress Tensor Measurements at the El Teniente Mine, Chile. *Proceedings of International Symposium on In Situ Rock Stress*, Trondheim, Norway, June 19 – 21, 2006.
- Windsor, C. R., P. Cavieres, E. Villaescusa, and J. Pereira. 2006b. Rock stress tensor measurements at the El Teniente mine, Chile. *Proceedings of International Symposium on In Situ Rock Stress*, Trondheim, Norway, June 19 – 21, 2006.
- Yu, H. S. 2006. *Plasticity and Geotechnics*. New York: Springer.

Zepeda, R. and R. Parraguez. 2008. Antecedentes de la aplicación del fracturamiento hidráulico en la mina El Teniente (Diablo Regimiento y Reservas Norte) y avance del FH en Pilar Norte. Internal report SGM-I-019/2008, División el Teniente, CODELCO – Chile.

Zuñiga, P. 1982. Alteración y mineralización hipógenas en el sector oeste del yacimiento El Teniente. Santiago, Universidad de Chile.

*Every reasonable effort has been made to acknowledge the owners of copyright material. I would be pleased to hear from any copyright owner who has been omitted or incorrectly acknowledged.*

## APPENDIX A - CONSTITUTIVE MODEL DESCRIPTION FOR THE CONTINUUM PARTS

Based on:

- Levkovitch, V., F. Reusch, and D. Beck. 2010. Application of a non-linear confinement sensitive constitutive model to mine scale simulations subject to varying levels of confining stress. *Proceedings of the European Rock Mechanics Symposium*. (Ed: In J. Zhao, V. Labiouse, J. Dudt and J. Mathier), Lausanne, Switzerland, 15-18 June, pp. 161-164.

Reusch, F., V. Levkovitch, and D. Beck. 2010. Multi-scale, non-linear numerical analysis of mining induced deformation in complex environments. *Proceedings of the European Rock Mechanics Symposium*. (Ed: In J. Zhao, V. Labiouse, J. Dudt and J. Mathier), Lausanne, Switzerland, 15-18 June, pp. 697-700

### Constitutive model description for the continuum parts

The relation between stress, strain, strength and degradation is described for the rock mass by the rock mass constitutive model. Generally, constitutive models for solid continua consist of 3 main parts: a yield criterion which describes the relation between stress and strength (HB for this project), a plastic strain potential, which describes how the material will deform as a consequence of changes in stress due to damage and a package of softening curves that describe how material properties are related to strain. The 3 parts may be linearly dependent or independent. Acknowledging these 3 parts is important: the yield criterion alone does not describe the workings of a model sufficiently.

Yield Criterion: In LR2, a generic strength criterion is used that can approximate almost any common rock mechanics yield criterion. The generic criterion that can approximate Hoek-Brown (in this case), Mohr-Coulomb or other criteria is the Menetrey/Willam strength criterion (1), described by the following function

$$\left[ \frac{q}{\sigma_{ci}} \right]^2 + m \left[ \frac{1}{3} \frac{q}{\sigma_{ci}} R(\theta, e) - \frac{p}{\sigma_{ci}} \right] - s = 0 \quad [1]$$

The material constants  $s$  and  $m$  are the measures of the cohesive and frictional strength, and  $\sigma_{ci}$  represents the uniaxial compressive strength. Further,  $p = -1/3 \mathbf{I} \cdot \boldsymbol{\sigma}$  is the hydrostatic pressure,  $q = \sqrt{3/2 \mathbf{S} \cdot \mathbf{S}}$  the Mises equivalent stress and  $r = \left[ 9/2 \mathbf{S} \cdot (\mathbf{S} \mathbf{S}) \right]^{1/3}$  the third stress invariant with  $\mathbf{S}$  being the deviatoric part of the Cauchy stress  $\boldsymbol{\sigma}$ . The dependence on the third invariant is introduced via the convex elliptic function in the deviatoric stress plane.

$$R(\theta, e) = \frac{4(1-e^2) \cos^2 \theta + (2e-1)^2}{2(1-e^2) \cos \theta + (2e-1) \sqrt{4(1-e^2) \cos^2 \theta + 5e^2 - 4e}} \quad [2]$$

Here, the variable  $\theta$ , defined via  $\cos 3\theta = (r/q)^3$ , is the deviatoric polar angle (also known as Lode angle) and the material constant  $e$  is the deviatoric eccentricity that describes the “out-of-roundedness” of the deviatoric trace of the function  $R(\theta, e)$  in terms of the ratio between the Mises stress along the extension meridian ( $\theta = 0$ ) and the compression meridian ( $\theta = \pi/3$ ). For  $\theta = 0$  and  $\theta = \pi/3$  the function becomes  $1/e$  and 1 respectively. The convexity of  $R(\theta, e)$  requires that  $0.5 \leq e \leq 1$ .

In the case of  $e = 0.5$  the Menetrey/Willam failure function represents a circumscribed approximation of the Hoek-Brown (2) strength criterion

$$\left( \frac{\sigma_1 - \sigma_3}{\sigma_{ci}} \right)^2 + m \frac{\sigma_3}{\sigma_{ci}} - s = 0, \quad [3]$$

where  $\sigma_1$  and  $\sigma_3$  are the major and minor principal stresses at failure. In order to recognize the similarity between the both criteria we rewrite the principal stresses representation using the relation between the stress invariants and the principal stresses

$$\sigma_1 = -p + \frac{2}{3}q \cos \theta \text{ and } \sigma_3 = -p + \frac{2}{3}q \cos \left( \theta + \frac{2}{3}\pi \right).$$

Inserting the upper expressions for the principal stresses into [3] one obtains the Hoek/Brown strength criterion in terms of the stress invariants

$$\left[ \frac{2}{\sqrt{3}} \frac{q}{\sigma_{ci}} \sin \left( \theta + \frac{\pi}{3} \right) \right]^2 + m \left[ \frac{2}{3} \frac{q}{\sigma_{ci}} \cos \theta - \frac{p}{\sigma_{ci}} \right] - s = 0. \quad [4]$$

$e = 0.5$  results in an exact match between the both criteria at the extension and compression meridians. For  $\theta = 0$  and  $\theta = \pi/3$  both expressions are reduced respectively to

$$\left[ \frac{q}{\sigma_{ci}} \right]^2 + m \left[ \frac{2}{3} \frac{q}{\sigma_{ci}} - \frac{p}{\sigma_{ci}} \right] - s = 0 \text{ and} \quad [5.1]$$

$$\left[ \frac{q}{\sigma_{ci}} \right]^2 + m \left[ \frac{1}{3} \frac{q}{\sigma_{ci}} - \frac{p}{\sigma_{ci}} \right] - s = 0. \quad [5.2]$$

Thus, for  $e = 0.5$  the Menetrey/Willam criterion can be considered as a circumscribed approximation of the Hoek/Brown function.

In contrast to the Hoek/Brown model that doesn't account for the intermediate principal stress, the dependence on  $\sigma_2$  in the case of the Menetrey/Willam criterion [1] is governed by the eccentricity parameter  $e$  and this can be very useful. Increasing eccentricity values cause a higher dependence on  $\sigma_2$  with the deviatoric trace of the Menetrey/Willam model approaching a circle.

Thus, the Menetrey/Willam model possesses a material parameter that can be adjusted to match the true triaxial failure data if this is required. For Ridgeway Deeps this feature was not used (the common form of HB was implemented), but these anisotropic effects may be important for more detailed, higher resolution projects in the future.

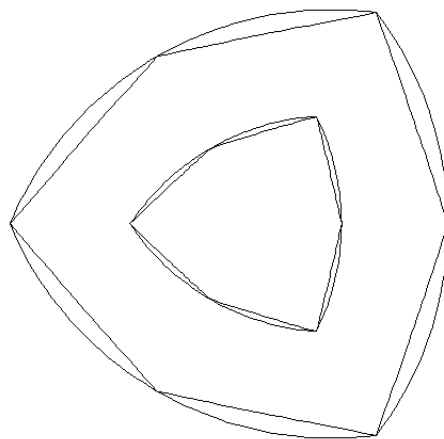


Figure 0-1 Comparison between the Menetrey/Willam failure model (smooth curves) and the 1980 Hoek-Brown criteria at two levels of confinement

In 1992 the original Hoek/Brown criterion was extended (3) by an additional parameter  $a$  to the following form

$$\left(\frac{\sigma_1 - \sigma_3}{\sigma_{ci}}\right)^{\frac{1}{a}} + m \frac{\sigma_3}{\sigma_{ci}} - s = 0, \quad [6]$$

that allows to change the curvature of the failure envelope, particularly in the very low normal stress range to account for very low or zero tensile strength in heavily jointed or very poor rock masses. A corresponding extension of the Menetrey/Willam model takes the form

$$\left[\frac{q}{\sigma_{ci}}\right]^{\frac{1}{a}} + m \left[\frac{1}{3} \frac{q}{\sigma_{ci}} R(\theta, e) - \frac{p}{\sigma_{ci}}\right] - s = 0, \quad [7]$$

which is implemented as a failure criterion in the framework of the LR2 model. Accordingly, the above failure function [7] can be considered as a circumscribed approximation of the 1992 Hoek/Brown (3) criterion.

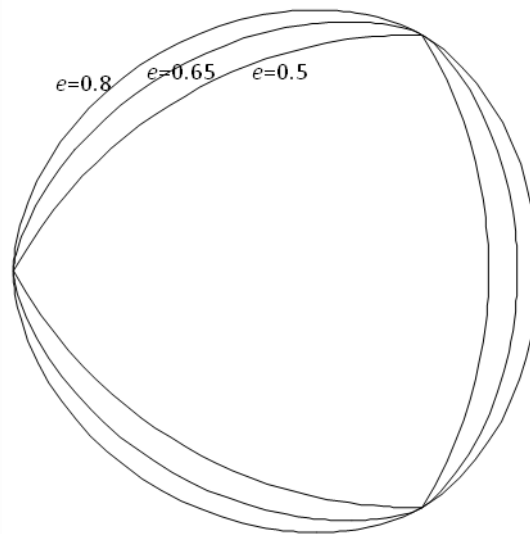


Figure 0-2 Deviatoric traces of the Menetrey/Willam failure function for three different eccentricity values.

The plastic strain potential is given by the relation

$$\mathbf{D}_p = \lambda \frac{\partial G}{\partial \boldsymbol{\sigma}}$$

where  $\lambda$  the accumulated equivalent plastic strain and  $G$  the flow potential

$$G = (A_f q)^b + m [B_f R(\theta, e) q - D_f p].$$

Here,  $D_f$  is the dilation parameter in the bulk. If this parameter is different from  $C_f$  the flow rule is non-associative which is the case for the most geotechnical materials.

Softening: The model is implemented in such a way that all the strength parameters as well as the dilation are prescribed as piecewise linear functions of accumulated plastic strain.

Jointed materials: The failure of the **jointed material** is described by the following sliding criterion

$$f = \tau - p_n \tan \beta - d$$

with  $d$  and  $\beta$  being the cohesion and the friction angle in the joint, respectively.

Further,  $\tau$  is the magnitude of the shear stress resolved onto the joint plane and  $p_n$  the normal stress acting across the joint. The plastic strain rate is given by the relation

$$\mathbf{D}_p = [\cos \psi \operatorname{sym}(\mathbf{s} \otimes \mathbf{n}) + \sin \psi \mathbf{n} \otimes \mathbf{n}] \dot{\lambda}$$

with  $\psi$  being the dilation angle in the joint. Further,  $\mathbf{n}$  is the unit normal vector of the joint plane and  $\mathbf{s}$  the unit vector into the direction of the resolve shear stress.

A key distinction of the ubiquitous joint formulation of LR2 is that yield may occur on joints or in the rock mass, not either.

#### 7.4 Representation of explicit structure

The behaviour of explicit discontinuities in LR2 and this project was approximated using traction-separation based cohesive elements.

The constitutive behaviour of these elements can be defined using the LR2 continuum-based constitutive model, or a constitutive model specified directly in terms of traction versus separation or a combination of both. A combination approach was used in this model.

In the combined approach, cohesive elements constrain initial stress-strain behavior of the contact at the discontinuity, but at a critical strain level the contact element formulation takes over. The contact elements allow separation of the two sides of the contact, and formation of particles bound by contact elements. The approach is taken because cohesive elements are very computationally efficient and Dissipated Plastic Energy at the contact is easily computed for such elements, whereas contact elements are required to account for the kinematics of large separation or dislocation.

## **APPENDIX B – ROCK MASS PROPERTIES USED IN THE NUMERICAL SIMULATION**

Key:

Material properties used during all modeling steps. From simulation M05 to M17

Appendix B: Rock mass properties used in the numerical simulation

Parameters		CMET	DACTIRE	DIORTIE	BRECCIA	HOST	SURFACE	FAULT
UCS [Mpa]		72,0	88,0	68,2	74,8	98,0	72,0	123,2
GSI		61,1	69,7	55,0	65,0	70,7	65,4	83,7
Eccentricity e		0,6	0,6	0,6	0,6	0,6	0,6	0,6
PS Level p	Trans	0,016728	0,014378	0,015357	0,012421	0,014378	0,014378	0,021074
	Res	0,045164	0,038822	0,041464	0,033536	0,038822	0,038822	0,056899
HB parameter s	Peak	8,59E-04	8,83E-04	1,32E-03	6,74E-04	1,52E-03	1,52E-03	8,74E-04
	Trans	8,59E-04	8,83E-04	1,32E-03	6,74E-04	1,52E-03	1,52E-03	8,74E-04
	Res	1,08E-03	1,10E-03	1,40E-03	9,00E-04	1,50E-03	1,50E-03	1,09E-03
LR2 dilatancy d	Peak	0,0556	0,0669	0,0726	0,0686	0,0817	0,0817	0,0363
	Trans	0,1350	0,0144	0,0154	0,0124	0,0144	0,0144	0,0211
	Res	0,0196	0,0199	0,0254	0,0163	0,0272	0,0272	0,0198
HB parameter mb	Peak	0,89	1,07	1,16	1,10	1,31	1,31	0,58
	Trans	0,89	1,07	1,16	1,10	1,31	1,31	0,58
	Res	0,63	0,64	0,81	0,52	0,87	0,87	0,63
Elastic modulus E [Pa]	Peak	1,01E+10	1,03E+10	1,31E+10	8,40E+09	1,40E+10	1,40E+10	1,02E+10
	v	0,23	0,23	0,24	0,23	0,25	0,25	0,23
HB parameter a		0,50144	0,50144	0,50144	0,50144	0,50144	0,50144	0,50144
Density		2700	2700	2700	2700	2700	2700	2700
Modulus of cave material Standard E [Pa]	Peak	2,02E+08	2,05E+08	2,61E+08	1,68E+08	2,80E+08	2,80E+08	2,04E+08
	v	0,20	0,20	0,20	0,20	0,20	0,20	0,20
Modulus of cave material Fast moving E [Pa]	Peak	5,04E+07	5,13E+07	6,53E+07	4,20E+07	7,00E+07	7,00E+07	5,10E+07
	v	0,00	0,00	0,00	0,00	0,00	0,00	0,00

**Table B.1:** Rock mass properties for Esmeralda used in M05.

Parameters		CMET	DACTIRE	DIORTIE	BRECCIA	HOST	SURFACE	FAULT
UCS [Mpa]		72,0	88,0	68,2	74,8	98,0	72,0	123,2
GSI		61,1	69,7	55,0	65,0	70,7	65,4	83,7
Eccentricity e		0,6	0,6	0,6	0,6	0,6	0,6	0,6
PS Level p	Trans	0,014322	0,013372	0,013847	0,011470	0,012896	0,012896	0,022405
	Res	0,038670	0,036103	0,037387	0,030968	0,034819	0,034819	0,060493
HB parameter s	Peak	1,93E-03	1,60E-03	2,82E-03	1,10E-03	3,41E-03	3,41E-03	1,76E-03
	Trans	1,93E-03	3,90E-03	8,76E-03	2,27E-03	1,15E-02	1,15E-02	4,46E-03
	Res	1,08E-03	1,10E-03	1,40E-03	9,00E-04	1,50E-03	1,50E-03	1,09E-03
LR2 dilatancy d	Peak	0,2100	0,1925	0,2450	0,1575	0,2625	0,2625	0,2013
	Trans	0,0756	0,0134	0,0138	0,0115	0,0129	0,0129	0,0224
	Res	0,0305	0,0279	0,0355	0,0228	0,0381	0,0381	0,0292
HB parameter mb	Peak	1,44	1,43	1,71	1,39	1,94	1,94	0,63
	Trans	1,44	2,48	3,24	2,28	3,81	3,81	1,11
	Res	0,97	0,89	1,14	0,73	1,22	1,22	0,93
Elastic modulus E [Pa]	Peak	1,57E+10	1,44E+10	1,83E+10	1,18E+10	1,96E+10	1,96E+10	1,50E+10
	v	0,25	0,25	0,26	0,24	0,26	0,26	0,25
HB parameter a		0,50052	0,50052	0,50052	0,50052	0,50052	0,50052	0,50052
Density		2700	2700	2700	2700	2700	2700	2700
Modulus of cave material Standard E [Pa]	Peak	3,14E+08	2,87E+08	3,66E+08	2,35E+08	3,92E+08	3,92E+08	3,00E+08
	v	0,20	0,20	0,20	0,20	0,20	0,20	0,20
Modulus of cave material Fast moving E [Pa]	Peak	7,84E+07	7,19E+07	9,15E+07	5,88E+07	9,80E+07	9,80E+07	7,51E+07
	v	0,00	0,00	0,00	0,00	0,00	0,00	0,00

**Table B.2:** Rock mass properties for Esmeralda used in M06.

Appendix B: Rock mass properties used in the numerical simulation

Parameters		BRECCIA	CMETFW	CMETHW	DACITA	DIORITE	LAMP	PORF	LAT	SECONDO	FAULTR	FAULTB	FAULTG
UCS [Mpa]		72,0	88,0	68,2	74,8	98,0	72,0	123,2	80,0	112,0	92,0	80,0	52,0
GSI		61,1	69,7	55,0	65,0	70,7	65,4	83,7	67,5	76,1	70,7	67,5	42,0
Eccentricity e		0,6	0,6	0,6	0,6	0,6	0,6	0,6	0,6	0,6	0,6	0,6	0,6
PS Level p	Trans	0,014531	0,012501	0,012248	0,013516	0,010979	0,013009	0,010979	0,012248	0,013009	0,018084	0,018084	0,018084
	Res	0,039235	0,033754	0,033069	0,036494	0,029643	0,035124	0,029643	0,033069	0,035124	0,048826	0,048826	0,048826
HB parameter s	Peak	9,07E-04	2,15E-03	2,40E-03	1,40E-03	4,11E-03	1,73E-03	4,11E-03	2,40E-03	1,73E-03	9,37E-04	1,46E-03	1,46E-03
	Trans	9,07E-04	2,15E-03	2,40E-03	1,40E-03	4,11E-03	1,73E-03	4,11E-03	2,40E-03	1,73E-03	9,37E-04	1,46E-03	1,46E-03
	Res	1,08E-03	1,10E-03	1,40E-03	9,00E-04	1,50E-03	1,50E-03	1,09E-03	1,08E-03	1,10E-03	1,40E-03	9,00E-04	1,50E-03
LR2 dilatancy d	Peak	0,1400	0,2200	0,2300	0,1800	0,2800	0,2000	0,2800	0,2300	0,2000	0,1430	0,1840	0,1840
	Trans	0,1400	0,0125	0,0122	0,0135	0,0110	0,0130	0,0110	0,0122	0,0130	0,0181	0,0181	0,0181
	Res	0,0504	0,0792	0,0828	0,0648	0,1008	0,0720	0,1008	0,0828	0,0720	0,0515	0,0662	0,0662
HB parameter mb	Peak	1,07	1,68	1,77	1,34	2,33	1,50	2,33	1,77	1,50	0,82	0,96	0,96
	Trans	1,07	1,68	1,77	1,34	2,33	1,50	2,33	1,77	1,50	0,82	0,96	0,96
	Res	0,65	1,02	1,07	0,84	1,30	0,93	1,30	1,07	0,93	0,66	0,85	0,85
Elastic modulus E [Pa]	Peak	1,05E+10	1,64E+10	1,72E+10	1,34E+10	2,09E+10	1,49E+10	2,09E+10	1,72E+10	1,49E+10	1,07E+10	1,37E+10	1,37E+10
	v	0,23	0,25	0,26	0,24	0,27	0,25	0,27	0,26	0,25	0,23	0,24	0,24
HB parameter a		0,50058	0,50058	0,50058	0,50058	0,50058	0,50058	0,50058	0,50058	0,50058	0,50058	0,50058	0,50058
Density		2700	2700	2700	2700	2700	2700	2700	2700	2700	2700	2700	2700
Modulus of cave material Standard	E [Pa]	2,09E+08	3,28E+08	3,43E+08	2,69E+08	4,18E+08	2,99E+08	4,18E+08	3,43E+08	2,99E+08	2,14E+08	2,75E+08	2,75E+08
	v	0,20	0,20	0,20	0,20	0,20	0,20	0,20	0,20	0,20	0,20	0,20	0,20
Modulus of cave material Fast moving	E [Pa]	5,23E+07	8,21E+07	8,59E+07	6,72E+07	1,05E+08	7,47E+07	1,05E+08	5,23E+07	8,21E+07	8,59E+07	6,72E+07	1,05E+08
	v	0,00	0,00	0,00	0,00	0,00	0,00	0,00	0,00	0,00	0,00	0,00	0,00

**Table B.3:** Rock mass properties for Esmeralda used in M07.

Appendix B: Rock mass properties used in the numerical simulation

Parameters		BRECCIA	CMETFW	CMETHW	DACITA	DIORITE	LAMP	PORF	LAT	SECONDO	FAULTR	FAULTB	FAULTG
UCS [Mpa]		72,0	88,0	68,2	74,8	98,0	72,0	123,2	80,0	112,0	92,0	80,0	52,0
GSI		61,1	69,7	55,0	65,0	70,7	65,4	83,7	67,5	76,1	70,7	67,5	42,0
Eccentricity e		0,6	0,6	0,6	0,6	0,6	0,6	0,6	0,6	0,6	0,6	0,6	0,6
PS Level p	Trans	0,014531	0,012501	0,012248	0,013516	0,010979	0,013009	0,010979	0,012248	0,013009	0,018084	0,018084	0,018084
	Res	0,039235	0,033754	0,033069	0,036494	0,029643	0,035124	0,029643	0,033069	0,035124	0,048826	0,048826	0,048826
HB parameter s	Peak	1,40E-03	2,15E-03	2,40E-03	1,40E-03	4,11E-03	1,73E-03	4,11E-03	2,40E-03	1,73E-03	9,37E-04	1,46E-03	1,46E-03
	Trans	1,40E-03	2,15E-03	2,40E-03	1,40E-03	4,11E-03	1,73E-03	4,11E-03	2,40E-03	1,73E-03	9,37E-04	1,46E-03	1,46E-03
	Res	1,08E-03	1,10E-03	1,40E-03	9,00E-04	1,50E-03	1,50E-03	1,09E-03	1,08E-03	1,10E-03	1,40E-03	9,00E-04	1,50E-03
LR2 dilatancy d	Peak	0,1800	0,2200	0,2300	0,1800	0,2800	0,2000	0,2800	0,2300	0,2000	0,1430	0,1840	0,1840
	Trans	0,1800	0,0125	0,0122	0,0135	0,0110	0,0130	0,0110	0,0122	0,0130	0,0181	0,0181	0,0181
	Res	0,0648	0,0792	0,0828	0,0648	0,1008	0,0720	0,1008	0,0828	0,0720	0,0515	0,0662	0,0662
HB parameter mb	Peak	1,26	1,68	1,77	1,34	2,33	1,50	2,33	1,77	1,50	0,82	0,96	0,96
	Trans	1,26	1,68	1,77	1,34	2,33	1,50	2,33	1,77	1,50	0,82	0,96	0,96
	Res	0,84	1,02	1,07	0,84	1,30	0,93	1,30	1,07	0,93	0,66	0,85	0,85
Elastic modulus E [Pa]	Peak	1,34E+10	1,64E+10	1,72E+10	1,34E+10	2,09E+10	1,49E+10	2,09E+10	1,72E+10	1,49E+10	1,07E+10	1,37E+10	1,37E+10
	v	0,24	0,25	0,26	0,24	0,27	0,25	0,27	0,26	0,25	0,23	0,24	0,24
HB parameter a		0,50058	0,50058	0,50058	0,50058	0,50058	0,50058	0,50058	0,50058	0,50058	0,50058	0,50058	0,50058
Density		2700	2700	2700	2700	2700	2700	2700	2700	2700	2700	2700	2700
Modulus of cave material Standard	E [Pa]	2,69E+08	3,28E+08	3,43E+08	2,69E+08	4,18E+08	2,99E+08	4,18E+08	3,43E+08	2,99E+08	2,14E+08	2,75E+08	2,75E+08
	v	0,20	0,20	0,20	0,20	0,20	0,20	0,20	0,20	0,20	0,20	0,20	0,20
Modulus of cave material Fast moving	E [Pa]	6,72E+07	8,21E+07	8,59E+07	6,72E+07	1,05E+08	7,47E+07	1,05E+08	8,59E+07	7,47E+07	5,34E+07	6,87E+07	6,87E+07
	v	0,00	0,00	0,00	0,00	0,00	0,00	0,00	0,00	0,00	0,00	0,00	0,00

**Table B.4:** Rock mass properties for Esmeralda used in M08.

Appendix B: Rock mass properties used in the numerical simulation

Parameters		BRECCIA	CMETFW	CMETHW	DACITA	DIORITE	LAMP	PORF	LAT	SECONDO	FAULTR	FAULTB	FAULTG
UCS [Mpa]		72,0	88,0	68,2	74,8	98,0	72,0	123,2	80,0	112,0	92,0	80,0	52,0
GSI		61,1	69,7	55,0	65,0	70,7	65,4	83,7	67,5	76,1	70,7	67,5	42,0
Eccentricity e		0,6	0,6	0,6	0,6	0,6	0,6	0,6	0,6	0,6	0,6	0,6	0,6
PS Level p	Trans	0,014531	0,012501	0,012248	0,013516	0,010979	0,013009	0,010979	0,012248	0,013009	0,018084	0,017175	0,018084
	Res	0,039235	0,033754	0,033069	0,036494	0,029643	0,035124	0,029643	0,033069	0,035124	0,048826	0,046372	0,048826
HB parameter s	Peak	1,40E-03	2,15E-03	2,40E-03	1,40E-03	4,11E-03	1,73E-03	4,11E-03	2,40E-03	1,73E-03	9,37E-04	1,73E-03	1,46E-03
	Trans	1,40E-03	2,15E-03	2,40E-03	1,40E-03	4,11E-03	1,73E-03	4,11E-03	2,40E-03	1,73E-03	9,37E-04	1,73E-03	1,46E-03
	Res	1,08E-03	1,10E-03	1,40E-03	9,00E-04	1,50E-03	1,50E-03	1,09E-03	1,08E-03	1,10E-03	1,40E-03	9,00E-04	1,50E-03
LR2 dilatancy d	Peak	0,1800	0,2200	0,2300	0,1800	0,2800	0,2000	0,2800	0,2300	0,2000	0,1430	0,2000	0,1840
	Trans	0,1800	0,0125	0,0122	0,0135	0,0110	0,0130	0,0110	0,0122	0,0130	0,0181	0,0172	0,0181
	Res	0,0648	0,0792	0,0828	0,0648	0,1008	0,0720	0,1008	0,0828	0,0720	0,0515	0,0720	0,0662
HB parameter mb	Peak	1,26	1,68	1,77	1,34	2,33	1,50	2,33	1,77	1,50	0,82	1,11	0,96
	Trans	1,26	1,68	1,77	1,34	2,33	1,50	2,33	1,77	1,50	0,82	1,11	0,96
	Res	0,84	1,02	1,07	0,84	1,30	0,93	1,30	1,07	0,93	0,66	0,93	0,85
Elastic modulus E [Pa]	Peak	1,34E+10	1,64E+10	1,72E+10	1,34E+10	2,09E+10	1,49E+10	2,09E+10	1,72E+10	1,49E+10	1,07E+10	1,49E+10	1,37E+10
	v	0,24	0,25	0,26	0,24	0,27	0,25	0,27	0,26	0,25	0,23	0,25	0,24
HB parameter a		0,50058	0,50058	0,50058	0,50058	0,50058	0,50058	0,50058	0,50058	0,50058	0,50058	0,50058	0,50058
Density		2700	2700	2700	2700	2700	2700	2700	2700	2700	2700	2700	2700
Modulus of cave material Standard	E [Pa]	2,69E+08	3,28E+08	3,43E+08	2,69E+08	4,18E+08	2,99E+08	4,18E+08	3,43E+08	2,99E+08	2,14E+08	2,99E+08	2,75E+08
	v	0,20	0,20	0,20	0,20	0,20	0,20	0,20	0,20	0,20	0,20	0,20	0,20
Modulus of cave material Collapse	E [Pa]	2,69E+08	3,28E+08	3,43E+08	2,69E+08	4,18E+08	2,99E+08	4,18E+08	3,43E+08	2,99E+08	2,14E+08	2,99E+08	2,75E+08
	v	0,20	0,20	0,20	0,20	0,20	0,20	0,20	0,20	0,20	0,20	0,20	0,20
Modulus of cave material Fast moving	E [Pa]	6,72E+07	8,21E+07	8,59E+07	6,72E+07	1,05E+08	7,47E+07	1,05E+08	8,59E+07	7,47E+07	5,34E+07	7,47E+07	6,87E+07
	v	0,20	0,20	0,20	0,20	0,20	0,20	0,20	0,20	0,20	0,20	0,20	0,20

**Table B.5:** Rock mass properties for Esmeralda used in M09.

Appendix B: Rock mass properties used in the numerical simulation

Parameters		BRECCIA	CMETFW	CMETHW	DACITA	DIORITE	LAMP	PORF	LAT	SECONDO	FAULTR	FAULTB	FAULTG
UCS [Mpa]		72,0	88,0	68,2	74,8	98,0	72,0	123,2	80,0	112,0	92,0	80,0	52,0
GSI		61,1	69,7	55,0	65,0	70,7	65,4	83,7	67,5	76,1	70,7	67,5	42,0
Eccentricity e		0,6	0,6	0,6	0,6	0,6	0,6	0,6	0,6	0,6	0,6	0,6	0,6
PS Level p	Trans	0,014531	0,012501	0,012248	0,013516	0,010979	0,013009	0,010979	0,012248	0,013009	0,018084	0,017175	0,018084
	Res	0,039235	0,033754	0,033069	0,036494	0,029643	0,035124	0,029643	0,033069	0,035124	0,048826	0,046372	0,048826
HB parameter s	Peak	1,40E-03	2,15E-03	2,40E-03	1,40E-03	4,11E-03	1,73E-03	4,11E-03	2,40E-03	1,73E-03	9,37E-04	1,73E-03	1,46E-03
	Trans	1,40E-03	2,15E-03	2,40E-03	1,40E-03	4,11E-03	1,73E-03	4,11E-03	2,40E-03	1,73E-03	9,37E-04	1,73E-03	1,46E-03
	Res	1,08E-03	1,10E-03	1,40E-03	9,00E-04	1,50E-03	1,50E-03	1,09E-03	1,08E-03	1,10E-03	1,40E-03	9,00E-04	1,50E-03
LR2 dilatancy d	Peak	0,1800	0,2200	0,2300	0,1800	0,2800	0,2000	0,2800	0,2300	0,2000	0,1430	0,2000	0,1840
	Trans	0,1800	0,0125	0,0122	0,0135	0,0110	0,0130	0,0110	0,0122	0,0130	0,0181	0,0172	0,0181
	Res	0,0648	0,0792	0,0828	0,0648	0,1008	0,0720	0,1008	0,0828	0,0720	0,0515	0,0720	0,0662
HB parameter mb	Peak	1,26	1,68	1,77	1,34	2,33	1,50	2,33	1,77	1,50	0,82	1,11	0,96
	Trans	1,26	1,68	1,77	1,34	2,33	1,50	2,33	1,77	1,50	0,82	1,11	0,96
	Res	0,84	1,02	1,07	0,84	1,30	0,93	1,30	1,07	0,93	0,66	0,93	0,85
Elastic modulus E [Pa]	Peak	1,34E+10	1,64E+10	1,72E+10	1,34E+10	2,09E+10	1,49E+10	2,09E+10	1,72E+10	1,49E+10	1,07E+10	1,49E+10	1,37E+10
	v	0,24	0,25	0,26	0,24	0,27	0,25	0,27	0,26	0,25	0,23	0,25	0,24
HB parameter a		0,50058	0,50058	0,50058	0,50058	0,50058	0,50058	0,50058	0,50058	0,50058	0,50058	0,50058	0,50058
Density		2700	2700	2700	2700	2700	2700	2700	2700	2700	2700	2700	2700
Modulus of cave material Standard E [Pa]	v	2,69E+08	3,28E+08	3,43E+08	2,69E+08	4,18E+08	2,99E+08	4,18E+08	3,43E+08	2,99E+08	2,14E+08	2,99E+08	2,75E+08
		0,20	0,20	0,20	0,20	0,20	0,20	0,20	0,20	0,20	0,20	0,20	0,20
Modulus of cave material Collapse E [Pa]	v	2,69E+08	3,28E+08	3,43E+08	2,69E+08	4,18E+08	2,99E+08	4,18E+08	3,43E+08	2,99E+08	2,14E+08	2,99E+08	2,75E+08
		0,20	0,20	0,20	0,20	0,20	0,20	0,20	0,20	0,20	0,20	0,20	0,20
Modulus of cave material Fast moving E [Pa]	v	6,72E+07	8,21E+07	8,59E+07	6,72E+07	1,05E+08	7,47E+07	1,05E+08	8,59E+07	7,47E+07	5,34E+07	7,47E+07	6,87E+07
		0,20	0,20	0,20	0,20	0,20	0,20	0,20	0,20	0,20	0,20	0,20	0,20

**Table B.6:** Rock mass properties for Esmeralda used in M10.

Appendix B: Rock mass properties used in the numerical simulation

Parameters		BRECCIA	CMETFW	CMETHW	DACITA	DIORITE	LAMP	PORF	LAT	SECONDO	FAULTR	FAULTB	FAULTG
UCS [Mpa]		72,0	88,0	68,2	74,8	98,0	72,0	123,2	80,0	112,0	92,0	80,0	52,0
GSI		61,1	69,7	55,0	65,0	70,7	65,4	83,7	67,5	76,1	70,7	67,5	42,0
Eccentricity e		0,6	0,6	0,6	0,6	0,6	0,6	0,6	0,6	0,6	0,6	0,6	0,6
PS Level p	Trans	0,014531	0,012501	0,012248	0,013516	0,009171	0,013009	0,010979	0,012248	0,013009	0,018084	0,017175	0,018084
	Res	0,039235	0,033754	0,033069	0,036494	0,024761	0,035124	0,029643	0,033069	0,035124	0,048826	0,046372	0,048826
HB parameter s	Peak	1,40E-03	2,15E-03	2,40E-03	1,40E-03	5,57E-03	1,73E-03	4,11E-03	2,40E-03	1,73E-03	9,37E-04	1,73E-03	1,46E-03
	Trans	1,40E-03	2,15E-03	2,40E-03	1,40E-03	5,57E-03	1,73E-03	4,11E-03	2,40E-03	1,73E-03	9,37E-04	1,73E-03	1,46E-03
	Res	1,08E-03	1,10E-03	1,40E-03	9,00E-04	1,50E-03	1,50E-03	1,09E-03	1,08E-03	1,10E-03	1,40E-03	9,00E-04	1,50E-03
LR2 dilatancy d	Peak	0,1800	0,2200	0,2300	0,1800	0,3080	0,2000	0,2800	0,2300	0,2000	0,1430	0,2000	0,1840
	Trans	0,1800	0,0125	0,0122	0,0135	0,0092	0,0130	0,0110	0,0122	0,0130	0,0181	0,0172	0,0181
	Res	0,0648	0,0792	0,0828	0,0648	0,1109	0,0720	0,1008	0,0828	0,0720	0,0515	0,0720	0,0662
HB parameter mb	Peak	1,26	1,68	1,77	1,34	2,87	1,50	2,33	1,77	1,50	0,82	1,11	0,96
	Trans	1,26	1,68	1,77	1,34	2,87	1,50	2,33	1,77	1,50	0,82	1,11	0,96
	Res	0,84	1,02	1,07	0,84	1,43	0,93	1,30	1,07	0,93	0,66	0,93	0,85
Elastic modulus E [Pa]	Peak	1,34E+10	1,64E+10	1,72E+10	1,34E+10	2,30E+10	1,49E+10	2,09E+10	1,72E+10	1,49E+10	1,07E+10	1,49E+10	1,37E+10
	v	0,24	0,25	0,26	0,24	0,27	0,25	0,27	0,26	0,25	0,23	0,25	0,24
HB parameter a		0,50058	0,50058	0,50058	0,50058	0,50058	0,50058	0,50058	0,50058	0,50058	0,50058	0,50058	0,50058
Density		2700	2700	2700	2700	2700	2700	2700	2700	2700	2700	2700	2700
Modulus of cave material Standard v	E [Pa]	5,38E+08	6,57E+08	6,87E+08	5,38E+08	9,20E+08	5,97E+08	8,36E+08	6,87E+08	5,97E+08	4,27E+08	5,97E+08	5,49E+08
	v	0,20	0,20	0,20	0,20	0,20	0,20	0,20	0,20	0,20	0,20	0,20	0,20
Modulus of cave material Collapse v	E [Pa]	2,69E+08	3,28E+08	3,43E+08	2,69E+08	4,60E+08	2,99E+08	4,18E+08	3,43E+08	2,99E+08	2,14E+08	2,99E+08	2,75E+08
	v	0,20	0,20	0,20	0,20	0,20	0,20	0,20	0,20	0,20	0,20	0,20	0,20
Modulus of cave material Fast moving v	E [Pa]	1,34E+08	1,64E+08	1,72E+08	1,34E+08	2,30E+08	1,49E+08	2,09E+08	1,72E+08	1,49E+08	1,07E+08	1,49E+08	1,37E+08
	v	0,20	0,20	0,20	0,20	0,20	0,20	0,20	0,20	0,20	0,20	0,20	0,20

**Table B.7:** Rock mass properties for Esmeralda used in M11.

Appendix B: Rock mass properties used in the numerical simulation

Parameters		BRECCIA	CMETFW	CMETFW_HIF	CMETFW_MIF	CMETHW	DACITA	DIORITE	LAMP	PORF	LAT	SECONDO	FAULTR	FAULTB	FAULTG
UCS [Mpa]		72,0	88,0	68,2	74,8	98,0	72,0	123,2	80,0	112,0	92,0	80,0	52,0	80,0	73,6
GSI		61,1	69,7	55,0	65,0	70,7	65,4	83,7	67,5	76,1	70,7	67,5	42,0	50,0	46,2
Eccentricity e		0,6	0,6	0,6	0,6	0,6	0,6	0,6	0,6	0,6	0,6	0,6	0,6	0,6	0,6
PS Level p	Trans	0,014531	0,012501	0,014985	0,014157	0,012248	0,013516	0,009171	0,013009	0,010979	0,012248	0,013009	0,019077	0,017175	0,018084
	Res	0,039235	0,033754	0,040461	0,038225	0,033069	0,036494	0,024761	0,035124	0,029643	0,033069	0,035124	0,051507	0,046372	0,048826
HB parameter s	Peak	1,40E-03	2,15E-03	1,26E-03	1,51E-03	2,82E-03	1,40E-03	5,57E-03	1,73E-03	4,11E-03	2,40E-03	1,73E-03	8,14E-04	1,73E-03	1,46E-03
	Trans	1,40E-03	2,82E-03	1,26E-03	1,51E-03	2,82E-03	1,40E-03	5,57E-03	1,73E-03	4,11E-03	2,40E-03	1,73E-03	8,14E-04	1,73E-03	1,46E-03
	Res	1,08E-03	1,96E-03	1,26E-03	1,50E-03	1,40E-03	9,00E-04	1,50E-03	1,50E-03	1,09E-03	1,08E-03	1,10E-03	1,40E-03	9,00E-04	1,50E-03
LR2 dilatancy d	Peak	0,1800	0,2200	0,1705	0,1870	0,2450	0,1800	0,3080	0,2000	0,2800	0,2300	0,2000	0,1300	0,2000	0,1840
	Trans	0,1800	0,0125	0,0150	0,0142	0,0122	0,0135	0,0092	0,0130	0,0110	0,0122	0,0130	0,0191	0,0172	0,0181
	Res	0,0648	0,0792	0,0614	0,0673	0,0882	0,0648	0,1109	0,0720	0,1008	0,0828	0,0720	0,0468	0,0720	0,0662
HB parameter mb	Peak	1,26	1,68	1,17	1,32	1,88	1,34	2,87	1,50	2,33	1,77	1,50	0,71	1,11	0,96
	Trans	1,26	1,68	1,17	1,32	1,88	1,34	2,87	1,50	2,33	1,77	1,50	0,71	1,11	0,96
	Res	0,84	1,02	0,79	0,87	1,14	0,84	1,43	0,93	1,30	1,07	0,93	0,60	0,93	0,85
Elastic modulus E [Pa]	Peak	1,34E+10	1,64E+10	1,64E+10	1,64E+10	1,83E+10	1,34E+10	2,30E+10	1,49E+10	2,09E+10	1,72E+10	1,49E+10	9,71E+09	1,49E+10	1,37E+10
	v	0,24	0,25	0,24	0,24	0,26	0,24	0,27	0,25	0,27	0,26	0,25	0,23	0,25	0,24
HB parameter a		0,50058	0,50058	0,50058	0,50058	0,50058	0,50058	0,50058	0,50058	0,50058	0,50058	0,50058	0,50058	0,50058	0,50058
Density		2700	2700	2700	2700	2700	2700	2700	2700	2700	2700	2700	2700	2700	2700
Modulus of cave material Standard	E [Pa]	4,03E+08	4,93E+08	4,93E+08	4,93E+08	5,49E+08	4,03E+08	6,90E+08	4,48E+08	6,27E+08	5,15E+08	4,48E+08	2,91E+08	4,48E+08	4,12E+08
	v	0,20	0,20	0,20	0,20	0,20	0,20	0,20	0,20	0,20	0,20	0,20	0,20	0,20	0,20
Modulus of cave material Collapse	E [Pa]	2,69E+08	3,28E+08	3,28E+08	3,28E+08	3,66E+08	2,69E+08	4,60E+08	2,99E+08	4,18E+08	3,43E+08	2,99E+08	1,94E+08	2,99E+08	2,75E+08
	v	0,20	0,20	0,20	0,20	0,20	0,20	0,20	0,20	0,20	0,20	0,20	0,20	0,20	0,20
Modulus of cave material Fast moving	E [Pa]	1,01E+08	1,23E+08	1,23E+08	1,23E+08	1,37E+08	1,01E+08	1,72E+08	1,12E+08	1,57E+08	1,29E+08	1,12E+08	7,28E+07	1,12E+08	1,03E+08
	v	0,20	0,20	0,20	0,20	0,20	0,20	0,20	0,20	0,20	0,20	0,20	0,20	0,20	0,20

Table B.8: Rock mass properties for Esmeralda used in M14.

Appendix B: Rock mass properties used in the numerical simulation

Parameters		BRECCIA	CMETFW	CMETFW_HIF	CMETFW_MIF	CMETHW	DACITA	DIORITE	LAMP	PORF	LAT	SECONDO	FAULTR	FAULTB	FAULTG
UCS [Mpa]		72,0	88,0	68,2	74,8	98,0	72,0	123,2	80,0	112,0	92,0	80,0	52,0	80,0	73,6
GSI		61,1	69,7	55,0	65,0	70,7	65,4	83,7	67,5	76,1	70,7	67,5	42,0	50,0	46,2
Eccentricity e		0,6	0,6	0,6	0,6	0,6	0,6	0,6	0,6	0,6	0,6	0,6	0,6	0,6	0,6
PS Level p	Trans	0,014531	0,012501	0,011876	0,011876	0,012248	0,013516	0,009171	0,013009	0,010979	0,012248	0,013009	0,019077	0,017175	0,018084
	Res	0,039235	0,033754	0,032066	0,032066	0,033069	0,036494	0,024761	0,035124	0,029643	0,033069	0,035124	0,051507	0,046372	0,048826
HB parameter s	Peak	1,40E-03	2,15E-03	1,26E-03	1,51E-03	2,82E-03	1,40E-03	5,57E-03	1,73E-03	4,11E-03	2,40E-03	1,73E-03	8,14E-04	1,73E-03	1,46E-03
	Trans	1,40E-03	2,82E-03	1,26E-03	1,51E-03	2,82E-03	1,40E-03	5,57E-03	1,73E-03	4,11E-03	2,40E-03	1,73E-03	8,14E-04	1,73E-03	1,46E-03
	Res	1,08E-03	1,96E-03	1,26E-03	1,50E-03	1,40E-03	9,00E-04	1,50E-03	1,50E-03	1,09E-03	1,08E-03	1,10E-03	1,40E-03	9,00E-04	1,50E-03
LR2 dilatancy d	Peak	0,1800	0,2200	0,1705	0,1870	0,2450	0,1800	0,3080	0,2000	0,2800	0,2300	0,2000	0,1300	0,2000	0,1840
	Trans	0,1800	0,0125	0,0119	0,0119	0,0122	0,0135	0,0092	0,0130	0,0110	0,0122	0,0130	0,0191	0,0172	0,0181
	Res	0,0648	0,0792	0,0614	0,0673	0,0882	0,0648	0,1109	0,0720	0,1008	0,0828	0,0720	0,0468	0,0720	0,0662
HB parameter mb	Peak	1,26	1,68	1,09	1,37	1,88	1,34	2,87	1,50	2,33	1,77	1,50	0,71	1,11	0,96
	Trans	1,26	1,68	1,09	1,37	1,88	1,34	2,87	1,50	2,33	1,77	1,50	0,71	1,11	0,96
	Res	0,84	1,02	0,79	0,87	1,14	0,84	1,43	0,93	1,30	1,07	0,93	0,60	0,93	0,85
Elastic modulus E [Pa]	Peak	1,34E+10	1,64E+10	1,64E+10	1,64E+10	1,83E+10	1,34E+10	2,30E+10	1,49E+10	2,09E+10	1,72E+10	1,49E+10	9,71E+09	1,49E+10	1,37E+10
	v	0,24	0,25	0,24	0,24	0,26	0,24	0,27	0,25	0,27	0,26	0,25	0,23	0,25	0,24
HB parameter a		0,50058	0,50058	0,50058	0,50058	0,50058	0,50058	0,50058	0,50058	0,50058	0,50058	0,50058	0,50058	0,50058	0,50058
Density		2700	2700	2700	2700	2700	2700	2700	2700	2700	2700	2700	2700	2700	2700
Modulus of cave material Standard v	E [Pa]	4,03E+08	4,93E+08	3,28E+08	3,28E+08	5,49E+08	4,03E+08	6,90E+08	4,48E+08	6,27E+08	5,15E+08	4,48E+08	2,91E+08	4,48E+08	4,12E+08
	v	0,20	0,20	0,20	0,20	0,20	0,20	0,20	0,20	0,20	0,20	0,20	0,20	0,20	0,20
Modulus of cave material Collapse v	E [Pa]	1,68E+08	2,05E+08	2,05E+08	2,05E+08	2,29E+08	1,68E+08	2,87E+08	1,87E+08	2,61E+08	2,15E+08	1,87E+08	1,21E+08	1,87E+08	1,72E+08
	v	0,20	0,20	0,20	0,20	0,20	0,20	0,20	0,20	0,20	0,20	0,20	0,20	0,20	0,20
Modulus of cave material Fast moving v	E [Pa]	1,01E+08	1,23E+08	8,21E+07	8,21E+07	1,37E+08	1,01E+08	1,72E+08	1,12E+08	1,57E+08	1,29E+08	1,12E+08	7,28E+07	1,12E+08	1,03E+08
	v	0,20	0,20	0,20	0,20	0,20	0,20	0,20	0,20	0,20	0,20	0,20	0,20	0,20	0,20

Table B.9: Rock mass properties for Esmeralda used in M15.

Appendix B: Rock mass properties used in the numerical simulation

Parameters		BRECCIA	CMETFW	CMETFW_HIF	CMETFW_MIF	CMETHW	DACITA	DIORITE	LAMP	PORF	LAT	SECONDO	FAULTR	FAULTB	FAULTG
UCS [Mpa]		72,0	88,0	68,2	74,8	98,0	72,0	123,2	80,0	112,0	92,0	80,0	52,0	80,0	73,6
GSI		61,1	69,7	55,0	65,0	70,7	65,4	83,7	67,5	76,1	70,7	67,5	42,0	50,0	46,2
Eccentricity e		0,6	0,6	0,6	0,6	0,6	0,6	0,6	0,6	0,6	0,6	0,6	0,6	0,6	0,6
PS Level p	Trans	0,014531	0,012501	0,011876	0,011876	0,012248	0,013516	0,009171	0,013009	0,010979	0,012248	0,013009	0,019077	0,017175	0,018084
	Res	0,039235	0,033754	0,032066	0,032066	0,033069	0,036494	0,024761	0,035124	0,029643	0,033069	0,035124	0,051507	0,046372	0,048826
HB parameter s	Peak	1,40E-03	2,15E-03	1,26E-03	1,51E-03	2,82E-03	1,40E-03	5,57E-03	1,73E-03	4,11E-03	2,40E-03	1,73E-03	8,14E-04	1,73E-03	1,46E-03
	Trans	1,40E-03	2,82E-03	1,26E-03	1,51E-03	2,82E-03	1,40E-03	5,57E-03	1,73E-03	4,11E-03	2,40E-03	1,73E-03	8,14E-04	1,73E-03	1,46E-03
	Res	1,08E-03	1,96E-03	1,26E-03	1,50E-03	1,40E-03	9,00E-04	1,50E-03	1,50E-03	1,09E-03	1,08E-03	1,10E-03	1,40E-03	9,00E-04	1,50E-03
LR2 dilatancy d	Peak	0,1800	0,2200	0,1705	0,1870	0,2450	0,1800	0,3080	0,2000	0,2800	0,2300	0,2000	0,1300	0,2000	0,1840
	Trans	0,1800	0,0125	0,0119	0,0119	0,0122	0,0135	0,0092	0,0130	0,0110	0,0122	0,0130	0,0191	0,0172	0,0181
	Res	0,0648	0,0792	0,0614	0,0673	0,0882	0,0648	0,1109	0,0720	0,1008	0,0828	0,0720	0,0468	0,0720	0,0662
HB parameter mb	Peak	1,26	1,68	1,09	1,37	1,88	1,34	2,87	1,50	2,33	1,77	1,50	0,71	1,11	0,96
	Trans	1,26	1,68	1,09	1,37	1,88	1,34	2,87	1,50	2,33	1,77	1,50	0,71	1,11	0,96
	Res	0,84	1,02	0,79	0,87	1,14	0,84	1,43	0,93	1,30	1,07	0,93	0,60	0,93	0,85
Elastic modulus E [Pa]	Peak	1,34E+10	1,64E+10	1,64E+10	1,64E+10	1,83E+10	1,34E+10	2,30E+10	1,49E+10	2,09E+10	1,72E+10	1,49E+10	9,71E+09	1,49E+10	1,37E+10
	v	0,24	0,25	0,24	0,24	0,26	0,24	0,27	0,25	0,27	0,26	0,25	0,23	0,25	0,24
HB parameter a		0,50058	0,50058	0,50058	0,50058	0,50058	0,50058	0,50058	0,50058	0,50058	0,50058	0,50058	0,50058	0,50058	0,50058
Density		2700	2700	2700	2700	2700	2700	2700	2700	2700	2700	2700	2700	2700	2700
Modulus of cave material Standard v	E [Pa]	4,03E+08	4,93E+08	3,28E+08	3,28E+08	5,49E+08	4,03E+08	6,90E+08	4,48E+08	6,27E+08	5,15E+08	4,48E+08	2,91E+08	4,48E+08	4,12E+08
	v	0,20	0,20	0,20	0,20	0,20	0,20	0,20	0,20	0,20	0,20	0,20	0,20	0,20	0,20
Modulus of cave material Collapse v	E [Pa]	2,69E+08	3,28E+08	3,28E+08	3,28E+08	3,66E+08	2,69E+08	4,60E+08	2,99E+08	4,18E+08	3,43E+08	2,99E+08	1,94E+08	2,99E+08	2,75E+08
	v	0,20	0,20	0,20	0,20	0,20	0,20	0,20	0,20	0,20	0,20	0,20	0,20	0,20	0,20
Modulus of cave material Fast moving v	E [Pa]	1,01E+08	1,23E+08	8,21E+07	8,21E+07	1,37E+08	1,01E+08	1,72E+08	1,12E+08	1,57E+08	1,29E+08	1,12E+08	7,28E+07	1,12E+08	1,03E+08
	v	0,20	0,20	0,20	0,20	0,20	0,20	0,20	0,20	0,20	0,20	0,20	0,20	0,20	0,20

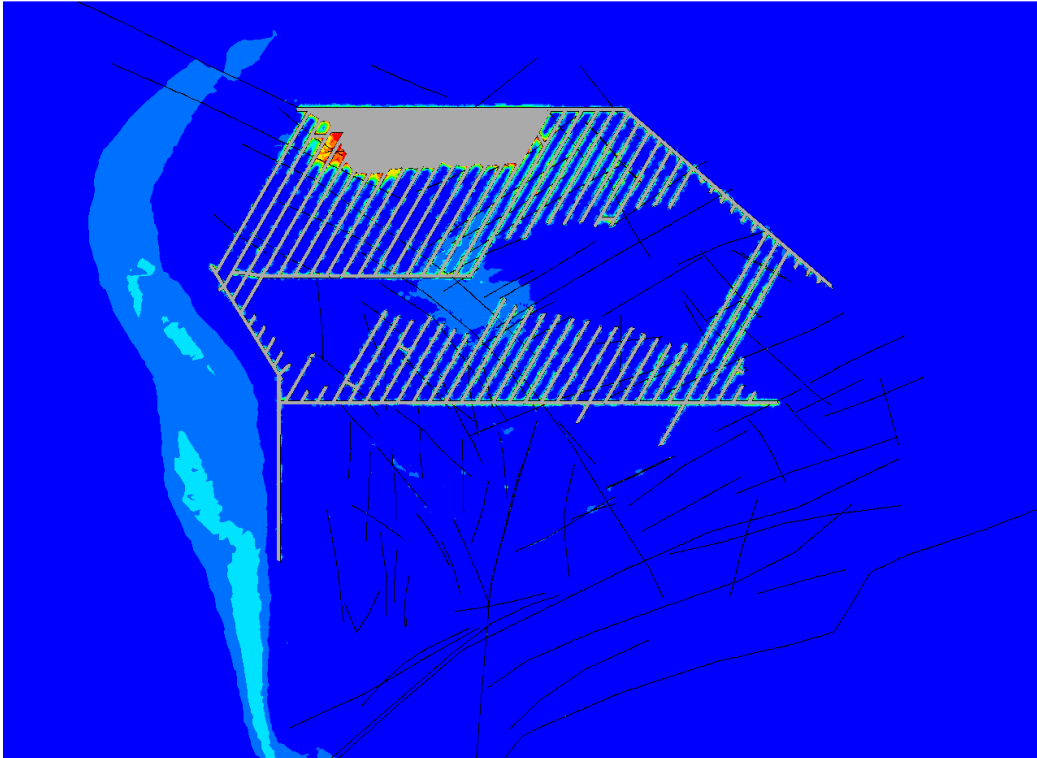
Table B.10: Rock mass properties for Esmeralda used in M16.

Appendix B: Rock mass properties used in the numerical simulation

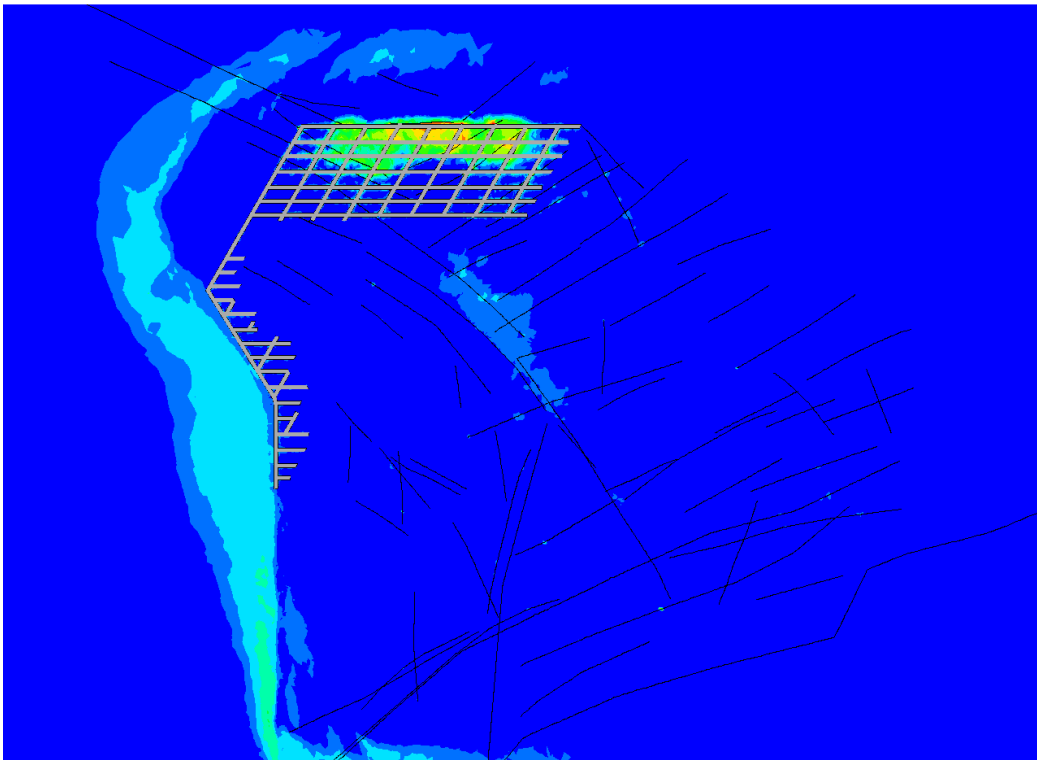
Parameters		BRECCIA	CMETFW	CMETFW_HIF	CMETFW_MIF	CMETHW	DACITA	DIORITE	LAMP	PORF	LAT	SECONDO	FAULTR	FAULTB	FAULTG
UCS [Mpa]		72,0	88,0	68,2	74,8	98,0	72,0	123,2	80,0	112,0	92,0	80,0	52,0	80,0	73,6
GSI		61,1	69,7	55,0	65,0	70,7	65,4	83,7	67,5	76,1	70,7	67,5	42,0	50,0	46,2
Eccentricity e		0,6	0,6	0,6	0,6	0,6	0,6	0,6	0,6	0,6	0,6	0,6	0,6	0,6	0,6
PS Level p	Trans	0,014531	0,012501	0,011876	0,011876	0,012248	0,013516	0,009171	0,013009	0,010979	0,012248	0,013009	0,019077	0,017175	0,018084
	Res	0,039235	0,033754	0,032066	0,032066	0,033069	0,036494	0,024761	0,035124	0,029643	0,033069	0,035124	0,051507	0,046372	0,048826
HB parameter s	Peak	1,40E-03	2,15E-03	1,26E-03	1,51E-03	2,82E-03	1,40E-03	5,57E-03	1,73E-03	4,11E-03	2,40E-03	1,73E-03	8,14E-04	1,73E-03	1,46E-03
	Trans	1,40E-03	2,82E-03	1,26E-03	1,51E-03	2,82E-03	1,40E-03	5,57E-03	1,73E-03	4,11E-03	2,40E-03	1,73E-03	8,14E-04	1,73E-03	1,46E-03
	Res	1,08E-03	1,96E-03	1,26E-03	1,50E-03	1,40E-03	9,00E-04	1,50E-03	1,50E-03	1,09E-03	1,08E-03	1,10E-03	1,40E-03	9,00E-04	1,50E-03
LR2 dilatancy d	Peak	0,1800	0,2200	0,1705	0,1870	0,2450	0,1800	0,3080	0,2000	0,2800	0,2300	0,2000	0,1300	0,2000	0,1840
	Trans	0,1800	0,0125	0,0119	0,0119	0,0122	0,0135	0,0092	0,0130	0,0110	0,0122	0,0130	0,0191	0,0172	0,0181
	Res	0,0648	0,0792	0,0614	0,0673	0,0882	0,0648	0,1109	0,0720	0,1008	0,0828	0,0720	0,0468	0,0720	0,0662
HB parameter mb	Peak	1,26	1,68	1,09	1,37	1,88	1,34	2,87	1,50	2,33	1,77	1,50	0,71	1,11	0,96
	Trans	1,26	1,68	1,09	1,37	1,88	1,34	2,87	1,50	2,33	1,77	1,50	0,71	1,11	0,96
	Res	0,84	1,02	0,79	0,87	1,14	0,84	1,43	0,93	1,30	1,07	0,93	0,60	0,93	0,85
Elastic modulus E [Pa]	Peak	1,34E+10	1,64E+10	1,64E+10	1,64E+10	1,83E+10	1,34E+10	2,30E+10	1,49E+10	2,09E+10	1,72E+10	1,49E+10	9,71E+09	1,49E+10	1,37E+10
	v	0,24	0,25	0,24	0,24	0,26	0,24	0,27	0,25	0,27	0,26	0,25	0,23	0,25	0,24
HB parameter a		0,50058	0,50058	0,50058	0,50058	0,50058	0,50058	0,50058	0,50058	0,50058	0,50058	0,50058	0,50058	0,50058	0,50058
Density		2700	2700	2700	2700	2700	2700	2700	2700	2700	2700	2700	2700	2700	2700
Modulus of cave material Standard	E [Pa]	4,03E+08	4,93E+08	3,28E+08	3,28E+08	5,49E+08	4,03E+08	6,90E+08	4,48E+08	6,27E+08	5,15E+08	4,48E+08	2,91E+08	4,48E+08	4,12E+08
	v	0,20	0,20	0,20	0,20	0,20	0,20	0,20	0,20	0,20	0,20	0,20	0,20	0,20	0,20
Modulus of cave material Collapse	E [Pa]	6,72E+08	8,21E+08	8,21E+08	8,21E+08	9,15E+08	6,72E+08	1,15E+09	7,47E+08	1,05E+09	8,59E+08	7,47E+08	4,85E+08	7,47E+08	6,87E+08
	v	0,20	0,20	0,20	0,20	0,20	0,20	0,20	0,20	0,20	0,20	0,20	0,20	0,20	0,20
Modulus of cave material Fast moving	E [Pa]	1,01E+08	1,23E+08	8,21E+07	8,21E+07	1,37E+08	1,01E+08	1,72E+08	1,12E+08	1,57E+08	1,29E+08	1,12E+08	7,28E+07	1,12E+08	1,03E+08
	v	0,20	0,20	0,20	0,20	0,20	0,20	0,20	0,20	0,20	0,20	0,20	0,20	0,20	0,20

Table B.11: Rock mass properties for Esmeralda used in M17.

**APPENDIX C – REPRESENTATIVE SUMMARY OF IMAGES FROM  
MODEL RESULTS FOR ESMERALDA SIMULATION**



**Figure C.1:** Plan view with Plastic strain distribution in Undercut level of Esmeralda operation, Step April 1997



**Figure C.2:** Plan view with Plastic strain distribution in Production level of Esmeralda operation, Step April 1997

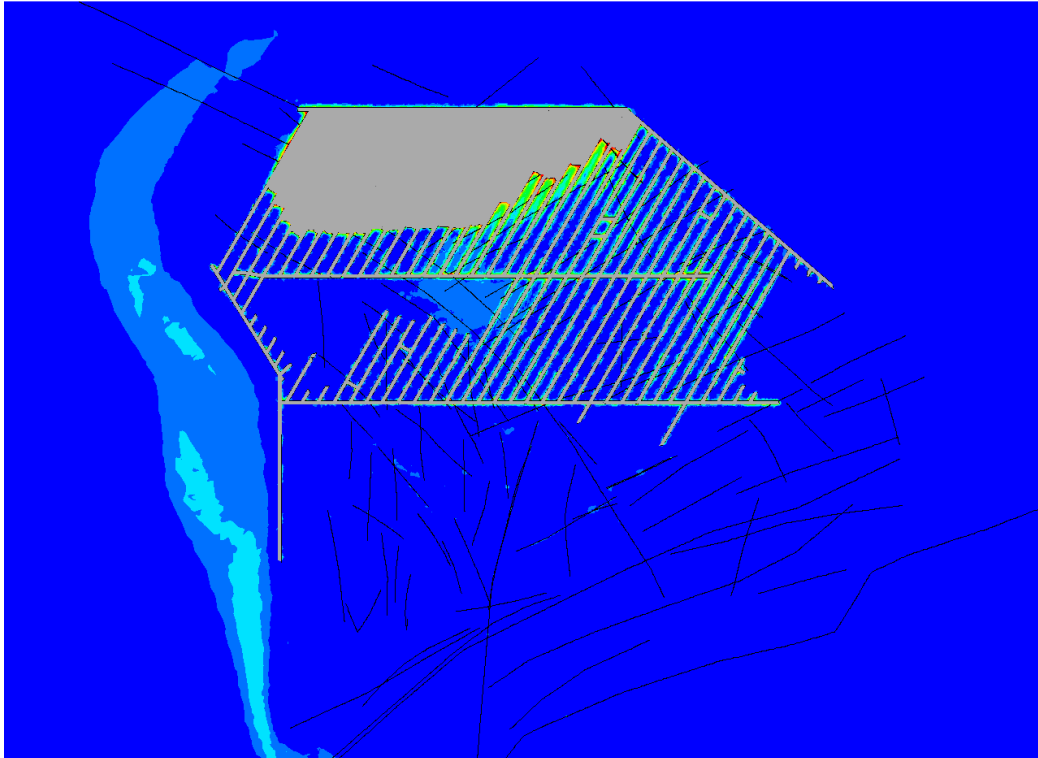


**Figure C.3:** Plan view with Plastic strain distribution in Undercut level of Esmeralda operation, Step March 1999

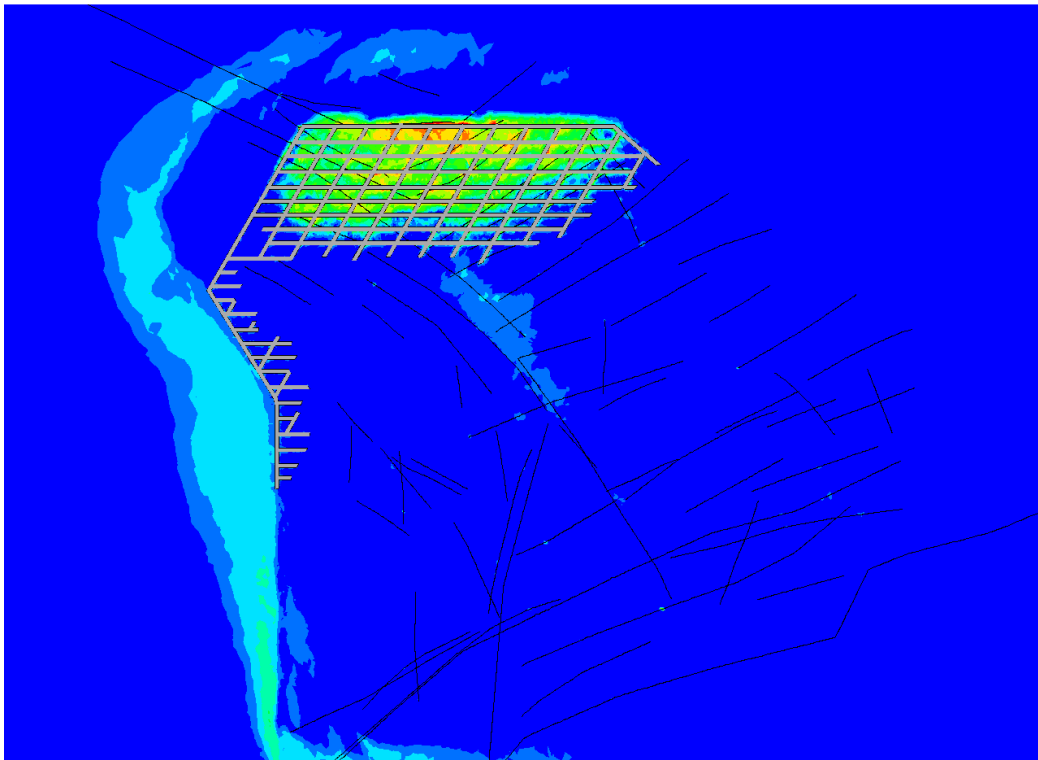


**Figure C.4:** Plan view with Plastic strain distribution in Production level of Esmeralda operation, Step March 1999

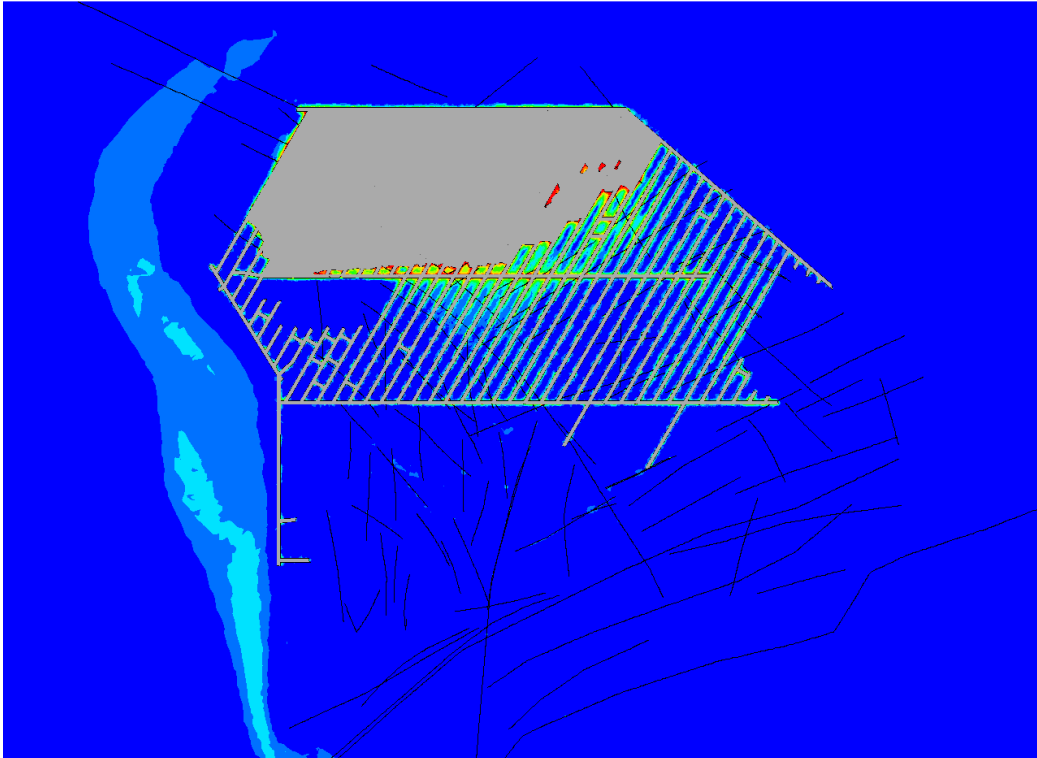


**Figure C.5:** Plan view with Plastic strain distribution in Undercut level of Esmeralda operation, Step March 2000

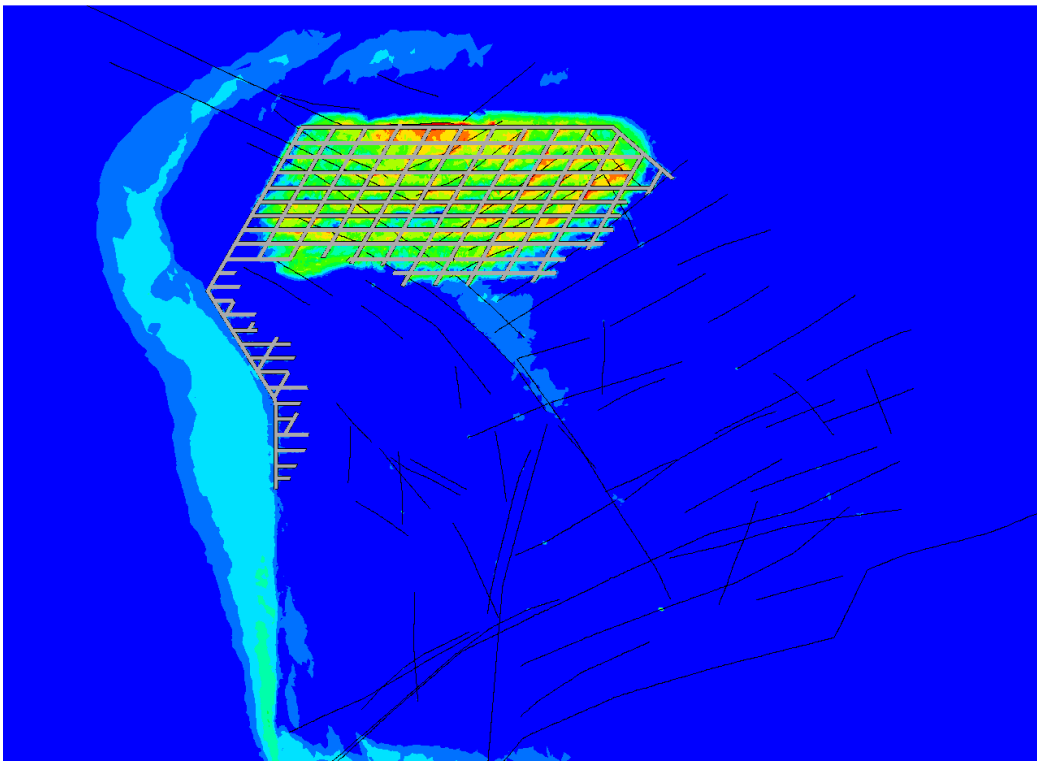


**Figure C.6:** Plan view with Plastic strain distribution in Production level of Esmeralda operation, Step March 2000

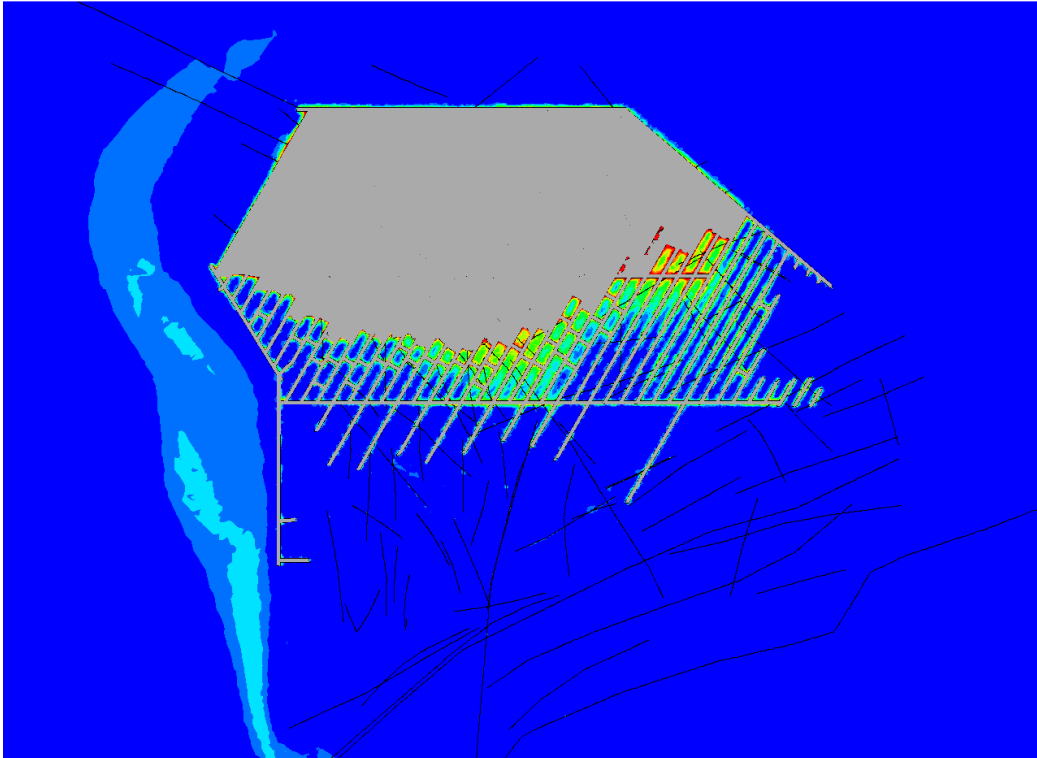


**Figure C.7:** Plan view with Plastic strain distribution in Undercut level of Esmeralda operation, Step April 2001

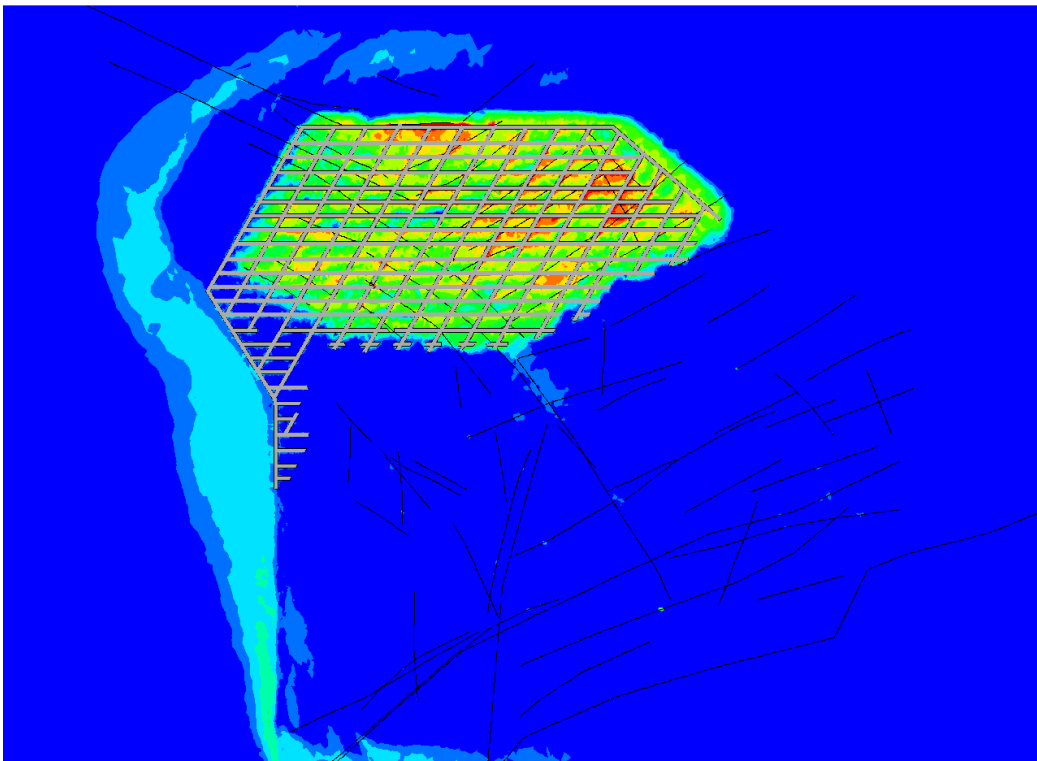


**Figure C.8:** Plan view with Plastic strain distribution in Production level of Esmeralda operation, Step April 2001

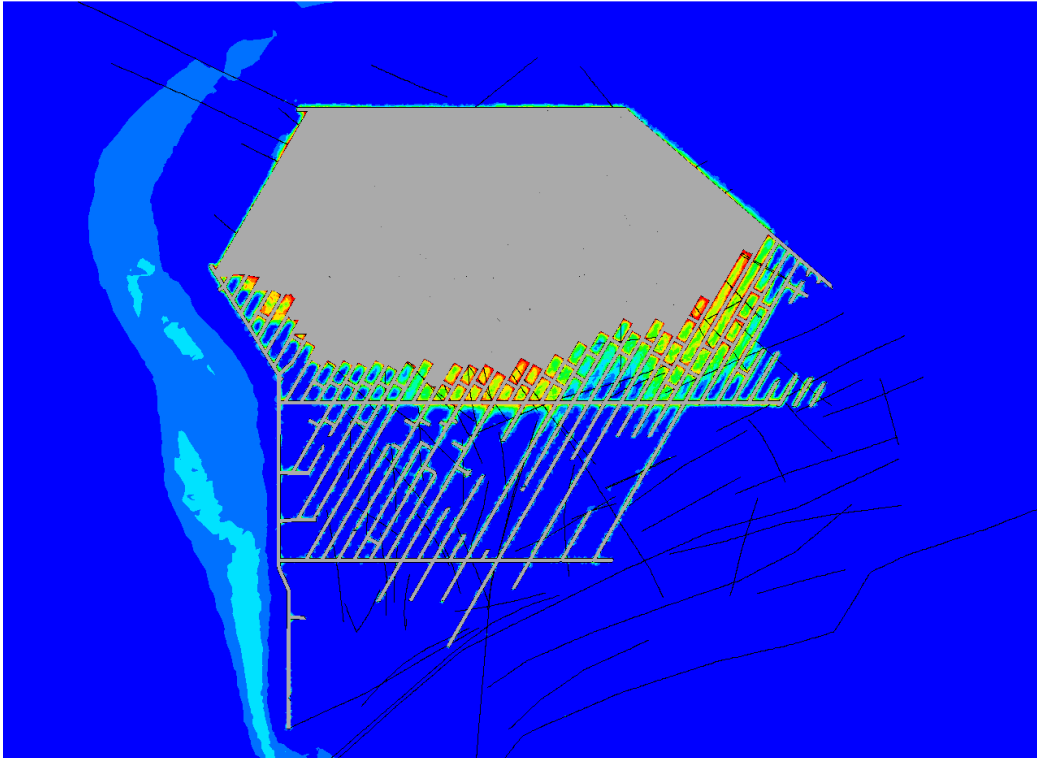


**Figure C.9:** Plan view with Plastic strain distribution in Undercut level of Esmeralda operation, Step July 2002

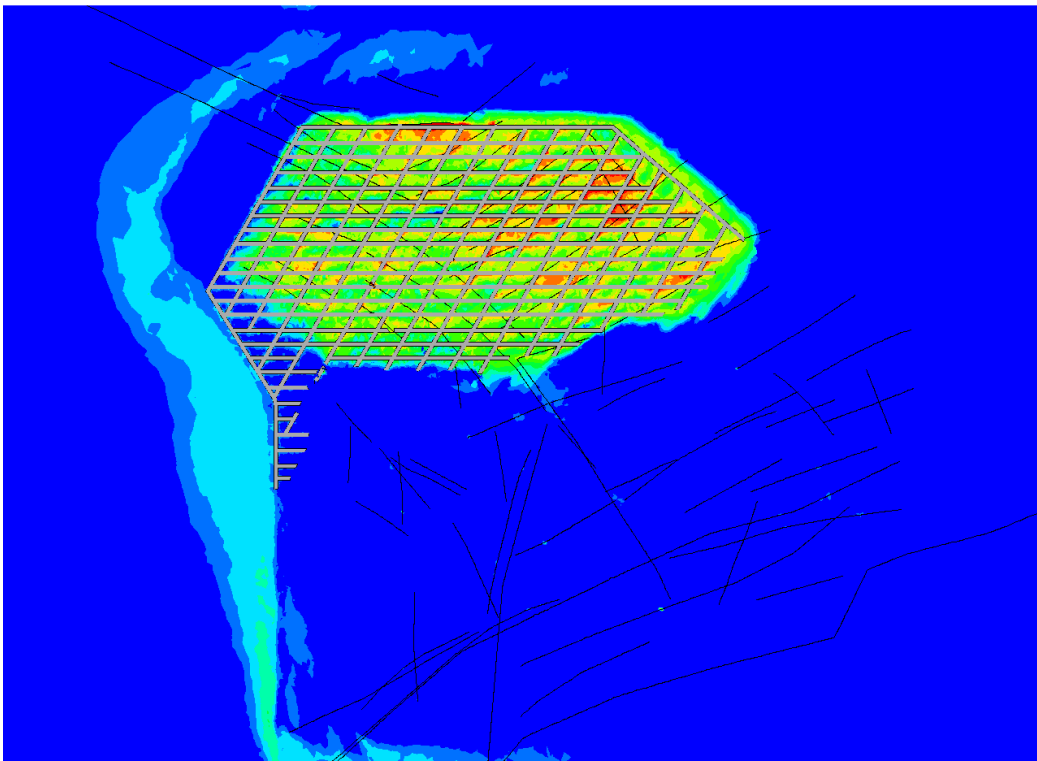


**Figure C.10:** Plan view with Plastic strain distribution in Production level of Esmeralda operation, Step July 2002

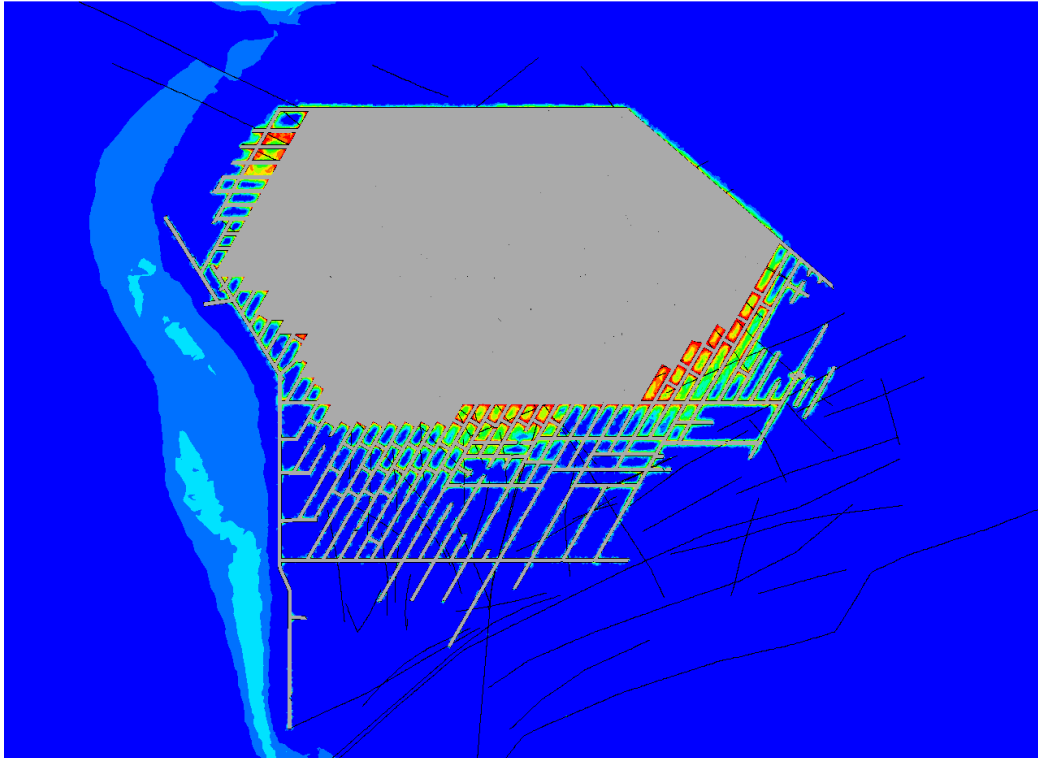


**Figure C.11:** Plan view with Plastic strain distribution in Undercut level of Esmeralda operation, Step April 2004

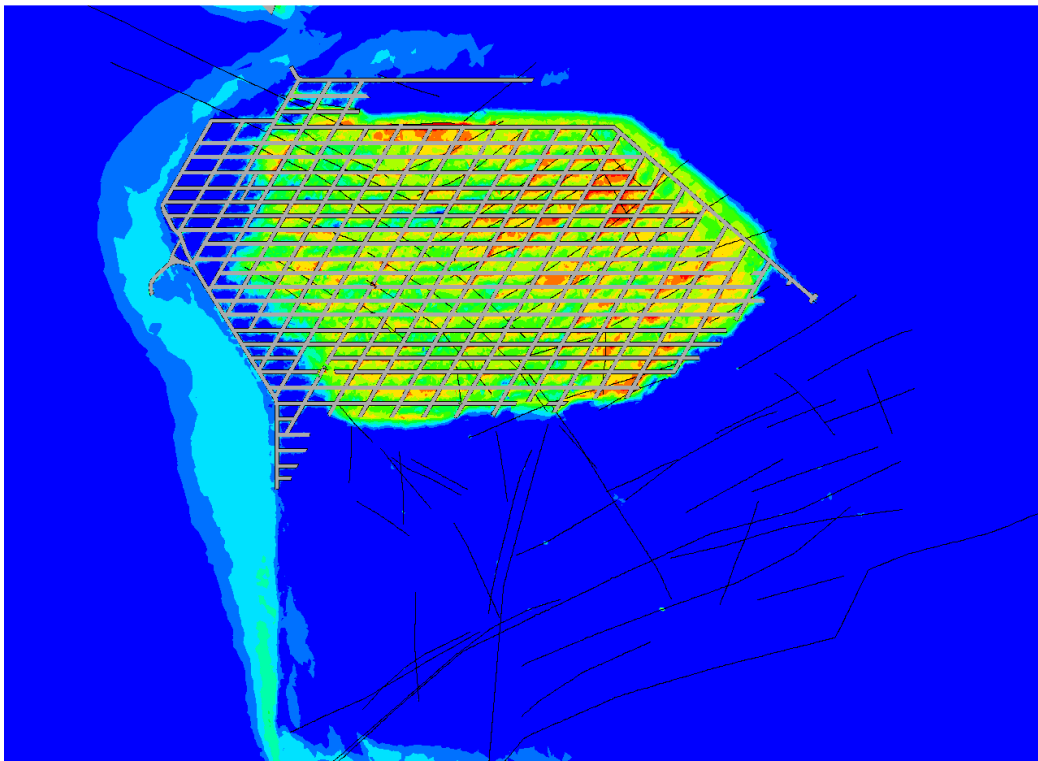


**Figure C.12:** Plan view with Plastic strain distribution in Production level of Esmeralda operation, Step April 2004

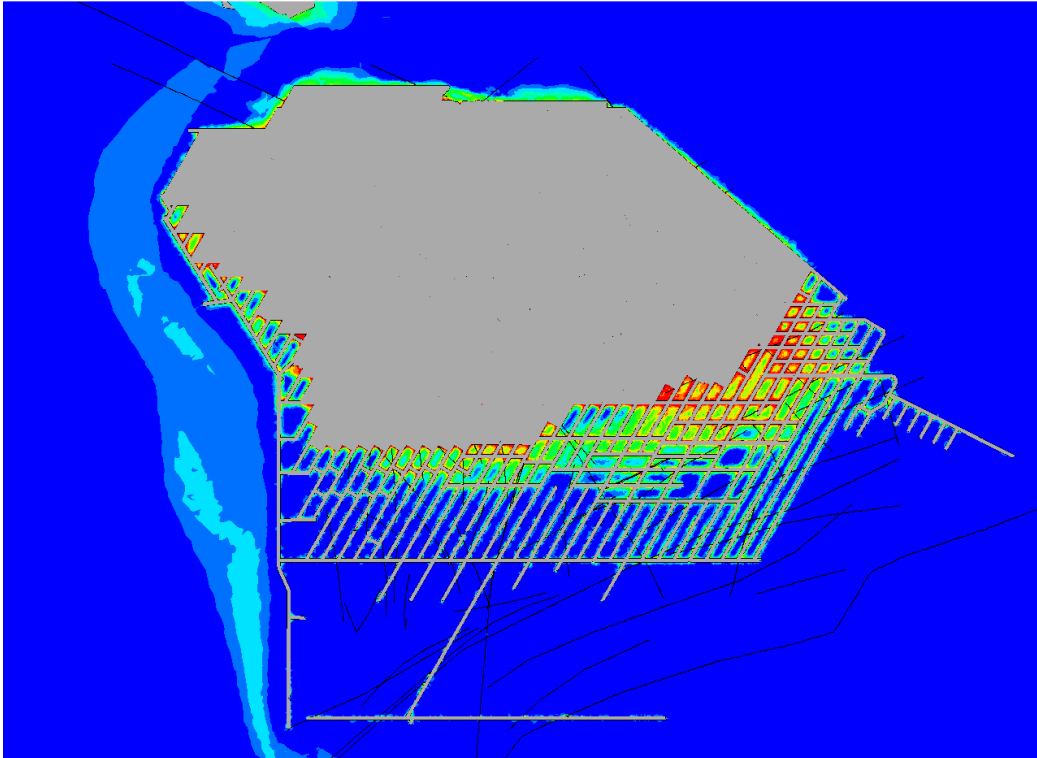


**Figure C.13:** Plan view with Plastic strain distribution in Undercut level of Esmeralda operation, Step March 2006

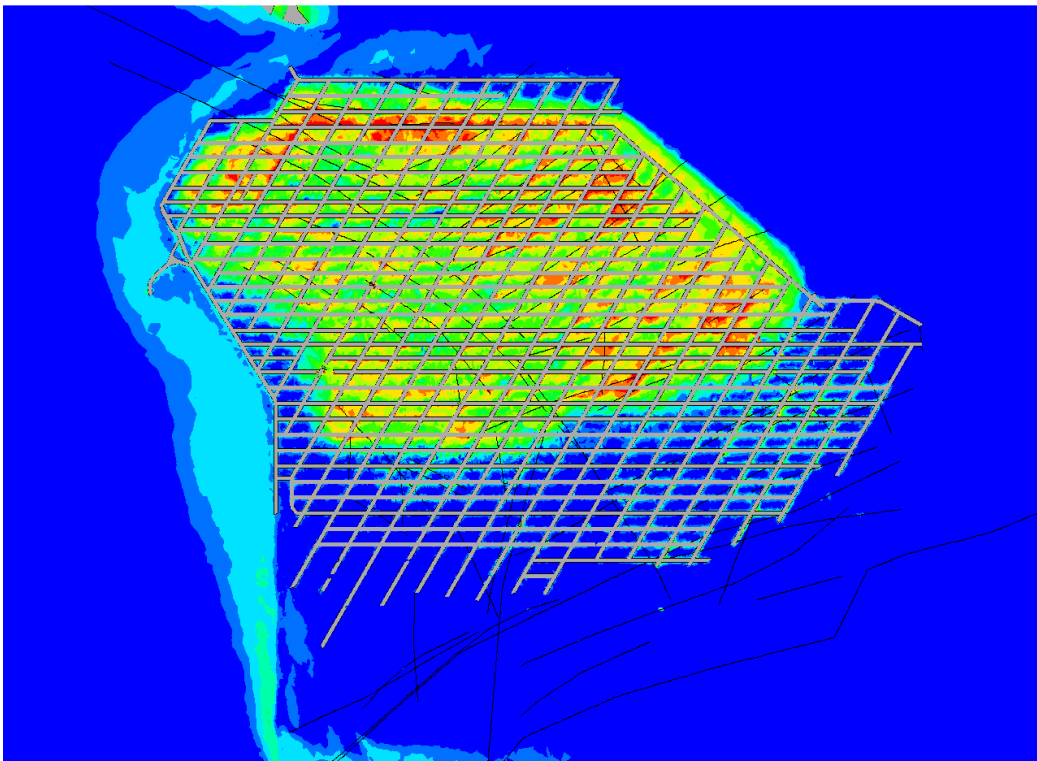


**Figure C.14:** Plan view with Plastic strain distribution in Production level of Esmeralda operation, Step April 2006

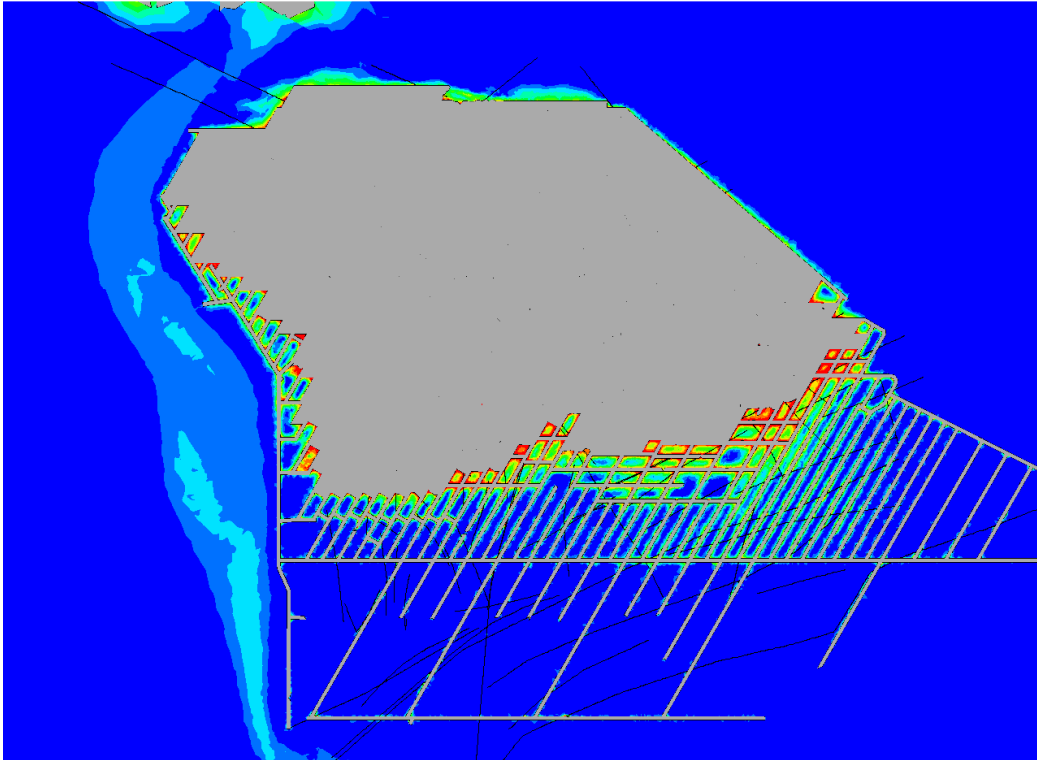


**Figure C.15:** Plan view with Plastic strain distribution in Undercut level of Esmeralda operation, Step March 2009

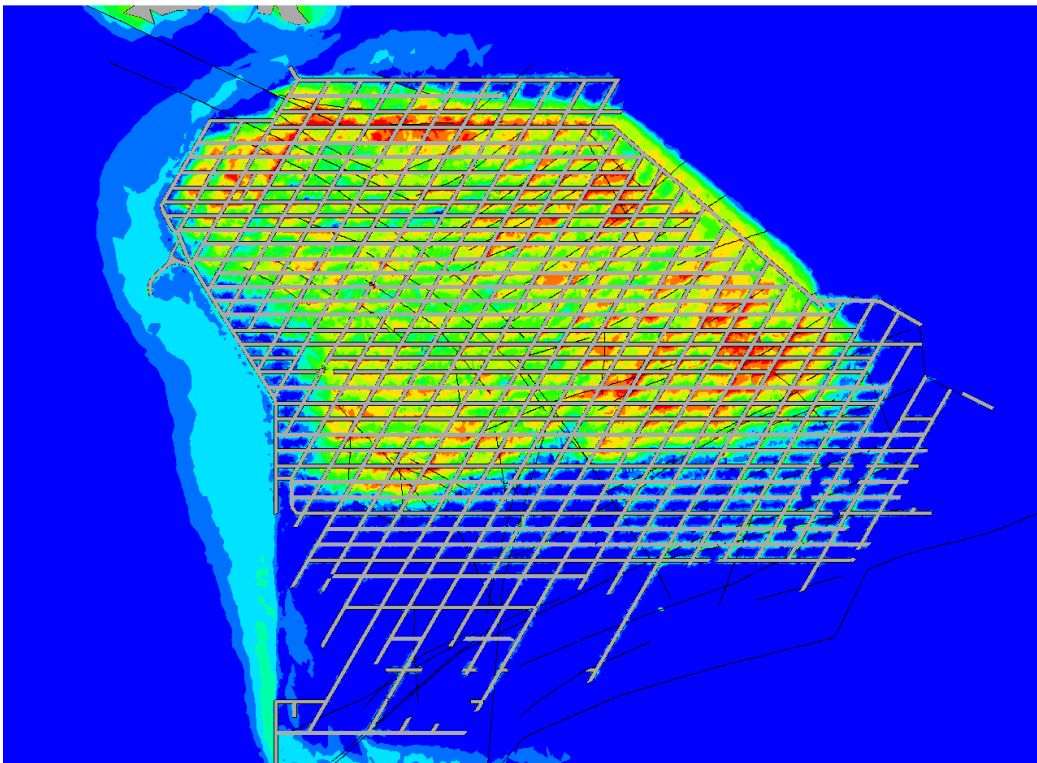


**Figure C.16:** Plan view with Plastic strain distribution in Production level of Esmeralda operation, Step April 2009

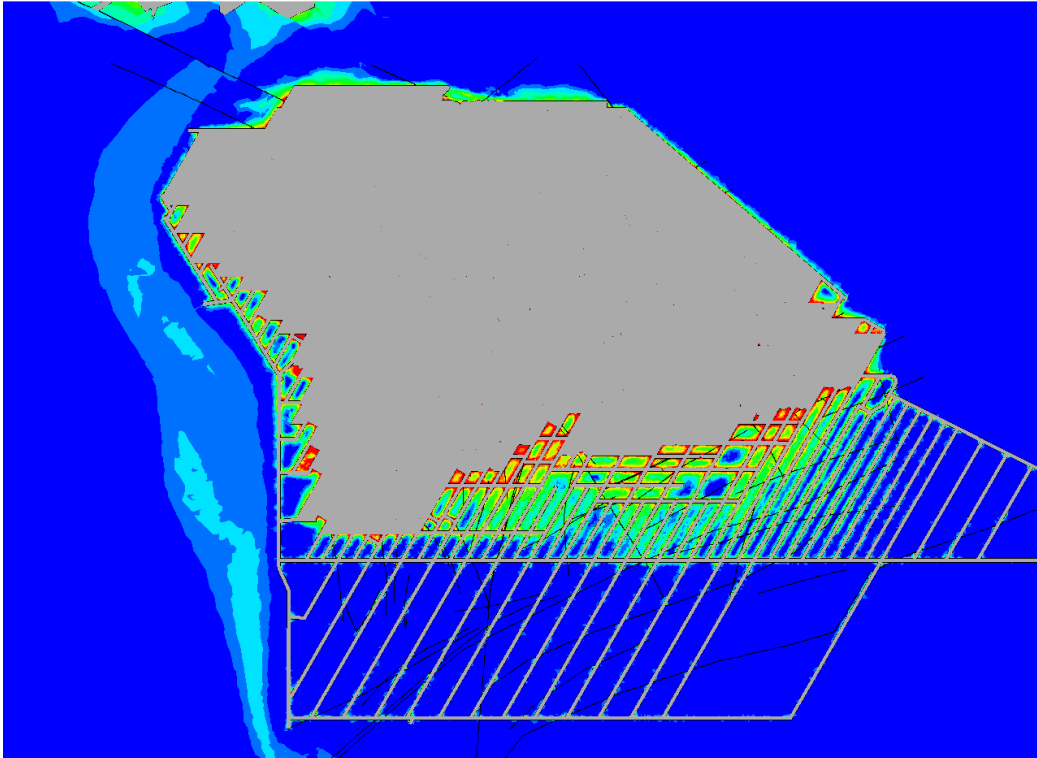


**Figure C.17:** Plan view with Plastic strain distribution in Undercut level of Esmeralda operation, Step June 2010

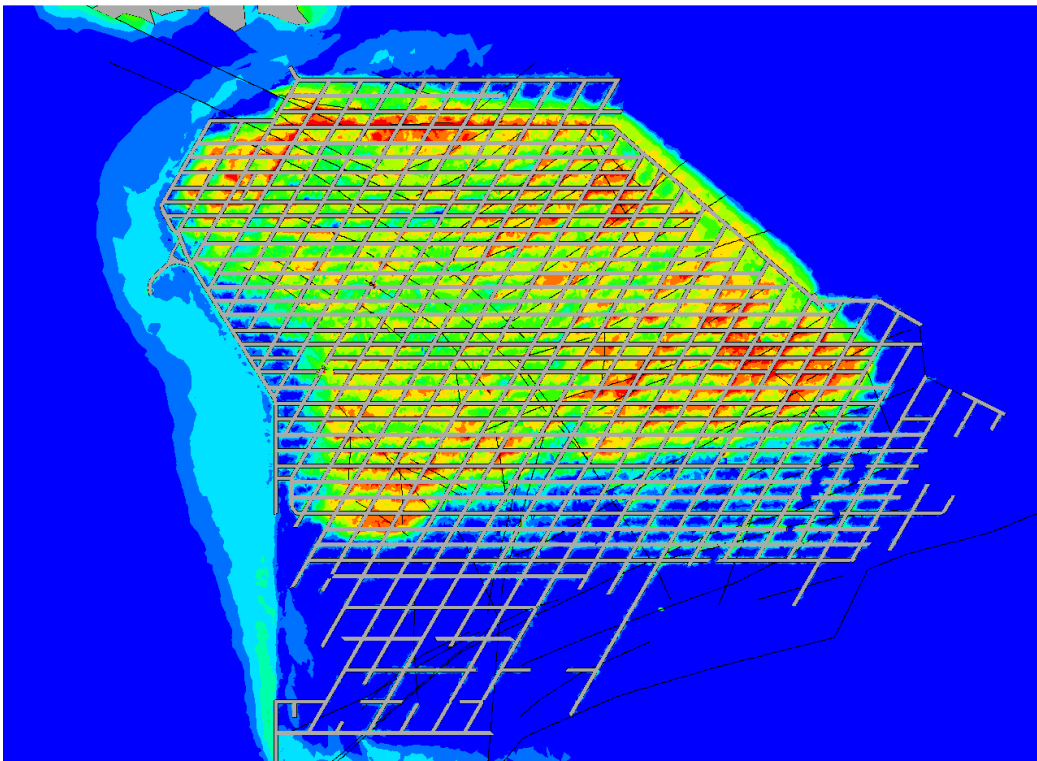


**Figure C.18:** Plan view with Plastic strain distribution in Production level of Esmeralda operation, Step June 2010

**APPENDIX D – BENCHMARK OF COLLAPSES FOR CODELCO  
UNDERGROUND OPERATIONS**

Appendix D: Benchmark of Collapse for Codelco underground operations

PRODUCTIVE SECTOR	COLLAPSE	UBICACIÓN			DATE		DAMAGE		A <sub>AFA</sub> (m <sup>2</sup> )	W <sub>F</sub> (m)	A <sub>AB</sub> (m <sup>2</sup> )	REFERENCE		
		DRIFT	TRENCHES	OP (s)	YEAR	MONTH	A <sub>AF</sub> (m <sup>2</sup> )	OP (s)						
TENIENTE 4 SUR	B	1	C-4	Z-1 a Z-3	1	1984	4	4500	2	4500	390	24206		
			C-5	Z-1 a Z-4	1									
			C-6	Z-4 a Z-6	0									
	B	2	C-7	Z-7 a Z-9	1	1985	10	1350	1	1350	400	48205		
	B	3	C-9	Z-12 a Z-16	1	1987	4	2425	2	6385	400	81924		
			4	C-7	Z-10 a Z-13			1					1860	
	BC	5	C-12	Z-16 a Z-19	0			7					2100	
C	6	C-15L	Z-20 a Z-40	1	1988	3	1620	3	5290	400	80931			
		C-11L	Z-20 a Z-22											
TENIENTE 4 SUR	C	6	C-11L	Z-23 a Z-40	1	1988	3	1620	8	15360	400	80931		
			7	C-16	Z-19 a Z-22			1					6	2050
			8	C-17L	Z-19 a Z-22			1					1	2130
		9	C-5L	Z-41 a Z-46	2	1989	2	9560	6	11690	400	67451		
			C-7L	Z-42 a Z-46	1									
			C-9L	Z-42 a Z-45	1									
			C-11L	Z-41 a Z-43	0									
		10	C-13L	Z-40 a Z-42	1	1990	5	7100	1	7100	700	80816		
			C-5L	Z-47	0									
				C-7L									Z-47	
C-9L	Z-40 a Z-41		0											
	Z-46 a Z-47													

OP (s): Damaged Ore Passes

A<sub>AF</sub>: Affected Area

A<sub>AFA</sub>: Annual Affected Area

W<sub>F</sub>: Width of Front

A<sub>AB</sub>: Open Area

Appendix D: Benchmark of Collapse for Codelco underground operations

PRODUCTIVE SECTOR		COLLAPSE	UBICACIÓN			DATE		DAMAGE		A <sub>AFA</sub> (m <sup>2</sup> )	W <sub>F</sub> (m)	A <sub>AB</sub> (m <sup>2</sup> )	REFERENCE			
			DRIFT	TRENCHES	OP (s)	YEAR	MONTH	A <sub>AF</sub> (m <sup>2</sup> )	OP (s)							
TENIENTE 4 SUR	C	10	C-11L	Z-44 a Z-48	1	1990	5	7100	2	7100	700	80816				
			C-13L	Z-43 a Z-47	0											
	CD	11	C-11L	Z-31 a Z-32	1	1991	1	7560	6	24250	700	93501				
	D		C-13L	Z-20 a Z-49												
CD		C-15L	Z-23 a Z-31	2												
TENIENTE 4 SUR	CD	11	C-15L	Z-32 a Z-47	2	1991	1	7560	4	32245	700	93501				
	C	12	C-10	Z-9 a Z-13	1	1991	9	6880								
			C-11	Z-9 a Z-13												
			C-12	Z-9 a Z-13												
		13	C-1L	Z-46 a Z-50	0	1991	10	2250								
	D	14	C-15L	Z-48 a Z-49	0	1992	1	670					0	810	700	94299
	C	15	C-19L	Z-21 a Z-23			3	140								
	D	16	C-17L	Z-47 a Z-50			1	2040								
C	17	C-3L	Z-31	2			510									

OP (s): Damaged Ore Passes

A<sub>AF</sub>: Affected Area

A<sub>AFA</sub>: Annual Affected Area

W<sub>F</sub>: Width of Front

A<sub>AB</sub>: Open Area

Appendix D: Benchmark of Collapse for Codelco underground operations

PRODUCTIVE SECTOR	COLLAPSE	UBICACIÓN			DATE		DAMAGE		A <sub>AFA</sub> (m <sup>2</sup> )	W <sub>F</sub> (m)	A <sub>AB</sub> (m <sup>2</sup> )	REFERENCE		
		DRIFT	TRENCHES	OP (s)	YEAR	MONTH	A <sub>AF</sub> (m <sup>2</sup> )	OP (s)						
TENIENTE 4 SUR	C	18	C-19L	Z-31 a Z-42	1	1993	9	1140	1	5065	700	Pasten (1999). Villegas (2008).		
	D	19	C-19L	Z-44 a Z-52		1994	2	3925	0	11055	700		98641	
		20	C-17L	Z-51 a Z-54	4			2080						
		21	C-15L	Z-50 a Z-53			2090							
		22	C-22L	Z-44 a Z-48	2960									
	C	23	C-5L	Z-51	0	1995	3	1020	3	9260	700		87621	
	D	24	C-9L	Z-52	1		4	1430						
25		C-25L	Z-31 a Z-40	1950										
TENIENTE 4 SUR	C	26	C-17L	Z-43	1	1995	6	1410	2	15332	700		87621	
	D	27	C-19L	Z-31 a Z-32	0		7	3450						
	CD		C-21L	Z-32 a Z-41	1									
	D		28	C-23L		Z-31	1		1	1510	0			
		C-29		Z-37 a Z-39	7	4610								
		29	C-3L	Z-55		1996		8	690					
			C-5L	Z-56										
			C-7L	Z-53										
		30	C-31L	Z-36	0	1997		12	1302	0		1302	700	84114
		31	C-11L	Z-50 a Z-51										
	C-13L		Z-50 a Z-52											
32	C-21L	Z-52 a Z-53	0	1999	6	1052	0	1052	700	76307				
33	C-13L	Z-58 a Z-59												

OP (s): Damaged Ore Passes

A<sub>AF</sub>: Affected Area

A<sub>AFA</sub>: Annual Affected Area

W<sub>F</sub>: Width of Front

A<sub>AB</sub>: Open Area

Appendix D: Benchmark of Collapse for Codelco underground operations

PRODUCTIVE SECTOR	COLLAPSE	UBICACIÓN			DATE		DAMAGE		A <sub>AFA</sub> (m <sup>2</sup> )	W <sub>F</sub> (m)	A <sub>AB</sub> (m <sup>2</sup> )	REFERENCE
		DRIFT	TRENCHES	OP (s)	YEAR	MONTH	A <sub>AF</sub> (m <sup>2</sup> )	OP (s)				
TENIENTE 4 SUR	D	34	C-9L	Z-57	1	2000	3	1557	1	1557	700	66600
			C-11L	Z-57								
			C-23L	Z-52	0							
		35	C-21L	Z-54 a Z-56								
		36	C-23L	Z-52 a Z-53	1	2001	6	1	1040	700	67900	1
		37	C-3L	Z-74 a Z-75	0	2003	7	0	3072	700	76713	0
		38	C-1R	Z-74 a Z-75			8					
		39	C-25L	Z-56 a Z-57			9					
		40	C-13L	Z-64 a Z-67	0	2003	10	1	4975	700	76713	1
		41	C-5L	Z-68 a Z-71			11					
			C-7L	Z-69 a Z-71								
		42	C-9L	Z-66 a Z-68	1	2004	5	1	4420	700	67821	1
C-11L	Z-65 a Z-68											
43	C-17L	Z-65 a Z-67	0		6							
RENO	Invariante	R-1	C-9	Z-21 a Z-27	1	2001	---	2070	1	2070	350	44656
		R-2	C-7	Z-30 a Z-32	1	2002	---	1300	1	1300	380	52047
		R-3	C-9	Z-16 a Z-20	0	2003	4	1280	0	1280	490	52400
		R-4	C-9	Z-28 a Z-29	0	2004	4	570	0	900	500	55539
		R-5	C-8	Z-28 a Z-29	0		8					

OP (s): Damaged Ore Passes

A<sub>AF</sub>: Affected Area

A<sub>AFA</sub>: Annual Affected Area

W<sub>F</sub>: Width of Front

A<sub>AB</sub>: Open Area

Appendix D: Benchmark of Collapse for Codelco underground operations

PRODUCTIVE SECTOR		COLLAPSE	UBICACIÓN			DATE		DAMAGE		A <sub>AFA</sub> (m <sup>2</sup> )	W <sub>F</sub> (m)	A <sub>AB</sub> (m <sup>2</sup> )	REFERENCE
			DRIFT	TRENCHES	OP (s)	YEAR	MONTH	A <sub>AF</sub> (m <sup>2</sup> )	OP (s)				
REGTO.	FW	R-1	C-31	Z-9 a Z-10	1	2003	6	650	1	650	135	35547	Pasten (1999). Villegas (2008).
		R-2	C-36	Z-14 a Z-16	1	2004	2	2000	1	2000	135	34017	
ESMERALDA	Central	E-1	C-17	Z-11 a Z-12	1	2001	11	1150	3	3500	585	59026	
		E-2	C-19	Z-11 a Z-12	1			1250					
		E-3	C-23	Z-8 a Z-9	1			1100					
		E-4	C-19	Z-10	0	2002	4	600	0	1370	585	70000	
			C-23	Z-7	0			770					
		E-5	C-19	Z-13 a Z-14	0	2003	4	562	2	6741	585	69877	
			C-21	Z-11 a Z-15	---			2247					
			C-23	Z-11 a Z-15	1			2247					
			C-25	Z-11 a Z-14	1			1124					
		E-6	C-17	Z-10 a Z-11	0	2004	5	561	---	---	585	---	
		---	C-19	Z-17 a Z-19	---		---	1800					
			C-21	Z-17 a Z-19	---		---	1800					
C-23	Z-17 a Z-19		---	---	1800								
C-25	Z-16 a Z-18		---	---	1800								
C-27	Z-17 a Z-19		---	---	1800								
C-29	Z-17 a Z-19		---	---	1800								

**OP (s):** Damaged Ore Passes

**A<sub>AF</sub>:** Affected Area

**A<sub>AFA</sub>:** Annual Affected Area

**W<sub>F</sub>:** Width of Front

**A<sub>AB</sub>:** Open Area

Appendix D: Benchmark of Collapse for Codelco underground operations

PRODUCTIVE SECTOR	COLLAPSE	UBICACIÓN			DATE		DAMAGE		A <sub>AFA</sub> (m <sup>2</sup> )	W <sub>F</sub> (m)	A <sub>AB</sub> (m <sup>2</sup> )	REFERENCE	
		DRIFT	TRENCHES	OP (s)	YEAR	MONTH	A <sub>AF</sub> (m <sup>2</sup> )	OP (s)					
ESMERALDA	Central	C-23	Z-24	0	2009	1		4	8850	617	56102	Dunlop et. al. (2010)	
		C-25	Z-24	0									
		C-31	Z-22 a Z-23	1									
		C-33	Z-21 a Z-23	1									
		C-35	Z-20 a Z-23	1									
		C-37	Z-20 a Z-23	1									
		C-39	Z-19 a Z-23	1	2010	6	6994	4	12727	617	45472		
		C-41	Z-18 a Z-22	1									
		C-43	Z-17 a Z-21	1									
		C-45	Z-17 a Z-21	1									
		C-23	Z-25 a Z-27	0		12	5733	0	12727	617	41814		
		C-25	Z-25 a Z-26	0									
		C-27	Z-24 a Z-26	0									
		C-29	Z-24 a Z-25	0									
		C-31	Z-24 a Z-25	0									
		C-33	Z-24 a Z-25	0									
		C-35	Z-24 a Z-25	0									
		C-37	Z-24	0									

OP (s): Damaged Ore Passes

A<sub>AF</sub>: Affected Area

A<sub>AFA</sub>: Annual Affected Area

W<sub>F</sub>: Width of Front

A<sub>AB</sub>: Open Area

Appendix D: Benchmark of Collapse for Codelco underground operations

PRODUCTIVE SECTOR	COLLAPSE	UBICACIÓN			DATE		DAMAGE		A <sub>AFA</sub> (m <sup>2</sup> )	W <sub>F</sub> (m)	A <sub>AB</sub> (m <sup>2</sup> )	REFERENCE	
		DRIFT	TRENCHES	OP (s)	YEAR	MONTH	A <sub>AF</sub> (m <sup>2</sup> )	OP (s)					
IVISIÓN ANDINA NIVEL 16 PRODUCCIÓN LHD III PANEL MINA RIO BLANCO.					1999						19726	Diaz, Espinoza & Karzulovic (2000)	
	4 y 5		CP-57			2000	6			5400		6580	Karzulovic & Lledó (2003).
			CP-61				7						
			CP-65				8						
	8		CP-51	BP-23 a BP-24		2002	9			1000			
			CP-53					10					
	9		CP-53	BP-18 a BP-19		2003	5			1400		6500	
			CP-53	BP-18 a BP-19			6						
			CP-57	BP-15 a BP-18			7						
			CP-53	BP-18 a BP-19									
			CP-55	BP-15 a BP-17			8						
			CP-57	BP-15 a BP-18									
			CP-53	BP-18 a BP-19			9						
			CP-55	BP-15 a BP-17									
			CP-57	BP-15 a BP-18									
			CP-61	BP-19 a BP-21			11						
			CP-53	BP-18 a BP-19									
			CP-55	BP-15 a BP-17									
			CP-57	BP-15 a BP-18									
		CP-61	BP-19 a BP-21										

OP (s): Damaged Ore Passes      A<sub>AF</sub>: Affected Area      A<sub>AFA</sub>: Annual Affected Area      W<sub>F</sub>: Width of Front      A<sub>AB</sub>: Open Area

Appendix D: Benchmark of Collapse for Codelco underground operations

PRODUCTIVE SECTOR	COLLAPSE	UBICACIÓN			DATE		DAMAGE		A <sub>AFA</sub> (m <sup>2</sup> )	W <sub>F</sub> (m)	A <sub>AB</sub> (m <sup>2</sup> )	REFERENCE	
		DRIFT	TRENCHES	OP (s)	YEAR	MONTH	A <sub>AF</sub> (m <sup>2</sup> )	OP (s)					
DIV. SALVADOR	INCA OESTE	XC - 18	Z - 21 a Z - 24		1999	12			400			De Nicola, Fishwick & Tapia (2000)	
		XC - 19	Z - 19 a Z - 24										
		XC - 20	Z - 17 a Z - 23										
		XC - 21	Z - 17 a Z - 22										
		XC - 16	Z - 14 a Z - 19	0	2006	10	1	5400					AS BULT DE COLAPSOS SECTOR INCA OESTE Y. SEPÚLVEDA O. F POBLETE V. (OCTUBRE DE 2012)
		XC - 17	Z - 19 a Z - 25	1		11							
		XC - 16	Z - 20 a Z - 23	1	2007	4	1	1350					
		XC - 16	Z - 24	0	2008	10	0	450					
		XC - 12	Z - 20 a Z - 21	0	2009	8	2	9900					
		XC - 13	Z - 17 a Z - 21	0		8							
		XC - 14	Z - 15 a Z - 21	1		8 y 11							
		XC - 15	Z - 13 a Z - 22	1		8 y 10							
	XC - 17	Z - 18	0										
	XC - 17	Z - 12 a Z - 17	1	2010		1	2700						
	XC - 15	Z - 23	0	2011		0	--						
	INCA CENTRAL	XC - 1	Z - 3 a Z - 7 Z - 4 a Z - 7		2005	1 2 4			1720				
XC - 2													
XC - 5													
UDC 1,2,4													

OP (s): Damaged Ore Passes

A<sub>AF</sub>: Affected Area

A<sub>AFA</sub>: Annual Affected Area

W<sub>F</sub>: Width of Front

A<sub>AB</sub>: Open Area

Appendix D: Benchmark of Collapse for Codelco underground operations

PRODUCTIVE SECTOR	COLLAPSE	UBICACIÓN			DATE		DAMAGE		A <sub>AFA</sub> (m <sup>2</sup> )	W <sub>F</sub> (m)	A <sub>AB</sub> (m <sup>2</sup> )	REFERENCE
		DRIFT	TRENCHES	OP (s)	YEAR	MONTH	A <sub>AF</sub> (m <sup>2</sup> )	OP (s)				
DIV. SALVADOR	INCA CENTRAL OESTE	XC - 10	Z - 25	0	2006			0	225			AS BULT DE COLAPSOS SECTOR INCA CENTRAL OESTE Y. SEPÚLVEDA O. F. POBLETE V. (OCTUBRE DE 2012)
		XC - 8	Z - 23	0	2007			2	2925			
		XC - 9	Z - 25 a Z - 26	1								
		XC - 10	Z - 26	1								
		XC - 11	Z - 25 a Z - 27	0								
		XC - 6	Z - 28 a Z - 30	0	2008			2	4670			
		XC - 7	Z - 30 a Z - 31	0								
		XC - 8	Z - 24 a Z - 25	1								
		XC - 9	Z - 23 a Z - 24	1								
		XC - 12	Z - 11 a Z - 15	0	2009			4	11824			
		XC - 8	Z - 22	0								
		XC - 11	Z - 22 a Z - 24	0								
			Z - 28 a Z - 29	1								
		XC - 12	Z - 23 a Z - 29	0								
		XC - 13	Z - 23 a Z - 28	1								
		XC - 14	Z - 26 a Z - 27	1	2010			1	5685			
		XC - 15	Z - 18 a Z - 29	1								
		XC - 7	Z - 28 a Z - 29	0								
		XC - 9	Z - 22	0								
		XC - 10	Z - 23 a Z - 24	0								
XC - 12	Z - 30 a Z - 31	0										
XC - 13	Z - 29 a Z - 30	0										
XC - 14	Z - 28 a Z - 30	0										
XC - 15	Z - 30	1										

OP (s): Damaged Ore Passes

A<sub>AF</sub>: Affected Area

A<sub>AFA</sub>: Annual Affected Area

W<sub>F</sub>: Width of Front

A<sub>AB</sub>: Open Area

Appendix D: Benchmark of Collapse for Codelco underground operations

PRODUCTIVE SECTOR		COLLAPSE	UBICACIÓN			DATE		DAMAGE		A <sub>AFA</sub> (m <sup>2</sup> )	W <sub>F</sub> (m)	A <sub>AB</sub> (m <sup>2</sup> )	REFERENCE
			DRIFT	TRENCHES	OP (s)	YEAR	MONTH	A <sub>AF</sub> (m <sup>2</sup> )	OP (s)				
DIV. SALVADOR	INCA CENTRAL OESTE		XC - 10	Z - 21 a Z - 22	0	2011			1	2139		AS BULT DE COLAPSOS SECTOR INCA CENTRAL OESTE Y. SEPÚLVEDA O. F. POBLETE V. (OCTUBRE DE 2012)	
			XC - 12	Z - 21 a Z - 22	0								
			XC - 15	Z - 31 a Z - 32	1								
			XC - 14	Z - 25	0	2012			563				

**OP (s):** Damaged Ore Passes

**A<sub>AF</sub>:** Affected Area

**A<sub>AFA</sub>:** Annual Affected Area

**W<sub>F</sub>:** Width of Front

**A<sub>AB</sub>:** Open Area

**APPENDIX E – MAPS OF OBSERVED DAMAGE ON UNDERCUT  
LEVEL ESMERALDA OPERATION FOR ALL  
EXTRACTION STEPS (1999 - 2009).**

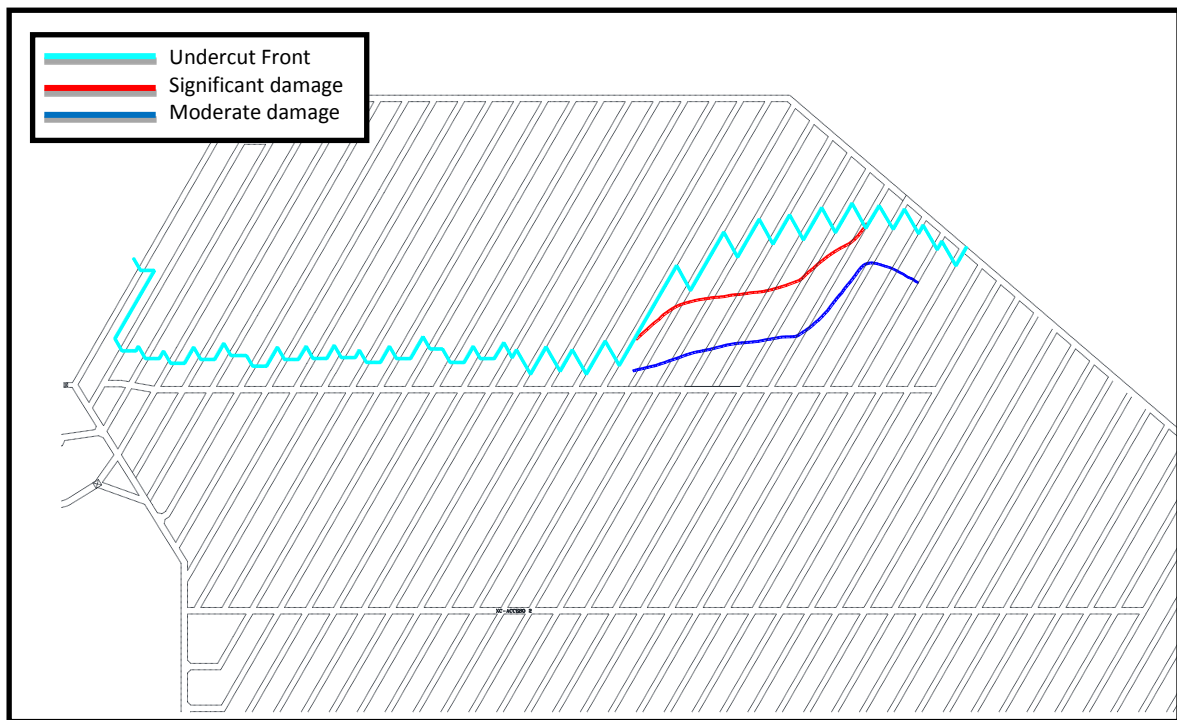


**Figure E.1:** Mapped damage located ahead of undercut front on UCL Esmeralda operation, Sept. 1999.

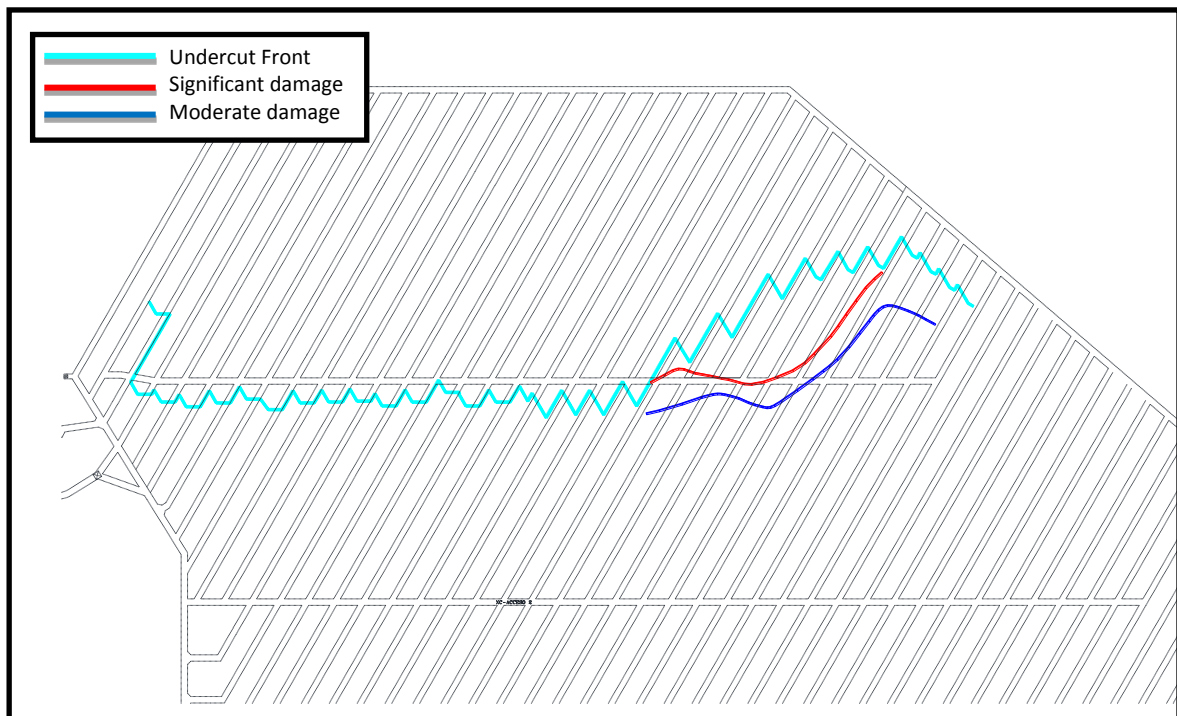


**Figure E.2:** Mapped damage located ahead of undercut front on UCL Esmeralda operation, Nov. 1999.

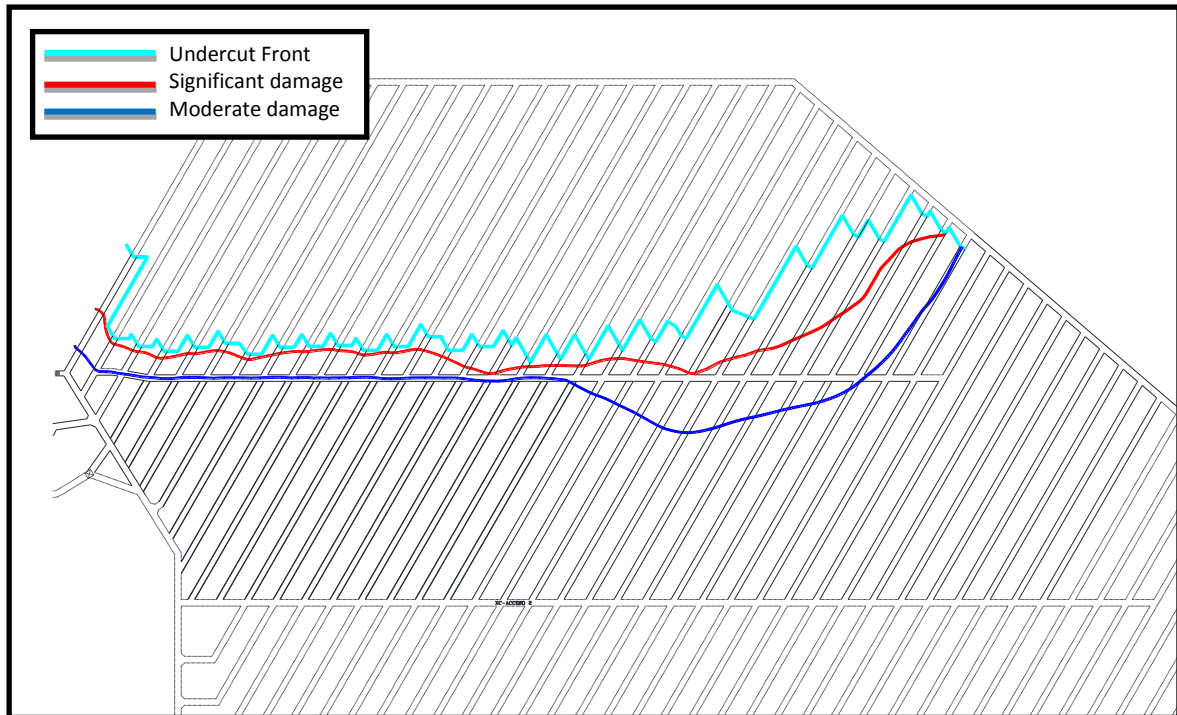


**Figure E.3:** Mapped damage located ahead of undercut front on UCL Esmeralda operation, Jan. 2000.

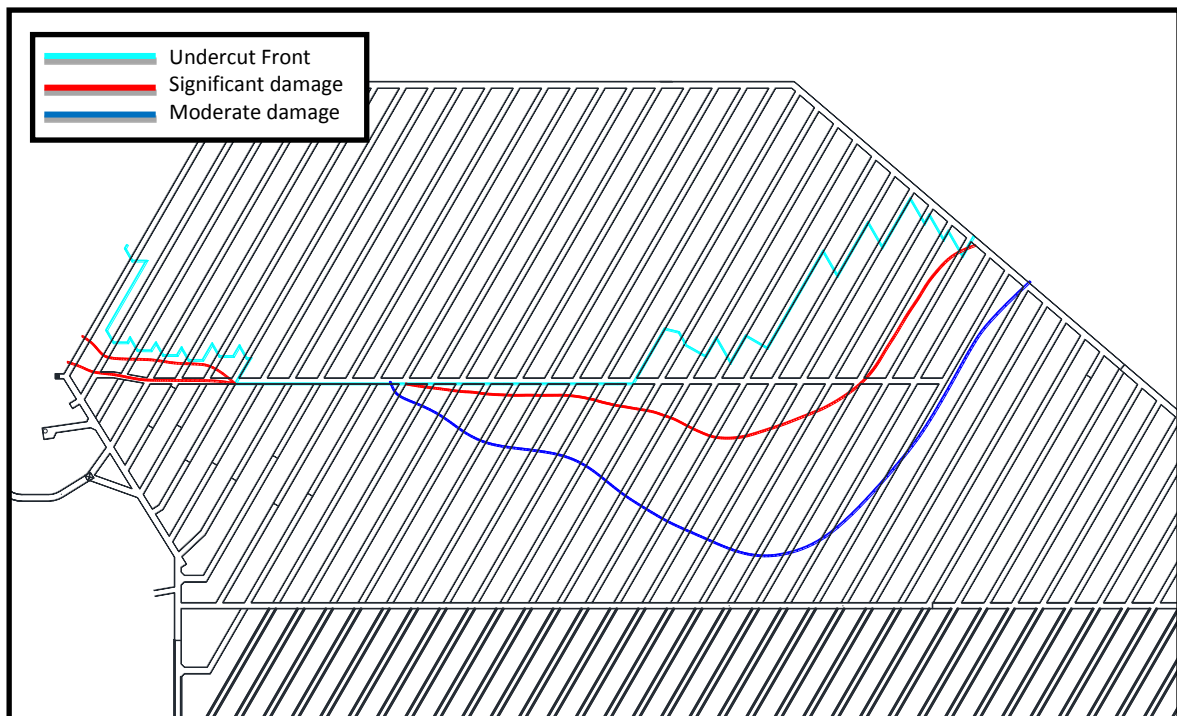


**Figure E.4:** Mapped damage located ahead of undercut front on UCL Esmeralda operation, April 2000.

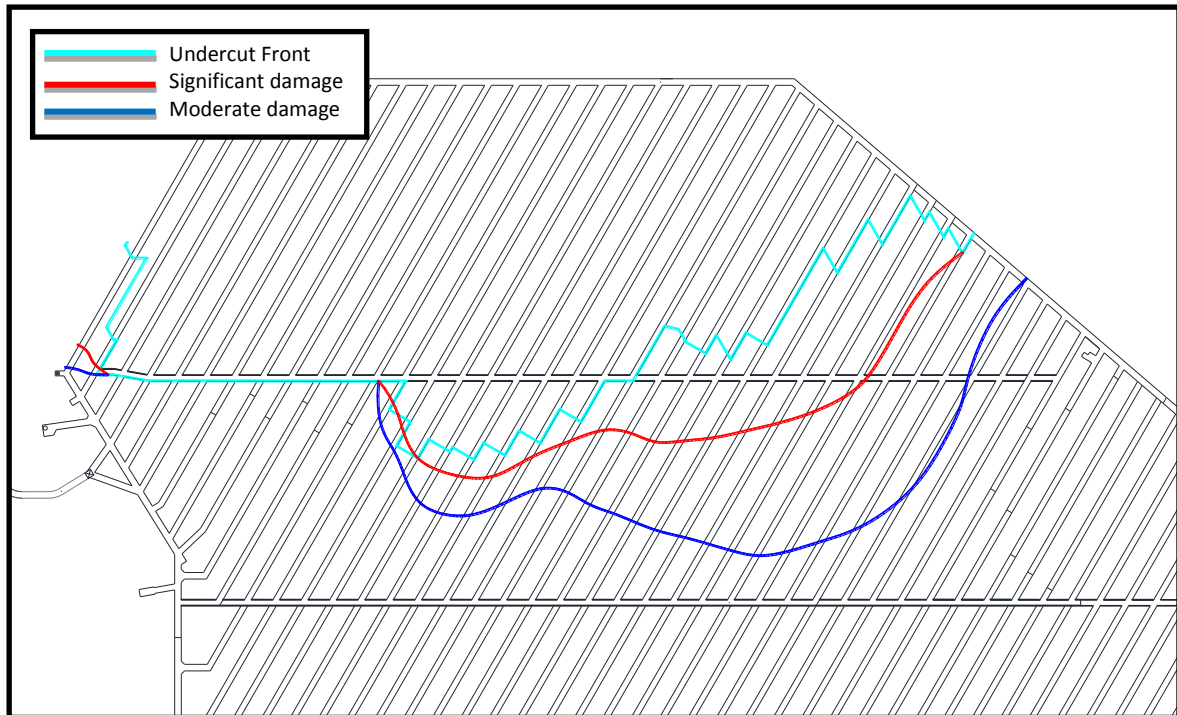


**Figure E.5:** Mapped damage located ahead of undercut front on UCL Esmeralda operation, July 2000.

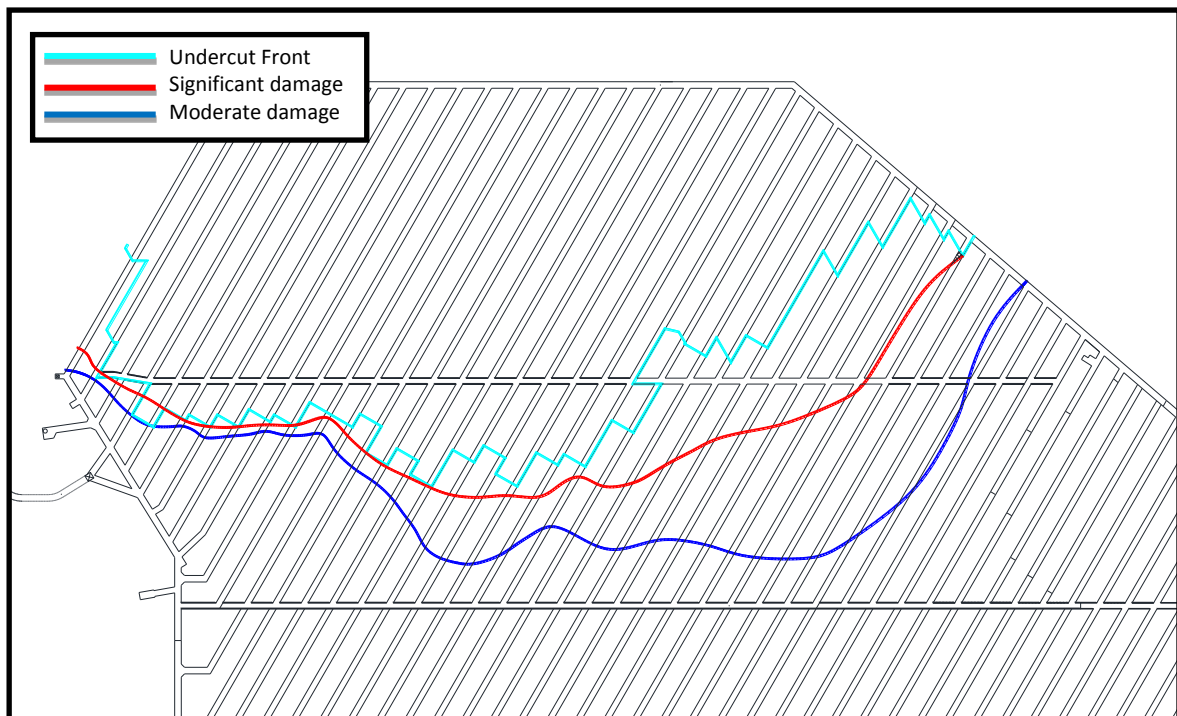


**Figure E.6:** Mapped damage located ahead of undercut front on UCL Esmeralda operation, Sept. 2000.

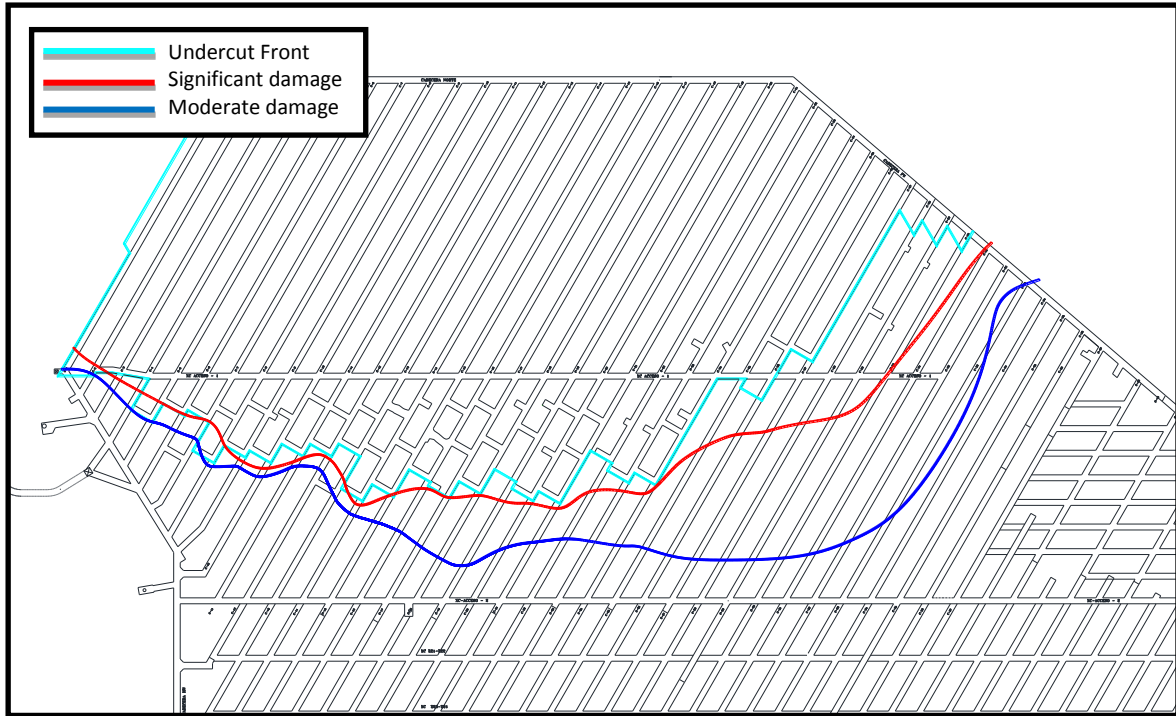


**Figure E.7:** Mapped damage located ahead of undercut front on UCL Esmeralda operation, Feb. 2001.

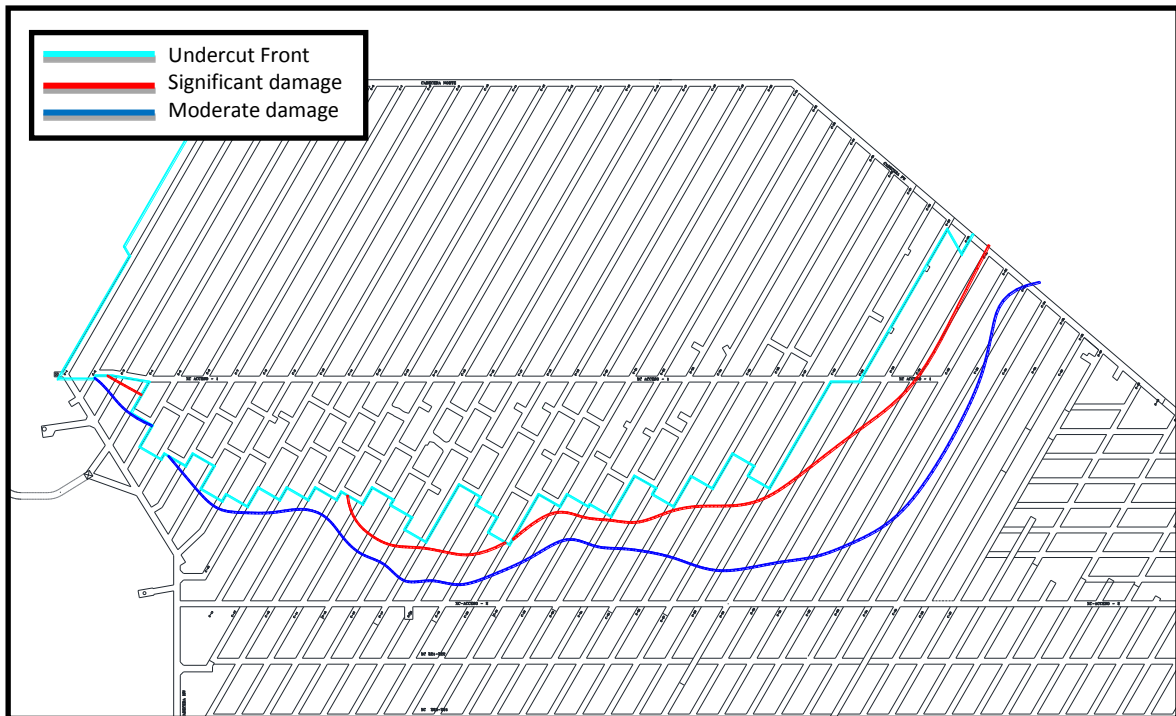


**Figure E.8:** Mapped damage located ahead of undercut front on UCL Esmeralda operation, July 2001.

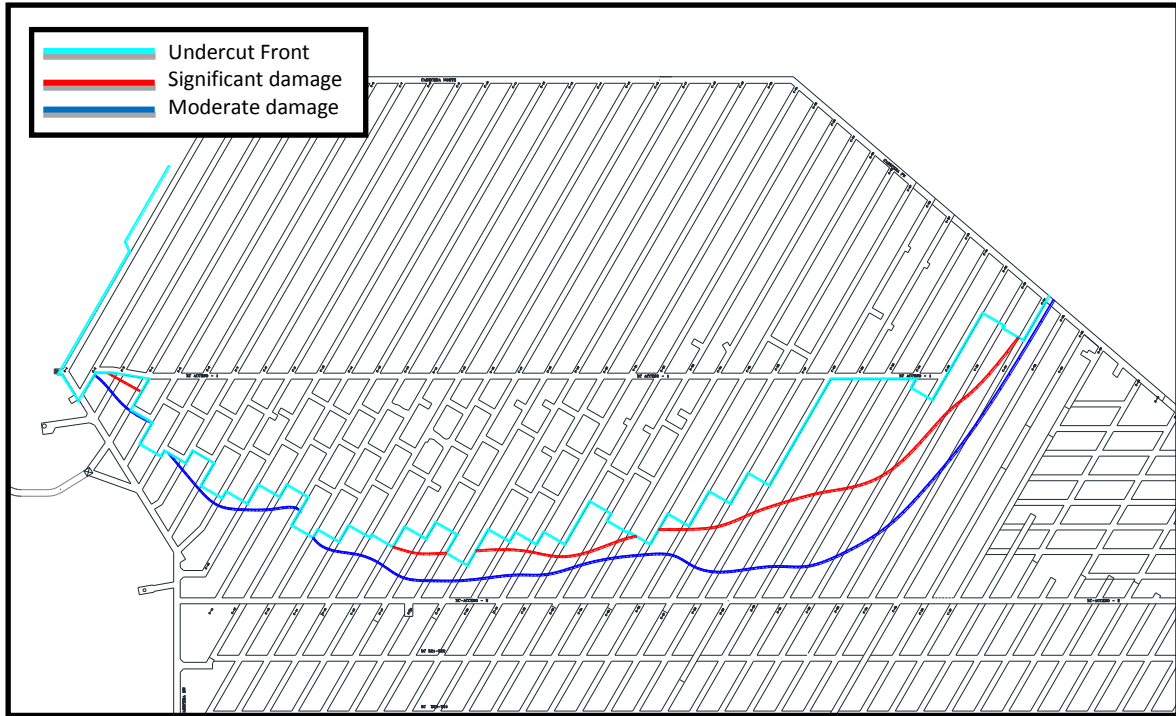


**Figure E.9:** Mapped damage located ahead of undercut front on UCL Esmeralda operation, Oct. 2001.

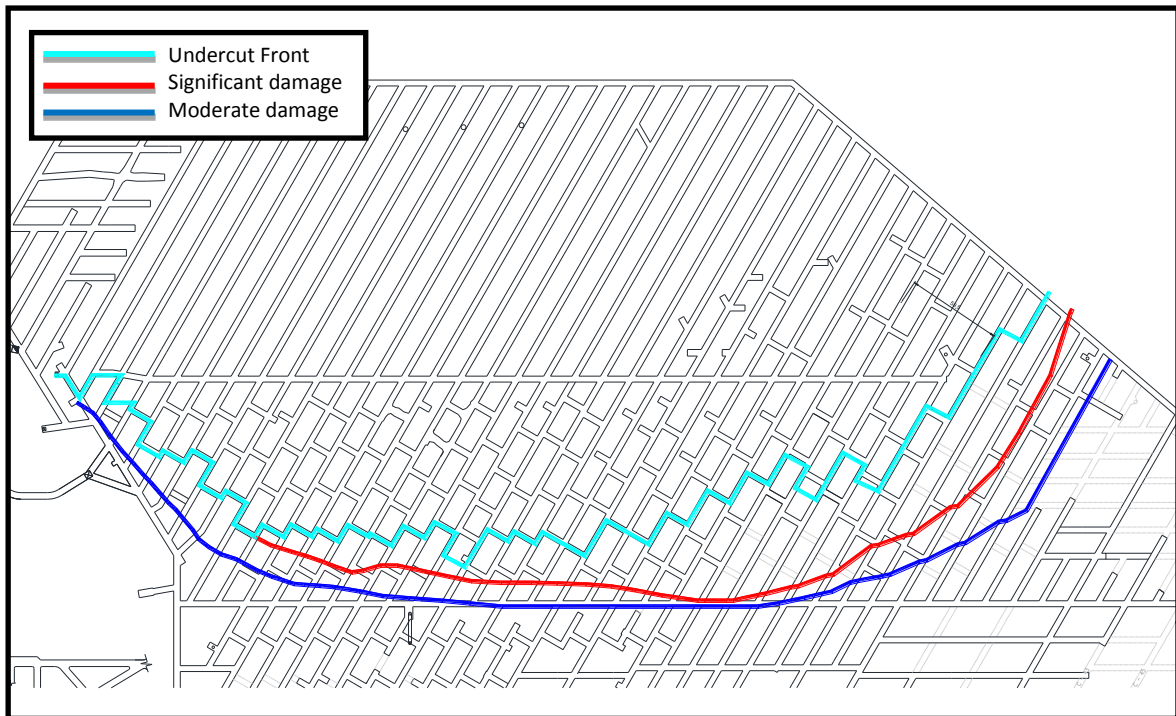


**Figure E.10:** Mapped damage located ahead of undercut front on UCL Esmeralda operation, Oct. 2002.

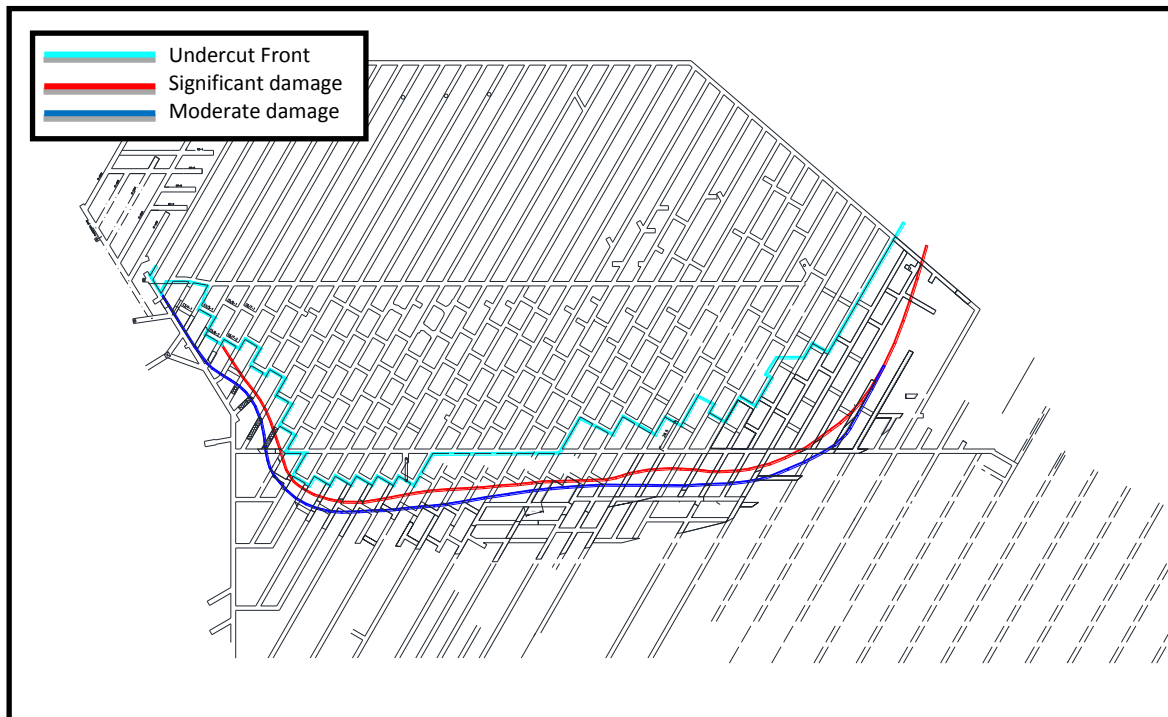


Figure E.11: Mapped damage located ahead of undercut front on UCL Esmeralda operation, Dec. 2003.

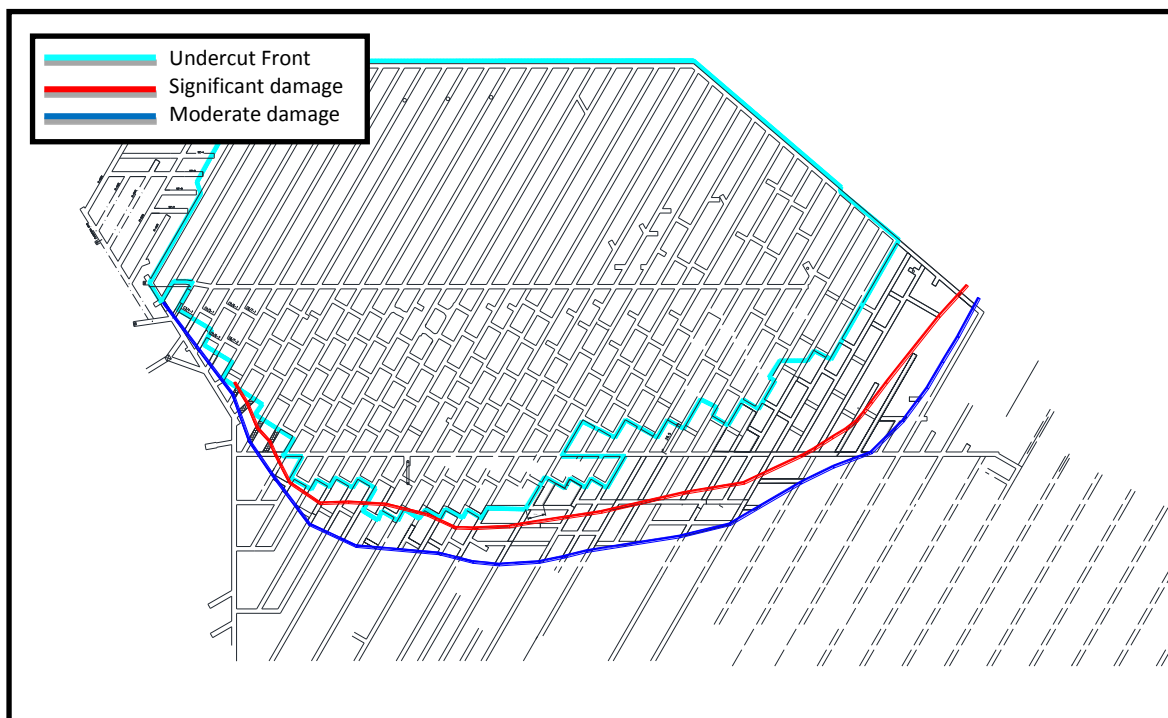
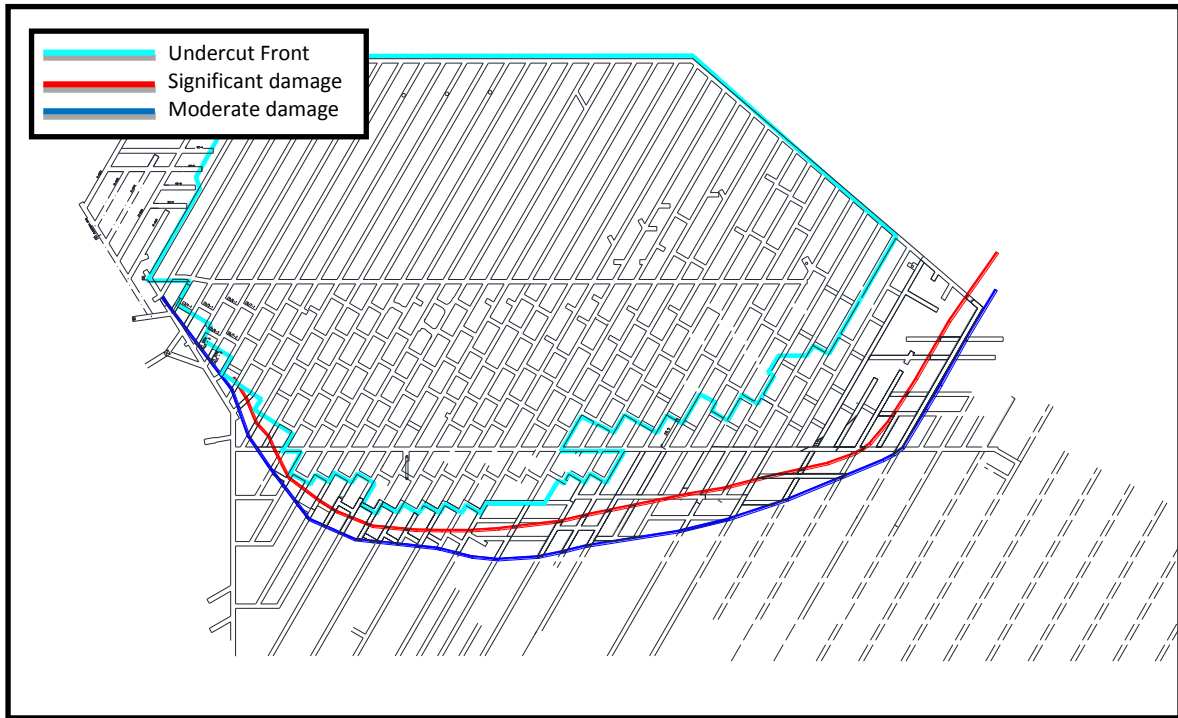
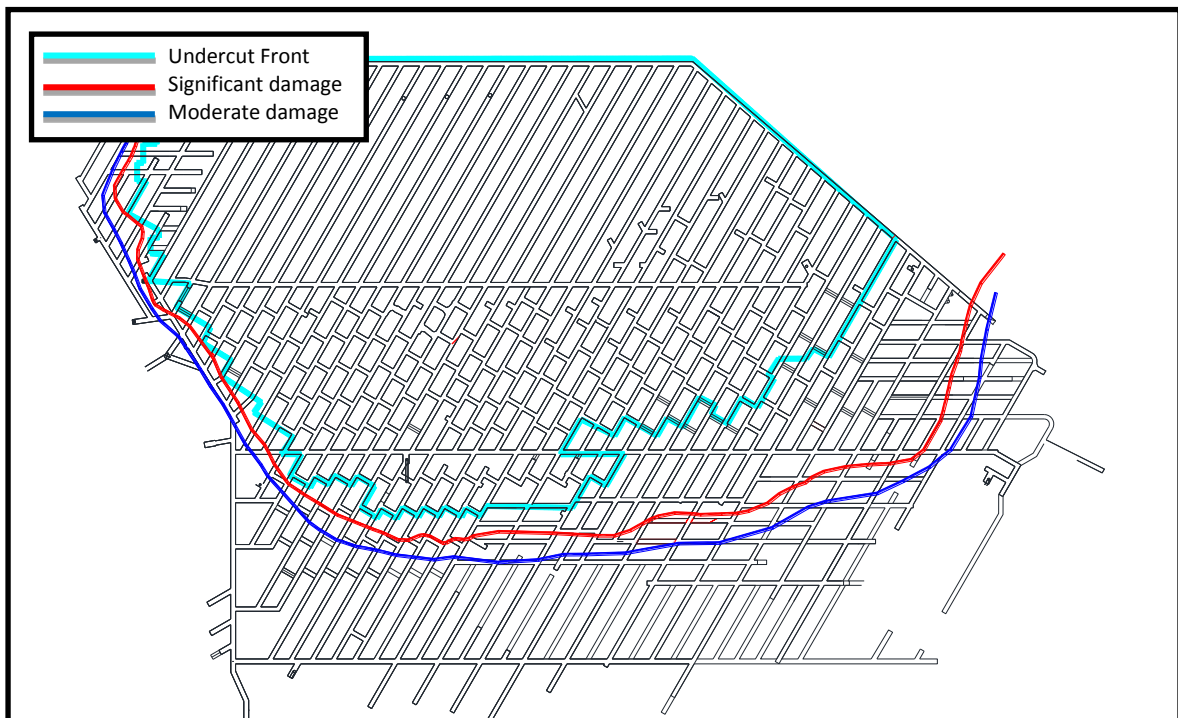


Figure E.12: Mapped damage located ahead of undercut front on UCL Esmeralda operation, July 2004.



**Figure E.13:** Mapped damage located ahead of undercut front on UCL Esmeralda operation, Nov. 2004.



**Figure E.14:** Mapped damage located ahead of undercut front on UCL Esmeralda operation, March 2005.

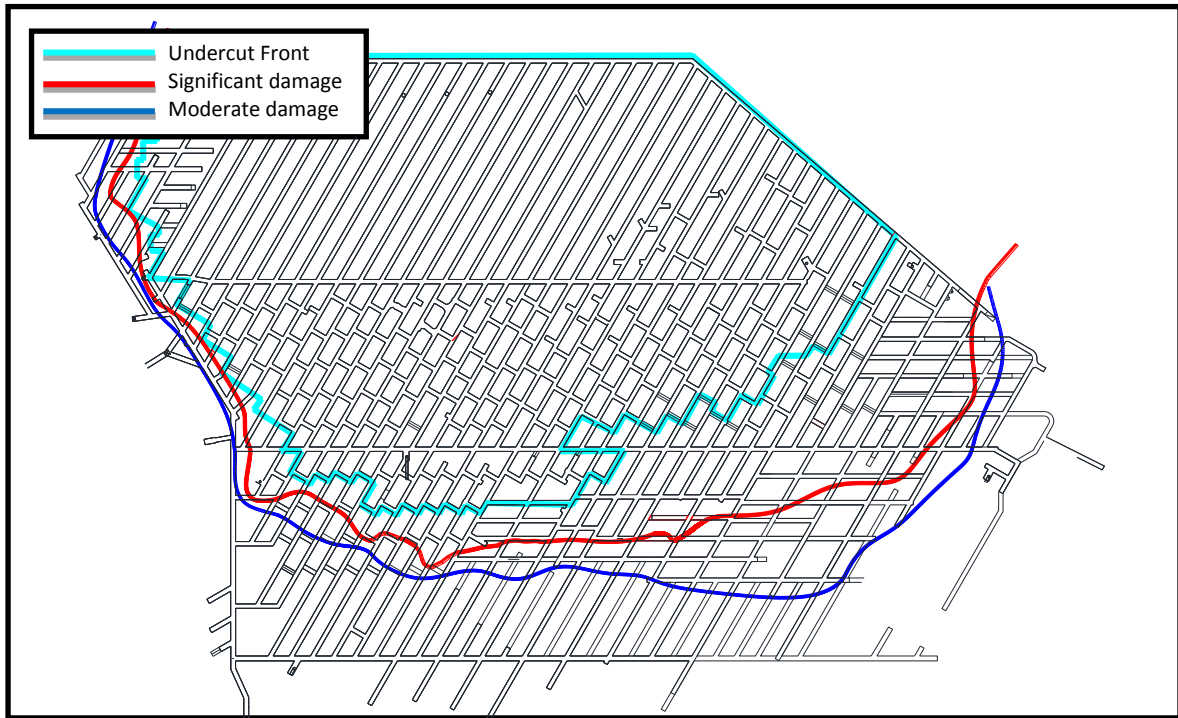


Figure E.15: Mapped damage located ahead of undercut front on UCL Esmeralda operation, April 2005.

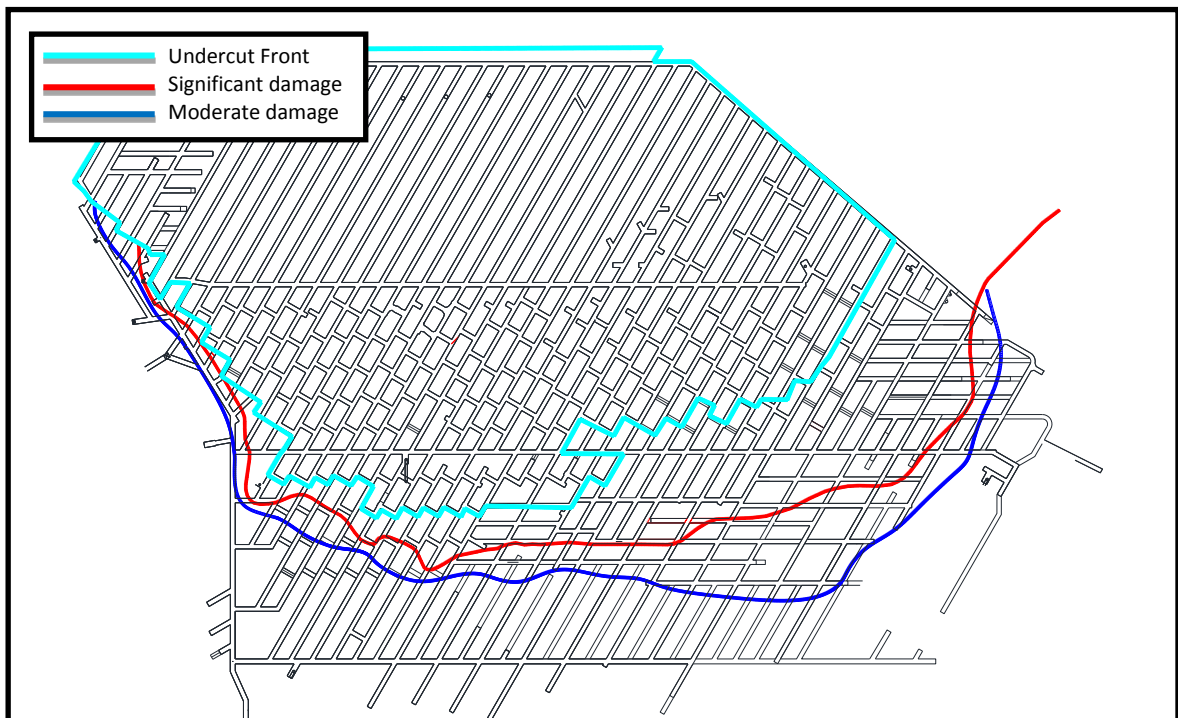


Figure E.16: Mapped damage located ahead of undercut front on UCL Esmeralda operation, Nov. 2005.

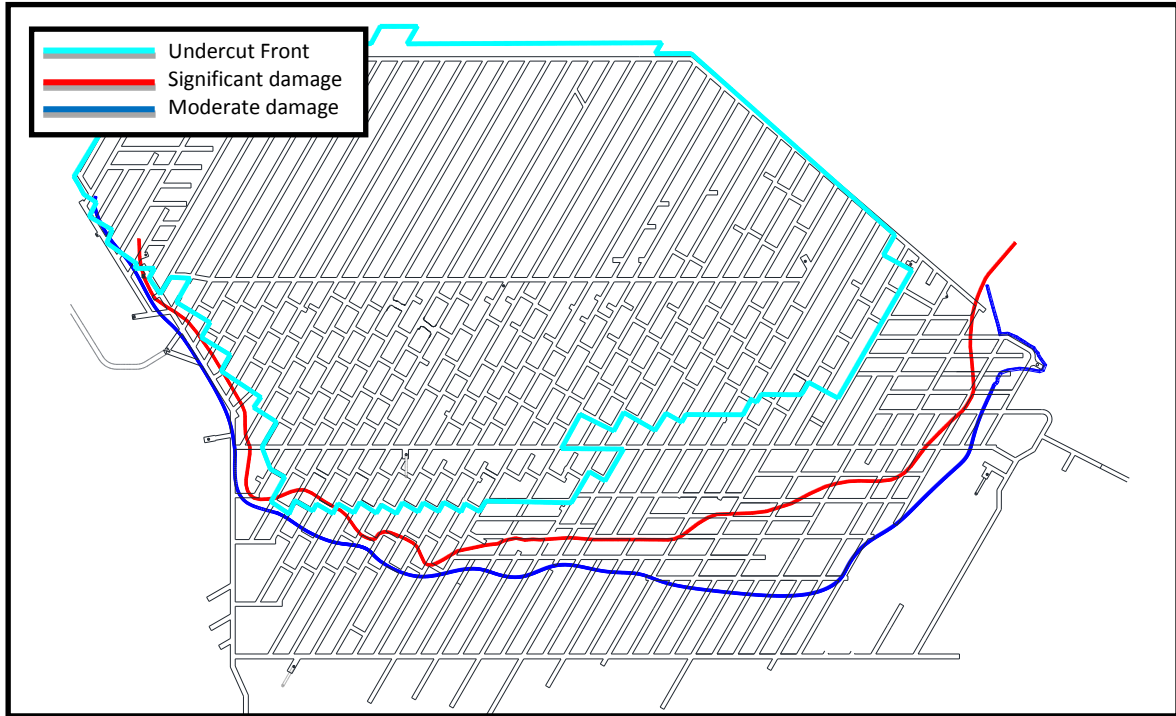


Figure E.17: Mapped damage located ahead of undercut front on UCL Esmeralda operation, March 2006.

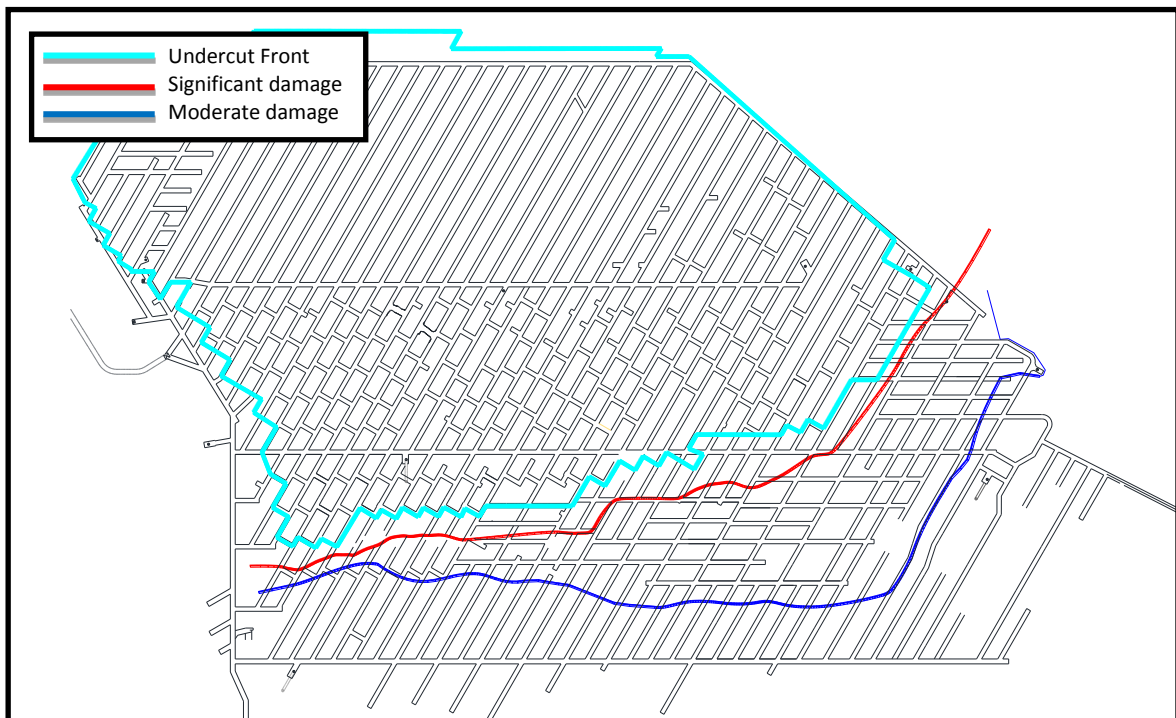
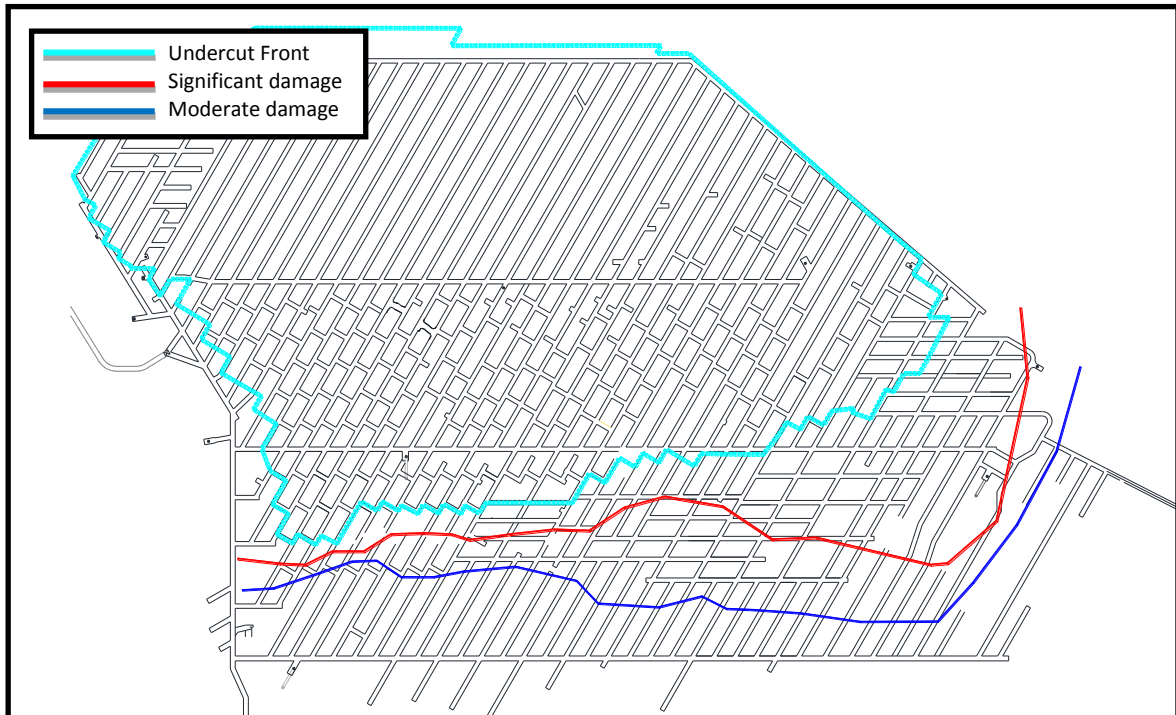
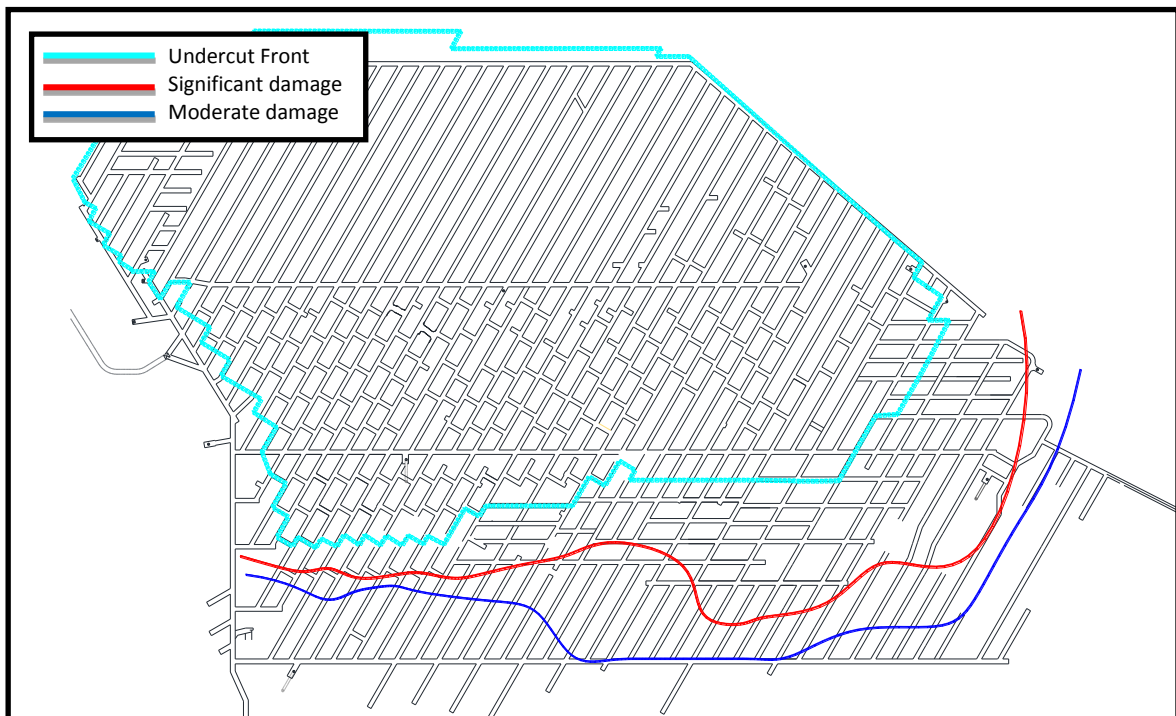


Figure E.18: Mapped damage located ahead of undercut front on UCL Esmeralda operation, May 2007.



**Figure E.19:** Mapped damage located ahead of undercut front on UCL Esmeralda operation, Nov. 2007.



**Figure E.20:** Mapped damage located ahead of undercut front on UCL Esmeralda operation, April 2008.

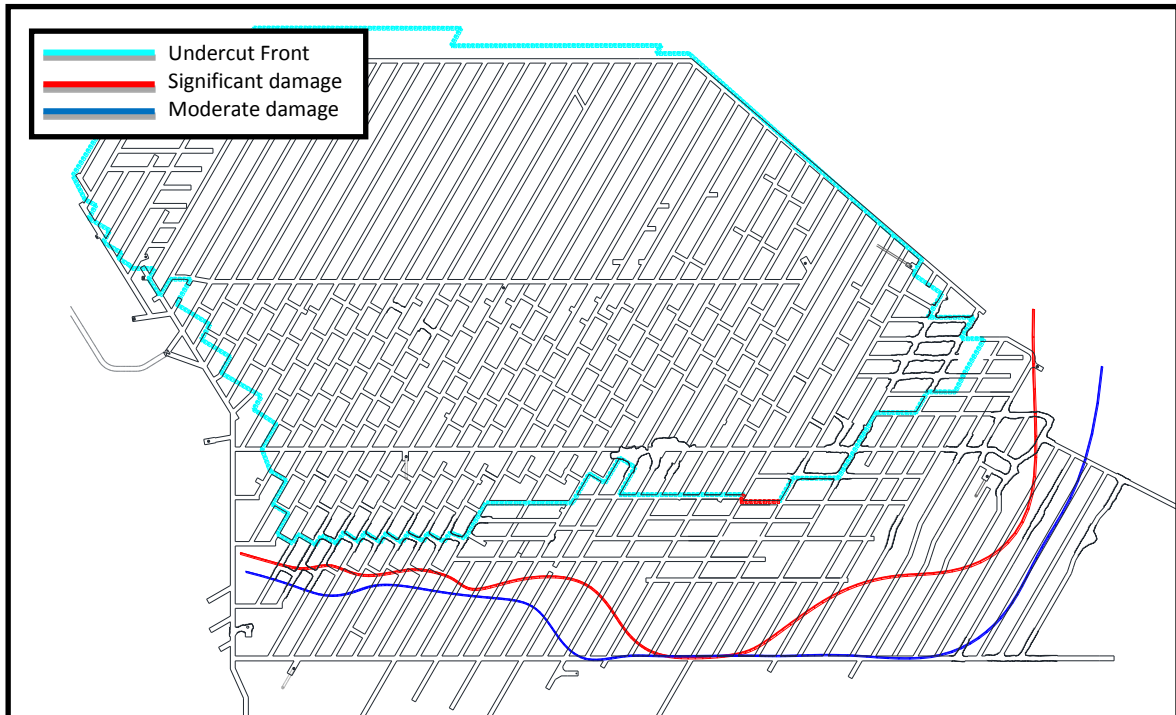


Figure E.21: Mapped damage located ahead of undercut front on UCL Esmeralda operation, July 2008.

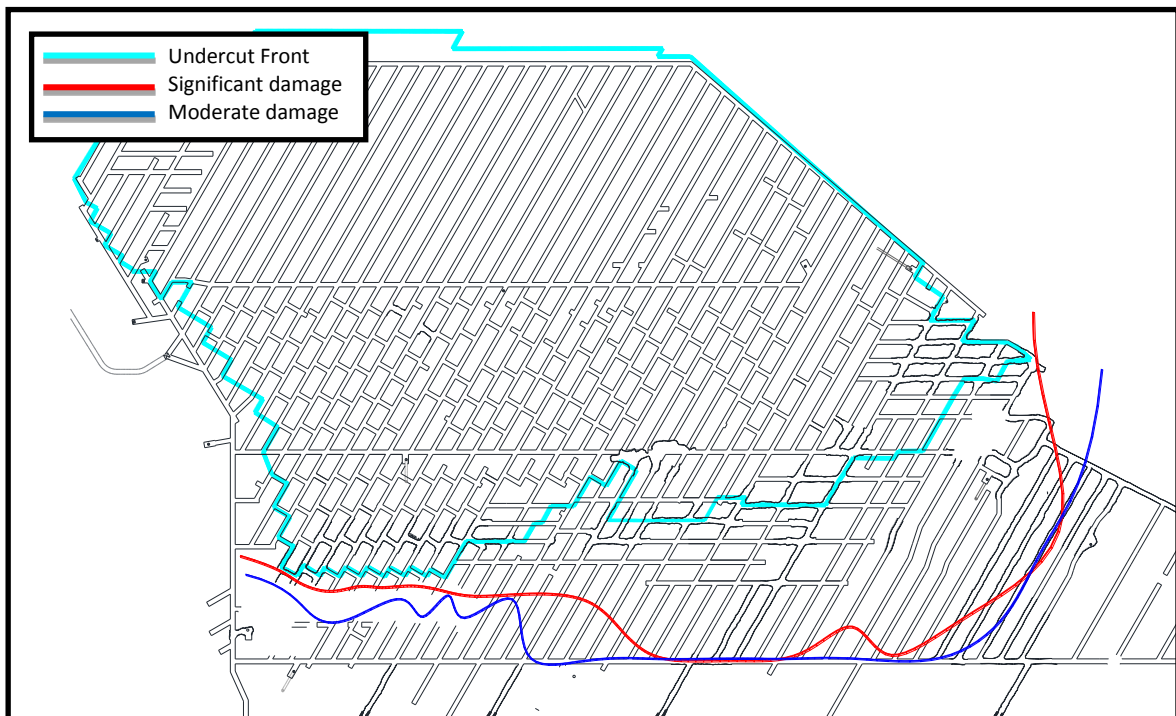


Figure E.22: Mapped damage located ahead of undercut front on UCL Esmeralda operation, Sept. 2009.